



HAL
open science

Identification des régulateurs de la sirtuine de type 1 (SIRT1) : acteur clé de l'altération osseuse et la capacité de différenciation des cellules stromales en situation de déficit énergétique (Anorexie Mentale)

Viktorija Avilkina

► **To cite this version:**

Viktorija Avilkina. Identification des régulateurs de la sirtuine de type 1 (SIRT1) : acteur clé de l'altération osseuse et la capacité de différenciation des cellules stromales en situation de déficit énergétique (Anorexie Mentale). Cellular Biology. Université du Littoral Côte d'Opale, 2023. English. NNT : 2023DUNK0653 . tel-04100417

HAL Id: tel-04100417

<https://theses.hal.science/tel-04100417>

Submitted on 17 May 2023

HAL is a multi-disciplinary open access archive for the deposit and dissemination of scientific research documents, whether they are published or not. The documents may come from teaching and research institutions in France or abroad, or from public or private research centers.

L'archive ouverte pluridisciplinaire **HAL**, est destinée au dépôt et à la diffusion de documents scientifiques de niveau recherche, publiés ou non, émanant des établissements d'enseignement et de recherche français ou étrangers, des laboratoires publics ou privés.



Thèse de Doctorat

Mention : Biologie-Santé

Spécialité : Aspects moléculaires et cellulaires de la biologie

présenté à *l'Ecole Doctorale en Sciences Technologie et Santé (ED 585)*

of l'Université du Littoral Côte d'Opale

par

Viktorija AVILKINA

pour obtenir le grade de Docteur de l'Université du Littoral Côte d'Opale

Regulators of Sirtuin Type 1 (SIRT1) : a key player in bone alterations and bone marrow stromal cells differentiation capacity in a mouse model of Anorexia nervosa

Soutenue le 7 Février 2023, après avis des rapporteurs, devant le jury d'examen :

M ^{me} S. BECK-CORMIER, Chargée de Recherche (Inserm) HDR, Univ. Nantes	Rapporteur
M ^{me} A. BOULOUMIÉ, Directrice de Recherche (Inserm) HDR, Univ. Toulouse	Rapporteur
M A. GUIGNANDON, Maître de Conférences HDR, Univ. Jean Monnet	Examineur
M W. CAWTHORN, Senior Lecturer, Univ. of Edinburgh	Examineur
M S. KAMEL, Professeur Praticien Hospitalier, Univ. de Picardie Jules Verne	Examineur
M ^{me} O. VILTART, Professeure, Univ. de Lille	Examineur
M C. CHAUVEAU, Professeur, Univ. du Littoral Côte d'Opale	Directeur de thèses
M ^{me} O. GHALI MHENNI, Maîtresse de Conférences, Univ. du Littoral Côte d'Opale	Co-directrice

“Когда наука достигает какой-либо вершины, с неё открывается обширная перспектива дальнейшего пути к новым вершинам, открываются новые дороги, по которым наука пойдёт дальше.”

- С. Вавилов

ACKNOWLEDGEMENTS

Most importantly, I would like to thank **Prof Christophe Chauveau** and **Dr Olfa Ghali Mhenni**, my supervisors, for welcoming me in the MAB Lab and for all help and support during these past 3 years. Thank you, **Dr Olfa Ghali Mhenni**, for being always available for me and for your help in day-to-day tasks, as well as help in work planning. Thank you, **Prof Christophe Chauveau**, for always asking the right questions and pushing this project further. Thank you for finding time in your busy schedule, as a head of the laboratory, to sit down and encourage productive discussion,

I would like to express my gratitude to **Dr Sarah Beck-Cornier**, from University of Nantes (Inserm, UMR_S 1229 RMeS), and **Dr Anne Bouloumié**, from University of Toulouse (Inserm, UMR_1048), for accepting the role of “reporteurs” to assess current manuscript. Additionally, I want to thank **Prof Saïd Kamel**, from University of Picardie Jules Verne (MP3CV), and **Prof Odile Viltart**, from University of Lille (UMR CNRS 9193), for kindly accepting to fulfil the role of “examineurs”. Moreover, my sincerely thank to **Dr William Cawthorn**, from University of Edinburgh, and **Dr Alain Guignandon**, from Saint Etienne University, for being the part of my annual committee, for your helpful comments and useful discussions. Also, I would like to thank you for kindly accepting the role of “examineurs”, during my thesis defence.

This work would not have been done, without technical support of **MAB Lab members**. Therefore, I would like to thank **Veronique Gaultier, Flore Miellot** and **Damien Leterme** for conduction mice experimentations during our long protocols, as well as performing mice sacrifice. Additional appreciation I would like to express to **Veronique, Flore and Severine Delplace** for help with histology and bone analysis. I was lucky to be surrounded by great fellow students, who always made my day. Thank you so much **Federica and Amelie** for sharing this experience with me, for always providing moral support, and thank you for this unforgettable time during the conferences.

Moreover, our **Lille part of MAB Lab**, played an important role in supporting this project, by delegating part of the work. Special thank you I want to say to **Dr Guillaume Falgayrac** for his patience during RAMAN spectroscopy training, as well as all his work done on adipocytes. Also, thank you to **Jerome Delattre**, who helped me with acquiring micro-CT data.

Additional acknowledgment I was to dedicate to **EGID lab**, University of Lille, who collaborated with us, and provided valuable results of RNA Sequencing. Special thank you to **Dr Amelie Bonnefond, Dr Mehdi Derhourhia and Dr Mickaël Canouil**, for all the work that you did.

I would also like to thank people who contributed towards construction of my scientific foundation, including knowledge and experience. Therefore, I am grateful to my personal tutor in Newcastle University, **Prof Craig Robson**, who always encouraged me to proceed in my dreams. Furthermore, thank you, **Prof John Loughlin**, for inviting me, a second year Baccalaureate student at the time, to your lab and introducing me to the world of research. Now looking back, I can reflect that my education started with you and first ever research project on osteoarthritic, and now my last research project (during the process of education) is concluding with bone research as well.

I believe that one of the biggest impacts on me, my way of thinking, my scientific knowledge and my foundation of laboratory expertise was given by already **Dr Yennifer Cortes-Arraya**. A PhD student at the time, in Roslin Institute, University of Edinburgh, she helped me a lot in guiding and teaching me throughout my Master Degree research project. She showed me all ups and downs of conducting a project, taught me all techniques she knew and helped me to make my final decision and proceed on to conducting PhD. Therefore, thank you, **Yennifer** for your patience and help.

My infinite gratitude, I would like to express to **my parents**, who always been incredibly supportive of me and my choices. Without your encouragement 10 years ago, to leave home and proceed my education abroad, I would never get to this point. Thank you for this decision, as I never had a moment in life when I regretted leaving home that early in life. Thank you for always providing a sense of security, as well as infinite and unconditional love, which allowed me to proceed my aspirations. Also, my deepest appreciation I want to express to my **grandmother Ija** and **grandparents Svetlana and Valentins**. I am incredibly lucky to have a loving and supporting family. Despite the initial criticism, I am happy with my decision to move to France, as here I found most valuable connections.

One of my most important connection established during this time in France was with you, **Enzo**. I never could imagine meeting my partner, here in Boulogne sur Mer, but here we are almost 3 years later. Thank you for being persistence and breaking the containment laws when pandemic hit us. Thank you for always being there with me, I definitely would have never survived French bureaucracy without your help. Most definitely, I would have not survived (actually) without my personal translator on these numerous doctors' appointments. I am incredibly thankful that I have you in my life and that we will close this chapter to start a new one together.

Another, very important for me, connection I found in this lab, straight after arrival to France. Therefore, I want to thank from the bottom of my heart, my friend, who managed to become my best friend after these 3 years – **Federica**. Without your help and support, this pandemic, as well as life after, would be definitely harder. Thank you for always being there with me and for me, for always being on my side. Thank you for all your help with experiments and with good advice. After all this time you showed that you are truly my best friend and this friendship will last forever.

Nevertheless, I want to thank my friends that are with me for well over a decade – **Anastasia, Marija and Alisa** (who is with me for 25 years). Our friendship has been tested through time and distance, but despite all obstacles, we always stayed connected. Thank you so much for always supporting me, and always making me feel loved. I am grateful to call you all my best friends, as I know that no matter what I can rely on you. Also, thank you, **Robin**, for staying my friend (lab partner for life) after all these years, even if our paths took us apart, you always found a moment to visit me.

In the end of these acknowledgments, I want to express my gratitude to all people who are surrounding me and say additional thank you to **Dr Jerome Eeckhoute**, who gave me an opportunity to conduct a Post-Doctoral project in his team.

Financements

Financement MESRI

Contrat doctoral de droit public

Du 18 novembre 2019 au 17 février 2023

Par Université du Littoral Côte d'Opale/la Région Haut de France

TABLE OF CONTENT

LIST OF FIGURES	10
LIST OF TABLES	14
LIST OF ABBREVIATIONS	15
FOREWORD.....	19
INTRODUCTION.....	20
1. Crosstalk between Bone and Adipose tissue	20
1.1 Skeleton.....	20
1.1.1 Bone development and remodelling	21
1.1.2 Bone functions	23
1.1.2i Bone function – haematopoiesis	23
1.1.2ii Bone function – energy metabolism	24
1.1.2iii Bone function – mineral metabolism.....	25
1.1.2iv Bone function – extraskeletal tissues.....	26
1.2 Adipose tissues.....	26
1.2.1 Adipose tissue functions	29
1.2.1i WAT function - lipogenesis, TAG synthesis and lipolysis	29
1.2.1ii WAT function - adiponectin and leptin secretion.....	33
1.2.1iii BAT function – thermogenesis.....	35
1.3 BMAT.....	36
1.3.1 BMAT study approach.....	37
1.3.2 BMAT functions	39
1.3.2i BMAT function - haematopoiesis.....	41
1.3.2ii BMAT function - bone turnover.....	42
1.3.2iii BMAT function – systemic	43
1.3.3 BMAT regulation.....	45
1.3.3i BMAT regulation - ageing.....	46
1.3.3ii BMAT regulation - menopause	47
1.3.3iii BMAT regulation - cancer.....	49
1.3.4 BMAT in metabolic disease.....	50
1.3.4i BMAT in diabetes.....	51
1.3.4ii BMAT in obesity	51
1.3.4iii BMAT in anorexia nervosa	51
Anorexia nervosa (AN) - characterisation	51
BMAT accumulation in AN – clinical studies.....	54
BMAT accumulation in AN – studies on animal models	56
2. Sirtuin Type 1 – metabolic regulator	60
2.1 Sirtuin family	60
Sirtuin family – function.....	61
2.2 SIRT1 structure and expression	64
2.2.1 Protein topology.....	65
2.2.2 Expression pattern.....	66
2.3 SIRT1 function.....	67
2.3.1 SIRT1 cellular function.....	68

Chromatin structure and gene transcription	68
DNA repair.....	69
Cell survival and apoptosis	69
Autophagy.....	70
Ion channel regulation.....	71
Inflammation.....	71
2.3.2 SIRT1 function in metabolic tissue.....	72
2.3.2i SIRT1 function in metabolic tissue - Pancreas.....	72
2.3.2ii SIRT1 function in metabolic tissue - Liver	74
2.3.2iii SIRT1 function in metabolic tissue - Adipose tissue	78
2.3.3 SIRT1 function in bone marrow	79
2.4 SIRT1 regulation of expression and activity	80
2.4.1 Transcriptional regulation of SIRT1	82
2.4.2 Post-transcriptional regulation of SIRT1	84
Non-coding RNAs	84
NAD ⁺ levels and small molecules	85
Protein-protein interactions.....	86
Protein PTMs	88

AIMS AND OBJECTIVES OF THE THESIS.....91

PART 1 – THE EFFECT OF SEVERITY LEVEL AND DURATION OF ENERGY DEFICIT ON BONE AND BONE MARROW STROMAL CELL (BMSC) DIFFERENTIATION IN ANOREXIA NERVOSA MOUSE MODEL92

I. INTRODUCTION	92
II. MATERIALS AND METHODS.....	102
1. Animals	102
2. Dual Energy X-Ray Absorptiometry (DEXA) Analysis	103
3. Mineralized Bone Micro-CT Analysis.....	103
4. Bone Marrow Adipose Tissue Content - Micro-CT Analysis	104
6. Primary Bone Marrow Stromal Cell Culture	105
7. ST2 Cell Line Culture in Nutrient Deficiency Medium	105
8. Raman Microspectroscopy.....	106
9. Mineralisation Quantification	107
10. RNA Sequencing and Data Analysis	107
11. RNA Extraction and Reverse Transcription	108
12. Real-Time PCR.....	108
13. SIRT1 ELISA Assay.....	109
14. Statistical Analysis.....	110
III. RESULTS	111
1. Circulating SIRT1 has a negative association with femoral head fat in AN patients 111	
2. Severity Level of Energy Deficit in Mice Affect Bone Phenotype and BMSC Differentiation Capacity.....	111
3. Duration of Energy Deficit in Mice Affect Bone Phenotype and BMSC Differentiation Capacity.....	122
4. Transcriptomic analysis of BMSCs extracted from 10-Week and 4-Week SBA Protocols (Cohort 1) by RNA Sequencing.....	131
5. Replication of Original Study – 10-Week and 4-Week SBA Protocols Cohort 2.	147

6. In vitro study on BMSCs differentiation capacity – development of medium mimicking nutrient deficiency	162
2. DISCUSSION AND CONCLUSIONS	166
PART II – IDENTIFICATION OF NEW POTENTIAL REGULATORS OF SIRT1 GENE EXPRESSION USING RNA SEQUENCING DATA	190
I. INTRODUCTION	190
II. MATERIALS AND METHODS.....	193
1. Animals	193
2. Primary Bone Marrow Stromal Cell and ST2 Cell Culture.....	193
3. RNA Sequencing and Data Analysis	193
4. RNA Extraction and Reverse Transcription	193
5. Real-Time PCR.....	194
6. siRNA Transfection	195
7. Statistical Analysis.....	195
III. RESULTS	196
Identification of new potential regulators of Sirt1 expression using RNA-seq data	196
IV. DISCUSSION AND CONCLUSIONS	204
PART 3 – FURTHER INVESTIGATION OF SIRT1 REGULATORS.....	207
I. INTRODUCTION	207
II. MATERIALS AND METHODS.....	213
1. Animals	213
2. Primary Bone Marrow Stromal Cell and ST2 Cell Culture.....	213
3. Drug Treatments	214
4. AMPK Activity Assay	214
5. siRNA Transfection	214
6. RNA Extraction and Reverse Transcription	215
7. Real-Time PCR.....	215
8. Protein Extraction	216
9. Western Blotting	216
10. Statistical Analysis.....	216
III. RESULTS	218
1. AMPK expression is modulated in long term SBA protocol (SBA 18%).....	218
2. In primary BMSCs and ST2 cells, AMPK α 1 is more abundant than AMPK α 2 ..	219
3. Suppression of AMPK activity by Dorsomorphin has a negative effect on Sirt1 expression	220
4. Only Prkaa1 suppression with small interference RNA (siRNA) affects Sirt1 expression	225
5. Induction of AMPK activity does not affect Sirt1 mRNA level.....	229
6. DISCUSSION AND CONCLUSIONS	232
OVERALL CONCLUSIONS AND PROSPECTIVES	235
LIST OF PUBLICATIONS AND COMMUNICATIONS.....	245
PROJECT SUMMARY IN FRENCH	247

BIBLIOGRAPHY263

LIST OF FIGURES

Figure 1. <i>In vitro</i> differentiation of human MSCs.	20
Figure 2. The schematic diagram of endochondral ossification process	21
Figure 3. The process of bone remodelling	21
Figure 4. Bone signalling molecules affecting body homeostasis	23
Figure 5. WAT, BAT, Beige AT and BMAT depots in humans and mice.	27
Figure 6. Summary de novo lipogenesis in WAT.....	30
Figure 7. Summary of triacylglycerol synthesis and lipolysis in WAT.....	32
Figure 8. Diagram of leptin regulated energy balance.....	34
Figure 9. Main mechanisms of adiponectin's functions on peripheral tissues to regulate metabolism and insulin sensitivity.....	35
Figure 10. Conversion of red marrow to yellow marrow.	37
Figure 11. Location and characteristics of mouse and human cBMAT and rBMAT.....	45
Figure 13. Sirtuin family structure.....	45
Figure 14. Enzymatic activity of sirtuin family members	62
Figure 15. Schematic diagram of SIRT1 isoforms.	64
Figure 16. Protein structure of human SIRT1	66
Figure 17. <i>Sirt1</i> mRNA expression overview	67
Figure 18. SIRT1 protein expression overview	67
Figure 19. Summary of SIRT1 function in pancreatic β -cells.....	74
Figure 20. Summary of glucose homeostasis in hepatocytes and involvement of SIRT1 this process.....	77
Figure 21. Potential mechanisms of CR-mediated regulation of SIRT1 activity.	81
Figure 22. Summary diagram of the miR-34a/p53/SIRT1 regulatory loop.....	85
Figure 23. Summary diagram of the regulation of SIRT1 expression and function.....	88
Figure 24. A workflow of RNA-seq.	98
Figure 25. Correlation analysis of SIRT1 plasma concentration and fat fraction in femoral neck on AN patients.....	111

Figure 26. Body and tissue mass, BMC, fat and lean mass in mice after 10 weeks of SBA protocols of different severity.	114
Figure 27. The results of micro-CT analysis of tibia, showing different bone parameters after exposure to 10 weeks of SBA protocols at different levels of severity.	115
Figure 28. Study of adipocyte first appearance, size and lipid unsaturation ratio in 10-week protocol groups.	117
Figure 29. 10-week SBA protocol induced changes in BMSC differentiation comparing to CT	119
Figure 30. 10-week SBA protocol induced a suppression of <i>Sirt1</i> mRNA level Figure 29. 10-week SBA protocol induced an alteration in osteoblastogenesis comparing to CT group. ...	120
Figure 31. 10-week SBA protocol induced a suppression of <i>Sirt1</i> mRNA level	121
Figure 32. Body mass, BMC, fat and lean mass in mice after 4 weeks of SBA protocol (cohort 1).....	124
Figure 33. The results of micro-CT analysis of tibia, showing different bone parameters after exposure to 4-week SBA protocol	125
Figure 34. Study of adipocyte first appearance, size and lipid unsaturation ratio in 4-week protocol groups.	127
Figure 35. Study of adipogenic marker gene expression in BMSCs.	128
Figure 36. Osteoblastogenic marker gene expression in BMSCs after 4-week SBA protocol.	129
Figure 37. <i>Sirt1</i> expression in BMSCs extracted from 4-week SBA protocol.	130
Figure 38. Volcano Plot of top altered genes in 10-week study	132
Figure 39. Most upregulated and downregulated pathways in 10-week SBA 18% condition.	137
Figure 40. Volcano Plot of top altered genes in 4-week study.	139
Figure 41. Most upregulated and downregulated pathways in 4-week SBA 18% condition	142
Figure 42. Volcano Plot of 10-week study that tags common adipogenic and osteoblastogenic marker genes.	144
Figure 43. Volcano Plot of 4-week study that tags common adipogenic and osteoblastogenic marker genes	146
Figure 44. Body mass, BMC, fat and lean mass in mice after 10 weeks of SBA protocol ...	149
Figure 45. Micro-CT analysis of tibia, showing different bone parameters after 10 weeks of SBA protocol.	150

Figure 46. Adipocyte first appearance, size and adipogenic gene expression in BMSCs extracted from mice of 10-week protocol.....	152
Figure 47. Osteoblastogenic gene expression in BMSCs extracted from mice of 10-week protocol.	152
Figure 48. <i>Sirt1</i> expression in BMSCs extracted from mice of 10-week protocol.....	153
Figure 49. Body mass, BMC, fat and lean mass in mice after 4 weeks of SBA protocol	156
Figure 50. Micro-CT analysis of tibia, showing different bone parameters after 4 weeks of SBA protocol.	158
Figure 51. Adipocyte first appearance, size and adipogenic gene expression in BMSCs extracted from mice of 4-week protocol.....	159
Figure 52. Osteoblastogenic gene expression in BMSCs extracted from mice of 4-week protocol	161
Figure 53. <i>Sirt1</i> expression in BMSCs extracted from mice of 4-week protocol.....	162
Figure 54. Adipogenic, osteoblastogenic genic markers and <i>Sirt1</i> mRNA level in ST2 treated with low FBS medium.	163
Figure 55. Adipogenic, osteoblastogenic genic markers and <i>Sirt1</i> mRNA level in primary mice BMSCs treated with low FBS medium.....	165
Figure 56. RANKL gene (<i>Tnfs11</i>) and OPG gene (<i>Tnfrsf11b</i>) relative mRNA level in BMSCs extracted from CT and SBA 18% mice from different studies.....	184
Figure 57. Mice body mass timeline.....	185
Figure 58. Schematic representation of siRNA action.....	191
Figure 59. Summary of RNA-seq data analysis to identify <i>Sirt1</i> related genes and Venn diagram of upregulated/downregulated pathways.	197
Figure 60. Summary of RNA-seq data analysis to identify <i>Sirt1</i> related genes and Venn diagram of upregulated/downregulated genes	199
Figure 61. Relative mRNA expression of RNA sequencing identified genes.	200
Figure 62. <i>Rb1</i> and <i>Sirt1</i> expression in ST2 cells after exposed to <i>Rb1</i> siRNA.....	203
Figure 63. AMPK activity regulation and function.	208
Figure 64. AMPK α -subunits structure and molecular regulation.	210
Figure 65. <i>Prkaa1</i> and <i>Prkaa2</i> expression in BMSCs extracted from SBA mice.....	218
Figure 66. Basal expression of <i>Prkaa1</i> and <i>Prkaa2</i> expression in BMSCs and ST2 cells....	220

Figure 67. AMPK activity assay results and <i>Sirt1</i> expression in ST2 cells and primary BMSCs exposed to 14h and 72h DM treatment.	222
Figure 68. <i>Prkaa1</i> and <i>Prkaa2</i> expression in primary BMSCs and ST2 cells exposed to 14h and 72h DM treatment.	224
Figure 69. <i>Prkaa1</i> , <i>Sirt1</i> and <i>Prkaa2</i> expression in ST2 cells after exposed to <i>Prkaa1</i> siRNA.	226
Figure 70. <i>Prkaa2</i> , <i>Sirt1</i> and <i>Prkaa1</i> expression in ST2 cells after exposed to <i>Prkaa2</i> siRNA.	227
Figure 71. <i>Prkaa1</i> and <i>Prkaa2</i> expression in ST2 cells after exposed to combination of <i>Prkaa1</i> and <i>Prkaa2</i> siRNA.	229
Figure 72. AMPK activity assay results and <i>Sirt1</i> expression in primary BMSCs exposed to 14h A-769662 treatment.	230
Figure 73. <i>Prkaa1</i> and <i>Prkaa2</i> expression in primary BMSCs exposed to 14h A-769662 treatment.	231
Figure 74. Project work overview and main questions addressed in this study.	235
Figure 75. Project work overview and main questions addressed in this study with answers.	238
Figure 76. Bone/BMA regulation in the context of energy deficit.	240

LIST OF TABLES

Table 1. Summary of AT subtypes.	28
Table 1. Summary of AT subtypes.	28
Table 2. Summary of studies conducted on AN patients.	56
Table 3. Summary of studies conducted on animal models of CR.	59
Table 4. Summary of SIRT1 mRNA and protein isoforms in humans.	64
Table 5. Details of lipid droplets studied in each condition of the 10-week and 4-week protocols (cohort 1).	107
Table 6. Primer sequences and conditions of quantitative RT-PCR (PART 1).	109
Table 7. Summary of gene function (10-week).	134
Table 8. Summary of gene function (4-week).	140
Table 9. Summary of results obtained from 10-week cohort 1, comparing CT and different weight loss groups (SBA 0%, 12%, 18%, 24%).	170
Table 10. Summary of results obtained from 10-week cohort 1 study and 10-week cohort 2 study, comparing CT and SBA 18% groups.	181
Table 11. Summary of results obtained from 4-week cohort 1 study and 4-week cohort 2 study, comparing CT and SBA 18% groups.	182
Table 12. Primer sequences and conditions of quantitative RT-PCR (PART 2).	194
Table 13. Summary of gene function.	202
Table 14. Primer sequences and conditions of quantitative RT-PCR (PART 3).	215

LIST OF ABBREVIATIONS

1,2-DAG – 1,2-Diacylglycerol	BAX – Bcl-2-associated X protein
1H-MRS – single-voxel proton spectroscopy	BBB – blood brain barrier
2-MAG – 2-monoacylglycerol	Beige AT – beige adipose tissue
3T3-L1 – extramedullary preadipocytes	BGLAP – osteocalcin gene
AA – amino acids	BK – calcium-activated potassium
AC – adenylyl cyclase	BM – bone marrow
Ac-CoA – acetyl-CoA	BMA – bone marrow adipocyte
ACC1 – acetyl-CoA carboxylase 1	BMA _d – BM adipocytes
ACLY – ATP-citrate lyase	BMAT – bone marrow adipose tissue
ACS – acyl-coenzyme A synthetase	BMC – bone mineral composition
ACSL1 – involving acyl-CoA synthetase long chain family member 1	BMD – bone mineral density
ADHR – autosomal dominant hypophosphatemic rickets	BMI – body mass index
AGPAT – acylglycerophosphate acyltransferase	BMP – bone morphogenic protein
AGRP – Agouti-related protein	BMS2 – bone marrow stromal cell line 2
AMP – adenosine monophosphate	BMSC – bone marrow stromal cell
AMPK – AMP protein kinase	Bv/Tv – bone volume per tissue volume
AN – anorexia nervosa	C3H10T1/2 – murine pluripotent mesenchymal cell line
AP-1 – activator protein 1	Ca ²⁺ – calcium ions
Arg – arginine	CACUL1 – Cdk2-associated cullin 1
AT – adipose tissue	cAMP – cyclic adenosine monophosphate
ATF4 – activating transcription factor 4	cBMAT – constitutive BMAT
Atg – autophagy protein	CE-CT – contrast enhanced micro-CT
ATGL – adipose triglyceride lipase	CEBP – CCAAT/enhancer-binding protein
ATM – ataxia telangiectasia mutated	CESA – contrast enhancing staining agents
ATP – adenosine triphosphate	CHK2 – checkpoint kinase 2
Av/Tv – adipocyte volume/tissue volume	ChORE – carbohydrate response element
BAT – brown adipose tissue	Chr – chromosome
	ChREBP – carbohydrate response element binding protein
	CNS – central nervous system
	COLL1 – collagen type 1

Cort.Th – Cort.Th
 CPT1 – carnitine palmitoyl transferase 1
 CR – caloric restriction
 CREB – cAMP-response-element-binding protein
 CRTC2 – CREB regulated transcription regulator 2
 CtIP – C-terminal binding protein 1 (CtBP1) interacting protein
 CTR – C-terminal regulatory segment
 CXCL – C-X-C motif chemokine ligand
 Cys – cystine
 DDR – DNA damage response
 DEXA – dual-energy x-ray absorptiometry
 DG – dentate gyrus
 DLX5 – distal-less homeobox 5 gene
 DNL – de novo lipogenesis
 DNMT – DNA methyltransferase
 DNMT1 – DNA methyltransferase 1
 DYRK – tyrosine-phosphorylated and regulated kinase
 EOD – every other day
 ER – endoplasmic reticulum
 ER α – oestrogen receptor alpha
 ETC – electron transport chain
 EV – Extracellular vesicle
 EZH2 – enhancer of zeste homologue 2
 FA – fatty acid
 FABP4 – fatty acid binding protein 4
 FACS – fluorescent-activated cell sorting
 FASN – fatty acid synthase
 FBS – foetal bovine serum
 FGF – fibroblast growth factor
 FGF23 – fibroblast growth factor 23
 FOXO – forkhead box O
 FSH – follicle stimulated hormone
 G-CSF – granulocyte colony-stimulating factor
 GCGR – glucagon receptor
 GCSF – granulocyte-colony stimulating factor
 GDH – glutamate dehydrogenase
 GH – growth hormone
 GlaOC – uncarboxylated OC
 GluOC – undercarboxylated OC
 GLUT4 – glucose transporter type 4
 Gly-3-P – sn-glycerol-3-phosphate
 GM-CSF – granulocyte-macrophage colony-stimulating factor
 GPAT – glycerol-3-phosphate acyltransferase
 H3 – histone
 HEK-293 – human embryonic kidney cell line
 HEK293 – human embryonic cell line
 Hf-WD-POM – Hafnium Wells-Dawson polyoxometalate
 HFD – high fat diet
 HIC1 – hypermethylated in cancer 1
 HIF1 – hypoxia inducible factor 1
 hMSCs – human mesenchymal stem cells
 HNF4 – hepatic nuclear factor 4
 HPG – hypothalamic-pituitary-gonadal
 HSC – haematopoietic stem cell
 HSCs – haematopoietic stem cells
 HSL – hormone sensitive lipase
 HUR – Human antigen R
 IB – inhibitor of B

IBXM – 3-isobutyl-methylxanthine
 IGF-1 – insulin like growth factor 1
 IKK – IB kinase
 IL – interleukin
 IR – insulin receptor
 IRI – ischemic renal injury
 IRS – insulin receptor substrate
 JAK2 – Janus kinase 2
 LC3 – 1A/1B-light chain 3
 LepR – leptin receptor
 Leu – leucin
 lncRNA – long ncRNA
 LPA – produce lysophosphatidic acid
 LXR – liver X receptor
 Lys – lysin
 MafA – MAF BZIP transcription factor A
 MAR1 – mating-type regulator
 MCD – malonyl-CoA decarboxylase
 MEF2 – MADS box transcription
 enhancer factor 2
 MGL – monoglyceride lipase
 micro-CT – x-ray microfocus computed
 tomography
 MIP-1 α – macrophage inflammatory
 protein 1 α
 miRNA – microRNA
 Mlx – Max-like protein X
 MMP9 – matrix metalloproteinase 9
 MRI – magnetic resonance imaging
 MSC – mesenchymal stem cell
 MST1 – mammalian Ste20 like kinase
 mTORC1 – mammalian target of
 rapamycin complex 1
 MyoD – myoblast determination protein 1
 NAD – nicotinamide adenine dinucleotide
 NAFLD – non-alcoholic fatty liver disease
 NAM – nicotinamide
 NAMPT – nicotinamide
 phosphoribosyltransferase
 NaPi-2a – type IIa sodium-phosphate co-
 transporter
 Nav1.5 – voltage-gated cardiac Na⁺
 channel
 NCoR – nuclear receptor co-repressor
 ncRNA – non-coding RNA
 NE – norepinephrine
 NeuroD – neurogenic differentiation factor
 NF κ B – nuclear factor kappa-light-chain-
 enhancer of activated B
 NPY – neuropeptide Y
 NTS – nuclear translocation signals
 OC – osteocalcin
 OL – osteocyte-less mice
 OPG – osteoprotegerin
 OsO₄ – osmium-tetroxide
 OVX – ovariectomised
 OXPHOS – oxidative phosphorylation
 P2Y₂ – purinergic receptor
 PA – phosphatidic acid
 PAP – Phosphatidic acid
 phosphohydrolases
 PARP – poly ADP-ribose polymerase
 PDFF – proton-density fat fraction
 PDX1 – pancreas/duodenum homeobox
 protein 1
 PEPCK1 – phosphoenolpyruvate
 carboxykinase
 PET – positron emission tomography

PI3K – phosphatidylinositol 3-kinase
 PKA – protein kinase A
 PKB – protein kinase B
 PLIN2 – perilipin 2
 PMOP – postmenopausal osteoporosis
 Pol I – RNA polymerase I
 POMC – pro-opiomelanocortin
 PP2A – protein phosphatase 2A
 PPARGC1a – PPAR γ coactivator 1 alpha
 PPAR γ – peroxisome proliferator-activated receptor gamma
 Prdm16 – PR domain containing 16
 Pref1 – pre-adipocyte marker
 PTECs – proximal tubular epithelial cells
 PTH – parathyroid hormone
 PTH – parathyroid hormone
 PTM – post transcriptional modifications
 RANKL – receptor activator of nuclear factor kappa-B ligand
 rBMAT – regulated BMAT
 rDNA – ribosomal DNA
 RLEB– v-Rel reticuloendotheliosis viral oncogene homolog B
 ROS – reactive oxygen species
 RUNX2 – runt-related transcription factor 2
 SBA – separation based anorexia
 SCD1 – stearoyl-CoA desaturase 1
 SCF – stem cell factor
 SCFs – stem cell factors
 Ser – serine
 SIR2 – silent information regulator 2
 SIRT1-v1 – SIRT1 isoform-1
 SOST – sclerostin
 SRE – serum responsive element
 SREBP-1c – sterol-regulatory element binding protein 1c
 SREBP1c – sterol regulatory element-binding protein
 STAT3 – signal transducer and activator of transcription 3
 SVF – stromal vascular fraction
 T1DM/T2DM – type 1/2 diabetes mellitus
 TAF168 – transcription initiation factor TFIID subunit
 TAG – triacylglycerol
 Tb.N – trabecular number
 Tb.Sp – trabecular spacing
 Tb.Th – trabecular thickness
 TCA – tricarboxylic acid cycle
 TFAM – mitochondrial transcription factor A
 TGF – transforming growth factor
 Thr – threonine
 TNAP – non-specific alkaline phosphatase
 TNAP – tissue non-specific alkaline phosphatase
 TNF – tumour necrosis factor
 TORC2 – rapamycin complex 2
 TRPV5 – transient receptor potential vanilloid-5
 UCP1 – uncoupling protein 1
 UTR – untranslated region
 WAT – white adipose tissue
 WFI – water-fat imaging
 Wnt – wingless-type family member
 Wnt11 – wingless-type family member 11
 X5P – xylulose-5-phosph

FOREWORD

This PhD project titled “Sirtuin Type 1 (SIRT1) – a key regulator in bone alterations and bone marrow differentiation capacity in mouse model of Anorexia Nervosa”, originated as a continuation of studies on separation based anorexia (SBA) mouse model, published by Zgheib *et al.* and Louvet *et al.* (1,2).

Based on previous findings, we hypothesised that SIRT1-mediated regulation of bone marrow stromal cell differentiation capacity can contribute towards an increase in bone marrow adiposity and loss of bone tissue. Understanding of potential mechanisms that are responsible for SIRT1 suppression during nutrient deficiency, in future, can lead to the development of new treatment strategies for anorexia induced bone loss.

This piece of work starts with general introduction on interaction between bone and adipose tissue within bone marrow, as well as description of SIRT1. It will be followed by the aims of thesis and objectives. Main body consists of 3 main parts – 1. Focuses on SBA model and associated changes in mice; 2. Describes preliminary results of RNA sequencing on BMSCs extracted from SBA mice; 3. Explores relationship between SIRT1 and AMPK. Each of the parts contain the discussion and conclusion sections.

The last part of the manuscript is general conclusion, where our findings would be presented in the context of previous work, highlight the contribution to the field, and we will try to answer the question – why there is an increase in bone marrow adipose tissue during severe nutrient deficiency?

INTRODUCTION

1. Crosstalk between Bone and Adipose tissue

Back in 1970 Friedenstein *et al.* published a discovery of cells harvested from bone marrow (BM), which have been shown an ability to form into fibroblastic colony forming cells (3). This was the first encounter with mesenchymal stem cells (MSCs) that led to the extensive research in this area and the discovery of other sources of adult MSCs. It was demonstrated that MSCs are able to differentiate in neurons, adipocytes, chondrocytes, osteoblast and myoblasts (Fig. 1) (4,5). The self-renewal capacity and differentiation abilities of MSCs allowed the development of various therapeutic purposes of this cell type (tissue regeneration, tissue repair) (6,7). A strong link exists between the adipose tissue (AT) and bone; therefore, an introduction will start with literature review of skeleton, different subtypes of adipose tissue and their interconnection.

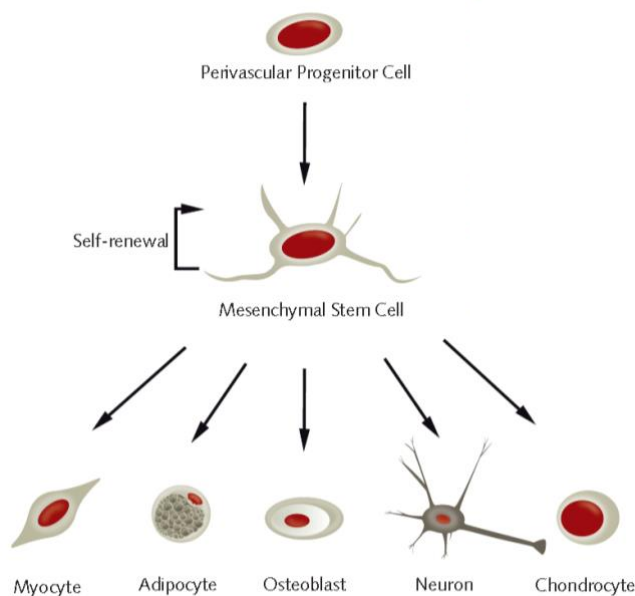


Figure 1. *In vitro* differentiation of human MSCs.

Under appropriate culture conditions, multipotent human mesenchymal stem cells can differentiate into osteoblasts, adipocytes, chondrocytes, myocytes and neurons. Adapted from Sigma Aldrich

(<https://www.sigmaaldrich.com/FR/fr/technical-documents/protocol/cell-culture-and-cell-culture-analysis/primary-cell-culture/mesenchymal-stem-cell-differentiation>)

1.1 Skeleton

A Skeleton serves a crucial function in providing a structural support for the body, movement abilities, internal organ protection, mineral reservoir and also provides the environment for haematopoiesis (8,9). Human skeleton consists of 213 bones and each bone undergoes

remodelling throughout the lifetime to adapt to biomechanical changes, as well as preventing damages to preserve the structural strength (10,11).

1.1.1 Bone development and remodelling

In mammalian skeleton, formation starts with migration of MSCs to the site of the future bone and form a highly dense cellular structure in its shape (12). The MSCs start to differentiate into chondrocytes within these structures to form a cartilage model of the future bone. The complex process of endochondral ossification is initiated in the primary ossification centre by the differentiation and proliferation of chondrocytes, which reach a hypertrophic state. The pre-osteoblast, osteoclast and endothelial cell invasion in the hypertrophic cartilage is leading to the cartilage resorption (13). With time of foetus growth and development, the primary ossification centre expands into cortical bone and blood vessels invade the mineralised matrix. Secondary ossification centres form in both ends of the developing bone and allows to form epiphyseal growth plate cartilage, which is responsible for longitudinal expansion of the bone (14–17).

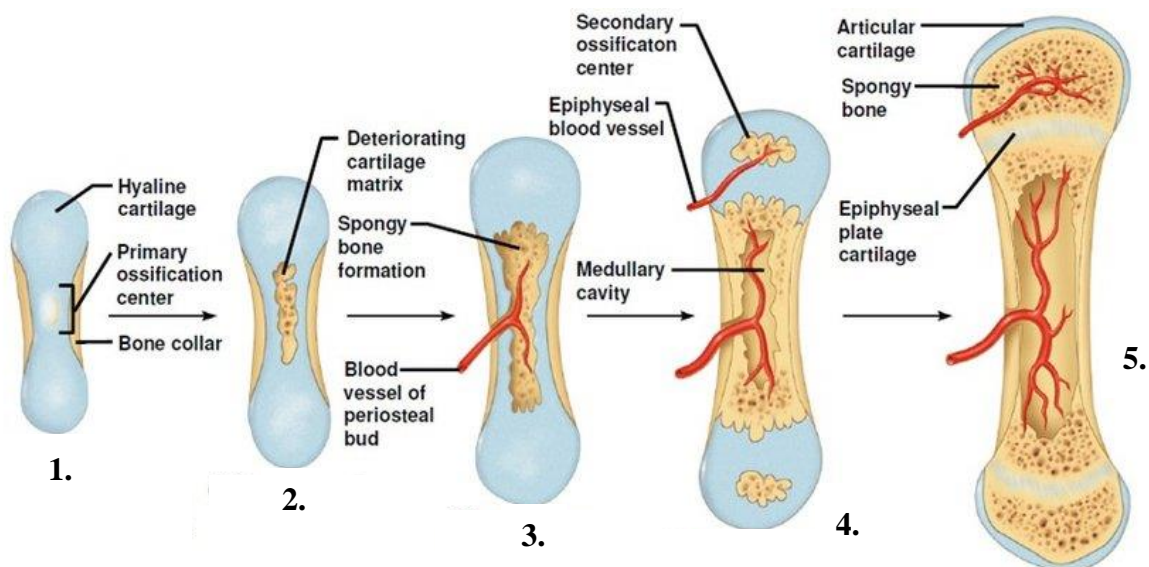


Figure 2. The schematic diagram of endochondral ossification process. 1. Formation of bone collar around hyaline cartilage model; 2. Cavitation of the hyaline cartilage within the cartilage model; 3. Invasion of internal cavities by the periosteal bud and spongy bone formation; 4. Formation of the medullary cavity as ossification continues, appearance of secondary ossification centres; 5. Ossification of the epiphyses; Adapted from Black *et al.* 2017 (17).

Fully developed mineralized tissue consists of four cell types – osteocytes, osteoblasts, osteoclasts and bone lining cells (18,19). Each type of these cells plays an important role in bone structure and remodelling, where osteoclasts perform bone resorption and osteoblast maintain bone deposition (10,20) (Fig. 3).

The bone remodelling cycle starts with recruitment and activation of mononuclear osteoclast precursors from the circulation to bind lining cell surface of the bone. This leads to the fusion of mononuclear cells to form multinucleated preosteoclast and their binding to bone matrix (22). In adult humans, the process of bone resorption takes place for approximately 2 to 4 weeks and is completed by osteoclast apoptosis (23). The reversal step of bone remodelling is a transition point between bone resorption and start of bone formation. The pre-osteoblast cells are being recruited to the resorption cavity to induce a process of new bone formation (11). After 4 to 6 weeks of new bone formation, osteoblasts secrete the collagenous matrix and induce matrix mineralisation (24). Furthermore, osteoblasts that were surrounded by the matrix become osteocytes, which form a network within the tissue (25). The cycle of bone remodelling is repeating constantly throughout the life; however, the trabecular bone balance is slightly negative, leading to bone thinning with age. A lot of various factors (age, sex, metabolic conditions) affect the bone thinning process and development of the disease.

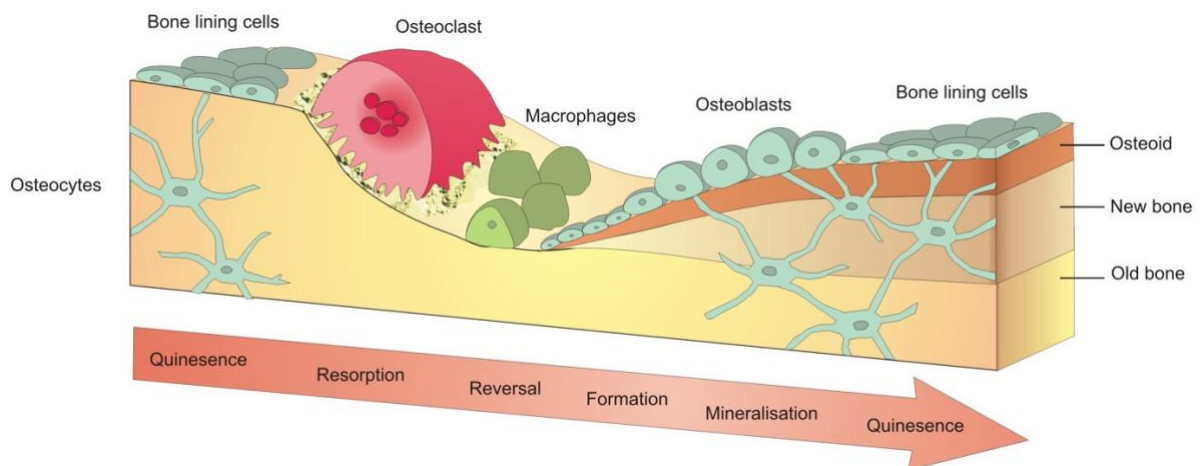


Figure 3. The process of bone remodelling. The old bone is resorbed by osteoclasts, following this macrophage like cells are found at the intermediate of the resorption site. This leads to the recruitment of osteoblast precursors, which proliferate and develop into mature osteoblasts. Mineralisation of matrix is taking place and this finalizes process of bone remodelling. Adapted from Biomedical Tissue Research, University of York (<https://www.york.ac.uk/res/bonefromblood/background/boneremodelling.html>)

1.1.2 Bone functions

Bone not only serves the function of structural support and muscle attachment point, but also it contributes to whole body homeostasis. Bone participates in maintenance of haematopoiesis and immune system activity, brain function and energy metabolism (26–28) (Fig. 4).

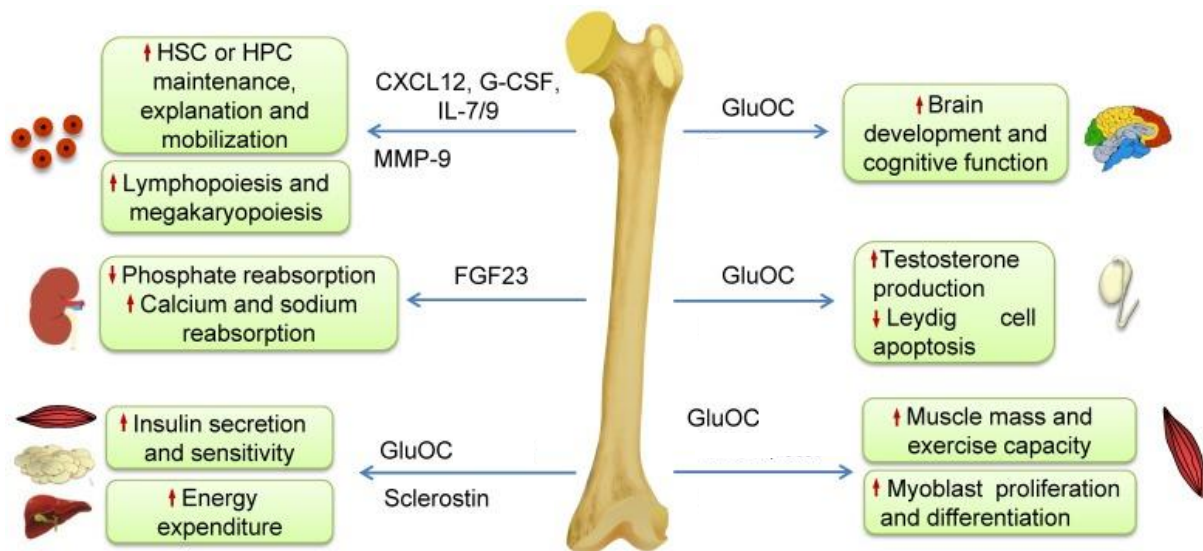


Figure 4. Bone signalling molecules affecting body homeostasis. Diagram shows molecules secreted by osteocytes, osteoblasts and osteoclasts that play important role in regulation of body homeostasis. Adapted from Su *et al.*, 2019 (28).

1.1.2i Bone function – haematopoiesis

The process of new blood and immune cell formation take place in BM. The close proximity of the bone cells and haematopoietic stem cells (HSCs) allows their communication, which was extensively studied in past years. Visualisation of HSCs using intravital microscopy showed an adjacent localisation of these cells to osteoblasts (29). Furthermore, runt-related transcription factor 2 (RUNX2) loss in mouse model resulted not only in failed skeleton development, but also in shift of haematopoiesis to extramedullary organs (spleen and liver), demonstrating the importance of mineralized tissue development for haematopoiesis (30,31).

Induced osteoblast deficiency in mice lead to the decrease in HSCs, linking the haematopoiesis and osteoblasts (32). Parathyroid hormone (PTH) signalling in osteoblasts results in an increase of both osteoblasts and HSCs (33). Close attachment between osteoblasts and HSCs allows the secretion of molecules, which maintain HSCs quiescence. This is achieved through osteoblast

production of wingless-type family member 11 (Wnt11), leading to initiation of Wnt signalling pathway in HSCs (34). Additionally, secreted thrombopoietin and angiopoietin-1 are also able to regulate quiescence in HSCs (35,36). Cells of osteoblast lineage produce C-X-C motif chemokine ligand 12 (CXCL12) and interleukin 7 (IL-7) in response to PTH signalling were shown to support B lymphopoiesis (Fig. 4) (33,37–39).

Other types of bone cells within the BM niche were also shown to be involved in the regulation of HSCs. BM engraftment of HSCs is partially dependent on calcium ions level (Ca^{2+}) within the microenvironment. One of the sources of Ca^{2+} is bone resorption by osteoclasts (40). Kollet *et al.* suggested that osteoclast produced cathepsin K protease mediates cleavage of CXCL12 chemokine and further result in mobilization of HSCs into the systemic circulation (41). Moreover, Kollet *et al.* observed that receptor activator of nuclear factor kappa-B ligand (RANKL)-stimulated osteoclast secrete matrix metalloprotease 9 (MMP9), which results in recruitment of the progenitors (Fig. 4) (41). Similarly to Kollet *et al.*, Heissig *et al.* demonstrated that matrix metalloproteinase 9 (MMP9) induces a release of stem cell factors (SCFs), which promote haematopoietic reconstitution (42). Loss of osteoclast activity was shown to result in defective HSC niche, due to the decrease in osteoblast differentiation (43). Also, osteocytes play an important role in maintaining haematopoiesis within BM, by promoting myeloid expansion through production of granulocyte-colony stimulating factor (G-CSF) (44). Sato *et al.* conducted a study on osteocyte-less (OL) mice and observed that this model exhibited lymphopenia, decreased number of lymphocytes (45). These studies clearly demonstrate the importance of bone cells in maintaining healthy haematopoiesis.

1.1.2ii Bone function – energy metabolism

Osteocalcin (OC) is a hormone secreted by osteoblasts, which alters whole body glucose metabolism (46). Uncarboxylated OC (GlaOC) is found to be embedded into the bone matrix. In the process of bone resorption, osteoclasts generate the acidic environment of resorption pit and promote the decarboxylation of GlaOC to undercarboxylated OC (GluOC), an active form of OC (47–49). The effect of OC on glucose homeostasis was firstly described in OC deficient mice study by Ducy *et al.* (50). Further research in this area revealed that OC is able to promote cell proliferation, leading to improved insulin production and secretion, and improve insulin sensitivity in metabolic tissue (liver, AT, muscle) (Fig. 4) (28,49). Additionally, a positive signalling loop exists between insulin signalling and OC production. Insulin signalling was

shown to induce osteoblastogenesis, in mice, insulin receptor (IR) deletion leads to impaired osteoblast differentiation and decrease in OC production (51). Furthermore, loss of IR induce production of osteoprotegerin (OPG), which inhibits osteoclast differentiation, reducing bone resorption and decreasing the circulating level of GluOC (52). The decrease of GluOC serum level will further result in decrease of insulin production.

Osteocytes are also participating in regulation of osteoanabolic capacity by upregulating Wnt/ β -catenin signalling and whole body energy metabolism through production of glycoprotein sclerostin (53). Sclerostin influences body composition by regulating anabolism and catabolism in AT (Fig. 4) (54,55). The treatment with sclerostin neutralising antibody in mouse model resulted in the reduction of white adipose tissue mass and improvement of insulin sensitivity (54).

1.1.2iii Bone function – mineral metabolism

Additionally, to whole body energy metabolism, bone serves an important role as an endocrine organ in regulation of systemic mineral metabolism. Osteoblast and osteocytes secrete fibroblast growth factor 23 (FGF23) hormone, member of FGF family (56). In the beginning of 21st century the mutation in FGF23 that resulted in glycoprotein gain of function, was found to be a genetic cause of autosomal dominant hypophosphatemic rickets (ADHR), a disease resulting in renal phosphate wasting (57). On the other hand, loss of function mutation in FGF23 cause the development of familial hyperphosphatemic tumoral calcinosis (TC). This disease is characterised by hyperphosphatemia, which takes place as a result of renal phosphate reabsorption, and by elevated vitamin D ($1\alpha,25$ -dihydroxyvitamin D_3) concentration (58–60). The main function of FGF23 in kidneys is the suppression of phosphate reabsorption from the urine and the suppression of vitamin D synthesis (61,62). Inhibition of phosphate reabsorption is taking place through suppressing the expression of the type IIa sodium-phosphate co-transporter (NaPi-2a) by binding to a FGFR1- α -Klotho co-receptor complex, that are located in the proximal tubules of the kidney (37–41)(63,64). These events lead to phosphate loss. Also, FGF23 promotes calcium reabsorption by acting upon the transient receptor potential vanilloid-5 (TRPV5), a channel located in distal renal tubules (65).

FGF23 also functions within the bone itself. It was reported that FGF23 within the bone cells is a transcriptional suppressor of tissue non-specific alkaline phosphatase (TNAP) (66). TNAP

is cleaving the mineralisation inhibitor pyrophosphate and therefore that it regulates bone mineralisation (67).

1.1.2iv Bone function – extraskkeletal tissues

Secreted by bone, OC (its active form GluOC) signalling affects various peripheral tissue. Muscle is not only using bone as an attachment point, but also bone signalling affects the IL-6 production in muscle cells. During exercise, the GluOC induced production of IL-6 results in enhanced uptake of fatty acids (FA) and glucose in myofibers, resulting in adaptation to exercise (Fig. 4) (68,69). Furthermore, administration of GluOC in high concentration to mice, resulted in muscle mass growth (70). OC was also shown to regulate the male fertility through the inhibition of Leydig cells apoptosis and promotion of testosterone production in testes (Fig. 4) (71).

In recent years, a role of OC in brain function and development had emerged. In mice, the maternal GluOC was found to cross the placental barrier, as well as blood brain barrier (BBB) in order to promote the brain development of cognitive functions in the foetus (72–74). Deletion of OC in adult mice (OC $-/-$) resulted in development of brain structure abnormalities, impairment of memory abilities and the level of neurotransmitters. The administration of OC in these mice improved the phenotype and memory deficit (72).

Based on the information above, it can be concluded that bone serves an important role not only in mobility and protection, but also in function maintenance of vital organs. In the same time this thesis focuses on the relationship between bone and adipose tissue, and changes in these relationships which results in development of bone disease, therefore it is important to thoroughly look at the bone function and development, as well as the AT.

1.2 Adipose tissues

The AT is an organ, which main function is to maintain energy homeostasis and serves a role of nutrient storage (75). In humans and rodents AT can be divided in four subtypes, white adipose tissue (WAT), brown adipose tissue (BAT), beige adipose tissue (Beige AT) and bone marrow adipose tissue (BMAT). AT subtypes are located around the body in distinct fat depots (Fig. 5). Visceral WAT depot surrounds internal organs and protects them, subcutaneous WAT

depot is predominantly located in abdominal and thoracic cavities. Inguinal AT is composed of both WAT and Beige AT, therefore is highly influenced by dietary and environmental factors (76). In humans, BAT is located in the deep sections of the neck. BMAT is located within limbs, as well as in the spine (77,78). Each of the AT subtype has its unique morphology, composition and localization, which facilitates its function (Table 1).

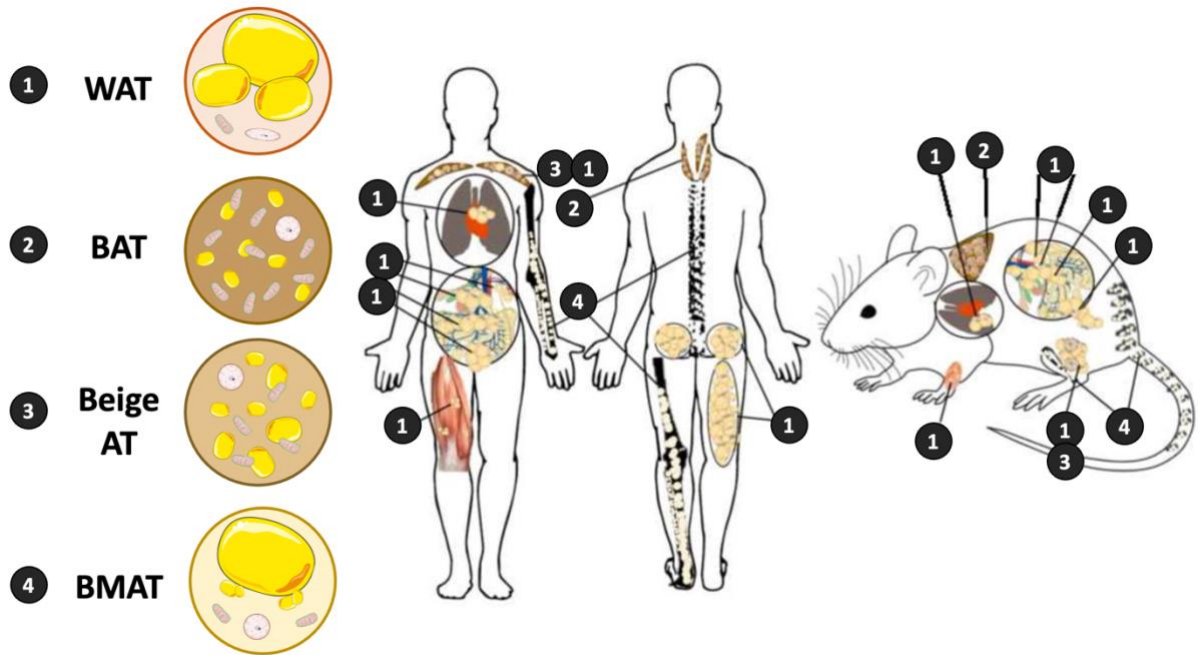
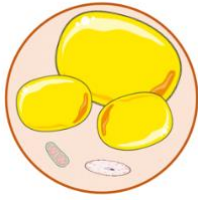
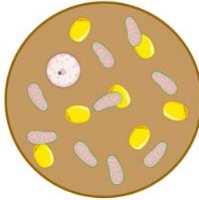
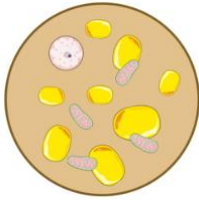



Figure 5. WAT, BAT, Beige AT and BMAT depots in humans and mice. In rodents and adult humans WAT depots are divided into visceral and subcutaneous AT. Visceral AT surrounds and protects vital organs, subcutaneous AT is predominantly located in abdominal and thoracic cavities. BAT is located in the deep sections of the neck (humans) and in the intrascapular region (rodents). BMAT in both humans and rodents is located within limbs, as well as in the spine. Adapted from Suchacki *et al.*, 2016 (76).

	White Adipose Tissue (WAT)	Brown Adipose Tissue (BAT)	Beige Adipose Tissue (Beige AT)	Bone Marrow Adipose Tissue (BMAT)
Morphology				
Localization	<ul style="list-style-type: none"> • Subcutaneous; • Visceral; (79) • Retroperitoneal; • Gluteal; (80) 	<ul style="list-style-type: none"> • Cervical; • Paravertebral; • Supraclavicular; • Axillary; • Suprarenal; • Peri-aortic; (81) 	<ul style="list-style-type: none"> • Within the WAT depots; (82) 	<ul style="list-style-type: none"> • Bone Marrow (ribs, sternum, vertebrae, medullary canal of long bones (tibia, femur, and humerus)) (83);
Composition	<ul style="list-style-type: none"> • Flattened nucleus; (84) • 90% of the cell volume is composed of lipid droplets; • Low mitochondria count; • Highly vascularized tissue; (79) 	<ul style="list-style-type: none"> • Rounded nucleus; • Small intracellular lipid droplets; • High density of mitochondria; (85) 	<ul style="list-style-type: none"> • Rounded nucleus; • Increased density of mitochondria upon stimulation; • Decrease of lipid droplet size upon stimulation; (84) 	<ul style="list-style-type: none"> • Increased lipid droplet volume; • Low mitochondria content; (83)
Function	<ul style="list-style-type: none"> • Lipogenesis; • FA oxidation; • Lipolysis; • Endocrine – Adiponectin, Leptin, Chemerin and Adipsin secretion; (79,86,87) 	<ul style="list-style-type: none"> • Heat Production; (85) 	<ul style="list-style-type: none"> • Exhibit WAT phenotype, but are thermogenic upon the cold stimulation; (88) 	<ul style="list-style-type: none"> • Lipid storage and lipolysis; • Bone metabolism; • Haematopoiesis; • Endocrine – Adiponectin and Leptin secretion; (83)

 - Nucleus;  - Mitochondria;  - Lipid Droplet;

Table 1. Summary of AT subtypes. Focusing on morphology, localization, composition and function of distinct adipose tissue depots. Summarises the diversity of adipose tissue function in human body.

Components of the diagram were taken from <https://smart.servier.com/>.

1.2.1 Adipose tissue functions

WAT depots account for most AT in the body and its primary function is fat storage in the form of lipid droplets. WAT stores excess energy from food consumption in a form of triacylglycerol (TAG) (89). Additionally, WAT acts as an endocrine organ and secretes various adipokines like adiponectin and leptin, which regulate the lipid and glucose metabolism in the body (90–92). The main function of BAT is to convert the TAG consumed within a diet and transfer it into the heat (93). This function is facilitated by high number of mitochondria within the BAT and expression of uncoupling protein 1 (UCP1) in these adipocytes (94). UCP1 serves role of proton channel within the mitochondria membrane and allows re-entry of protons back into matrix, by this process adenosine triphosphate (ATP) is not produced, but allows the conversion of chemical energy into the heat energy (95). The intermediate tissue, between WAT and BAT, was shown to be Beige AT (88). This subtype of adipocytes was shown to be derived from and within WAT sub-population, but have thermogenic parameters of BAT, as well as expression of UCP1 protein (96,97). Beige AT is able to switch between thermogenic and fat storage phenotype depending on environmental conditions, therefore, it is able to perform all functions of WAT and BAT described before (98). Finally, BMAT for a long time was considered as a space filler within bone cavity, without distinct function and origin. Beresford *et al.* in 1992 demonstrated that bone and adipose tissue derives from same precursor cells – bone marrow stromal cells (BMSCs) (99). Due to BMAT heterogeneous origin and gene expression profile similar with Beige AT, it was classified as distinct AT type (100,101).

1.2.1i WAT function - lipogenesis, TAG synthesis and lipolysis

The process of lipogenesis in AT starts with glucose sensing and uptake via glucose transporter type 4 (GLUT4) (102). In the process of glycolysis, glucose is broken down into metabolites and pyruvate, which both play a role in *de novo* lipogenesis (DNL). Pyruvates undergo tricarboxylic acid cycle (TCA) cycle in mitochondria to produce the citrate, leading to its transport into cytoplasm of AT and initiation of lipogenesis. The cascade of DNL starts with release of acetyl-CoA (Ac-CoA) by ATP-citrate lyase (ACLY) enzyme (103). During next step, acetyl-CoA carboxylase 1 (ACC1) enzyme converts Ac-CoA into malonyl-CoA (104). After fatty acid synthase (FASN) converts malonyl-CoA into palmitate and at last palmitate is transformed into FA by stearoyl-CoA desaturase 1 (SCD1) (105,106). Meanwhile, the

metabolites produced in the process of glycolysis are also participating in DNL. The intermediate metabolite xylulose-5-phosphate (X5P) acts as an activator of protein phosphatase 2A (PP2A) (107). It was shown that PP2A dephosphorylates carbohydrate response element binding protein- (ChREBP-) at serine 196 (Ser196) and threonine 666 (Thr666) residues and facilitate its translocation to the nucleus (108). ChREBP- together with Max-like protein X (Mlx) binds carbohydrate response element (ChORE) and initiate transcription of ChREBP-, which subsequently induce expression of target genes that are participating in DNL (ACLY, ACC1, FASN, SCD1) (Fig. 6) (109,110).

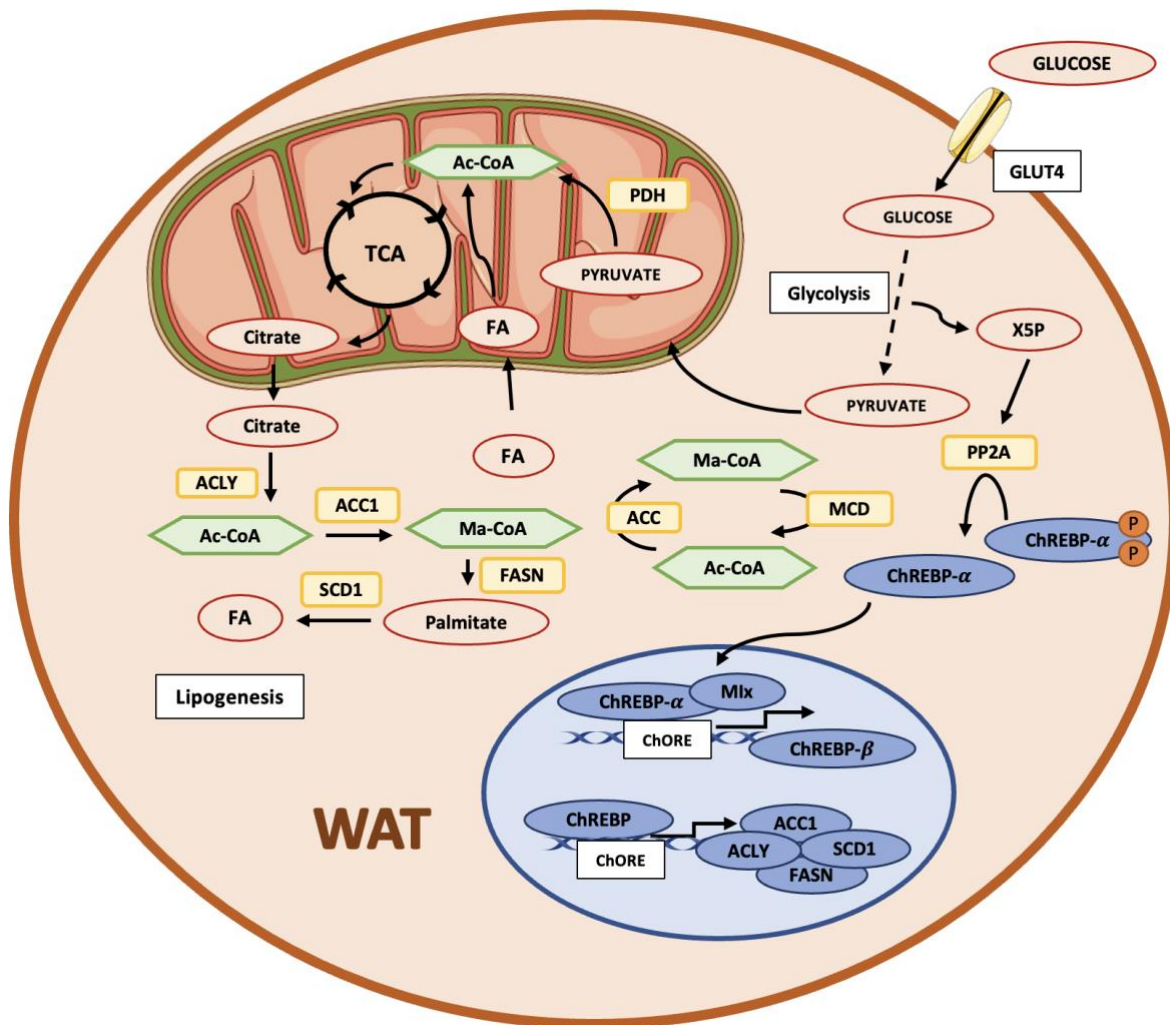


Figure 6. Summary de novo lipogenesis in WAT. Diagram shows the metabolism of glucose, which facilitates DNL, as well as activation of target genes necessary for the process of lipogenesis. Components of the diagram were taken from <https://smart.servier.com/>. Glucose transporter type 4 (GLUT4); xylulose-5-phosphate (X5P); protein phosphatase 2A (PP2A); carbohydrate response element binding protein- α (ChREBP- α); Max-like protein X (Mlx); carbohydrate response element (ChORE); ATP-citrate lyase (ACLY); acetyl-CoA carboxylase 1 (ACC1); stearoyl-CoA desaturase 1 (SCD1); fatty acid synthase (FASN); fatty acid (FA); acetyl-CoA carboxylase (ACC); malonyl-CoA decarboxylase (MCD); triacylglycerol (TAG).

Newly synthesised FA are transferred into endoplasmic reticulum (ER), where TAG synthesis is taking place (111). In the cascade of the enzymatic reactions on the *sn*-glycerol-3-phosphate (Gly-3-P) backbone glycerol-3-phosphate acyltransferase (GPAT) attaches FA-CoA to produce lysophosphatidic acid (LPA) (112). After an acylglycerophosphate acyltransferase (AGPAT) facilitates the attachment of another FA-CoA to form phosphatidic acid (PA) (113). Phosphatidic acid phosphohydrolases (PAP) enzyme catalyses the PA to generate 1,2-Diacylglycerol (1,2-DAG) (114). At last 1,2-DAG is acetylated by diacylglycerol acyltransferases (DGAT) and attach last FA-CoA, forming TAG, which is later stored in the lipid droplets (115,116). TAG is derived not only from FA produced in the process of DNL, but also through the uptake from the bloodstream. After food consumption, FA are absorbed in small intestine into the bloodstream, they enter adipocyte through CD36 transporter and after are stored in a form of TGA (Fig. 7) (117,118).

During feeding, when blood glucose rise, pancreatic β -cells sense the change in glucose gradient and secrete insulin into the bloodstream (119). Insulin binding to IR on the surface of AT and induce downstream signalling. These events activate insulin receptor substrate (IRS), which further phosphorylates phosphatidylinositol 3-kinase (PI3K) and protein kinase B (PKB/AKT) (120,121). Activation of mammalian target of rapamycin complex 1 (mTORC1) by PKB/AKT, induce the translocation of sterol regulatory element-binding protein (SREBP1c) into the cell nucleus, where it binds to the serum responsive element (SRE) to induce the expression of DNL genes (122,123). mTORC1 is also involved in suppressing the activity of adipose triglyceride lipase (ATGL) and block the lipolysis (124). Furthermore, PKB/AKT is involved in blocking protein kinase A (PKA), that induces lipolysis. Additionally, both ATGL and hormone sensitive lipase (HSL) are repressed by PKB/AKT, stopping the lipolysis in AT (125).

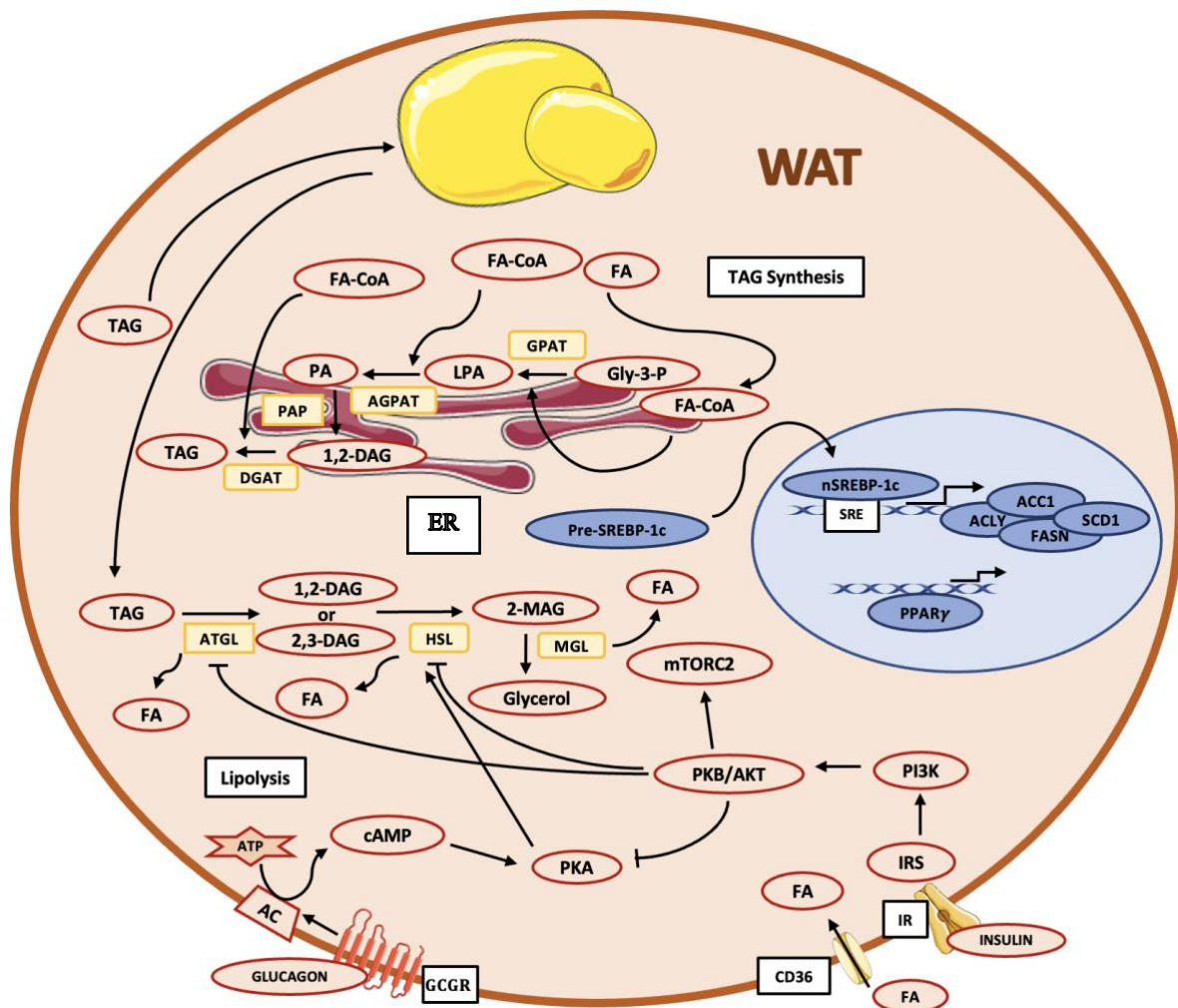


Figure 7. Summary of triacylglycerol synthesis and lipolysis in WAT. Diagram shows the TGA synthesis and lipolysis, which are induced or suppressed by insulin or glucagon signalling, in response to feeding condition.

Components of the diagram were taken from <https://smart.servier.com/>.

Insulin receptor (IR); insulin receptor substrate (IRS); phosphatidylinositol 3-kinase (PI3K); protein kinase B (PKB/AKT); rapamycin complex 1 (mTORC1); element-binding protein (SREBP1c); serum responsive element (SRE); ATP-citrate lyase (ACLY); acetyl-CoA carboxylase 1 (ACC1); stearoyl-CoA desaturase 1 (SCD1); fatty acid synthase (FASN); endoplasmic reticulum (ER); *sn*-glycerol-3-phosphate (Gly-3-P); glycerol-3-phosphate acyltransferase (GPAT); lysophosphatidic acid (LPA); acylglycerophosphate acyltransferase (AGPAT); phosphatidic acid (PA); Phosphatidic acid phosphohydrolases (PAP); 1,2-Diacylglycerol (1,2-DAG); 2,3-Diacylglycerol (2,3-DAG); diacylglycerol acyltransferases (DGAT); glucagon receptor (GCGR); adenylyl cyclase (AC); cyclic adenosine monophosphate (cAMP); protein kinase A (PKA); hormone sensitive lipase (HLS); adipose triglyceride lipase (ATGL); 2-monoacylglycerol (2-MAG); monoglyceride lipase (MGL); triacylglycerol (TAG); peroxisome proliferator-activated receptor gamma (PPAR γ).

In a period of energy demand, glucagon is secreted by pancreatic α -cells in response to low blood glucose level (126). Binding of glucagon to the glucagon receptor (GCGR) on the adipocyte surface triggers the G-protein coupled activation and interaction with adenylyl cyclase (AC), which converts ATP into cyclic adenosine monophosphate (cAMP) (127). Increase in intracellular cAMP level results in activation of PKA (128). PKA facilitates activation of HLS, a key enzyme in TAG lipolysis (129,130). Overall, lipolysis starts with hydrolysis of TAG by ATGL to form 1,2-DAG or 2,3-DAG. After HLS breaks it down to 2-monoacylglycerol (2-MAG). Next step is driven by monoglyceride lipase (MGL), to produce glycerol and FA (131). However, the involvement of glucagon in lipolysis induction in human AT is highly questioned. Numerous studies in rodents demonstrated glucagon promoting activation of HLS (132,133). In the same time, some studies in humans did not demonstrate any effect on lipolysis in response to glucagon (134,135). Recently, Periera *et al.* showed that the expression level of GCGR on the surface of human AT is low, but after exposure to high glucagon concentration the increase in lipolysis was observed (136). A variety of other lipolytic hormones was established to play role in induction of lipolysis in WAT – norepinephrine (NE), is a primary activator of fasting induced lipolysis (137). Also, adrenocorticotrophic hormone (ACTH) and GH have been shown to induce lipolysis (138).

1.2.1ii WAT function - adiponectin and leptin secretion

Initially, adipose tissue was considered primarily an energy storage unit, however after Friedman *et al.* discovery of leptin this misconception was disproved (139). This hormone is secreted by AT in response to changes in nutrient availability and thus modulates the food intake (Fig. 8) (140,141). Leptin acts in the hypothalamus by blocking the food intake, through inhibition of neuropeptide Y and Agouti-related protein (NPY/AGRP) neurons and activation of anorexigenic pro-opiomelanocortin (POMC) neurons (68–70)(142). Through activity in the sympathetic nervous system, leptin regulated lipolysis in AT (143). Also in liver, leptin indirectly is activating AMP protein kinase (AMPK), which induce intracellular signalling cascade and result in suppression of SREBP1c and subsequent decrease in lipogenic gene expression (144,145). The activation of AMPK in liver inhibits DNL by phosphorylating ACC1 enzyme and blocking its activity (146). Additionally, in muscle cells leptin is also regulating the glucose uptake and fatty acid oxidation (147,148). High blood circulating leptin level is positively associated with increase in body mass index (BMI), as its preliminary function is to decrease the fat content (149). The leptin production in anorexia nervosa (AN)

patients was significantly reduced in several studies, which was predictable, as leptin level in positively associated with BMI (150).

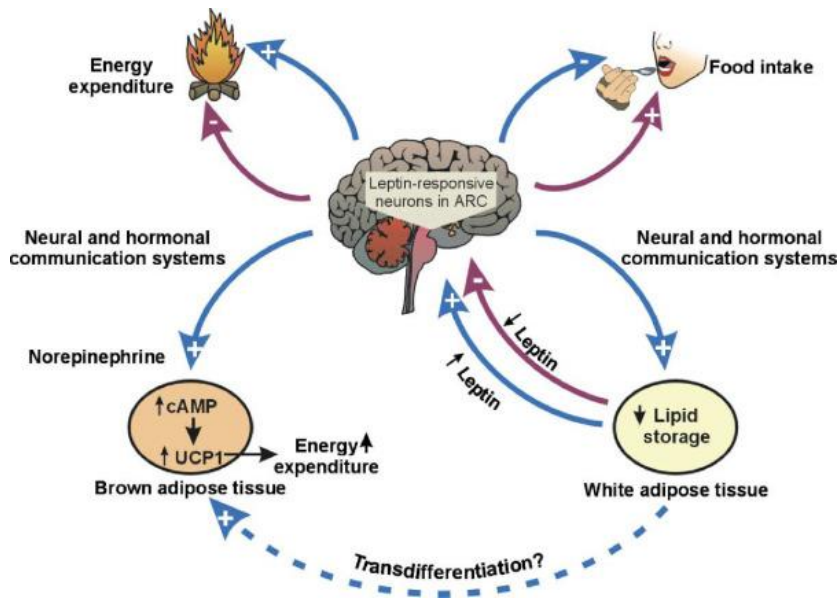


Figure 8. Diagram of leptin regulated energy balance. Leptin regulates its own expression, food intake and energy expenditure. From Gettys, 2004 (138).

On the other hand, in individuals with high BMI, the adiponectin was shown to be decreased, as secretion of this adipokine is associated with caloric restriction (CR) (151,152). First, adiponectin activates the AMPK signalling pathway in the liver, resulting in upregulation of carbohydrate breakdown and FA oxidation, as well as protection against insulin resistance (Fig. 9) (153,154). This is achieved not only through activation of AMPK pathway, but also via induction of PPAR expression (155). It also, facilitates glucose and FA uptake in muscle cell, in order to provide them with sufficient energy source (156,157). Moreover, adiponectin improves insulin production and secretion by pancreatic β -cells (158). However, adiponectin can also work in an autocrine manner and promote the adipogenesis in AT, by inducing PPAR expression (159).

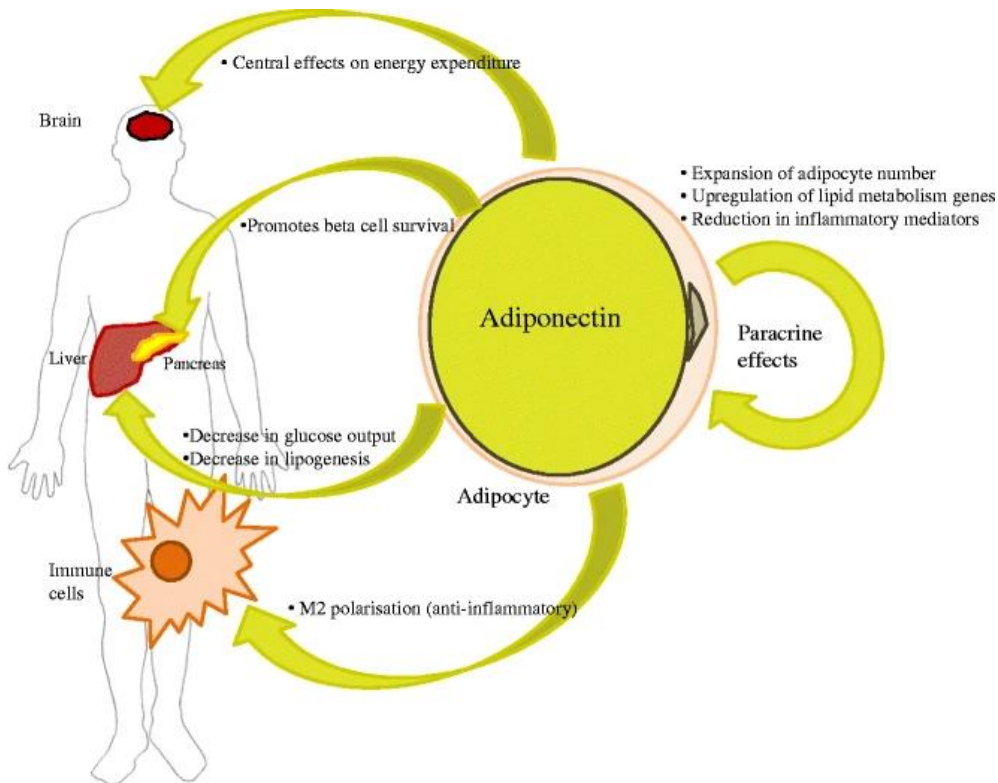


Figure 9. Main mechanisms of adiponectin's functions on peripheral tissues to regulate metabolism and insulin sensitivity. From Turer and Scherer, 2012 (154).

1.2.1iii BAT function – thermogenesis

In BAT development, peroxisome proliferator-activated receptor gamma (PPAR γ) suppression results in recruitment of the PR domain containing 16 (Prdm16), which induces the transcription of BAT genes and results in AT browning. The thermogenesis in BAT starts with decrease in body temperature, which triggers the NE production in hypothalamus (160). This neurotransmitter is binding β -adrenergic receptors on the surface of BAT and triggers the G protein coupled receptor activation and AC activation (161). AC converts ATP into cAMP, which activates PKA (128). PKA facilitates phosphorylation and activation of cAMP-response-element-binding protein (CREB), that binds to UCP1 gene promoter and induce its transcription (162). UCP1 acts with the mitochondria of BAT, where it serves a role of a channel. UCP1 transfers the H⁺ proton, produced by a series of reactions in electron transport chain (ETC), into inner mitochondria matrix, independently of ATP production (93,163). In the process of energy transduction, heat is produced.

Additionally, UCP1 requires FA binding in order to be activated (95). PKA also induces HSL enzymatic activity and increase the rate of lipolysis in BAT, but this way FA content is increased and is used to activate UCP1 and to produce Ac-CoA by -oxidation (164,165).

1.3 BMAT

In the end of 20th century it was found that BMAT, as well as bone cells are derives from same precursor cells population – BMSCs (99). Back in 1991, Caplan *et al.* for the first time established a term of MCS, referring to stem cell population within BM (166). The initial naming of this class of cell was based upon their differentiation capacity into multiple tissue types beyond the skeletal lineage (including skeletal muscle, myocardium, smooth muscle) (167). After the discovery of different MSC sources (synovial, dental pulp or adipose tissue), BM specific population of cell with MSC like differentiation ability, currently are referred as BMSCs (168–171).

BMSCs are considered to be a highly heterogeneous population of the cells. Cells are typically isolated by plating to the *in vitro* culture plates, due to their ability to adhere to plastic surface (172,173). Also, BMSC population can be isolated though negative sorting by fluorescent-activated cell sorting (FACS), using haematopoietic lineage marker CD45 (174). Currently, BMSCs specific marker was not identified, therefore, markers of MSC that cross-react with BMSC population can be used (e.g., CD271/CD63/W8-B2/MSCA-1 in humans) (175). Kuznetsov *et al.* study showed by single cell colony analysis, that only low percentage of extracted cells are able to exhibit a stem cell differentiation capacity into trilineage (osteoblast, adipocyte and chondrocyte) and furthermore, form a heterotopic bone marrow organ when cells are implanted *in vivo* (176). The rest of the cell population is considered to be a lineage committed cells (177). These subpopulations of the cells, are likely to function as a haematopoiesis support or immune system regulators (non-progenitor function of BMSC population) (178).

Overall, BM is a dynamic tissue that consists of BMAT together with haematopoietic and variety of stem cells, enclosed in complex extracellular matrix. BMAT is a distinct type of AT, which is saturated within BM cavity and composes 70% of whole BM volume. In adult human, BMAT account approximately 10% of total fat composition (76,179). One of the first

documented observation of BMAT was dated back in 19th century, when Ernest Neumann identified “large yellow cells” during the trabecular bone autopsy (180). Later this finding was confirmed by various investigators (181–183). The interest in BMAT origin and function rose throughout the years and development of technologies in medical research (positron emission tomography (PET) and magnetic resonance imaging (MRI) scans) allowed the non-invasive study on BMAT (184,185). Currently, it is established that in human BMAT starts to develop only postnatally at the distal ends of long bones. Therefore, the red haematopoietic marrow, which was prenatally composing BM, is slowly replaced by BMAT and BM is converted into yellow marrow (Fig. 10) (186,187).

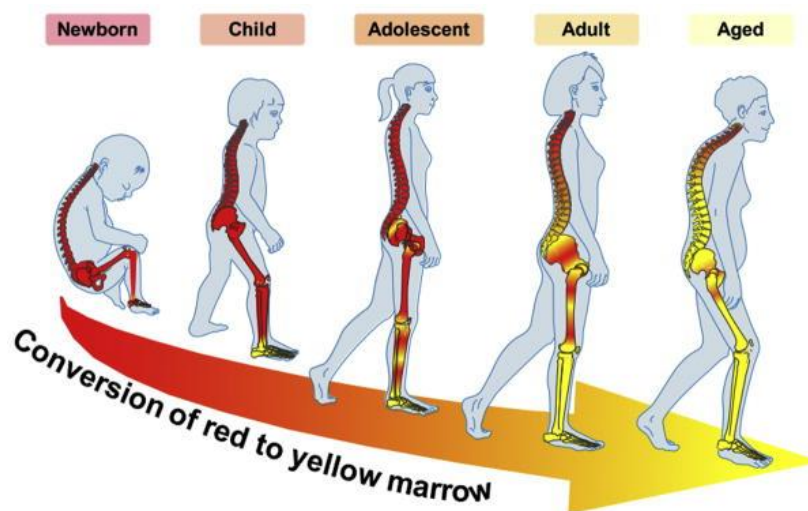


Figure 10. Conversion of red marrow to yellow marrow. Diagram shows the gradual replacement of red (haematopoietic) marrow by yellow (adipose tissue) marrow in the process of aging. From Li *et al.*, 2018 (182).

In the process of ageing, BMAT expansion was found to be associated with development of bone pathologies (188,189). Additionally, increase in BMAT was observed in menopausal women, due to the oestrogen deficiency, leading to development of osteoporosis and other bone associated conditions (190,191).

1.3.1 BMAT study approach

Advances in technologies lead to the breakthrough in characterisation of BMAT and in understanding its function. In particular, the histological analysis brought a historical value in understanding composition of BMAT. Therefore, histomorphometry is one of the most important aspects in standardised methodology in BMAT research (192). Recently,

methodologies working group from the Bone Marrow Adiposity Society published a review article covering the most recent models and techniques in BMAT research (192).

Dr Parfitt publication “Terminology and symbols in bone morphometry” was a base for first guidelines on bone histomorphometry (193). This technique can be described as a method to quantify the components of marrow to assess quality of bone and changes in cells size or number. Histomorphometry is based on 5 main steps – 1. sample preparation; 2. decalcification; 3. embedding; 4. staining; 5. quantification (192). Despite the scientific value of this technique, it has few limitations, as being time-consuming and requiring the microscopy and in most of the cases manual quantification. Moreover, it relies on interpretation of a user and therefore control of quality is required. The process of detection of BM adipocytes (BMAds) and their quantification can be challenging due to their close connection in adipocytic areas (192).

To overcome the challenges of this 2D technique, more recently appeared the use of 3D imaging to quantify and establish BM adiposity (BMA) distribution within BM. X-ray microfocus computed tomography (micro-CT) is currently the most powerful tool to study mineralised tissue (194). However, the limitation of this technology is low specificity for soft tissue, which doesn't allow to study the BMAT within the bone. This problem was solved with development of contrast enhanced micro-CT (CE-CT) (195). With a help of contrast enhancing staining agents (CESA), it allows to bind to tissue *ex vivo* and visualise BMAT. Scheller *et al.* reported the use of osmium-tetroxide (OsO₄) as a CESA, in study and quantification of BMAT using CE-CT (196–198). This type of staining is continued to be widely used, however it is highly toxic and should be appropriately handled (199,200). This limitation was improved by Kerckhofs *et al.*, who reported the study on visualisation of bone mineral structure and soft tissue using Hafnium Wells-Dawson polyoxometalate (Hf-WD-POM) (201). This technique allows not only to perform 3D CE-CT, but also subsequently perform immunostaining and histology, with non-toxic material for safer manipulations.

In clinical studies, it is crucial to use non-invasive imaging. Currently, MRI is widely used as *in vivo* BMAT study tool (202,203). It allows to quantify changes in BMAT volume in response to treatments, dietary adjustments or exercise (204,205). The measurements in rodents are more challenging due to their small size, therefore most of the *in vivo* studies using MRI are conducted on human subjects. In order to quantify BMAT in these studies, a proton-density fat

fraction (PDFF) biomarker can be used. It measures the unconfounded fat signal in relation to the sum of the unconfounded fat together with water signals (202,206,207). The challenge is to minimize the number of confounding factors and focus only on lipid proton signals. Therefore, more accurate quantifying techniques emerged - single-voxel proton spectroscopy (¹H-MRS) and chemical shift encoding-based water-fat imaging (WFI) techniques (206). Moreover, recently high-resolution peripheral quantitative computed tomography (HR-pQCT) is used to accurately quantify BMAT in humans (208).

To study the BMAT subtypes, localisation and function at the cellular level, it is crucial to establish *in vitro* systems. BM is a complex microenvironment, which consist of various cell types, therefore it is difficult to isolate BMAdS from BM. This led to the development of *in vitro* adipogenic differentiation protocols, to study BMAdS derived from BMSCs. This method is based on isolation of a stromal vascular fraction (SVF) that is plated on the plastic and expanded in tissue culture. The monolayer of adherent cells represents the fraction of BMSCs, which are treated with a cocktail of molecules inducing adipogenic differentiation. The validation of obtained BMAdS is done through fluorescent dyes to detect the formation of lipid droplets (Nile Red, Oil Red O) or the detection of adipocyte specific gene and protein expression (RT-qPCR, Western Blotting, RNA sequencing). Additionally, cells can be characterised base on surface markers by flow cytometry (192).

1.3.2 BMAT functions

With the developing interest in BMAT research and with advancing of experimental techniques, a broad range of BMAT function was established. BMAT stores significant amount of fat and expresses IR, these parameters link BMAT with energy metabolism (209). FA and lipids stored in BMAT can be used to produce ATP for osteoblasts (210). It was also shown that BMAT not only interacts with tissue within the closed system of BM, but also function as an endocrine organ that is participating in regulation of whole body metabolism (83,211,212).

In regard to fatty acid uptake and lipid storage, BMAT lipid droplets are made up of a core of neutral lipids such as TAG and cholesteryl esters that is surrounded by a phospholipid monolayer with embedded proteins (213–215). As a result, bone marrow adipocytes must first acquire fatty acid substrates before being esterified and stored. These fatty acids, like those found in other adipose depots, are assumed to be obtained either by absorption from the

circulation or through de novo synthesis from glucose substrates. When fatty acids enter the cell, they must be esterified to glycerol or cholesterol via a two-step, ATP-dependent mechanism catalysed by acyl-coenzyme A synthetase (ACS) and involving acyl-CoA synthetase long chain family member 1 (ACSL1), ACSL3, and ACSL4 (213). When these fatty acids are activated, they might begin to be integrated into the lipid droplet core. TAGs are by far the most prevalent lipid detected in MAT, despite the fact that the relative proportions of TAGs and cholesteryl esters might fluctuate (213–215). PLIN1 has been discovered as a component of bone marrow adipocytes by immunohistochemistry as well as western blot analysis (216). In other adipose depots, tiny lipid droplets are assumed to be covered with perilipin 2 (PLIN2) and PLIN3, and when the droplet grows larger, they are replaced by PLIN1 (217,218). Despite the fact that marrow adipocytes are distinct and much remains unknown about marrow adipocyte lipid droplets, their biogenesis appears to include similar machinery seen in classic WAT. However, study by Attane *et al.* suggested that BMAT exhibit a distinct lipid metabolism characteristics comparing to WAT (219). They showed that BMAT has a reduced level of lipolytic activity and the metabolism in this tissue is focused on cholesterol (219).

Once lipid droplets form in BMAd, they may function as a source of stored energy or ATP. When cellular energy is required, whether by BMAd or other cells, lipid droplets are thought to be broken down into free fatty acids by lipolysis. BMAT lipolysis was previously undervalued and rarely explored. For example, histological investigation of BMAT would frequently offer some insight on the number or volume of marrow adipocytes/lipid droplets, but because to the nature of lipid flow, it was impossible to determine whether this was due to increased fatty acid storage or decreased lipolysis. BMAT has recently been revealed to undergo cytoplasmic lipase-mediated lipolysis, this distinct depot appears to be less susceptible to β -adrenergic stimulation than WAT (216). As a result, although lipolysis seems to occur in BMAd similarly to other adipose depots, the stimulus or response may be exclusive to this depot.

BMAd use FA for their own ATP generation. Because BMAT in the distal tibia, proximal tibia, and femur has a high amount of long-chain fatty acids, it is hypothesised that predominantly β -oxidation occurs in these sites (215,220). Acetyl-coenzyme A is joining the TCA cycle and undergo oxidative phosphorylation, resulting in the production of ATP. This

ATP may now supply the bone with the energy necessary for cellular operation and maintenance.

1.3.2i BMAT function - haematopoiesis

Haematopoiesis can be divided into five branches – myelopoiesis, lymphopoiesis, erythropoiesis, thrombopoiesis and HSC self-renewal (221). Haematopoiesis occurs in close proximity to stroma cells, which provide the support for HSC self-renewal and differentiation (222). BM stroma consist of stromal fibroblasts, endothelial cells, smooth muscle cells, reticular cells, osteoblasts and adipocytes (223,224). BMAdS are the most abundant cell type within the BM stroma and in the process of ageing BMAT, within yellow marrow, gradually replace the red haematopoietic marrow, potentially affecting the HSCs expansion (225). Indeed, the accumulation of BMAT was shown to correlate with a decrease in HSCs and induces the reversible quiescence of HSCs within yellow marrow (226). However, recently it was highlighted that the role of BMAT in inhibition or maintenance of haematopoiesis is still considered disputable (226,227).

The transwells co-culture experiments, showed that *in vitro* in the presence of BMAdS, HSCs has a reduced expansion ability. On the other hand, inhibition of BMAT *in vivo*, results in reconstitution of haematopoiesis and leukocyte formation. These findings suggest that BMAdS secrete the signalling molecules that induce inhibition of haematopoiesis and lymphopoiesis (226). Accumulation of BMAT during high fat diet *in vivo*, found to rapidly reduce B lymphopoiesis (228). Additionally, *in vitro*, BMAT secreted paracrine factors were found to inhibit lymphopoiesis, through suppression of proliferation and maturation of lymphoid progenitors (229).

Contradictory, BMAT expansion and further increased level of BMAT secreted adipokine (adiponectin), are reported to be involved in pathological and normal regulation of haematopoiesis (179,230). Adiponectin is able to regulate the HSCs quiescence and therefore promote haematopoiesis (231). Study on mice, demonstrated that BMAT produced adiponectin signalling activates p38 MAPK pathways in HSCs and stimulate their multipotency (232). The haematological malignancies were found to be associated with low

level of adiponectin within interstitial fluids (233). Additionally, reduced BMAT in subjects with haematological malignancies and low level of local adiponectin reduce the macrophage secreted tumour necrosis factor, leading to reduced protection from inflammatory environment and increased risk of cancer development (234). Several types of haematopoietic cells were reported to express leptin receptor, suggesting the role of BMAT derived leptin on haematopoiesis, however current findings are contradictory (235). A number of studies on leptin or leptin receptor deficient mice exhibited impaired haematopoiesis, reduced number of circulating lymphocytes and inability to recover lymphopoiesis following the irradiation (236–239). However, *in vitro*, in murine and human derived BM cells, leptin stimulation failed to induce cell proliferation or survival (240). Another BMAT secreted cytokine, stem cell factor, signals to HSCs through binding the c-Kit receptor and promote cell proliferation and survival (241). Moreover, complete BMAT depletion in BMAd-Cre mice was shown to result in significant reduction of HSCs population without affecting mature cells, suggesting that BMAd lipolysis is required to fuel myelopoiesis (242).

1.3.2ii BMAT function - bone turnover

It is well established that adipocytes are able to inhibit the osteoblast activity. Co-culture of primary osteoblast with mature adipocytes results in suppression of osteoblastogenesis (243). It was suggested that this effect of adipocytes on osteoblast takes place due to lipotoxicity of FA (244). Finding from clinical and animal studies, demonstrated a negative correlation between BMAT and bone mass (189,245). In BMAd-Cre model, where mice lack specifically BMAT, Li *et al.* demonstrated an increase in cortical bone formation and trabecular bone formation was enhanced in caudal vertebrae of mice (242,246). BMAd and osteoblasts derive from the same precursor cells BMSCs, therefore the inverse relationships between these cell types might be driven by external stimulation of BMSCs to favour particular fate (247,248). Furthermore, similarly to WAT, BMAT functions as an endocrine organ secreting adipokine - leptin (179,229,249). BMAT secreted leptin is involved in suppression of bone formation through activation of Janus kinase 2 (JAK2)/ signal transducer and activator of transcription 3 (STAT3) signalling pathway in BMSCs (250).

On the other hand, various research articles showed the BMAT contribution to osteoclastogenesis. In the process of adipogenesis, the transcription factors CCAAT/enhancer-binding protein beta (CEBP β) and CEBP δ bind to the receptor activator for RANKL promoter

and facilitate its expression (251). Using flow cytometry, it was identified that RANKL expressed cells were also positive for pre-adipocyte marker (Pref1) and were capable of generating osteoclast from macrophages (251). *In vitro* study on mature adipocytes derived from bone marrow stromal cell line 2 (BMS2) were demonstrated to support osteoclast differentiation and function (252). Additionally, BMAT was shown to secrete chemokines C-X-C motif chemokine ligand 1 and 2 (CXCL1, CXCL2), which are promoting osteoclastogenesis in the context of metastatic prostate cancer (253). Leptin secretion by BMAT and its further signalling in brain stem increases sympathetic activity, however currently the degree of BMAT contribution to circulating leptin level is poorly understood (254). This leads to support of bone resorption through an activating transcription factor 4 (ATF4) – mediated process and decreases bone formation through CREB (255,256). Leptin receptor (LepR) was shown to be expressed in BMSCs and it was suggested that leptin signalling in these stem cells suppresses adipogenic differentiation and activates osteogenic (257,258). In leptin deficient mouse models (ob/ob mice), the administration of leptin at different sites resulted in decreased size and number of adipocytes within the BM (259–261).

Extracellular vesicles (EVs), or exosomes, released by adipocytes might potentially have a negative effect on the osteogenesis in co-culture system (262,263). These EVs contain various transcripts that are adipose tissue specific – PPAR γ , leptin or micro-RNAs (miR-138, miR-30c, miR-31, miR-125a and b) (262). Secretion of these EVs can potentially affect the phenotype of osteoblasts.

Recently, Li *et al.* demonstrated that lipolysis in BMAd is required for regeneration of trabecular bone, suggesting that BMAd is playing a positive role in bone homeostasis (246).

1.3.2iii BMAT function – systemic

As was mentioned before, BMAT is another source of circulating adipokines – adiponectin and leptin (249,264,265). Secreted adipokines regulate local and systemic bone homeostasis and energy metabolism. It was established that in WAT, adiponectin secretion promotes insulin sensitivity and protects against inflammation. However, Cawthorn *et al.* demonstrated that in CR condition BMAT secretion of circulating adiponectin is greater than from WAT (179). Additionally, BMAT and circulating adiponectin were found to be increased in other conditions, like type 1 diabetes mellitus (T1DM), ageing or oestrogen deficiency (266–269).

Moreover, in the study of Cawthorn *et al.* it has been shown that skeletal muscle CR-adaptation was impaired in *Ocn-Wnt10b* mice (overexpress *Wnt10b* from osteoblast), which are resistant to CR-induced BMAT expansion and hyperadiponectinaemia (179). More specifically, in the adiponectin suppression condition, it was observed that in skeletal muscles expression of mitochondrial transcripts (PPARG coactivator 1 alpha (*Ppargc1a*), mitochondrial transcription factor A (*Tfam*) and acyl-CoA dehydrogenase medium chain (*Acadm*)) was absent (179). Other studies have shown the positive effect of adiponectin on mitochondrial biogenesis (270). Furthermore, adiponectin is involved in regulation of systemic functions – glucose tolerance, insulin sensitivity in metabolic tissue, improved cardiovascular function and anti-inflammatory (157).

Leptin is known to form a sense of satiety in the brain and store energy in peripheral tissue (271). In 1998, for the first time, it was confirmed that *in vitro* primary BMAT cells express leptin (249). Later, multiple studies confirmed that *in vitro* human primary BMAds and BMSC-derived BMAds are able to express leptin and further secrete it into the system (272–274). The level of leptin secretion in BMAT and WAT differs in different species. In male C57BL/6J mice, Liu *et al.* demonstrated using microarray analysis that BMAT expressed lower level of leptin comparing to epididymal WAT (267). Cawthorn *et al.* described that in rabbit model, BMAT secreted similar amount of leptin as, inguinal WAT and perirenal WAT (179).

In contrast to WAT, Liu *et al.* transcriptomic analysis demonstrated that BMAT can be characterised by transcription of elevated level of inflammatory response genes – tumour necrosis factor α (TNF- α) and IL-6 or IL-1 (267). In the study of Tencerova *et al.*, BMAT exhibited higher expression level of TNF- α and IL-1 comparing to WAT in C57BL/6J mice (275). Interestingly, high fat diet and development of obesity in mice induced the increase of inflammatory cytokines in visceral AT, but in BMAT their decrease was observed (275). These results suggest that BMAT exhibits different inflammatory response to other AT depots. Human BMSC-derived adipocytes were also shown to secrete macrophage inflammatory protein 1 α (MIP-1 α), granulocyte colony-stimulating factor (G-CSF) and granulocyte-macrophage colony-stimulating factor (GM-CSF) (276). Furthermore, it was found that murine BMSC-derived adipocytes produce CXCL1 and CXCL2, allowing to regulate immune response (253). Overall, BMAT was found to secrete a range of pro-inflammatory factors, which are involved in regulation of bone and haematopoiesis, as well as whole body homeostasis (277–279).

1.3.3 BMAT regulation

With the development of new techniques described above, further characterisation of BMAT allowed to distinguish the presence of two different BMAT subtypes. For the first time, Tavassoli *et al.* defined two distinct groups of adipocytes that diverge in their location within BM, their cellular properties and composition, as well as their regulation (280,281). Adipocytes firstly appears in distal part of the skeleton (distal tibia or caudal vertebra) are identified as constitutive BMAT (cBMAT) within yellow marrow. This type of BMAT contain large adipocyte size, and they predominantly consist of unsaturated lipids (Fig. 11) (196). On the other hand, different type of BMAT is present in the lumbar and thoracic vertebrae, in the limb skeleton (proximal tibiae or in distal femur), hip and ribs, and is interspersed between haematopoietic cells (196,242,282). It forms later in life and appears in more scattered way comparing to cBMAT. This type of BMAT is referred as regulated BMAT (rBMAT) and it has been shown to consist from smaller adipocytes and saturated lipids (Fig. 11) (196).

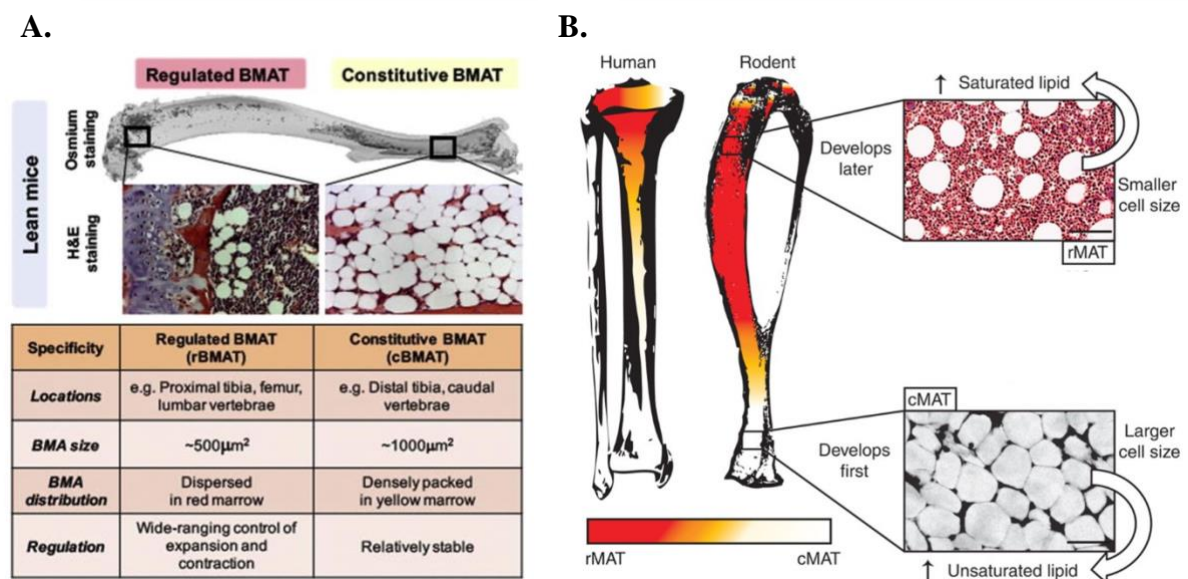


Figure 11. Location and characteristics of mouse and human cBMAT and rBMAT. A. Mice tibiae were studied using osmium staining and haematoxylin and eosin (H&E) staining shows difference between cBMAT and rBMAT, properties are summarised in the table. Adapted from Li *et al.*, 2018 (182); B. Summary of cBMAT and rBMAT in the mice tibia/femur junction and in the human proximal tibia metaphysis or femur. Adapted from Scheller *et al.*, 2015 (259). Bone marrow adipose tissue (BMAT); marrow adipose tissue (MAT).

Studies on the adult mice revealed that females exhibit higher level of rBMAT comparing to males. However, the cBMAT was found to be similar between sexes (101,196,283). Furthermore, the ovariectomy in rodents cause a dramatic increase in BMAT, interestingly that rBMAT expansion in this condition was greater than cBMAT (101,284). rBMAT and total BMAT appears to be regulated by various changes in the body – nutrient availability, environment or endocrine factors. In particular, studies have shown that specifically rBMAT population is expended in response to CR, ovariectomy and irradiation, which is typically associated with bone loss and abnormal haematopoiesis (285).

A 21-day cold exposure resulted in extensive rBMAT loss in mice tibia (196). Another negative regulator of rBMAT is the exercise or mechanical loading. Extensive research on this topic demonstrated that mice, which were undergoing exercise, exhibited a decrease in BMAT within proximal tibia and in whole bone (204,286–289). Endocrine signalling of PTH also is able to affect BMAT. Deletion of PTH/PTHrP receptor in BMSCs, was shown to have a positive effect on BMAT accumulation (290). Furthermore, the administration of PTH can reduce an increase in BMAT in mice (290). Interestingly, in BMAd-Cre mice, Depletion of very abundant cBMAT resulted in increased cortical bone in the distal tibia and trabecular bone in the caudal vertebrae, whereas loss of less abundant rBMAT resulted in minor or no effects on proximal tibial trabecular bone (242). Based on these findings, it can be concluded that various factors cause changes in BMAT, and it demonstrates the plasticity of rBMAT, as well as BMAT tissue overall.

1.3.3i BMAT regulation - ageing

Since 1882 various studies of the qualitative changes in the human marrow have been published, when Ernst Neumann noted that there is trabecular bone shrinkage with age and that most of the bone marrow in the axial skeleton consists of AT that does not participate in haematopoiesis. Many other researchers confirmed the same findings (181–183,189). These initial histomorphometric findings in elderly and osteoporotic individuals were validated in subsequent research utilising other techniques (190,291). Changes in marrow, including a rapid increase in BMAT content, are noted in female participants between the ages of 55 and 65, but the increase in male subjects is much more gradual, however it is continuous (190). In recent years, a lot of attention was given to the role of BMAT in the development of age related osteoporosis (292). Due to the fact that both adipocytes and osteoblasts are derived from

BMSCs, it was assumed that increase in adipogenesis is associated with a suppression of osteoblastogenesis (293–297). Studies in haploinsufficiency of PPAR γ , indicated a promotion of bone formation through enhanced osteoblastogenesis, combined with suppression of adipogenesis (298,299). In contrast, in the process of ageing, the increased expression of PPAR γ was observed in the BM leads to enhanced adipogenesis and reduced osteogenesis (300). Studies in BMSC cultures from senescent accelerated mouse models (SAMP-6) and normal aged mice revealed increased adipocyte differentiation, through increased expression of *Pparg2*, and decreased osteoblastogenesis, through decreased expression of *Runx2*, distal-less homeobox 5 gene (*Dlx5*), collagen type 1 (*Coll1a1*), osteocalcin (*Bglap*) (301,302). Additionally, several studies have demonstrated the relevance of PPAR γ activation in the age-related rise of BMAT and reduced osteoblastogenesis. PPAR γ and CEBP levels were shown to be higher in aged mice BM (251). An increase in production of endogenous PPAR γ 2 ligands could explain the observed phenotype, the increase in BM adipogenesis and subsequent reduction of osteoblastogenesis. Examples of these ligands are - dietary lipids, dyslipidemia, hyperlipidemia, and the use of medications such as lipid lowering agents, glucocorticoids, and thiazolidinediones (303). Moreover, Chandra *et al.* study supported the idea that accumulation of BMAd is leading to the depletion of BMSCs pool through contribution towards age-associated cell senescence, as well as lineage switching towards adipogenesis in ageing environment (304–307).

Overall, this research indicates that BMAT appears to be associated to age-related bone loss; nevertheless, the cause of BMAT throughout ageing remained unclear. Woods *et al.* in their association study showed that in men there were no associations between BMAT and changes in bone density or strength (308). However, in older women, they found a strong association between BMAT and greater loss of trabecular bone at the spine and femoral neck, and greater loss of spine compressive strength (308). Highlighting the role of menopause on woman bone health.

1.3.3ii BMAT regulation - menopause

Multiple studies established a correlation between increased BMA volume and bone loss at multiple sites, in older woman and in ovariectomised (OVX) animal models (190,205,214,308–313). Recently, Woods *et al.* described that higher BMAT predicts trabecular bone loss at the spine and femoral neck in older women, as well as reductions in spine compressive

strength.(308). Oestrogen treatment reduces BMA while increasing bone mass in oestrogen-deficient humans and animals (311,314). These data suggest that BMAT plays a role in bone loss caused by oestrogen discontinuation, but it is unclear if this is a causative link. Therefore, it should be noted that before defining the involvement of BMAT in postmenopausal osteoporosis (PMOP) pathophysiology, the molecular processes of abnormal BMAT growth following oestrogen removal must be understood.

One of the potential mechanisms of BMAT accumulation in PMOP, is through the imbalance in BMSCs differentiation capacity. Oestrogen has a considerable influence on the final differentiation of BMSCs into osteoblasts or adipocytes. According to several research studies, oestrogen enhances osteogenic differentiation while suppressing adipogenic differentiation in BMSCs via multiple mechanisms (315–317). Kumar *et al.* found that oestradiol inhibits adipogenesis in the bone marrow stromal cell line ST2 by increasing transforming growth factor (TGF)-mediated connective tissue growth factor (CTGF) production (315). Rooney *et al.* demonstrated that silencing oestrogen receptor alpha (ER α) induces BMAd proliferation, indicating that ER α is involved in BMSCs fate decision by oestrogen signalling (318). Furthermore, oestrogen can inhibit the synthesis of sclerostin (SOST) by osteogenic cells (319,320). In PMOP women, oestrogen deprivation resulted in increased BMA and concomitantly higher SOST levels (321). SOST has been demonstrated to enhance adipogenic differentiation of MSCs, resulting in BMAT growth and bone loss (322). Also, oestrogen deficient triggers overproduction of TNF- α , which leads to suppression of osteogenesis with subsequent upregulation of adipogenesis, through upregulation of purinergic receptor (P2Y2) in BMSCs (323).

Due to the endocrine feedback of the gonadal-pituitary axis, decreasing oestrogen concentrations correspond with increasing follicle stimulated hormone (FSH) concentrations. Recent research found that inhibiting FSH binding to its receptor with an antibody prevented the growth of BMAT following ovariectomy, and that therapy with this antibody in sham-operated animals reduced marrow adipose tissue (324). They demonstrated that both adipocytes and BMSCs express the FSH receptor and that FSH receptor defective animals had enhanced adipogenesis in BMSCs, implying that postmenopausal high FSH leads to increased BMSC adipogenesis. Additionally, FSH has been shown to have a direct effect on bone, independently of oestrogen (325). The FSH receptor was found to be present on osteoclasts,

and has been associated with positive regulation of osteoclast differentiation (326). Therefore, it can be suggested that FSH has a direct negative effect on bone volume.

Oestrogen deficiency, has also been shown to induce trans-differentiation *in vitro*. Foo *et al.* described that lack of oestrogen induces trans-differentiation of hFOB 1.19, a human pre-osteoblast cell line, into adipocytes via down-regulation of β -catenin signalling (327). Similar findings were obtained by Gao *et al.*, where through the canonical Wnt signalling pathway, 17-estradiol resulted in reduction of the osteo-adipogenic trans-differentiation of MC3T3-E1 cells in a dose-dependent manner. They also discovered that MSC-derived osteoblasts in OVX mice had more trans-differentiation potential into the adipocytic lineage than the sham group (328). Overall, an increase in osteo-adipogenic trans-differentiation during menopause may lead to increasing MAT content while decreasing bone production.

Longitudinal studies, revealing changes in both BMD and BMAT in response to therapies for low bone mass, support the link between BMAT and BMD. Teriparatide (recombinant human PTH) treatment of postmenopausal women for one year resulted in reduced vertebral BMAT while increasing lumbar spine BMD (329). Following 12 months of oestrogen replacement therapy, there was a reduction in adipocyte volume/tissue volume (AV/TV) in postmenopausal women (330). In animal models, *in vitro* studies demonstrated a decrease in BMAT in OVX rats, which were treated with raloxifene, a modulator of ER widely used in osteoporosis treatment (331). However, the same treatment in postmenopausal women did not induce significant changes in BMAT volume, despite 2 year exposure (313).

1.3.3iii BMAT regulation - cancer

The interaction of tumour cells, osteoclasts, and osteoblasts is well recognised, but the association between BMAT, multiple myeloma, and breast or prostate cancer metastases has only just begun to be appreciated. Lately, multiple research teams have published excellent overviews of the expanding data, which is linking BMAT to tumour growth and the development of related bone disease (332–335).

Breast and prostate cancer are both solid tumours that primarily spread to the BM. Adipocytes in the BM may be implicated in the recruitment and proliferation of certain tumour forms. Previous *in vitro* investigations found that BMAds enhance tumour development and

metastasis of prostate cancer through FA production and hypoxia inducible factor 1 α (HIF-1 α) activation (336,337). Moreover, mice studies on melanoma, showed that cancer cells induce lipolysis in BMAdS, on the other hand BMAdS were found to secrete factors that promote cancer cell growth (338). Clinical studies on breast cancer patients, showed higher level of BMA comparing to matching healthy controls (73% BMA in cancer patients vs. 60% in control individuals) (339). These findings suggest that breast cancer is related with increased BMA, despite the fact that these individuals did not have metastatic illness.

Changes in the BM are caused by haematological malignancies, and it has long been recognised that BMA is raised in aplastic anaemia and decreased in leukaemia (340). This was formerly assumed to be related to the lack or increase of haematological cancer cells, but this has lately been challenged. Indeed, it is currently recognised that bone marrow adipocytes play an active part in the pathogenesis of haematological neoplastic illness (341). *In vitro* studies have revealed that human BMAdS actively stimulate leukemic development via lipid transfer and mediator release (342,343). Furthermore, pharmacological reduction of lipid transfer between BMAdS and leukemic blasts by inhibition of fatty acid binding protein 4 (FABP4), which is required for lipid transport, results in lowered tumour survival *in vitro*, in the same time increasing leukemic mouse survival *in vivo* (342). Likewise, inhibiting carnitine palmitoyl transferase 1 (CPT1), which is required for fatty acid entrance into the mitochondria, reduced the survival of human leukaemia cells *in vitro*, showing that fatty acids constitute an essential source of energy for these cells. Despite the fact that these animal and *in vitro* findings are encouraging, no human clinical trials have yet been published.

1.3.4 BMAT in metabolic disease

It was described above, BMAT is a dynamic tissue that is involved in overall metabolic homeostasis and is strongly correlated with skeletal health. The BMAT correlation with low bone mass has been observed in various healthy individuals study groups – Caucasian woman (344), in young, middle-aged and elderly mixed population (345–347). In addition to data presented on healthy individuals, abnormalities in bone observed during process of ageing or metabolic disease were associated with BMAT accumulation within BM cavity (191). Effect of ageing on altered bone architecture and increase in BMAT was widely described in both sex (190,348,349). It was found that in females accumulation of BMAT takes place rapidly between age of 55 and 65, however in male the increase is gradual throughout the life (190).

In ageing woman, gonadal deficiency or menopause, leads to the development of imbalance between BMAT and bone (309). Furthermore, the increase in BMAs number has been observed in different metabolic and nutrient associated disease.

1.3.4i BMAT in diabetes

Diabetes, both T1DM and T2DM, are metabolic conditions during which patients experience increased risk of bone fracture due to bone loss (350–352). Mouse models of T1DM were characterised by attenuation of insulin production, reduced body weight, hyperglycaemia and bone loss (353). Additionally, these animal models exhibited an increase in BMAT (352,354–356). However, in clinical study on T1DM patients, MRI indicated slight shift in amount of BMAT within BM comparing to controls, but within normal range (357,358). Therefore, more human studies required to understand the presence of BMAT alterations in T1DM patients. In T2DM studies, it was concluded that increase in patient fracture risk is independent of bone mineral density or BMAT (359–361). Interestingly, Goulding *et al.* showed that in patients with T2DM, there was no increase in BMAT observed, however, the level of saturate lipids in BM was higher than in controls (362). Furthermore, T2DM patients who experienced a fracture had the highest level of saturated FA (362).

1.3.4ii BMAT in obesity

Similarly to diabetes, obesity was found to affect bone mass (209). In obese premenopausal woman, it was found that amount of visceral AT correlated with BMAT, and these findings were associated with decrease in bone mineral density (BMD) (363). *In vitro* studies on BMSCs extracted from overweight subjects were committed to adipogenic differentiation, suggesting that circulating factors affect stem cell fate and lead to increase in BMAT (364,365).

1.3.4iii BMAT in anorexia nervosa

Anorexia nervosa (AN) - characterisation

Another nutrition associated disease that was found to result in bone loss is AN. Anorexia is a psychiatric disorder characterised by extrema level of self-imposed starvation and CR, which results in weight loss (366,367). Unfortunately, this disease becoming increasingly common in

modern society and occurs in almost 4% of young females (368–370). Furthermore, cases of AN among male population are increasing as well (368,371).

This psychiatric disease results in severe weight loss, patient mean body weight was shown to be only approximately 70% of healthy body weight controls and was frequently associated with chronic stress (372,373). The severity level of the disease consequences was linked to its duration (374). Commonly, AN patients exhibit nutritionally acquired growth hormone (GH) resistance (375,376). Hepatic GH resistance was confirmed, through the administration of supraphysiologic doses of recombinant human GH to AN patients, which did not result in an increase in output of insulin-like growth factor 1 (IGF-1) (375). The consequences of GH resistance were evident in young male patients with AN, who were found to be shorter comparing to control individuals (377). In the same time, data on young females with AN is contradictory, as studies reported variability in their data (378–380). Furthermore, alterations in adipokine (adiponectin and leptin) production were observed in adults and adolescents with AN. Affected individuals have low levels of leptin comparing to healthy subjects (381,382). Decreased leptin secretion reflects a decrease in fat depots. Additionally, reduced leptin concentration results in dysfunction of hypothalamic-pituitary-gonadal (HPG) axis and impaired gonadotropin secretion leading to amenorrhoea in females (381,383). Reports state that AN induces an increase in adiponectin comparing to controls, which also potentially can result in impaired gonadotropin secretion (384,385). Further, in post-menopausal women and elderly men, high circulating adiponectin level was associated with reduced BMD, through decrease in OPG and an increase in osteoclast activity (386,387). This suggests that AN associated increase in adiponectin can contribute to the decrease in BMD. Another serious consequence of AN in females with amenorrhoea, as a result of compensatory response to negative energy balance (388).

AN is associated with approximate 7-fold increase in bone fracture risk, which is caused by significant bone loss and imbalance in bone turnover (389–391). Most of the fracture risk was found to be associated with reduction in BMD; in clinical study it was identified that 38% of AN patients had T scores less than -2.5 and 92% of patients had T score less than -1 (negative T scores indicate the bone is weaker than normal) (392). These complications, which affect almost 50% of AN patients, may not be reversible and can be associated with life-long risks of spinal vertebrae compression fracture and long bone fracture (393).

The reduction of BMD in AN patients can be classified in two main types – osteopenia and osteoporosis (394). Osteopenia is a mild form of the disease, that is defined by bone densitometry with T score between -1 to -2.5 (395). In case when osteopenia is not addressed, it can quickly progress into the more severe form of osteoporosis. This severe degree of BMD loss is characterised by T score lower than -2.5 (396). AN associated osteoporosis in younger individuals can result in increased long-term or life-long fracture risk and loss of height due to spinal compression fractures with chronic back pains (394). Due to the seriousness of AN consequences, the treatment of patients should be carefully addressed.

Currently, osteopenia patient's treatment focuses on weight restoration and supplementary intake of vitamin D and calcium, without osteoporosis medications (397). On the other hand, vitamin D or calcium intake is not sufficient enough to reverse consequences of osteoporosis, therefore stronger medication and treatment plan required. For adult AN patients with osteoporosis, bisphosphate agents (alendronate or risedronate) are orally administered (398). These agents act as inhibitors of bone resorption and bone turnover, leading to reduction of bone loss and around 4% restoration in BMD (399). However, this treatment exhibits side serious effects in some of the patients, therefore is not considered to be the best treatment option (399). On the market there are three other medications to treat adult AN related osteoporosis – teriparatide, denosumab and transdermal oestrogen therapy (394). Teriparatide is an analogue of PTH, which increases new bone formation. The clinical trial study with AN and osteoporotic patients showed a remarkable 10% increase in BMD following 6-month teriparatide treatment (400). However, this treatment requires daily injections during 2 years, which make them practically difficult. Denosumab is a biological agent used in treatment of osteoporosis and in post-menopausal woman it has a positive effect on BMD, but no studies on AN patients were conducted (401). Amenorrhoea has been also shown to be associated with severe bone loss in AN patients, therefore it is treated with high oestrogen doses given in birth control pills (402). In AN adolescent patients oestrogen replacement increased BMD, but dosage was not high enough to mimic healthy puberty (403). AN studies on bisphosphate agents described the controversial finding (398,404,405).

In summary, current treatments of severe bone loss in AN patients requires improvements, therefore it is important to study molecular mechanisms of bone loss within BM in CR context. This will allow to develop new therapy strategies and reverse osteoporosis in AN patients.

BMAT accumulation in AN – clinical studies

AN leads to the acute decrease in peripheral adipose tissue, but paradoxically an increase in BMAT was observed in AN patients (406,407). In a healthy individual, BMAT comprises 10% of total fat, but in people with AN the BMAT can take up around 31% of total body AT (406). Previously, Bredella *et al.* conducted a small cohort study on 10 AN and 10 normal weight individuals, where they emphasised the difference in BM fat content between the two study groups (245). Women with AN had more lumbar and femoral BM fat than controls, and BM fat was negatively correlated to BMD. In addition, AN patients with amenorrhoea had significantly greater BMA than anorexia patients with regular menstrual cycles, which might be owing to the cumulative effect of oestrogen withdrawal on BMA. Second study of Bredella *et al.*, focused of slightly bigger cohort of premenopausal AN patients (14 women, mean age 29.5 ± 7.1 years) and compared them with 12 normal weight controls (aged 20-45). Using ¹H-MR spectroscopy and dual-energy x-ray absorptiometry (DEXA) analysis of the bone and BM content, they confirmed the existence of negative correlation between lumbar spine BMD and total femoral fat content. Also, in long bones on AN patient, hip BMD was inversely associated with total femoral fat content (406). However, not only the amount of femoral fat was found to have a negative correlation with BMD, but also the quality of formed lipids. The degree of marrow FA saturation correlates adversely with BMD, suggesting that saturated fats may affect BMD in the context of AN (406).

Range of studies were performed to identify the correlation between BMAT, BMI and BMD. Difference between studied groups was observed, mainly due to the subject age and the severity of AN (408). Larger study, which was conducted by Ecklund *et al.* described that in 70 adolescent subjects, with different severity level of AN, BMAT accumulation was strongly associated with their age – 16 (or less) years old subjects displayed a positive tendency between BMAT, BMI and BMD. On the other hand, patients who were 17 years old (or more) had higher level of BMAT when the severity of the disease was increased (subjects with lower BMI). This study had shown a strong age association with BM fat. A trend of increasing BM fat throughout the childhood, adolescence and adulthood was previously described, and this study confirmed that association in AN patients (408,409). Moreover, it has been shown that BMD exhibited negative association with BM fat in older subjects, once again providing evidence of BMA negative effect on bone (408).

Another study on 47 adolescent subjects (14-24 years old) with AN confirmed the increase in BMAT comparing to 55 age matching controls. Also, inverse relationship between BMAT and BMD in spine and long bones was described (410). This particular study looked at bone strength of AN patients, and they found a positive association between strength and lean mass, as well as bone microarchitectural parameters. Predictably, BMAT was estimated to be inversely correlated with bone strength and BMD (410).

Recently, Bard *et al.* had a close look at femoral head composition in AN patients, as well as recovered individuals (411). This study covered a comparatively large cohort of patients, 40 underweight and 36 weight recovered AN patients were contrasted to 10 normal weigh women. The team identified that BM fat fraction in AN patients was higher than in controls. Moreover, the unsaturation level of this fat also has been found to be lower in underweight individuals, as well as recovered AN patients, supporting findings of Bredella *et al.* (406). Study of multiple locations in the hip showed an inverse connection between BM fat percentage and lipid unsaturation levels. Overall, this study emphasised that there are complex relationships between BMA, BMD, and body fat.

Similar findings were observed in older, pre-menopausal woman (25-31 years old) (412). 26 AN subjects and 20 normal weight controls have been followed for 12 months. Initial findings stated that BMAT level was associated with decrease in BMD in AN patients. However, after short weight gain, both BMAT and BMD were increase in same subjects (412). These longitudinal results show the dynamic character of this fat deposit and give more evidence for its potential function in mineral metabolism. Unfortunately, very limited number of studies provided a follow-up data on AN patients after recovery.

Bredella <i>et al.</i> 2009	Bredella <i>et al.</i> 2014	Ecklund <i>et al.</i> 2017	Singhal <i>et al.</i> 2018	Badr <i>et al.</i> 2019	Fazeli <i>et al.</i> 2019
20 subjects (10CT; 10AN)	26 subjects (12CT; 14AN)	40 subjects (20CT; 20AN)	102 subjects (55CT; 47AN)	86 subjects (10CT; 76AN (40UW + 36WR))	46 subjects (20CT; 26AN)
20-42 years old	20-45 years old	13-18 years old	14-24 years old	18-35 years old	24-32 years old
BMI AN – 17.6 BMI CT – 21.9	BMI AN – 17.7 BMI CT – 22.1	BMI AN – 16.9 BMI CT – 22.3	BMI AN – 18.4 BMI CT – 22.1	BMI AN – 15.4 BMI CT – 20.2	BMI AN – 16.7 BMI CT – 22.6
BMD AN – 0.97 BMD CT – 1.14	BMD AN – 0.66 BMD CT – 0.82	N/A	BMD AN – 297.5 BMD CT – 328.0	BMD AN – 0.67 BMD CT – N/A	BMD AN – 0.77 BMD CT – 0.96
BMA Femur AN – 7.11 CT – 4.05	BMA Femur AN – 10.8 CT – 5.1	Red Marrow (T_1 value), lower in AN subjects	BMA L4 AN – 0.89 CT – 0.52	BMFF AN – 0.91 CT – 0.82	BMA L4 AN – 0.98 CT – 0.48
Patients with amenorrhoea had significantly greater BMA	Marrow FA saturation correlates adversely with BMD	Showed a trend of increasing BM fat throughout the childhood	Positive association between bone strength and lean mass	AN subjects had lower unsaturation level of BMAds	Short term weight gain caused BMAT and BMD increase

Table 2. Summary of studies conducted on AN patients. Table highlights 6 recent studies on AN patients, describing the number of participants, their body parameters and association between studied parameters. CT – control; AN – anorexia nervosa; BMI – body mass index; BMD – bone mineral density; BMA – bone marrow adiposity; BMFF – bone marrow fat fraction;

BMAT accumulation in AN – studies on animal models

In order to better understand the process of BMAT accumulation in condition of food deprivation, various studies on animal models were conducted. The first published paper in the topic of CR in animal models was by Hamrick *et al.* in 2008 (413). In this study, experimental design was focused on 14-week-old male mice, which were exposed to 10% food restriction for 1 week, then it was increased to 25% for another week and at last it was risen up to 40% restriction for another 8 weeks. This gradual increase in food restriction during 10 weeks resulted in significant decrease of body weight (-33% vs. CT), fat and lean mass in mice (vs. CT) (413). Unfortunately, no data was provided on mice initial weigh, therefore mice body weigh change throughout the protocol cannot be estimated. Interestingly, that whole body BMD, did not change in CR mice, but spine BMD and trabecular bone were increases in this condition. Only femur BMD, cortical thickness and fracture strength decreased dramatically in

CR mice (vs. CT). Importantly, these bone alterations in CR mice took place in the environment that lacked BMAds (413).

Later, Devlin *et al.* conducted a study on young C57BL/6J male mice (3-week-old), where they were exposed to 30% CR for 9 weeks (414). This protocol induced slow weight gain in CR mice (+88% vs. day 0) and resulted in bone and BMA alterations. Cortical and trabecular bone acquisition were both impaired by CR, including whole-body BMD and bone mineral composition (BMC), trabecular bone volume percentage, cortical bone area, as well as bending strength. Histomorphometry revealed that CR mice had decreased bone production and increased bone resorption. Moreover, CR mice had significantly greater BMA (+794% vs. CT) (414).

One of the Cawthorn *et al.* studies focused on 15-week-old male rabbits, which were fed 30% CR diet for 7 weeks. This particular diet was previously shown to induce BMAT expansion in animal models (179,414). Additionally, in this study they explored the effect of extensive CR on bone and BMAT, where young male rabbits (6-week-old) were fed 50-70% lower than *ad libitum* controls, for 7 weeks (415,416). Unexpectedly, neither moderate (30% CR), nor extensive (50-70% CR) protocols, did not cause an expansion of BMAT, in opposite these protocols resulted in BMAT loss (283). The initial study of Cawthorn *et al.* on 9-week-old female and male C57BL/6J mice, which was firstly published in 2014, animals were exposed to 30% CR for 6 weeks (179). This study focused on establishing the correlation between BMAT expansion and an increase in circulating adiponectin (417–419). They discovered that BMAT expansion significantly contributes to increased serum adiponectin during CR. These data demonstrate that BMAT is a key source of circulating adiponectin in lean conditions, and that BMAT can act beyond the skeleton to have systemic effects via endocrine activities (179). Replication of the study described above, where female C57BL/6J mice were exposed to 30% CR, resulted in an increased BMAT at the proximal tibia (283). In this study, Cawthorn *et al.* also concluded that changes in BMAT can be associated with glucocorticoids, as they were increased in mice and unchanged in rabbit model (283).

Scheller *et al.* conducted a study on acute short (48h) fasting in 16-week-old male rats and 18-week-old female (216). Animals did not have access to food for 48h, in prior to the sacrifice. Results showed that short-term fasting induced a decrease in BMAds cell size by 18% in males

and 34% in females, within proximal tibia. This study suggested that BMAT lipolysis is required to fuel BM in acute energy deprivation (216).

Another study on extended CR used 4-week-old female and male C57BL/6J mice and CR mice received ad libitum food, but only every other day (EOD) (420). This protocol lasted for 9 months and after bone mineralisation content was quantified. Unfortunately, BMA in this study was not quantified. Female EOD mice gained 31% of weight (vs. day 0) and male EOD mice gained 21% of weight (vs. day 0). In contrast, CT groups gained 46% for males and 42% for female mice (vs. day 0). Results showed that prolonged EOD treatment did not result in significant mineral loss. Starting an EOD feeding pattern in maturity did not worsen the loss of mineral content with age, but rather improved the reduction of mineral deposits in animals with low mineral density (420).

Recently, Duque *et al.* conducted a study on 2-month-old male Sprague-Dawley rats, who were individually housed and were fed chow diet (421). After 8 months, rats were randomized into CT and CR groups (40% CR feeding). After 10 months of protocol, rats were sacrificed. Results demonstrated that CR mice had a significant decrease in body weight (vs. CT), as well as reduction in bone volume per tissue volume (Bv/Tv) (-20% vs. CT) in proximal tibia. CR group contained significantly higher BMADs number comparing to the CT group. Interestingly, circulating leptin level was found to be decreased in CR rats, probably due to the decrease in AT mass outside the bone (421).

One of our recent studies demonstrated that long term (8-week) Separation Based Anorexia (SBA) model protocol in 7-week-old C57BL/6J female mice results in reduction of bone parameters and BMD with subsequent increase in BMA (2). Overall, it was found that effect of CR on BMAT is specie specific, can depend on a strain and also sex of the model.

	Specie	Age (Day 0)	Protocol Length	CR or FR Severity	BW Change	Bone Changes (vs CT)	BMA Changes (vs CT)
Hamrick <i>et al.</i>, 2008	Mouse	14-week-old	10-week	10% (1W) + 25% (1W) + 40% (8W)	-33% (vs CT)	Femur BMC -21%	No BMAds
Devlin <i>et al.</i>, 2010	Mouse	3-week-old	9-week	30% FR	+88% (vs D0)	Femur Bv/Tv -11%	BMA +794%
Baek <i>et al.</i>, 2012	Rat	6-month-old	12-week	40% FR	-20% (vs D0)	Tibia BMD +5%	BMA +94%
Cawthorn <i>et al.</i>, 2014	Mouse	9-week-old	6-week	30% FR	Decrease (vs D0)	-	BMA Increase
Cawthorn <i>et al.</i>, 2016	Rabbit	15-week-old	7-week	30%/50-70% CR	-	Bv/Tv -20%	No Change
Piotrowska <i>et al.</i>, 2020	Mouse	3-week-old	9-month	EOD Feeding	+26% (vs D0)	No Mineral Loss	-
Duque <i>et al.</i>, 2020	Rat	10-month-old	10-month	40% CR	-20% (vs CT)	Tibia Bv/Tv -20%	BMAds N. +400%

Table 3. Summary of studies conducted on animal models of CR. Table highlights 7 recent studies on CR animal models, describing the specie, their age, protocol length, protocol severity and its effect on animal body parameters.

CT – control; FR – food restriction; EOD – every other day feeding; BW – body weight; BMD – bone mineral density; BMC – bone mineral composition; Bv/Tv – bone volume fraction; BMA – bone marrow adiposity; BMFF – bone marrow fat fraction; BMAds – bone marrow adipocytes

2. Sirtuin Type 1 – metabolic regulator

Sirtuin Type 1 (SIRT1) is a nicotinamide adenine dinucleotide (NAD⁺)-dependent deacetylase, the mammalian homolog of yeast silent information regulator 2 (SIR2) (422). It affects a variety of cellular processes by regulation of protein activity (targeting forkhead box O (FOXOs), nuclear factor kappa-light-chain-enhancer of activated B (NFκB), PGC-1α, etc.) and gene expression through deacetylation of histones (H3 and H4) (422). In mammals, SIRT1 is one of seven members of sirtuin family, a conserved family of proteins found in all domains of life (423).

2.1 Sirtuin family

For the first time Klar *et al.* in 1979, described a mutation in mating-type regulator (MAR1) loci, which resulted in sterility of *Saccharomyces cerevisiae* through silencing the mating-type loci HMR and HML (424). Later, other sterility causing mutations were discovered by Rine *et al.*, the responsible gene in these studies was named silent information regulator 1 - 4 (SIR1-4), which replaced old nomenclature (425–427). Further studies revealed that yeast SIR2 functions as histone deacetylase, which is dependent on NAD⁺ as a co-factor (428). Furthermore, experiments in yeast demonstrated the role of sirtuins in ageing, through a model of replicative life span (429). Later it was confirmed that SIR2 has a conserved functional role in ageing in a wide range of organisms from bacteria to mammals (430). Throughout the years, interest in SIR grown and by 1999 Roy A. Frye identified five human homologues of SIR2, naming them sirtuins (431). At the moment, seven members of sirtuin family have been identified (SIRT1-7), where human SIRT1 is evolutionary closest to yeast SIR2 (432,433).

Seven members of sirtuin family in humans are found in distinct compartments within the cell. SIRT6 and SIRT7 are predominantly found in cell nucleus, whereas SIRT1 and SIRT2 could be found both in nucleus and cytoplasm (423,434,435). SIRT3, SIRT4 and SIRT5 were found to contain the mitochondrial targeting sequence on the N-terminal end and were characterised to function within the mitochondrial matrix (436–438). Despite the differences in N- and C-termini, all family members contain highly conserved NAD⁺ - binding and catalytic domain (439,440) (Fig. 13).

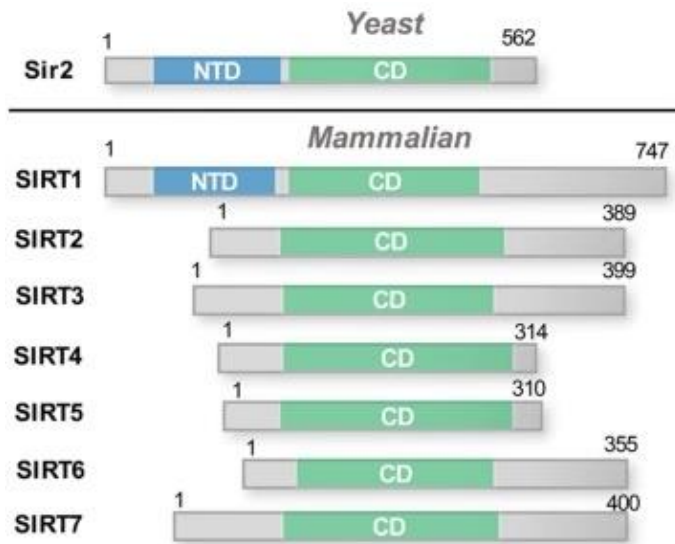


Figure 13. Sirtuin family structure. Comparison of yeast SIR2 and mammalian sirtuin family members, which share conserved catalytic domain (CD). SIRT1 exhibit particular structural similarities with SIR2, due to the presence of N-terminal domain (NTD). Adapted from Hou *et al.*, 2016 (425).

Sirtuin family – function

Tsang *et al.* has identified a ribosyltransfer reaction catalyzed by cobB, the bacterial homologue of SIR2 (441). This discovery was followed by characterisation of sirtuin activity and their NAD⁺-dependent deacetylation, with few exceptions (428,442–444). Unlike most of the members of mammalian sirtuin family, SIRT4 functions as NAD⁺-dependent mono-ADP-ribosyltransferase (437). Furthermore, SIRT1 and SIRT6 have been shown to conduct both auto-ADP-ribosyltransferase and deacetylase activities (423,445–447) (Fig. 14). Acetylated histones (H1, H3, and H4) have been shown to be targets for sirtuin histone deacetylase (HDAC) activity. In particular, lysine 16 (Lys16) of H4 is an important residue in sirtuin-mediated suppression of gene expression (448,449). Sirtuin activity as deacetylases allows them to modify protein activity and regulate various *in vivo* processes, including cell survival, mediation of cell metabolism and suppression of inflammation, resulting in promotion of longevity and protection against the cancer (423,450–454).

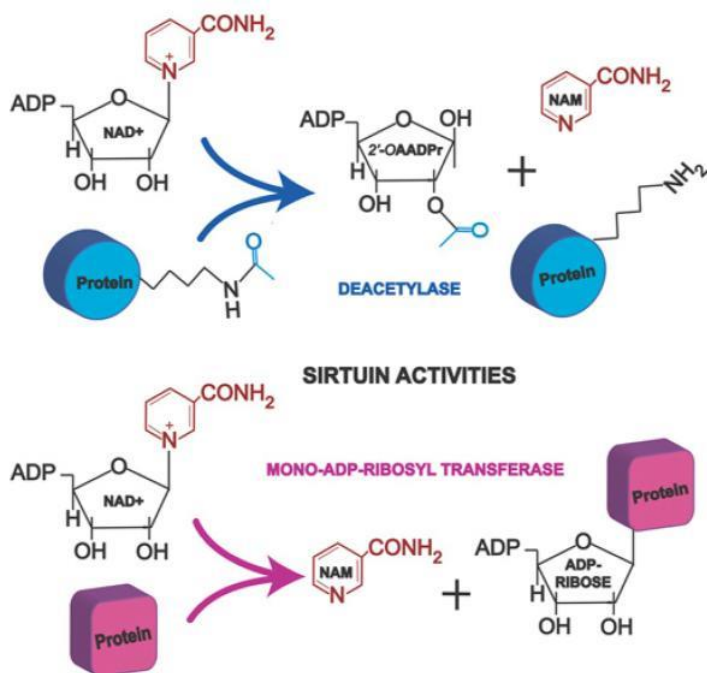


Figure 14. Enzymatic activity of sirtuin family members. Sirtuins are able to perform NAD⁺-dependent deacetylation, as well as mono-ADP-ribosyl transferase activity, which allows them to regulate wide range of cellular mechanisms. From Michan and Sinclair, 2009 (415). Nicotinamide (NAM).

In cytoplasm, SIRT2 was found to be co-localised with microtubule network and together with HDAC6 regulate level of tubulin acetylation (455,456). More importantly, SIRT2 functions as a regulator of mitotic progression during the cell cycle (455,457,458). During cell cycle, SIRT2 was shown to be associated with centrosome and mitotic spindles, which suggests that this protein plays a role in chromosome condensation and completion of mitosis (434). However, more recent findings emphasised the role of SIRT2 in halting cell division, when DNA damage emerges (459). This protects the cell from wrong replication. Moreover, in adipose tissue, SIRT2 is the most abundant member of sirtuin family, and it negatively regulates adipogenesis through deacetylation of FOXO1 (460,461). Additionally, SIRT2 blocks the process of *de novo* lipogenesis by targeting ACLY for degradation (Fig. 6) (462,463). The anti-inflammatory effect of SIRT2 was also described (464).

SIRT3 is one out of three members of sirtuin family who is located within the mitochondria, where it regulates diverse mitochondrial function, including ATP production, reactive oxygen species (ROS) management, activation of FA metabolism through β -oxidation, inhibition of lipogenesis and regulation of cell death (465–467). In pancreas, it plays an important role in facilitating insulin secretion under high glucose condition (468,469). Furthermore, it was demonstrated that SIRT3 is involved in BAT differentiation and in BAT thermogenesis, where SIRT3 is associated with *Ucp1* gene expression (470–472).

In contrast with SIRT3, SIRT4 was shown to suppress insulin secretion in pancreatic cells (437,473–475). Moreover, SIRT4 suppresses glutamate dehydrogenase (GDH) activity and reduce glutamate metabolism, subsequently reducing insulin secretion (437,476–478). Another SIRT4 target in pancreatic β -cells is pyruvate dehydrogenase (PDH), the main producer of Ac-CoA from pyruvate. Suppression of this enzyme results in decreased accessibility of Ac-CoA to the TCA cycle, reduced ETC activity and reduced ATP production, generating insufficient insulin secretion (479). In liver SIRT4 opposing function to other members of sirtuin family and plays role in decrease of FAO during high fat diet (480,481). In WAT, SIRT4 has been shown to upregulate lipogenesis by suppressing FA β -oxidation through blocking malonyl-CoA decarboxylase (MCD) enzyme activity (480,482).

The last mitochondrial enzyme in sirtuin family is SIRT5 (483). Recently, it was described that SIRT5 in proximal tubular epithelial cells (PTECs) is required for normal ATP production in the context of ischemic renal injury (IRI) (484). In addition, Zhou *et al.* has shown that SIRT5 may have a cardioprotective effect in the response to acute ischaemia, which is conducted through liver-cardiac crosstalk mechanism (485). SIRT5 is also serving as a post-translational modifier of proteins, maintaining desuccinylation, demalonylation and deglutarulation (486–488).

SIRT6 is a predominantly nuclear protein that is associated with regulation of chromatin structure and targeting H3K9Ac and H3K56Ac (489,490). It aids in protection against DNA damage by regulating DNA repair factor C-terminal binding protein 1 (CtBP1) interacting protein (CtIP) and suppress genomic instability through base-excision repair and DNA-end resection (491,492). It was outlined that SIRT6 activity attenuates NF κ B signalling pathways, by binding directly affecting RelA subunit (493,494). In pancreatic β -cells, SIRT6 facilitates insulin secretion, through promotion of glucose oxidation and facilitation of calcium influx (495–497). In liver, SIRT6 deletion results in decrease in FAO, suggesting that SIRT6 can be involved in FA β -oxidation (498,499). Overall, due to its functions (deacetylation, gene promoter binding, direct physical interaction) SIRT6 plays an important role in inflammation, stress response, genomic stability and metabolism (500–502).

SIRT7 is associated with regulation of ribosomal DNA (rDNA) transcription in mammalian cells (503,504). Overexpression of SIRT7 resulted in increased RNA polymerase I (Pol I)-

mediated gene transcription, and SIRT7 knockdown resulted in decrease of Pol I activity (505). In nucleus SIRT7 serves as a component of Pol I transcriptional machinery (506,507). SIRT7 was described to suppress the ER stress and is able to reverse fatty liver in obese models (508).

2.2 SIRT1 structure and expression

As it was described above, mammalian SIRT1 is evolutionally the closest homologue of yeast SIR2, which is located and functions predominantly in cell nucleus and was established to have both auto-ADP-ribosyltransferase and NAD⁺-dependent deacetylase activity (432,435,447). In humans *Sirt1* gene is located at chromosome (Chr) 10q21.3 in the region ranging from 67884669 bp to 67918390 bp, and it has been described to have three alternative splicing isoforms (431,509). SIRT1 isoform-1 (SIRT1-v1) was established to be a close homolog of SIR2 and has been widely described throughout the years (510). The other two isoforms are subsequently referred as SIRT1-v2 and SIRT1-v3 (Table 4).

Gene	Chromosome	Isoform	mRNA Accession#	Exon-Skipping	Protein Accession#	Amino Acid	Sirtuin Domain		
							from-to	Length	% (SIRT/Total)
SIRT1	10	V1	NM_012238		NP_036370	747	244–498	254	34.0
		V2	NM_001142498	ex1, ex3	NP_001135970	452	1–203	202	44.7
		V3	NM_001314049	ex1, ex2, ex3	NP_001300978	444	1–195	194	43.7

Table 4. Summary of SIRT1 mRNA and protein isoforms in humans. Summary contains a Genbank accession number for each mRNA and protein isoform. Comparing to SIRT1-v1, the rest of isoforms appear to be shortened due to axon skipping. Adapted from Zhang *et al.*, 2021 (501).

SIRT1-v2 and SIRT1-v3 were shown to contain shorter sequence comparing to SIRT1-v1, as exon skipping events took place during the production of these variants (509). The most important structural and functional difference between SIRT1-v1 and other two isoforms is presence of two nuclear translocation signals (NTS), which allow SIRT1-v1 to enter the nucleus and conduct there its activity (509) (Fig. 15).

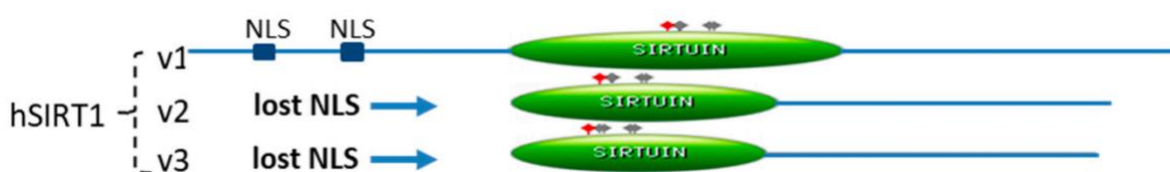


Figure 15. Schematic diagram of SIRT1 isoforms. In contrast with SIRT1-v1 other two structural isoforms lack nucleus localisation signal (NLS). Adapted from Zhang *et al.*, 2021 (501).

In current project main focus of the study is SIRT1-v1, therefore in all the rest of manuscript information will be provided referring to SIRT1-v1, which will be simply called SIRT1.

2.2.1 Protein topology

In order to improve the understanding of SIRT1 function and activity, crystal structure have provided insight into substrate and co-factor binding, as well as catalysis (511,512). Human SIRT1 protein consists of 747 amino acids (AA), out of which 277 residues are composing the catalytic core (509,513). SIRT1 catalytic domain contains the canonical sirtuin fold that was firstly described in archaea (SIR2.Af1.NAD⁺) and is composed of two subdomains (513,514). One part is a large NAD⁺-binding subdomain with a Rossmann fold super-secondary structure and a small subdomain consisting of Zn²⁺-binding site and helical module (513) (Fig. 16). Substrate binding results in dramatic changes in interactions between large and small subunits, causing the closure of SIRT1 catalytic domain (Fig. 16A). Additionally, previous findings have shown that N- and C-terminal region plays an important role in SIRT1 activity (515,516). Pan *et al.* demonstrated that conserved catalytic core of SIRT1 protein alone has low catalytic activity, but presence of N- and C-terminal regions improve the protein catalytic activity by 12-45 fold (516). They also concluded that N-terminal domain contributes towards catalytic rate and C-terminal domain mainly contributes to *K_m* (affinity of enzymes for their substrate) for NAD⁺ (516). Furthermore, crystal structure of SIRT1 had revealed that C-terminal regulatory segment (CTR) binding site is located on the lower edge of NAD⁺-binding domain, which complements the β -sheet of the Rossmann fold, leading to inhibition of catalytic properties of the enzyme by blocking NAD⁺-binding site (513,517) (Fig. 16).

It was widely described that SIRT1 has hundreds of substrates, including proteins that play central roles in regulatory mechanism, like histones, FOXOs, p53, NF κ B (518–520). Recently, Hendler *et al.* explored the question of how SIRT1 is able to recognise target acetyl-lysine residues in such a wide variety of different substrates (521). Using the bioinformatic-experimental approach workflow to identify key residues in SIRT1 that are important for its multispecificity. This method allowed to identify key residues on the active site of SIRT1, for example amino acids arginine (Arg446) and leucine (Leu450) in SIRT1 are essential for p53 deacetylation activity (521). In future this approach could also reveal the importance of SIRT1 structural dynamics and furthermore, conformational changes to conduct substrate recognition (521).

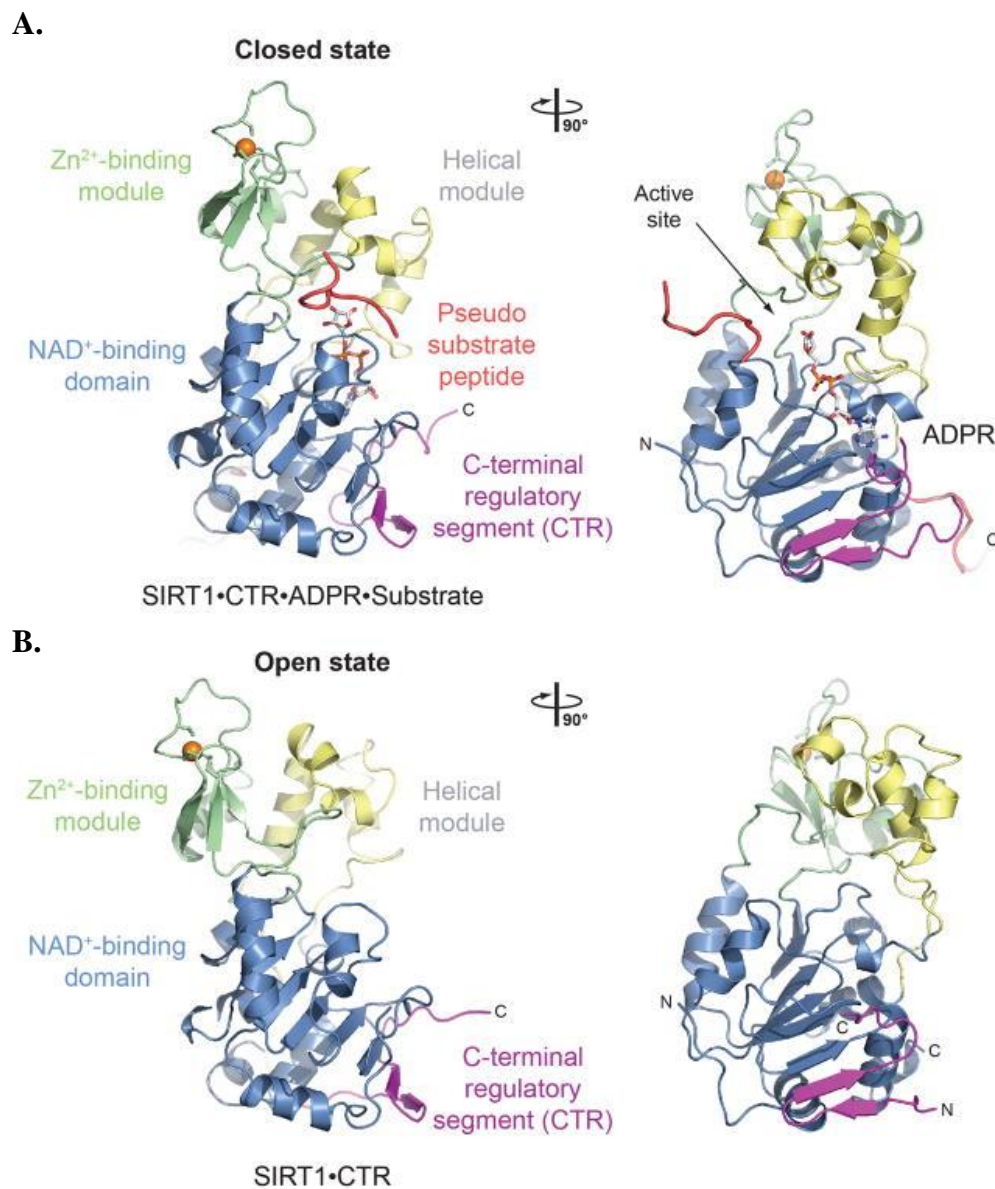


Figure 16. Protein structure of human SIRT1. A. Structure of SIRT1 complex in presence of substrate (closed state); B. Structure of SIRT1 heterodimer with CTR in inactive (open) state. From Davenport *et al.*, 2014 (505).

2.2.2 Expression pattern

The multispecificity of SIRT1 catalytic subunit allows it to act upon various protein in various tissues. In humans, *Sirt1* mRNA was characterised to be expressed in 55 tissue types, with low tissue specificity (Fig. 17). Based on the data provided by the Hyman Protein Atlas, it can be observed that *Sirt1* mRNA has higher expression pattern in adrenal gland, testis and ovary (Fig. 17).

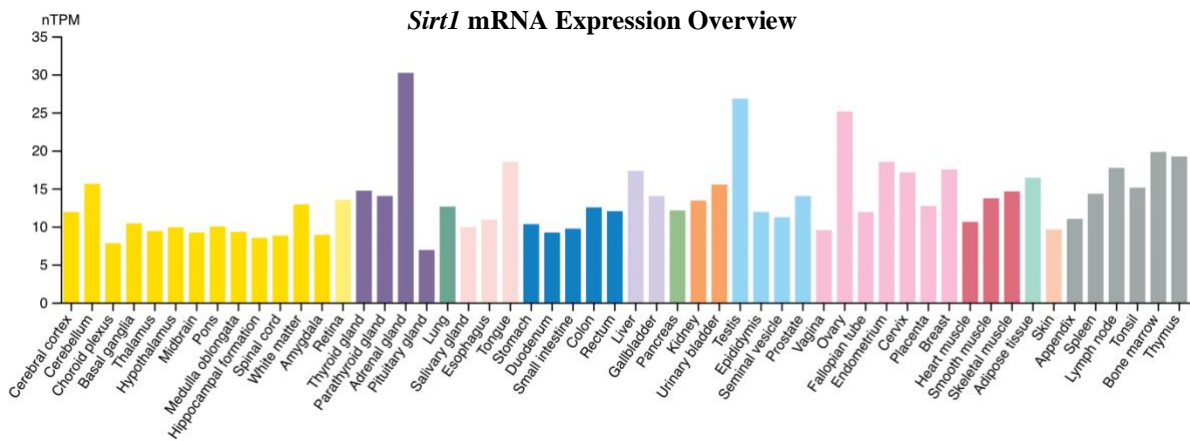


Figure 17. Sirt1 mRNA expression overview. Graph is based on consensus dataset, which consists of normalised expression (normalised protein coding transcripts per million - nTPM) levels for 55 tissue types, created by combining the HPA and GTEx transcriptomics datasets. Data is color-coded that is based on tissue groups, each consisting of tissues with functional features in common. From the Human Protein Atlas (<https://www.proteinatlas.org/ENSG00000096717-SIRT1/tissue>).

On the other hand, protein expression pattern showed that SIRT1 protein is not present in all 44 tissues studied (Fig. 18). SIRT1 was found to be expressed at high level only in adrenal gland, testis, placenta and lymph nodes (Fig.18). It can be remarked that limited amount of *Sirt1* mRNA is translated into the protein under the basal conditions.

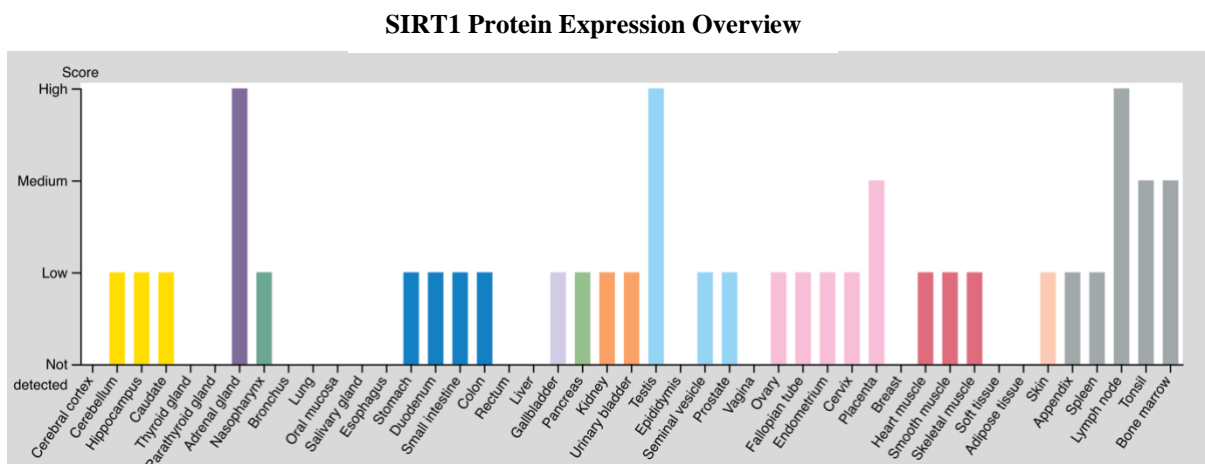


Figure 18. SIRT1 protein expression overview. Graph is based on protein expression data of 44 tissues. Color-coding is based on tissue groups, each consisting of tissues with functional features in common. Mouse-over function shows protein score for analysed cell types in a selected tissue. From the Human Protein Atlas (<https://www.proteinatlas.org/ENSG00000096717-SIRT1/tissue>).

2.3 SIRT1 function

SIRT1 is the most extensively studied member of sirtuin family and it is characterised to be a class III histone deacetylase that can deacetylate histone and also non-histone protein targets (522,523). First, SIRT1 non-histone substrate was identified by Muth *et al.*, who showed that deacetylation of TATA binding protein-associated factor 168 (TAF168), a transcription factor regulating RNA polymerase I complex (RNA Pol I), inhibits its transcriptional initiation *in vitro* (524). SIRT1 multispecificity allows having a wide list of targets, which are implicated in variety of cellular processes.

2.3.1 SIRT1 cellular function

Chromatin structure and gene transcription

Similar to SIR2 in yeast, mammalian SIRT1 facilitates the organisation of heterochromatin structure, which is associated with histone hypoacetylation and leading to gene transcription suppression. In this process the main SIRT1 target is lysine residue at the position 9 (Lys9) or position 26 (Lys26) of H1, position 14 (Lys14) of H3 and position 16 (Lys16) of H4 (522,525,526). The reduced expression level of *Sirt1* in human cells using the RNA interference technique induced the hyperacetylation of both H3K9 and H4K16, confirming histone deacetylase function of SIRT1 (449). Additionally, SIRT1 mediated histone deacetylation has been shown to regulate genome stability, through deacetylation of N-terminus tails of histones (H1K26, H2A.Z, H3K9, H3K56 and H4K16) (428,449,525,526). Furthermore, SIRT1 is known to regulate gene expression not only through chromatin structure modification, but also by regulation of various transcription factors. As was mentioned before, SIRT1-mediated deacetylation of transcription initiation factor TFIID subunit (TAF168), results in the reduction of its DNA binding affinity and leads to suppression of RNA Pol I transcription *in vitro* (524). In 2005, Bouras *et al.* demonstrated that in human embryonic kidney cell line (HEK-293) SIRT1 deacetylates p300 at Lys1020 and Lys1024 residues, resulting in the negative regulation of this histone acetyltransferase (527). Since p300 is an important transcription regulator, its alterations by SIRT1 play an important role in downstream changes in metabolism and cell differentiation (527).

Another example of transcription regulation by SIRT1 is formation of complex with muscle specific transcription factor myoblast determination protein 1 (MyoD), which leads to SIRT1-mediated deacetylation of H3K9ac and H3K14ac in the myogenin and myosin heavy chain

promoters and inhibition of muscle specific gene expression (528). Regulation of muscle differentiation by SIRT1 is also achieved through alteration in MADS box transcription enhancer factor 2 (MEF2) activity. Deacetylation of Lys424 on MEF2 by SIRT1 leads to inhibition of its activity (529). Additionally, it was shown that SIRT1 regulated the activity of FOXO transcription factors and in skeletal muscle cells SIRT1 overexpression deacetylated FOXO3 and blocks the transcription of atrophy-related genes (530).

DNA repair

SIRT1 plays an important role in DNA damage response (DDR) and subsequent protection against DNA damage, as a histone deacetylase at the DNA damage site, as well as protein deacetylase regulating DNA repair and DDR (531–535). In human fibroblasts, it was described that SIRT1 impairs the production of UV-induced 6-4 phosphoprotein and Pt-GG phosphoprotein lesions, which can induce cell apoptosis, by deacetylation of histones and maintaining condensed heterochromatin structure (536). Chromatin modification has been shown to influence temporal and spatial control of DNA damage repair (537). Oberdoerffer *et al.* demonstrated that SIRT1 plays an important role in efficient repair of double-stranded breaks (DSB), by promoting repair through ataxia telangiectasia mutated (ATM) signalling pathway (538). SIRT1 together with enhancer of zeste homologue 2 (EZH2), DNA methyltransferase 1 (DNMT1) and 3B (DNMT3B) are recruited to the site of DSB and inducing hypoacetylated H4K16, H3K9me2/me3, and H3K27me3, result in maintenance of compacted chromatin structure (533). Moreover, SIRT1 is directly related to the DDR and is able to recruit repair proteins to DSB sites and modulate their activity by deacetylating them (539). For example, repair proteins like KU70 and members of FOXO family, were shown to be activated by SIRT1 through the direct deacetylation, in the context of DNA damage (532,540–544).

Cell survival and apoptosis

A second protein that was described as a non-histone target of SIRT1 deacetylase activity was tumour suppressor p53 (545). SIRT1 has been shown to deacetylate a variety of lysine residues of p53 in mice (Lys317, Lys370, Lys379) and humans (Lys320, Lys373, Lys382) (545,546). SIRT1 facilitates the suppression of p53 transactivation activity, thereby leads to apoptosis suppression in the context of DNA damage or oxidative stress (545,547). In addition, SIRT1-

dependent deacetylation of p53 regulated its localisation and in this way controls cell fate decision. In absence of SIRT1, translocation of p53 to the nucleus is decreased, which results in protein accumulation and passage to mitochondria, where it induces the apoptotic pathway (548).

The other regulatory mechanism through which SIRT1 manage cell survival, is by deacetylating a DNA-repair factor KU70, an inhibitor of Bcl-2-associated X protein (BAX)-mediated apoptosis. In response to stress, this mechanism prevent apoptosis triggering in HEK-293 cells (21).

SIRT1 and E2F1, a regulator of cell proliferation and cell cycle, form a negative regulatory loop (549,550). E2F1 induces *Sirt1* expression by direct binding to the promoter region, whereas SIRT1 plays the role as an inhibitor E2F1 apoptotic function (550).

Another type of tumour suppressor, p73, was also described as a target of SIRT1 deacetylation. Similar to p53, deacetylated p73 loses its transcriptional activity and results in apoptosis inhibition (551,552).

SIRT1 is able to improve cell survival by regulating FOXO transcription factors. Three FOXO proteins (FOXO1, FOXO3A and FOXO4) has been shown to undergo SIRT1-mediated deacetylation upon binding to LXXLL motif (in FOXO1) (553–556). SIRT1 reduces apoptosis by affecting function of FOXO3A in neurons and fibroblasts (542,557,558).

Autophagy

In response to environmental stress, like nutrient deficiency, cells induce autophagy, as a protection mechanism (559,560). During the starvation, SIRT1 level and activity is increased leading to deacetylation of autophagy proteins and subsequent induction of the autophagy process (21,561,562). SIRT1 targets are autophagy proteins (Atg) 7 and 8, which were found to be deacetylated *in vitro*. Targeting *Sirt1* gene expression or cell treatment with SIRT1 inhibitors, showed a remarkable increase in Atg7 acetylation (561). Moreover, deacetylation of microtubule-associated protein 1A/1B-light chain 3 (LC3) at Lys49 and Lys51 residue by SIRT1 was found to initiate the process of autophagy under starvation (563).

Ion channel regulation

SIRT1 was also found to regulate ion channels. In the heart, it was found that SIRT1 deacetylation of voltage-gated cardiac Na⁺ channel (Nav1.5) at Lys1479 position, serves an essential function in regulating Na⁺ current and overall cardiac electrical activity (564). SIRT1 deficiency in cardiac myocytes has been shown to impair the regulation of intracellular Ca²⁺ and Na⁺, therefore inducing cardiac dysfunction and arrhythmogenesis (565). In addition, it was demonstrated, in mouse model of anxiety and stress, that in dentate gyrus (DG), part of hippocampal formation, SIRT1-mediated deacetylation of large conductance calcium-activated potassium (BK) channel results in rapid modulation of DG function during maladaptive stress response (566).

Inflammation

It was widely described in the literature that SIRT1 possesses strong anti-inflammatory effects, by inhibiting expression of factors involved in inflammation. In the acute inflammatory response like sepsis, SIRT1 was shown to deacetylate H3K16 in the promoter region of cytokines IL-1 and TNF- α , suppressing their expression (567,568). Furthermore, SIRT1 is able to reduce histone acetylation of IL-6 promoter region, subsequently by reducing its expression level (569).

NF κ B signalling plays one of the central roles in inflammation and is a widely studied pathway. It is composed of NF κ B1, NF κ B2, p65, RELB proto-oncogene and c-REL proto-oncogene (570). In an inactive state, NF κ B is a part of cytoplasmic complex, bound by a member of inhibitor of B (IB) family. During the inflammatory response, IB kinase (IKK) phosphorylates IB and targets it for degradation. Free NF κ B is translocated into nucleus and initiate inflammatory response gene transcription (571). SIRT1 directly inhibits NF κ B-mediated inflammatory response by deacetylating p65 subunit of NF κ B complex and suppressing its DNA binding ability (520,572–574). Subsequent studies confirmed that SIRT1 suppress NF κ B activity through reduction of p65 acetylation at Lys310 residue and by accelerating its ubiquitination and degradation (575,576). Additionally, SIRT1 is able to inhibit degradation of IB, therefore maintaining NF κ B in an inactive state (577). Indirectly, SIRT1 negatively modulates NF κ B activity through positive regulation of AMPK (578). Overexpression of

SIRT1 can result in establishment of interactions between peroxisome proliferator-activated receptor (PPAR) and p65, inhibiting NF κ B-mediated cytokine production (579).

Moreover, HIF-1 α is known as an important transcription factor involved in inflammatory response and oxidative stress. Indeed, it has been reported for the first time, that SIRT1 deacetylase activity directly regulates acetylation status of Lys374 residue on HIF-1 α protein. This posttranslational modification results in failed recruitment of p300 and inactivation of HIF-1 α (580,581).

Finally, activator protein 1 (AP-1) a transcription factor is a regulator of inflammation and immunity, formed by c-Jun and c-Fos. Upon activation, AP-1 promotes transcription of inflammatory factors like IL-2, IL-8 and TNF- α (582). SIRT1 is able to impair AP-1 transcriptional activity through direct deacetylation of C-terminus of c-Jun (583,584).

2.3.2 SIRT1 function in metabolic tissue

Extensive amount of research articles described importance of SIRT1 in metabolic organs, its role in an insulin production and sensitivity, FA metabolism (585). In this context, we have recently published a revue describing the role of SIRT1 in these metabolic organs and their crosstalk impacting bone homeostasis (586).

2.3.2i SIRT1 function in metabolic tissue - Pancreas

In pancreatic β -islets, SIRT1 overexpression studies demonstrated raise of insulin secretion (587). Furthermore, β -cells specific SIRT1 knockout models displayed reduced glucose stimulated insulin secretion, suggesting that this protein is required for efficient function of the cells (588). SIRT1 knockout mice exhibited high levels of UCP2 in the mitochondria of β -cells. In this tissue, UCP2 suppresses the production of ATP in response to high glucose (589). This changes the ATP/ADP gradient and leads to block of insulin granule secretion. Bordone *et al.* demonstrated that in the nucleus of INS-1 cell line, SIRT1 binds directly the UCP2 promoter region and suppresses its expression (Fig. 19). The decreased expression of UCP2 is followed by an increases in ATP/ADP gradient and stimulation of insulin secretion mechanism (590). Along with UCP2 suppression, SIRT1 regulates a variety of genes involved in insulin

expression and glucose uptake. SIRT1 is able to activate the expression of insulin gene *via* regulation of its transcription factors. FOXO1 was found to suppress MAF BZIP transcription factor A (MAfA) and neurogenic differentiation factor (NeuroD) transcription factors, which induce transcription of insulin gene. SIRT1-mediated deacetylation of FOXO1 and its subsequent suppression results in increased production of MAfA and NeuroD, and induction of insulin production (591) (Fig.19). Also, activation of SIRT1 by resveratrol showed an upregulation of pancreas/duodenum homeobox protein 1 (PDX1), which plays a critical role in insulin gene expression, as well as GLUT1/2 expression, facilitating glucose uptake (592). A potential mechanism of PDX1 enhancement by SIRT1, is through SIRT1 deacetylation and activation of forkhead transcription factor FOXA2, which is necessary for activation of PDX1 transcription in β -cells (593). It is well characterised that SIRT1 expression is upregulated in pancreas during the CR (594). Recent study about CR effect on β -cell function in mouse model demonstrated an increased insulin secretion, confirming positive effect of CR on body metabolism (595). This effect of CR might be explained by upregulation of SIRT1 expression; however, the direct connection is not established.

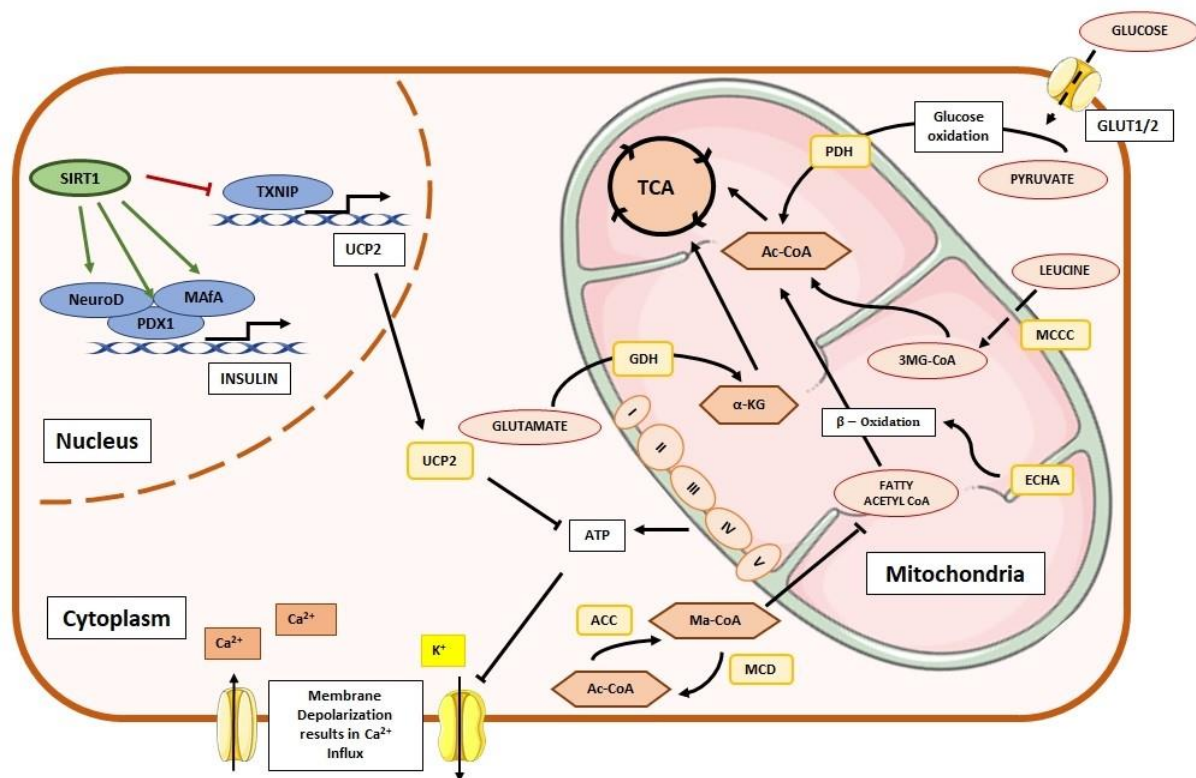


Figure 19. Summary of SIRT1 function in pancreatic β -cells. Diagram shows the insulin secretion mechanism in β -cells and how SIRT1 is involved in regulation of this process.

Components of the diagram were taken from <https://smart.servier.com/>.

Sirtuin types 1 (SIRT1); pancreatic and duodenal homeobox 1 (PDX1); glucose transporter 2 (GLUT2); thioredoxin interacting protein (TXNIP); uncoupling protein 2 (UCP2); neurogenic differentiation (NeuroD); MAF BZIP transcription factor A (MAF A); pyruvate dehydrogenase (PDH); acetyl-CoA (Ac-CoA); glutamate dehydrogenase (GDH); α -ketoglutarate (α -KG); adenosine triphosphate (ATP); acetyl CoA carboxylase (ACC); malonyl-CoA decarboxylase (MCD); enoyl-CoA hydratase (ECHA); 3-methylglutaconyl-CoA (MG-CoA); methylcrotonoyl-CoA carboxylase (MCCC); tricarboxylic acid cycle (TCA).

2.3.2ii SIRT1 function in metabolic tissue - Liver

The main player in regulation of glucose metabolism in liver is SIRT1. In mouse model, liver specific deletion of SIRT1 results in hyperglycaemia and development of insulin resistance in hepatocytes (596). The micro-RNA miR-181a mediated decrease in SIRT1 activity results in hepatic insulin resistance, and suppression of miR-181a cause an improvement of insulin sensitivity in these cells (597). Various animal studies of hepatic SIRT1 activation reported a positive effect on insulin sensitivity and protection from insulin resistance in response to high caloric diet (598–602). Activation of SIRT1 by metformin or resveratrol in human hepatocyte cell line (HepG2), contributed towards improvement of insulin resistance (603–605). Additionally, study on human embryonic cell line (HEK293) demonstrated an interaction

between SIRT1 and PI3K protein in insulin signalling pathway, through this SIRT1 positively modulates insulin signalling (606). All these data demonstrate that SIRT1 have beneficial effects on insulin sensitivity in hepatic cells.

Additionally, sirtuin family member play important role in regulation of glucose homeostasis in liver under different nutrition conditions (607). CR has been shown to stimulate the expression and activity of SIRT1 in various mammalian tissues, such as liver and white adipose tissue (21,594). This can be explained by the increased NAD^+/NADH ration in cytoplasm and mitochondria of cells upon fasting (608). On the early stages of CR or nutrient deficiency, the increased SIRT1 level results in a decreased PGC-1 acetylation *via* direct protein interactions. This result in transcriptional upregulation of gluconeogenic genes like FOXO1 and hepatic nuclear factor 4 (HNF4), that enhance *de novo* glucose synthesis by hepatocytes (609–611) (Fig. 20). Also, SIRT1 deacetylates the lysine residue on the DNA binding domain of FOXO1 gene, resulting in an increase of its DNA binding ability (558,612,613). The rise of FOXO1 protein activity on early stages of fasting, leads to binding of this transcription factor to the promoter region of several gluconeogenic genes, by this promoting their expression and improve hepatic glucose output (614–617). Another mechanism associated with induction of gluconeogenesis by SIRT1 is suppression of STAT3 (Fig. 20). In normal nutrition condition STAT3 plays a role in downregulation of glucose production in liver, however on early stages of caloric deprivation, the deacetylation of STAT3 protein by SIRT1 induced its inactivation, causing an increase in gluconeogenesis (618).

During the extension of CR time, SIRT1 changes its mode of action. SIRT1 deacetylates and deactivates CREB regulated transcription regulator 2 (CRTC2) protein (Fig. 20). Under normal conditions, glucagon signalling induces the dephosphorylation and nuclear translocation of CRTC2, where it upregulated gluconeogenic gene expression (619). Therefore, during extended nutrient insufficiency, SIRT1 downregulates gluconeogenesis. Another mechanism of SIRT1 action is through deacetylating factors like target of rapamycin complex 2 (TORC2) and CREB binding protein (CBP), which are involved in regulation of key gluconeogenesis promoter cAMP response element binding protein (CREBP) (619). The SIRT1 deacetylation cause an indirect decrease in CREB protein expression (Fig. 20). However, SIRT1 is able to bind CREB directly and deacetylates the Lys136 residue, deactivating the protein (620). CREB functions as a transcription factor for phosphoenolpyruvate carboxykinase (PEPCK1), downregulation of CREB function causes a decrease in PEPCK1 transcription and subsequent

reduction of hepatic gluconeogenesis (621). Also, SIRT1 is able to suppress PEPCK1 function by deacetylating and downregulating FOXO3 (557).

SIRT1 is strongly associated with FAO in liver. Multiple knockout studies showed that the absence of liver specific SIRT1 causes the development of hepatic steatosis, characterised by fat accumulation in liver (596,611,622). During the CR, SIRT1 upregulates the FAO in hepatocytes by deacetylation and subsequent activation of PGC-1 α and PPAR α . The nuclear protein PPAR α upregulates the expression of proteins, which are involved in fatty acid β -oxidation (622,623). Additionally, SIRT1 is involved in cholesterol homeostasis. This function of SIRT1 is achieved by downregulation of lipogenic gene like sterol-regulatory element binding protein 1c (SREBP-1c) (624,625). SIRT1 was found to bind and deacetylate other isoforms of SEBP protein, targeting these proteins for degradation and subsequently reducing the hepatic lipogenesis and fat storage (626,627). It was established that SIRT1 is able to upregulate genes involved in lipolysis, by deacetylating and upregulating liver X receptor (LXR) (628). LXRs are ligand activated transcription factors that are involved in upregulation of fatty acid metabolism genes, as well as cholesterol metabolism (629). In the SIRT1 knockout mice, the levels of the cholesterol in liver were elevated, demonstrating the importance of SIRT1 in cholesterol homeostasis (627,630). The reactivation of SIRT1/AMPK pathway in liver exposed to high fat diet (HFD), results in protection from lipid dysregulation and further development of non-alcoholic fatty liver disease (NAFLD) (631).

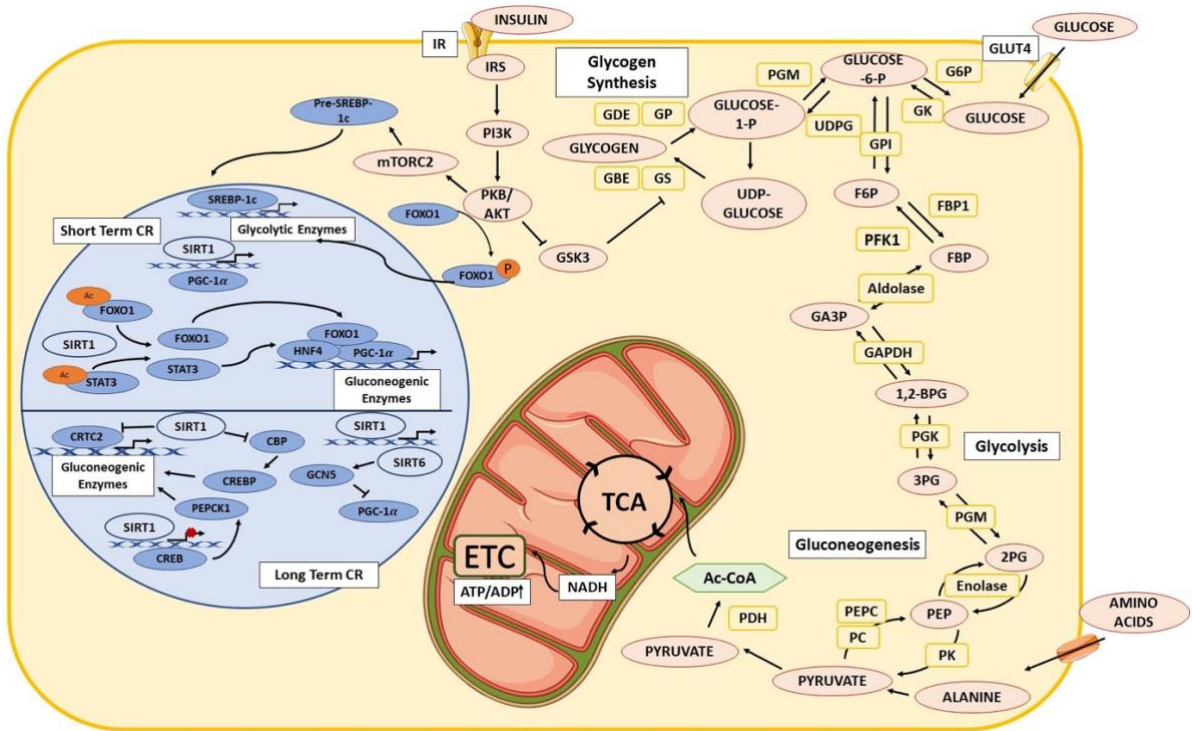


Figure 20. Summary of glucose homeostasis in hepatocytes and involvement of SIRT1 this process. Diagram resembles insulin signalling pathway, glycogen synthesis, as well as gluconeogenesis and glycolysis in liver hepatic cells. Additionally, SIRT1 function in cell nucleus is shown during short term and long-term CR.

Components of the diagram were taken from <https://smart.servier.com/>.

Sirtuin type 1 (SIRT1); forkhead box O1 (FOXO1); signal transducer and activator of transcription 3 (STAT3); hepatic nuclear factor 4 (HNF4); PPAR γ coactivator 1 α (PGC-1 α); sterol-regulatory element binding protein 1c (SREBP-1c); CREB regulated transcription regulator 2 (CRTC2); CREB binding protein (CBP); cAMP response element binding protein (CREB/CREBP); general control non-depressible 5 (GCN5); rapamycin complex 2 (mTORC2); protein kinase B (PKB/AKT); insulin receptor (IR); insulin receptor substrate (IRS); phosphatidylinositol 3-kinase (PI3K); glycogen synthase kinase 3 (GSK3); glycogen branching enzyme (GBE); glycogen synthase (GS); glycogen debranching enzyme (GDE); P-glycoprotein (GP); phosphoglucomutase (PGM); uridine diphosphate glucose (UDPG); glycosylphosphatidylinositol (GPI); glycerol kinase (GK); glucose-6-phosphate dehydrogenase (G6P); 6-O-phosphono-beta-D-fructofuranose (F6P); phosphofructokinase-1 (PFK1); fructose 1,6-bisphosphate (FBP); glyceraldehyde 3-phosphate (GA3P); glyceraldehyde-3-phosphate dehydrogenase (GAPDH); 2,3-bisphosphoglyceric acid (1,2-BPG); phosphoglycerate kinase (PGK); 3-Phosphoglyceric acid (3PG); phosphoglycerate mutase (PGM); 2-phosphoglyceric acid (2PG); phosphoenolpyruvate (PEP); pyruvate kinase (PK); phosphoenolpyruvate carboxylase (PEPC); pyruvate carboxylase (PC); pyruvate dehydrogenase (PDH); acetyl-CoA (Ac-CoA); tricarboxylic acid cycle (TCA); electron transport chain (ETC);

2.3.2iii SIRT1 function in metabolic tissue - Adipose tissue

In WAT, SIRT1 is involved in various stages of its differentiation, adipogenesis, metabolism and endocrine activity. The main regulator of adipose tissue differentiation is PPAR γ (632). The knockout of AT specific SIRT1 was associated with enhanced PPAR γ activity in these cells (633). Multiple studies demonstrated that SIRT1 upregulation in WAT, results in PPAR γ suppression and subsequent inhibition of adipogenesis (634). Additionally, it was established that SIRT1 deacetylates PPAR γ at Lys268 and Lys293 residues, by this inhibiting its transcription factor activity (634,635). Moreover, it was shown that SIRT1 binds to PPAR γ co-factor, nuclear receptor co-repressor (NCoR) and facilitate the suppression of PPAR γ expression (636). SIRT1 mediated suppression of PPAR γ , not only affect the adipose differentiation, but also FA transport. Through downstream regulation of fatty-acid-binding protein (aP2), SIRT1 facilitates reduction of fat storage during the CR (634,637,638). In the process of DNL, enzyme ACLY serves an important role in the first step of FA production. It is known that ACLY is acetylated and activated in response to glucose uptake (639). SIRT1 induced deacetylation of ACLY results in decrease of its activity (463). SIRT1 plays a role in regulation of adiponectin secretion. With low nutrient availability in 3T3-L1 cell line, SIRT1 levels rise and suppress PPAR γ expression. This cause decrease in downstream gene transcription like ER oxidoreductin 1 like protein (Ero1-L), which is important for ER function and protein folding (640). The result of these events is impaired production of adiponectin (641). Despite this, another study by Qiao *et al.*, showed that SIRT1 activates adiponectin gene transcription through enhancing FOXO1 and C/EBP- binding to adiponectin gene promoter region and facilitates its expression (642).

The activation of BAT gene expression in pre adipocytes, it is a novel approach in reversing the obesity and its consequences (643–645). In the differentiation of BAT, SIRT1 plays an important role as a transcriptional mediator. SIRT1 not only functions as transcription regulator of PPAR γ , but also as PPAR γ deacetylase at Lys293 and Lys268 residues. This results in deactivation of the PPAR γ , as well as recruitment of PR domain containing 16 (Prdm16), which induces transcription of BAT genes and results in AT browning (635). In 3T3-L1 preadipocyte cell line, silencing of SIRT1 cause upregulation of WAT specific genes (pantothenate kinase 3 (Pank3), angiotensinogen (Agt)) and inflammatory markers, at the expense of BAT marker genes (Prdm16) (646). Overall, SIRT1 has been shown to induce beiging of AT.

2.3.3 SIRT1 function in bone marrow

Within BM niche, studies on SIRT1 conclude its role in HSC maturation and differentiation. The *Sirt1* gene knockdown in haematopoietic system was shown to cause significant decline in lymphoid compartment, aberrant HSC expansion, genomic instability and anaemia (647–649). Activators of SIRT1, resveratrol and SRT3025, have been shown to alter a number of HSCs and modulate its deacetylase capacity *in vivo* and *in vitro* (650,651). However, recently Park *et al.* showed that BM specific (osteoblast) deletion of *Sirt1* did not alter blood cell production, nor lineage distribution or HSC maturation (652). These findings suggest that SIRT1 does not play a crucial role in haematopoietic niche of BM. Furthermore, SIRT1 role in HSC ageing was poorly described. Wang *et al.* demonstrated that *Sirt1* knockout suppressed gene activation in ageing HSCs, predominantly it affected genes involved in regulation of protein synthesis and metabolism. They showed that SIRT1 inhibition leads to suppression of growth and survival of human B/myeloid mixed phenotype acute leukaemia (653). Overall, these results propose that SIRT1 might be a potential therapeutic target for modulating activity of HSCs in the process of ageing.

Currently, some studies are focusing on understanding the relationship between sirtuin family and BMAT function, especially BMAT expansion during the CR. The SIRT1 was shown to play a role in BMSCs differentiation capacity (654). *In vitro* studies on murine pluripotent mesenchymal cell line (C3H10T1/2) and human mesenchymal stem cells (hMSCs) from bone marrow, demonstrated that SIRT1 pharmacological activation downregulated adipogenic differentiation (655–657). BMSCs containing SIRT1 deletion exhibited defect in self-renewal capacity, as well as reduction of osteoblast differentiation, without affecting adipogenic differentiation (658). Moreover, recently it was confirmed that during severe long-term CR, the SIRT1 expression level in BMSCs decreases. Reduction in SIRT1 potentially leads to BMAT expansion, through BMSCs preferential differentiation into adipocytes (2). This study suggests that SIRT1 can be able to downregulate BMAT expansion during long term CR.

It is also reported that thermogenic genes are dependent on SIRT1 expression. Indeed, SIRT1 haplo-insufficiency in mice resulted in decreased expression of thermogenic genes in tibial BMAT, like 3AR, Prdm16 or PGC-1. Additionally, overexpression of SIRT1 in CH310T1/2 cell line, resulted in increased expression of Prdm16 or PGC-1, characteristic of BAT (654).

2.4 SIRT1 regulation of expression and activity

Highly diverse role of SIRT1 activity in various cellular and metabolic processes is modulated in response to environmental stimuli (cell stress, CR, overnutrition, etc.) through transcription, translation and post-translational regulation (659–662).

In the context of cellular stress, it was described that the cysteine residues of SIRT1 are susceptible to oxidation under oxidative stress, which could impact SIRT1 activity and SIRT1 degradation in the proteasomes (663–666). During the inflammatory response, SIRT1 inhibits NF κ B signalling and lowers inflammation, but when the exposure to high levels of H₂O₂ or harsh oxidative stress is prolonged, it reduces *Sirt1* expression and protein function (667,668). In WAT, liver and skeletal muscles of mice, Cai *et al.* discovered that prolonged oral administration of pro-oxidative advanced glycation end-products (AGE) significantly lowered SIRT1 protein levels (666). This alteration was linked to increased adiposity and insulin resistance, both of which are common hallmarks of type 2 diabetes. Additionally, both oxidative and aldehyde stress could enhance carbonylation and alkylation of SIRT1 cysteine groups, causing SIRT1 protein breakdown in the proteasomes of metabolic tissue (664). Caito *et al.* described that in the context of redox state, SIRT1 protein loss takes place (664,669). Furthermore, oxidative stress can lower NAD⁺ levels and consequently impede SIRT1 activity (663). These findings show that the SIRT1 enzyme may be a target of oxidative changes and become inhibited under oxidative stress.

Excessive formation of oxidants, development of cellular stress and reduction of NAD⁺/NADH ratio, can be attributed to high nutrient consumption during metabolic conditions like obesity (670–673). Overload of nutrients is broken down through glycolysis and further TCA cycle, leading to NAD⁺ oxidation to NADH, contributing to elevated NADH in cytosol (674). This leads to reduction in SIRT1 activity (675). In the same time the overproduction of NADH and its passages through mitochondrial oxidative phosphorylation (OXPHOS) complexes, results in electron leakage and elevated ROS production, facilitating development of oxidized state in the surrounding environment. As it was mentioned above, oxidative stress negatively affects *Sirt1* gene expression and SIRT1 protein posttranslational modifications (676). In mice, Noriega *et al.* showed that negative control of *Sirt1* transcription is achieved through activation of carbohydrate ChREBP that binds *Sirt1* promoter site (677–679). Decrease in *Sirt1* gene expression during nutrient overconsumption was observed in various metabolic

tissue, like pancreas islets, β -cells, liver and adipose tissue (680–682). These mechanistic disruptions have been linked to a variety of metabolic disorders, including insulin resistance together with type 2 diabetes, and non-alcoholic fatty liver disease (683–686).

In reverse, nutrient deprivation or exposure to CR has been shown to have a positive impact on SIRT1 activity and *Sirt1* gene expression. Guarente *et al.* postulated that the metabolic change from fermentation to respiration in *Saccharomyces cerevisiae*, which occurs in response to CR, resulted in higher NAD⁺ intracellular levels, which in turn increases Sir2 activity (687) (Fig. 21). The increased respiratory activity would reduce NADH, which acts as a competitive inhibitor of Sir2 deacetylase activity (675,688). Alternatively, Sinclair *et al.* hypothesised that CR boosts Sir2 activity by reducing intracellular amounts of nicotinamide (NAM), a by-product of the Sir2-catalyzed deacetylation process, which suppresses Sir2 deacetylase activity (689). The decrease in nicotinamide concentration would be caused by an increase in PNC1 (pyrazinamidase and nicotinamidase 1) levels, a nicotinamidase enzyme that catalyses the first reaction leading to NAD⁺ regeneration from NAM (690). A similar mechanism of CR-mediated SIRT1 regulation can be observed in higher eukaryotes, where nicotinamide phosphoribosyltransferase (NAMPT) enzyme is responsible for NAD⁺ resynthesis from NAM (691–693) (Fig. 21). Numerous studies have provided evidence of NAMPT importance in regulation of NAD⁺ levels and SIRT1 function in mammalian (pancreatic β -cells, myoblasts, fibroblast) (694–696).

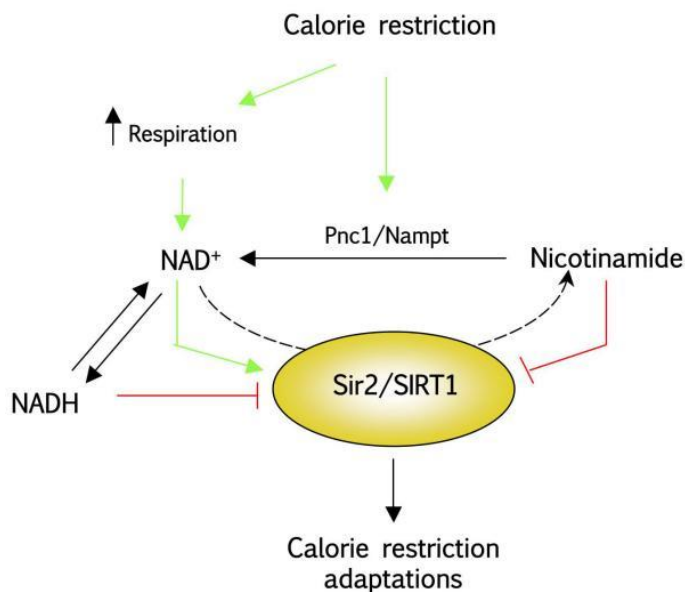


Figure 21. Potential mechanisms of CR-mediated regulation of SIRT1 activity. CR is able to positively regulate SIRT1 activity through increasing respiration and NAMPT activity, therefore increasing NAD⁺/NADH ratio. From Canto *et al.*, 2009 (592).

2.4.1 Transcriptional regulation of SIRT1

Transcription of *Sirt1* gene is regulated both by epigenetic modifications, and a wide range of transcription factors.

DNA methylation of CpG islands in gene promoter region by DNA methyltransferase (DNMT) has a negative correlation with this gene transcription (697). In various disease, it was found that reduction in *Sirt1* expression is associated with DNA hypermethylation. In oral epithelial cells extracted from oral cancer patients, *Sirt1* was found to be hypermethylated and downregulated in response to arecoline exposure (698). In hearts of gestational diabetes rat model, *Sirt1* expression level was shown to be significantly reduced comparing to control animals (699). *In vitro* study on suppression of DNMT3A by the DNA methylation inhibitor 5-azacytidine (5-AZA) resulted in an increase in SIRT1 protein, suggesting that transcription of *Sirt1* was affected by DNMT3A (699).

Voelter-Mahlknecht *et al.* back in 2006, isolated, cloned and characterised human *Sirt1* gene, concluding that promoter region of this gene contains NFκB binding site (700). Later, Zhang *et al.* conducted the study where they demonstrated that overexpression of NFκB p65 subunit, results in upregulation of *Sirt1* gene expression and SIRT1 protein level (701). Using electrophoretic mobility shift assay, Katto *et al.* confirmed direct binding of NFκB to the *Sirt1* promoter region (702). In the process of inflammation, activation of NFκB and its subunits has been shown to directly bind and promote *Sirt1* gene expression, which in return will initiate negative regulation of NFκB activity through its deacetylation (701,702). In overnutrition context, it is demonstrated that PPARγ can inhibit *Sirt1* expression through binding to PPAR response element and recruitment of SIRT1 to this site could facilitate its autoregulation (703,704). Furthermore, p53 was also found to have a reciprocal regulation with SIRT1 (704). In the nucleus, p53 binds directly to two response elements within the promoter region of *Sirt1* and facilitate its suppression (705). The knockout of p53 (*Trp53*) in mice resulted in increased level of SIRT1 in several tissue types and in tumour cell line suppression of p53 induced overexpression of *Sirt1* gene (704,706).

Another tumour suppressor that was identified to negatively control *Sirt1* expression was hypermethylated in cancer 1 (HIC1). Together with C-terminal binding protein 1 (CTBP1), HIC1 form a co-repressor complex, which binds and upstream enhancer element of *Sirt1* gene

promoter and facilitates the suppression of the transcription (707,708). HIC1 serves an important function as tumour suppressor. In the process of cell ageing, hypermethylation of HIC1 promoter induces the suppression of its expression. However, decrease in HIC1, removes SIRT1 repression and further leads to promotion of tumour gene expression (708–710). In prostate cancer mouse models, as well as patients, HIC1 reduction results in a significant upregulation of *Sirt1* during tumorigenesis (711). In the hypoxic condition, the initiation of HIC1/CTPB1 complex results in binding to *Sirt1* promoter and gene repression (580,712). However, hypoxia was also described to upregulate *Sirt1* expression through HIF-1 α binding to HER5 response element (713).

Furthermore, transcriptional regulation of *Sirt1* is achieved through another negative feedback loop. It was described that DNA damage by cancer drug etoposide results in E2F1-dependent induction of *Sirt1* gene expression (550,714). On the other hand, SIRT1 is able to deacetylate E2F1 and inhibit its activity, forming a feedback loop between these two proteins. Due to the fact that E2F1 is an activator of apoptotic genes like *Tp53* or *Tp73*, the activation of *Sirt1* transcription and negative feedback loop initiation might be a protective mechanism against the aberrant apoptosis in response to DNA damage.

Both p53 and FOXO3a share the same binding site on the promoter region of *Sirt1* gene, therefore similarly to p53, FOXO3a can regulate *Sirt1* transcription (704). It was described that acute nutritional stress resulted in FOXO3a nuclear translocation, where it binds p53, dissociates an inhibitory complex and restores *Sirt1* expression (704). In the same time SIRT1-mediated deacetylation of FOXO3a enabling its function in various biological processes (557,715).

Also, SIRT1 - c-myc have established a negative feedback loop, which is involved in multiple biological processes. Binding to *Sirt1* promoter allows c-myc to induce *Sirt1* expression. In return, SIRT1 deacetylase activity is able to destabilise c-myc protein and reduce its enhancer activity (716).

In liver, age-dependent downregulation of *Sirt1* is described to be maintained through C/EBP-HDAC1 complex (717). On the other hand, during adipogenesis C/EBP induced expression of *Sirt1* through c/EBP binding site on the *Sirt1* promoter (718).

2.4.2 Post-transcriptional regulation of SIRT1

Additional to transcriptional regulation, SIRT1 is tightly regulated at post-transcriptional level. Therefore, following gene transcription, SIRT1 is regulated through alterations in mRNA stability. Human antigen R (HUR) protein is a tumour suppressor and regulates the gene transcription through targeting of mRNA. HUR binds 3' untranslated region (UTR) of *Sirt1* mRNA and by this improves its stability (719). In the process of cell ageing and cell senescence, HUR level was shown to be reduced, which correlates with a decrease in SIRT1 production. Abdelmohsen *et al.* reported that in senescing cells, HUR phosphorylation by checkpoint kinase 2 (CHK2) disrupts the interaction between HUR and *Sirt1* mRNA, resulting in decreased SIRT1 protein level (719).

Non-coding RNAs

Post-transcriptional regulation of SIRT1 is achieved through numerous types of non-coding RNAs (ncRNAs), in particular by microRNAs (miRNAs). miRNAs bind to the 3'UTR of a target mRNA, causing transcriptional repression of the gene or targeting the mRNA for degradation (720). Wide range of miRNAs were described to target SIRT1 protein expression – miR-34, miR-143, miR-9, miR-132, miR-217 (721). Most well described miRNA, which regulates SIRT1, is miR-34a (722). It binds 3'UTR of *Sirt1* mRNA and suppresses transcription without targeting mRNA for degradation. miR-34a transcription is directly promoted by p53, resulting in a formation of feedback loop between miR-34a, SIRT1 and p53 (722) (Fig. 22). As it was described above, p53 inhibits *Sirt1* gene transcription by binding directly to the promoter region. At the same time, p53 promotes miR-34a expression, that will repress *Sirt1* mRNA. In return, SIRT1 was shown to deacetylate p53 protein and reduce its activity, as well as repress miR-34a expression through a direct binding to its promoter (704,723–725).

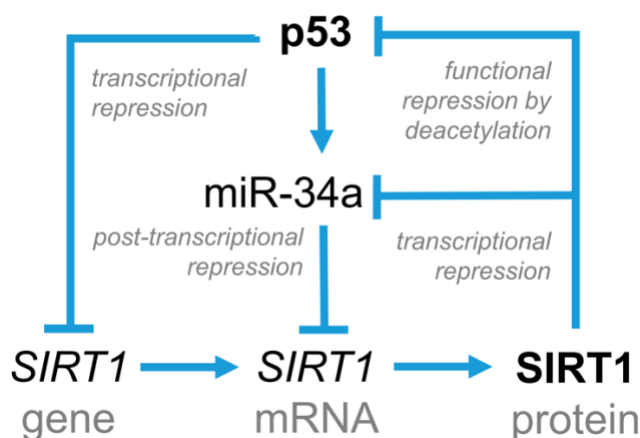


Figure 22. Summary diagram of the miR-34a/p53/SIRT1 regulatory loop. p53 promotes expression of miR-34a, which targets SIRT1 mRNA and blocks its translation. Also, p53 binds to the promoter of the *Sirt1* gene and suppresses its transcription. In turn, SIRT1 deacetylates p53, repressing its activity, and inhibits expression of miR-34a. From Buler *et al.*, 2016 (655).

Furthermore, miR-34a is not only able to suppress *Sirt1* transcription, but also SIRT1 activity. NAMPT, an enzyme involved in the NAD⁺ salvaging pathway, was found to be suppressed by miR-34a (726). An increase in miR-34a production results in a decrease in intracellular level of NAD⁺ and subsequently reduces the activity of SIRT1 (726,727).

In addition, long ncRNAs (lncRNAs) can regulate *Sirt1* translation (728–731). Wang *et al.* described that antisense (AS) lncRNA consists of *Sirt1* mRNA complementary sequence, which allows it to compete with miR-34a for binding to 3' region of *Sirt1* and suppression of its further translation (732). On the other hand, Li *et al.* recently demonstrated that a complex of SIRT1-AS-lncRNA can bind *Sirt1* mRNA and facilitate its stability, promoting SIRT1 translation (733).

NAD⁺ levels and small molecules

Catalytic activity of SIRT1 depends upon the availability of NAD⁺, therefore SIRT1 activity is increased in the conditions when intracellular level of NAD⁺ is high (fasting or caloric restriction, exercise or late acute inflammation) (734–736). Conditions like obesity, ageing or early acute inflammation are associated with low NAD⁺/NADH ratio, which was found to cause significant decrease in SIRT1-mediated deacetylation (735–738). DNA repair enzyme poly ADP-ribose polymerase (PARP) mediates poly-ADP-ribosylation of proteins with the consumption of NAD⁺. PARP1 is recruited to DNA damage site and binds DNA break, this event is followed by recruitment of NAD⁺-dependent ADP ribose unit, and related enzymes that are required for DNA damage repair (739). Bai *et al.* showed that in BAT and muscle cells, depletion or inhibition of PARP1 is associated with SIRT1 activity increase, both *in vitro* and

in vivo (740). Therefore, it might be concluded that PARP1 mediated consumption of NAD⁺, can play a role in regulation of SIRT1 activity.

Discovery of small molecules that are able to modulate SIRT1 activity, allowed to conduct various studies on mimicking physiological alterations of SIRT1. Inhibition of SIRT1 protein can be achieved through exposure to splitomicin, sirtinol, NAM, MC2141 or EX-527, as well as other analogues of sirtinol (741–744). NAM was described to bind SIRT1 C-pocket and reverse the primary catalytic step (745,746). In opposition, plant-derived metabolites, for example stilbenes, flavones and anthocyanidins were found to allosterically bind and lead to activation of SIRT1 *in vitro* (747). Additionally, resveratrol, SRT1720 and STT2183 were shown to have an activating effect of SIRT1 (602,747–749). Resveratrol was characterised as the most potent natural activator of SIRT1 deacetylase (750,751). Indeed, it was recently demonstrated, that *Sirt1* down-regulation in BMSCs achieved through sirtinol treatment, can be reversed by resveratrol, and it further leads to a decrease in adipogenesis and increase in osteogenesis (2).

Protein-protein interactions

Devenport *et al.* aimed to shed light on regulation of SIRT1 activity, through the study of crystal structure of SIRT1 in complex with CTR. They established an inhibitory role of the CTR, in the closed SIRT1.CTR.ADPR. structure, through influencing the conformational changes in SIRT1 protein, that are required for substrate turnover (Fig. 16) (513). A number of proteins were identified to bind directly to SIRT1 and modulate its stability and activity. Multiprotein complex with cyclic adenosine monophosphate (cAMP) was reported to boost the stability and deacetylase activity of SIRT1 (752). Active regulator of SIRT1 (AROS), positively regulates SIRT1 activity through direct binding to a site distal of SIRT1 catalytic domain (753,754). Kim *et al.* confirmed the interaction between AROS and SIRT1, leading to an improved SIRT1 activity and inhibition of p53-mediated transcription (753). Kakkola *et al.* describes AROS as a SIRT1 agonist, by conducting *in vitro* activity assays (755). However, in tumour cells, it was shown that AROS is a weak activator of SIRT1, suggesting that AROS regulatory function is different in various cellular contexts (756).

SIRT1 is able to form complexes in a substrate specific manner with other partner proteins. In the form of complex, SIRT1 activity or substrate recognition is altered, as well as recruitment

of SIRT1 to the specific site of DNA promoters or other proteins. Complex including four and a half LIM domain protein 2 (FHL2), SIRT1-FOXO1-FHL2 and SIRT1-p53-necdin were shown to improve SIRT1 interactions with FOXO1 and p53 substrates, additionally to its improved deacetylase activity (757,758). SIRT1-STAT3-USP22 (ubiquitin specific peptidase 22) complex reformation results in elevated SIRT1 stability (759). Another SIRT1 complex with p53, SIRT1-p53-PML IV, induces inhibition of p53 through deacetylation and recruitment of SIRT1 and p53 to the nuclear bodies of promyelocytic leukaemia protein (PML) (760). The recruitment of SIRT1 to PPAR γ promoter region and improvement of PPAR γ substrate binding to SIRT1, is mediated through interaction of SIRT1 with Cdk2-associated cullin 1 (CACUL1) (761). Moreover, there are a number of other SIRT1 complexes with substrate-specific activity - SIRT1-PGC-1 α -FOXO3a, SIRT1-PGC-1 α -HNF4 α , SIRT1-FOXO3a-NRF1 and SIRT1-FOXO1-Pml (591,610,762).

Moreover, the inhibitor of SIRT1 - deleted in breast cancer 1 (DBC1) was described to bind catalytic core domain of SIRT1 protein and negatively regulate the activity through obscuring the association between SIRT1 activity (ESA) motif and catalytic domain (515,763–765). DBC1 emerges to be an important compound in DNA damage response. In the context of genotoxic stress, phosphorylation of DBC1 improves its bonding affinity to SIRT1 and inhibits the deacetylase activity (766). Through DBC1-mediated suppression of SIRT1 function, the activity and expression of p53 and FOXO3 are modulated (763,764). A schematic diagram showing the regulation of SIRT1 expression and function is shown below of this section.

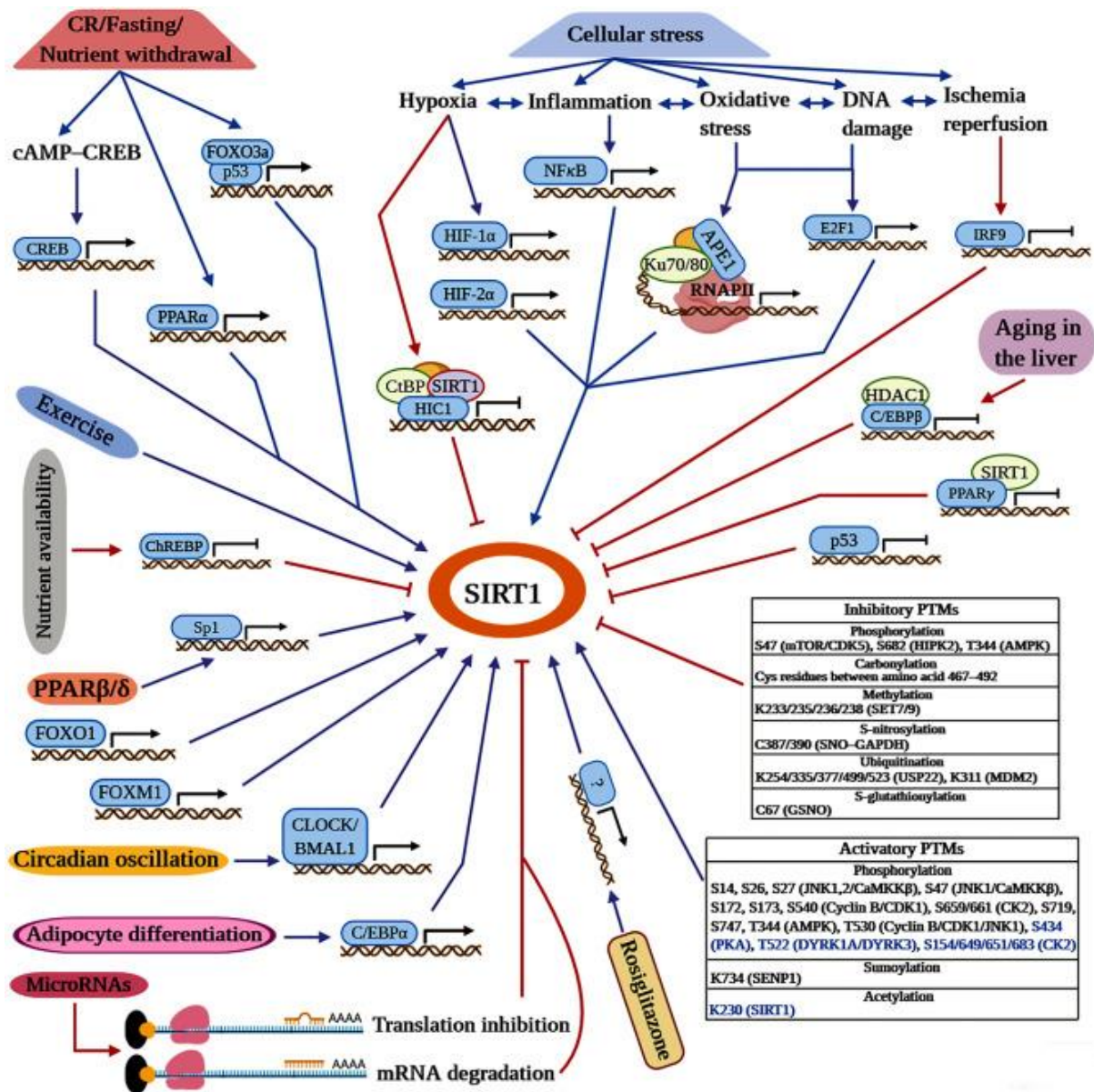


Figure 23. Summary diagram of the regulation of SIRT1 expression and function. Regulation occurs at multiple levels by transcription factors, microRNAs and PTMs. From Shahgaldi *et al.*, 2021 (654).

Protein PTMs

It was described that SIRT1 has at least 13 residues that are targets of post transcriptional modifications (PTM), in particular to phosphorylation, which modifies its activity.

Several kinases were reported to phosphorylate threonine residues of SIRT1 protein. AMPK is another metabolic sensor in cells, as it is sensing changes in the level of ATP and directly phosphorylates metabolic enzymes (767). It interacts with SIRT1 catalytic domain and

facilitates Thr344 phosphorylation, leading to inhibition of SIRT1-mediated deacetylation (768). Additionally, AMPK can modulate SIRT1 stability, through phosphorylation and activation of DBC1 (769). On the other hand, CDK1 is able to increase SIRT1 activity through Thr530 phosphorylation (770). Dual specificity tyrosine-phosphorylated and regulated kinase (DYRK) family is highly conserved and its members DYRK1a, DYRK2 and DYRK3 are known to phosphorylate broad set of proteins (771,772). Both, DYRK1a and DYRK3, were found to interact with SIRT1 (773). They are able to phosphorylate Thr522 and thereby promote deacetylation of p53. Lu *et al.* concluded that Thr522 phosphorylation is crucial in regulation of SIRT1 tissue specific activity (774). DYRK2 was also reported by Utani *et al.* to modulate DNA synthesis and prevent DNA damage by phosphorylating SIRT1 Thr530 residue (775). In addition, serine phosphorylation of SIRT1 protein plays an important role in regulation of its function. Enhancement of SIRT1 activity can be achieved through casein kinase 2 (CK2)-mediated phosphorylation of various serine residues (Ser154, Ser649, Ser651, Ser683) or CDK1-mediated phosphorylation of Ser540 (770,776). On the other hand, CDK2 is able to negatively regulate SIRT1 activity by phosphorylating Ser164 (777). Another mechanism of SIRT1 negative regulation in the context of DNA damage is phosphorylation of Ser682 residue by homeodomain-interacting protein kinase 2 (HIPK2) (778). Furthermore, phosphorylation at this site induces disruption in AROS binding to SIRT1, thus upregulates p53 activity and drives DNA-damage induced cell apoptosis. However, AMPK-mediated phosphorylation of Ser27 cause reduction of DBC1 binding affinity to SIRT1, leading to enhanced SIRT1 activity (779). Other positive regulators of SIRT1 in c-Jun N-terminal kinase 1 and 2 (JNK1 and JNK2), which facilitates Ser47 and Ser27 phosphorylation and further stability of SIRT1 (780–782). Conserved sites of SIRT1 catalytic domain contain two main phosphorylation sites tyrosine (Tyr) 280 and Tyr301, which are both targets of Janus kinase 1 (JAK1) enzymatic activity. These particular PTMs are crucial for SIRT1-mediated deacetylation of STAT3 transcription factor (783). Overall, SIRT1 phosphorylation plays a very important role in its deacetylase activity and stability.

Another PTM, which was found to regulate SIRT1 protein stability, is ubiquitination. In the series of enzymatic reactions, ubiquitin binds to the target protein and results in its degradation, leading to reduced downstream effect of this protein. Ubiquitination of SIRT1 was found to be associated with different cellular contexts. For example, in liver, during lipid metabolism, SIRT1 ubiquitination by mammalian Ste20 like kinase (MST1) represses its activity (784). Shen *et al.* reported that in the context of colorectal cancer, autophagy genes are inhibited

through the activity of ubiquitin-conjugating E2 enzyme variant protein 1 (Ube2v1) and degradation of SIRT1 (785). Additionally, Yu *et al.* showed that SMURF2-mediated ubiquitination and subsequent degradation of SIRT1, decreases the proliferation of colorectal cancer (786). In response to DNA damage, SIRT1 is ubiquitinated by MDM2 E3 ligase and Lys311, however in this context SIRT1 is not degraded, but its nuclear translocation is inhibited (787). Also, ubiquitin-specific peptidase 22 (USP22) and the E3 ubiquitin ligase CHFR regulate SIRT1 stability by targeting it for degradation (759,788). These studies suggest that SIRT1 ubiquitination plays a key role in regulation of DNA damage and cancer.

Furthermore, glycosylation of C-terminus end of SIRT1 protein can regulate its activity. Han *et al.* showed that both *in vitro* and *in vivo*, O-GlcNacylation of Ser549 residue results in upregulation of SIRT1 deacetylase activity, protecting cells against apoptosis (789). In opposition, Chattopadhyay *et al.* found that N-terminus glycosylation of SIRT1 can target it for degradation through ubiquitination in the overnutrition condition (790). Another PTM has a positive regulatory effect on SIRT1 activity. In normal physiological condition, simulation of Lys734 residue preserved SIRT1 deacetylase activity. Desumoylation of SIRT1 at this site by senstrin-specific protease 1 (SEN1) reduces its activity *in vitro* (668). Oxidative stress also enhances interaction between SIRT1 and SEN1 and inducing p53-mediated apoptosis (791). At last, S-nitrosylation PTM is adding nitrosyl group to the reactive thiol group of cystine (Cys) and results in formation of S-nitrosothiol (SNO). This PTM was described to regulate protein localization, stability and also activity in different cellular processes (792,793). S-nitrosylation of GAPDH facilitates its translocation to nucleus, where it transfers nitric oxide group to SIRT1 Cys387 and Cys390 (794). It was described that SNO-SIRT1 exhibits reduced deacetylase activity, in response to stress and inflammation (795,796). All together, these results confirm the importance and tight regulation of SIRT1 activity and stability by various PTMs.

AIMS AND OBJECTIVES OF THE THESIS

This project was originated from the establishment of SBA mouse model, which mimics the consequences of AN. Recently, our research group demonstrated that mice exposed to long term weight loss of 18% from initial weight (SBA 18% protocol) exhibit not only alterations in BMC and bone parameters, but also increase in BMA, similarly to AN patients (2). Knowing adipocytes and osteoblasts are derived from same precursor cells - BMSCs, it was hypothesised that reduction of bone mass and accumulation of BMAT can take place due to changes in BMSC differentiation potential. Additionally, in the same study it was shown that shift in BMSCs differentiation potential favouring adipogenic lineage, can potentially take place through the observed suppression of *Sirt1* mRNA and SIRT1 protein level in SBA mice (2).

SIRT1 is well known to support osteoblastogenic lineage and subsequently suppress adipogenic differentiation of BMSCs. Observed suppression of *Sirt1* expression, which potentially lead to the changes in BMSCs fate decision, lead to the hypothesis that SIRT1 plays central role in regulation of cell differentiation within BM. For that reason, this project focuses on identification of potential regulators of *Sirt1* expression in BMSCs extracted from weight lost mice.

Therefore, **the first objective of this work was to replicate initial study on mice weight loss, to determine does the severity level and length of SBA protocol affect mice body parameters, BMSCs differentiation capacity and *Sirt1* expression.** This was achieved by replicating the SBA study using long term (10-week) and short term (4-week) protocols, as well as testing different severity of weight loss in mice (0%, 12%, 18%, 24% d).

The second aim was to determine molecular mechanism of *Sirt1* expression regulation in SBA derived BMSCs, which was achieved through comparing transcriptomics of BMSCs extracted from 10-week SBA mice or 4-week SBA mice and comparing them with cells from control animals. Moreover, **we explored interaction between AMPK and SIRT1,** which was previously described in the literature, through regulation of AMPK activity and expression.

PART 1 – THE EFFECT OF SEVERITY LEVEL AND DURATION OF ENERGY DEFICIT ON BONE AND BONE MARROW STROMAL CELL (BMSC) DIFFERENTIATION IN ANOREXIA NERVOSA MOUSE MODEL

I. INTRODUCTION

State of art of SBA model

AN is characterised by the starvation leading to severe CR, and which subsequently results in weight loss (366,367). Currently, this condition is predominant in female population and occurs with prevalence of 4% among young females (368–370). The consequences of AN in young individuals could be very severe and are associated with alterations in female reproduction system, GH intolerance, leptin deficiency and bone loss with subsequent increase in BMA in some individuals (375,381,383,400,406). In some of the cases, bone fragility was found to be irreversible, despite the weight gain in subjects (393). In order to study the consequences of AN and develop appropriate treatment strategies, it is important to conduct studies on animal models. In the literature, some attempts to develop a model exhibiting AN consequences were described.

In the introduction section it was highlighted that currently in literature a variety of different CR protocols are done, on different animal models and both male and female subjects. Overall, it can be concluded that effect of CR on bone and BMA is specie specific, can depend on a strain and also sex of the model. Multiple studies described, tend to use male species of mice or rabbits to study the consequences of CR on bone and BMA, results of which cannot be applicable to female AN subjects (415,416,421). Other, that study female species, widely used CR model consist of control condition (*ad libitum* feeding) and CR condition (70% or 60% of *ad libitum* feeding). This model is considered to have a moderate effect on animals, as CR condition is determined according to average food intake of the control condition, which in its turn results in the animal being 30% overfed (797–800). Moreover, some of the studies reported that animals fed 40% *ad libitum* diet, exhibited weight gain (vs day 0) (283). However, in case of increased CR severity (30% *ad libitum* diet), animal weight loss was reported to be reduces (vs day 0) (283). Nevertheless, these studies demonstrated that CR is able to induce alterations in body composition, endocrine function and reproduction system (414,801,802). Moreover, most of CR studies lack the stress component, as AN is associated with chronic stress that can

influence metabolic processes (373). Due to lack of the consistency in data, it is difficult to draw the conclusions about optimal CR protocol, that can mimic the consequences in AN.

On the other hand, Van Leeuwen *et al.* and Hao *et al.* described a different approach to induce mouse body weight loss, the model of separation, which induced a weight loss in mice (803,804). The weight loss in this model was achieved through an increase in metabolic demands of animals. Mice were housed in a cage fitted with six individual Plexiglas partitions, which restricted their physical contact, nevertheless, allowing to smell and see their neighbours. Results showed that separation stress significantly decreased the weight of the mice. Moreover, similarly to AN patients, mice exhibited a significant decrease in dopamine and norepinephrine, which indicates undergoing stress (803,805,806). Findings of these studies have highlighted an importance of stress component in AN associated changes in central nervous system (CNS) and the efficiency of mouse separation model in mimicking the AN-associated stress.

Zgheib *et al.* conducted the study, where they compared the effect of three different types of weight loss protocols on mice body and bone changes (1). Weight loss was induced through either mouse separation, as it was previously done by Van Leeuwen *et al.* and Hao *et al.*, through time restricted feeding, as well as both conditions applied together. This study demonstrated that combination of separation, which increases metabolic demand of mice, and reduction of energy intake by decreasing food availability time, results in efficient weight loss in mice. It was called Separation Based Anorexia (SBA) model, and it exhibited physiological changes that mimicked those described in AN patients (1).

By the end of 10 weeks, Zgheib *et al.* described alterations in mice induced by this protocol (1). First of all, SBA protocol induced a desired 25% weight loss (vs. D0) in animals with mean body weight decrease of 40% comparing to CT group, without inducing a visual distress. This resulted in 35% decrease in fat mass and 9% decrease in lean mass (vs. D0). Also, significant decrease in BMC was observed in SBA mice. Studying plasma of SBA mice, Zgheib *et al.* demonstrated a significant reduction of circulating leptin, similarly to data obtained from AN patient studies (381,383). Another characteristic of AN that was exhibited in SBA mice is alterations in GH/IGF-1 axis. In AN patients the potential GH resistance is observed, as high GH level in plasma is associated with low IGF-1 levels (375,376). Plasma samples extracted from SBA mice contained almost 10-fold increase in GH (vs. CT) and nearly 2-fold decrease

in IGF-1 (vs. CT). Moreover, SBA protocol induced alterations in reproductive system of mice, as it caused significant reduction in ovary size as well as oestrous cycle frequency alterations. Suggesting that SBA protocol is able to mimic changes in reproductive system observed in AN patients and other CR animal models (801,807). Overall, this study demonstrated that SBA model is a valuable model of long-term effect of weight loss that have close resemblance with symptoms observed in AN.

Objectives of the in vivo study

In prior to current project, Louvet *et al.* demonstrated that 8 weeks of an SBA protocol, inducing moderate weight loss (18%) in mice comparing to their initial weight, is associated with an increase in BMA, bone loss and changes in BMSC fate decision (2). Changes in BMSCs differentiation capacity were established through stem cell extraction and co-differentiation study. Firstly, BMSC heterogeneous population was extracted from mice tibia and femur. This is achieved through the protocol that was described by Ghali *et al.* (808). After, to understand the preference of BMSCs to commit to adipogenic or osteoblastogenic fate, Ghali *et al.* developed a co-differentiation medium (808). Cell differentiation potential was assessed through staining, as well as through study of marker gene expression. For adipogenic differentiation, mRNA level of - peroxisome proliferator-activated receptor gamma transcription factor, which initiates transcription of other adipose tissue genes (*Pparg2*); glucose transporter type 4 gene that facilitates glucose uptake (*Glut4*); and adipose tissue secreted adipokines, adiponectin (*Adipoq*) and leptin (*Lep*) were determined. For osteoblastogenic differentiation mRNA level of - runt-related transcription factor 2, responsible for transcription of osteoblast related genes (*Runx2*); osterix transcription factor required for osteoblast differentiation (*Sp7*); alkaline phosphatase which plays a key role in bone mineralisation (*Alp*) and osteoblast secreted osteocalcin, which is required for bone remodelling and metabolism (*Bglap*) were studied (808). Overall, Louvet *et al.* described the negative effect of 18% weight loss in mice on bone parameters (reduced Tb.Th and Cort.Th), that was associated with an increase in BMA. Moreover, studying BMSCs differentiation, it was found that cells exhibit preference for adipogenesis at the expense of osteoblastogenesis, which potentially can take place due to the decrease in *Sirt* gene and SIRT1 protein expression (2).

Previously, *in vitro* studies showed that SIRT1 is involved in regulation of BMSC cell renewal capacity, as well as induction of osteoblastogenic differentiation in these cells (658). Nutrient deprivation or exposure to CR has been shown to have a positive impact on SIRT1 activity and *Sirt1* gene expression in pancreatic β -cells, myoblasts or fibroblast (668,694,809). Several studies in AN patients, showed an increase in plasma circulating level of SIRT1 (810,811).

However, study in the bone marrow showed that during severe long term of CR, the SIRT1 expression level is decreased and potentially contributes to decrease in BMAT expansion (2). Nevertheless, study by Louvet *et al.* confirmed the involvement of SIRT1 decrease in an increase in BMA with subsequent loss of bone, allowing the development of current work.

This part of the project focuses on confirmation of previously published data. Furthermore, it was hypothesised that these changes in bone and BMSCs could potentially depend on the severity of weight loss and the length of SBA protocol. To verify these hypotheses, we studied bone, BMA, BMSC differentiation capacity and *Sirt1* mRNA expression after a 10-week induction of 4 different levels of body weight loss (0%, -12%, -18% and -24%) relative to mice at day 0. The same parameters were also analysed after a 4-week SBA protocol, with 18% of weight loss in mice.

To complete the transcriptomic study of BMSCs extracted from SBA mice, RNA Sequencing analysis was conducted on cells extracted from CT and SBA 18% weight loss mice after 10-week and 4-week protocols.

Explore transcriptomic changes using RNA Sequencing

Study of cell transcriptomics is essential in understanding and interpreting the functional components of genome, as well as the molecular components of cells and tissues. This could be further applied to study development or disease. RNA sequencing (RNA-seq) is a deep-sequencing technology, that allows to establish transcriptome profile and provides accurate measurements of transcripts levels (812–814). Currently, it is used in a variety of research studies, as well as clinical settings. For example, many aspects of cancer research and therapy have made use of RNA sequencing, including biomarker discovery and characterization of cancer heterogeneity or evolution, cancer immune microenvironment and immunotherapy (815–819). RNA-seq methods, in particular, give a large amount of data on the gene expression

levels of many species across multiple conditions at high resolution (820,821). This knowledge naturally led to the notion of differently expressed genes (DEGs), which are genes whose expression levels have been found to be significantly different between several conditions.

RNA-seq allows for analysis of the transcriptome in a rather unbiased way, it provides a single base pair resolution, a tremendous dynamic detection range (>8,000 fold), and low background signals. Additionally, RNA-seq can show transcriptional start sites, exposing alternative promoter use, mRNA isoforms produced from alternative splicing, and premature transcription termination at the 3' end, which is important for mRNA stability (822–826).

The process of RNA-seq starts with RNA isolation from the samples and transformation of RNA population to cDNA fragment library through reverse transcription, containing adaptor sequence at both ends (Fig. 51). Adaptors are artificial DNA fragments that are inserted prior to sequencing to guarantee that the DNA fragment being sequenced adheres to the sequencing flow cell. These adaptors are usually sequenced and would have been deleted from the reads (827). Then, each molecule is sequenced in a high-throughput manner, with or without amplification, to acquire short sequences from one end (single-end sequencing) or both ends (pair-end sequencing).

There are several approaches of conducting sequencing of produced library (Illumina, Pacific Bioscience and Oxford Nanopore), in our study the Illumina approach has been used, therefore we would focus on its underlining steps. After a library of cDNA is produced, using adaptor sequence, fragments are hybridised to the flow cell surface. In the process of bridge amplification, each bound fragment is amplified into the cluster. Next, the process of sequencing starts with addition of fluorescently labelled nucleotides, and incorporation of these nucleotides to each fragment of the cluster. Every cycle of sequencing, a digital image of clusters is obtained and the emission wavelength and intensity of incorporated nucleotides allow to identify the base. These cycles are repeated until the end of the read length and the process of genome alignment can start. Using a single-end reading approach, the sequencer reads a fragment from one end to the other to generate the base pair sequence. It begins with one read in one direction, then it concludes this direction at the chosen read duration, and following process begins a new round of reading from the other end of the fragment (828). Alternatively, paired-end reading enhances the capacity to determine the relative locations of

different reads in the genome, making it far more successful than single-end reading in resolving structural rearrangements such as gene insertions, deletions, or inversions. It can also help with repeated region assembling (828). However, this level of precision may not be necessary for some types of research, and paired-end reads are more expensive and time-consuming to do, comparing to single-end reads. Our data was obtained and mapped through pair-end reading, therefore its precision rate is high.

After sequencing, the obtained reads are either matched to a reference genome or transcripts (mapping), or they are constructed from scratch without the assistance of the genomic sequence, allowing to create a genome-scale transcription map that includes the transcriptional organization or level of expression for each gene (assembly) (812,819,829). The fact that RNA-seq allows to assemble *de novo* genome transcript makes it especially appealing for non-model organisms whose genomic sequences have not yet been identified (830). Moreover, RNA-seq has been shown to have a high level of accuracy in quantification of gene expression level, which was confirmed not only by qPCR, but also by spike-in RNA controls of known concentration (831,832).

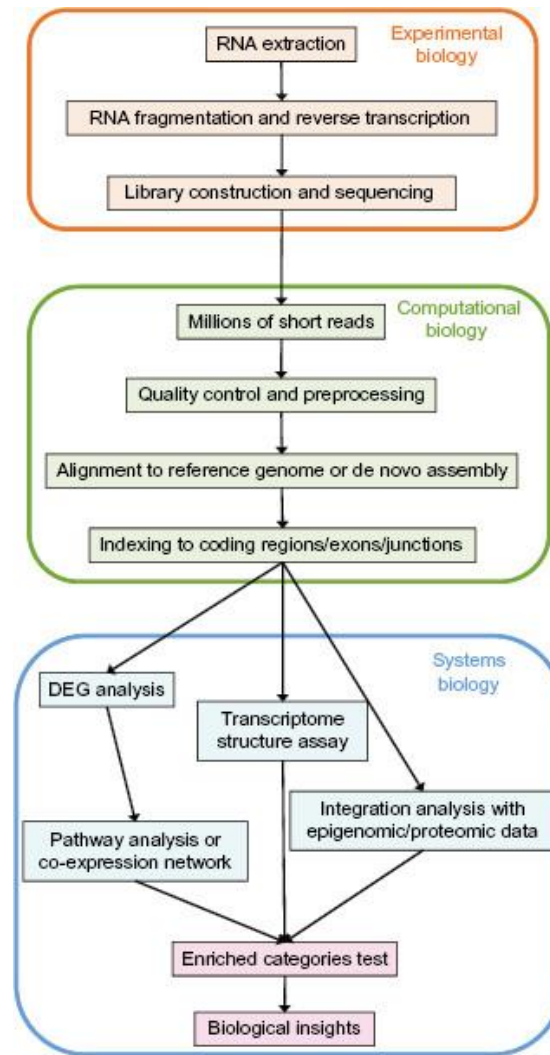


Figure 24. A workflow of RNA-seq. Summary of key steps of RNA-seq, starting from sample isolation and generation of cDNA, followed by sequencing, further genome mapping and data analysis. Taken from Han *et al.*, 2015 (924).

DGE tools conduct statistical tests based on quantification of expressed genes obtained from computational analyses of raw RNA-seq reads, like mapping and assembly (833–839). The mapping process involves comparison of qualified reads, obtained through sequencing of a sample of interest, to an already known reference genome or transcriptome. Depending on the experimental goal, the mapped reads for each sample are then indexed into gene-level, exon-level, or transcript-level categories to measure the abundance of each of these categories (840). The assembly method involves building a data set of transcripts expression level without pre-existing reference genome, which is much more challenging than mapping process, however with software tools like RNA-Seq by Expectation Maximization (RSEM), it is possible to have an accurate estimate (841). This allows to compare transcriptomics of two distinct populations

and develop deeper understanding of cell changes in the context of disease, drug treatment or metabolic state.

In the current part of the study, the main interest is to complete our knowledge about SBA induced changes in BMSCs. Most importantly, to determine transcriptomic differences between BMSCs extracted from CT and SBA 18% weight loss mice from 10-week, as well as 4-week studies.

In vitro studies on nutrient deficiency

The effect of CR or nutrient deficiency was described not only in animal models, but also in the *in vitro* cell culture models (842–845). Most of the *in vitro* experiments consist of cell exposure to the serum extracted from CR treated animals (rates, mice, apes), which results in alterations of cell biology, similarly to *in vivo* studies (842,843,845,846). However, another way to study CR *in vitro*, is to reduce cells glucose or nutrient availability (844). In these experiments, cells are exposed to low glucose growth medium, which induces changes in cell biology (844). Li and Tollefsbol showed that mimicking CR through glucose restriction in human lung fibroblasts (WI-38, IMR-90 and MRC-5) results in increased expression of *Sirt1* in these cells (847). Based on these findings, that *in vitro* model can mimic *in vivo* alterations, it was hypothesised that CR in BMSCs model, potentially can mimic consequences of SBA mouse model on cell differentiation capacity. As it was mentioned before, *in vivo* long term energy deficit induced by SBA protocol resulted in alterations of BMSC differentiation capacity favouring adipogenesis and suppressing *Sirt1* mRNA expression in these cells (2). Therefore, it was hypothesised that *in vitro* reduction of nutrient availability in prior to co-differentiation might affect BMSC fate decision. Thus, growth medium containing reduced serum concentration (7% and 5% FBS) would be tested both on cell line and primary mouse BMSCs.

To examine the *in vitro* CR on cell differentiation capacity, preliminary studies were conducted using mice stromal cell line. Several immortalised cell lines are currently used, including C3H10T1/2, TBR32-2, MC3T3-G2/PA6, ST2, HS-5 and HS-27A (848–852). Upon stimulation by bone morphogenic proteins (BMPs), more specifically by BMP-2, C3H10T1/2, ST2 and MC3T3-G2/PA6 cell lines had increased alkaline phosphatase (ALP) activity (849,853). However, comparing to MC3T3-G2/PA6 cell line, ST2 cells exhibited more

elevated increase (853). In addition, BMP-2 exposure induced the osteocalcin expression in ST2 cells and not in MC3T3-G2/PA6 cell line (853). Upon transplantation of ST2 cells into peritoneal cavities of athymic mice and their treatment with BMP-2, cells generated mineralized bone in the chambers, confirming the osteoblast differentiation ability of ST2 cell line (853). Abdallah *et al.* described some limitations of ST2 cell line comparing to primary extracted mouse BMSCs (854). Primary cells displayed a higher rate of osteoblast differentiation potential and responsiveness to osteogenic factors including BMPs, IGF-1, PDGF, TGF β 1,3, FGF, cAMP, Wnt3a and VEGF, comparing to ST2 cell line (854). Despite this, multiple studies described the osteoblastic potential of ST2 cells (855,856).

Moreover, it was widely described that upon stimulation, ST2 cell line can differentiate into adipocyte lineage (34–37). Indeed, it was demonstrated that upon treatment with cocktail containing insulin, dexamethasone and 3-isobutyl-methylxanthine (IBXM), ST2 cell line is able to differentiate into adipocytes (860). They exhibit accumulation of triglycerides and expression of adipogenic transcription factors (*Pparg2*, *Cebpa*). In contrast to MC3T3-G2/PA6 cell line, ST2 cells can respond to the adipogenic effects of insulin, similarly to the extramedullary preadipocytes (3T3-L1) (860).

Furthermore, ST2, HS-5 and HS-27A cell lines were shown to have immunoregulatory function (861,862). For example, ST2 cells are able to support the differentiation of monocytes, alveolar macrophages and HPCs into osteoclast, in the co-culture studies (862,863). ST2 cells exhibit positive regulation of thymocyte differentiation, additionally provide the support for B-cell and T-cell development (851,864). Overall, ST2 cell line is not only able to fulfil differentiation into adipocytes and osteoblast, but also provide a support for haematopoiesis, by this representing functional components of BM microenvironment. Therefore, in current study, this cell type is used as model of mouse BMSCs.

In this study, firstly, different concentration of foetal bovine serum (FBS) in MEM growth medium were tested. The ability of ST2 cell line to amplify in low nutrient availability condition was examined. Preliminary study focused on five different FBS concentrations (0%, 1%, 3%, 5% and 7%) and cell proliferation was studied comparing to standard 10% FBS concentration, which was used as a control. Results showed that 0%, 1% and 3% FBS in growth medium are not sufficient to maintain normal cell survival. Therefore, the rest of the study was focused on 5% and 7% FBS concentrations.

Overall, this part of the research project aims to explore the effect of severity level (0%, 12%, 18% and 24% weight loss in mice) and duration of SBA protocol (10-week or 4-week) on body and bone parameters of mice, as well as *Sirt1* mRNA expression and differentiation capacity of extracted BMSCs from control and SBA groups. Additionally, we aim to develop the *in vitro* nutrient deficiency model, that can induce changes in BMSC differentiation and affect *Sirt1* mRNA expression. This is done, in order to explore regulation of *Sirt1* expression in nutrient deprivation.

II. MATERIALS AND METHODS

1. Animals

Seven-week-old female C57BL/6J mice purchased from Charles River Laboratories (St Germain sur l'Abresle, France) were used for the separation-based anorexia (SBA) model (1). Mice were housed 6 per cage in a controlled room temperature ($22^{\circ}\text{C} \pm 1^{\circ}\text{C}$) under a 12-hour dark/light cycle (lights off at 10 a.m.) and with free access to water. Before induction of the SBA protocol, mice were acclimatized for 7 days, therefore SBA protocols started at 8-week-old. At this age, mice become sexually mature and their development is resembling to that of young women with onset of AN (865). At this age, mouse skeleton is still developing, but slowly and so protocols can impact remodelling but also maturation of the skeleton, like for anorexia for women. The SBA protocol was generated for 10 weeks (cohort 1) and aimed to induce 4 different weight loss conditions in randomly allocated mice – no weight loss (SBA 0%), a light 12% weight loss (SBA 12%) (achieved 12.97%), a moderate body weight loss of 18% (SBA 18%) (achieved 17.27%) and severe weight loss of 24% (SBA 24%) (achieved 23.17%), relative to day 0 (D0). A time restricted-feeding was used to induce weight loss in mice, a food access time was gradually reduced from 6 h to 2 h per day during the protocol, depending on the desired weight loss to achieve. Mice allocated to severe, moderate, and light weight loss groups had reduced food availability and time dependent on the progression of weight loss. For no weight loss group, the time of the feeding was not decreased dramatically, in order to maintain the initial mouse weight. Furthermore, throughout the protocol mice of SBA groups, were kept in the separate sections of the cage with free access to water and this encouraged the increased energy expenditure by thermogenesis. The SBA mice were gathered together in regular cages for the periods of feeding. The CT group was housed in standard conditions in collective cages, with water and food provided ad libitum. This study was specifically approved by the Committee on the Ethics of Animal Experiments (CEEA) of Nord-Pas de Calais, France (permit number: CEEA#2016070717275082).

Additionally, a 4-week SBA protocol (cohort 1) was performed using seven-week-old female C57BL/6J mice, similar to the 10-week protocol. After one week of acclimatization, the SBA protocol was generated for 4 weeks to achieve moderate weight loss of 18% (SBA 18%) (achieved 18.75%) in mice relative to their weight at D0. This study was specifically approved

by the Committee on the Ethics of Animal Experiments (CEEA) of Nord-Pas de Calais, France (permit number: CEEA#2016070717275082).

Replication of 10-week and 4-week protocol was conducted (cohort 2). Similar to the previous cohort (cohort 1), this study was performed using seven-week-old female C57BL/6J mice, which were housed for 7 days in prior to protocol start. The protocol was generated to achieve 18% weight loss during two different protocol lengths. In 10-week cohort 2 study mice achieved -18.0% weight loss vs D0 and in 4-week cohort 2 study mice achieved -18.1% of weight loss vs D0. This study was specifically approved by the Committee on the Ethics of Animal Experiments (CEEA) of Nord-Pas de Calais, France (permit number: CEEA#2016070717275082).

2. Dual Energy X-Ray Absorptiometry (DEXA) Analysis

The fat mass, lean mass, and bone mineral content (BMC) of mice were analysed between 09:00 and 11:00 by using the DEXA Lunar PIXImus Mouse Densitometer (GE Healthcare, Madison, WI). Intramouse coefficients of variation were <5% (1).

3. Mineralized Bone Micro-CT Analysis

Tibiae extracted from CT and SBA mice were scanned using a Skyscan 1172 microCT device (Bruker MicroCT, Kontich, Belgium). The software suite provided by the manufacturer was used for image acquisition, reconstruction, analysis, and 3D visualisation (Skyscan 1172, NRecon, Dataviewer, CTAn, CTVox™). Analysis of the tibia trabecular bone volume/tissue volume (Bv/Tv) ratio, cortical thickness (Cort.Th), trabecular thickness (Tb.Th), trabecular number (Tb.N) and trabecular spacing (Tb.Sp) of all animals were determined in a 0.5mm region beginning 250mm proximal to the proximal growth plate. More detailed description for the quantification of 3D microarchitecture of trabecular bone has been previously presented (866).

4. Bone Marrow Adipose Tissue Content - Micro-CT Analysis

In the proximal tibia, BMAT was analysed and quantified by micro-CT using a previously published protocol (867). After the first micro-CT scan, tibiae were decalcified in 4% formic acid/10% NBF (1:1), pH 7.4, for 48 h. Then bones were rinsed in distilled water and stained in the fume hood for 48 h in the aqueous staining solution (1% osmium tetroxide solution stabilized in a 2.5% dichromate potassium) at room temperature. Then, bones were rinsed for 48 h at room temperature in PBS with regular renewal of the solution. Osmium-stained bones were then stored at 4 °C in PBS until the second micro-CT acquisition. The study focused on quantifying the percentage of the ratio of adipocyte volume to marrow volume (% Ad.V/Ma.V). The data are presented in the form of the percentage of BMAT volume in marrow volume.

5. Bone Marrow Adipose Tissue Content – Perilipin Immunohistochemistry

Embedding and sectioning of tibia from CT and SBA 18% mouse starts with fixation in cold 10% neutral buffered formalin for 24 hours. These undecalcified tibias were dehydrated through increasing alcohol series, infiltrated then embedded in Technovit 9100 resin (Heraeus Kulzer) (868). Tibias were sectioned with a microtome (RM2255, Leica Biosystems) at a thickness of 6 µm. The sections were placed on gelatine-coated slides and dried 48h at 37°C. Sections were deplasticised in acetone, then rehydrated and stained with perilipin immunohistochemistry.

The procedure was carried out at room temperature except for the primary antibody incubation at +4°C. After encircling sections with a water-repellant wax pen, sections were rinsed for 2 changes of 2 minutes in 0.1M PBS and slides were placed in a humidified chamber. To block the endogenous peroxidases activity, sections were incubated in 3% H₂O₂ (prepared in PBS) for 20min, followed by 3 washing for 5 minutes in 0.1M PBS. Sections were then incubated in 10% goat normal serum (Agilent/DAKO, Ref. X090710-8), 4% BSA (Sigma-Aldrich, Ref. A9647) and 0.1M PBS to block nonspecific binding for 1h. The next day, sections were washed 3 times for 5 mins in 0.1M PBS. Then, samples were incubated 1h in the secondary biotinylated antibody (Agilent/DAKO, Ref. E043201-8) diluted at 1:500 in the dilution buffer. The sections were blot dried and incubate 45mins with the streptavidin-HRP (Agilent/DAKO, Ref. P039701-2) diluted at 1:400 in PBS. Finally, sections were washed 3 times of 5 mins in 0.1M PBS and

incubate 5 mins in DAB solution (Sigma-Aldrich, ref. D4293-50SET). The reaction was stopped by placing the slides in tap water for 5 min.

Image acquisition was performed on an Axiokop40 microscope (Zeiss, Germany) using Histolab and Archimed software (Excilone). Two sections at 256 μ m distance from each other in the middle shaft of the tibia were used to perform study of the bone marrow adipocytes density. Adipocytes at proximal tibias were measured in an area from 200 to 1000 microns below the growth plate. The number of adipocytes per marrow area (N. Ad/Ma.Ar) (cells/mm²) was measured by tracing adipocytes with ImageJ software (NIH).

6. Primary Bone Marrow Stromal Cell Culture

Primary bone marrow cells were harvested from the tibiae and femurs of CT and SBA mice, as it was described in Ghali *et al.* study (808). Cells were plated for 48 hours adhesion and for 7-10 days to reach full confluence in MEM medium (PAN BIOTECH; P04-21050) with 15% foetal bovine serum (PAN BIOTECH; P30-3306), 1% penicillin/streptomycin (PAN BIOTECH; P04-85100) and 1% stable glutamine (PANBIOTECH; P06-07100). After, plated BMSC population was differentiated into both osteoblasts and adipocytes according to the co-differentiation protocol described in a previously published article (808). The medium containing co-differentiation inducers was replaced every two days during the 14 days of the co-differentiation experiment. This medium combines standard osteoblastogenic medium with Dexamethasone. Ghali *et al.* showed that addition of 100 nM of dexamethasone into osteoblastogenic medium containing 50 μ g/ml of ascorbic acid and 10 mM of β -glycerophosphate, supports adipocyte and osteoblast differentiation in mouse primary of BMSCs (808). This culture duration was chosen because of its brevity, which allowed for minimizing the time for cells to change after leaving the *in vivo* state.

7. ST2 Cell Line Culture in Nutrient Deficiency Medium

ST2 cells were obtained from Deutsche Sammlung von Mikroorganismen und Zellkulturen (Lot 5, 27-01-2016) and incubated at 37°C and 5% CO₂, in MEM medium (PAN BIOTECH; P04-21050) supplemented with different concentration of foetal bovine serum (PAN BIOTECH; P30-3306) (5%, 7% and 10%), 1% penicillin/streptomycin (PAN BIOTECH; P04-85100) and 1% stable glutamine (PANBIOTECH; P06-07100). After cells reached

confluence and were exposed to reduced nutrient medium for 5 days, the standard co-differentiation protocol was initiated (808).

8. Raman Microspectroscopy

For Raman microspectroscopy, extracted BMSC population was plated on calcium fluoride (CaF₂) substrate, which is adapted to Raman analysis. The analysis of samples was conducted using LabRAM HR800 (Jobin-Yvon, France) instrument equipped with an XYZ motorized stage and a diode laser $\lambda=785$ nm. The Raman spectrometer was coupled with a microscope (BX40, Olympus). Raman acquisitions were performed with a water objective 100x lens (Nikon, numerical aperture = 1.1 Japan). The water immersion objective focused the laser on the cell within the micrometre scale on the centre of individual lipid droplets, where one spectrum corresponds to one adipocyte lipid droplet. A total of 1,252 lipid droplets were acquired over 109 adipocytes in 10-week cohort 1 study (Table 5), representing an average of 83.4 lipid droplets analysed per well and an average of 7.2 adipocytes analysed per well. In 4-week cohort 1 study, a total of 154 lipid droplets were analysed in 43 adipocytes (Table 5).

Spectral acquisition was performed in the 400-1800 cm⁻¹ range. The Raman signal was collected by a multichannel CCD detector (1024 × 256 pixels). The acquisition time was set at 60 s averaged 2 times per spectrum (total acquisition time = 120 sec). Raman spectra were processed using Labspec software (HORIBA, Jobin-Yvon, France). A Savitzky–Golay smoothing filter was applied to all Raman spectra. The band areas were integrated over defined Raman shift regions in the spectrum using a sum filter. The filter calculates the areas within the chosen borders and the background is subtracted by taking the baseline from the first to the second border. The band area was estimated at 1441 cm⁻¹ (peak-ROI 1400-1500 cm⁻¹) and 1654 cm⁻¹ (peak-ROI 1620-1694 cm⁻¹). The Raman bands at 1441 cm⁻¹ and 1654 cm⁻¹ are assigned to vibrations CH₂ and C=C, respectively (31). The unsaturation ratio was calculated as the ratio of band areas 1654 cm⁻¹/1441 cm⁻¹ (31).

Condition	Number of lipid droplets = number spectra over 3 wells	Number of adipocytes analysed over 3 wells per condition
10-week (cohort 1)		
CT	519	41
SBA24%	111	13
SBA18%	299	30
SBA12%	134	10
SBA0%	189	15
Total	1252	109
4-week (cohort 1)		
CT	45	18
SBA18%	109	25
Total	154	43

Table 5. Details of lipid droplets studied in each condition of the 10-week and 4-week protocols (cohort 1).

9. Mineralisation Quantification

For the samples of 10-week cohort 1 study, mineralisation level was quantified using the same protocol previously described by Bruedigam *et al.* (869). Briefly, cells were harvested in a solution of PBS 1X/Triton 0.2%/HCl 6 M and disrupted by sonication. After, 5 μ l of HCl 6 M was added to 95 μ l of each sample and incubated overnight at 4°C. Following by centrifugation at 1500 \times g for 5 min, the protein content was determined using the DC protein assay kit BioRad. The mineralisation content was quantified spectrophotometrically around 595nm.

10. RNA Sequencing and Data Analysis

Library preparation for mRNA sequencing (mRNA-seq) was done using the KAPA mRNA HyperPrep Kit, following the manufacturer's instructions. The sequencing of libraries was done using the NovaSeq6000 system (SP flow cell; 2x100 bp mode). RSEM counts data were imported in R v4.1.2 for data processing and all statistical analyses. In addition to bioinformatics quality-control, a principal component analysis was performed to identify outliers and/or technical bias from known technical variables. No outliers were identified and none of the technical variables were found significant on the first three principal components, accounting for 59.16 % of the variance. Differential expression analyses were performed using

the Bioconductor R package DESeq2 (v1.34.0) on genes exhibiting an average count strictly greater than one, a median count strictly greater than zero and a non-null variance across the samples used in the analysis. Results were annotated with genes symbol (HGNC), UniProt Swiss-Prot IDs, and Entrez gene IDs using the Bioconductor R package biomaRt (v2.50.2). Over-representation analyses (ORA) were performed using the Bioconductor R package clusterProfiler (v4.2.2) and the following databases: Reactome, Gene Ontology Biological Process, Gene Ontology Cellular Component, Gene Ontology Molecular Function, and KEGG. Differentially expressed genes were considered in ORA if Benjamini-Hochberg false discovery rate were below 5 %, and pathway enrichments were considered significant for a Benjamini-Hochberg false discovery rate below 5 %.

11. RNA Extraction and Reverse Transcription

Total RNA was extracted from BMSC and ST2 cell cultures using Extract-all (Eurobio, Les Ulis, France). At the end of cell culture, 1ml of Extract-all was added per 1 well of a 24-well plate and samples were transferred to a 1.5 ml collecting tube. Next step was to add 200µl of chloroform (Thermo Scientific; J67241.AP) per each tube and spin samples at 4°C and 12 000 g for 15 min. The upper aqueous phase containing RNA was removed and the rest of the protocol was conducted according to RNeasy Mini Kit (QIAGEN; 74104) manufacturer's protocol. Total RNA was quantified using the NanoDrop 2000 spectrophotometer (Thermo Scientific, Labteck, Palaiseau, France).

12. Real-Time PCR

Reverse transcription of samples was conducted using the Maxima First Standard cDNA Synthesis Kit for RT-qPCR (Thermofisher; K1642) manufacturer's protocol. Quantitative PCR (qPCR) experiment required 5µl of PowerUp SYRB Green Master Mix (Applied Biosystems; A25742), 1µl of upstream primer, 1µl of downstream primer and 2µl of water, per reaction (870). The sequences of the primers (TibMolBiol, Berlin, Germany), annealing temperature and GenBank reference for each of the genes analysed with efficiency test are shown in Table 6.

Gene	Primer Sequences	Annealing temperature	Product length	GenBank
<i>18S</i>	F: ATTCCGATAACGAACGAGAC R: GCTTATGACCCGCACTTACT	60 °C	297 bp	X03205
<i>Gapdh</i>	F: GGCATTGCTCTCAATGACAA R: TGTGAGGGAGATGCTCAGTG	62 °C	200 bp	NM_008084
<i>Pparg2</i>	F: TCGCTGATGCACTGCCTATG R: GAGAGGTCCACAGAGCTGATT	60 °C	103 bp	NM_011146
<i>Adipoq</i>	F: TGTTCCTCTTAATCCTGCCCA R: CCAACCTGCACAAGTTCCTT	60 °C	104 bp	NM_009605
<i>Lep</i>	F: GAGACCCCTGTGTCTGGTTC R: CTGCGTGTGTGAAATGTCATTG	60 °C	139 bp	NM_008493
<i>Glut4</i>	F: ACTCTTGCCACACAGGCTCT R: AATGGAGACTGATGCGCTCT	62 °C	174 bp	NM_009204
<i>Runx2</i>	F: GCCGGGAATGATGAGAACTA R: GGACCGTCCACTGTCACCTT	62 °C	200 bp	NM_001146038.2
<i>Bglap</i>	F: AAGCAGGAGGGCAATAAGGT R: CGTTTGTAGCGGTCTTCA	60 °C	364 bp	L24431
<i>Sp7</i>	F: ATGGCGTCCTCTCTGCTTG R: TGAAAGGTCAGCGTATGGCTT	54 °C	237 bp	NM_130458
<i>Coll1a1</i>	F: GGTGAGCCTGGTCAAACGG R: ACTGTGTCCTTTCACGCCTT	60 °C	189 bp	NM_007743
<i>Sirt1</i>	F: TAGGGAACCTTTGCCTCATC R: GGCATATTCACCACCTAGCC	51 °C	100 bp	NM_019812.2

Table 6. Primer sequences and conditions of quantitative RT-PCR (PART 1).

13. SIRT1 ELISA Assay

Plasma was extracted from 64 AN patients from Lille University hospital, which were investigated using MRI and DXA scans (411). Subjects, aged between 18 and 35 years old, had an average BMI of 16.94. These samples were used to conduct the quantification of blood circulating level of SIRT1.

SIRT1 concentration was determined by a monoclonal antibody-based ELISA method using a commercially available human SIRT1 ELISA kit (MyBioSource, Cod. GDMBS705558). Kit precision was estimated with an inter- and intraassay coefficient of variation of 10 and 8%, respectively, and a detection range of 0.156ng/ml – 10ng/ml. An equal quantity of primary mouse anti-human SIRT1 monoclonal IgG was used to coat microtiter plates. Following the washing step, secondary avidin conjugated horseradish peroxidase was added to wells. After one hour of incubation, washings of the wells were performed. In each well, 100 µl of standard and plasma samples were pipetted. Seven different concentrations of purified SIRT1 (0.15,

0.312, 0.625, 1.25, 2.5, 5.0, and 10 ng/ml) were used to plot a standard curve. Absorbance was measured in each well using a spectrophotometric plate reader at a single wave of 450 nm.

14. Statistical Analysis

The 10-week (cohort 1) study was performed with 6 specimens per condition, except of mineralisation experiment, which had 4 replicated per group. The 4-week (cohort 1) study was performed with 5 individuals per condition. Cohort 2 experiments for both 10-week and 4-week protocols used 12 mice per condition. The median and interquartile range were calculated for the groups. Due to the low number of replicates, the normality of the data could not be tested. In 10-week (cohort 1) study and siRNA experiments we performed Kruskal-Wallis One-Way ANOVA test, to show the significance between all the conditions. Additionally, we conducted Dunn's test in order to see the relationships between specific pairs of conditions. For the rest of the studies, we performed Mann–Whitney's test to see the statistically significant relationship between the two particular conditions. All tests were performed using GraphPad Prism software. Differences with $p < 0.05$ were considered statistically significant.

III.RESULTS

1. Circulating SIRT1 has a negative association with femoral head fat in AN patients

With help of Lille University hospital, we obtained the plasma samples from AN patients, as well as data of fat fraction in femoral neck of individuals. AN patient plasma samples were used to quantify blood circulating SIRT1 level. These data were used to conduct the correlation analysis, between SIRT1 plasma concentration and femoral neck fat fraction. Results showed a negative association between these two parameters (Fig. 25). This suggests that lack of SIRT1 can be involved in fat accumulation in BM, emphasising the importance of SIRT1 investigation in SBA mouse model.

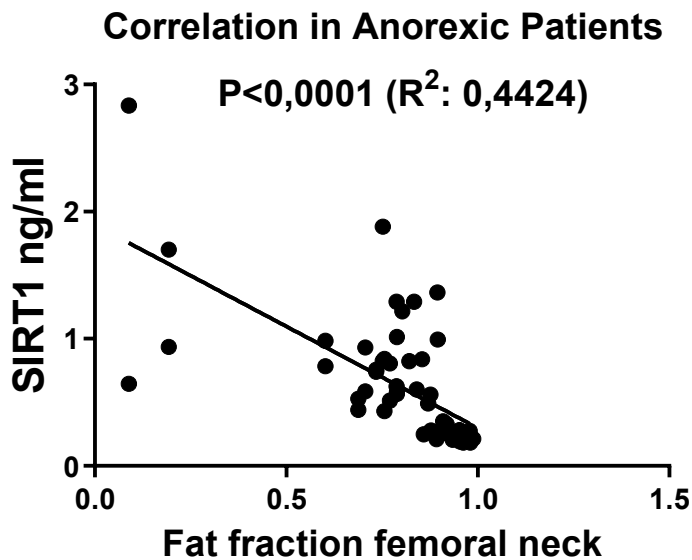


Figure 25. Correlation analysis of SIRT1 plasma concentration and fat fraction in femoral neck on AN patients. Negative correlation between circulating SIRT1 concentration and femoral neck fat fraction, suggests close relationship between femoral neck BMA and lack of SIRT1.

2. Severity Level of Energy Deficit in Mice Affect Bone Phenotype and BMSC Differentiation Capacity

The 10-week SBA protocols induced a significant decrease in mouse body weight (12%, 18%, 24%) and altered fat, lean mass and bone mineral content

To study the effect of energy deficit severity on bone and BMSCs, we performed four different SBA protocols on female mice. The weight loss of 0%, 12%, 18% and 24% from the initial mouse weight, was induced over 10 weeks. Prior to the study, mice were randomised into five experimental groups that did not display significant differences in body weight at day 0. Mice

from the control group (*ad libitum* and not separated) displayed a significant body weight increase (+22.42% vs. D0) after 10 weeks (Fig. 26A). In the SBA 0% group, no significant weight change (+4.39% vs. D0) was observed, as this condition did not imply weight change (Fig. 26A). In all other SBA groups, we observed a significant decrease in weight after 2 weeks of protocol and this decrease was maintained until the end of the 10 weeks (SBA 12% (-12.97%) vs. D0; SBA 18% (-17.27%) vs. D0; and SBA 24% (-23.17%) vs. D0) ($p < 0.005$ vs. D0) (Fig. 26A). After quantifying average cumulative food consumption, we observed that mice from SBA groups all exhibit higher or same amount of food consumed (vs. CT), suggesting that SBA protocol induces increase in energy expenditure leading to weight loss (Fig. 26D). Following mice sacrifice, after 68 days of SBA protocol, adipose tissue and liver weigh were measured. In moderate (18%) and severe (24%) weight loss groups exhibited a 77% and 79% decrease (vs. CT) in subcutaneous adipose tissue (SCAT), respectively (Fig. 26C). Moreover, visceral adipose tissue (VAT) weight was dramatically decreased in these weight loss groups (SBA18% -95% vs. CT; SBA 24%: -94% vs. CT) (Fig. 26C). Moreover, only in 12% SBA group we saw a significant increase in total liver weight (14% vs CT) (Fig. 26C). Decrease in adipose tissue depots could be also seen through the reduction in total mice fat composition (59-64%, $p = 0.0001$ vs. CT) (Fig. 25E). Also, decrease in lean mass in mice from the SBA groups 12% (-19% vs. CT) and 24% (-22% vs. CT) was determined. Interestingly, this parameter was significantly reduced only in weight loss conditions, while in the SBA 18% group, lean mass just showed a tendency to decrease without statistically significant change (Fig. 26F). Reduction in lean mass can be potentially associated with significant reduction in BMC. The results of DEXA analysis showed a significant decrease in total body bone mineral content (BMC) only in light (12%) and moderate (18%) weight loss conditions (SBA 12% -17% vs. CT; SBA 18% -15% vs. CT) (Fig. 26G). The study of the BMC at specific sites, revealed that all three weight loss conditions induced a significant decrease in femur BMC - SBA 12% (-27% vs. CT), 18% (-29% vs. CT) and 24% (-30% vs. CT) (Fig. 26H). However, only the SBA 18% group showed a significant decrease in the BMC of lumbar vertebrae (L3-L5) (SBA 18% -23% vs. CT) (Fig. 26I). Overall, these data highlight that lean mass and fat mass parameters can be potentially associated with BMC under weight loss conditions, as a significant decrease in whole-body BMC or femoral/vertebral BMC together with lean and fat mass was observed only in the weight loss mice.

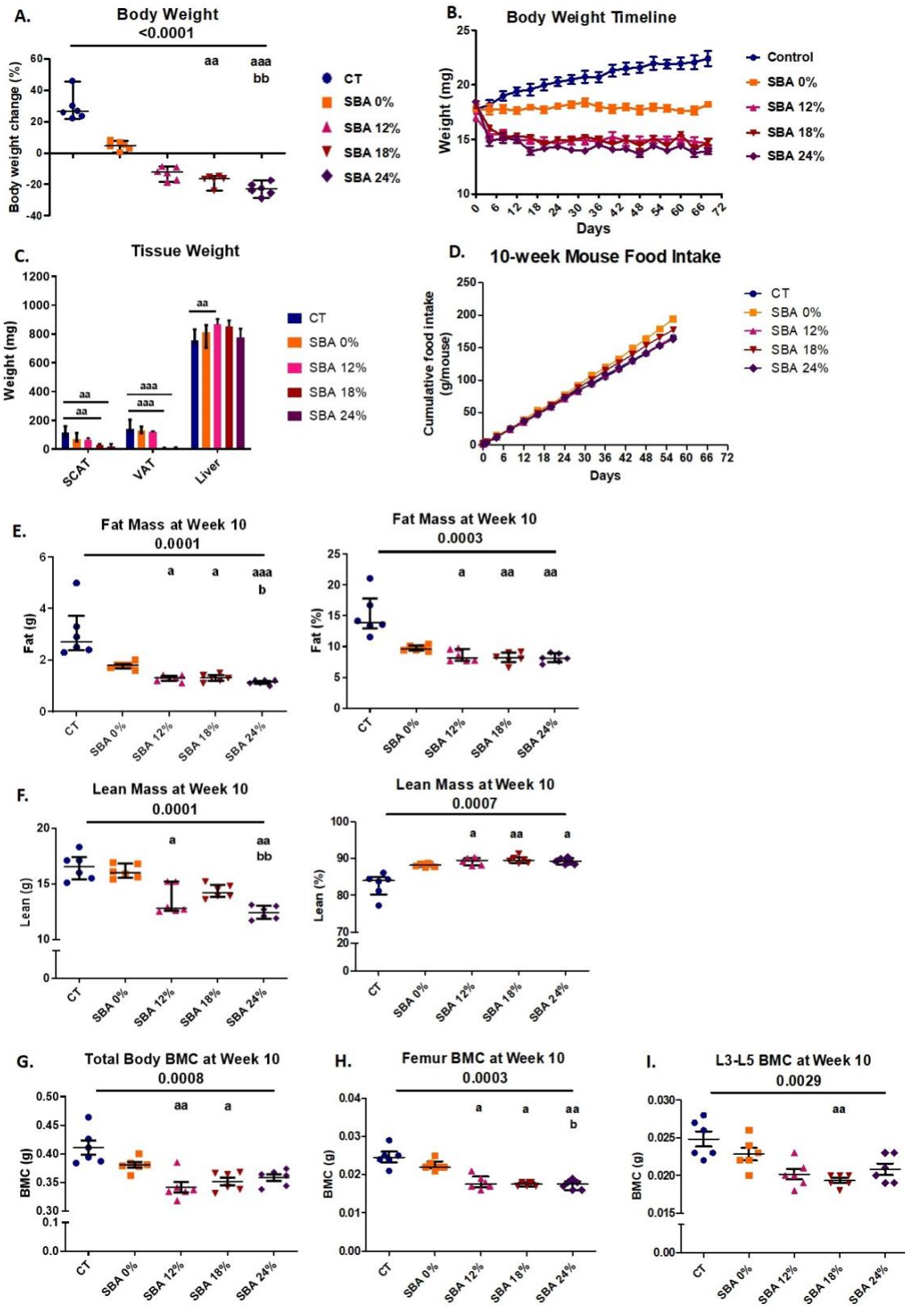


Figure 26. Body and tissue mass, BMC, fat and lean mass in mice after 10 weeks of SBA protocols of different severity. The body weight and composition analysis were performed on standard condition (CT), constant weight group (SBA 0%) and three weight loss groups with different severity levels (SBA 12%, 18% and 24%). A. Graph represents a percentage body weight loss on mice between day 0 and 10 weeks of SBA protocol; B. Body weight timeline was presented for each of SBA condition, represents average mouse body weight for every 6 days of the protocol (starting at day 0 and ending at day 68); C. Mice tissue weight after 10-week protocol – subcutaneous adipose tissue (SCAT), visceral adipose tissue (VAT), total liver and liver right lobe (RL); D. Cumulative food intake was recorded, as the sum of the mean food intake per mouse from day 1 to day 60; E-F. Fat mass and lean mass content, respectively, were evaluated for each mouse and condition after 10 weeks of SBA protocol, data presented in grams (g) and in % of total mice weight (fat + lean + total BMC); G-I. Study of total mouse body mineral content (BMC), femur BMC and vertebra (L3-L5) BMC, respectively, were evaluated for each animal and each condition after 10 weeks of SBA protocol. Data represent median and interquartile range; n=6. Statistical analysis was performed using Kruskal-Wallis One-Way ANOVA test and Dunn's test; a - $p < 0.05$, aa - $p < 0.005$ and aaa - $p < 0.0005$ when compared to the CT group (b – when compared to the SBA 0% group).

Only 18% and 24% weight loss groups resulted in a significant decrease in trabecular and cortical thickness, without an increase in bone marrow adiposity

To determine the effect of SBA severity on bone microarchitecture, we conducted proximal tibia micro-CT analysis. Bone volume fraction (Bv/Tv) showing the volume of mineralized trabecular bone on the total marrow cavity volume was not affected by the SBA protocols (Fig. 27A). Trabecular thickness (Tb.Th) was significantly decreased only under severe weight loss conditions (SBA 24%: -29% vs. CT) (Fig. 27B). In contrast with the trabecular bone thickness, the trabecular number (Tb.N) was shown to display a tendency to exhibit higher level (+42%) in the severe energy deficit condition (24% weight loss), with no effect in other conditions (Fig. 27C). Furthermore, trabecular spacing (Tb.Sp.) was significantly lower only in the SBA 24% condition (-18% vs. CT), suggesting the potential association between low Tb.Th, high Tb.N and further low Tb.Sp (Fig. 27D). This potentially shows that reduction of Tb.Th in SBA 24% condition was compensated with an increase in Tb.N, furthermore the increase in Tb.N led to reduction of Tb.Sp (Fig. 27). Bone fragility was assessed through the study of cortical thickness (Cort.Th), which was affected by the 18% and 24% SBA protocols. Indeed, the 18% and 24% weight loss in mice resulted in 16% and 17% decreases in this parameter, respectively ($p = 0.0001$ vs. CT) (Fig. 27E). After having a closer look at the average tibia diameters, we observed that in SBA 18% weight loss group displays a low diameter of periosteum (-5.5% vs. CT), which was accompanied by a 4.5% increase (vs. CT) in endosteum, subsequently leading to loss in Cort.Th (Fig. 27H,I). Similarly, significant reduction of Cort.Th in SBA 24% group can be explained by a 5.3% decrease (vs. CT) in outer tibia diameter and 5.4% increase in inner tibia diameter (vs. CT), indicating a loss in bone wall thickness (Fig. 27H,I).

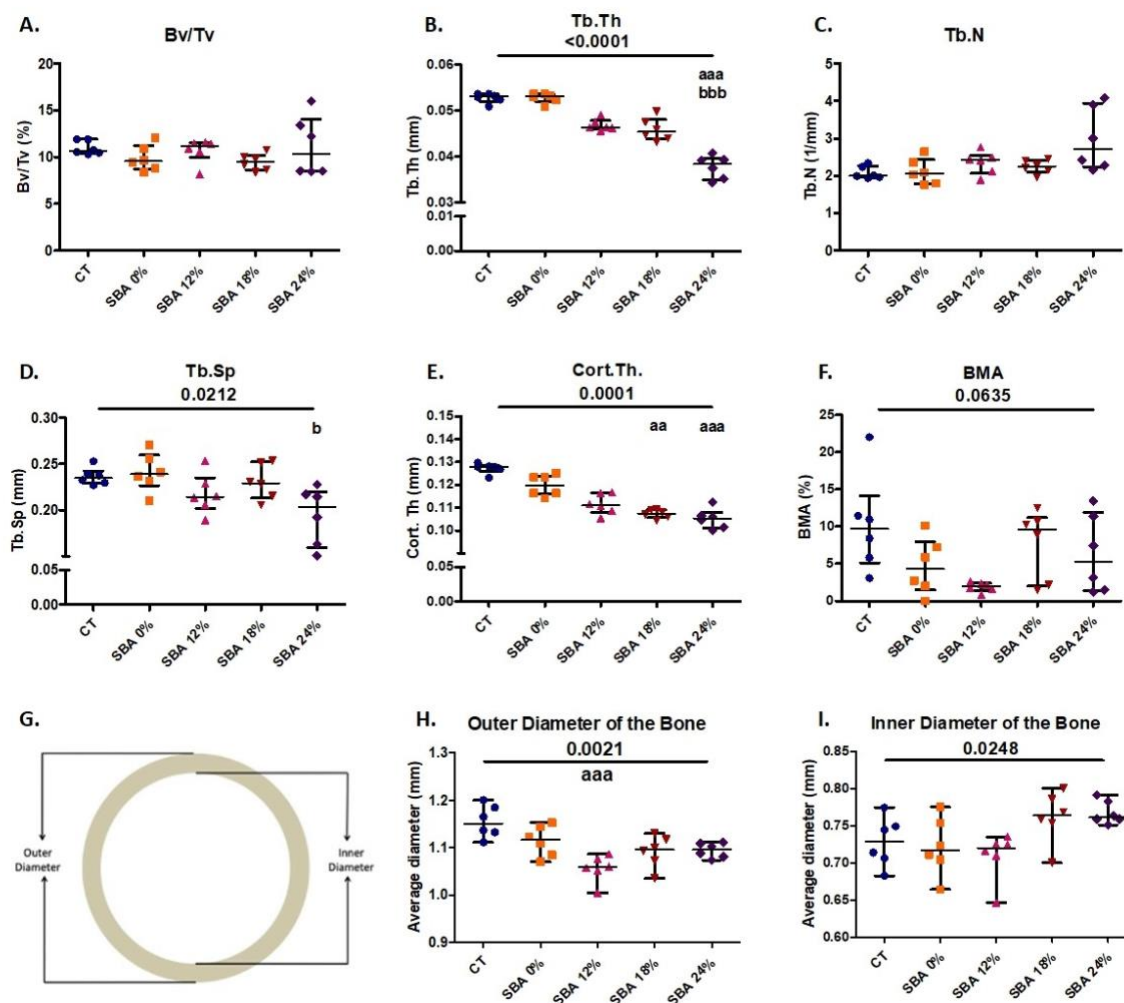
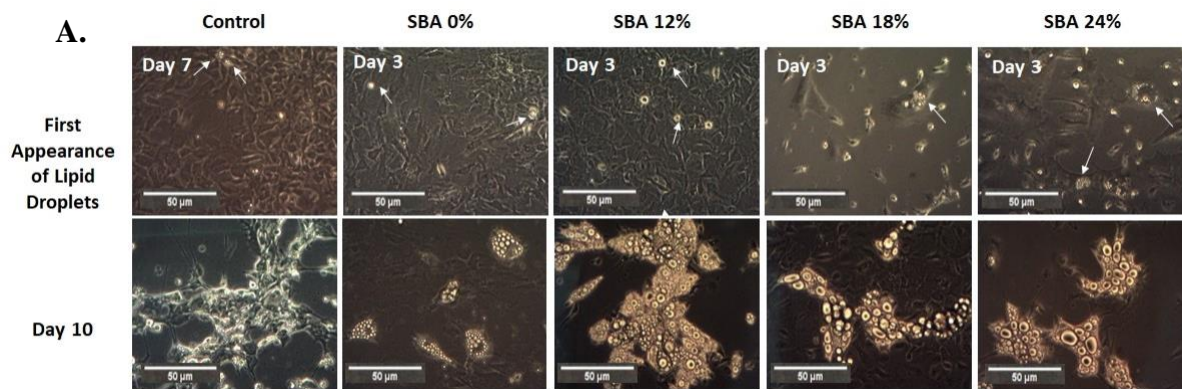


Figure 27. The results of micro-CT analysis of tibia, showing different bone parameters after exposure to 10 weeks of SBA protocols at different levels of severity. A. Bone volume fraction (Bv/Tv) was expressed as a percentage on mineralized tissue in each condition after 10 weeks; B-E. Trabecular thickness (Tb.Th), trabecular number (Tb.N) and trabecular spacing (Tb.Sp), and cortical thickness (Cort.Th), respectively, were evaluated for each animal and each condition after 10 weeks of SBA protocol (expressed in millimetres); F. Bone marrow adiposity (BMA) was calculated as a percentage of BMAT volume in marrow volume; G. Bone cross-section depicting the inner diameter (endosteum) and outer diameter (periosteum) measured for bone thickness, taken from Lapointe *et al.*, 2020 (877); H-I. Average tibia diameter measured including inner section and bone area (outer diameter), and diameter of inner section specifically, respectively. Data represent median and interquartile range; n=6. Statistical analysis was performed using Kruskal-Wallis One-Way ANOVA test and Dunn's test; a - $p<0.05$, aa - $p<0.005$ and aaa - $p<0.0005$ when compared to the CT group (b – when compared to the SBA 0% group).

These results demonstrated the potential link between moderate and severe energy deficit and low Cort.Th. The results of BMA showed a high heterogeneity of the samples in each group. Statistically, there is no significant effect of the severity, but a strong tendency ($p=0.0635$). Because of the heterogeneity inside each group, the number of samples has to be increase, in orde to reach a significance. However, only the SBA 12% group exhibited a tendency of BMA decrease by 82% (vs. CT, $p=0.0637$) after conducting Kruskal-Wallis test (Fig. 27F).

SBA protocol resulted in rapid adipogenesis of BMSCs and weight loss conditions were associated with a decrease in lipid unsaturation levels

During 14 days of the co-differentiation experiment, cells extracted from SBA and control mice were observed under light microscopy. BMSCs extracted from CT mice started to form lipid droplets after the 7th day of co-differentiation. Cells extracted from SBA mice (0%, 12%, 18% and 24%) showed the first appearance of lipid droplets much faster, after the 3rd day of co-differentiation induction (Fig. 28A). This finding suggests that the SBA protocol induces *in vivo* changes in BMSC commitment and that these cells are potentially committed to differentiating into adipocytes. After qualitative study (microscopic observations) of adipocytes on day 10 of differentiation experiment, BMSCs extracted from the SBA 12%, 18% and 24% groups globally seemed to generate greater number and larger adipocytes compared to the CT or SBA 0% groups (Fig. 28A).



B. RAMAN Spectroscopy of 10-week Day 14 Samples

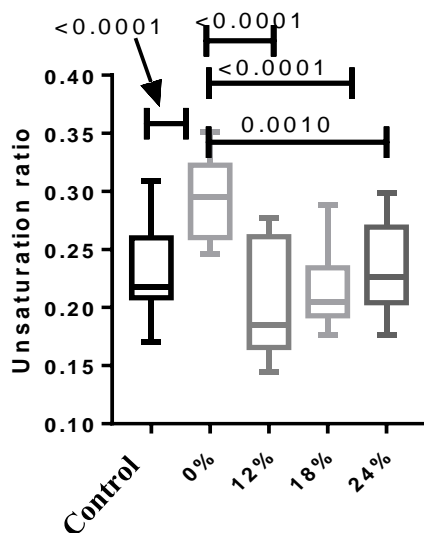


Figure 28. Study of adipocyte first appearance, size and lipid unsaturation ratio in 10-week protocol groups. A. Light microscope images of cells from each condition were taken on different points of differentiation showing the first appearance of lipid droplets and adipocytes at day 10; B. Lipid droplet unsaturation ratio was compared between four SBA groups and the control. The results showed that there is a significant decrease in unsaturation ratio in weight loss groups when compared to the 0% group. The control group did not show a significant difference with weight loss groups (SBA 12%, 18%, 24%). Data represent median and interquartile range; $n=6$. Statistical analysis was performed using Mann–Whitney’s test.

Additionally, Raman spectroscopy analysis was performed for more detailed characterisation of the adipocytes from different groups. The lipid unsaturation levels in the SBA 12%, 18% and 24% groups were significantly lower than those in the SBA 0% group, showing that the severity of energy deficit can lead to a decrease in lipid unsaturation levels (Fig. 28B).

Moderate and severe weight loss conditions (SBA 18% and 24%) resulted in an increase in adipogenic and subsequent decrease in osteoblastogenic potential of BMSCs

In order to confirm the commitment of BMSCs to the adipocyte lineage, the mRNA levels of adipogenic markers in the SBA and CT groups were analysed. The mRNA level of marker genes was measured after 48 hours of cell adhesion and after 14 days of co-differentiation. Interestingly, after 48 hours of adhesion in a standard medium, the unstimulated BMSCs from mice of SBA 24% protocols already exhibited high levels of peroxisome proliferator-activated receptor gamma 2 (*Pparg2*) mRNA (+125% vs. CT), showing a potential commitment to adipogenic differentiation prior to co-differentiation stimulation, and thus suggesting that already *in vivo* BMSCs express early adipogenic markers (Fig. 29A). The SBA 12% and 24% conditions, also showed significant increase in *Pparg2* relative mRNA level (vs. SBA 0%) (Fig. 29A). Furthermore, *Pparg2* mRNA levels were similarly enhanced after induction of co-differentiation in severe weight loss group (SBA 24%: +236% vs. CT) (Fig. 29B). Additionally, the SBA 18% group demonstrated the highest upregulation of *Pparg2* after 14 days of co-differentiation (+ 285% vs. CT and vs. SBA 0%) (Fig. 29B). Other marker genes characterising cell commitment to adipogenic differentiation (leptin (*Lep*)) and glucose transporter member 4 (*Glut4*)) exhibited an increase in the moderate and severe weight loss groups (SBA 18% - *Lep* +1292% vs CT, *Glut4* +807% vs. CT; SBA 24% - *Lep* +1864% vs. CT) (Fig. 29C, E). The adiponectin (*Adipoq*) mRNA level was found to be upregulated only in the SBA 18% group (+53% vs. SBA 0%) (Fig. 29D). However, the 12% weight loss condition displayed the lowest mRNA level of *Adipoq* (Fig. 29D).

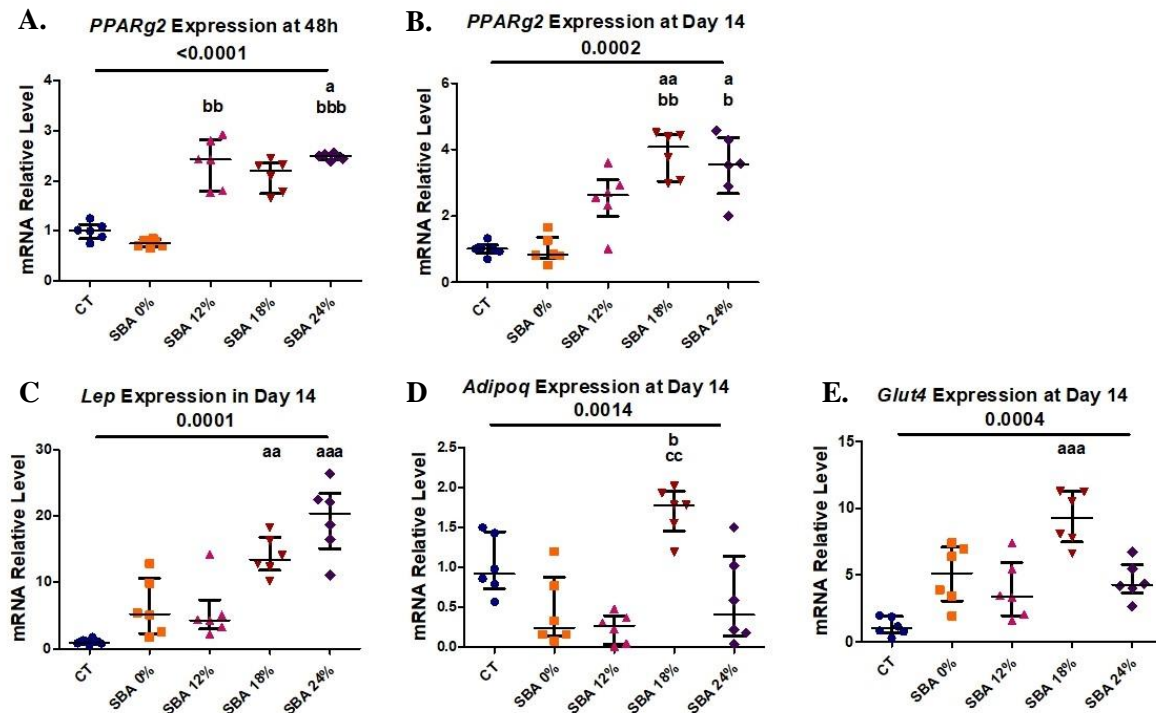


Figure 29. 10-week SBA protocol induced changes in BMSC differentiation comparing to CT. A-B. Relative mRNA expression level of early adipogenic marker gene (*Pparg2*) in CT and SBA groups (0%, 12%, 18%, 24%), cells were cultured for 48 hours in standard growth medium or were exposed to co-differentiation medium for 14 days, respectively; C-E. Relative mRNA expression level of other adipogenic marker genes (*Lep*, *Adipoq*, and *Glut4*, respectively) in CT and SBA groups (0%, 12%, 18%, 24%) after exposure to co-differentiation medium during 14 days. Data represent median and interquartile range; n=6. Statistical analysis was performed using Kruskal-Wallis One-Way ANOVA test and Dunn’s test; a - $p < 0.05$, aa - $p < 0.005$ and aaa - $p < 0.0005$ when compared to the CT group (b – when compared to the SBA 0% group; c – when compared to SBA 12% group). Peroxisome proliferator-activated receptor gamma 2 (*Pparg2*), leptin (*Lep*), adiponectin (*Adipoq*), facilitated glucose transporter member 4 (*Glut4*).

In this study, our aim was to determine whether the severity of SBA causes an imbalance in BMSC lineage commitment, as we initially hypothesised that upregulation of adipogenesis is achieved at the expense of osteoblastogenesis. Thus, after 14 days of co-differentiation, the mineralisation level of CT and SBA cells was studied by quantifying the calcium to protein ratio. The results demonstrated a strong alteration of mineralisation capabilities in moderate and severe weight loss conditions (18% and 24%, on average -82% vs. CT) (Fig. 30A). However, this trend was not statistically significant. Only 18% weight loss condition exhibited significant decrease in mineralisation (vs SBA 0%). The mRNA level analysis showed that the early marker of osteoblastogenesis (runt-related transcription factor 2 (*Runx2*)) was significantly reduced in severe weight loss condition (SBA 24% -55% vs. CT) at 48 hours after cell plating in standard medium (Fig. 30B). Also, after 14 days of exposure to co-differentiation

medium both moderate and severe weight loss conditions induced changes in *Runx2* mRNA level (SBA 18% -75% vs. CT; SBA 24% -70% vs. CT) (Fig.30B, C). Interestingly, further study of other markers of osteoblastogenesis (collagen1A1 (*Coll1a1*), osteocalcin (*Bglap*) and osterix (*Sp7*)) at the end of co-differentiation revealed a reduction in mRNA levels only in the moderate and severe weight loss groups (*Coll1a1* - SBA 18% -77% vs SBA 0%, SBA 24% - 83% vs. SBA 12%; *Bglap* - SBA 18% -73%, SBA 24% -72% vs. CT; *Sp7* - SBA 18% -81%, SBA 24% -77% vs. CT) (Fig. 30D-F). Overall, the results suggest that an increase in adipogenesis occurs at the expense of osteoblastogenesis and that BMSCs extracted from SBA mice are apparently more committed to adipogenic lineage.

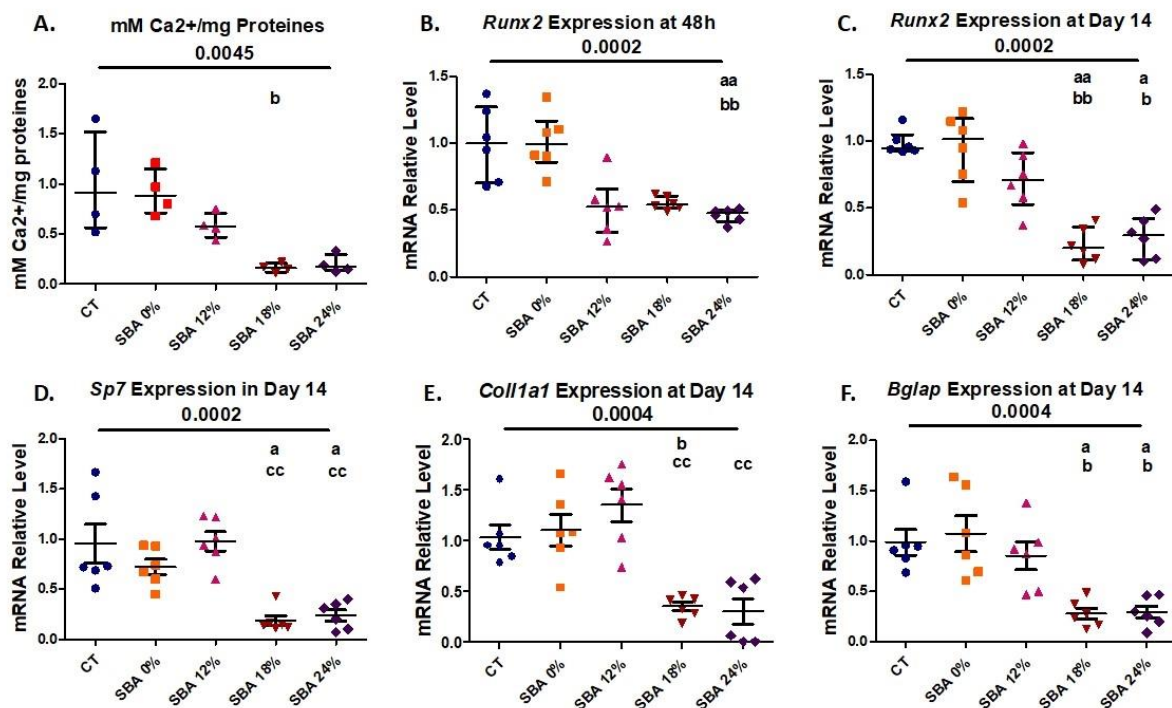


Figure 30. 10-week SBA protocol induced an alteration in osteoblastogenesis comparing to CT group. A. Mineralisation level of CT and SBA groups (0%, 12%, 18%, 24%) quantified by measuring the calcium to protein ratio; B-C. Relative mRNA expression level of early osteoblastogenic marker gene (*Runx2*) in CT and SBA groups (0%, 12%, 18%, 24%), cells were cultured for 48 hours in standard growth medium and for 14 days were exposed to co-differentiation medium, respectively; D-F. Relative mRNA expression level of other osteoblastogenic marker genes (*Sp7*, *Coll1a1*, and *Bglap*, respectively) in CT and SBA groups (0%, 12%, 18%, 24%) after exposure to co-differentiation medium for 14 days. Data represent median and interquartile range; Mineralisation study n=4, qPCR n=6. Statistical analysis was performed using Kruskal-Wallis One-Way ANOVA test and Dunn's test; a - p<0.05, aa - p<0.005 when compared to the CT group (b – when compared to the SBA 0% group; c – when compared to SBA 12% group). Runt-related transcription factor 2 (*Runx2*), osterix (*Sp7*), collagen1a1 (*Coll1a1*), osteocalcin (*Bglap*).

Alterations in BMSC differentiation capacity can be associated with a decrease in Sirt1 expression level

Recently, Louvet *et al.* demonstrated that the 18% SBA protocol causes change in BMSC lineage commitment towards adipogenesis and a decrease in *Sirt1* mRNA level and activity, which was concluded to be a potential regulator of BMSC differentiation (2). In the present study, we examined the impact of weight loss severity on the expression level of *Sirt1* mRNA. The results of the SBA 18% weight loss protocol showed a 67% decrease (vs. CT) in *Sirt1* mRNA in BMSCs after 48 hours of adhesion in growth medium and a 75% decrease (vs. CT) after 14 days of co-differentiation (Fig. 31). These findings confirmed previously published data. Additionally, the *Sirt1* mRNA level was significantly altered in the 24% group (-60% vs. CT) after 48 hours of cell adhesion and after 14 days of co-differentiation (-68% vs. CT) (Fig. 31). So, decrease in *Sirt1* mRNA levels under moderate and severe weight loss conditions could be associated with an increase in adipogenic mRNA markers and a subsequent downregulation of osteoblastogenesis in BMSCs.

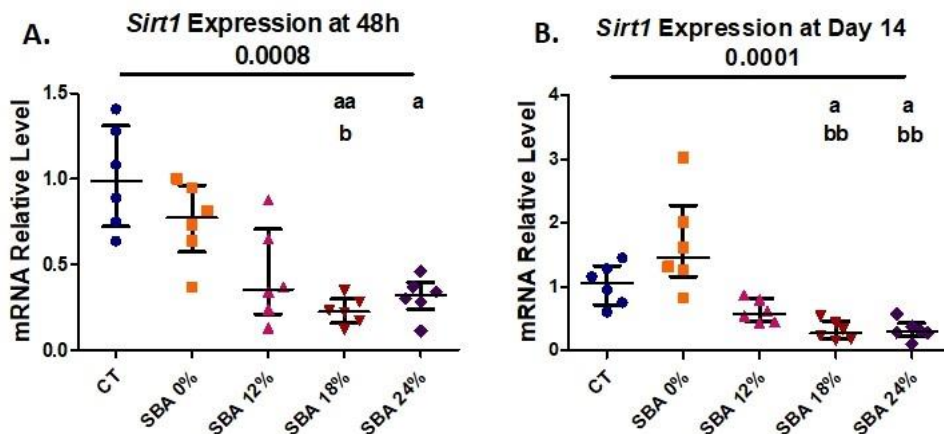


Figure 31. 10-week SBA protocol induced a suppression of *Sirt1* mRNA level. A-B. Relative mRNA expression level of sirtuin type 1 (*Sirt1*) in CT and SBA groups (0%, 12%, 18%, 24%), cells were cultured for 48 hours in standard growth medium and for 14 days were exposed to co-differentiation medium, respectively. Data represent median and interquartile range; n=6. Statistical analysis was performed using Kruskal-Wallis One-Way ANOVA test and Dunn's test; a - $p < 0.05$, aa - $p < 0.005$ when compared to the CT group (b – when compared to the SBA 0% group).

3. Duration of Energy Deficit in Mice Affect Bone Phenotype and BMSC Differentiation Capacity

The short term (4-week) SBA protocol induced a significant decrease in mouse body weight (18%) and was shown to cause changes only in fat mass

Long-term SBA protocols (10-week) have been shown to induce changes in bone and mouse BMSC differentiation capacity. However, we were interested in the effect of duration of energy deficit on the mouse bone composition and BMSC differentiation capacity. Therefore, we conducted a 4-week SBA protocol. In the 10-week study detailed above, the SBA 18% group exhibited alterations in bone parameters and in BMSC differentiation capacity, confirming the hypothesis that adipogenesis is upregulated in these cells at the expense of osteoblastogenesis. Based on these findings, we compared CT mice with 18% weight loss mice after exposure to the SBA protocol for 4 weeks.

Six days after the beginning of the protocol, SBA mice reached the targeted body weight loss of 18% (-18.8% vs. D0) after 4 weeks (Fig. 32A,B). After studying weight differences between CT and SBA 18% groups at the end of 4-week protocol, we observed that SBA group weight was lower than CT group just by 18% (Fig. 32B). The weight of fat depots, SCAT and VAT, was reduced by 38% and 85% (vs. CT), respectively (Fig. 32C). Average cumulative food consumption of mice was found to be slightly higher in SBA group comparing to control mice after 10 days of SBA protocol (Fig. 32D). This suggests that the level of energy expenditure in SBA mice is significantly higher than in CT, as despite an increase in mouse food consumption, we observe a decrease of 18% in mouse body weight (vs. D0). Interestingly, in contrast with 10-week protocol, 18% weight loss in mice during a short period of time resulted in increase in liver mass. Total liver mass was increased by 20% (vs. CT) (Fig. 32C). After the study of body composition, it was concluded that the 4-week SBA protocol induced alterations only in mice fat mass (-50% vs. CT), with no change in BMC or lean mass (Fig. 32E-I).

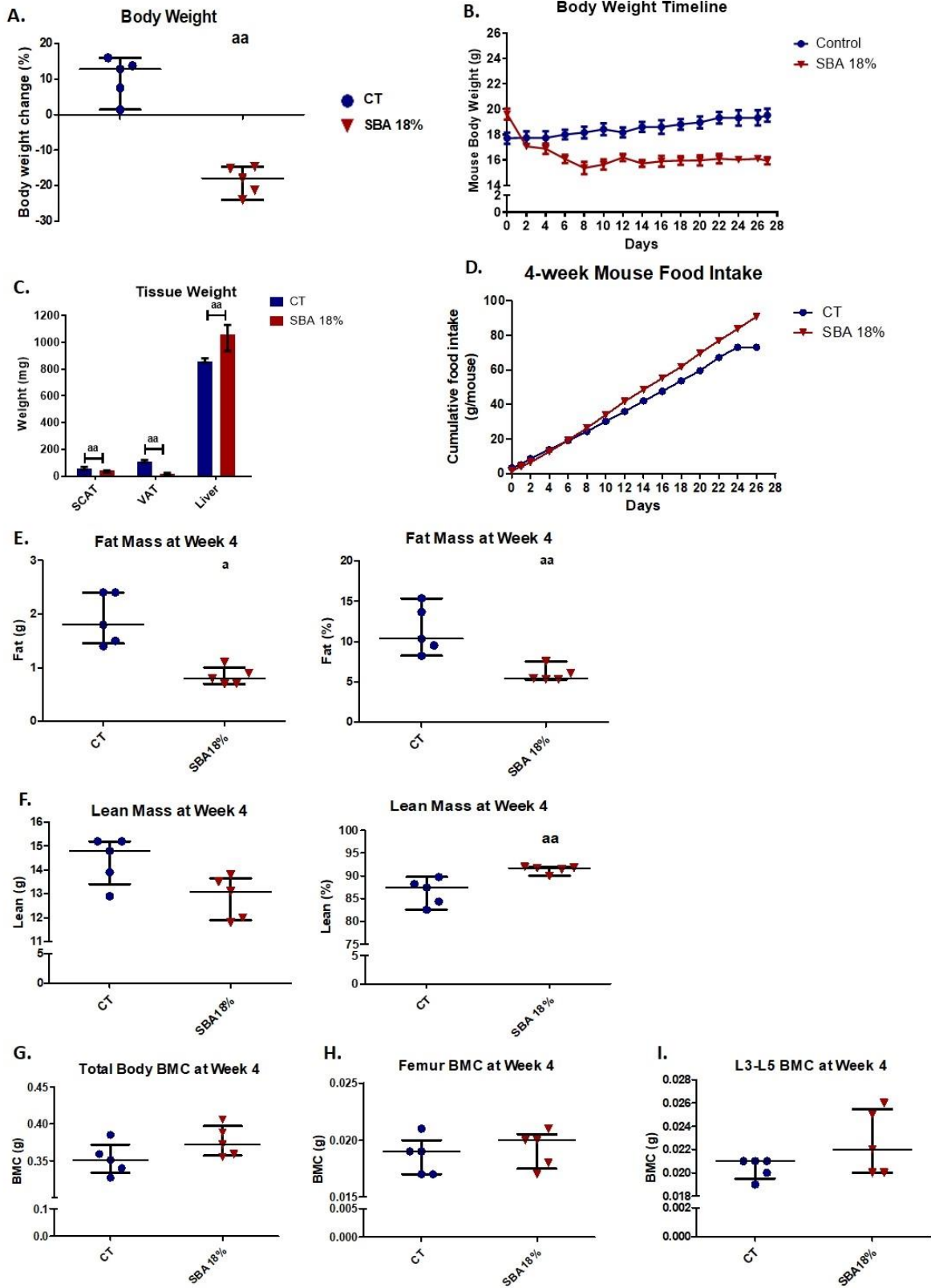


Figure 32. Body mass, BMC, fat and lean mass in mice after 4 weeks of SBA protocol (cohort 1). The body weight and composition analysis were performed on standard condition (CT) and weight loss group (SBA 18%). A. Graph represents a percentage body weight loss on mice between day 0 and 4 weeks of SBA protocol; B. Body weight timeline was presented for each of SBA condition, represents average mouse body weight for every 2 days of the protocol (starting at day 0 and ending at day 28); C. Mice tissue weight after 4-week protocol – subcutaneous adipose tissue (SCAT), visceral adipose tissue (VAT), total liver; D. Cumulative food intake was recorded, as the sum of the mean food intake per mouse from day 1 to day 27. F-E. Fat mass and lean mass content, respectively was evaluated for each mouse and condition after 4 weeks of SBA protocol, data presented in grams (g) and in % of total mice weight (fat + lean + total BMC); G-I. Study of total mouse body mineral content (BMC), femur BMC and vertebra (L3-L5) BMC, respectively, evaluated for each animal and each condition after 4 weeks of SBA protocol. Data represent median and interquartile range; n=5. Statistical analysis was performed using Mann–Whitney’s test; a - $p < 0.05$, aa - $p < 0.005$, when compared to the CT group.

The 4-week SBA protocol induced a significant decrease in trabecular thickness, without affecting other bone parameters or BMA

Additionally, the bone microarchitecture results showed that the short SBA protocol induced changes in Tb.Th (-16% vs. CT), a very sensitive parameter, but did not lead to alterations in Bv/Tv, Tb.N, Tb.Sp or Cort.Th (Fig. 33A-E). Looking in detailed on tibia diameter, it can be observed that there in an increase in endosteum diameter, indicating potential bone resorption taking place (Fig. 33H). However, lack of change in Cort.Th can be explained through an increase in periosteum diameter, which results in compensation (Fig. 33G). Moreover, bone marrow adiposity was not affected by the 4-week SBA protocol (Fig. 33F). Thus, the 4 weeks of the protocol were not enough to induce major changes in bone microarchitecture parameters, unlike the 10-week duration.

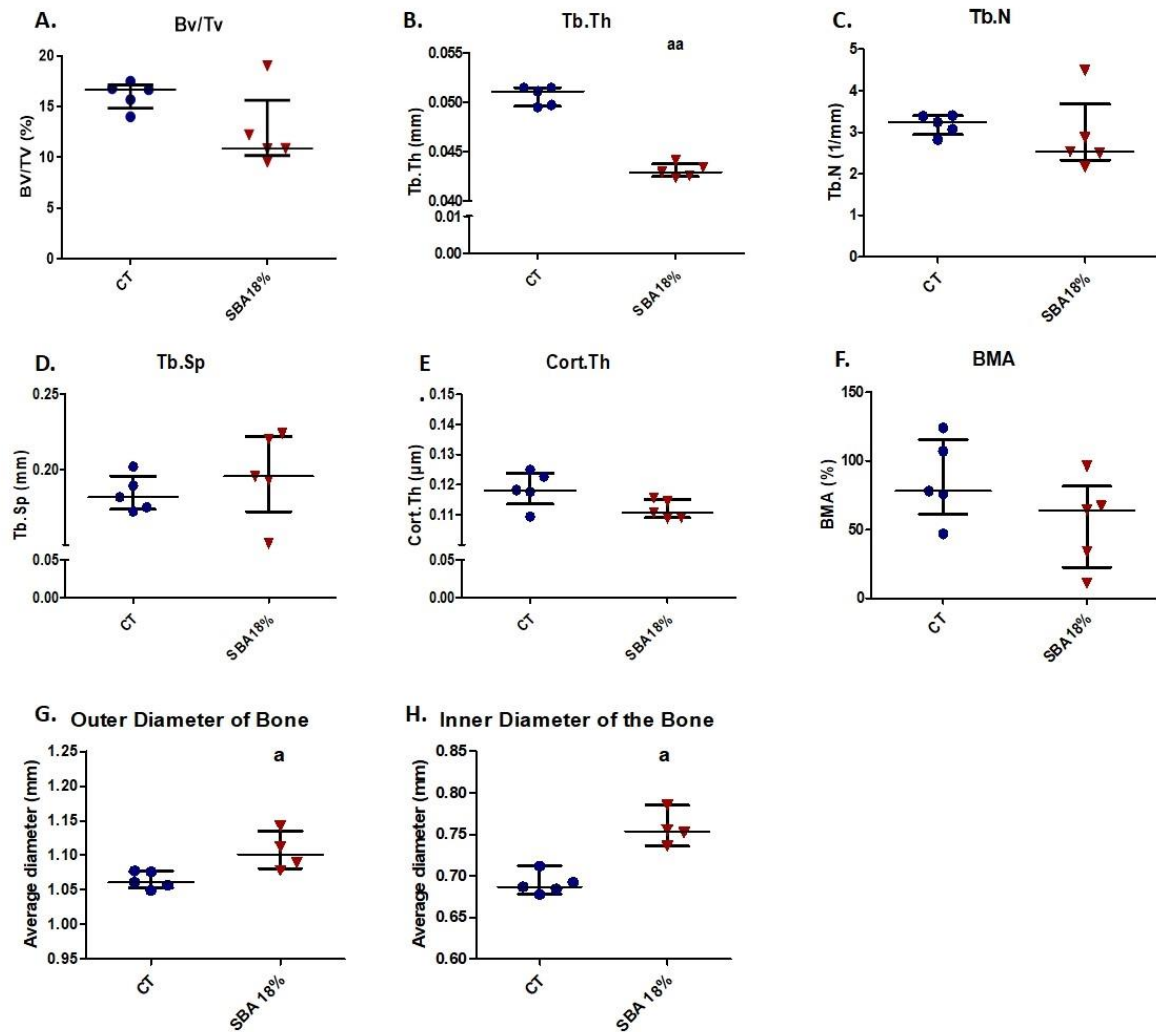
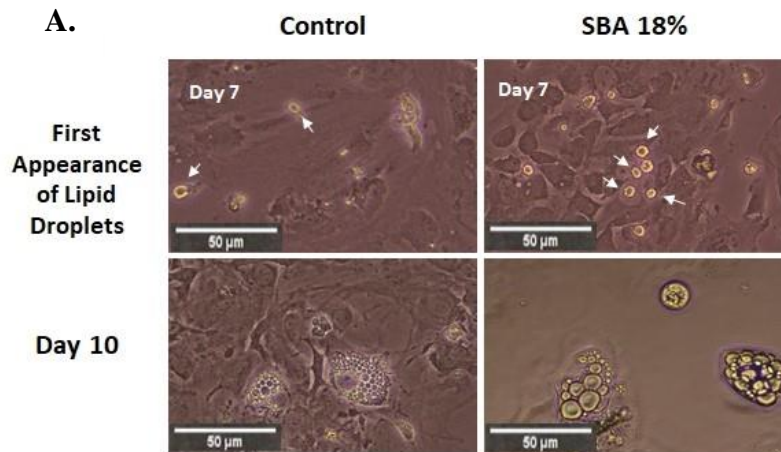


Figure 33. The results of micro-CT analysis of tibia, showing different bone parameters after exposure to 4-week SBA protocol. A. Bone volume fraction (Bv/Tv) was expressed as a percentage on mineralized tissue in each condition after 4 weeks; B-E. Trabecular thickness (Tb.Th), trabecular number (Tb.N) and trabecular spacing (Tb.Sp), and cortical thickness (Cort.Th), respectively, were evaluated for each animal and each condition after 4 weeks of SBA protocol (expressed in millimetres); F. Bone marrow adiposity (BMA) was calculated as a percentage of BMAT in marrow volume; G-H. Average tibia diameter measured including inner section and bone area (outer diameter), and diameter of inner section specifically, respectively. Data represent median and interquartile range; n=5. Statistical analysis was performed using Mann-Whitney's test. In C, aa - $p < 0.005$ when compared to CT group.

Reduced length of SBA protocol did not result in alterations of BMSC differentiation capacity

BMSCs were extracted from bone marrow and co-differentiation into osteoblasts and adipocytes was induced. This, followed by the cells study under a light microscope. Images showed that the first appearance of lipid droplets took place on the 7th day of co-differentiation in both the CT and SBA 18% groups (Fig. 34A). Additionally, after 10 days of co-differentiation, there was no difference observed in the accumulation of adipocytes in SBA 18% vs. CT (Fig. 34A). Therefore, the 4-week SBA protocol did not induce a shift of BMSCs towards adipocyte differentiation and did not induce changes in lipid accumulation capacities, as it was suggested by the results of the 10-week experiments.

Furthermore, similarly to the 10-week protocol, analysis of lipid unsaturation level by Raman spectroscopy showed no difference in lipid unsaturation levels between the control and SBA 18% groups after 4 weeks (Fig. 34B).



B.
**RAMAN Spectroscopy of
 4-week Day 14 Samples**

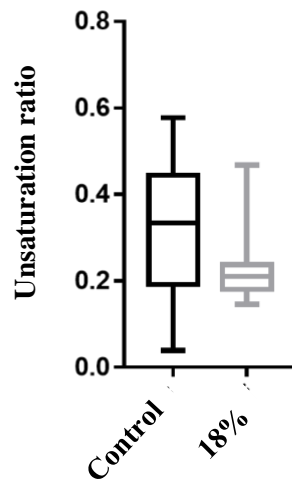


Figure 34. Study of adipocyte first appearance, size and lipid unsaturation ratio in 4-week protocol groups. A. Light microscope images of cells from each condition were taken on different points of differentiation showing the first appearance of lipid droplets and adipocytes at day 10; B. Lipid droplet unsaturation ratio was compared between the 18% SBA group and the control, and no difference was found between the two groups. Data represent median and interquartile range; n=5. Statistical analysis was performed using Mann–Whitney’s test.

Similar to the 10-week SBA study, we analysed the relative mRNA levels of adipogenic/osteoblastogenic genes in extracted BMSCs. The results of the early adipogenic marker gene (*Pparg2*) showed that after 48 hours of proliferation in standard growth medium, BMSCs extracted from SBA 18% mice had significantly increased expression levels (+350% vs. CT) (Fig. 35A). However, this upregulation of *Pparg2* expression was not long term, and after 14 days of co-differentiation, there was no significant difference observed between the two conditions (Fig. 35B). The analysis of mature adipocyte marker genes (*Lep*, *Adipoq*, *Plin1*) demonstrated no change in the SBA 18% group compared to the CT group after 14 days of co-differentiation (Fig. 35C-F).

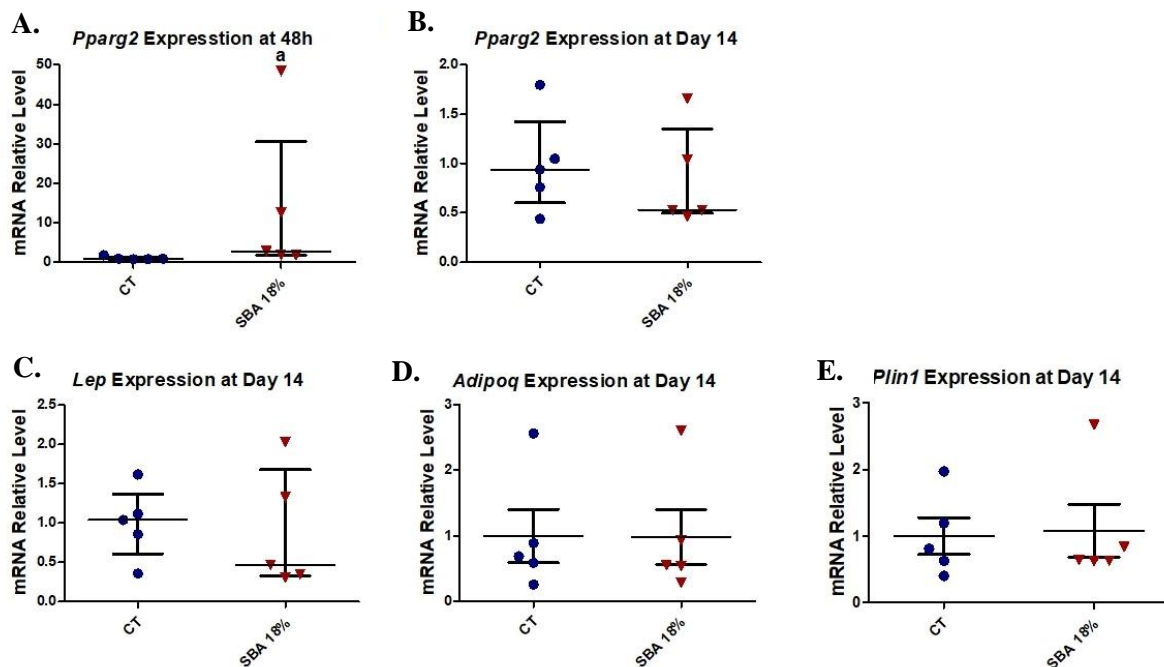


Figure 35. Study of adipogenic marker gene expression in BMSCs. A-B. Relative mRNA expression level of early adipogenic marker gene (*Pparg2*) in CT and SBA (18%) groups, cells were cultured for 48 hours in standard growth medium and for 14 days were exposed to co-differentiation medium, respectively; C-E. Relative mRNA expression level of other adipogenic marker genes (*Lep*, *Adipoq* and *Plin1*, respectively) in CT and SBA groups (18%) after exposure to co-differentiation medium for 14 days. Data represents median and interquartile range; n=5. Statistical analysis was performed using Mann–Whitney’s test. In B, a - p<0.05 when compared to CT group. Peroxisome proliferator-activated receptor gamma 2 (*Pparg2*), leptin (*Lep*), adiponectin (*Adipoq*), perilipin (*Plin1*).

After, the expression level of osteoblastogenic marker genes was determined in the CT and SBA 18% groups. The early osteoblastogenic marker (*Runx2*) was not affected by 4 weeks of protocol after 48 hours of incubation in proliferation medium or after 14 days of exposure to co-differentiation medium (Fig. 36A,B). Moreover, other osteoblastogenic marker genes (*Sp7*, *Colla1*, *Bglap*) were also not altered by the short-term SBA protocol (Fig. 36C-E). The results of this study suggest that the 4-week protocol does not induce alterations in BMSC differentiation capacity.

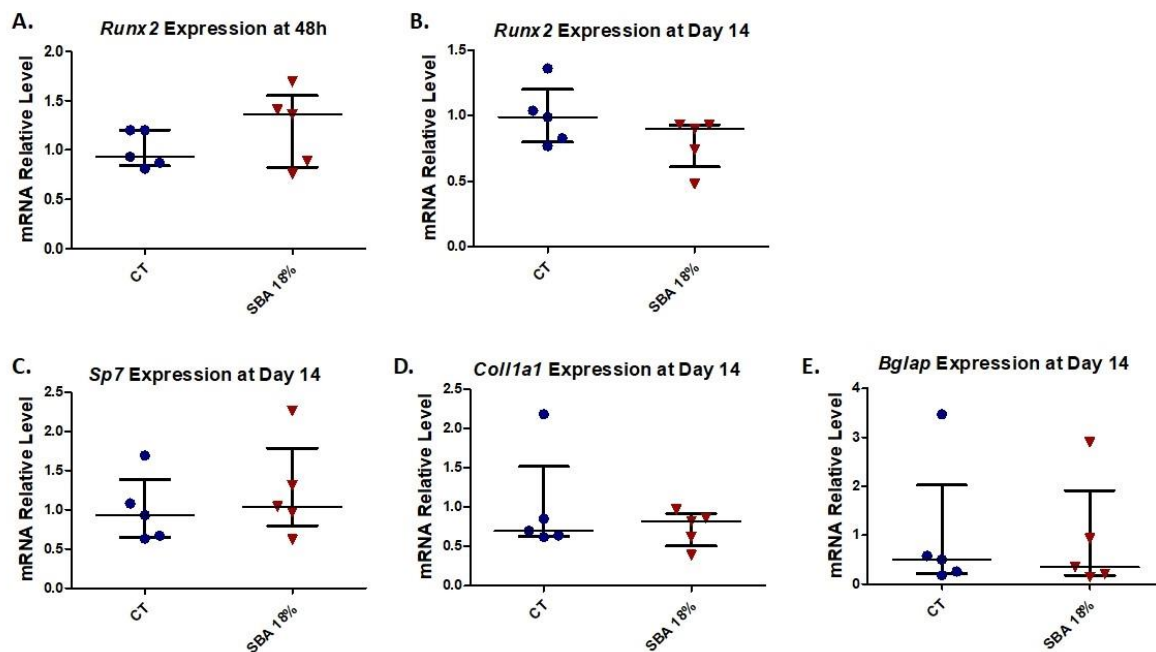


Figure 36. Osteoblastogenic marker gene expression in BMSCs after 4-week SBA protocol. A-B. Relative mRNA expression level of early osteoblastogenic marker gene (RUNX2) in CT and SBA groups (18%), respectively, cells were cultured for 48 hours in standard growth medium and for 14 days were exposed to co-differentiation medium, respectively; C-E. Relative mRNA expression level of other osteoblastogenic marker genes (*Sp7*, *Coll1a1* and *Bglap*, respectively) in CT and SBA (18%) groups after exposure to co-differentiation medium for 14 days. Data represent median and interquartile range; n=5. Statistical analysis was performed using Mann–Whitney’s test. Runt-related transcription factor 2 (*Runx2*), osterix (*Sp7*), collagen1a1 (*Coll1a1*), osteocalcin (*Bglap*).

4-week SBA protocol did not cause change in *Sirt1* expression

To confirm the association between *Sirt1* expression and BMSC lineage commitment, we examined relative mRNA levels in the 4-week SBA 18% group vs. the CT group. The findings showed that the expression of *Sirt1* was not affected by the short SBA protocol, further suggesting its involvement in BMSC fate decisions (Fig. 37).

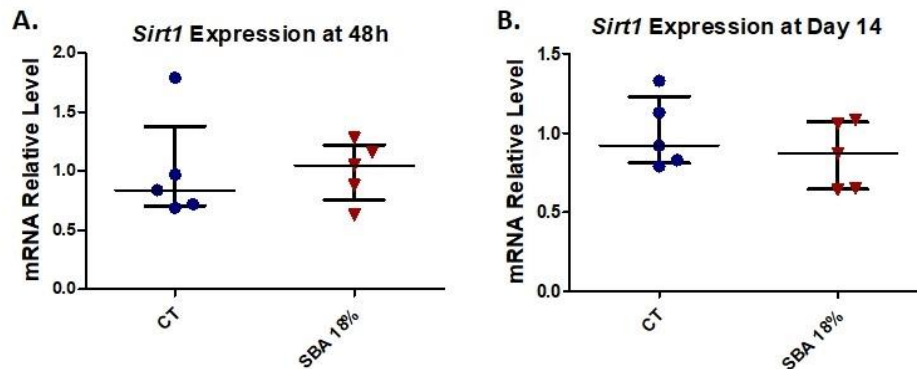


Figure 37. *Sirt1* expression in BMSCs extracted from 4-week SBA protocol. A-B. Relative mRNA expression level of sirtuin type 1 (*Sirt1*) in CT and SBA groups (18%), cells were cultured for 48 hours in standard growth medium and for 14 days were exposed to co-differentiation medium, respectively. Data represent median and interquartile range; n=5. Statistical analysis was performed using Mann–Whitney’s test.



Severity Level and Duration of Energy Deficit in Mice Affect Bone Phenotype and Bone Marrow Stromal Cell Differentiation Capacity

Viktorija Avilkina¹, Damien Leterme¹, Guillaume Falgayrac², Jérôme Delattre², Flore Miellot¹, Véronique Gauthier¹, Christophe Chauveau^{1*} and Olfa Ghali Mhenni^{1*}

¹ MAB Lab ULR4490, Univ Littoral Côte d'Opale, Boulogne-sur-Mer, France, ² MAB Lab ULR4490, Univ Lille Nord de France, Lille, France

OPEN ACCESS

Edited by:

Sarah Beck-Cormier,
U1229 Médecine Régénératrice et
Squelette (RMeS) (INSERM), France

Reviewed by:

William Peter Cawthorn,
University of Edinburgh,
United Kingdom
Noriaki Ono,
University of Texas Health Science
Center at Houston, United States

*Correspondence:

Christophe Chauveau
christophe.chauveau@univ-littoral.fr
Olfa Ghali Mhenni
olfa.ghali@univ-littoral.fr

Specialty section:

This article was submitted to
Bone Research,
a section of the journal
Frontiers in Endocrinology

Received: 21 February 2022

Accepted: 25 April 2022

Published: 06 June 2022

Citation:

Avilkina V, Leterme D, Falgayrac G,
Delattre J, Miellot F, Gauthier V,
Chauveau C and Ghali Mhenni O
(2022) Severity Level and Duration of
Energy Deficit in Mice Affect Bone
Phenotype and Bone Marrow Stromal
Cell Differentiation Capacity.
Front. Endocrinol. 13:880503.
doi: 10.3389/fendo.2022.880503

Anorexia nervosa is known to induce changes in bone parameters and an increase in bone marrow adiposity (BMA) that depend on the duration and seriousness of the disease. Previous studies have found that bone loss is associated with BMA accumulation. Sirtuin of type 1 (Sirt1), a histone deacetylase that is partly regulated by energy balance, was shown to have pro-osteoblastogenic and anti-adipogenic effects. To study the effects of the severity and duration of energy deficits related to bone loss, a mouse model of separation-based anorexia (SBA) was established. We recently demonstrated that moderate body weight loss (18%) 8-week SBA protocol in mice resulted in an increase in BMA, bone loss, and a significant reduction in Sirt1 expression in bone marrow stromal cells (BMSCs) extracted from SBA mice. We hypothesized that Sirt1 deficit in BMSCs is associated with bone and BMA alterations and could potentially depend on the severity of weight loss and the length of SBA protocol. We studied bone parameters, BMA, BMSC differentiation capacity, and Sirt1 expression after induction of 4 different levels of body weight loss (0%, 12%, 18%, 24%), after 4 or 10 weeks of the SBA protocol. Our results demonstrated that 10 week SBA protocols associated with body weight loss (12%, 18%, 24%) induced a significant decrease in bone parameters without any increase in BMA. BMSCs extracted from 12% and 18% SBA groups showed a significant decrease in Sirt1 mRNA levels before and after co-differentiation. For these two groups, decrease in Sirt1 was associated with a significant increase in the mRNA level of adipogenic markers and a reduction of osteoblastogenesis. Inducing an 18% body weight loss, we tested a short SBA protocol (4-week). We demonstrated that a 4-week SBA protocol caused a significant decrease in Tb.Th only, without change in other bone parameters, BMA, Sirt1 expression, or differentiation capacity of BMSCs. In conclusion, this study showed, for the first time, that the duration and severity of energy deficits are critical for changes in bone parameters, BMSC differentiation, and Sirt1 expression. Furthermore, we showed that in this context, Sirt1 expression could impact BMSC differentiation with further effects on bone phenotype.

Keywords: energy deficit, bone, bone marrow adiposity, sirtuin type 1 (SIRT1), bone marrow stromal cell (BMSC), differentiation

INTRODUCTION

Anorexia nervosa (AN) is a disorder with psychiatric origins characterized by inadequate dietary intake resulting in low body weight. Many studies have demonstrated that a higher volume of bone marrow adipose tissue (BMAT) is present in anorexic patients than in normal-weight controls (1–3). This high level of BMAT is often associated with a decline in bone mass, resulting in increased fracture risk (4, 5). Recently, a negative correlation was shown between the fraction of fat in the bone marrow cavity and the bone mineral density (BMD) at the femoral neck and at the hip of anorexic patients in multiple anatomical subregions, even after weight recovery (6).

Marrow adipocytes originate from skeletal stem cells (SSCs) that also function as precursors to muscle, cartilage, and bone-forming osteoblasts (7–9). Moreover, it has been shown that the accumulation of marrow adipocytes, which is observed in bone loss situations, is potentially caused by a shift in the commitment of SSCs from the osteogenic pathway to the adipogenic pathway (10). This finding suggested the existence of a competitive relationship between these two pathways. Furthermore, bone marrow stromal cells (BMSCs), which include SSCs from aged mice express more adipocytic transcripts and fewer osteoblastic transcripts than BMSCs extracted from young animals (11).

The differentiation of SSCs towards the adipocytic or osteoblastic pathway could be influenced by many modulators of signalling pathways, such as glucocorticoids, Wnts, and bone morphogenetic proteins (12–14). Moreover, the histone deacetylase (HDAC) family was also shown to influence the fate of differentiating mesenchymal progenitor cells by removing acetyl groups from lysine residues in histones and other proteins, thus, altering chromatin structure, gene expression, and protein activity (15, 16).

Sirtuin type 1 (Sirt1) is classified as a class III HDAC and is known to be involved in the extension of lifespan in mammals and other organisms and in protection against age-associated diseases (such as diabetes and obesity) (17). Additionally, Sirt1 is involved in the regulation of BMSC differentiation into either osteoblasts or adipocytes. Indeed, several studies have demonstrated that activation of Sirt1 promotes osteoblastic differentiation (18–21), while a decrease in Sirt1 expression induces adipocytic differentiation (22, 23). Interestingly, caloric restriction (CR) has been shown to stimulate the expression and activity of Sirt1 in various mammalian tissues, such as liver and white adipose tissue. Also, CR has been shown to induce a decrease in the level of Sirt1 mRNA in the cerebellum and midbrain (24, 25).

Recently, we demonstrated that 8 weeks of a separation-based anorexia (SBA) protocol, inducing medium weight loss (18%) vs day 0 of experiment in mice, is associated with an increase in bone marrow adiposity (BMA), bone loss, and a significant reduction in Sirt1 expression in BMSCs extracted from SBA mice (26). We hypothesized that Sirt1 deficit in BMSCs is involved in bone and BMA alterations and could potentially depend on the severity of weight loss and the length of SBA protocol. To verify these hypotheses, we characterized bone and BMA, and determined BMSC differentiation capacity and Sirt1 expression after a 10-week induction of 4 different levels of body

weight changes (0%, -12%, -18% and -24%) relative to mice at Day 0. The same parameters were also analyzed after a 4-week SBA protocol with 18% weight loss.

MATERIALS AND METHODS

Animals

Seven-week-old female C57BL/6J mice purchased from Charles River Laboratories (St Germain sur l'Abresle, France) were used for the separation-based anorexia (SBA) model (27). This particular mouse strain was chosen because of its use in various studies related to calorie restriction-induced bone alterations. Additionally, C57BL/6J mice exhibit a medium level of BMA, which allows us to detect any change in this parameter.

Mice were housed 6 per cage in a controlled room temperature (22°C±1°C) under a 12-hour dark/light cycle (lights off at 10 a.m.) and with free access to water. Before induction of the SBA protocol, mice were acclimatized for one week. The SBA protocol was generated for ten weeks and aimed to induce 4 different weight loss conditions in randomly allocated mice – no weight loss (SBA 0%), a light 12% weight loss (SBA 12%) (achieved 12.97%), a moderate body weight loss of 18% (SBA 18%) (achieved 17.27%) and severe weight loss of 24% (SBA 24%) (achieved 23.17%), relative to Day 0 (D0). A time restricted-feeding was used to induce weight loss in mice, a food access time was gradually reduced from 6 h to 2 h per day during the protocol, depending on the desired weight loss to achieve. Mice allocated to severe, moderate, and light weight loss groups had reduced food availability and time dependent on the progression of weight loss. For no weight loss group the time of the feeding was not decreased dramatically, in order to maintain the initial mice weight. Furthermore, throughout the protocol mice of SBA groups were kept in the separate sections of the cage with free access to water and this encouraged the increased energy expenditure by thermogenesis. The SBA mice were gathered together in regular cages for the periods of feeding. The CT group was housed in standard conditions in collective cages with water and food provided *ad libitum*. This study was specifically approved by the Committee on the Ethics of Animal Experiments (CEEA) of Nord-Pas de Calais, France (permit number: CEEA#2016070717275082).

Additionally, a 4-week SBA protocol was performed using seven-week-old female C57BL/6J mice, similar to the 10-week protocol. After one week of acclimatization, the SBA protocol was generated for 4 weeks to achieve moderate weight loss of 18% (SBA 18%) (achieved 18.75%) in mice relative to their weight at D0. This study was specifically approved by the Committee on the Ethics of Animal Experiments (CEEA) of Nord-Pas de Calais, France (permit number: CEEA#2016070717275082).

Dual Energy X-Ray Absorptiometry (DEXA) Analysis

The fat mass, lean mass, and bone mineral content (BMC) of mice were analyzed using the Lunar PIXImus Mouse Densitometer (GE Healthcare, Madison, WI) according to a previously described protocol (27).

Mineralized Bone Micro-CT Analysis

Tibiae extracted from CT and SBA mice were scanned using a Skyscan 1172 microCT device (Bruker MicroCT, Kontich, Belgium). The software suite provided by the manufacturer was used for image acquisition, reconstruction, analysis, and 3D visualisation (Skyscan 1172[®], NRecon[®], Dataviewer, CTAn[®], CTVox[™]). Analysis of the tibia trabecular bone volume/tissue volume (BV/TV) ratio, cortical thickness (Cort.Th), trabecular thickness (Tb.Th), trabecular number (Tb.N) and trabecular spacing (Tb.Sp) of all animals were determined in a 0.5mm region beginning 250mm proximal to the proximal growth plate. More detailed description for the quantification of 3D microarchitecture of trabecular bone has been previously presented (28).

Bone Marrow Adipose Tissue Content - Micro-CT Analysis

The BMAT and bone parameters analyzed by micro-CT of all mice were quantified using a previously published protocol (29) in the proximal tibia. To quantify the BMAT content, the same region of interest (ROI) was used as in the analysis of mineralized bone. After the first micro-CT scan, tibiae were decalcified in 4% formic acid/10% NBF (1:1), pH 7.4, for 48 h. Then bones were rinsed in distilled water and stained in the fume hood for 48 h in the aqueous staining solution (1% osmium tetroxide solution stabilized in a 2.5% dichromate potassium) at room temperature. Then, bones were rinsed for 48 h at room temperature in PBS with regular renewal of the solution. Osmium-stained bones were then stored at 4°C in PBS until the second micro-CT acquisition. The study focused on quantifying the percentage of the ratio of adipocyte volume to marrow volume (% Ad.V/Ma.V). The data are presented in the form of the percentage of BMAT volume in marrow volume.

Primary Bone Marrow Cell Cultures

Primary bone marrow cells were harvested from the tibiae and femurs of CT and SBA mice and grown for 7-10 days in aMEM media (PAN BIOTECH; P04-21050) with 15% fetal bovine serum (PAN BIOTECH; P30-3306), 1% penicillin/streptomycin (PAN BIOTECH; P04-85100) and 1% stable glutamine (PAN BIOTECH; P06-07100). After reaching full confluency, the plated BMSC population was differentiated into both osteoblasts and adipocytes according to the co-differentiation protocol described in a previously published article (30). The media containing co-differentiation inducers was replaced every two days during the 14 days of the co-differentiation experiment. This culture duration was chosen because of its brevity, which allowed for minimizing the time for cells to change after leaving the *in vivo* state.

Raman Microspectroscopy

Cells were plated on calcium fluoride (CaF₂) substrate, which is adapted to Raman analysis. The Raman microspectrometer was a LabRAM HR800 (Jobin-Yvon, France) instrument equipped with an XYZ motorized stage and a diode laser $\lambda=785$ nm. The Raman spectrometer was coupled with a microscope (BX40, Olympus). Raman acquisitions were performed with a water objective 100x lens (Nikon, numerical aperture = 1.1 Japan). The water immersion

objective focused the laser on the cell within the micrometre scale on the centre of individual lipid droplets, where one spectrum corresponds to one adipocyte lipid droplet. A total of 1,252 lipid droplets were acquired over 109 adipocytes (Table 1), representing an average of 83.4 lipid droplets analyzed per well and an average of 7.2 adipocytes analyzed per well. Spectral acquisition was performed in the 400-1800 cm⁻¹ range. The Raman signal was collected by a multichannel CCD detector (1024×256 pixels). The acquisition time was set at 60 s averaged 2 times per spectrum (total acquisition time = 120 sec). Raman spectra were processed using Labspec software (HORIBA, Jobin-Yvon, France). A Savitzky-Golay smoothing filter was applied to all Raman spectra. The band areas were integrated over defined Raman shift regions in the spectrum using a sum filter. The filter calculates the areas within the chosen borders and the background is subtracted by taking the baseline from the first to the second border. The band area was estimated at 1441 cm⁻¹ (peak-ROI 1400-1500 cm⁻¹) and 1654 cm⁻¹ (peak-ROI 1620-1694 cm⁻¹). The Raman bands at 1441 cm⁻¹ and 1654 cm⁻¹ are assigned to vibrations CH₂ and C=C, respectively (31). The unsaturation ratio was calculated as the ratio of band areas 1654 cm⁻¹/1441 cm⁻¹ (31).

Mineralization Quantification

The sample mineralization level was quantified using the same protocol previously described (30). Briefly, cells were harvested in a solution of PBS 1X/Triton 0.2%/HCl 6 M and disrupted by sonication. After, 5 ml of HCl 6 M was added to 95 ml of each sample and incubated overnight at 4°C. Following by centrifugation at 1500 × g for 5 min, the protein content was determined using the DC protein assay kit BioRad. The mineralization content was quantified.

RNA Extraction, Reverse Transcription and Real-Time PCR

Total RNA was extracted from BMSC cultures by the previously described protocol (30). Reverse transcription and RT-PCR were performed as previously described (32). The sequences of the primers (TibMolBiol, Berlin, Germany), annealing temperature, product length, and GenBank reference for each of the analyzed genes are shown in Table 2.

TABLE 1 | Details of lipid droplets studied in each condition of the 10-week and 4-week protocols.

Condition	Number of lipid droplets = number spectra over 3 wells	Number of adipocytes analysed over 3 wells per condition
10-week		
CT	519	41
SBA24%	111	13
SBA18%	299	30
SBA12%	134	10
SBA0%	189	15
Total	1252	109
4-week		
CT	45	18
SBA18%	109	25
Total	154	43

Statistical Analysis

The 10-week study was performed with 6 samples per condition, except for the mineralization experiment, which had 4 replicated per group. The 4-week study was performed with 5 samples per condition. The median and interquartile range were calculated for the groups. Due to the low number of replicates, the normality of the data could not be tested. In 10-week study, we performed Kruskal-Wallis One-Way ANOVA test to show the significance between all the conditions. Additionally, we conducted Dunn's test in order to see the relationships between specific pairs of conditions. For the 4-week studies we performed Mann-Whitney's test to see the statistically significant relationship between the two particular conditions. All tests were performed using GraphPad Prism software. Differences with $p < 0.05$ were considered statistically significant.

RESULTS

The 10-Week SBA Protocols Induced a Significant Decrease in Mouse Body Weight (12%, 18%, 24%) and Were Shown to Cause Changes Not Only in Fat Mass But Also in Lean Mass and Bone Mineral Composition

To study the effect of energy deficit severity on bone and BMSCs, we performed four different SBA protocols on female mice. We induced 0%, 12%, 18%, and 24% weight loss from the initial mouse weight over 10 weeks. Prior to the study, mice were randomized into five experimental groups that did not display significant differences in body weight at Day 0. Mice from the control group (*ad libitum* and not separated) displayed a

significant body weight increase (+22.42% vs. D0) after 10 weeks (Figure 1A). In the SBA 0% group, no significant weight change (+4.39% vs. D0) was observed, as this condition did not imply weight change (Figure 1A). In all other SBA groups, we observed a significant decrease in weight after 2 weeks of protocol and this decrease was maintained until the end of the 10 weeks (SBA 12% (-12.97%) vs. D0; SBA 18% (-17.27%) vs. D0; and SBA 24% (-23.17%) vs. D0) ($p < 0.005$ vs. D0). The results of DEXA analysis showed a significant decrease in total body bone mineral content (BMC) only in light (12%) and moderate (18%) weight loss conditions (SBA 12% -17% vs. CT; SBA 18% -15% vs. CT) (Figure 1B). The study of the BMC at specific sites, revealed that all three weight loss conditions induced a significant decrease in femur BMC - SBA 12% (-27% vs. CT), 18% (-29% vs. CT) and 24% (-30% vs. CT) (Figure 1C). However, only the SBA 18% group showed a significant decrease in the BMC of lumbar vertebrae (L3-L5) (SBA 18% -23% vs. CT) (Figure 1D). The BMC decrease was potentially associated with a decrease in lean absolute mass in mice from the SBA groups 12% (-19% vs. CT) and 24% (-22% vs. CT). This parameter was significantly reduced only in weight loss conditions, while in the SBA 18% group, lean absolute mass just showed a tendency to decrease without statistically significant change (Figure 1E). However, study of lean percentage (%) of total mouse mass, showed a significant increase in all three weight loss conditions (SBA 12%, 18% and 24%). This was due to a significant decrease in fat mass in same conditions (on average -53% vs. CT). Fat absolute mass in weight loss conditions exhibited a great decrease (59-64%, $p < 0.0001$ vs. CT) (Figure 1F). These data highlight that absolute lean mass and fat mass parameters can be associated with BMD under weight loss conditions, as a significant decrease in whole-body

TABLE 2 | Primer sequences and conditions of quantitative RT-PCR.

Gene	Primer Sequences	Annealing temperature	Product length	GenBank
<i>18S</i>	F: ATTCCGATAACGAACGAGAC R: GCTTATGACCCGCACTTACT	60°C	297 bp	X03205
<i>Gapdh</i>	F: GGCATTGCTCTCAATGACAA R: TGTGAGGGAGATGCTCAGTG	62°C	200 bp	NM_008084
<i>Pparg2</i>	F: TCGCTGATGCACTGCCTATG R: GAGAGGTCCACAGAGCTGATT	60°C	103 bp	NM_011146
<i>Adipoq</i>	F: TGTTCTCTTAATCCTGCCCA R: CCAACCTGCACAAGTTCCTT	60°C	104 bp	NM_009605
<i>Lep</i>	F: GAGACCCCTGTGTCGGTTC R: CTGCGTGTGTGAAATGTCATTG	60°C	139 bp	NM_008493
<i>Plin1</i>	F: CACCATCTCTACCCGCCTTC R: GGGTGTTGGCGGCATATTC	58°C	149 bp	NM_001113471.1
<i>Glut4</i>	F: ACTCTTGCCACACAGGCTCT R: AATGGAGACTGATGCGCTCT	62°C	174 bp	NM_009204
<i>Runx2</i>	F: GCCGGGAATGATGAGAATA R: GGACCGTCCACTGTCACTTT	62°C	200 bp	NM_001146038.2
<i>Bglap</i>	F: AAGCAGGAGGGCAATAAGGT R: CGTTTGTAGGCGGTCTTCA	60°C	364 bp	L24431
<i>Sp7</i>	F: ATGGCGTCTCTCTGCTTG R: TGAAGGTGACGCTATGGCTT	54°C	237 bp	NM_130458
<i>Col1a1</i>	F: GGTGAGCCTGGTCAAACGG R: ACTGTGCTCTTTCAGCCTTT	60°C	189 bp	NM_007743
<i>Sirt1</i>	F: TAGGGAACCTTTGCCTCATC R: GGCATATTCACCACCTAGCC	51°C	100 bp	NM_019812.2

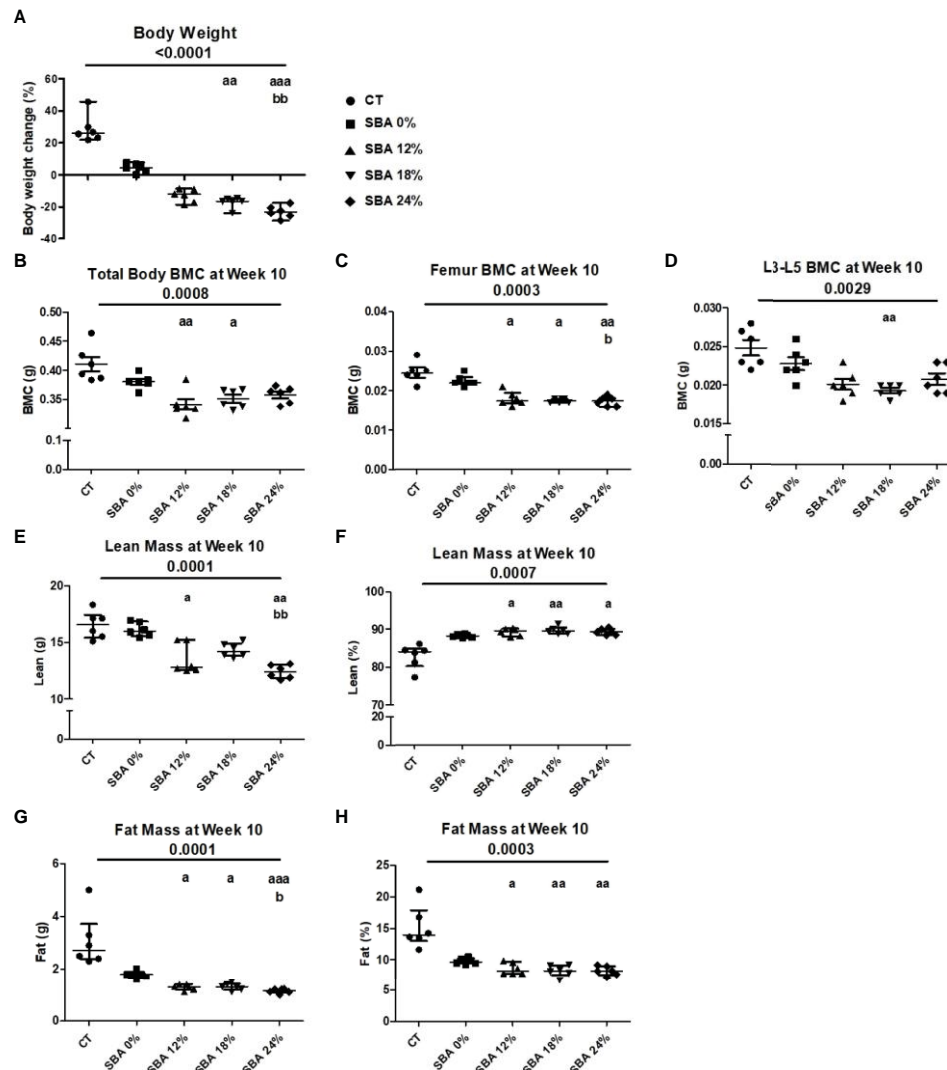


FIGURE 1 | Body mass, BMC, fat and lean mass in mice after 10 weeks of SBA protocols of different severity. The body weight and composition analysis were performed on standard condition (CT), constant weight group (SBA 0%) and three weight loss groups with different severity levels (SBA 12%, 18% and 24%). (A) Graph represents a percentage body weight loss on mice between day 0 and 10 weeks of SBA protocol; (B-D) Study of total mouse body mineral content (BMC), femur BMC and vertebra (L3-L5) BMC, respectively, were evaluated for each animal and each condition after 10 weeks of SBA protocol.; (E, F) Lean mass content presented in grams and % of total mass, respectively, was evaluated for each mouse and condition after 4 weeks of SBA protocol; (G, H) Fat mass content presented in grams and % of total mass, respectively, was evaluated for each mouse and condition after 4 weeks of SBA protocol. Data represent median and interquartile range; $n = 6$. Statistical analysis was performed using Kruskal-Wallis One-Way ANOVA test and Dunn's test; $a - p < 0.05$, $aa - p < 0.005$ and $aaa - p < 0.0005$ when compared to the CT group ($b -$ when compared to the SBA 0% group).

BMC or femoral/vertebral BMC together with lean and fat mass was observed only in the weight loss mice.

The 18% and 24% SBA Protocols Resulted in a Significant Decrease in Trabecular and Cortical Thickness, Without Any Increase in Bone Marrow Adiposity

To determine the effect of SBA severity on bone microarchitecture, we conducted proximal tibia micro-CT analysis. Bone volume fraction (BV/TV) showing the relative volume of mineralized trabecular bone was not affected by the

SBA protocols (Figure 2A). Trabecular thickness (Tb.Th) was significantly decreased only under severe weight loss conditions (SBA 24%: -29% vs. CT) (Figure 2B). In contrast with the thickness of the trabecular bone, the trabecular number (Tb.N) and trabecular spacing (Tb.Sp) were not significantly affected, even for the 24% group (Figures 2C, D). One of the bone fragility parameters was assessed through the study of cortical thickness (Cort.Th), which is affected by the SBA protocol. Indeed, the SBA 18% and 24% caused 16% and 17% decreases in this parameter, respectively ($p < 0.0001$ vs. CT) (Figure 2E), demonstrating the potential link between moderate and severe energy deficit and

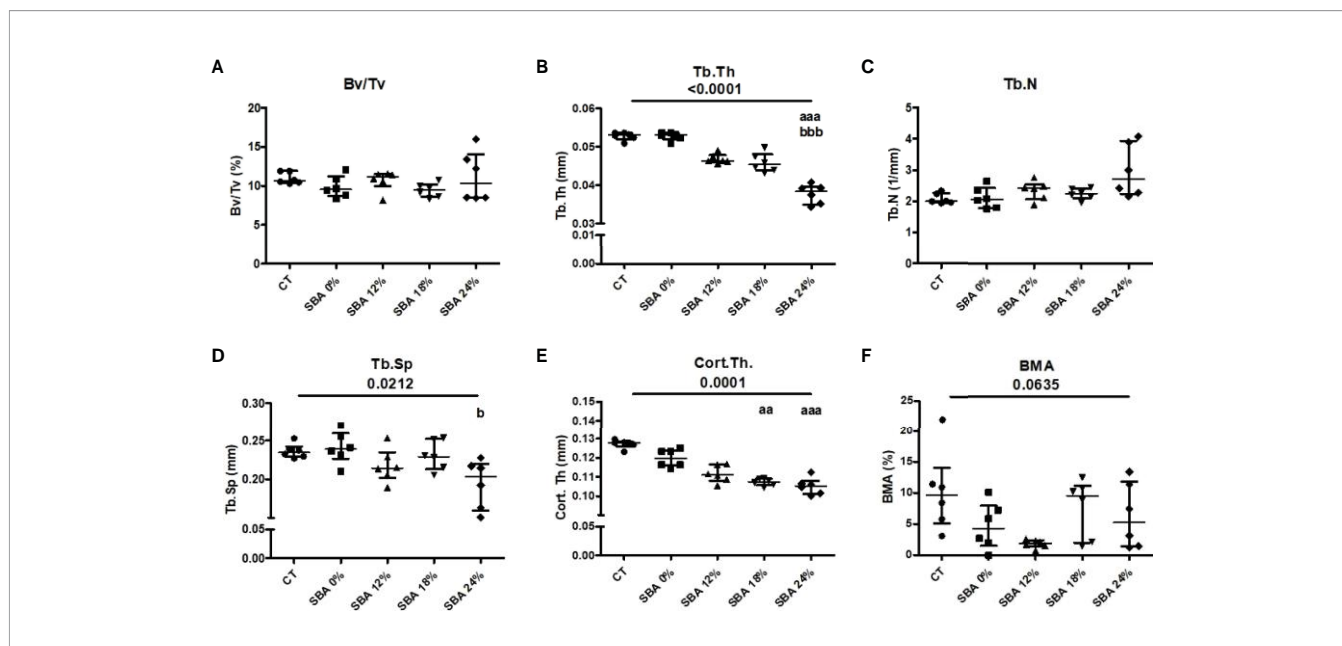


FIGURE 2 | The results of micro-CT analysis of tibia, showing different bone parameters after exposure to 10 weeks of SBA protocols at different levels of severity. (A) Bone volume fraction (BV/TV) was expressed as a percentage on mineralized tissue in each condition after 10 weeks; (B-E) Trabecular thickness (Tb.Th), trabecular number (Tb.N) and trabecular spacing (Tb.Sp), and cortical thickness (Cort.Th), respectively, were evaluated for each animal and each condition after 10 weeks of SBA protocol (expressed in millimetres); (F) Bone marrow adiposity (BMA) was calculated as a percentage of BMAT volume in marrow volume. Data represent median and interquartile range; n = 6. Statistical analysis was performed using Kruskal-Wallis One-Way ANOVA test and Dunn’s test; a - p < 0.05, aa - p < 0.005 and aaa - p < 0.0005 when compared to the CT group (b - when compared to the SBA 0% group).

decrease in Cort.Th. The results of bone marrow adiposity (BMA) showed a high heterogeneity of the samples in each group. Only the SBA 12% group exhibited a tendency of BMA decrease by 82% (p<0.1, Figure 2F).

SBA Protocol Resulted in Rapid Adipogenesis of BMSCs and Weight Loss Conditions Were Associated With a Decrease in Lipid Unsaturation Levels

Throughout the co-differentiation experiment, cells extracted from SBA and control mice were observed under light microscopy.

BMSCs extracted from CT mice started to form lipid droplets after the 7th day of co-differentiation. Cells extracted from SBA mice (0%, 12%, 18%, and 24%) showed the first appearance of lipid droplets much faster, after the 3rd day of co-differentiation (Figure 3). This finding suggests that the SBA protocol induces *in vivo* changes in BMSC commitment and that these cells are potentially committed to differentiating into adipocytes. After qualitative study (microscopic observations) of adipocytes on Day 10 of differentiation, BMSCs extracted from the SBA 12%, 18%, and 24% groups globally seemed to generate more numerous and larger adipocytes compared to the CT or SBA 0% groups

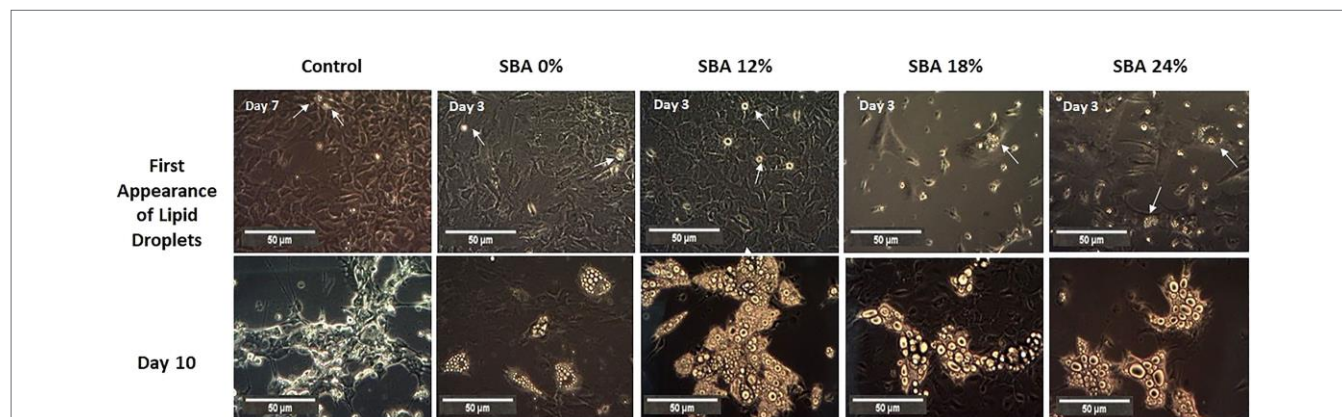


FIGURE 3 | Overview of adipocyte first appearance and size. A. Light microscope images of cells from each condition were taken on different points of differentiation showing the first appearance of lipid droplets and adipocytes at day 10.

(Figure 3). Additionally, Raman spectroscopy analysis was performed to characterize more of the adipocytes from different groups. The lipid unsaturation levels in the SBA 12%, 18%, and 24% groups were significantly lower than those in the SBA 0% group, showing that the severity of energy deficit can lead to a decrease in lipid unsaturation levels (Supplementary Figure 1).

Only SBA 18% and 24% Protocols Resulted in an Increase in Adipogenesis and Subsequent Decrease in Osteoblastogenesis

To confirm the commitment of BMSCs to the adipocyte lineage, the mRNA levels of adipocytic markers in the SBA and CT groups were analyzed. The marker gene relative mRNA level was measured 48 hours after plating (adherent cells) and at day 14 of co-differentiation. This culture duration was chosen because of its brevity, which minimized the time for cells to change after leaving the *in vivo* state. Interestingly, after 48 hours of adhesion in a standard medium, the unstimulated BMSCs from mice of SBA 24% protocols already exhibited high levels of peroxisome proliferator-activated receptor gamma 2 (*Pparg2*) mRNA (+125% vs CT) (Figure 4A), showing a potential commitment to adipogenic differentiation prior to co-differentiation stimulation and thus probably *in vivo*. The SBA 0% group showed similar expression level of *Pparg2* to CT and SBA 12% and 24% conditions, also showed significant increase in *Pparg2*

relative mRNA level vs. SBA 0%. Furthermore, *Pparg2* mRNA levels were similarly enhanced after 14 days of co-differentiation in severe weight loss group (SBA 24%: +236% vs. CT) (Figure 4B). Additionally, the SBA 18% group demonstrated the highest upregulation of *Pparg2* (+285% vs. CT and vs. SBA 0%) (Figure 4B). Other marker genes characterizing cell commitment to adipogenic differentiation (leptin (*Lep*) and facilitated glucose transporter member 4 (*Glut4*)) exhibited an increase in the moderate and severe weight loss groups (SBA 18% - *Lep* +1292% vs CT, *Glut4* +807% vs. CT; SBA 24% - *Lep* +1864% vs. CT) (Figures 4C, E). The adiponectin (*Adipoq*) mRNA level was found to be upregulated only in the SBA 18% group (+53% vs. SBA 0%) (Figure 4D). However, the 12% weight loss condition displayed the lowest mRNA level of *Adipoq* (Figure 4D).

In our study, we wanted to determine whether the severity of SBA causes an imbalance in BMSC lineage commitment and whether upregulation of adipogenesis is achieved at the expense of osteoblastogenesis. Thus, after 14 days of co-differentiation, the mineralization level of CT and SBA cells was studied by quantifying the calcium to protein ratio. The results demonstrated a strong alteration of mineralization capabilities in moderate and severe weight loss SBA conditions (18% and 24%, on average -82% vs. CT) (Figure 5A). However, this trend was not significant. Only 18% weigh loss condition exhibited significant decrease in mineralization vs. SBA 0%. The mRNA level analysis showed that the early marker of osteoblastogenesis [run-related transcription factor 2 (*Runx2*)] was significantly

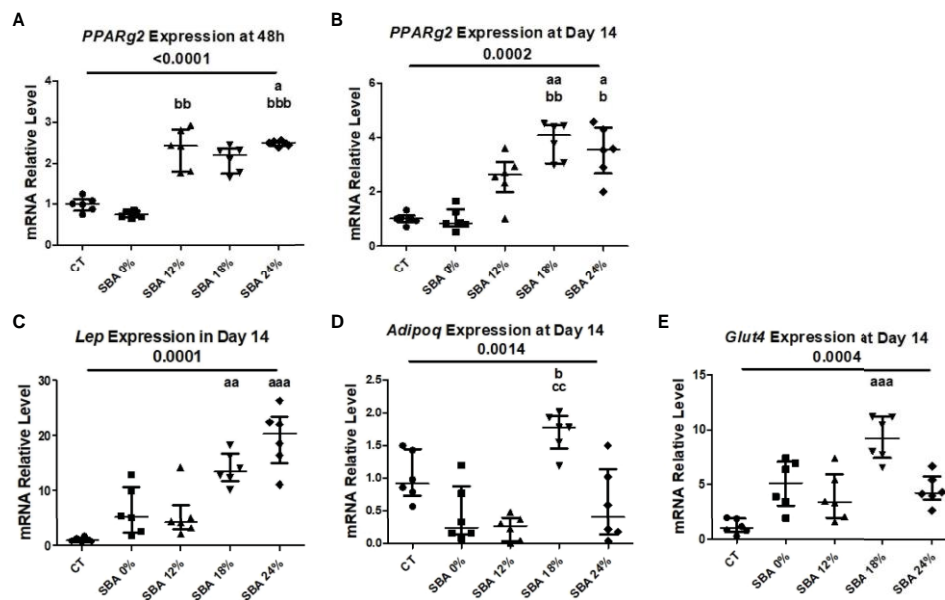


FIGURE 4 | 10-week SBA protocol induced an increase in adipogenesis. (A, B) Relative mRNA expression level of early adipogenic marker gene (*Pparg2*) in CT and SBA groups (0%, 12%, 18%, 24%), cells were cultured for 48 hours in standard growth media and for 14 days were exposed to co-differentiation media, respectively; (C-E) Relative mRNA expression level of other adipogenic marker genes (*Lep*, *Adipoq*, and *Glut4*, respectively) in CT and SBA groups (0%, 12%, 18%, 24%) after exposure to co-differentiation media during 14 days. Data represent median and interquartile range; n=6. Statistical analysis was performed using Kruskal-Wallis One-Way ANOVA test and Dunn's test; a - $p < 0.05$, aa - $p < 0.005$ and aaa - $p < 0.0005$ when compared to the CT group (b - when compared to the SBA 0% group; c - when compared to SBA 12% group). Peroxisome proliferator-activated receptor gamma 2 (*Pparg2*), leptin (*Lep*), adiponectin (*Adipoq*), facilitated glucose transporter member 4 (*Glut4*).

reduced in severe weight loss condition (SBA 24% -55% vs. CT) 48 hours after cell plating in standard media and after 14 days in co-differentiation medium both moderate and severe conditions induced changes in *Runx2* mRNA level (SBA 18% -75% vs. CT; SBA 24% -70% vs. CT) (Figures 5B, C). Interestingly, further study of other markers of osteoblastogenesis [collagen1A1 (*Col1a1*), osteocalcin (*Bglap*) and osterix (*Sp7*)] at the end of co-differentiation revealed a reduction in mRNA levels only in the moderate and severe weight loss groups (*Col1a1* - SBA 18% -77% vs SBA 0%, SBA 24% -83% vs. SBA 12%; *Bglap* - SBA 18% -73%, SBA 24% -72% vs. CT; *Sp7* - SBA 18% -81%, SBA 24% -77% vs. CT) (Figures 5D–F). Moreover, the results suggest that an increase in adipogenesis occurs at the expense of osteoblastogenesis and that BMSCs extracted from SBA mice are apparently more committed to adipogenic lineage.

Recently, we demonstrated that the 18% SBA protocol favors BMSC lineage commitment towards adipogenesis and a decrease in *Sirt1* level and activity, a potential regulator of BMSC differentiation (26). In the present study, we examined the impact of weight loss severity on the expression level of *Sirt1* mRNA. The results of the SBA 18% protocol showed a 67% decrease (vs. CT) in *Sirt1* mRNA in BMSCs after 48 hours of adhesion in growth media and a 75% decrease (vs. CT) after 14 days of co-differentiation (Figure 6). This finding confirmed our previously published data. Additionally, the *Sirt1* mRNA level was significantly altered in the 24% groups (-60% vs. CT) after 48

hours of adhesion and after 14 days of co-differentiation (-68% vs. CT) (Figure 6). So, decrease in *Sirt1* mRNA levels under moderate and severe weight loss conditions could be associated with an increase in adipogenic mRNA markers and a subsequent downregulation of osteoblastogenesis in BMSCs.

The 4-Week SBA Protocol Induced a Significant Decrease in Mouse Body Weight (18%) and Was Shown to Cause Changes Only in Fat Mass and Trabecular Thickness

Long-term SBA protocols (10-week duration) have been shown to induce changes in mouse BMSC differentiation capacity; however, we were interested in the duration of energy deficit affecting the mouse bone composition and BMSC differentiation capacity. Therefore, we conducted a 4-week SBA protocol. In the 10-week study detailed above, the SBA 18% group exhibited alterations in bone parameters and in BMSC differentiation capacity, confirming the hypothesis that adipogenesis is upregulated in these cells at the expense of osteoblastogenesis. Based on these findings, we compared CT mice with 18% weight loss mice after exposure to the SBA protocol for 4 weeks.

The mouse body weight showed a significant decrease in percentage body weight loss in the SBA 18% group vs. CT (Figure 7A). After the study of body composition, it was concluded that the 4-week SBA protocol induced alterations in

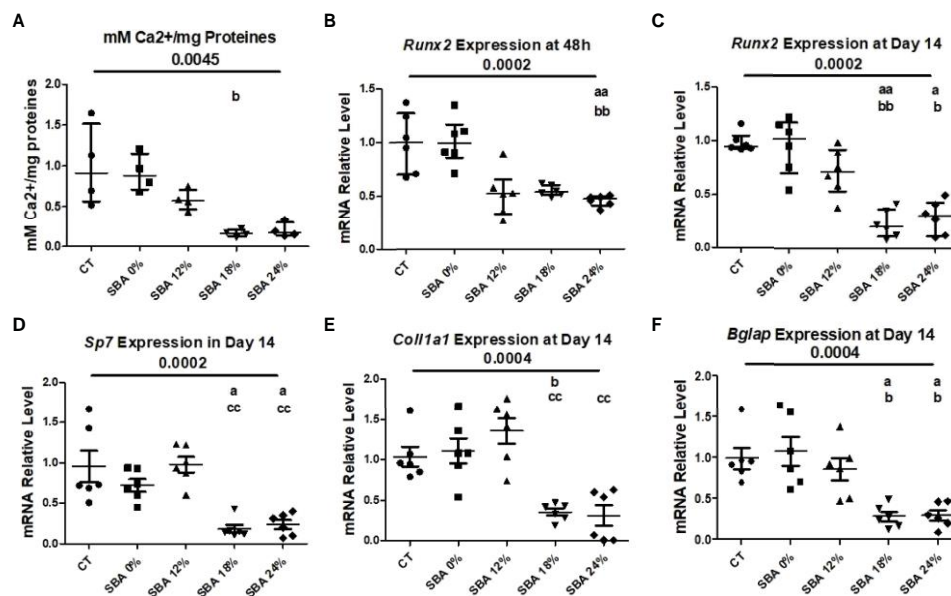


FIGURE 5 | 10-week SBA protocol induced a decrease in osteoblastogenesis. (A) Mineralization level of CT and SBA groups (0%, 12%, 18%, 24%) quantified by measuring the calcium to protein ratio; (B, C) Relative mRNA expression level of early osteoblastogenic marker gene (*Runx2*) in CT and SBA groups (0%, 12%, 18%, 24%), cells were cultured for 48 hours in standard growth media and for 14 days were exposed to co-differentiation media, respectively; (D-F) Relative mRNA expression level of other osteoblastogenic marker genes (*Sp7*, *Col1a1*, and *Bglap*, respectively) in CT and SBA groups (0%, 12%, 18%, 24%) after exposure to co-differentiation media for 14 days. Data represent median and interquartile range; Mineralisation study n = 4, qPCR n = 6. Statistical analysis was performed using Kruskal-Wallis One-Way ANOVA test and Dunn's test; a - $p < 0.05$, aa - $p < 0.005$ when compared to the CT group (b - when compared to the SBA 0% group; c - when compared to SBA 12% group). Runt-related transcription factor 2 (*Runx2*), osterix (*Sp7*), collagen1a1 (*Col1a1*), osteocalcin (*Bglap*). *Sirt1* is sustainably decreased in BMSCs from SBA mice (18% and 24%).

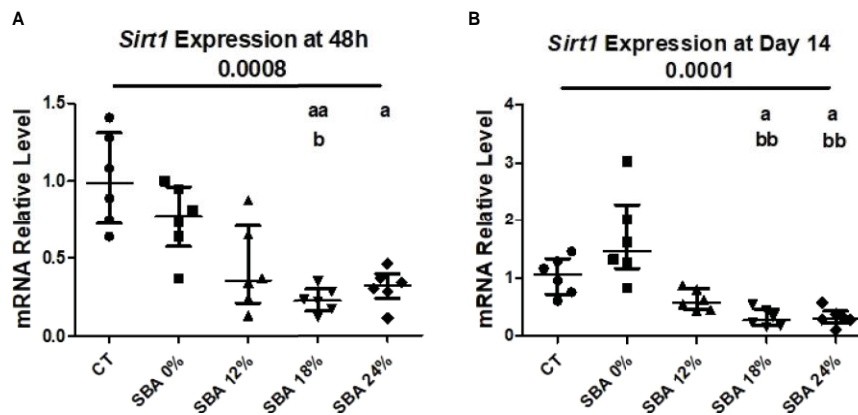


FIGURE 6 | 10-week SBA protocol induced a suppression of SIRT1 mRNA level. (A, B) Relative mRNA expression level of sirtuin type 1 (*Sirt1*) in CT and SBA groups (0%, 12%, 18%, 24%), cells were cultured for 48 hours in standard growth media and for 14 days were exposed to co-differentiation media, respectively.

Data represent median and interquartile range; $n = 6$. Statistical analysis was performed using Kruskal-Wallis One-Way ANOVA test and Dunn's test; $a - p < 0.05$, $aa - p < 0.005$ when compared to the CT group ($b -$ when compared to the SBA 0% group).

mouse fat absolute mass (-50% vs. CT), with no change in BMC or lean absolute mass (Figure 7). However, the significant decrease in fat % of total mouse weight was accompanied with significant increase in lean % mass (Figures 7C, E).

Furthermore, the bone microarchitecture results showed that the short SBA protocol induced changes in Tb.Th (-16% vs. CT) (Figure 7B) to a similar extent as the 10-week 18% weight loss protocol (Figure 2B). The 4-week SBA protocol also had no effect on BV/TV, Tb.N and Tb.Sp (Figures 8A, B, D), similar to SBA 18% group in 10-week protocol (Figure 2). However, in contrast with 10-week protocol, short duration of SBA had no effect on Cort.Th (Figure 8E). Additionally, bone marrow adiposity was not affected by the 4-week SBA protocol (Figure 8F). Thus, the 4-week protocol was not enough to induce changes in cortical bone microarchitecture, unlike the 10-week protocol.

Reduced Length of SBA Protocol Did Not Result in Alterations of BMSC Differentiation Capacity or Changes in Sirt1 Expression

After BMSCs were extracted from bone marrow and co-differentiation was induced, the cells were studied under a light microscope. Images showed that the first appearance of lipid droplets took place on the 7th day of co-differentiation in both the CT and SBA 18% groups (Figure 9A). Additionally, after 10 days of differentiation, there was no difference observed in the accumulation of adipocytes in SBA 18% vs. CT (Figure 9A). Therefore, the 4-week SBA protocol did not induce a shift of BMSCs towards adipocyte differentiation, as suggested by the results of the 10-week experiments. Similarly, it did not induce changes in lipid accumulation capacities. Raman spectroscopy showed no difference in lipid unsaturation levels between the control and SBA 18% groups (Supplementary Figure 2). Similar to the 10-week SBA study, we analyzed the relative mRNA levels of adipogenic/osteoblastogenic genes in extracted BMSCs. The

results of the early adipogenic marker gene (*Pparg2*) showed that after 48 hours of proliferation in standard growth media, BMSCs extracted from SBA 18% mice had significantly increased expression levels ($+350\%$ vs. CT) (Figure 9B). However, this upregulation of *Pparg2* expression was not long term and after 14 days of co-differentiation, there was no significant difference observed between the two conditions (Figure 9C). The analysis of late adipogenic marker genes (*Lep*, *Adipoq*, *Plin1*) demonstrated no change in the SBA 18% group compared to the CT group after 14 days of co-differentiation (Figures 9D–F).

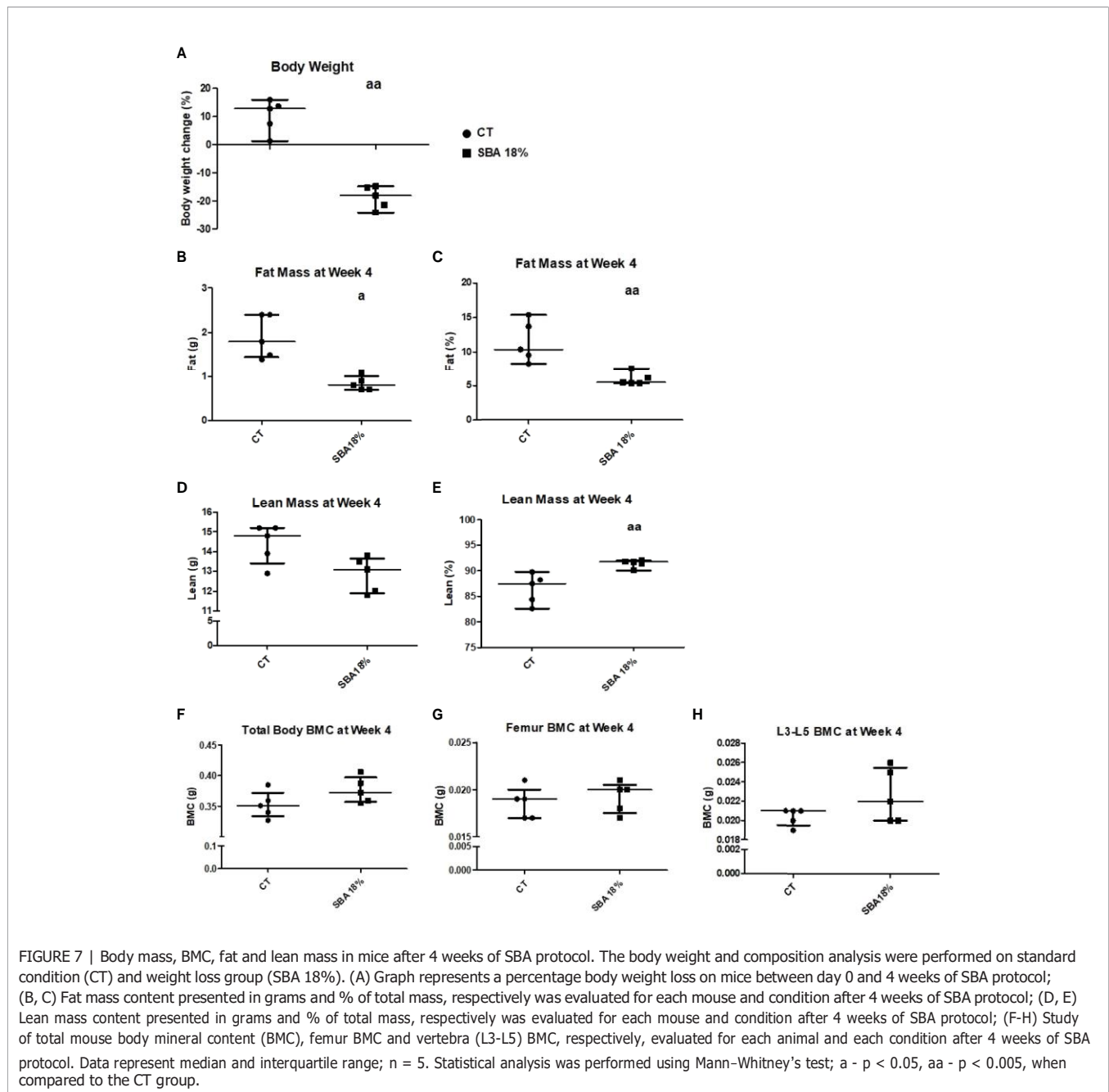
The next step was to determine the expression level of osteoblastic marker genes in the CT and SBA 18% groups. The early osteoblastogenic marker (*Runx2*) was not affected by 4 weeks of CR after 48 hours of incubation in proliferation media or after 14 days of exposure to co-differentiation media (Figures 10A, B). Moreover, other osteoblastogenic marker genes (*Coll1a1*, *Sp7* and *Bglap*) were also not altered by the short-term SBA protocol (Figures 10C–E). The results of this study suggest that the 4-week protocol does not induce alterations in BMSC differentiation capacity.

To confirm the association between *Sirt1* expression and BMSC lineage commitment, we examined relative mRNA levels in the 4-week SBA 18% group vs. the CT group. The findings showed that the expression of *Sirt1* was not affected by the short SBA protocol, further suggesting its involvement in BMSC fate decisions (Figure 11).

DISCUSSION

Ten Weeks of 18% and 24% Body Weight Loss Induce an Alteration of Bone Mineral Content Without Increase in Bone Marrow Adiposity

We recently demonstrated that a long-term energy deficit characterized by a moderate weight loss (18%) in mice is



associated with bone loss and an increase in BMA (26). In this study, we sought to determine the impact of a different degree of severity on bone architecture, BMA, and then to identify the potential molecular mechanisms involved in BMA regulation in this context. The mice were exposed for 10 weeks to a separation-induced increase in energy expenditure and a time-restricted feeding that prevented compensatory feeding and resulted in significant weight loss (SBA) (27). Results of mice body parameters showed similar fat mass decrease in all SBA groups compared to the control group. The 12%, 18%, and 24% groups displayed a decrease in BMC at least in femur. These results suggest that a significant weight loss over a long period of time

(10 weeks) is required to induce changes in mineralized bone (Figure 1). Moreover, these bone changes are not directly related to fat mass because they are not shown in the 0% group. This was already shown in adult male mice by Mitchell et al. (33). They demonstrated that different levels of CR 10%, 20%, 30%, and 40% in male mice induced body weight losses of around 0%, 11%, 22%, and 28%, respectively after 12 weeks (33). These weight changes were associated to fat mass decrease of approximately 12% for 10% CR and 30 to 35% for the other groups. In this study, no significant changes in BMC, trabecular bone microarchitecture, and cortical bone were detected. Unfortunately, BMA was not determined. The conflicting

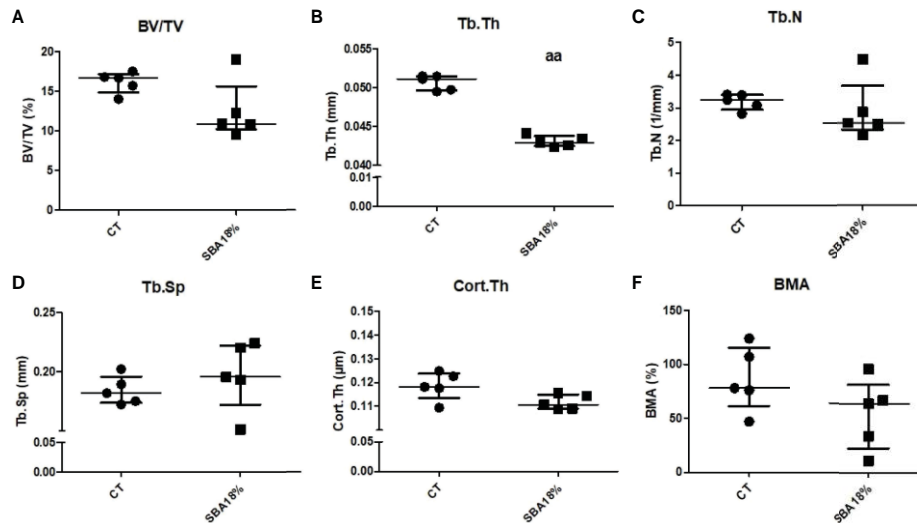


FIGURE 8 | The results of micro-CT analysis of tibia, showing different bone parameters after exposure to 4 weeks of SBA protocol. (A) Bone volume fraction (BV/TV) was expressed as a percentage on mineralized tissue in each condition after 4 weeks; (B-E) Trabecular thickness (Tb.Th), trabecular number (Tb.N) and trabecular spacing (Tb.Sp), and cortical thickness (Cort.Th), respectively, were evaluated for each animal and each condition after 4 weeks of SBA protocol (expressed in millimetres); (F) Bone marrow adiposity (BMA) was calculated as a percentage of BMAT in marrow volume. Data represent median and interquartile range; $n = 5$. Statistical analysis was performed using Mann-Whitney's test. In C, aa - $p < 0.005$ when compared to CT group.

results on bone in the present study and that of Mitchell could be due to sex, age, and protocol differences. Furthermore, Mitchell's study also showed the lack of relationship between fat mass decrease and bone in energy deficit experiment.

Previously, we showed that the SBA protocol of 18% weight loss results in an increase in BMA (26). Interestingly, in the current study, BMA appeared to be altered only in one weight loss condition. BMA displayed a decrease (not significant) in SBA mice with a light weight loss (12%) (Figure 2F). Firstly, the apparent discrepancy between the two studies could be explained by the fact that we observed a high heterogeneity in BMA among mice of the same group. Secondly, in the first study, BMA was assessed using histological (2D) approaches with slices focused on a specific area of the proximal tibia and with a specific orientation, while this study used 3D assessment on a larger volume including the area analyzed in the previous study. So, the increase observed in a specific area and the lack of significant changes observed on the large volume suggest that very localized changes could occur in the density of adipocytes in the marrow. Various studies demonstrated an increase in BMA associated with bone alteration in anorexic patients (9, 10, 13). In rodent, models of food or calorie restriction demonstrated that 9 weeks of a 30% restriction on food in 3-week-old male mice induced low BV/TV (-11%), Cort.Th (-27%), and body weight (-40%), which were accompanied with high BMA (700%) compared to CT mice (34). Also, it has been shown that 6 weeks of a 30% calorie-restricted diet in 9-week-old female mice induced an increase in tibia BMA (700%) compared to that in the *ad libitum* group (35). Interestingly, in these two studies, the high increase in BMA was associated with a body weight increase of 80% vs. day 0 (34) or a final body weight similar to that of day 0 of the

experiment (35). The difference in our BMA results compared to these two studies (34, 35) may be explained by the fact that we used young adult female mice, while the first one investigated growing male mice (34) and by the difference in body weight loss relative to that on day 0 (33, 34). In addition, it is reported that an extensive CR in rabbits can cause a loss of BMAT (34). A similar finding has been observed with severe anorexic patients (36). Thus, the sex of animals and level of body weight loss may strongly affect BMA. In contrast, a calorie restriction protocol (low carbohydrate feeding) for 12 weeks on 6-month-old Sprague-Dawley female rats, demonstrated that restricted rats displayed body weight loss (20% vs. day 0 and 25% vs. CT rats), a low volumetric BMD at the proximal tibia (-14%) and only a two-fold increase in BMA measured at the distal femur (37). More recently, male Sprague-Dawley rats (8 months old) exposed to 40% calorie restriction during 12 months, displayed 40% body weight loss vs. CT rats, which resulted in a decrease in the bone mineral index (30% vs. CT rats) and an increase in BMA at the proximal tibia (20% vs. CT rats) (38). Conversely, 10 weeks of CR in 14-week-old male mice led to a body weight loss of 30% (relative to CT mice) and a total disappearance of bone marrow adipocytes in the distal femur (34). Altogether, these data suggest that restriction-induced changes in BMA and bone quality may be modulated by severity of protocol, body weight loss, age, sex, and duration of restriction.

Ten Weeks of 18% and 24% Body Weight Loss Induce an Imbalance Between Osteoblastogenesis and Adipogenesis

Due to the fact that, in the current study, bone alterations were not associated to a high BMA, we hypothesised that the

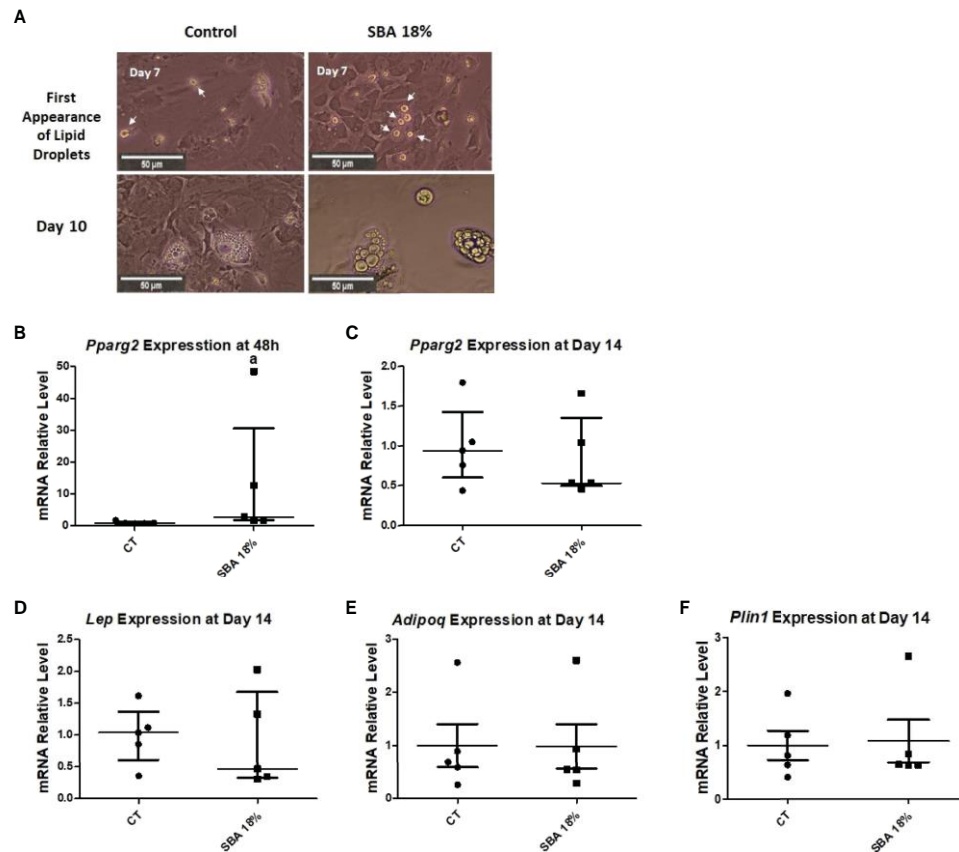


FIGURE 9 | Study of adipocyte first appearance, size and adipogenic gene expression in BMSCs. (A) Light microscopic images of cells from each condition were taken at different time points of co-differentiation showing the first appearance of lipid droplets (day 7) and adipocytes at Day 10; (B, C) Relative mRNA expression level of early adipogenic marker gene (*Pparg2*) in CT and SBA (18%) groups, cells were cultured for 48 hours in standard growth media and for 14 days were exposed to co-differentiation media, respectively; (D-F) Relative mRNA expression level of other adipogenic marker genes (leptin, adiponectin, and perilipin, respectively) in CT and SBA groups (18%) after exposure to co-differentiation media for 14 days. Data represents median and interquartile range; $n = 5$. Statistical analysis was performed using Mann-Whitney's test. In (B), $a - p < 0.05$ when compared to CT group. Peroxisome proliferator-activated receptor gamma 2 (*Pparg2*), leptin (*Lep*), adiponectin (*Adipoq*), perilipin (*Plin1*).

commitment of BMSCs towards the adipogenic pathway could impact bone mass even if adipocytes are not able to reach a mature state. Therefore, it was important to study BMSC differentiation to obtain a more precise understanding of the cell commitment towards the adipogenic or osteoblastogenic pathway.

Given that osteoblasts and adipocytes are derived from a common mesenchymal progenitor, skeletal stem cells (39, 40), we tested the hypothesis that the degree of severity of body weight loss could impact the differentiation capacity of BMSCs extracted from SBA mice. After just 48 hours of adhesion in a standard proliferative medium, the unstimulated BMSCs from SBA mice with body weight loss (12%, 18%, and 24%) exhibited high levels of *Pparg2* mRNA even if not significantly for the 18% group (Figure 4A). This finding suggests that extracted BMSCs display commitment to the adipocytic lineage. As shown in Figures 3 and 4, SBA weight loss protocols enhance BMSC adipogenesis *in vitro*, especially for SBA 18% and 24% groups. The mRNA level of adiponectin was dramatically decreased in SBA mice with light

weight loss (12%) and this finding could be associated with a significant decrease in BMA under the same weight loss conditions. Significant loss of mature adipocytes *in vivo* could potentially affect the level of adiponectin production and *Adipoq* mRNA levels (41). Raman spectroscopy analysis (Supplementary Figure 1) further revealed that SBA protocol results in a decrease of unsaturated lipids ratio in BMSC-derived adipocytes. This suggests that energy deficit induces a long-lasting alteration of lipid quality regardless the level of body weight loss. Our analysis of osteoblastogenesis in BMSCs (Figure 5) suggests that only 18% and 24% weight loss groups induce significant and long-lasting changes in osteoblastogenesis *in vitro*.

Findings above led us to conclude that there potentially exists a preferential commitment of BMSCs extracted from SBA mice to the adipogenic pathway. Results show that adipogenesis and osteoblastogenesis seem to be affected by the severity of energy deficit and that at least an 18% weight loss is required to observe these alterations.

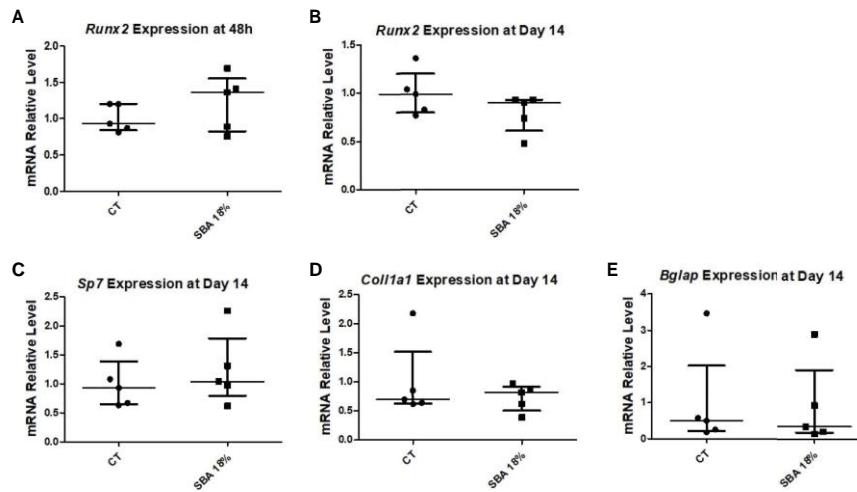


FIGURE 10 | 4-week SBA protocol did not induce changes in osteoblastogenesis. (A, B) Relative mRNA expression level of early osteoblastogenic marker gene (RUNX2) in CT and SBA groups (18%), respectively, cells were cultured for 48 hours in standard growth media and for 14 days were exposed to co-differentiation media, respectively; (C-E) Relative mRNA expression level of other osteoblastogenic marker genes (osterix, collagen1, and osteocalcin, respectively) in CT and SBA (18%) groups after exposure to co-differentiation media for 14 days. Data represent median and interquartile range; $n = 5$. Statistical analysis was performed using Mann-Whitney's test. Runt-related transcription factor 2 (*Runx2*), osterix (*Sp7*), collagen1a1 (*Col1a1*), osteocalcin (*Bglap*).

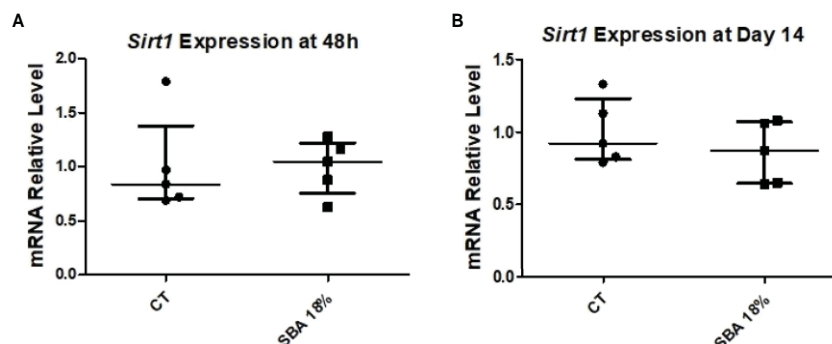


FIGURE 11 | 4-week SBA protocol induced no change in *Sirt1* expression. (A, B) Relative mRNA expression level of sirtuin type 1 (*Sirt1*) in CT and SBA groups (18%), cells were cultured for 48 hours in standard growth media and for 14 days were exposed to co-differentiation media, respectively. Data represent median and interquartile range; $n = 5$. Statistical analysis was performed using Mann-Whitney's test.

Sirt1 Is Sustainably Altered in BMSCs From 18% and 24% Groups at 10 Weeks

To determine the potential molecular mechanism involved in the regulation of BMSC differentiation in SBA mice, the relative mRNA level of *Sirt1* was measured. Indeed, we recently demonstrated that 18% weight loss in mice is associated with the downregulation of the expression and activity of *Sirt1* and further, possibly leads to an increase in adipogenesis at the expense of osteoblastogenesis (26). In the current study, we hypothesized that *Sirt1* could be altered by the degree of severity of energy deficit, leading to an imbalance between osteoblastogenesis and adipogenesis. It is important to note that *Sirt1* is widely known for its pro-osteoblastic and anti-adipogenic effects (18–23). Indeed, *in vivo* activation of *Sirt1* restores bone mass, structure, and biomechanical properties in ovariectomized

female mice (42) and it protects against age-associated bone loss in male mice (43). *In vitro* studies demonstrated that activation of *Sirt1* promotes osteoblastogenic differentiation at the expense of adipogenesis (18–21). Interestingly, our results demonstrated that BMSCs from SBA mice with moderate and severe weight loss (18% and 24%) presented a substantial low *Sirt1* mRNA level after 48 hours of culture and after 14 days of co-differentiation (Figure 6). These findings suggest that the decrease in *Sirt1* expression could be responsible for the observed increase in adipogenesis at the expense of osteoblastogenesis in these two groups.

Other studies have shown that CR can stimulate the expression and activity of *Sirt1* in various mammalian tissues, such as the liver or white adipose tissue (24, 25). It was also shown that CR decreases the mRNA level of *Sirt1* in the cerebellum and midbrain (44),

suggesting tissue-dependent regulation of the expression. More recently, in contrast to our study, it was demonstrated that 12 months of 40% calorie restriction of male Sprague–Dawley rats (8 months old) induced an upregulation in protein expression of *Sirt1* in bone marrow fat compared to that in *ad libitum* animals (38). This discrepancy between our results and others from Cohen et al. (24) and (38) could be explained by changes in calorie or food restriction protocols, mouse strain or species, age, and sex. Indeed, twelve-month-old male rats were used in Cohen et al. studies and calorie restriction involved a daily food allotment of 60% of that eaten by the *ad libitum* animals immediately after weaning (24). In our study, eight-week-old female C57BL/6J mice were submitted to the 10-week SBA protocol. Furthermore, the weight loss of mice in each protocol of calorie restriction could also explain this discrepancy. Indeed, contrary to our protocol, which induces 12%, 18%, and 24% weight loss in mice, there is no information on weight loss in the study by Cohen et al. (24) and there was a 40% lower weight (vs CT) in the study by Duque et al. (38). Thus, the loss of Sirt1 seems to be closely associated to bone and BMSCs alterations and could explain the strong and long-lasting commitment of BMSCs towards the adipogenic pathway in SBA mice.

In our study, 18% is considered moderate weight loss, which is associated with a decrease in all parameters of body composition (low fat mass, tendency to low lean mass, low total body BMC, low femur and lumbar spine BMC) and cortical bone thickness. Furthermore, only in this weight loss category we found an upregulation of most of the adipocyte markers analyzed (*Pparg2*, *Lep*, and *Glut4*) and a downregulation of most of the osteoblast markers analyzed (*Runx2*, *Sp7*, and *Bglap*). In addition, this weight loss group displayed a strong decrease in *Sirt1* mRNA level. Considering these results, the rest of the study was dedicated to focusing on SBA 18% and investigating the effect of a short duration of SBA protocol (4 weeks) on body composition, bone architecture, BMA, BMSC differentiation and *Sirt1* expression.

A Short Duration of Moderate Weight Loss Did Not Affect Bone Architecture, BMA, BMSC Differentiation or Sirt1 Expression

Four weeks of the SBA protocol induced only a decrease in fat mass (Figure 7B) and Tb.Th (Figure 8B) without affecting the other parameters of bone architecture and BMA (Figure 8). Selective change in Tb.Th does not seem to be associated with an overall bone alteration. Moreover, this short duration did not impact BMSC differentiation towards adipogenic lineage or osteoblastogenic lineage nor did it affect the unsaturation ratio of lipid droplets (Figures 9–11, Supplementary Figure 2). Interestingly, this lack of effects on bone and BMSCs differentiation is associated with a lack of effects on Sirt1 mRNA level. This strengthens the hypothesis of a direct involvement of Sirt1 alteration on BMSCs fate decision and bone. Altogether, these results suggest that in addition to the degree of severity, the duration of energy deficit could play an important role in regulating bone architecture, BMA, and BMSC differentiation, which requires long-term protocols to be altered. This line of inquiry will be required in the future to determine when the first alterations in bone, BMA, and *Sirt1* expression can occur in our SBA model.

CONCLUSION

The present study demonstrated, for the first time, the impact of severity and length of energy deficit on bone and BMSCs differentiation capacity. The data from two groups (moderate and severe weight loss) support the hypothesis that there is a link between decrease in Sirt1 mRNA levels and alterations in bone and BMSCs differentiation capacity. A comparison of the 10-week SBA protocol to the 4-week SBA protocol strengthens this hypothesis. Finally, bone alterations appear to be totally disconnected from BMA changes in this model, probably because the increase in the number of BM pre-adipocytes, which takes place at the expense of osteoblastogenesis and does not result in an increase in mature adipocytes.

In vivo changes in BMSCs engagement in the adipogenic pathway remain to be specified using FACS analysis. Furthermore, the molecular mechanisms responsible for Sirt1 long lasting downregulation will be explored through the RNA sequencing approach.

DATA AVAILABILITY STATEMENT

The original contributions presented in the study are included in the article/Supplementary Material. Further inquiries can be directed to the corresponding authors.

ETHICS STATEMENT

The animal study was reviewed and approved by the Committee on the Ethics of Animal Experiments (CEEA) of Nord-Pas de Calais, France (permit number: CEEA#2016070717275082).

AUTHOR CONTRIBUTIONS

CC, OG, and VA contributed to the conception and design of the work. VA carried out all the cell cultures experiments, qPCR and their analysis. DL and VG contributed to sample collection during mice sacrifice. JD and FM contributed to acquisition and analysis of the microCT data. GF performed the Raman analysis. VA, OG, and CC contributed to statistical analysis. VA and OG wrote the manuscript. CC and OG contributed to the review and editing the manuscript. All authors contributed to the article and approved the submitted version.

FUNDING

VA is supported by Université du Littoral Côte d'Opale and Région Hauts-de-France.

SUPPLEMENTARY MATERIAL

The Supplementary Material for this article can be found online at: <https://www.frontiersin.org/articles/10.3389/fendo.2022.880503/full#supplementary-material>

REFERENCES

- Bredella MA, Fazeli PK, Miller KK, Misra M, Torriani M, Thomas BJ, et al. Increased Bone Marrow Fat in Anorexia Nervosa. *J Clin Endocrinol Metab* (2009) 94(6):2129–36. doi: 10.1210/jc.2008-2532
- Ecklund K, Vajapeyam S, Feldman HA, Buzney CD, Mulkern RV, Kleinman PK, et al. Bone Marrow Changes in Adolescent Girls With Anorexia Nervosa. *J Bone Mineral Res* (2010) 25(2):298–304. doi: 10.1359/jbmr.090805
- Mayo-Smith W, Rosenthal DI, Goodsitt MM, Klibanski A. Intravertebral Fat Measurement With Quantitative CT in Patients With Cushing Disease and Anorexia Nervosa. *Radiology* (1989) 170(3):835–8. doi: 10.1148/radiology.170.3.2916039
- Miller KK, Grinspoon SK, Ciampa J, Hier J, Herzog D, Klibanski A. Medical Findings in Outpatients With Anorexia Nervosa. *Arch Intern Med* (2005) 165(5):561–6. doi: 10.1001/archinte.165.5.561
- Grinspoon S, Thomas E, Pitts S, Gross E, Mickley D, Miller K, et al. Prevalence and Predictive Factors for Regional Osteopenia in Women With Anorexia Nervosa. *Ann Intern Med* (2000) 133(10):790–4. doi: 10.7326/0003-4819-133-10-200011210-00011
- Badr S, Legroux-Gérot I, Vignau J, Chauveau C, Ruschke S, Karampinos DC, et al. Comparison of Regional Bone Marrow Adiposity Characteristics at the Hip of Underweight and Weight-Recovered Women With Anorexia Nervosa Using Magnetic Resonance Spectroscopy. *Bone* (2019) 127:135–45. doi: 10.1016/j.bone.2019.05.033
- OWEN M. Marrow Stromal Stem Cells. *J Cell Sci* (1988) 1988 (Supplement_10):63–76. doi: 10.1242/jcs.1988.Supplement_10.5
- Nishimura R, Hata K, Ikeda F, Ichida F, Shimoyama A, Matsubara T, et al. Signal Transduction and Transcriptional Regulation During Mesenchymal Cell Differentiation. *J Bone Mineral Metab* (2008) 26(3):203. doi: 10.1007/s00774-007-0824-2
- Pittenger Mark F, Mackay Alastair M, Beck Stephen C, Jaiswal Rama K, Douglas R, Mosca Joseph D, et al. Multilineage Potential of Adult Human Mesenchymal Stem Cells. *Science* (1999) 284(5411):143–7. doi: 10.1126/science.284.5411.143
- Beresford JN, Bennett JH, Devlin C, Leboy PS, Owen ME. Evidence for an Inverse Relationship Between the Differentiation of Adipocytic and Osteogenic Cells in Rat Marrow Stromal Cell Cultures. *J Cell Sci* (1992) 102(2):341. doi: 10.1242/jcs.102.2.341
- Moerman EJ, Teng K, Lipschitz DA, Lecka-Czernik B. Aging Activates Adipogenic and Suppresses Osteogenic Programs in Mesenchymal Marrow Stroma/Stem Cells: The Role of PPAR-Gamma2 Transcription Factor and TGF-Beta/BMP Signaling Pathways. *Aging Cell* (2004) 3(6):379–89. doi: 10.1111/j.1474-9728.2004.00127.x
- Li J, Zhang N, Huang X, Xu J, Fernandes JC, Dai K, et al. Dexamethasone Shifts Bone Marrow Stromal Cells From Osteoblasts to Adipocytes by C/EBPalpha Promoter Methylation. *Cell Death Disease* (2013) 4(10):e832–2. doi: 10.1038/cddis.2013.348
- Song L, Liu M, Ono N, Bringhurst FR, Kronenberg HM, Guo J. Loss of Wnt/b-Catenin Signaling Causes Cell Fate Shift of Preosteoblasts From Osteoblasts to Adipocytes. *J Bone Miner Res* (2012) 27(11):2344–58. doi: 10.1002/jbmr.1694
- Skillington J, Choy L, Derynck R. Bone Morphogenetic Protein and Retinoic Acid Signaling Cooperate to Induce Osteoblast Differentiation of Preadipocytes. *J Cell Biol* (2002) 159(1):135–46. doi: 10.1083/jcb.200204060
- Bradley EW, McGee-Lawrence ME, Westendorf JJ. Hdac-Mediated Control of Endochondral and Intramembranous Ossification. *Crit Rev Eukaryot Gene Expr* (2011) 21(2):101–13. doi: 10.1615/critrevueukargeneexpr.v2
- McGee-Lawrence ME, Carpio LR, Schulze RJ, Pierce JL, McNiven MA, Farr JN, et al. Hdac3 Deficiency Increases Marrow Adiposity and Induces Lipid Storage and Glucocorticoid Metabolism in Osteochondroprogenitor Cells. *J Bone Miner Res* (2016) 31(1):116–28. doi: 10.1002/jbmr.2602
- Bordone L, Cohen D, Robinson A, Motta MC, Van Veen E, Czopik A, et al. SIRT1 Transgenic Mice Show Phenotypes Resembling Calorie Restriction. *Aging Cell* (2007) 6(6):759–67. doi: 10.1111/j.1474-9726.2007.00335.x
- Bäckesjö C-M, Li Y, Lindgren U, Haldosen L-A. Activation of Sirt1 Decreases Adipocyte Formation During Osteoblast Differentiation of Mesenchymal Stem Cells. *J Bone Mineral Res* (2006) 21(7):993–1002. doi: 10.1359/jbmr.060415
- Simic P, Zainabadi K, Bell E, Sykes DB, Saez B, Lotinun S, et al. SIRT1 Regulates Differentiation of Mesenchymal Stem Cells by Deacetylating b-Catenin. *EMBO Mol Med* (2013) 5(3):430–40. doi: 10.1002/emmm.201201606
- Shakibaei M, Shayan P, Busch F, Aldinger C, Buhmann C, Lueders C, et al. Resveratrol Mediated Modulation of Sirt-1/Runx2 Promotes Osteogenic Differentiation of Mesenchymal Stem Cells: Potential Role of Runx2 Deacetylation. *PLoS One* (2012) 7(4):e35712–2. doi: 10.1371/journal.pone.0035712
- Tseng P-C, Hou S-M, Chen R-J, Peng H-W, Hsieh C-F, Kuo M-L, et al. Resveratrol Promotes Osteogenesis of Human Mesenchymal Stem Cells by Upregulating RUNX2 Gene Expression via the SIRT1/FOXO3A Axis. *J Bone Mineral Res* (2011) 26(10):2552–63. doi: 10.1002/jbmr.460
- Chiara B, Ilaria C, Antonietta C, Francesca C, Marco M, Lucia A, et al. SIRT1 Inhibition Affects Angiogenic Properties of Human MSCs. *BioMed Res Int* (2014) 2014:783459. doi: 10.1155/2014/783459
- Orecchia A, Scarponi C, Di Felice F, Cesarini E, Avitabile S, Mai A, et al. Sirtinol Treatment Reduces Inflammation in Human Dermal Microvascular Endothelial Cells. *PLoS One* (2011) 6(9):e24307. doi: 10.1371/journal.pone.0024307
- Cohen HY, Miller C, Bitterman KJ, Wall NR, Hekking B, Kessler B, et al. Calorie Restriction Promotes Mammalian Cell Survival by Inducing the SIRT1 Deacetylase. *Science* (2004) 305(5682):390. doi: 10.1126/science.1099196
- Zainabadi K, Liu CJ, Caldwell ALM, Guarente L. SIRT1 is a Positive Regulator of *In Vivo* Bone Mass and a Therapeutic Target for Osteoporosis. *PLoS One* (2017) 12(9):e0185236–e0185236. doi: 10.1371/journal.pone.0185236
- Louvet L, Leterme D, Delplace S, Miellot F, Marchandise P, Gauthier V, et al. Sirtuin 1 Deficiency Decreases Bone Mass and Increases Bone Marrow Adiposity in a Mouse Model of Chronic Energy Deficiency. *Bone* (2020) 136:115361. doi: 10.1016/j.bone.2020.115361
- Zgheib S, Méquignon M, Lucas S, Leterme D, Ghali O, Tolle V, et al. Long-Term Physiological Alterations and Recovery in a Mouse Model of Separation Associated With Time-Restricted Feeding: A Tool to Study Anorexia Nervosa Related Consequences. *PLoS One* (2014) 9(8):e103775. doi: 10.1371/journal.pone.0103775
- Coutel X, Olejnik C, Marchandise P, Delattre J, Béhal H, Kerckhofs G, et al. A Novel microCT Method for Bone and Marrow Adipose Tissue Alignment Identifies Key Differences Between Mandible and Tibia in Rats. *Calcified Tissue Int* (2018) 103(2):189–97. doi: 10.1007/s00223-018-0397-1
- Coutel X, Delattre J, Marchandise P, Falgayrac G, Béhal H, Kerckhofs G, et al. Mandibular Bone is Protected Against Microarchitectural Alterations and Bone Marrow Adipose Conversion in Ovariectomized Rats. *Bone* (2019) 127:343–52. doi: 10.1016/j.bone.2019.06.031
- Ghali O, Broux O, Falgayrac G, Haren N, van Leeuwen JPTM, Penel G, et al. Dexamethasone in Osteogenic Medium Strongly Induces Adipocyte Differentiation of Mouse Bone Marrow Stromal Cells and Increases Osteoblast Differentiation. *BMC Cell Biol* (2015) 16:9–9. doi: 10.1186/s12860-015-0056-6
- Czamara K, Majzner K, Pacia MZ, Kochan K, Kaczor A, Baranska M. Raman Spectroscopy of Lipids: A Review. *J Raman Spectroscopy* (2015) 46(1):4–20. doi: 10.1002/jrs.4607
- Ghali O, Chauveau C, Hardouin P, Broux O, Devedjian J-C. TNF- α 's Effects on Proliferation and Apoptosis in Human Mesenchymal Stem Cells Depend on RUNX2 Expression. *J Bone Mineral Res* (2010) 25(7):1616–26. doi: 10.1002/jbmr.52
- Mitchell SE, Tang Z, Kerbois C, Delville C, Konstantopulos P, Bruel A, et al. The Effects of Graded Levels of Calorie Restriction: I. Impact of Short Term Calorie and Protein Restriction on Body Composition in the C57BL/6 Mouse. *Oncotarget* (2015) 6(18):15902–30. doi: 10.18632/oncotarget.4142
- Devlin MJ, Cloutier AM, Thomas NA, Panus DA, Lotinun S, Pinz I, et al. Caloric Restriction Leads to High Marrow Adiposity and Low Bone Mass in Growing Mice. *J Bone Miner Res* (2010) 25(9):2078–88. doi: 10.1002/jbmr.82
- Cawthorn WP, Scheller EL, Parlee SD, Pham HA, Learman BS, Redshaw CMH, et al. Expansion of Bone Marrow Adipose Tissue During Caloric Restriction Is Associated With Increased Circulating Glucocorticoids and Not With Hypoleptinemia. *Endocrinology* (2016) 157(2):508–21. doi: 10.1210/en.2015-1477
- Abella E, Feliu E, Granada I, MilláF, Oriol A, Ribera JM, et al. Bone Marrow Changes in Anorexia Nervosa Are Correlated With the Amount of Weight

- Loss and Not With Other Clinical Findings. *Am J Clin Pathol* (2002) 118 (4):582–8. doi: 10.1309/2Y7X-YDXK-006B-XLT2
37. Baek K, Bloomfield SA. Blocking β -Adrenergic Signaling Attenuates Reductions in Circulating Leptin, Cancellous Bone Mass, and Marrow Adiposity Seen With Dietary Energy Restriction. *J Appl Physiol* (2012) 113 (11):1792–801. doi: 10.1152/jappphysiol.00187.2012
38. Duque G, Al Saedi A, Rivas D, Miard S, Ferland G, Picard F, et al. Differential Effects of Long-Term Caloric Restriction and Dietary Protein Source on Bone and Marrow Fat of the Aging Rat. *J Gerontol A Biol Sci Med Sci* (2020) 75 (11):2031–6. doi: 10.1093/gerona/glaa093
39. Bianco P, Robey PG, Saggio I, Riminucci M. 'Mesenchymal' Stem Cells in Human Bone Marrow (Skeletal Stem Cells): A Critical Discussion of Their Nature, Identity, and Significance in Incurable Skeletal Disease. *Hum Gene Ther* (2010) 21(9):1057–66. doi: 10.1089/hum.2010.136
40. Vashi AV, Keramidaris E, Abberton KM, Morrison WA, Wilson JL, O'Connor AJ, et al. Adipose Differentiation of Bone Marrow-Derived Mesenchymal Stem Cells Using Pluronic F-127 Hydrogel *In Vitro*. *Biomaterials* (2008) 29(5):573–9. doi: 10.1016/j.biomaterials.2007.10.017
41. Cawthorn WP, Scheller EL, Learman BS, Parlee SD, Simon BR, Mori H, et al. Bone Marrow Adipose Tissue Is an Endocrine Organ That Contributes to Increased Circulating Adiponectin During Caloric Restriction. *Cell Metab* (2014) 20(2):368–75. doi: 10.1016/j.cmet.2014.06.003
42. Artsi H, Cohen-Kfir E, Gurt I, Shahar R, Bajayo A, Kalish N, et al. The Sirtuin1 Activator SRT3025 Down-Regulates Sclerostin and Rescues Ovariectomy-Induced Bone Loss and Biomechanical Deterioration in Female Mice. *Endocrinology* (2014) 155(9):3508–15. doi: 10.1210/en.2014-1334
43. Herranz D, Muñoz-Martin M, Cañamero M, Mulero F, Martinez-Pastor B, Fernandez-Capetillo O, et al. Sirt1 Improves Healthy Ageing and Protects From Metabolic Syndrome-Associated Cancer. *Nat Commun* (2010) 1(1):3. doi: 10.1038/ncomms1001
44. Chen D, Steele AD, Hutter G, Bruno J, Govindarajan A, Easlon E, et al. The Role of Calorie Restriction and SIRT1 in Prion-Mediated Neurodegeneration. *Exp Gerontol* (2008) 43(12):1086–93. doi: 10.1016/j.exger.2008.08.050

Conflict of Interest: The authors declare that the research was conducted in the absence of any commercial or financial relationships that could be construed as a potential conflict of interest.

Publisher's Note: All claims expressed in this article are solely those of the authors and do not necessarily represent those of their affiliated organizations, or those of the publisher, the editors and the reviewers. Any product that may be evaluated in this article, or claim that may be made by its manufacturer, is not guaranteed or endorsed by the publisher.

Copyright © 2022 Avilkina, Leterme, Falgayrac, Delattre, Miellot, Gauthier, Chauveau and Ghali Mhennii. This is an open-access article distributed under the terms of the Creative Commons Attribution License (CC BY). The use, distribution or reproduction in other forums is permitted, provided the original author(s) and the copyright owner(s) are credited and that the original publication in this journal is cited, in accordance with accepted academic practice. No use, distribution or reproduction is permitted which does not comply with these terms.

4. Transcriptomic analysis of BMSCs extracted from 10-Week and 4-Week SBA Protocols (Cohort 1) by RNA Sequencing

Differentially expressed genes in 10-week SBA study (cohort 1)

In order to understand the transcriptomic differences between BMSCs extracted from SBA 18% weight loss and CT mice in two different protocols (10-week and 4-week cohort 1), RNA-seq analysis was conducted in undifferentiated BMSCs. Cells were extracted from SBA 18% and CT mice BM, and plated for 48h. This was done to separate haematopoietic cells from a heterogeneous population of BMSCs. Despite cell plating, we considered that adherent cells after 48 hours represent cell population within BM on mice. The experiment and analysis of data were performed with help of the Phillipe Froguel team (Amélie Bonnefond, Mehdi Derhourhi and Mickaël Canouil) from European Genomic Institute for Diabetes (EGID, Université de Lille). The current section focuses on preliminary analysis of RNA-seq data, describing basic findings of differentially expressed genes and pathways (based on lowest p-value) between SBA 18% and CT conditions, in the context of 10-week or 4-week SBA protocols.

Volcano Plot

Model: group

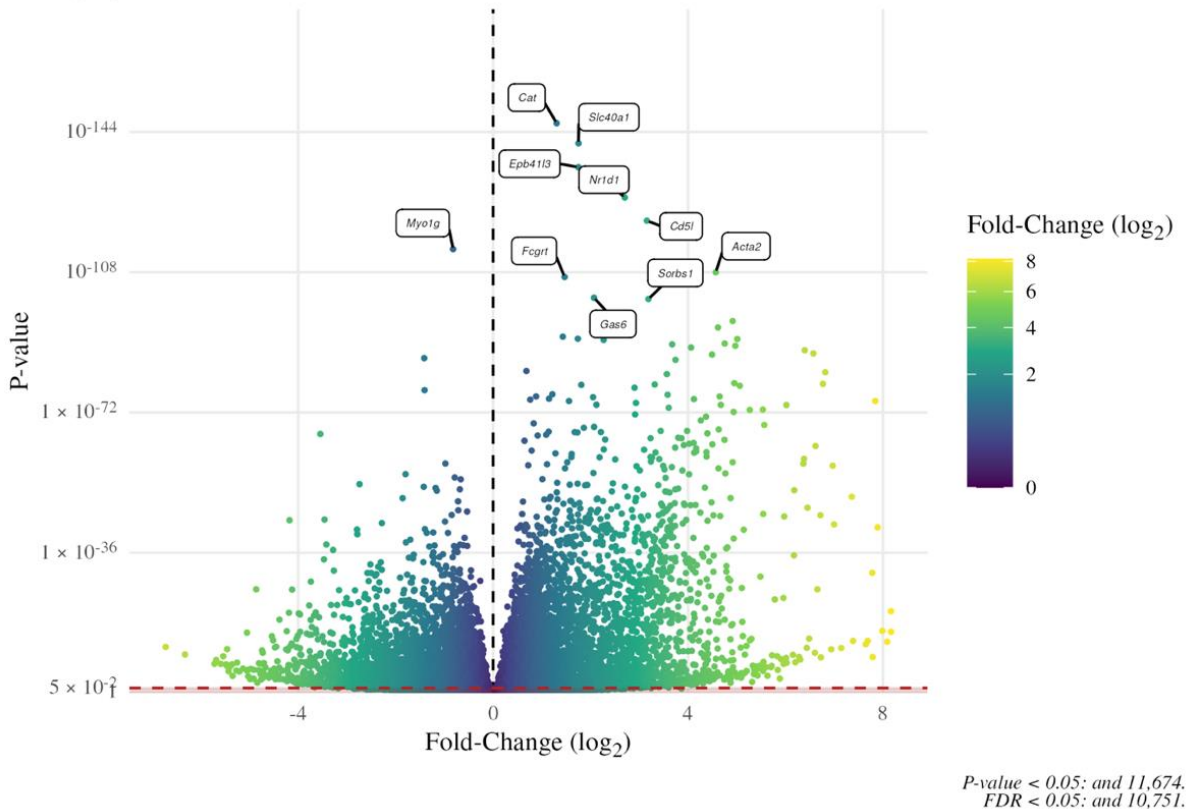


Figure 38. Volcano Plot of top altered genes in 10-week study. Summary of most upregulated and downregulated genes in 10-week SBA study, where negative log₂ is downregulated genes in SBA 18% condition and positive log₂ values are upregulated genes in SBA 18% group.

To investigate the difference between CT and SBA 18% mice, we firstly focused on studying differentially expressed genes. Overall, 10 751 genes were identified to be statistically significantly altered in 10-week SBA 18% group. This analysis was conducted based on transcriptome wide association study (TWAS) data in order to establish differentially expressed genes between two conditions (SBA 18% vs. CT). After removing duplicated and non-identified genes, we quantified that in the SBA 18% weight loss mice, extracted BMSCs contained 3 664 genes, which were found to be significantly upregulated and 4 451 genes were significantly downregulated.

In a first approach, to better understand changes that take place in cells from SBA 18% weight loss mice comparing to CT, the most significantly upregulated and downregulated genes were identified, based on p-value (Fig. 38). This approach was taken as low p-value represents in our heterogeneous cell population, highlighted genes having a high probability to consistently

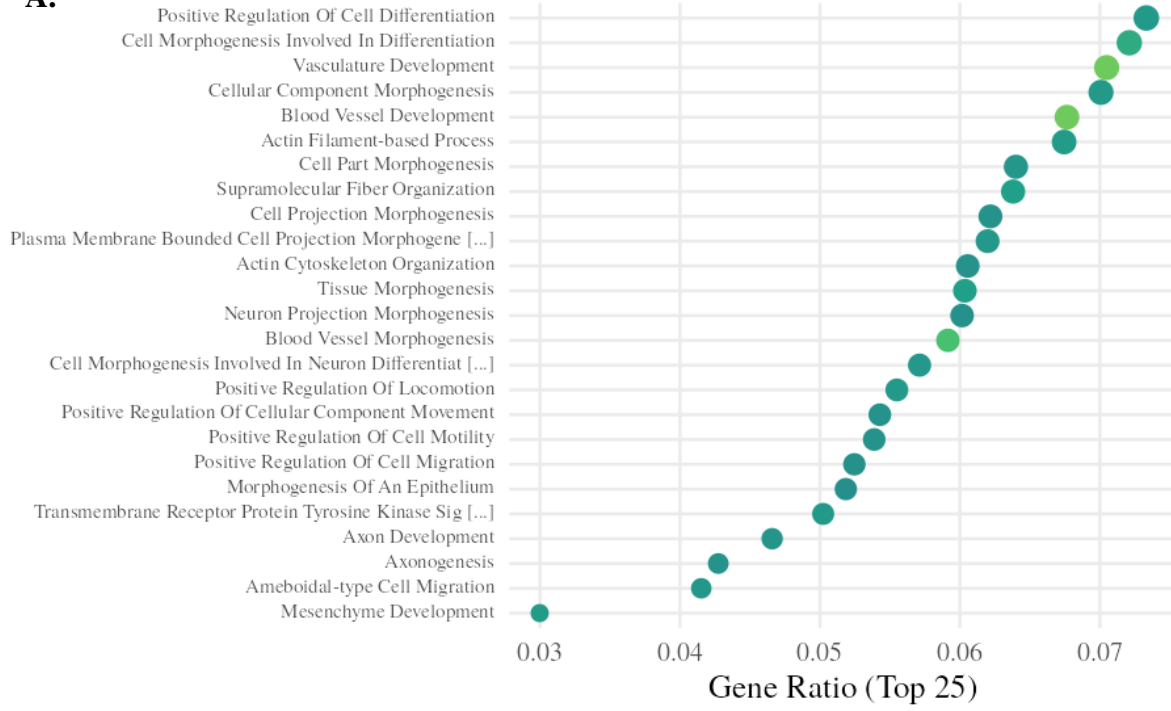
changes within the population and between our replicates (n=6). Genes with lowest p-value changes are briefly described in table 8, with their main associated functions. This preliminary analysis showed that lowest p-value among statistically downregulated genes (vs. CT) was found to be in membrane-associated class I myosin (*Myo1g*), which is known to regulate immune response through induction of T-cell migration and phagocytosis (Table 8) (871,872). But the fold change for this gene is very modest, like for the most significantly upregulated gene. Indeed, catalase (*Cat*) was found to exhibit lowest p-value among upregulated genes in SBA 18% condition, and it is involved in protection against oxidative stress (873). It was also discovered to have a positive effect on haematopoiesis, including granulocyte production (Table 8) (874). Actin alpha 2 (*Acta2*) gene, also exhibited one of the lowest p-value, which was combined with comparatively high fold change value ($\log_2 = 4.5$), suggesting that the level of *Acta2* mRNA production is highly increased in SBA 18% group comparing to CT (Fig. 38). *Acta2* encodes smooth muscle α -2 actin (SM α -2 actin) protein that is important for cell movement, found predominantly in smooth muscle cell lining of the internal organs (intestine, stomach, blood vessels) (Table 7) (875). SM α -2 actin positive cells were shown to be present in BM as well, they have monocyte/macrophage lineage origin and are involved in vascular remodelling (876). Strong increase in *Acta2* expression in SBA 18% derived from BMSCs could be potentially associated with upregulation of cellular function connected with actin filaments and cell mobility. As it can be observed, some of the highlighted genes do not exhibit a large fold change (positive or negative), meaning that change in their expression rate might be not biologically significant, therefore deeper analysis of the data would be required in order to highlight genes with the largest fold change in combination with low p-value, to study genes that are biologically altered in extracted BMSCs and play valuable role in SBA induced alterations.

Gene	Full Name	Function
Immune system		
<i>Myo1g</i>	Membrane-associated Class I Myosin	Unconventional myosin required during immune response for detection of rare antigen-presenting cells by regulating T-cell migration.
<i>Fcgrt</i>	Fc Gamma Receptor and Transporter	The encoded protein transfers immunoglobulin G antibodies from mother to foetus across the placenta. This protein also binds immunoglobulin G to protect the antibody from degradation.
<i>Slc40a1</i>	Solute Carrier Family 40 Member 1	Major iron transporter that plays a key role in balancing cellular and systemic iron levels. Known to be expressed in monocytes and macrophages.
Glucose/lipid metabolism		
<i>Sorbs1</i>	Sorbin and SH3 Domain Containing	Gene encodes a CBL-associated protein which functions in the signalling and stimulation of insulin. Required for insulin-stimulated glucose transport.
<i>Nr1d1</i>	Nuclear Receptor Subfamily 1 Group D Member 1	Transcriptional repressor which coordinates circadian rhythm and metabolic pathways in a heme-dependent manner. Regulates lipid metabolism by repressing the expression of apolipoprotein C3 (APOC3) and by influencing the activity of SREBPs. Moreover, represses insulin induced gene 2 (INSIG2) which interferes with the proteolytic activation of SREBPs which in turn govern the rhythmic expression of enzymes with key functions in sterol and fatty acid synthesis.
<i>Cd5l</i>	CD5 Molecule Like	Acts as a key regulator of lipid synthesis: mainly expressed by macrophages in lymphoid and inflamed tissues and regulates mechanisms in inflammatory responses, such as infection or atherosclerosis.
Oxidative-stress-response		
<i>Cat</i>	Catalase	An antioxidant enzyme in the body's defence against oxidative stress. It converts the reactive oxygen species hydrogen peroxide to water and oxygen and thereby mitigates the toxic effects of hydrogen peroxide.
Cell mobility and structure		
<i>Acta2</i>	Actin Alpha 2	Highly conserved protein that is involved in cell mobility, structure, integrity, and intercellular signalling.
<i>Epb41l3</i>	Erythrocyte Membrane Protein Band 4.1 Like 3	Predicted to enable cytoskeletal protein-membrane anchor activity and a structural constituent of cytoskeleton.
Cell proliferation		
<i>Gas6</i>	Growth Arrest Specific 6	Encoded protein thought to be involved in the stimulation of cell proliferation.

Table 7. Summary of gene function (10-week). Table summarises a name and function of genes, which were identified by RNA sequencing as top upregulated (green) and downregulated (red) genes in 10-week SBA 18% condition. Information is taken from genecards.org.

To see wider picture of events taking place after SBA protocol induction, obtained gene expression data was used to conduct ORA using gene ontology (GO) Biological Processes database to identify the top affected pathways in SBA 18% group (vs CT). This analysis combines upregulated/downregulated genes according to previously described database of pathways (GO Biological Processes), then it quantifies the proportion of upregulated and downregulated genes present in a particular pathway. If the number of upregulated genes is greater, it draws the conclusion that this pathway is also upregulated. When there is a balance between upregulated and downregulated genes from one given pathway, this pathway is counted in up- and in downregulated pathways at the same time. Results on the analysis showed that in BMSCs from 10-week protocol, significantly upregulated genes were allocated to 963 pathways. In the diagram, we presented the top 25 pathways that contain the highest number of genes, and these genes exhibit low p-value (Fig. 39A). Most of the displayed upregulated pathways are involved in cell differentiation and morphogenesis (vs. CT) (Fig. 39A). In particular, activation of actin filament processes, axonogenesis and regulation of cellular component movement were increased, suggesting that cells within this population are undergoing reorganisation and restructuring (Fig. 39A).

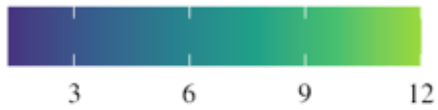
A.



Number of Genes

● 100 ● 200 ● 300

$-\log_{10}(\text{FDR})$
(Benjamini-Hochberg)



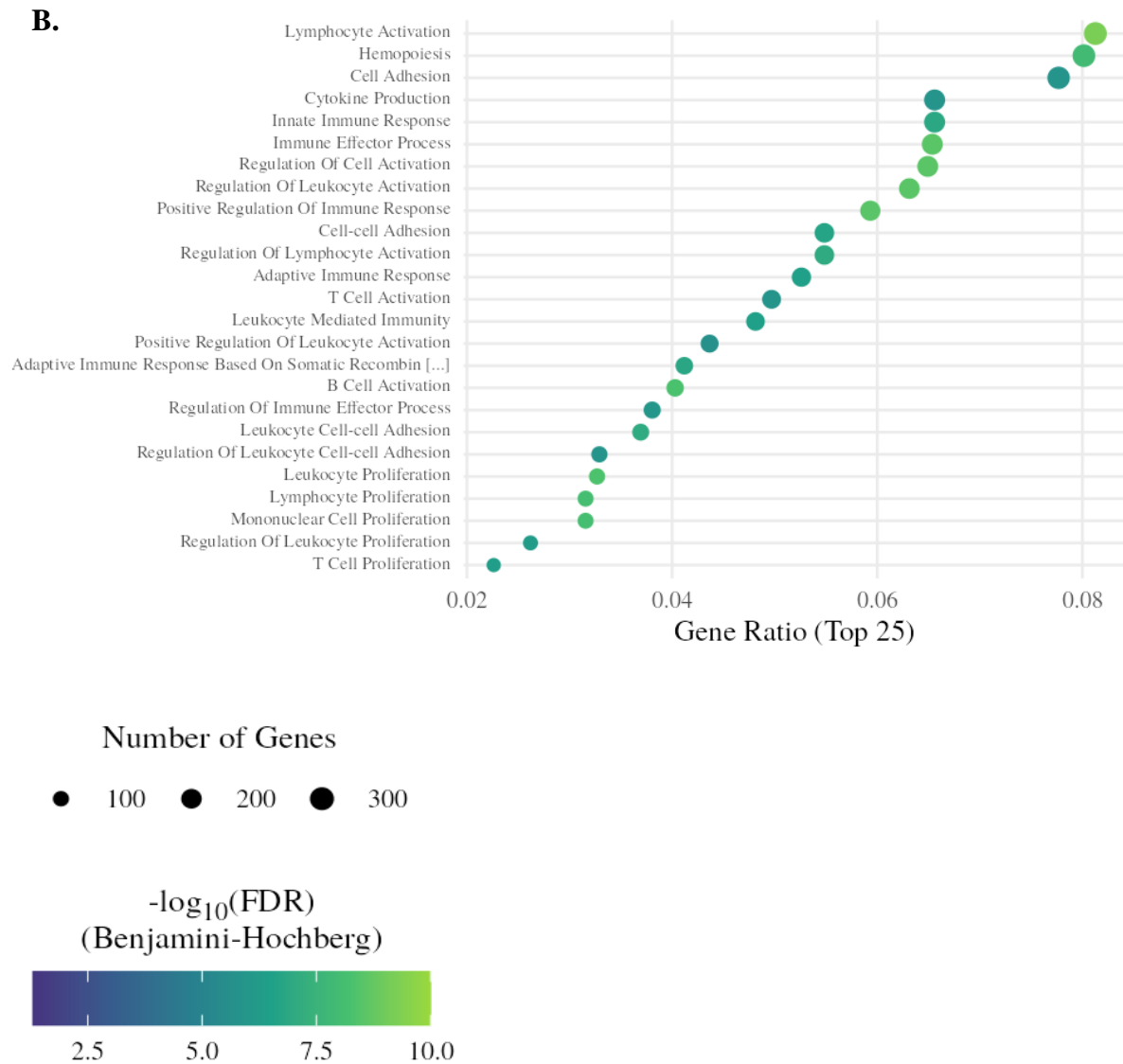


Figure 39. Most upregulated and downregulated pathways in 10-week SBA 18% condition. A-B. Using over-representation test, top 25 significantly upregulated and downregulated (respectively) pathways in BMSCs extracted from SBA18% (vs CT) based on Gene Ontology Biological Processes database.

Meanwhile, significantly downregulated genes in BMSCs extracted from SBA 18% weight loss mice, were identified to be present among 82 pathways. Top significantly downregulated pathways in 10-week SBA protocol were found to be associated with haematopoiesis and immune response (Fig. 39B). More specifically, we found that in SBA 18% condition BMSCs exhibit a downregulation in pathways associated with lymphocyte activation, cytokine production, immune cell proliferation and innate immune response (Fig. 39B). This potentially indicates that our heterogeneous population of extracted BMSCs contains a significant population of haematopoietic cells.

Differentially expressed genes in 4-week SBA study (cohort 1)

The next step was to explore results of RNA-seq in BMSCs extracted from 4-week SBA 18% weight loss mice and compare them to cells extracted from CT mice. Similar to previous section, we firstly focused on studying differentially expressed genes and found that 1 816 genes were statistically significantly altered in 4-week SBA 18% group. In the SBA 18% weight loss mice, extracted BMSCs, 889 genes were found to be significantly upregulated and 927 genes were significantly downregulated.

Identically to 10-week data analysis, in 4-week samples we explored changes associated with the lowest p-values. (Fig. 40). Genes with lowest p-value changes are briefly described in table 9, with their main associated functions. Neurexin 1 (*Nrxn1*) exhibited lowest p-value among significantly downregulated genes (vs. CT), it is characterised to play the major role in the neural system (877). It appears to be regulating synapse formation, which shows itself through participation in calcium signalling, synaptogenesis, and heterogeneous cell-to-cell adhesion—all of which are mediated by a variety of ligands (877). Interestingly, in BM, *Nrxn1* was found to suppress proliferation of haematopoietic progenitors (878). Kinzfohl *et al.* has shown that *in vivo* injection of recombinant NXPH1 caused myelo- and lymphosuppression in the BM (878) (Table 8). Therefore, it can be hypothesised that strong suppression of *Nrxn1* in BMSCs can give a positive effect on haematopoiesis.

Volcano Plot

Model: group

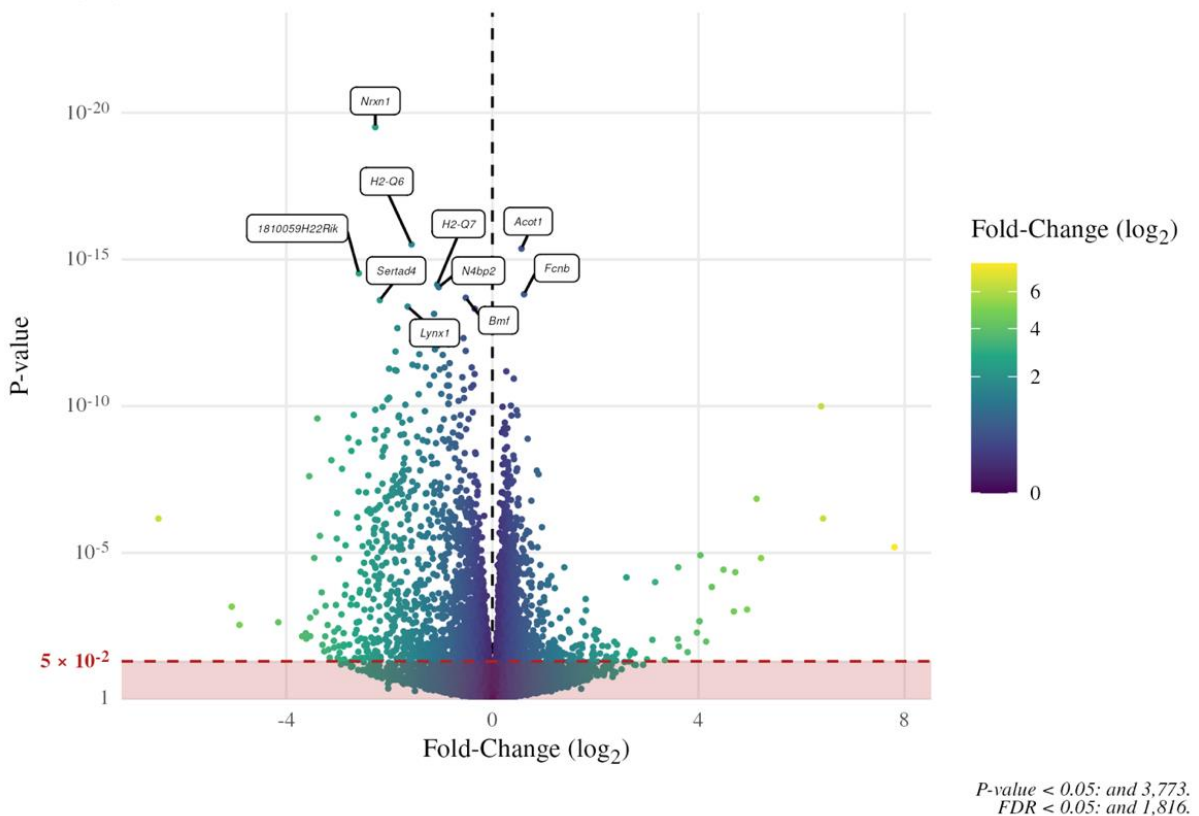


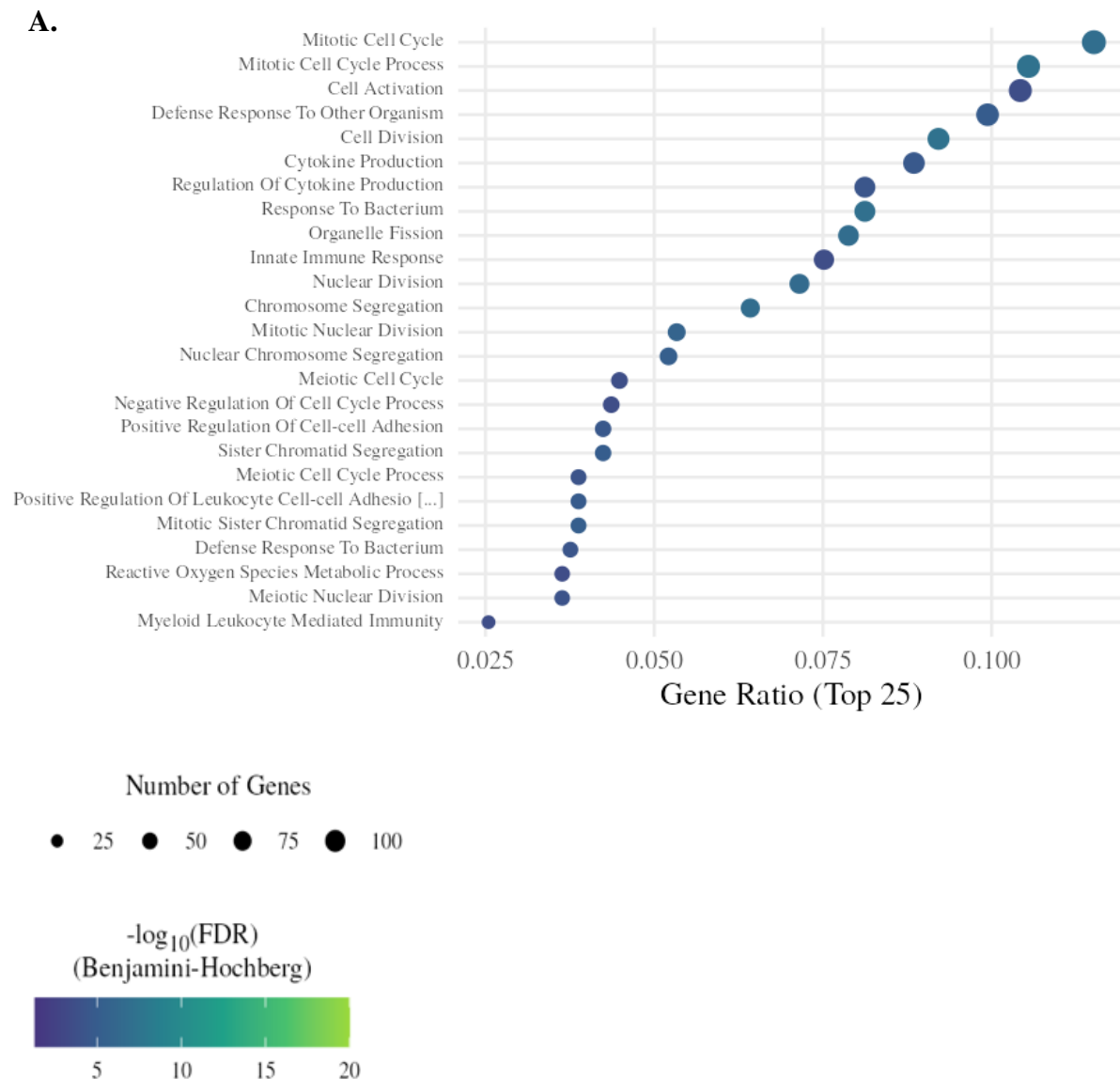
Figure 40. Volcano Plot of top altered genes in 4-week study. Summary of most upregulated and downregulated genes in 4-week SBA study, where negative \log_2 is downregulated genes in SBA 18% condition and positive \log_2 values are upregulated genes in SBA 18%.

Moreover, RNA-seq data showed that one of the highest negative \log_2 and low p-value were in RIKEN cDNA 1810059H22 (*1810059H22Rik*) gene, suggesting that its level in highly decreased in SBA 18% group comparing to CT (Fig. 40). Currently, not much information is known about this gene, only that it is an orthologous to human C9orf40 (chromosome 9 open reading frame 40) (Table 8). Additionally, RNA-seq data exposed that highest positive \log_2 and low p-value were in acetyl-CoA thioesterase 1 (*Acot1*) gene, indicating that its level in highly increased in SBA 18% group comparing to CT (Fig. 40). This gene codes for a protein that is involved in metabolism of long-chain FA (879) (Table 8). ACOT1 was found to regulate lipid metabolism in type 2 diabetes (880). Moreover, ACOT1 has been shown to play a central role in regulating hepatic fatty acid oxidation, oxidative stress, and inflammation during fasting (881).

Gene	Full Name	Function
Nervous system		
<i>Nrxn1</i>	Neurexin 1	Gene encodes a single-pass type I membrane protein that belongs to the neurexin family, which are cell-surface receptors that bind neuroligins to form Ca ²⁺ -dependent neurexin/neuroligin complexes at synapses in the central nervous system.
<i>Lynx1</i>	Ly6/Neurotoxin 1	Acts in different tissues through interaction to nicotinic acetylcholine receptors (nAChRs). Modulates functional properties of nicotinic acetylcholine receptors (nAChRs) to prevent excessive excitation, and hence neurodegeneration
Immune system		
<i>H2-Q6</i>	Histocompatibility 2, Q Region Locus 6	This locus controls a lymph node and splenic lymphocyte antigen detection. Orthologue of human HLA-A (major histocompatibility complex, class I, A) - playing a central role in the immune system by presenting peptides derived from the endoplasmic reticulum lumen that can be recognized by cytotoxic T cells.
<i>H2-Q7</i>	Histocompatibility 2, Q Region Locus 7	Predicted to be part of MHC class I protein complex and MHC class Ib protein complex. Orthologous to human HLA-E,F,G (major histocompatibility complex, class I, E, F, G).
<i>Fcnb</i>	Ficolin B	Is a homologue of human ficolin-1, that plays an important role in innate immunity
Not defined		
<i>Sertad4</i>	SERTA Domain Containing 4	Ortholog of human SERTAD4, interacts with bisphenol A and cisplatin.
<i>1810059H22 Rik</i>	RIKEN cDNA 1810059H22 gene	Orthologous to human C9orf40 (chromosome 9 open reading frame 40).
DNA repairs and apoptosis		
<i>N4bp2</i>	NEDD4 Binding Protein 2	This protein binds and hydrolyses ATP, may function as a 5'-polynucleotide kinase, and has the capacity to be a ubiquitylation substrate. This protein may play a role in transcription-coupled DNA repair or genetic recombination.
<i>Bmf</i>	Bcl2 Modifying Factor	BCL2 family members form hetero- or homodimers and act as anti- or pro-apoptotic regulators that are involved in a wide variety of cellular activities. This protein contains a single BCL2 homology domain 3 (BH3), and has been shown to bind BCL2 proteins and function as an apoptotic activator.
FA oxidation		
<i>Acot1</i>	Acetyl-CoA Thioesterase 1	This gene is involved in acyl-CoA metabolic process; long-chain fatty acid metabolic process; and very long-chain fatty acid metabolic process.

Table 8. Summary of gene function (4-week). Table summarises a name and function of genes, which were identified by RNA sequencing as top upregulated (green) and downregulated (red) genes in 4-week SBA 18% condition. Information is taken from genecards.org and informatics.jax.org.

Next, we focused on identifying the wider picture of events taking place after short term SBA protocol induction. Similar to 10-week data analysis, obtained data in 4-week study was used to conduct ORA using gene ontology (GO) Biological Processes database to identify the top affected pathways in SBA 18% group (vs CT). Result of the analysis indicated that significantly upregulated genes were related to 419 pathways. The top 25 of upregulated pathways were found to be related to mitotic cellular division and also in cytokine production (Fig. 41A). Similarly, to 10-week finding, RNA-seq data showed that in SBA 18% condition exposure for 4 weeks, results in downregulation of the immune response and immune cell activation in extracted BMSCs (Fig. 41B). Leukocyte and lymphocyte activation, adaptive immune response were found to be significantly altered (Fig. 41B).



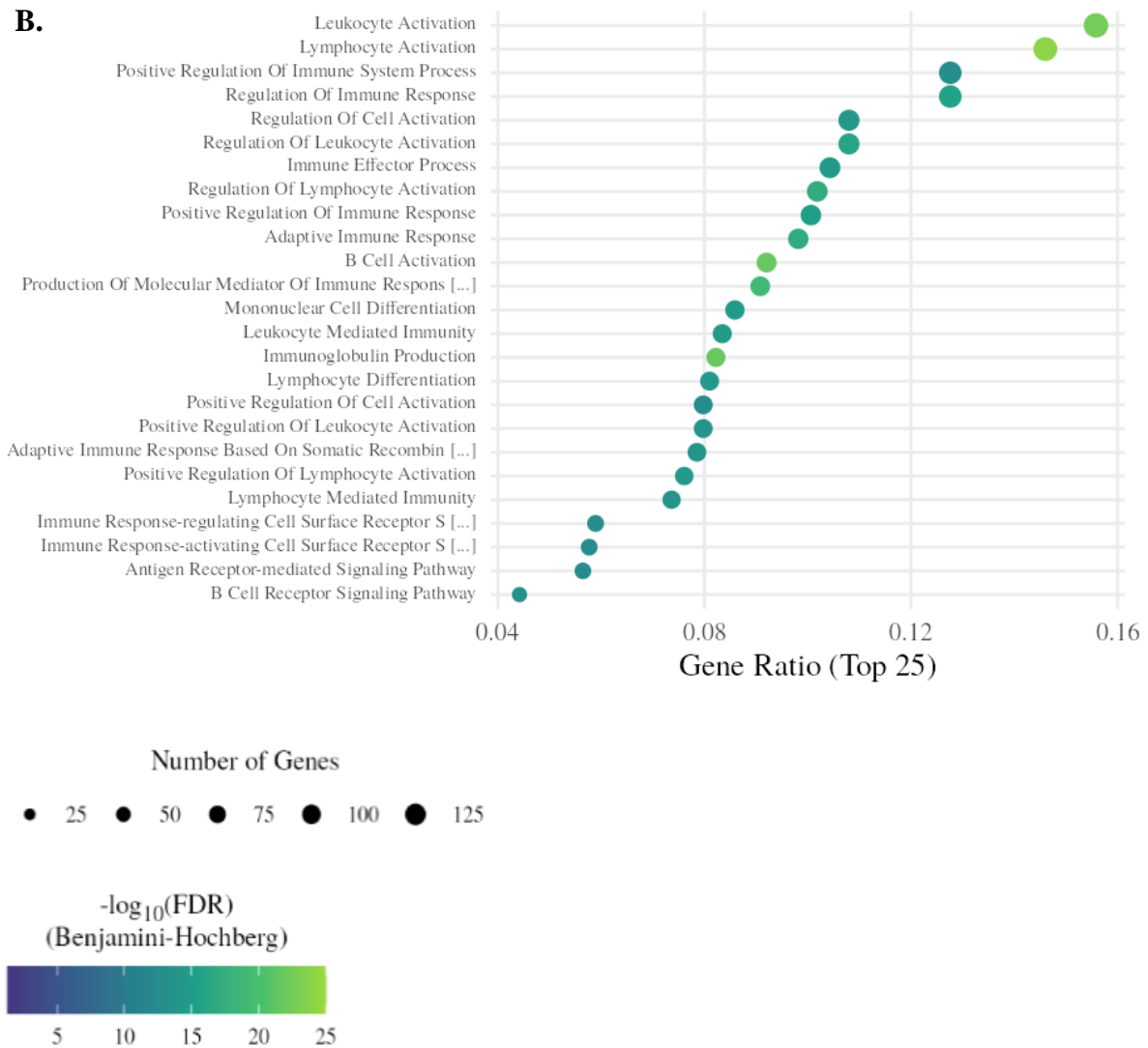


Figure 41. Most upregulated and downregulated pathways in 4-week SBA 18% condition. A-B. Using over-representation test, top 25 significantly upregulated and downregulated (respectively) pathways in BMSCs extracted from SBA18% (vs CT) based on Gene Ontology Biological Processes database.

To do a deeper analysis of affected pathways and their link with SBA protocols, we tried to determine which alteration pathways are similarly affected after both durations and which are more specific of the 4-week duration or the 10-week duration. When we compared upregulated pathway of 10-week with 4-week, we concluded that the main difference between conditions is that 10-week upregulated pathways are involved predominantly in the process of cell differentiation and tissue morphogenesis. On the other hand, closer look on 4-week results revealed that upregulated pathways are involved in the process of cell division and mitosis. This suggests that BMSCs extracted from 10-week SBA mice exhibit the mesenchymal

development and are undergoing the process of cell differentiation, whereas BMSCs from 4-week SBA mice are just undergoing cell proliferation. After close comparison of downregulated pathways, we found that some pathways are shared between 10-week and 4-week groups, however, in 10-week group BMSCs exhibit decrease in myeloid cell proliferation, but in 4-week group BMSCs display a decrease in lymphocyte activation.

Overall, the results of 4-week study resemble similarities with 10-week study, as in both condition haematopoiesis related processes were significantly downregulated in cells from weight loss condition. This result might indicate that in the process of BMSCs isolation, large fraction of attached cells exhibits haematopoietic and myeloid lineage, indicating that assessment of cell subpopulation withing BMSCs culture is required. The process of cells plating also induced increase in cell adhesion in both 10-week and 4-week BMSCs. Adhesion to the well, induced cell proliferation and potentially resulted in observed upregulation in mitosis, organelle morphogenesis and chromosome segregation.

Expression of genes involved in adipogenesis and osteoblastogenesis in 10-week and 4-week SBA studies (cohort 1)

In this thesis work, the main focus of interest is the switch in BMSC differentiation capacity, induced by significant weight loss in mice. Therefore, the findings of RNA sequencing were summarised in the form of Volcano plot, which represents downregulated/upregulated genes involved in adipogenic and osteoblastogenic differentiations in 10-week study (Fig. 42A,B). As it was expected, most of adipogenic marker genes in SBA 18% condition are found to have elevated mRNA count (vs. CT) (Fig. 42A). Only *Slc2a4* gene that codes for GLUT4 transporter was found to be decrease, however the level of its mRNA was found to be low (SBA18% - TPM = 0,086). Additionally, in PART1 we described that the lack of BMA increase in 10-week cohort 1 study could be due to the potential increase in adipocyte progenitors or MALPs, without increase in mature adipocytes. Therefore, we looked at the expression level of *Zfp423* gene mRNA, as it was described to be a pre-adipocyte marker. We identified that this marker is upregulated only in 10-week SBA 18% weight loss samples (308% vs. CT), indicating that there is a potential increase in pre-adipocyte number, which remains to be confirmed with flow cytometry analysis in a further study.

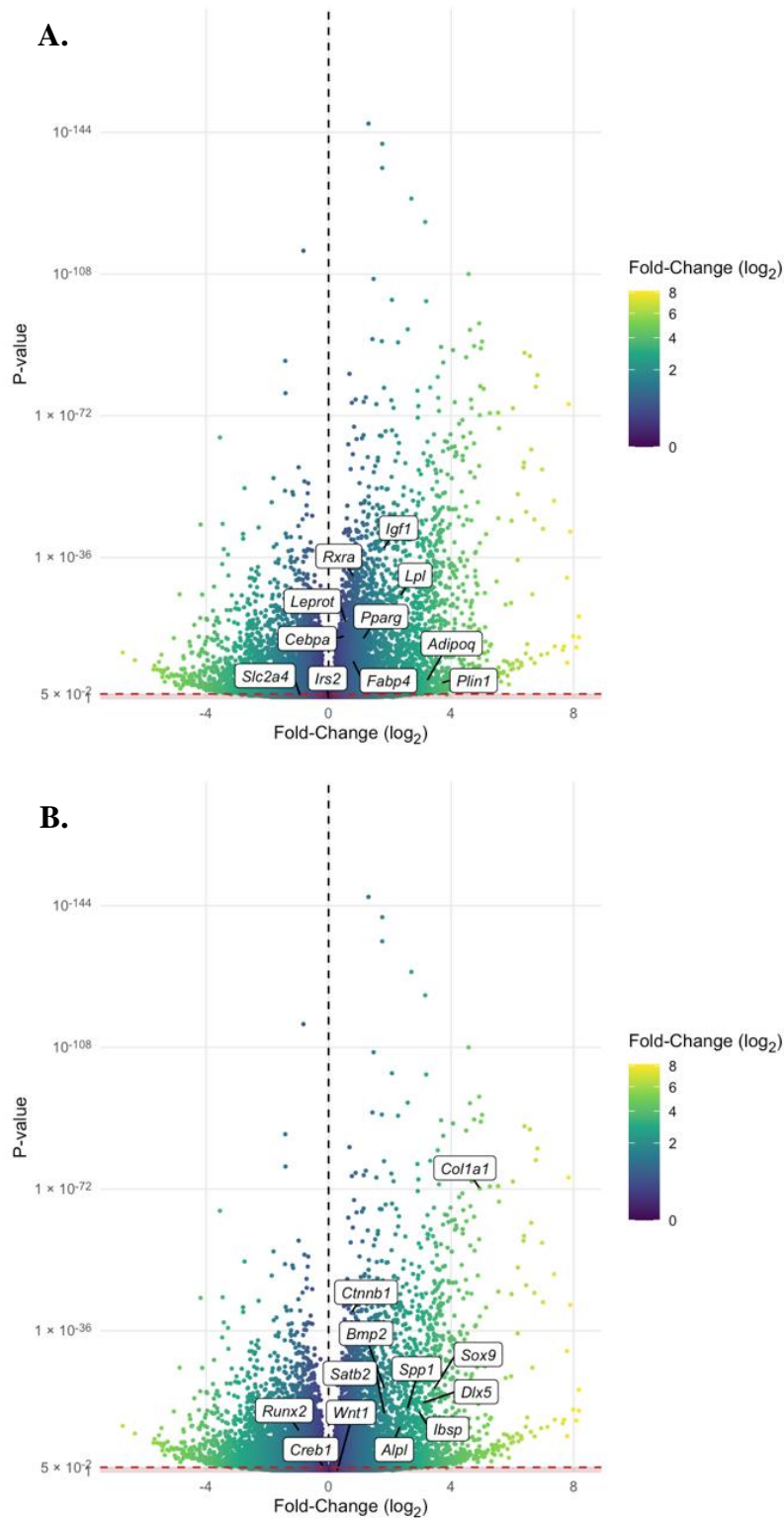


Figure 42. Volcano Plot of 10-week study that tags common adipogenic and osteoblastogenic marker genes. A. Summary of common adipogenic marker genes in 10-week SBA study, where negative \log_2 is downregulated genes in SBA 18% condition and positive \log_2 values are upregulated genes; B. Summary of common osteoblastogenic marker genes in 10-week SBA study, where negative \log_2 is downregulated genes in SBA 18% condition and positive \log_2 values are upregulated genes.

Among osteoblastogenic markers, *Runx2* and *Creb1* mRNA level were decreased in BMSCs extracted from weight loss mice, suggesting the suppression of early osteoblastogenic markers (Fig. 42B). To our surprise, early osteogenic marker, osterix (*Sp7*), was not found in the RNA database. Despite this, available data confirms the decrease in *Runx2* mRNA level already revealed in these cells using q-PCR and in the same cells after co-differentiation (882). But at the same time, it was surprising to discover that multiple osteoblastogenic markers are also upregulated in same BMSCs extracted from 10-week SBA 18% weight loss mice (Fig. 42B).

After studying the expression level of adipogenic and osteoblastogenic genes in 4-week group, results showed that a lot of genes were not detected, indicating that this genes were not present in the dataset, in this group and some of the changes were not statistically significant (Fig. 43A,B). In SBA 18% group, *Adipoq* and *Plin1* were shown to be significantly increased, together with slight upregulation of *Lpl* and *Igf1* (Fig. 43A). Osteoblastogenesis markers exhibited very low mRNA count with no statistically significant changes (Fig. 43B). These results complemented initial findings of this 4-week cohort, that 18% weight loss in mice, did not alter differentiation capacity of BMSCs.

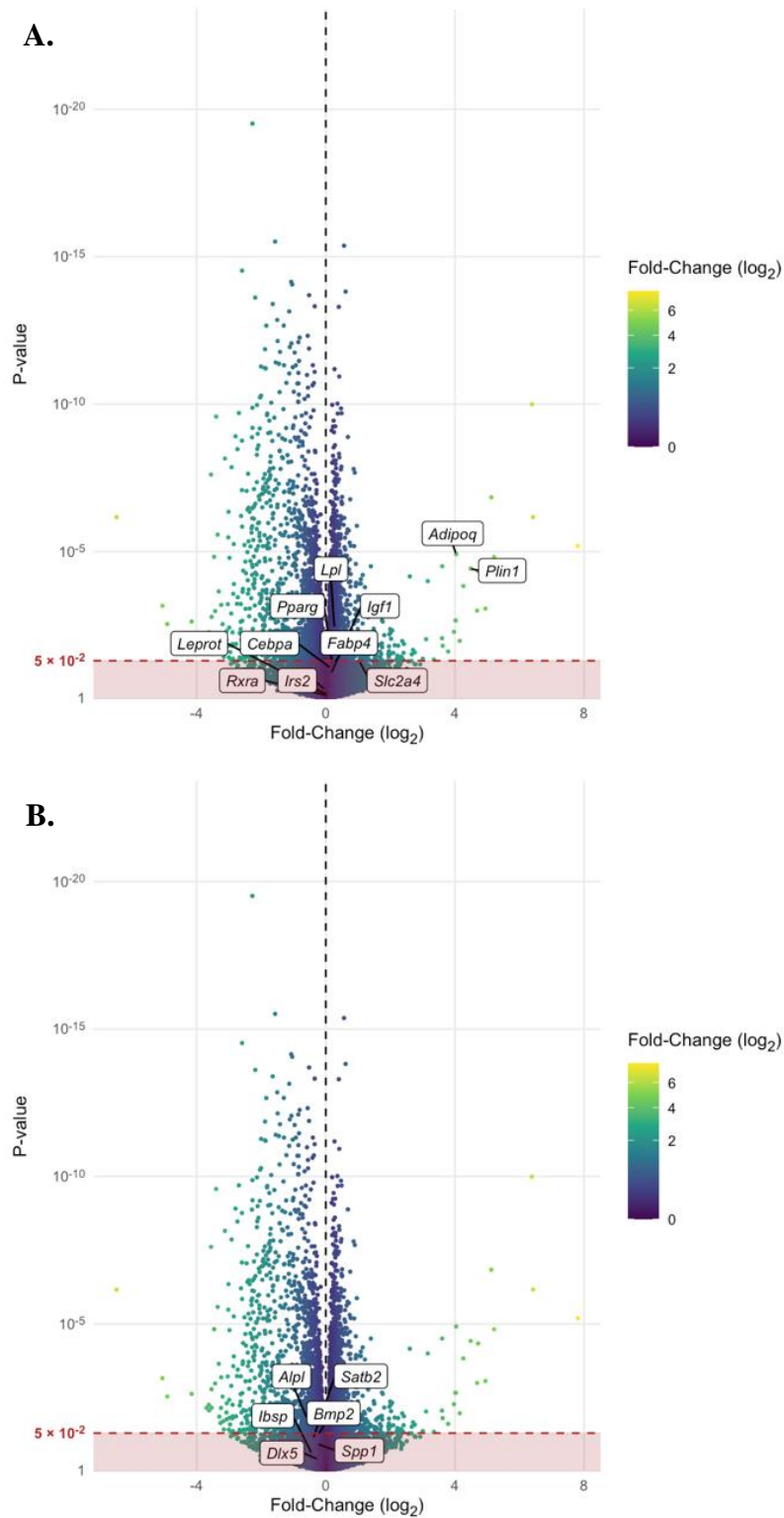


Figure 43. Volcano Plot of 4-week study that tags common adipogenic and osteoblastogenic marker genes. A. Summary of common adipogenic marker genes in 4-week SBA study, where negative log₂ is downregulated genes in SBA 18% condition and positive log₂ values are upregulated genes; B. Summary of common osteoblastogenic marker genes in 4-week SBA study, where negative log₂ is downregulated genes in SBA 18% condition and positive log₂ values are upregulated genes.

5. Replication of Original Study – 10-Week and 4-Week SBA Protocols Cohort 2

Replication of 10-week 18% weight loss SBA protocol resulted in reduced fat mass and bone mineral density, without affecting lean mass

In order to confirm and strengthen the finding of previous cohort, as well as, to test possible cohort effect in this study, we replicated 10-week and 4-week SBA protocols. In the current study, we focused on 18% weight loss condition and increased mice cohort to 12 subjects per condition. Result of mouse body weight, after completion of 10-week SBA protocol, showed an 18.02% decrease in SBA group (vs D0) and 22.1% increase in the CT group (vs D0) (Fig. 44A). Furthermore, the 18% SBA group exhibit 35.3% lower body weight than CT at the last day of SBA protocol (Fig. 44B). After mice sacrifice, study of mouse tissue weight showed that there is a significant decrease in SCAT and VAT (-67% and -72% vs. CT, respectively), without change in liver mass, similarly to SBA 18% group in previous cohort (cohort 1) (Fig. 44C). A significant reduction in uterus weight (-38% vs. CT) was also observed, suggesting alteration of the reproductive functions (Fig. 44C). When we studied average cumulative food consumption in SBA mice comparing to CT, we saw that there was no difference between the two groups, indicating that CT and SBA mice had very different energy expenditure rate (Fig. 44D). Separation induced stress and thermogenesis, allowed to 18% weight loss in mice, without change in food consumption rate (Fig. 44D). Characterisation of body parameters was done at the whole-body level, using DEXA (PIXIMUS) revealed that 10-week energy deficiency (SBA 18%) resulted in a 51% decrease in global fat mass (vs. CT) and had no effect upon lean mass (vs. CT) (Fig.44E). Similar changes in lean and fat mass were observed in this group from the previous cohort, with the exception that previously lean mass demonstrated a tendency to decrease in this condition (Fig. 26F). Additionally, PIXIMUS analysis of the skeleton confirmed previous findings from cohort 1, we observed significant decrease in total BMC (-16% vs. CT) and in femur BMC (-26% vs. CT) (Fig. 44G-I). Only, 10-week duration induced significant decrease in vertebra BMC (L3-L5) in cohort 1, however this time vertebrae BMC was not affected by SBA protocol (Fig. 44I).

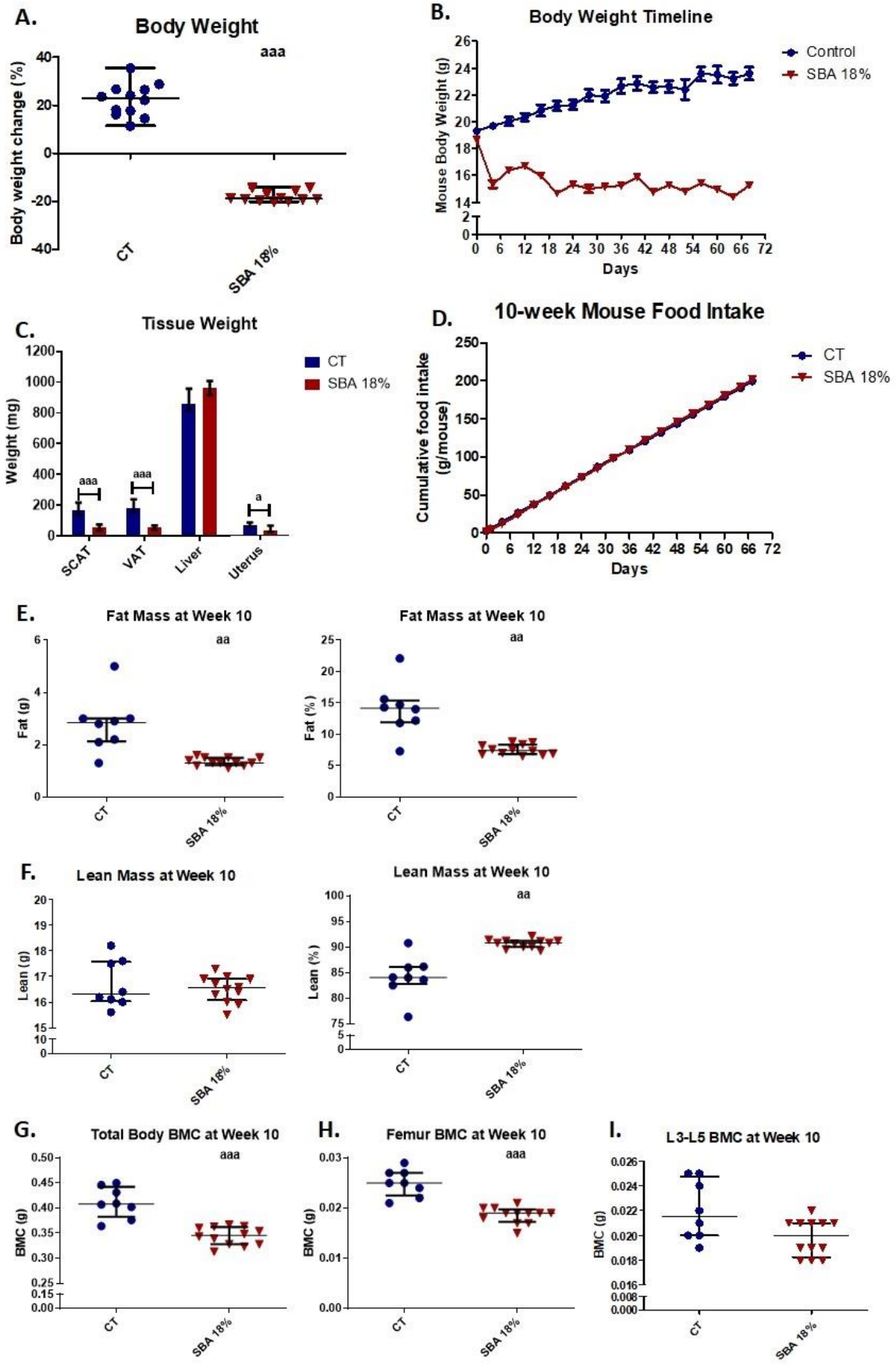


Figure 44. Body mass, BMC, fat and lean mass in mice after 10 weeks of SBA protocol.

The body weight and composition analysis were performed on standard condition (CT) and weight loss group (SBA 18%). A. Graph represents a percentage body weight loss on mice between day 0 and 10 weeks of SBA protocol; B. Body weight timeline was presented for each of SBA condition, with average mouse body weight for every 6 days of the protocol (starting at day 0 and ending at day 68); C. After mice sacrifice, subcutaneous fat tissue (SCAT), visceral adipose tissue (VAT), liver weight, as well as uterus weight was measured; D. Cumulative food intake was recorded, as the sum of the mean food intake per mouse from day 1 to day 67; E-F. DEXA assessment of fat mass and lean mass content respectively evaluated for each mouse and condition after 10 weeks of SBA protocol (expressed in grams (g) and in % of total weight); G-I. DEXA assessment of total mice body bone mineral content (BMC), femur BMC and vertebra (L5-L7) BMC respectively, evaluated for each animal and each condition after 10 weeks of SBA protocol (expressed in grams). Data represents mean and interquartile range; n=12. Statistical analysis was performed using Mann-Whitney's test; a - $p < 0.05$, aa - $p < 0.005$, aaa - $p < 0.0005$.

10-week cohort 2 of SBA 18% weight loss results in significant changes in mice bone parameters

Study of bone microarchitecture in control samples and SBA 18% samples, showed just a 5% lowering in bone volume fraction (Bv/Tv) (vs. CT) and 19% reduction in Tb.Th (vs. CT) in weight loss condition (Fig. 45A, B). Interestingly, in previously described data (10-week cohort 1) these parameters were not altered in 18% SBA condition (Fig. 26A-B). Moreover, replication of 10-week study showed a significantly low Cort.Th (-12% vs. CT) in 18% weight loss group, which was subsequently lower than 16% decrease in 10-week initial study (cohort 1) (Fig. 45E). In current cohort (cohort 2), trabecular number (Tb.N) and trabecular spacing (Tb.Sp) were not affected by 18% weight loss (Fig. 45C,D). Moreover, outer tibia diameter, which includes periosteum, was found to be decreased in SBA 18% condition (-7% vs. CT), and endosteum diameter was not changes (Fig. 45F,G). These results suggest that decrease in bone formation could be responsible for alterations in Cort.Th. Overall, results show that moderate weight loss in mice induced significant changes in bone parameters and bone mineral density, without affecting lean mass.

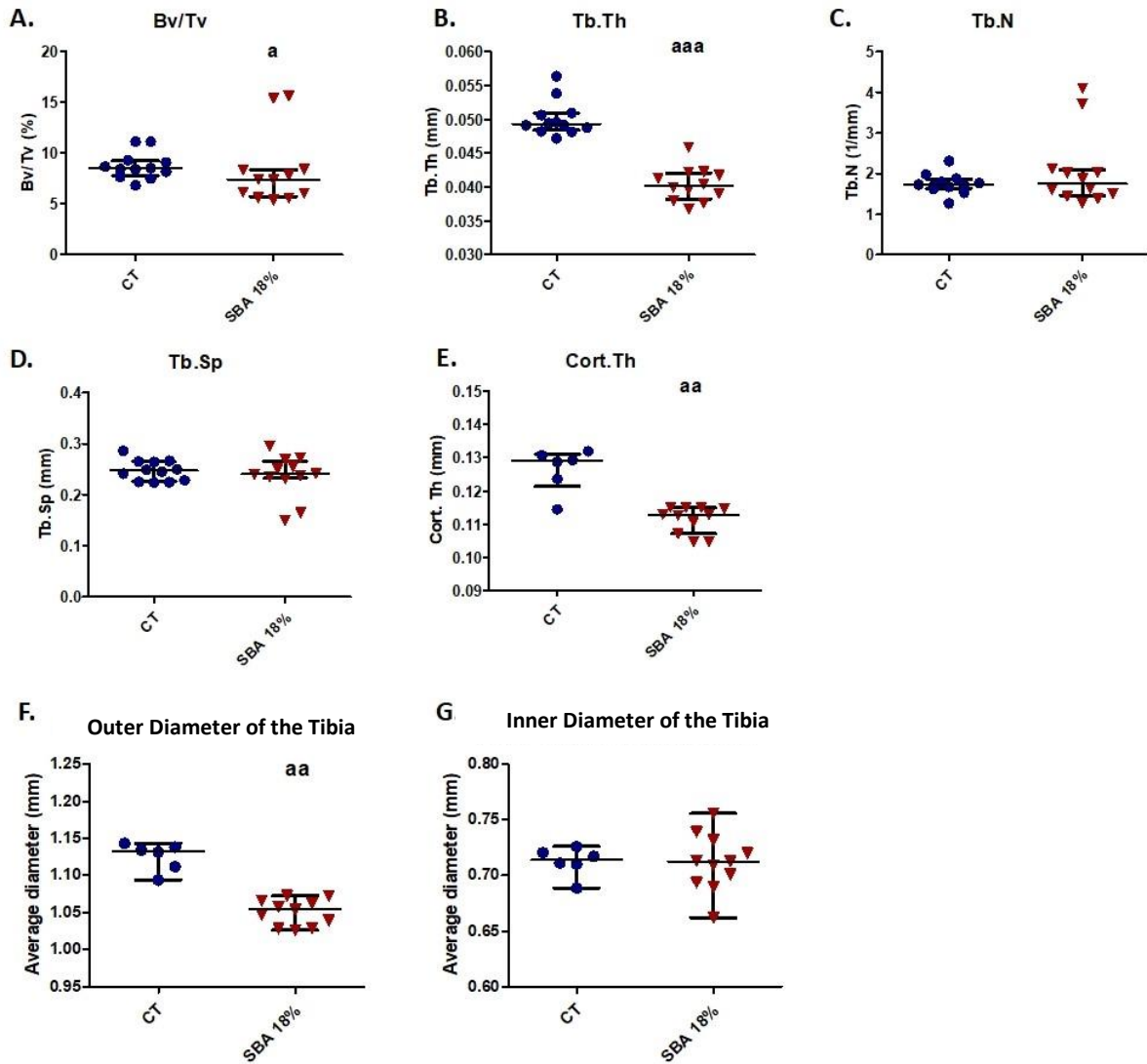


Figure 45. Micro-CT analysis of tibia, showing different bone parameters after 10 weeks of SBA protocol. A. Bone volume fraction (Bv/Tv) was expressed as a percentage of mineralized tissue; B-E. Trabecular thickness (Tb.Th.), trabecular number (Tb.N.), trabecular spacing (Tb.Sp.) and cortical thickness (Cort.Th.), respectively, were evaluated for each animal and each condition (expressed in millimetres); F-G. Average tibia diameter measured including inner section at bone area (outer diameter) and diameter of inner section specifically, respectively. Data represents mean and interquartile range; n=12, Cort.Th CT n=6. Statistical analysis was performed using Mann-Whitney's test; a - p<0.05, aa - p<0.005, aaa - p<0.0005.

10-week cohort 2 weight loss condition, did not induce changes in of BMSC differentiation capacity, nor in *Sirt1* expression in primary BMSCs

Next step of the study was to extract mice primary BMSC from CT and SBA 18% mice groups, plate them for 48h adhesion and for 14 days of co-differentiation. Results of light microscopy demonstrated an early appearance of lipid droplets in the SBA 18% condition (day 3), comparing to cells extracted from CT mice (day 5), confirming previous observations (Fig. 46A). However, towards the day 10 of co-differentiation, CT cells acquired similar quantity of adipocytes to SBA 18% group. In order to confirm similarities between CT and SBA 18% groups, relative mRNA level of adipogenic and osteoblastogenic marker genes was analysed.

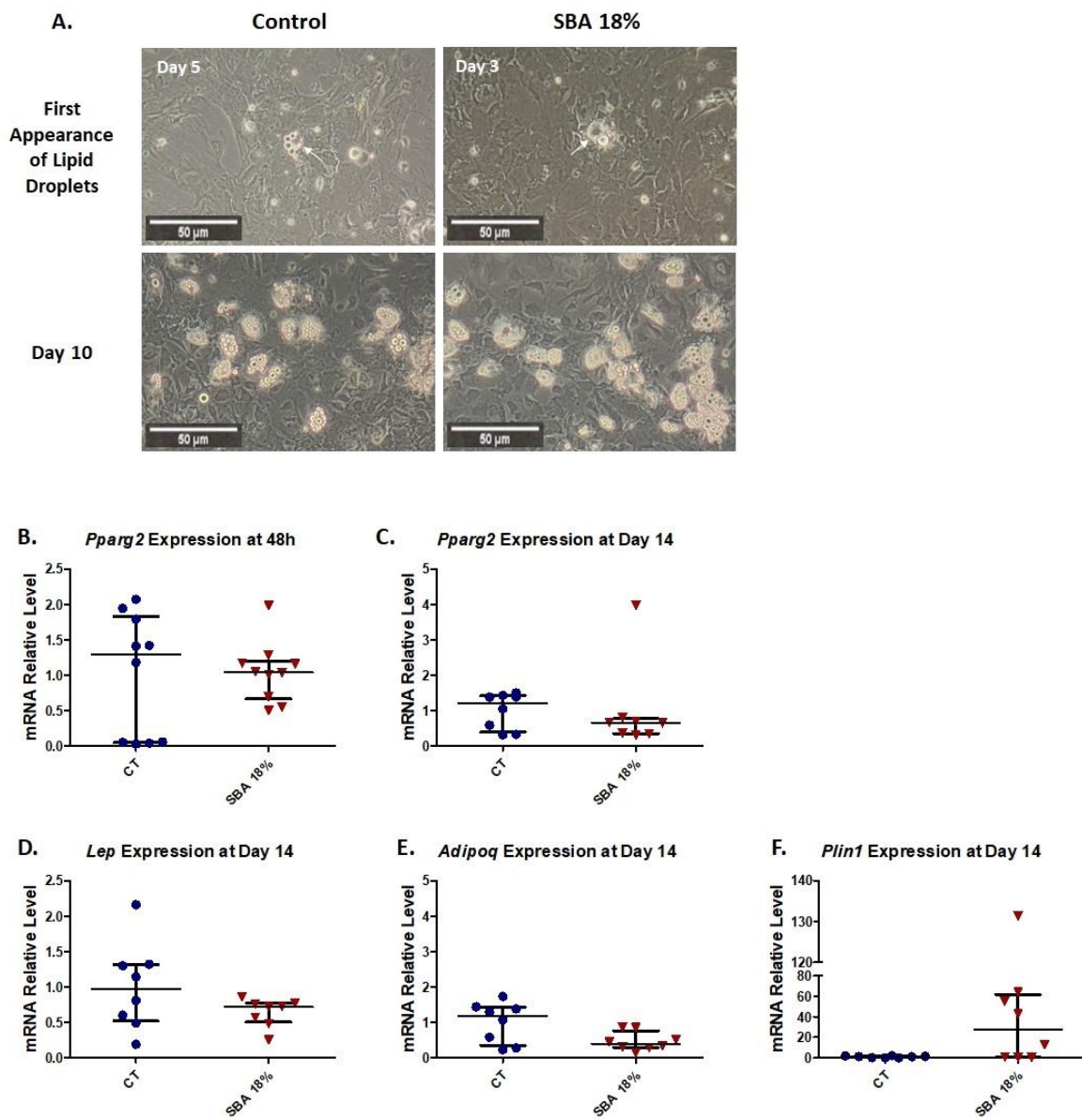


Figure 46. Adipocyte first appearance, size and adipogenic gene expression in BMSCs extracted from mice of 10-week protocol. A. Light microscope observation of cells from each condition were taken on different points of differentiation showing first appearance of lipid droplets (day 5 or day 3) and adipocytes at day 10 of co-differentiation induction; B-C. Relative mRNA expression level of early adipogenic marker gene (*Pparg2*) in CT and SBA group (18%), which were cultured for 48 hours in standard growth medium, as well as after 14 days of exposure to co-differentiation medium, respectively; D-F. Relative mRNA expression level of late adipogenic marker genes (leptin (*Lep*), adiponectin (*Adipoq*), perilipin (*Plin1*), respectively) in CT and SBA group (18%) after exposure to co-differentiation medium during 14 days. Data represents mean and interquartile range; n=8. Statistical analysis was performed using Mann-Whitney's test.

Surprisingly, 10-week protocol of 18% weight loss in mice (cohort 1) exhibited drastically different results to same condition in cohort 1. Replication of 10-week weight loss in mice did not result in alteration of early adipogenic marker (*Pparg2*) after 48h of adhesion or after 14 days of co-differentiation in extracted BMSCs (Fig. 46B, C). Furthermore, other adipogenic markers – leptin (*Lep*), adiponectin (*Adipoq*) and perilipin (*Plin1*), were also not affected by moderate weight loss in mice (vs. CT) (Fig. 46D-F). These results confirm the light microscopy observation, which suggest that in this cohort, 18% weight loss and CT groups have no difference in the rate of adipogenesis.

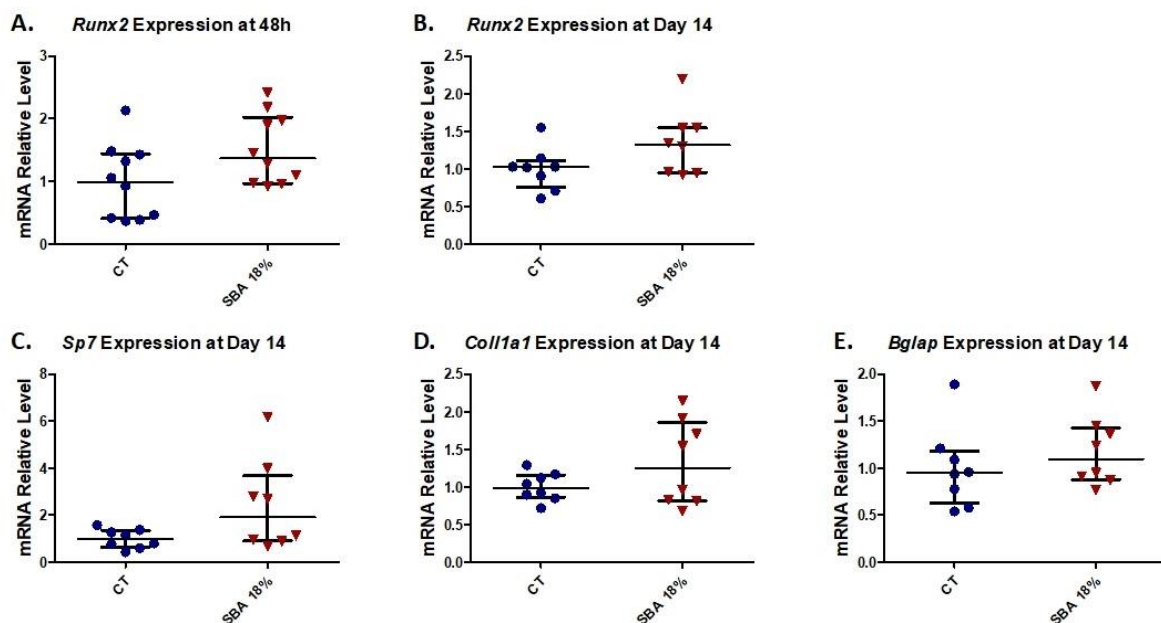


Figure 47. Osteoblastogenic gene expression in BMSCs extracted from mice of 10-week protocol. A-B. Relative mRNA expression level of early osteoblastogenic marker gene (*Runx2*) in CT and SBA group (18%), which were cultured for 48 hours in standard growth medium, as well as after 14 days of exposure to co-differentiation medium, respectively; C-E. Relative mRNA expression level of other osteoblastogenic marker gene (osterix (*Sp7*), collagen1a1 (*Coll1a1*) and osteocalcin (*Bglap*), respectively) in CT and SBA group (18%) after exposure to co-differentiation medium during 14 days. Data represents mean and interquartile range; n=8. Statistical analysis was performed using Mann-Whitney's test.

Second step was to look at osteoblastogenic genes relative mRNA level. Early osteoblastogenic marker *Runx2* was not altered in 10-week SBA protocol, neither after 48 hours of cell adhesion in proliferation medium, nor after 14 days of exposure to co-differentiation medium (vs. CT) (Fig. 47A, B). Moreover, relative mRNA level of other osteoblastogenic marker genes (*Sp7*, *Coll1a1* and *Bglap*) were not suppressed in 18% weight loss group (Fig. 47C-E). Results of this study suggest that in current cohort, 10-week protocol (cohort 2) does not induce alterations in BMSC differentiation capacity, which contradicts with previous findings in cohort 1.

After studying the relative mRNA level of *Sirt1* in BMSCs extracted from CT and SBA 18% mice, we observed that there was no difference between SBA 18% group and CT group, after 48h of adhesion or 14 days of co-differentiation (Fig. 48). Therefore, lack of changes in BMSC differentiation capacity in SBA 18% group was accompanied by no change in *Sirt1* mRNA level. This suggests that BMSCs differentiation is potentially dependent on *Sirt1* expression. Results of this 10-week cohort suggest that changes in bone parameters do not have a connection with BMSC differentiation capacity or *Sirt1* expression level.

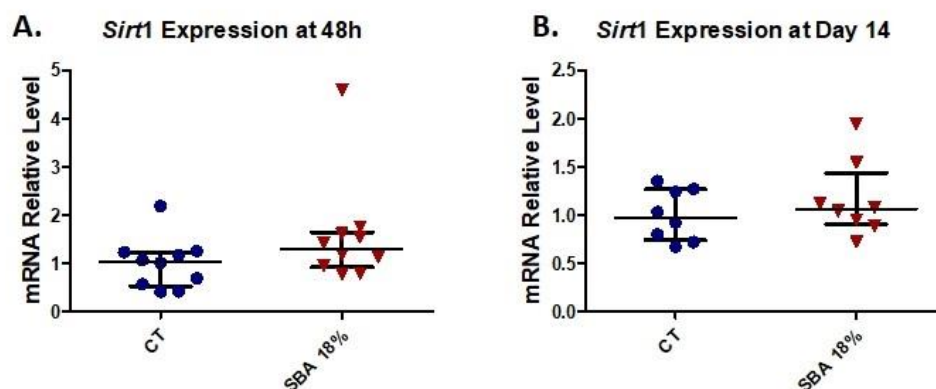


Figure 48. *Sirt1* expression in BMSCs extracted from mice of 10-week protocol. A-B. Relative mRNA level of sirtuin type 1 (*Sirt1*) in CT and SBA groups (18%), which were cultured for 48 hours in standard growth medium, as well as after 14 days of exposure to co-differentiation medium, respectively. Data represents mean and interquartile range; n=8. Statistical analysis was performed using Mann-Whitney's test.

Replication of 4-week SBA 18% study showed significant decrease not only in fat mass, but also in BMC

Similar to 10-week cohort 2 study, the 4-week SBA 18% weight loss protocol was conducted with increased number of mice (n=12). Results of the weight loss showed that SBA 18% group lost 18.1% from initial weight and CT group gained 12.5% (vs D0) (Fig. 49A). At the last day of 4-week protocol, mice from SBA 18% group had 26.3% lower weight than CT condition, which is bigger difference between SBA 18% and CT than was observed in first cohort of 4-week protocol (18.4% vs. CT) (Fig. 49B). The adipose tissue depots (SCAT and VAT) were significantly decreased in weight loss group (-63% and -80% vs. CT, respectively) after 4-week protocol (Figure 49C). In this cohort, decrease in adipose depots mass was significantly greater comparing to findings of cohort 1. Consequently, it can be concluded that greater difference in mice total weight between SBA 18% and CT can be associated with greater decrease in fat depots. Likewise, long SBA protocol (cohort 2), short term nutrient deficiency (cohort 2) induced a 63% reduction in uterus weight (Figure 49C). Furthermore, liver total weight was increased by 20% in weight loss mice, then in CT mice (Fig. 49C). Interestingly, liver weight was found to be altered in both cohorts of short-term SBA protocol (4-week), but 10-week SBA 18% weight loss group (cohort 1 and 2) did not result in liver mass alterations. Average food consumption in mice, exhibited an increase in SBA group comparing to CT, after 6 days of the weight loss protocol (Fig. 49D). These observations resembled initial results of 4-week cohort 1 study and also suggest an increase in energy expenditure in SBA mice, comparing to CT.

Due to the significant decrease in mice weight (vs. D0) and in SCAT and VAT tissue weight, SBA mice showed a significantly reduced fat mass (g and %) (-56% vs. CT) (Fig. 49E). In the same time, no changes in lean mass (g) were observed (vs. CT) after weight loss induction (Fig. 49F). After examining BMC, it was evident that within the current cohort we observed a decrease in total body BMC by 7% (vs. CT), as well as vertebrae BMC, also by 7% (vs. CT) (Fig. 49G, I). These findings contradict with preliminary results published in journal of *Frontiers in Endocrinology*, where 4-week protocol did not induce any changes in BMC of mice (882).

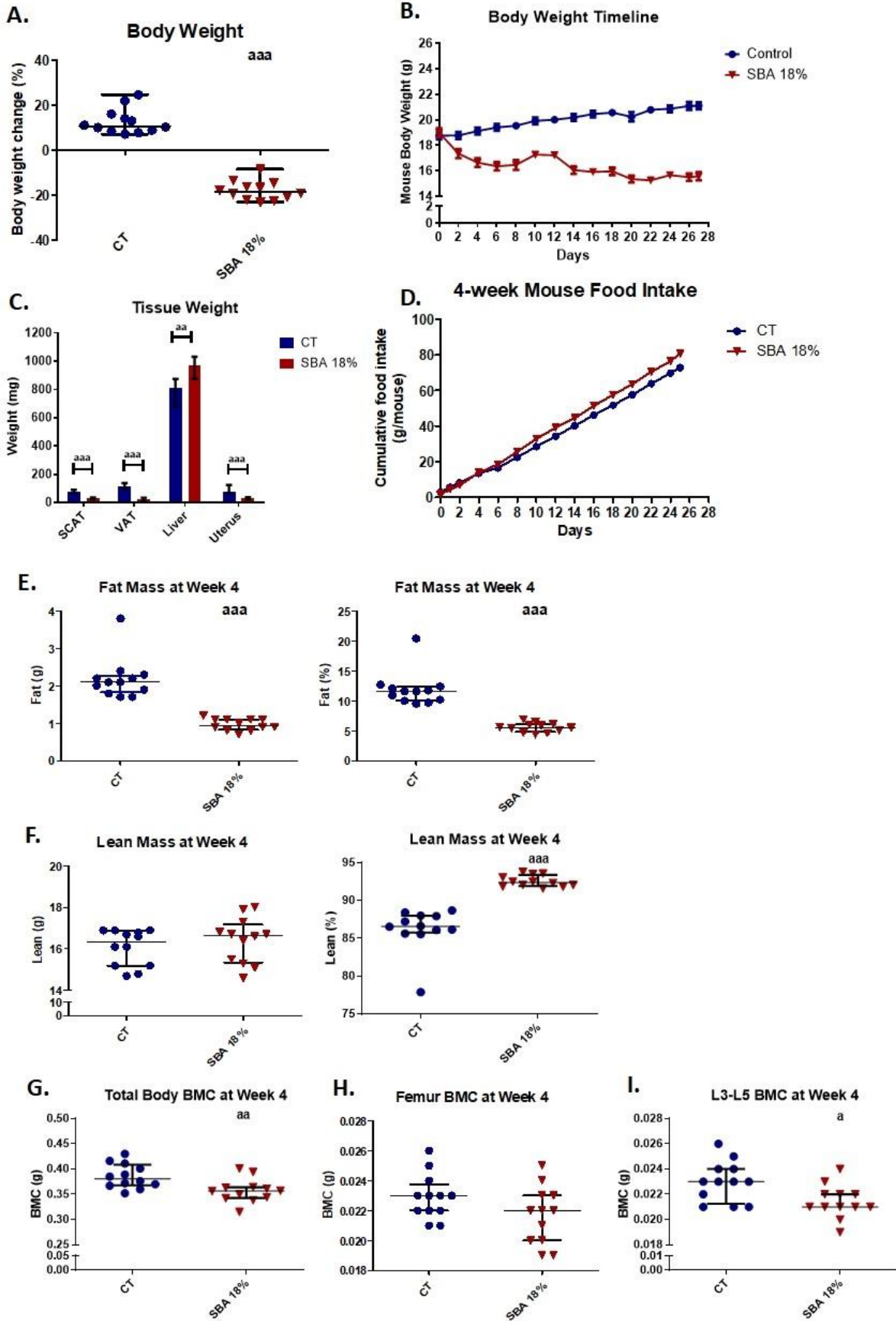


Figure 49. Body mass, BMC, fat and lean mass in mice after 4 weeks of SBA protocol.

The body weight and composition analysis were performed on standard condition (CT) and weight loss group (SBA 18%). A. Graph represents a percentage body weight loss on mice between day 0 and 4 weeks of SBA protocol; B. Body weight of individual mice is recorded daily before eating period, the 18.1% of weight loss (vs D0) was achieved in SBA 18% group and 12.5% weight increase (vs D0) was observed in CT group; C. After mice sacrifice, subcutaneous fat tissue (SCAT), visceral adipose tissue (VAT), liver total and right lobe (RL) weight, as well as uterus weigh was measured; D. Cumulative food intake was recorded, as the sum of the mean food intake per mouse from day 1 to day 27; E-F. Fat mass and lean mass content rwas evaluated for each mice and condition after 10 weeks of SBA protocol (expressed in grammes and in % of total weight), respectively; G-I. Study of total mice body mineral content (BMC), femur BMC and vertebra (L5-L7) BMC respectively, were evaluated for each animal and each condition after 4 weeks of SBA protocol (expressed in grams); Data represents mean and interquartile range; n=12. Statistical analysis was performed using Mann-Whitney's test; a - $p < 0.05$, aa - $p < 0.005$, aaa - $p < 0.0005$.

Sort-term nutrient deficiency (cohort 2) resulted in alterations of bone parameters

Initial findings of 4-week study have demonstrated that only Tb.Th was altered by short term nutrient deficiency (882). However, in current cohort it was observed that not only Tb.Th is reduced in SBA 18% weight loss group (-19% vs. CT), but also Bv/Tv was reduced by 29% in SBA group vs. CT (Fig. 50A, B). Bone fragility parameter (Cort.Th) was also reduced by 5% in nutrient deficiency mice (Fig. 50E). Additionally, an increase in Tb.Sp (+6% vs. CT) was induced by significant reduced number of trabeculae (Tb.N) (-13% vs. CT) and Tb.Th (Fig. 50B-D). Similar to 10-week cohort 2 study, bone outer (periosteum) and inner (endosteum) diameter were measured. Results exhibited a significant decrease in outer tibia diameter, without changes in endosteum, emphasising the decrease in bone formation, which can potentially contribute to the decrease in Cort.Th (Fig. 50G,H). Preliminary results of BMA, demonstrated a tendency of 25% increase in SBA 18% mice ($p=0.1775$ vs. CT), indicating that current 4-week cohort might have resulted not only in bone alterations but also in BMA (Fig. 50H). Moreover, we conducted histological analysis on the bone slides using perilipin in order to study BM on single cell resolution and look for changes in BMAds morphology. We found that an increase in BMA could be a result of increased BMAds number, as average diameter and area of single adipocyte was found to have a tendency to be reduced (-14% and -27% vs. CT, respectively $p=0.1225$) (Fig. 50I-K). Overall, the results of 4-week study on body and bone parameters showed a significant alteration in SBA 18% group, which are similar to 10-week findings. Moreover, data from the current cohort contradict the initial finding of 4-week study (882).

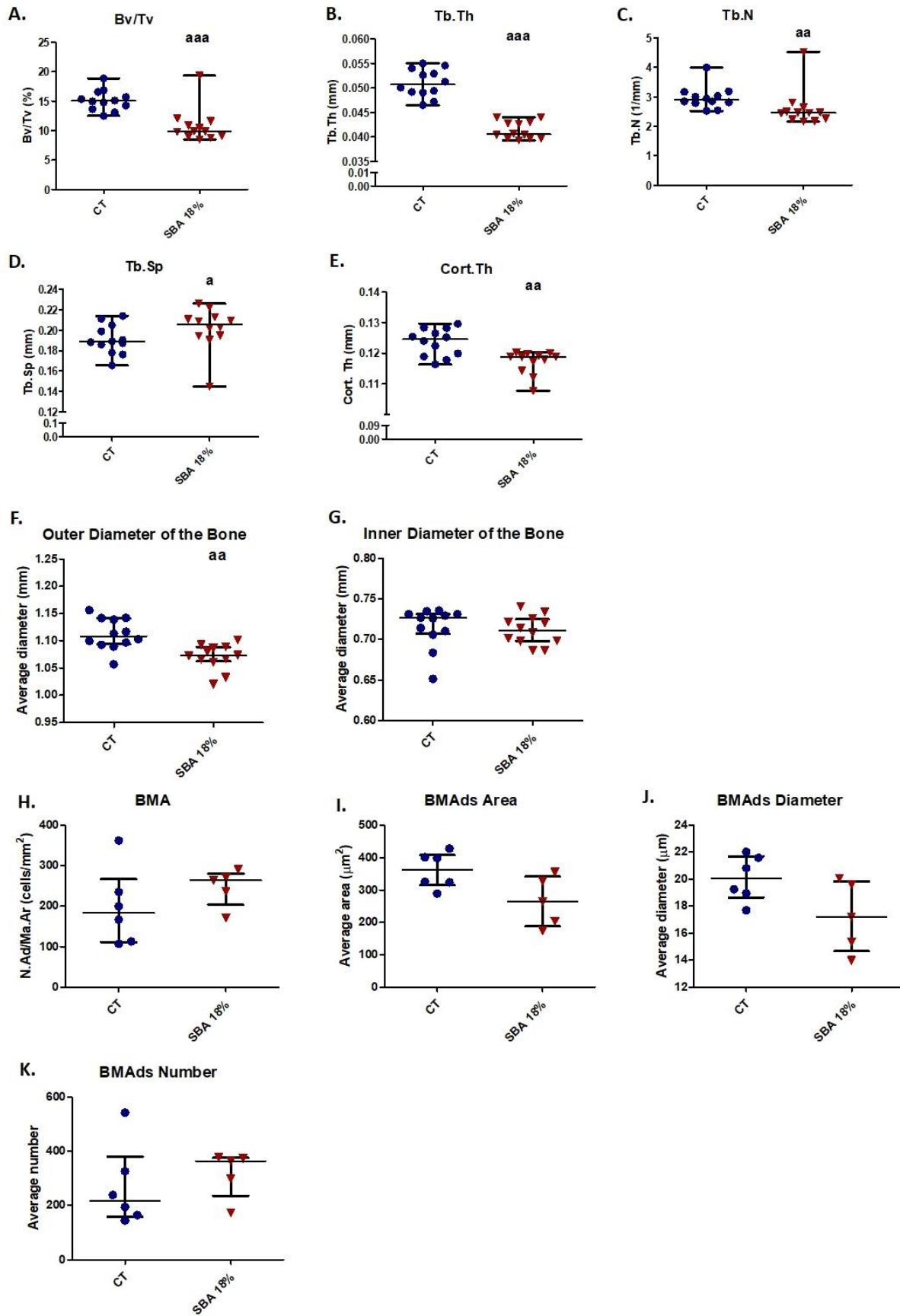


Figure 50. Micro-CT analysis of tibia, showing different bone parameters after 4 weeks of SBA protocol. A. Bone volume fraction (Bv/Tv) was expressed as a percentage of mineralized tissue; B-E. Trabecular thickness (Tb.Th.), trabecular number (Tb.N.), trabecular spacing (Tb.Sp.) and cortical thickness (Cort.Th.), respectively, were evaluated for each animal and each condition (expressed in millimetres); F-G. Average tibia diameter measured including inner section at bone area (outer diameter) and diameter of inner section specifically, respectively; H. Number of adipocytes per marrow area (N.Ad/Ma.Ar) was determined by histological analysis of tibias of CT and SBA mice; I-K. Average area of adipocytes, their average diameter and average number in SBA 18% mice and CT mice, respectively. Data represents mean and interquartile range; n=12, BMA n=5-6; Statistical analysis was performed using Mann-Whitney's test; a - $p < 0.05$, aa - $p < 0.005$, aaa - $p < 0.0005$.

In current 4-week study (cohort 2), BMSCs from SBA 18% condition did not exhibit changes in adipogenesis, but increase in osteoblastogenesis was observed

In order to understand the connection between alterations in the bone and BMSC differentiation capacity, the study proceeded on to *in vitro* experiment in extracted BMSCs. Induction of co-differentiation protocol in extracted BMSCs indicated that there was no difference in first lipid droplet appearance (day 3) between CT and SBA 18% groups (Fig. 51A). At day 10 of co-differentiation, it was visually evident that CT condition had higher overall number of adipocytes with greater size of lipid droplets (Fig. 51A), which was not seen in 4-week cohort 1 study.

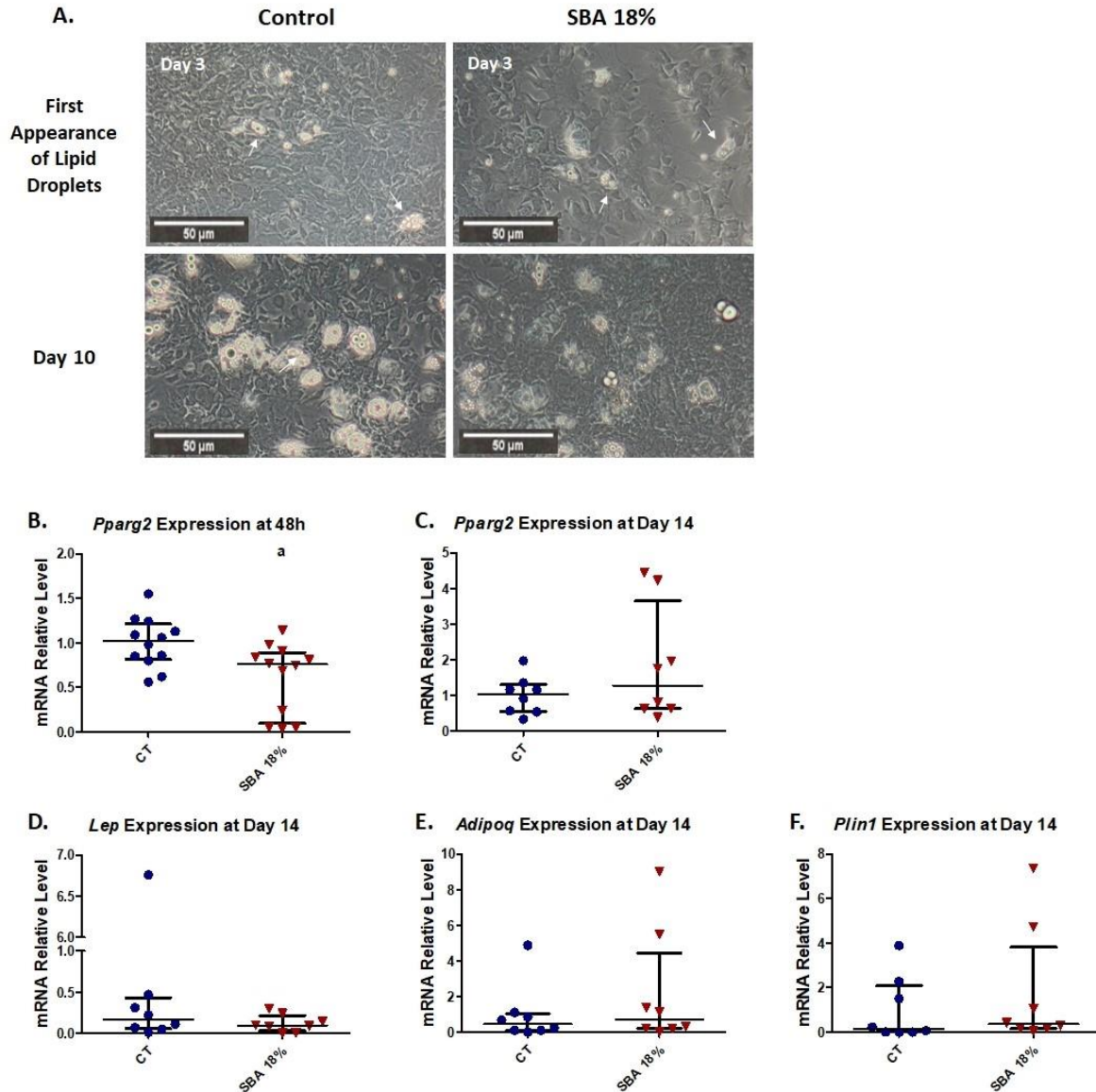


Figure 51. Adipocyte first appearance, size and adipogenic gene expression in BMSCs extracted from mice of 4-week protocol. A. Light microscope observation of cells from each condition were taken on different points of differentiation showing first appearance of lipid droplets (day 3) and adipocytes at day 10 of co-differentiation induction; B-C. Relative mRNA expression level of early adipogenic marker gene (*Pparg2*) in CT and SBA group (18%), which were cultured for 48 hours in standard growth medium, as well as after 14 days of exposure to co-differentiation medium, respectively; D-F. Relative mRNA expression level of late adipogenic marker gene (leptin (*Lep*), adiponectin (*Adipoq*), perilipin (*Plin1*), respectively) in CT and SBA group (18%) after exposure to co-differentiation medium during 14 days. Data represents mean \pm Interquartile range; n=8. Statistical analysis was performed using Mann-Whitney's test; a - $p < 0.05$.

The results of adipogenic marker gene expression partially confirmed, reduced rate of adipogenesis in SBA 18% condition vs. CT. Relative gene expression analysis shown that early adipogenic marker gene (*Pparg2*) was significantly decreased in SBA 18% BMSCs after 48h of adherence (Fig. 51B). Suggesting the reduced level of adipogenic commitment of BMSCs in current cohort. However, this effect of *Pparg2* relative mRNA level was not observed after 14 days of co-differentiation (Fig. 51C). After analysis of relative mRNA level of late adipogenic markers (*Lep*, *Adipoq*, *Plin1*), it was evident that 4-week SBA 18% weight loss protocol (cohort 2) did not induce changes in BMSCs differentiation into adipogenic lineage (Fig. 51D-F).

On the other hand, study of osteoblastogenic marker genes showed unexpected results. *Runx2* relative mRNA level was not changed in BMSC from SBA mice after 48 hours of cell adhesion. However, after 14 days of co-differentiation, *Runx2* mRNA level was 171% higher than in CT group (Fig. 52A,B). In addition, another early marker of osteoblastogenesis (*Sp7*) was dramatically increased (+934% vs. CT) in BMSCs extracted from SBA mice, comparing to CT group (Fig. 52C). Moreover, *Col1a1* mRNA level was also increased by 160% in SBA 18% condition (vs. CT) (Fig. 52D). On the other hand, in this cohort, we show a strong decrease in the mRNA expression of osteocalcin which is a late marker of osteoblastic differentiation and also reflects the osteoblastic function. Therefore, we conclude that in the current cohort, increase in early markers of osteoblastogenesis did not affect the capacity of BMSC to differentiate into adipogenic pathways.

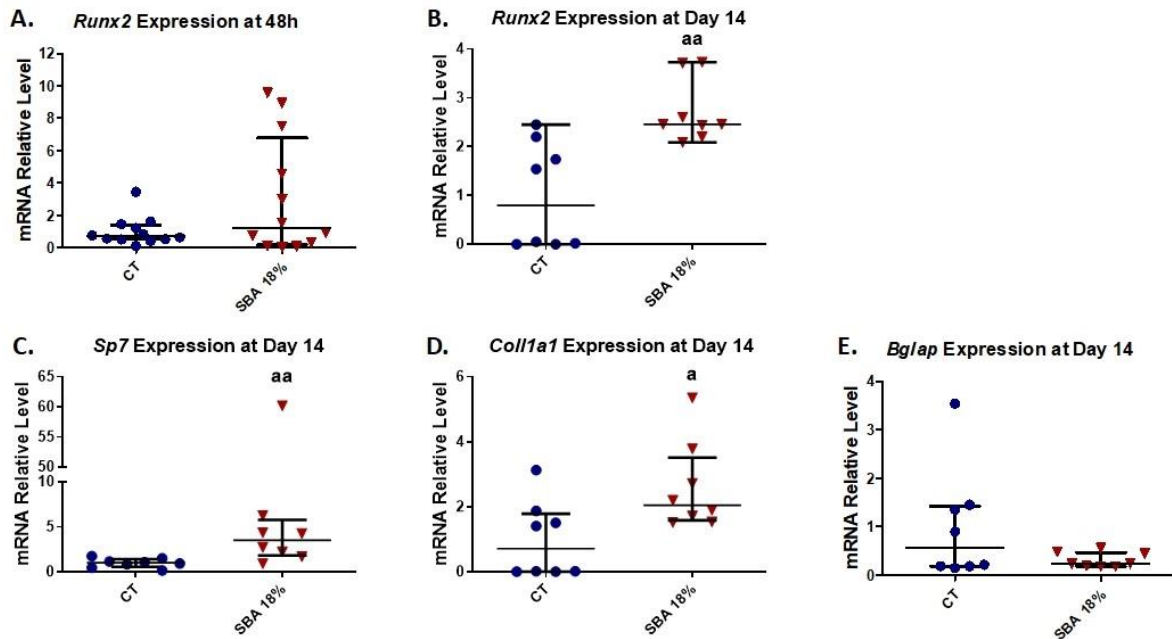


Figure 52. Osteoblastogenic gene expression in BMSCs extracted from mice of 4-week protocol. A-B. Relative mRNA expression level of early osteoblastogenic marker gene (*Runx2*) in CT and SBA group (18%), which were cultured for 48 hours in standard growth medium, as well as after 14 days of exposure to co-differentiation medium, respectively; C-E. Relative mRNA expression level of other osteoblastogenic marker gene (osteix (*Sp7*)) collagen1a1 (*Coll1a1*) and osteocalcin (*Bglap*), respectively) in CT and SBA group (18%) after exposure to co-differentiation medium during 14 days. Data represents mean \pm Interquartile range; n=8. Statistical analysis was performed using Mann-Whitney's test; a - p<0.05, aa - p<0.005.

After studying the expression of *Sirt1* in BMSCs extracted from CT and SBA 18% mice, it was concluded that there is no change in relative mRNA level in weight loss condition (vs CT) (Fig. 53). The finding of 4-week study demonstrated a contradictory result from previous cohort. Furthermore, upregulation of osteogenic markers in differentiated BMSCs was not accompanied by an upregulation of *Sirt1*, showing the lack of correlation between *Sirt1* expression and differentiation potential of BMSCs. Additionally, changes in bone parameters were also not related to *Sirt1* expression or shift in BMSCs differentiation capacity. Overall, this cohort showed inconsistencies in the results.

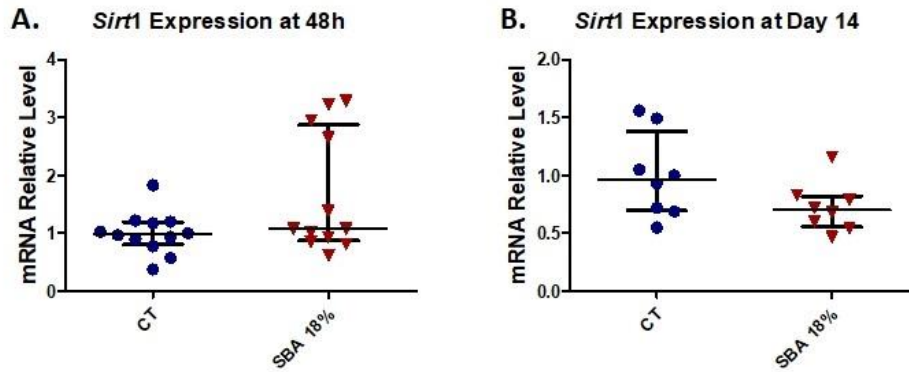


Figure 53. *Sirt1* expression in BMSCs extracted from mice of 4-week protocol. A-B. Relative mRNA level of sirtuin type 1 (*Sirt1*) in CT and SBA groups (18%), which were cultured for 48 hours in standard growth medium, as well as after 14 days of exposure to co-differentiation medium, respectively. Data represents mean \pm Interquartile range; n=8. Statistical analysis was performed using Mann-Whitney's test.

6. *In vitro* study on BMSCs differentiation capacity – development of medium mimicking nutrient deficiency

*In ST2 cell line, exposure to low FBS medium resulted in decrease of *Sirt1* and early osteoblastogenic marker*

After conducting the treatment with low FBS medium (5% FBS and 7% FBS) for 5 days, followed by co-differentiation of ST2 cells in the 10% FBS medium, mRNA relative expression of *Sirt1* and adipogenic/ osteoblastogenic genes was studied. Results showed that the FBS dose dependent decrease in *Sirt1* mRNA was achieved, additionally, exposure to 5% FBS resulted in long term statistically significant suppression of *Sirt1* mRNA (-34% vs. 10% FBS) (Fig. 54A). Results of adipogenic marker genes (*Pparg2*, *Lep* and *Adipoq*) study, showed that there is no change in their mRNA expression level (Fig. 54B-D). Out of osteoblastogenic genes, only early marker (*Runx2*) was decreased by 39% (vs. FBS 7%), the rest of osteoblastogenic markers (*Coll1a1*, *Bglap*) were not affected (Fig. 54E-G). These findings suggest that short (5 day) malnutrition of cells, through treatment with low FBS medium, can result in long term changes in *Sirt1* expression and lead to the decrease in *Runx2*, a key factor in osteoblastogenesis. Most importantly, these changes in relative mRNA level were affected, despite a restoration of FBS concentration during 14-day co-differentiation experiment.

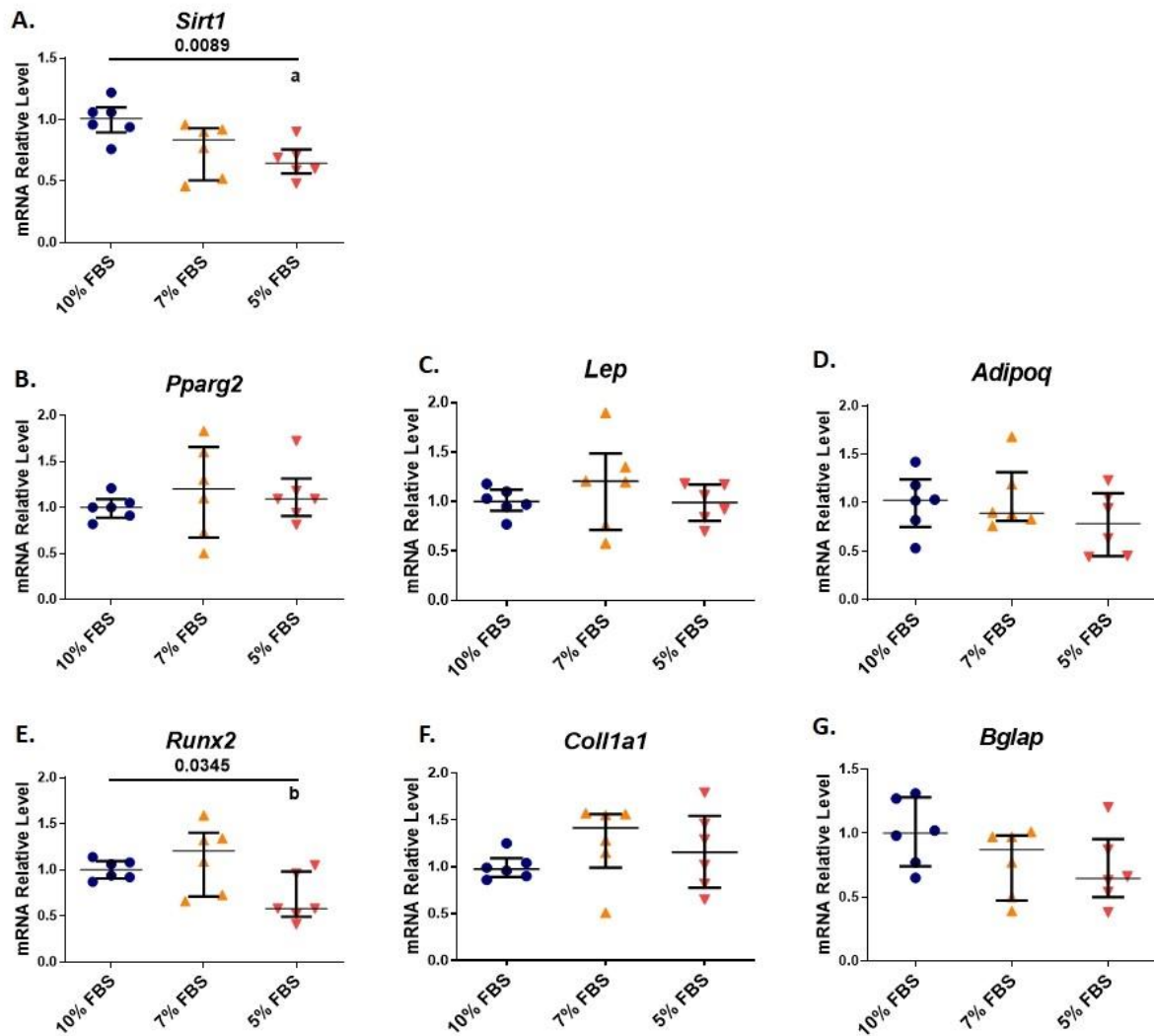


Figure 54. Adipogenic, osteoblastogenic genes and *Sirt1* mRNA level in ST2 treated with low FBS medium. A. Relative mRNA expression level of *Sirt1* in 10% FBS medium (control), 5% and 7% FBS (reduced nutrient) after 14 days of exposure to co-differentiation medium. B-D. Relative mRNA level of *Pparg2*, *Lep* and *Adipoq* in 10% FBS medium (control), 5% and 7% FBS (reduced nutrient) after 14 days of exposure to co-differentiation medium; E-G. Relative mRNA expression level of *Runx2*, *Coll1a1* and *Bglap* in 10% FBS medium (control), 5% and 7% FBS (reduced nutrient) after 14 days of exposure to co-differentiation medium; Data represent median and interquartile range, n=6. Statistical analysis was performed using Kruskal-Wallis One-Way ANOVA test and Dunn's test; a - p<0.05 when compared to the FBS 10% group (b – when compared to the FBS 7% group).

Exposure of primary mice BMSCs to low FBS medium did not affect Sirt1 expression or change in adipogenic marker genes mRNA

In order to test and confirm findings of ST2 cell experiment, the same conditions were tested on primary mouse BMSCs, extracted from 7-week-old C57L/6J mice. Similar to previous experiment, cells were exposed to 5% and 7% FBS growth medium for 5 days. Following the treatment, cells were co-differentiated using standard growth medium (10% FBS). Quantitative-PCR analysis of the samples showed that mRNA relative level of *Sirt1* in not significantly altered, but the decrease in FBS 5% group by 27% (vs. FBS 10%) can be observed (Fig. 55A). Adipogenic marker genes (*Pparg2*, *Lep* and *Adipoq*) exhibit no difference between reduced nutrient conditions (5% and 7% FBS) and the control (10% FBS), similarly to results in ST2 cells (Fig. 55B-D). Suggesting that reduction of serum in cell growth medium does not affect BMSC differentiation into adipocytes in 10% FBS differentiating medium. Or the changes induced by low FBS levels are normalized by the subsequent exposure to 10% FBS during the codifferentiation step. Additionally, study of osteoblastogenic markers (*Runx2*, *Coll1a1* and *Bglap*) showed that according to Kruskal-Wallis statistical analysis in BMSCs treated with low serum medium globally has an effect on *Coll1a1* mRNA, but without a significant specific effect of one concentration (Fig. 55E-G). Potentially, as increase in sample size can exhibit more clear results. Other osteoblastogenic marker expression was not affected (Fig. 55E-G). These findings suggest that modulation of nutrient availability *in vitro* can result in decreased expression of *Sirt1* mRNA and can also modestly affect some osteoblastogenic markers expression without compromising osteoblastogenesis as a whole, and without modulating adipogenesis in ST2 cell line or primary mouse BMSCs. These results must be analysed keeping in mind that after exposure to low FBS concentrations, all cells were subsequently exposed to 10% FBS containing medium during the differentiation step. This was necessary to maintain an efficient induction of differentiation, but could suppress or diminish not robust effects of initial low FBS exposure.

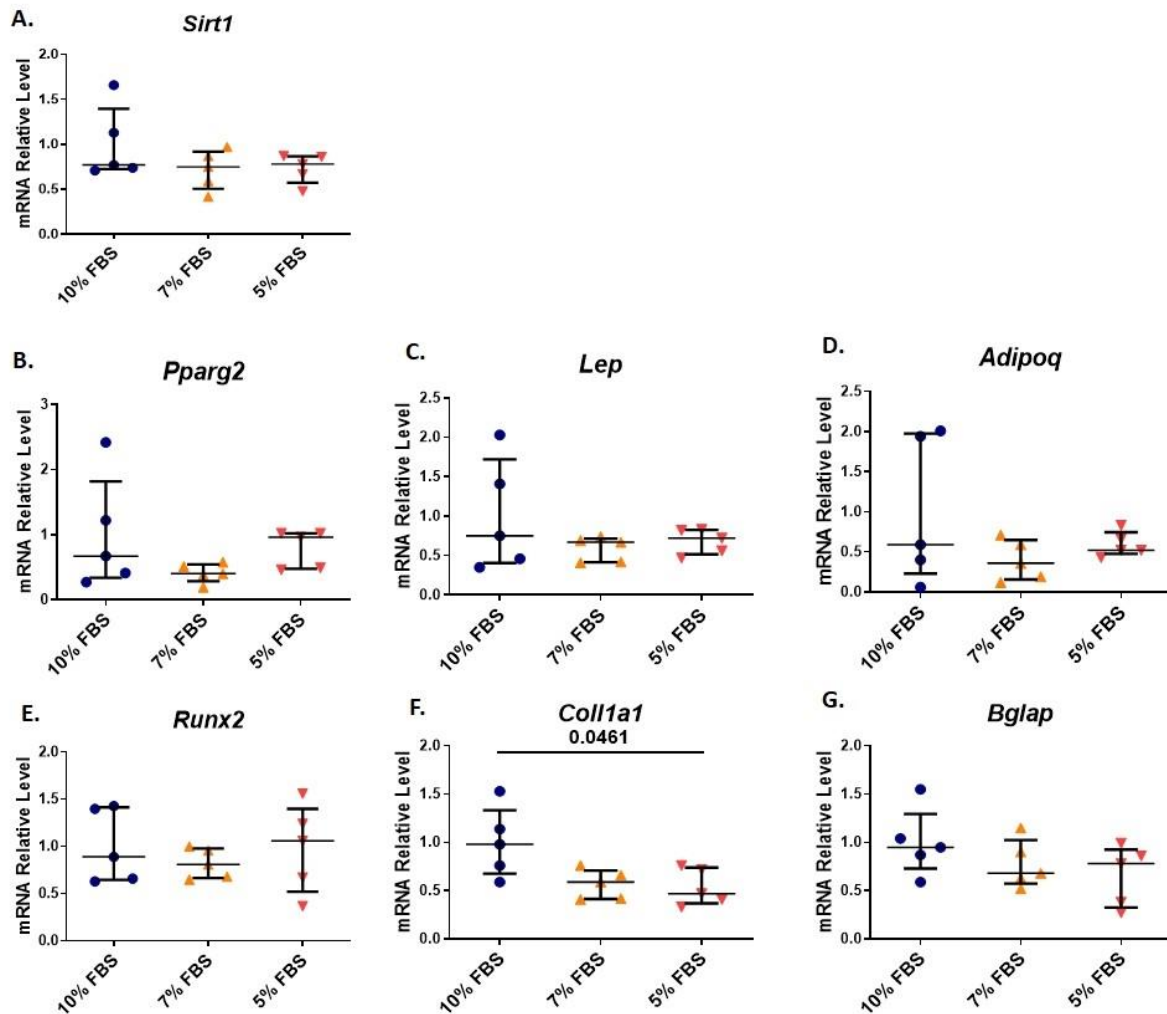


Figure 55. Adipogenic, osteoblastogenic genic markers and *Sirt1* mRNA level in primary mice BMSCs treated with low FBS medium. A. Relative mRNA expression level of *Sirt1* in 10% FBS medium (control), 5% and 7% FBS (reduced nutrient) after 14 days of exposure to co-differentiation medium. B-D. Relative mRNA level of *Pparg2*, *Lep* and *Adipoq* in 10% FBS medium (control), 5% and 7% FBS (reduced nutrient) after 14 days of exposure to co-differentiation medium; E-G. Relative mRNA expression level of *Runx2*, *Coll1a1* and *Bglap* in 10% FBS medium (control), 5% and 7% FBS (reduced nutrient) after 14 days of exposure to co-differentiation medium; Data represent median and interquartile range, n=5. Statistical analysis was performed using Kruskal-Wallis One-Way ANOVA test and Dunn's test.

2. DISCUSSION AND CONCLUSIONS

In AN patients SIRT1 negatively associated with femoral neck fat fraction

Interest in SIRT1-mediated regulation of BMSCs capacity in long term and severe nutrient deficiency condition was brought out, as bone loss and BMA gain was associated with decrease of BMSC *Sirt1* mRNA and SIRT1 protein expression (2,883). Moreover, our study in AN patient plasma showed a negative correlation between SIRT1 protein circulating level and fat in femoral neck (Fig. 25). This data strengthens our hypothesis of potential association between SIRT1 and AN-induced bone loss, as well as BMA increase. Replication of anorexia consequences in mouse model allows us to explore molecular changes that potentially take place in long term, severe nutrient deficiency.

Initial study on the effects of severity of energy deficiency on mice showed that ten weeks of 18% and 24% body weight loss induce an alteration of bone mineral content without increase in bone marrow adiposity

In our animal model, it was recently demonstrated that a long-term (10-week) energy deficit characterised by a moderate weight loss (18% vs. D0) in female mice is associated with a bone loss and an increase in bone marrow adiposity (BMA) (2). In this study we sought to determine the impact of a different degree of severity on bone architecture, BMA, and then to identify the potential molecular mechanisms involved in BMA regulation in this context. The mice were exposed for 10 weeks to a separation-induced increase in energy expenditure and a time-restricted feeding that prevented compensatory feeding and resulted in significant weight loss (SBA) (1). Results of mice body parameters showed similar fat mass decrease in all SBA groups compared to control one. The 12%, 18% and 24% groups displayed a decrease in bone mineral content (BMC) at least in femur. These results suggest that even for a long protocol a significant weight loss is required to induce changes in mineralised bone (Fig. 26), as the stable body weight group (SBA 0%) did not show any bone alteration. Moreover, these bone changes are not directly related to fat mass, because they are not shown in the 0% group. This was already shown in adult male mice by Mitchell *et al.* (884). They demonstrated that different levels of CR 10%, 20%, 30% and 40% in male mice induced body weight losses of around 0%, 11%, 22% and 28% (vs. CT), respectively after 12 weeks (884). These weight changes were associated to fat mass decrease of approximately 12% for 10% CR and 30 to 35% for the other groups. In this study, no significant changes in BMC, trabecular bone microarchitecture and

cortical bone were detected. Unfortunately, BMA was not determined. The conflicting results on bone in the present study and that of Mitchell's could be due to gender, age and protocol differences. However, Mitchell *et al.* study showed the lack of relationship between fat mass decrease and bone in energy deficit experiment.

Previously, using histological approaches, we showed that the SBA protocol of 18% weight loss results in an increase in BMA (2). Interestingly, in the current study, the BMA was altered only in one weight loss condition. Indeed, BMA displayed a tendency to decrease in SBA mice with a light weight loss (12%) (Fig. 27F). Moderate and severe weight loss groups exhibited no change in BMA vs. CT (Fig. 27F). Nevertheless, in 18% and 24% weight loss groups decrease in bone parameters was observed, suggesting that negative alteration in bone take place without accumulation of mature adipocytes in bone marrow cavity (Fig. 27). The results of BMA in the current study were obtained using osmium tetroxide staining followed by micro-CT analysis of the ratio between adipocyte volume and total bone marrow volume. Current technique allows staining of the mature adipocytes with osmium tetroxide in decalcified bone, without staining other cells in BM cavity (885). After, using the micro-CT scanner, this method provides a 3D map of the BMAT throughout the medullary cavity, above the growth plate, in the secondary centre of ossification (885,886). This approach provides reproducible and quantitative study of BMAT in a chosen volume of BM, however, it has its limitations.

Firstly, similarly to histological approaches, micro-CT analysis of adipocyte stained with osmium tetroxide focuses on mature adipose tissue, not taking into account pre-adipocyte cell fraction. Recently, in work of Zhong *et al.* it was described that population of marrow adipogenic lineage precursors (MALPs) are the most abundant cellular component of BMAT (887). Moreover, this cell population was found to secrete the greatest number of factors and at the highest level among other none mesenchymal lineage cells (887). These cells are able to act upon osteoblastogenesis, osteoclastogenesis and haematopoiesis within BM. Ablation of MALPs in young mice results in rapid and great bone formation (888–890). Single cell RNA sequencing (scRNA-seq) analysis showed that MALPs are expressing *Rankl*, colony stimulating factor 1 (*Csf1*) and other osteoclast regulatory factors (*Il7* or *Il34*) (891). This cell type was described as a stimulator of osteoclastogenesis (891,891–894). Altogether, MALPs are playing an important role in bone homeostasis and their accumulation within BM can potentially be associated with decreased bone formation and increased bone resorption. Therefore, it would be interesting to study the content of extracted BMSC population from CT

and SBA mice by Flow Cytometry or scRNA-seq, in order to identify the MALPs (Zfp423⁺) population size in these conditions. It will help us to determine if MALPs play a role in bone loss in the context of energy deficit.

Secondly, osmium tetroxide is a highly toxic substance that should be maintained with strict precision. However, new staining methods has been reported by Kerckhofs *et al.*, where they developed a technique to simultaneously visualise mineralised and soft tissue within BM (201). Utilising the Hafnium Wells-Dawson polyoxometalate (Hf-WD-POM), as contrast enhancing staining agent, and combining it with high resolution scanning (2 voxel size), allows to visualise adipocytes at single cell level. Using this technology, BMAT fraction within bone can be measured, but also it allows quantification of adipocyte number, diameter and density (192,201,895). Therefore, the apparent discrepancy between the current and Louvet's studies could be explained by the fact that we observed a high heterogeneity in BMA among mice of the same group (2). Secondly, in the first study of Louvet *et al.*, BMA was assessed using histological (2D) approach with few slides focused on a specific area of the proximal tibia with a specific orientation, while current study used 3D assessment on a large volume including the analysed in the previous study. So, the increase observed in a specific area and the lack of significant changes observed on the larger volume, suggests that highly localised changes could occur in the density of adipocytes in the marrow, which are not representative of what happens in the proximal BM cavity.

Nevertheless, various studies demonstrated an increase in BMA associated with bone alteration in anorexic patients . In rodent, models of food or calorie restriction demonstrated that 9 weeks of a 30% restriction on food in 3-week-old male mice induced low Bv/Tv (-11%), Cort.Th (-27%), and body weight (-40%), which were accompanied by high BMA (+700%) compared to CT mice (414). Also, it has been shown that 6 weeks of a 30% calorie-restricted diet in 9-week-old female mice, induced an increase in tibia BMA (700%) compared to that in the *ad libitum* group (283). Interestingly, in these two studies, the high increase in BMA was associated with a body weight increase of 80% vs. day 0 or a final body weight similar to that of day 0 of the experiment (283,414). The difference in our BMA results compared to these two studies may be explained by the fact that we used young adult female mice, while the first one investigated growing male mice, and by the difference in body weight loss relative to that on day 0 (283,414). In addition, it is reported that an extensive CR in rabbits can cause a loss of BMAT (283). Similar finding has been observed with severe anorexic patients (407). Thus, the gender

of animals and level of body weight loss may strongly affect BMA. In contrast, a calorie restriction protocol (low carbohydrate feeding) for 12 weeks on 6-month-old Sprague–Dawley female rats, demonstrated that restricted rats displayed body weight loss (-20% vs. D0 and -25% vs. CT), a low volumetric BMC at the proximal tibia (-14%) and only a two-fold increase in BMA measured at the distal femur (898). More recently, male Sprague–Dawley rats (8 months old) exposed to 40% calorie restriction during 12 months, displayed 40% body weight loss vs. CT rats, which resulted in a decrease in the bone mineral index (-30% vs. CT) and an increase in BMA at the proximal tibia (20% vs. CT) (421). On the other hand, 10 weeks of CR in 14-week-old male mice led to a body weight loss of 30% (relative to CT) and a total disappearance of bone marrow adipocytes in the distal femur (414). Altogether, these data suggest that restriction-induced changes in BMA and bone quality may be modulated by severity of protocol, body weight loss, age, sex and duration of restriction.

	SBA 0%	SBA 12%	SBA 18%	SBA 24%
Body Parameters				
Body Weight (vs D0)	+4.39%	-12.97%	-17.27%	-23.17%
Fat Mass (vs CT)	n/s	-59%	-59%	-64%
Lean Mass (vs CT)	n/s	-19%	n/s	-22%
Total BMC (vs CT)	n/s	-17%	-15%	n/s
Bone Parameters				
Bv.Tv (vs CT)	n/s	n/s	n/s	n/s
Tb.Th (vs CT)	n/s	n/s	n/s	-29%
Tb.N (vs CT)	n/s	n/s	n/s	+42%
Tb.Sp (vs CT)	n/s	n/s	n/s	-18%
Cort.Th (vs CT)	n/s	n/s	-16%	-17%
Periosteum (vs CT)	n/s	-6.9%	-5.5%	-5.3%
Endosteum (vs CT)	n/s	n/s	n/s	n/s
BMA (%) (vs CT)	n/s	-82%	n/s	n/s
Lipid Droplet Appearance (CT – D7)	Day 3	Day 3	Day 3	Day 3
BMSCs Co-Differentiation Marker Genes				
<i>Pparg2</i> 48h (vs CT)	n/s	n/s	+50%	+125%
<i>Pparg2</i> 14D (vs CT)	n/s	n/s	+285%	+236%
<i>Lep</i> 14D (vs CT)	n/s	n/s	+1292%	+1864%
<i>Adipoq</i> 14D (vs CT)	n/s	n/s	+53%	-60%
<i>Runx2</i> 48h (vs CT)	n/s	n/s	-44%	-55%
<i>Runx2</i> 14D (vs CT)	n/s	n/s	-75%	-70%
<i>Sp7</i> 14D (vs CT)	n/s	n/s	-81%	-77%
<i>Bglap</i> 14D (vs CT)	n/s	n/s	-73%	-72%
<i>Sirt1</i> 48h (vs CT)	n/s	n/s	-67%	-60%
<i>Sirt1</i> 14D (vs CT)	n/s	n/s	-75%	-68%

Table 9. Summary of results obtained from 10-week cohort 1, comparing CT and different weight loss groups (SBA 0%, 12%, 18%, 24%).

Ten weeks of 18% and 24% body weight loss induce an imbalance between osteoblastogenesis and adipogenesis

Due to the fact that in the current study, bone alterations were not associated to a high BMA, we hypothesised that the commitment of BMSCs towards the adipogenic pathway could impact bone mass even if adipocytes are not able to reach a mature state. Therefore, it was important to study BMSC differentiation potential to obtain a more precise understanding of the cell commitment towards the adipogenic or osteoblastogenic pathway.

Given that osteoblasts and adipocytes are derived from a common progenitor, BMSCs, we tested the hypothesis that the degree of severity of body weight loss could impact the differentiation capacity of BMSCs extracted from SBA mice (899). After just 48 hours of adhesion in a standard proliferative medium, the unstimulated BMSCs from SBA weight loss mice (12%, 18% and 24%) exhibited high levels of *PPAR γ 2* mRNA, even if an increase was not significant for the 18% group (Fig. 29A). This finding suggests that extracted BMSCs display commitment to the adipocytic lineage. Then, the exposure to co-differentiation medium, which induces both adipogenesis and osteoblastogenesis simultaneously, resulted in fast adipogenesis in BMSCs extracted from all SBA mice groups comparing to BMSCs from CT mice (808) (Fig. 28A). Indeed, lipid droplets appeared after 3 days after induction of co-differentiation in cells of SBA groups, while it took 7 days for BMSCs from CT mice (Fig. 25A). This rapid adipogenesis was associated with increased mRNA production of adipocyte markers *Pparg2* and *Lep* in 18% and 24% groups (Fig. 29B,C). Also, *Glut4* mRNA level was increased in the 18% weight loss group after 14 days of co-differentiation (Fig. 29E). The mRNA level of adiponectin was dramatically decreased in SBA mice with light weight loss (12%), and this finding could be associated with a significant decrease in BMA under the same weight loss conditions (Fig. 29D). Significant loss of mature adipocytes *in vivo* could potentially affect the level of adiponectin production and *Adipoq* mRNA levels (179).

Additionally, to characterise *in vitro* adipocytes, the lipid droplets of BMSCs (from SBA and CT mice) derived adipocytes were analysed using Raman spectroscopy (Fig. 28B). The unsaturated ratio of lipids was decreased in the SBA groups (12%, 18% and 24%) compared to the SBA 0% group after 14 days of co-differentiation. These results suggest that energy deficit related to SBA protocol, induced a long-lasting alteration of lipid quality regardless of the level of body weight loss.

After only 48 hours of adhesion in a standard proliferative medium, the unstimulated BMSCs from SBA mice (12%, 18% and 24%) presented significant reduction or decreasing tendency in *Runx2* mRNA (Fig. 30B). After 14 days in co-differentiation medium, BMSCs from 18% and 24% groups displayed a major alteration of early and late osteoblast markers (Fig. 30C-F). Furthermore, BMSCs from these two groups displayed deeply altered osteoblastic functions, such as mineralisation capabilities, compared to CT BMSCs (Fig. 30A). These results suggest that only SBA 18% and 24% weight loss groups induced significant and long-lasting changes in osteoblastogenesis *in vitro*.

Findings above led us to conclude that there potentially exists a preferential commitment of BMSCs extracted from SBA mice to the adipogenic pathway. Results show that adipogenesis and osteoblastogenesis seems to be affected by the severity of energy deficit, and that at least an 18% weight loss is required to observe these alterations. Moreover, potential presence of MALPs in our extracted BMSCs heterogeneous population can also contribute towards an increased adipogenesis, as well as upregulated adipogenic marker gene expression (887).

Sirt1 is sustainably altered in BMSCs from 18% and 24% groups in the initial study on 10 weeks cohort 1 SBA mice

To determine the potential molecular mechanism involved in the regulation of BMSC differentiation in SBA mice, the relative mRNA level of *Sirt1* was measured. Indeed, we recently demonstrated that 18% weight loss in mice is associated with the downregulation of the expression and activity of *Sirt1* and further possibly leads to an increase in adipogenesis at the expense of osteoblastogenesis (2). In the current study, we hypothesised that *Sirt1* could be altered according to the degree of severity of energy deficit, leading to an imbalance between osteoblastogenesis and adipogenesis. It is important to note that *Sirt1* is widely known for its pro-osteoblastic and anti-adipogenic effects (655,658,900–903). Indeed, *in vivo*, activation of *Sirt1* restores bone mass, structure, and biomechanical properties in ovariectomised female mice (904), and it protects against age-associated bone loss in male mice (905). *In vitro* studies demonstrated that activation of *Sirt1* promotes osteoblastogenic differentiation at the expense of adipogenesis (655,658,900,901). Interestingly, our results demonstrated that BMSCs from SBA mice with moderate and severe weight loss (18% and 24%) presented a substantial low *Sirt1* mRNA level after 48 hours of culture and after 14 days of co-differentiation (Fig. 31).

These findings suggest that the decrease in *Sirt1* expression could be responsible for the observed increase in adipogenesis at the expense of osteoblastogenesis in these two groups.

Other studies have shown that CR can stimulate the expression and activity of *Sirt1* in various mammalian tissues, such as the liver or white adipose tissue (21,906). It was also shown that CR decreases the mRNA level of *Sirt1* in the cerebellum and midbrain (907), suggesting tissue-dependent regulation of the expression. More recently, in contrast to our study, it was demonstrated that 12 months of 40% calorie restriction of male Sprague–Dawley rats (8 months old) induced an upregulation in protein expression of *Sirt1* in bone marrow fat comparing to that in *ad libitum* animals (421). This discrepancy between our results and findings of Cohen *et al.* could be explained by changes in calorie or food restriction protocols, mouse strain or species, age and gender (21,421). Indeed, twelve-month-old male rats were used in Cohen *et al.* study, and calorie restriction involved a daily food allotment of 60% of that eaten by the *ad libitum* animals immediately after weaning (21). In our study, eight-week-old female C57BL/6J mice were submitted to the 10-week SBA protocol. Furthermore, the weight loss of mice in each protocol of calorie restriction could also explain this discrepancy. Indeed, contrary to our protocol, which induces 12%, 18% and 24% weight loss in mice, there is no information on weight loss in the study by Cohen *et al.*, and there was a 40% weight loss (vs CT) in the study by Duque *et al.* (21,421). Thus, the loss of *Sirt1* seems to be closely associated to bone and BMSCs alterations and could explain the strong and long-lasting commitment of BMSCs towards the adipogenic pathway in SBA mice. Furthermore, in other types of mouse model, the association between decrease in SIRT1 production and increase in BMAT was observed. Elbaz *et al.* have shown that young (5 months) and old (23 months) post ovariectomy (OVX) mice exhibits 200% and 80% increase in BMAds number, respectively (314). This increase in BMAds number was associated with significant decrease in *Sirt1* expression, as well as SIRT1 protein level. Interestingly, the supplementation of oestrogen in OVX mice resulted in restoration of *Sirt1* gene expression and SIRT1 protein level, showing an involvement of oestrogen in regulation of SIRT1 production (314). Therefore in future, it would have been interesting to study the circulating oestrogen level in SBA mouse model.

In our study, 18% is considered moderate weight loss, which is associated with a decrease in all parameters of body composition (low fat mass, tendency to low lean mass, low total body BMC, low femur and lumbar spine BMC) and cortical bone thickness. Furthermore, only in this weight loss category we found an upregulation of most of the adipocyte markers analysed

(*Pparg2*, *Lep* and *Glut4*) and a downregulation of most of the osteoblast markers analysed (*Runx2*, *Sp7* and *Bglap*). In addition, this weight loss group displayed a strong decrease in *Sirt1* mRNA level. Considering these results, the rest of the *in vivo* and *ex vivo* studies were dedicated to focusing on SBA 18% and investigate the effect of a short duration of SBA protocol (4 weeks) on body composition, bone architecture, BMA, BMSC differentiation and *Sirt1* expression.

Preliminary study on the short duration of moderate weight loss showed changes in body parameters, without affecting bone architecture, BMA, BMSC differentiation or Sirt1 expression

Four weeks of the SBA protocol induced a significant decrease in SCAT and VAT tissue (g), leading to a significant decrease in fat mass (g), without affecting lean mass (g) (Fig. 32C-E). Mice organ weight study highlighted that in 4-week SBA protocol group, liver weight is significantly increased comparing to controls (Fig. 32C). This change in liver mass was abolished after 10-week of time-restricted feeding in SBA 18% weight loss group (Fig. 26C). Mequinion *et al.* reported that after 35 days of quantitative food restriction combined with voluntary exercise, mice exhibit a shift in energy metabolism (908). Anticipative activity, physical activity before feeding, was present in mice on day 15 of the study and was completely absent by day 45. This change was associated with a moderate but significant increase in body weight. This suggests that during the long term energy deficit, mice can adapt and change their energy use, as well as energy storage (908). We observed that in short term energy deficit study the adaptation to reduced food intake and exposure to isolation leads to the increase in liver weight but after 10 weeks of acclimatisation the liver weight normalises. Previously, Kostogryz *et al.* described that 70% *ad libitum* feeding in young (2 months old) ApoE/LDLr-/- (arthrosclerosis model) mice for 8 weeks, resulted in an 11% increase in liver weight (vs. CT) (909). One of the main reasons for liver weight increase is liver fat accumulation. Excess dietary fat, increased transport of free fatty acids (FFA) to the liver, insufficient fatty acid oxidation, and enhanced de novo lipogenesis are some of the factors behind fat build-up in the liver (910). 5-week CR (70% *ad libitum*) male mouse model (10-week-old), in Bruss *et al.* study, displayed unexpected metabolic rhythm defined by periods of increased FA synthesis alternated with periods of FA oxidation that is disproportionate to dietary FA intake (911). Therefore, the fast depletion of SCAT and VAT leading to potential increase in FFA release due to the lipolysis (912,913), in combination with increased food intake in the SBA 18% weight loss mice (vs. CT), could lead to the accumulation of liver fat, and higher liver weight

in 4-week SBA condition. In the current study, mice exhibited a decrease only in Tb.Th without affecting the other parameters of bone architecture and BMA (Fig. 33). Selective change in Tb.Th does not seem to be associated to an overall bone alteration. Moreover, this short duration did not impact BMSC differentiation towards adipogenic lineage or osteoblastogenic lineage, nor did it affect the unsaturation ratio of lipid droplets (Fig. 34-36). Interestingly, this lack of effects on bone and BMSCs differentiation is associated with a lack of effects on *Sirt1* mRNA level (Fig. 37). This strengthens the hypothesis of a direct involvement of SIRT1 alteration on BMSCs fate decision and bone. In order to improve our understanding about BMSC differentiation capacity and its alterations in response to energy deficit, it is important to characterise the content of BMSC heterogeneous population. The following step will be to identify CD45⁻CD31⁻Sca1⁺CD24⁺ cell population that display trilineage differentiation using flow cytometry. Also, it would be necessary to study the adipogenic progenitor population CD45⁻CD31⁻Sca1⁺CD24⁻ (349). Moreover, it would be compelling to determine the number of cell population expressing Zfp423⁺ marker of MALPs and cells expressing pre-osteoblast markers (CD90, alkaline phosphatase (ALP)) (914,915). Comparison of the cell population size between BMSCs extracted from CT mice and SBA 18% weight loss mice, as well as between short term (4-week) and long term (10-week) protocols, will allow us to determine the nature of changes responsible for the difference in cell commitment.

Altogether, these results suggest that in addition to the degree of severity, the duration of energy deficit could play an important role in regulating bone architecture, BMA, and BMSC differentiation, which requires long-term protocols to be altered. This line of inquiry will be required in future to determine when the first alterations in bone, BMA and *Sirt1* expression can occur in our SBA model, and if the minimal duration of protocol depends on the severity to observe these alterations.

Differentially expressed genes in 10-week and 4-week SBA study (cohort 1) exhibit decrease in haematopoiesis related pathways and increase in cell morphogenesis and migration

Our recently published data highlights the effect of SBA protocol duration on bone and BMSC differentiation capacity, as well as *Sirt1* expression in extracted BMSCs (882). Therefore, to improve our understanding of the molecular events that take place in BMSCs extracted from long term (10-week) and from short term (4-week) protocols, RNA-seq was performed. The aim of this study was to determine differentially expressed genes in BMSCs extracted from

SBA18% and CT mice, which were exposed to different lengths of SBA protocol, and were after plate for 48h of cell adhesion. With obtained data, we seek to understand transcriptomic changes that take place in cells in the context of energy deficiency and to identify new potential regulators of *Sirt1*.

Based on the preliminary findings and results of ORA, using GO Biological Processes database, it was identified that top upregulated pathways (based on lowest p-value and number of genes present) in both 10-week and 4-week studies, were related to cell differentiation, division and mitosis (Fig. 39A, 41A). Nevertheless, pathways upregulated in SBA 18% condition of 10- and 4-week groups were similar, when we looked more specifically on the two datasets together it became clear that BMSCs of 10-week exhibit increase in cell differentiation and more specifically in mesenchyme development. In the same time, BMSCs from 4-week group displayed upregulation of cell proliferation and mitosis. These events could be explained by the fact that in the BMSC isolation process, extracted cells were plated for 48h, in prior to RNA extraction. Therefore, active cell division can be related to cell proliferation in the plate. However, it should be noted that cells from 10-week SBA 18% mice were also undergoing cell differentiation process, suggesting that these cells were programmed for differentiation in prior to cell plating.

On the other hand, downregulated pathways in SBA 18% group (vs. CT) in 10-week study, were shown to be involved in haematopoiesis and immune cell activation (Fig. 39B). Unexpectedly, 4-week SBA protocol revealed alterations in immune system activation, similarly to 10-week study (Fig. 41B). Only difference that can be observed between BMSCs from 10- and 4-week studies in that cells from 10-week study displayed a downregulation in myeloid cell maturation, and cells from 4-week study demonstrated a downregulation in lymphocyte activation. Interestingly, it was previously described that AN patients tend to develop leukopenia, with a prevalence of 29-39% (916). Leukopenia can be defined as a blood condition that is characterised by low count of white blood cells, resulting in increased infection rate in affected individuals (917). Moreover, a severe consequence of this condition could be development of bone marrow atrophy, leading to AN patients suffering from a gelatinous bone marrow transformation (918). These findings of RNA-seq analysis suggests that SBA mice exhibit at least partially similar consequences of significant weight loss to AN patients.

BMSCs themselves were described to support and improve haematopoiesis (919). In various model organisms, the haematopoietic support capacity of BMSCs was described (920–925). In particular, co-transplantation studies of BMSCs and HSCs in Rhesus macaques and in mice studies showed improves the grafting of hematopoietic cells (920,923). BMSCs are also the primary source of SCF and CXCL12, which are required for HSC maintenance (926). Additionally, a distinct subset of BMSCs within the total cell population has different functions in regulating HSCs (927). A small subset of BMSCs (NG2⁺ LepR⁻ cells) found in small arterioles near the endosteal region have been shown to contribute to arteriolar niches that keep HSCs quiescent. The other component of BMSCs (NG2⁻ LepR⁺ cells) is thought to form perisinusoidal niches that promote HSC proliferation in the BM (927). These findings highlighted the critical role of BMSCs in BM haematopoiesis. BM stromal cells, including osteoblasts derived from BMSCs, are known to form the haematopoietic microenvironment and were described to promote haematopoiesis (928). Calvi *et al.* discovered a positive link between osteoblast lineage cells and HSC numbers (33). Moreover, ablation of osteoblasts has been shown to cause severe decrease in HSCs number (32). Therefore, the decrease in haematopoiesis, which was observed in SBA 18% weight loss samples, could be explained by the loss of bone mass in these mice.

Furthermore, these findings rise the importance of studying the origin of heterogeneous adherent cells, present after plating the content of mice BM. In the current study, isolation of primary BMSCs was achieved through cell plating and elimination of haematopoietic cells was done by medium replacement after 24h of cell culture. This type of cell isolation was claimed to allow extraction of total BM cell mixed population, which includes adipocyte and osteoblast precursor cells, as well as osteoclastogenic cells (929). Therefore, fraction of haematopoietic cells could be still present in the total BMSC population. Back in 1994, Gordon *et al.* demonstrated that the human bone marrow mononuclear cell fraction can adhere to plastic after a 2-hour incubation period, and it contains hematopoietic progenitor cells capable of sustaining haematopoiesis for at least 5 weeks in a long-term culture (930). A number of other studies proclaim the presence of CD45⁺ haematopoietic cells in BMSCs culture (931–934). Also, Guo *et al.* stated that isolation of BMSCs is commonly relied on adhesion to tissue culture plastic; however, in mouse models, excessive hematopoietic contamination is a considerable obstruction (932). Altogether, the results of RNA-seq can be influenced by the presence of haematopoietic cell population. To quantify the BMSCs proportion and other cells subpopulations in mice BM extracts after SBA protocol induction (vs. CT), flow cytometry

analysis should be conducted, which is one of the limiting points in this study. It would be interesting to quantify cell population that exhibit adipogenic and osteoblastogenic potential. We suppose that SBA protocol can not only alter BMSCs fate decision, but also alter proliferation of BMSCs. Recently, it was demonstrated that stem cells extracted from human deciduous teeth, which exhibit differentiation potential into osteoblasts and adipocytes, undergo low proliferation rate under exposure to nutrient deprived medium (935). For this, previously published markers by Schulz *et al.* could be used, as they described a tri-potent, perivascular population with stem cell-like characteristics (CD45⁻CD31⁻Sca1⁺CD24⁺) (349). Also, it would be useful to characterise cell population expressing cell surface markers like CD105, CD90, CD29 and CD44 (936,937). Besides, we are intent to study cells committed to adipogenic lineage adipogenic (CD45⁻CD31⁻Sca1⁺CD24⁻), as our initial hypothesis was that energy deficit protocol results in changes in BMSCs commitment in favour of adipogenesis (349). (349). In addition, RNA-seq results showed an upregulation in pre-adipocyte marker (*Zfp423*) expression that can potentially indicate an increased ratio of pre-adipocytes in 10-week SBA 18% weight loss condition vs. CT. In order to confirm these findings, it will be necessary to study the *Zfp423* surface marker in extracted BMSCs using flow cytometry.

Expression of some genes involved in osteoblastogenesis was increased in 10-week SBA studies (cohort 1)

After studying the expression of common adipogenic and osteoblastogenic marker genes in 10-week protocol, it was observed that in SBA 18% condition after 48h of cell adhesion, a lot of late osteoblastogenic markers were upregulated (Fig. 42B). However, *Runx2* mRNA level was significantly reduced and further co-differentiation of these cells showed reduced commitment to osteoblast fate (Fig. 30B,C). Indicating that the rest of potentially upregulated osteoblastogenic markers in extracted BMSCs did not contribute towards osteoblastogenic cell commitment. This indicates a potential change in cell expression profile after induction of co-differentiation. Nevertheless, more in depth bioinformatic analysis is required to explore the full potential of obtained data.

Overall, RNA-seq technology has its limitations. Library construction could be challenging. Many short reads that are identical to each other, for example, can be obtained from amplified cDNA libraries. Moreover, to be compatible with most deep-sequencing technologies, larger RNA molecules must be fragmented into smaller pieces (200-500 bp) (832). Also, RNA-Seq

faces a number of informatics challenges, including the development of efficient methods for storing, retrieving, and processing large amounts of data, which must be overcome in order to reduce errors in image analysis and base-calling and eliminate low-quality reads (812,938–940). In general, the more complex the transcriptome and the larger the genome, the more sequencing depth is required for optimal coverage, which has consequences for cost (941).

An alternative strategy to study the differentially expressed genes in heterogeneous cell population like adherent cells from bone marrow is single cell RNA-seq (scRNA-seq). In recent years, scRNA-seq has been applied to a variety of species, most notably to human tissues (both normal and malignant), and these studies have revealed significant cell-to-cell gene expression diversity (942–946). Single-cell methods offer the benefit of identifying heterogeneity among individual cells, differentiating a limited number of cells, and outlining cell maps, when compared to classical sequencing technique (947,948). Additionally, it allows conducting differential expression analysis, which is extremely beneficial for identifying genes that are significantly differentially expressed between not only groups of cells, but also between various subpopulations (949).

Replication of 10-week moderate weight loss study resulted in significant alterations in bone without affecting BMSCs differentiation capacity or Sirt1 expression

After studying mice body parameters and BMC, results of 10-week SBA 18% weight loss group cohort 2 display changes similar to the same condition in cohort 1, suggesting that long term SBA protocol is able to consistently induce decrease in fat mass and loss in BMC (Fig. 26, Fig. 44). In the replicated study, extracted tissue mass was measured and results reveal the similar changes in SCAT and VAT, as well as lack of alteration in liver mass, to cohort 1 study. Additional parameter was studied in cohort 2, uterus mass was found to be significantly decreased in mice of weight loss condition (Fig. 44C). In anorexic patients, the oestradiol deficiency and amenorrhoea were described (807,950–952). Furthermore, Zgheib *et al.* study, in which SBA protocol was characterised, reported the decrease in ovary length and width, as well as the interruption of oestrous cycle upon exposure to 10-week 24% weight loss, confirming findings of current 10-week SBA 18% protocol (1). Therefore, SBA mice display alteration of reproductive functions as AN patients do. The decrease in oestrogen is strongly associated with reduced bone formation and increased bone resorption (953). Deficiency in oestrogen signalling leads to decrease in BMP signalling and subsequent decrease in pre-

osteoblast differentiation into mature osteoblasts (954,955). Moreover, oestrogen reduction diminishes production of osteoprotegerin (OPG) and promotes receptor activator of NF- κ B ligand (RANKL), further resulting in increased osteoclast maturation and bone resorption (953,954). However, in the current scenario, inflammation plays a central role in activation of bone resorption. Previous meta-analyses found that TNF- α , IL1 β , IL6, and TNF-receptor-II are considerably elevated in AN (956–958). Ochi *et al.* have demonstrated a TNF- α contribution to inflammatory bone loss by enhancing the osteoclastogenic potential of osteoclast precursor cells (959). Therefore, loss of BMC in SBA 18% weight loss group mice could potentially be affected by decrease in uterus size and its possible reduction in hormonal secretion. However, to confirm these finding, it would be necessary to explore the inflammatory markers in SBA model. To identify the origin of bone loss in the current cohort, we looked at endosteum and periosteum diameters. We found that only average tibia periosteum diameters were decreased (Fig. 45G), suggesting that decrease in bone Cort.Th take place potentially due to the reduction in bone formation and not through activated bone resorption (960). Reduction in BMC was accompanied by decrease in bone volume fraction (Bv/Tv), Tb.Th and Cort.Th, confirming previously published data on the effect of 18% weight loss in mice on bone parameters (Fig. 45) (2,882).

Moreover, analysis of BMA is crucial in deciphering at least some mechanisms of bone loss in 10-week cohort 2, however, currently this data is not available, as it is under process of analysis. In contrast with previous cohort, where micro-CT with osmium tetroxide staining was used to quantify the total volume of BMA, in cohort 2 the histological analysis of bone slides was done using perilipin staining of lipid droplet coating. Labelling the lipid droplet surface allows to determine not only the count of adipocytes in BM, but also to study its morphology (219,229). This experiment will improve our understanding of lipid content, size and location within BM. Nevertheless, this technique has its disadvantages, as the study uses bone sections and does not allow to quantify the whole BMAT volume to BM volume ratio. Therefore, potential solution to obtain whole BMAT volume data and study lipids at high resolution in future, would be to use Hf-WD-POM use Hf-WD-POM contrast enhancing staining agent and scanning combination (201).

10-week SBA Protocol	COHORT 1	COHORT 2
Mice Wight Loss		
Final BW loss vs D0	-17.27%	-18.02%
Delta final BW CT/SBA	-38%	-35.3%
CT Final Body Weight Gain (vs. D0)	22.4%	22.1%
Cumutative Food Intake (SBA 18% vs. CT)	7%	ns
Ratio between Body Weight Change and Food Intake	CT 1% Weight Gain : 8.1g Consumed Food SBA 18% -1% Weight Loss : 10.3g Consumed Food	CT 1% Weight Gain : 8.9g Consumed Food SBA 18% -1% Weight Loss : 11.2g Consumed Food
Body parameters		
VAT weight (SBA 18%)	-95%	-72%
SCAT weight (SBA 18%)	-77%	-67%
Liver weight (SBA 18%)	ns	ns
Fat mass (g)	59%	-51%
Lean mass (g)	ns	ns
Total BMC	-15%	-16%
Femur BMC	-29%	-26%
Lumbar BMC	-23%	ns
Bone Parameters		
Bv/Tv	ns	-5%
Tb.Th	ns	-19%
Tb.N	ns	ns
Tb.Sp	ns	ns
Cort.Th	-16%	-12%
Outer Diameter of the Bone	-5.5%	-7%
Inner Diameter of the Bone	4.5%	ns
BMA	ns	N/A
BMAds Area	N/A	N/A
BMAds Diameter	N/A	N/A
BMAds Number	N/A	N/A
BMSCs Differentiation		
Day of lipid droplet appearance	Day 7 for CT / Day 3 for SBA 18%	Day 5 for CT / Day 3 for SBA 18%
Adipogenic markers 48h		
<i>Pparg2</i>	ns (+50%)	ns
Adipogenic markers D14		
<i>Pparg2</i>	285%	ns
<i>Plin1</i>	N/A	ns
<i>Adipoq</i>	53%	ns
<i>Lep</i>	1292%	ns
<i>Glut4</i>	807%	N/A
Osteoblastogenic markers 48h		
<i>Runx2</i>	ns (+50%)	ns
Osteoblastogenic markers D14		
<i>Runx2</i>	-75%	ns
<i>Sp7</i>	-81%	ns
<i>Coll1a1</i>	-77%	ns
<i>Bglap</i>	-73%	ns
<i>Sirt1</i> 48h	-67%	ns
<i>Sirt1</i> D14	-75%	ns

Table 10. Summary of results obtained from 10-week cohort 1 study and 10-week cohort 2 study, comparing CT and SBA 18% groups.

4-week SBA Protocol	COHORT 1	COHORT 2
Mice Wight Loss		
Final Body Weight loss vs D0	-18.8%	-18.1%
Delta final BW CT/SBA	-18%	-26.3%
CT Final Body Weight Gain (vs. D0)	10.2%	12.5%
Cumutative Food Intake (SBA 18% vs. CT)	19.19%	10.63%
Ratio between Body Weight and Food Intake	CT 1% Weight Gain : 6.1g Consumed Food SBA 18% -1% Weigh Loss : 4.5g Consumed Food	CT 1% Weight Gain : 7.5g Consumed Food SBA 18% -1% Weigh Loss : 4.8g Consumed Food
Body parameters		
VAT weight (SBA 18%)	-85%	-80%
SCAT weight (SBA 18%)	-38%	-63%
Liver weight (SBA 18%)	20%	20%
Fat mass (g)	-50%	-56%
Lean mass (g)	ns	ns
Total BMC	ns	-7%
Femur BMC	ns	ns
Lumbar BMC	ns	-7%
Bone Parameters		
Bv/Tv	ns	-29%
Tb.Th	-16%	-19%
Tb.N	ns	-13%
Tb.Sp	ns	6%
Cort.Th	ns	-5%
Outer Diameter of the Bone	4%	-4%
Inner Diameter of the Bone	9%	ns
BMA	ns	25% (p=0.1775)
BMAds Area	N/A	-27% (p=0.1255)
BMAds Diameter	N/A	-14% (p=0.1225)
BMAds Number	N/A	18% (p=0.3250)
BMSCs Differentiation		
Day of lipid droplet appearance	Day 7 for CT / Day 7 for SBA 18%	Day 3 for CT / Day 3 for SBA 18%
Adipogenic markers 48h		
<i>Pparg2</i>	350%	-39.46%
Adipogenic markers D14		
<i>Pparg2</i>	ns	ns
<i>Plin1</i>	ns	ns
<i>Adipoq</i>	ns	ns
<i>Lep</i>	ns	ns
Osteoblastogenic markers 48h		
<i>Runx2</i>	ns	ns
Osteoblastogenic markers D14		
<i>Runx2</i>	ns	171%
<i>Sp7</i>	ns	934%
<i>Coll1a1</i>	ns	160%
<i>Bglap</i>	ns	ns
<i>Sirt1</i> 48h	ns	ns
<i>Sirt1</i> D14	ns	ns

Table 11. Summary of results obtained from 4-week cohort 1 study and 4-week cohort 2 study, comparing CT and SBA 18% groups.

Study of BMSC differentiation capacity, highlighted that cells extracted from SBA 18% group exhibit rapid appearance of lipid droplets (day 3) comparing to the control cells (day 5) in response to co-differentiation medium exposure (Fig. 46A). Despite accelerated lipid droplet appearance, relative gene expression analysis of adipogenic markers in weight loss group showed no changes in cohort 2 (Fig. 46B-F). Neither osteoblastogenic marker genes were altered in these cells (Fig. 47). Lack of changes in adipogenic/osteoblastogenic gene expression was associated with no modification in *Sirt1* mRNA level (Fig. 48). On the one hand, these findings, again, confirm the importance of *Sirt1* in BMSC differentiation capacity, similarly to 4-week cohort 1 experiment. On the other hand, these findings lead to assumption that alterations in bone and BMC are not related to the level of *Sirt1* expression, nor to a switch in BMSCs differentiation capacity. One of the reasons that these results took place could be due to the close proximity to partially contaminated cells. During the co-differentiation experiment the bacterial contamination in multiple wells of 12-well plate was observed, therefore, RNA was extracted from cells only from wells, which did not display visual signs of contamination. Despite the avoidance of contaminated samples, it is still possible that gene expression profile of selected cells can be altered by close proximity to affected cells. In 10-week cohort 2 change in bone parameters were shown to be not connected to BMSCs differentiation capacity, but could potentially take place through increase in bone resorption makers. As was mentioned above, reduction in uterus size can potentially lead to reduced production of oestrogen and increase in bone resorption. First of all, it would be necessary to confirm the reduction in oestrogen production by quantification of circulating oestrogen in mice plasma using ELISA assay (961). In order to determine if there was an increase in bone resorption, RANKL (*Tnfs11*) and OPG (*Tnfrsf11b*) mRNA level was studied in BMSCs extracted from CT and SBA 18% mice of 10-week cohort 2 study. Results showed no increase in *Tnfs11* relative mRNA level, however, *Tnfrsf11b* mRNA was found to significantly increased (+1800% vs. CT) in SBA 18% group from cohort 1 (Fig. 56A,C). This, together with findings of periosteum diameter decrease and endosteum diameter increase (Fig. 27H,I), suggests that bone resorption is decreased in 10-week cohort 1 mice and reduction in bone parameters can take place though decrease in new bone formation. A further step would be to quantify the size of bone resorption site in bone samples, using the histomorphometry (962,963).

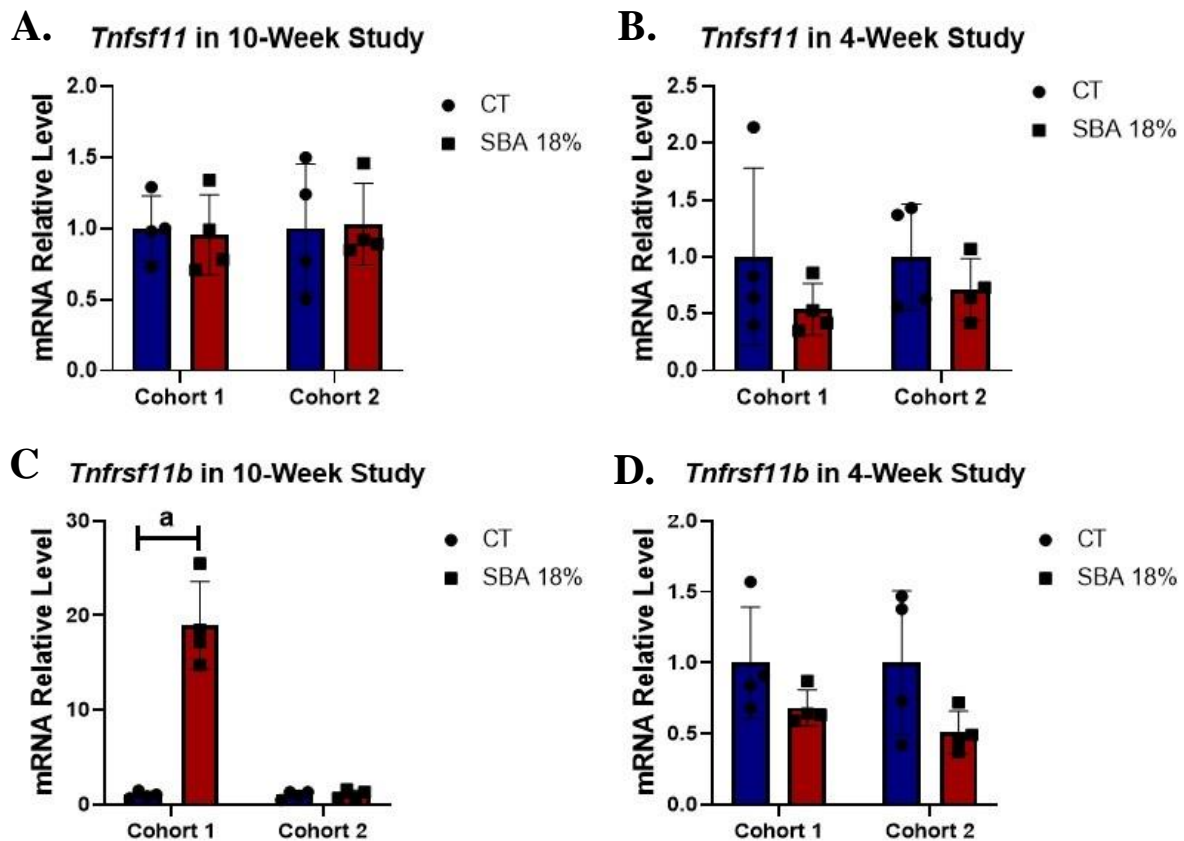


Figure 56. RANKL gene (*Tnfs11*) and OPG gene (*Tnfrsf11b*) relative mRNA level in BMSCs extracted from CT and SBA 18% mice from different studies. A. Relative mRNA expression level of *Tnfs11* in BMSCs extracted from CT and SBA 18% weight loss mice in 10-week cohort 1 and cohort 2; B. Relative mRNA expression level of *Tnfs11* in BMSCs extracted from CT and SBA 18% weight loss mice in 4-week cohort 1 and cohort 2. C. Relative mRNA expression level of *Tnfrsf11b* in BMSCs extracted from CT and SBA 18% weight loss mice in 10-week cohort 1 and cohort 2; D. Relative mRNA expression level of *Tnfrsf11b* in BMSCs extracted from CT and SBA 18% weight loss mice in 4-week cohort 1 and cohort 2; Data represent mean and SD; n=4. Statistical analysis was performed using Two-Way ANOVA test; a – p<0.05.d

Findings of 10-week cohort 2 study contradict initial results of 10-week cohort 1. This discrepancy in results could be also explained by dynamics in weight loss in different cohorts. In current cohort (cohort 2) in first 4 days of 10-week protocol, SBA 18% weight loss group mice experienced a drastic weight loss (17.7%), which was followed by (8.8%) weight gain, this shock could have potentially affected BMSCs transcriptomics and change cell behaviour. Results of 10-week cohort 1 demonstrated more consistent weight loss throughout 10 weeks, without extreme weight losses and gains (Fig. 57A). When we looked at overall food consumption ratio, we could see that in both cohorts, mice consumed similar amount of food, which resulted in 18% weight loss, suggesting that energy expenditure rate was not affected. At the end of 10-week protocol cohort 1 the difference in weight between CT and SBA 18%

groups was 34.2%, which is similar to cohort 2 finding (-35.3%). This implies that the discrepancy in BMSC marker gene expression between two cohorts is not due to difference in final mouse weight in CT and SBA 18% groups.

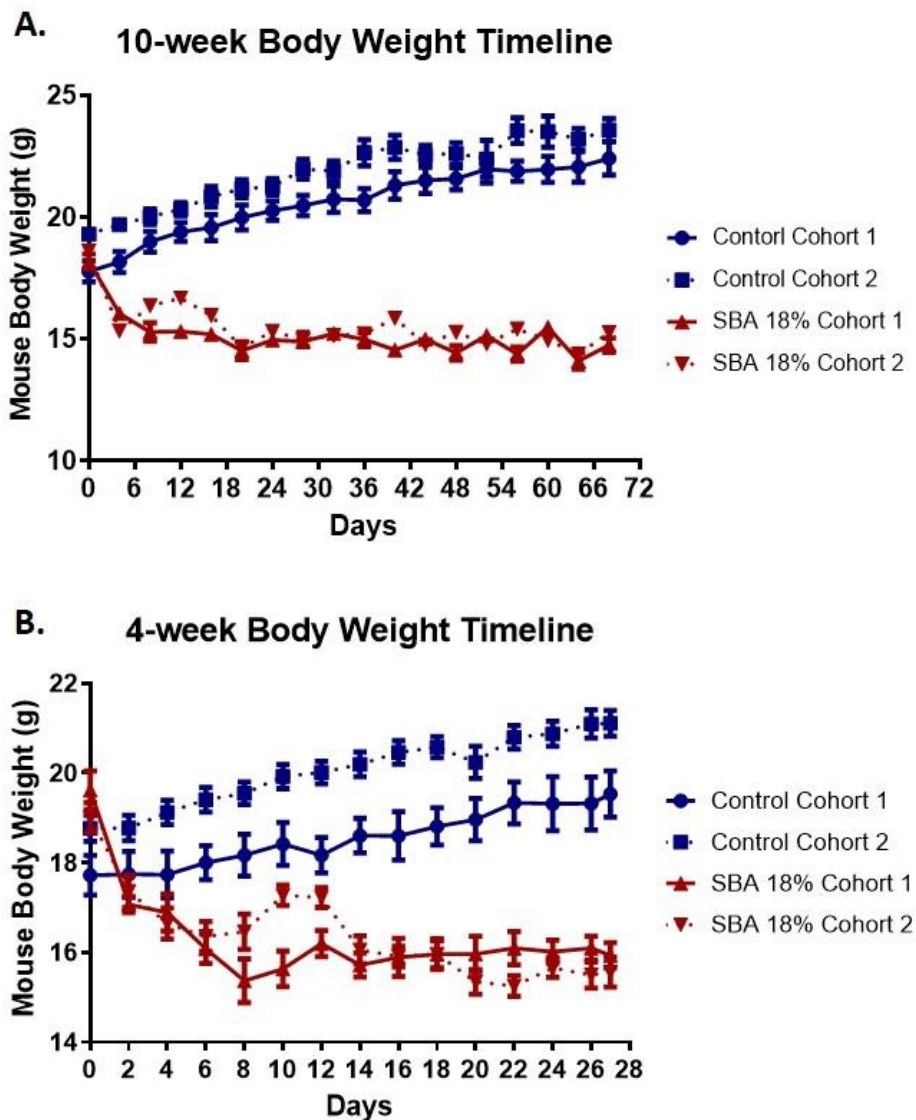


Figure 57. Mice body mass timeline. A. Body weight of individual mice is recorded daily before eating period for 10 weeks in cohort 1 and cohort 2; B. Body weight of individual mice is recorded daily before eating period for 4 weeks in cohort 1 and cohort 2. Data represents mean and interquartile range; n=12.

Replication of short-term SBA protocol (4-week) resulted in significant decrease in mice fat depots (SCAT and VAT), as well as alterations in liver mass (Fig. 49C). Both 4-week cohorts exhibited increased liver weight by 20% in moderate weight loss condition (vs. CT), confirming previously described data and suggesting that changes in mice energy consumption

and metabolism are taking place throughout SBA protocol. In this cohort, 4-week energy deficit caused decrease in total BMC and vertebral BMC, contradicting the initial findings in 4-week cohort 1 (Fig. 49G,I) (882). Concurrently, the reduction of BMC could be potentially connected with reduced uterus size, observed in SBA 18% weight loss group (Fig. 49C). As stated above, reduction in oestrogen signalling can lead to switch in bone turnover (953). In addition, decrease in BMC was accompanied by significant alterations in bone parameters (Fig. 50). Not only bone volume fraction and Cort.Th were reduced in SBA 18% group, but decrease in Tb.Th and Tb.N was accompanied by a significant increase in Tb.Sp (Fig. 50). These findings suggest that 4-week SBA protocol could induce alterations in the body and bone parameters to similar 10-week protocol. Interestingly, after quantifying BMA we found in both cohort 1 and cohort 2 change in volume was not significant. However, in cohort 2 SBA 18% we observed a positive tendency of 25% increase in BMA ($p=0.1775$ vs. CT), suggesting that changes in bone parameters could take place due to an increase in quantity of mature BMAds (882). Difference in BMA between two cohorts could be explained through different methodology of BMA quantification. In cohort 1 CT analysis of whole bone BMA was used, but in cohort 2 histological analysis of bone slides ($n=2$, in metaphasis of proximal tibia) was used. Change of quantification protocol was done to improve our understanding of adipocyte morphology within BM. From perilipin staining we were able to observe that 25% increase in BMA in SBA 18% group could take place due to an increase in BMAds number, however cell area and diameter were found to be reduced (vs. CT) (Fig. 50I-K). Reduction of BMAds size could be explained by possible increase in lipolysis in these cells. Recently, in 2019, Sheller *et al.* showed that 48-hour fasting in male and female Sprague-Dawley rats (16 to 20 weeks old) resulted in a decrease in tibia BMAds size (216). Moreover, they highlighted that only rBMAT from proximal tibia responded on CL316,243-induced (β 3-adrenergic receptor agonist) lipolysis, with no effect in distal cBMAT. This suggests that in our cohort 2 we are looking at BMAT, size of which could be reduced through the lipolysis. However, to improve the quantification of BMA it will be necessary to increase a slide number, as it is hard to predict in which confirmation of adipocyte they are cut. Further, stereological analysis of slides can be applied. With high number of slides this method will allow the 3D interpretation of 2D cross-sections, it is extracting quantitative information about 3D material from 2D samples (964–966). In simpler terms, stereology is a statistical inference of geometric parameters from sampled information, using the software analytical tools like MicroBrightfield (MBF Bioscience) it can predict a 3D shape of histological slides. Therefore, this technique can improve our estimation of BMAds diameter and area. On the other hand, development of Hf-

WD-POM contrast enhancing staining agent and scanning combination, which was described above, can also provide a single cell resolution on total BMAT. At the last day of preliminary study (4-week cohort 1), SBA 18% mice group exhibited 18% decrease in weight comparing to control mice (Fig. 57B). However, in the following cohort (4-week cohort 2), SBA 18% group displayed 26% decrease vs. control on the last day of SBA experiment (Fig. 50B). Therefore, discrepancy in findings between 4-week cohort 1 and cohort 2 could take place due to differences in weight loss in mice vs. CT.

In the same time, these changes in bone are not correlated with switch in BMSC differentiation capacity or *Sirt1* expression. No changes in lipid droplet appearance and no statistically significant changes were observed in adipogenic markers expression, from SBA 18% weight loss mice extracted BMSCs, after 14 days of co-differentiation (Fig. 51). Surprisingly, significant increase in early osteoblastogenic marker genes (*Runx2* and *Sp7*) was observed in cells of SBA 18% group vs. CT at the last day of co-differentiation experiment (Fig. 52B,C). Change in osteoblastogenic gene expression contradicted with findings of bone parameters in mice, leading to the hypothesis that changes in BMSCs commitment took place in the end of SBA protocol and did not affect bone microarchitecture. Additionally, the presence of partial cell contamination could affect BMSCs transcriptomics. Once again, this particular cohort suggests that BMSC differentiation capacity is not associated with changes in BMC and bone microarchitecture. Moreover, no change in adipogenic gene expression was accompanied by slight increase in BMA. Therefore, decrease in bone parameters also might take place due to increase in bone resorption. Results of gene expression analysis showed no change in *Tnfs11* relative mRNA level and in *Tnfrsf11b* mRNA, indicating that there is no increase RANKL production in BMSCs (Fig. 56B,D). For that reason, further quantification of bone resorption site is required, as other factors like inflammation can induce the osteoclast activity (962,963).

The discrepancy in data could also be explained by the period when the SBA protocol took place. It was shown in some studies that seasonal variation in mice behaviour can take place, therefore it could potentially affect the results of SBA protocol (967). The 4-week cohort 1 experiment took place in June/July, whereas 4-week cohort 2 experiment was conducted in September/October. Likewise, 10-week cohort 2 BMSCs, some cells in 4-week cohort 2 protocol were in close proximity to contaminated wells. Despite the fact that cells used in the experiment did not show visual signs of contamination, we couldn't exclude the fact that their gene expression profile could have been affected. Overall, current 10-week and 4-week studies

showed similar effect in bone alterations, without affecting *Sirt1* relative mRNA level or BMSCs fate decision. Therefore, in order to reconfirm the results, replication of 10-week and 4-week SBA protocol with a particular attention to weight loss dynamics is required. As well as, careful mouse allocation to CT and SBA groups, in order for both groups to have similar average weights at day 0 and avoid replication of 4-week cohort 1 results.

Low serum growth medium results in reduced Sirt1 expression in ST2 cells and affects early osteoblast markers

The next step of the project was to test the effect of reduced nutrient availability on the differentiation capacity of ST2 cells and primary mouse BMSCs, mimicking nutrient deficiency *in vitro*. After testing several conditions (FBS 5% medium and FBS 7% medium), it was shown that 5-day treatment with reduced serum (FBS 5%), *Sirt1* mRNA level significantly decrease in ST2 cell line (Fig. 54A). Also, *Runx2* mRNA level was affected by reduction of serum concentration (-39% vs. FBS 7%) (Fig. 54E). In primary mice BMSCs, *Sirt1* mRNA level exhibited a 27% decrease in FBS 5% group (vs. FBS 10%), suggesting a negative tendency of *Sirt1* expression ($p > 0.9999$) (Fig. 55A). Moreover, statistically significant decrease in *Coll1a1* was observed in BMSCs treated with reduced serum medium (vs. FBS 10%) (Fig. 55F). SIRT1 is known to function as a metabolic sensor, as it requires NAD^+ in order to conduct enzymatic activity (968). Therefore, modulation of nutrient availability can potentially affect SIRT1 activity, as well as expression through other transcription factors. Schwartz *et al.* demonstrated in fibroblast cell line, that cell expansion in medium containing 2% FBS results in 7-fold reduction in $\text{NAD}^+:\text{NADH}$ ratio, comparing to cell grown in 10% FBS medium (969). Reduction in NAD^+ availability can decrease SIRT1 activity and result in decreased *Runx2* mRNA level. Besides the effect on $\text{NAD}^+:\text{NADH}$ ration, reduced serum concentration (FBS 5%) was shown to decrease ATP production rate (vs. FBS 10%) in epithelial cell line (IPEC-J2) (970). Decrease in ATP production can result in decreased enzymatic activity in cells (971). For example, AMPK requires ATP in order to conduct its phosphatase activity and also, it was describes that AMPK is involved in regulation of SIRT1 activity and potentially could be indirectly involved in regulation of *Sirt1* transcription, for example through decrease phosphorylation and activation of E2F1 that lead to reduced induction of *Sirt1* expression (972–976). Additionally, it would be useful to study cell gene expression profile straight after 5-day exposure to low FBS medium, to see effect of nutrient deficiency avoiding restoration effect of co-differentiation medium with 10% FBS.

In current study, gene transcription analysis was performed only after low FBS treatment and further induction of co-differentiation. Therefore, in future it would be necessary to examine gene expression profile in ST2 cell line or primary BMSCs after 5-day exposure to low serum medium, as well as conducting full co-differentiation experiment using FBS 7% and FBS 5% conditions. This will allow us to further explore effects of serum concentration on cell differentiation and potentially improve the existing protocol.

PART II – IDENTIFICATION OF NEW POTENTIAL REGULATORS OF SIRT1 GENE EXPRESSION USING RNA SEQUENCING DATA

I. INTRODUCTION

RNA-seq results were used not only to identify transcriptomic differences between BMSCs extracted from CT and SBA 18% mice. The main objective of this approach is to identify new genes (not yet described in the literature) involved in the regulation of *Sirt1* mRNA. Findings of this study, should be confirmed using functional test. One of the available approaches to conduct functional test is using RNA interference (RNAi).

RNAi is the biological process by which double-stranded RNA (dsRNA) drives gene expression suppression by targeting complementary mRNA for further degradation. It was firstly demonstrated in *Caenorhabditis elegans*, by Fire *et al.* in 1998, where gene expression is regulated by dsRNA (977,978). Later, in 1999, small interference RNA (siRNA) were also discovered in plants and were found to regulate gene expression through guided sequence-dependent cleavage on the mRNA (979). With this discovery, siRNAs became firmly embedded in our view of the gene regulatory landscape, as protector of genome integrity in response to foreign or invasive nucleic acids such as transposons, transgenes, and viruses (980). Elbashir *et al.* had successfully demonstrated the relevance of the use of synthetic siRNAs for silencing and for characterisation of the siRNA structure and mode of action, which led to further development of RNAi applications (981).

With growing understanding of the molecular processes of endogenous RNA interference, siRNAs are emerging as a tool for various experimental procedures and as novel nucleic acid therapies in the treatment of incurable disorders such as some types of cancer (982–984). In general, siRNA consists of 21–23 nucleotides with 3' two-nucleotide overhangs, and it interacts with and activates the RNA-induced silencing complex (RISC) (985) (Fig. 58). The RISC component, endonuclease argonaute 2 (AGO2), cleaves the sense strand of the siRNA while the antisense strand stays attached to the RISC. The guide strand then directs the active RISC to its target mRNA for cleavage by AGO2. Because the guide strand of siRNA only attaches to mRNA that is completely complementary to it, only mRNA of the gene of interest would be targeted for degradation and therefore, expression of this gene would be silenced (985–987).

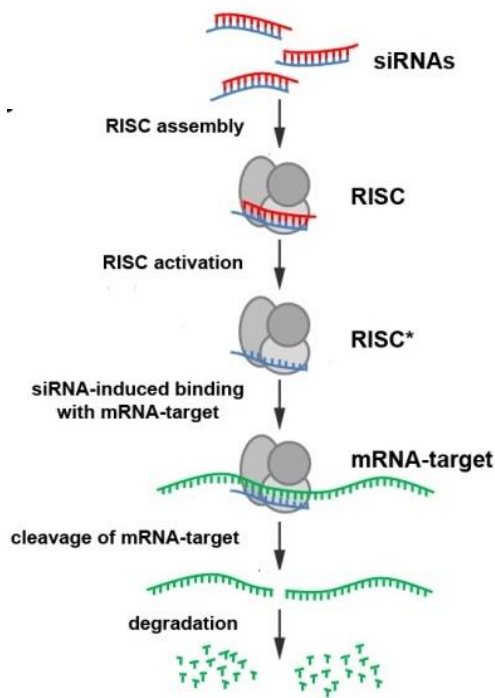


Figure 58. Schematic representation of siRNA action. Summary of key steps of effector step, including RISC complex assembly, activation of the complex and further targeting mRNA. Adapted from Petrova *et al.*, 2013 (933).

Gene specific knockout using siRNA allows inexpensive and fast test of protein function *in vitro*. Transfection of siRNA can be achieved using cationic lipids, which have long hydrophobic chains and positively charged head groups, facilitating their binding to the negatively charged siRNA, forming a lipid bilayer that the cell subsequently endocytosis (988).

Before discovery of siRNA, as a useful tool to conduct gene silencing studies, chemically modified antisense oligodeoxyribonucleic acids (ODNs) were used (989). They are 20 nucleotides long and function by hybridising to pre-mRNA and mRNA to provide a substrate for ribonuclease H (RNase H), which specifically breaks the RNA strand of the produced RNA-DNA duplexes (990). However, several studies suggested that siRNAs are significantly more effective and long-lasting than other forms of ODN (991–995). ODNs have the potential for non-specific impacts on gene expression, particularly when phosphorothioate-mediated, and they can be harmful by binding endogenous proteins (996). The high concentration of ODNs required to induce gene-silencing action magnifies the problem. For example, through the engagement of Toll-like receptors (TLRs), ODNs containing the CpG motif have been demonstrated to stimulate the production of IFNs and other innate immune responses (997–999). On the other hand, the low quantity of siRNA necessary for efficient gene silencing, as well as the fact that siRNAs are selectively and fast integrated into RISC, reduces the possibility of non-specific protein binding. Multiple studies have shown that transfection of siRNAs at low doses has no global, non-specific impact on gene expression (1000–1002).

For all these reasons, to exploit RNA-seq data and perform functional tests, we choose a strategy based on siRNA. Thus, we used siRNA probes specific to our gene of interest, after silencing the expression of this gene in cells, we studied the effect of this treatment on *Sirt1* relative mRNA level.

II. MATERIALS AND METHODS

1. Animals

Seven-week-old female C57BL/6J mice purchased from Charles River Laboratories (St Germain sur l'Abresle, France) were used for the separation-based anorexia (SBA) model (1). SBA protocol was performed similarly to the method described in PART 1, Materials and Methods section 1. This study was specifically approved by the Committee on the Ethics of Animal Experiments (CEEA) of Nord-Pas de Calais, France (permit number: CEEA#2016070717275082).

2. Primary Bone Marrow Stromal Cell and ST2 Cell Culture

Primary bone marrow cells were harvested from the tibiae and femurs of CT and SBA mice, as it was described in Ghali *et al.* study (808). Cells were plated for 48 hours adhesion in MEM medium (PAN BIOTECH; P04-21050) with 15% foetal bovine serum (PAN BIOTECH; P30-3306), 1% penicillin/streptomycin (PAN BIOTECH; P04-85100) and 1% stable glutamine (PANBIOTECH; P06-07100). ST2 cells were obtained from DSMZ (ST2, ACC 333, Lot5) and incubated at 37°C and 5% CO₂, in MEM medium (PAN BIOTECH; P04-21050) supplemented with 10% foetal bovine serum (PAN BIOTECH; P30-3306), 1% penicillin/streptomycin (PAN BIOTECH; P04-85100) and 1% stable glutamine (PANBIOTECH; P06-07100).

3. RNA Sequencing and Data Analysis

The process of RNA-seq and data analysis was described in PART 1, Materials and Methods section 10. In current study we used same data that was obtained previously.

4. RNA Extraction and Reverse Transcription

Total RNA was extracted from BMSC culture using Extract-all (Eurobio, Les Ulis, France). At the end of cell culture, 1ml of Extract-all was added per 1 well of a 24-well plate and samples were transferred to a 1.5 ml collecting tube. Next step was to add 200 µl of chloroform (Thermo Scientific; J67241.AP) per each tube and spin samples at 4°C and 12 000 g for 15 min. The

upper aqueous phase containing RNA was removed and the rest of the protocol was conducted according to RNeasy Mini Kit (QIAGEN; 74104) manufacturer's protocol. Total RNA was quantified using the NanoDrop 2000 spectrophotometer (Thermo Scientific, Labteck, Palaiseau, France).

5. Real-Time PCR

Reverse transcription of samples was conducted using the Maxima First Standard cDNA Synthesis Kit for RT-qPCR (Thermofisher; K1642) manufacturer's protocol. Quantitative PCR (qPCR) experiment required was conducted according to protocol in PART 1, Materials and Methods section 11. The sequences of the primers (TibMolBiol, Berlin, Germany), annealing temperature and GenBank reference for each of the genes analysed with efficiency test are shown in Table 12.

Gene	Primer Sequences	Annealing temperature	GenBank
<i>18S</i>	F: ATTCCGATAACGAACGAGAC R: GCTTATGACCCGCACTTACT	60 °C	X03205
<i>Gapdh</i>	F: GGCATTGCTCTCAATGACAA R: TGTGAGGGAGATGCTCAGTG	62 °C	NM_008084
<i>Daxx</i>	F: ACCCTGTGACCCCCAGTATG R: TCGCAGAATTTCCCGTCC	60 °C	NC_000083.7
<i>Esr1</i>	F: TCTGCCAAGGAGACTCGCTACT R: GGTGCATTGGTTTGTAGCTGGAC	60 °C	NM_007956
<i>Fiz1</i>	F: TGTAGCGAATGTGGCAAGAGTTTC R: AGGGCTTTTCACCAGTGTGGAC	60 °C	NM_001110328
<i>Cebpb</i>	F: CAAGCTGAGCGACGAGTACA R: AGCTGCTCCACCTTCTTCTG	61 °C	NM_009883.4
<i>Hif1a</i>	F: CCTGCACTGAATCAAGAGGTTGC R: CCATCAGAAGGACTTGCTGGCT	60 °C	NM_010431
<i>Rara</i>	F: AAATCATCCGGCTACCACT R: TCTGGATGCTTCGTCGGAA	60 °C	NM_009024
<i>Rbl</i>	F: GGAATTCGGCGTGTGCCATCAATG R: AGCTCTCAAGAGCTCAGACTCATGG	60 °C	NM_009029
<i>Rleb</i>	F: CCTCTTCCCTGTCACTAACGGTCTC R: ACGCTGCTTTGGCTGCTCTGTGATG	60 °C	NM_009046
<i>Smcr8</i>	F: GGTGCATTGGTTTGTAGCTGGAC R: GGCAAGCCTCACAGTACCAT	60 °C	NM_001085440.1

Table 12. Primer sequences and conditions of quantitative RT-PCR (PART 2).

6. siRNA Transfection

ST2 cells were transfected with small interfering RNA (siRNA), targeting *Rb1* (ref. 4390771), as well as non-targeting (siRNA negative control (siRNA neg), ref. 4390846) purchased from Ambion (Life Technology Inc.). siRNA targeting *Rb1* and siRNA neg were transfected to ST2 cells at a final concentration of 25nM, using Lipofectamine (Invitrogen, ref. 13778-030). Transfection solution was prepared in Opti-MEM reduced serum medium (Gibco, ref. 31985-062), four conditions were used in the study – Opti-MEM, Opti-MEM + Lipofectamine, Opti-MEM + Lipofectamine + siRNA neg, Opti-MEM + Lipofectamine + siRNA (*Rb1*). When ST2 cells reached 80% confluency, standard growth medium was changed to Opti-MEM, with or without transfection agents. Cells were incubated in transfection solution for 72 hours or for 7 days, without medium change.

7. Statistical Analysis

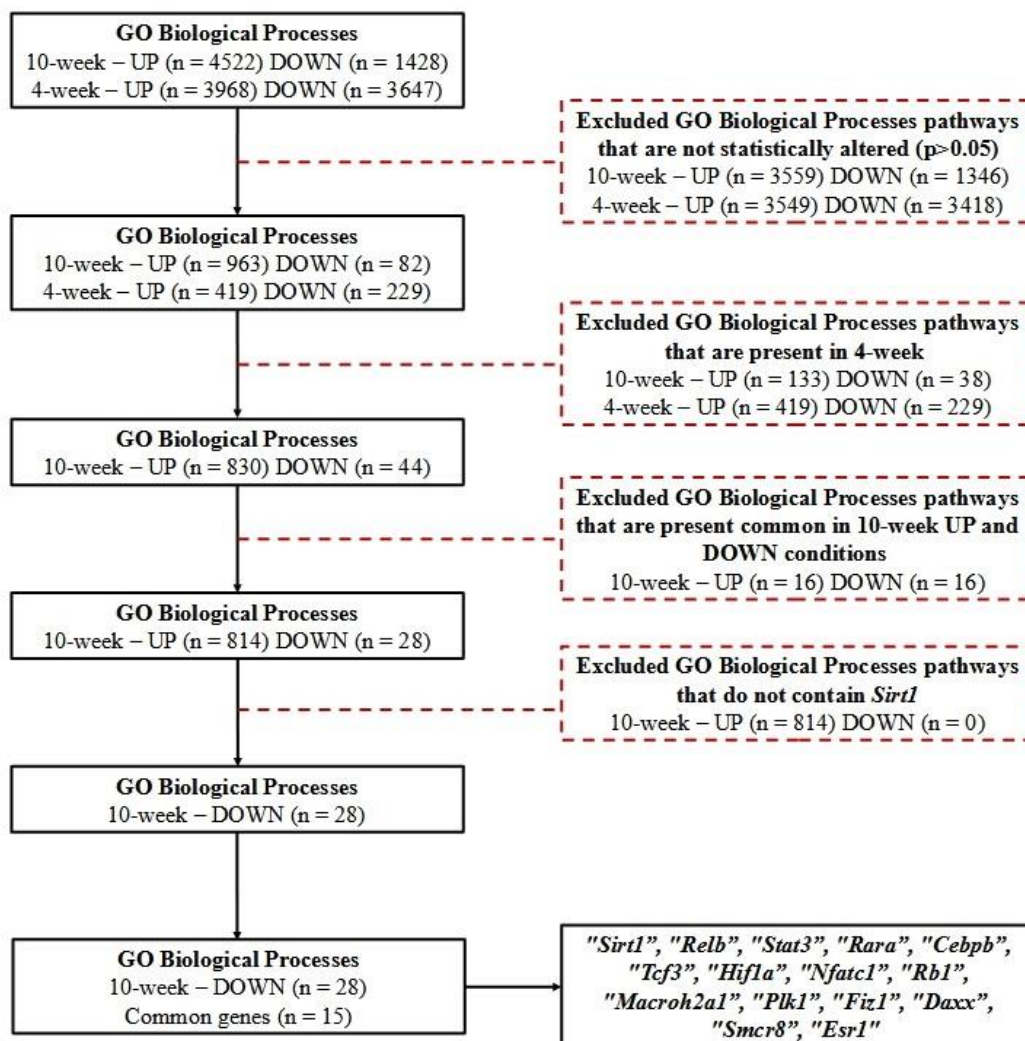
The 10-week (cohort 1) study was performed with 6 samples per condition. The 4-week (cohort 1) study was performed with 5 samples per condition. The median and interquartile range were calculated for the groups. Due to the low number of replicates, the normality of the data could not be tested. In siRNA transfection study we performed Kruskal-Wallis One-Way ANOVA test, to show the significance between all the conditions. Additionally, we conducted Dunn's test in order to see the relationships between specific pairs of conditions. For gene expression assessment, we performed Mann-Whitney's test to see the statistically significant relationship between the two particular conditions. All tests were performed using GraphPad Prism software. Differences with $p < 0.05$ were considered statistically significant.

III. RESULTS

Identification of new potential regulators of *Sirt1* expression using RNA-seq data

RNA-seq analysis of SBA 18% vs CT groups was also conducted to identify new potential regulators of *Sirt1* expression, which could be responsible for decrease in *Sirt1* mRNA in BMSCs. In order to narrow down the search and find genes that are potentially associated with *Sirt1* mRNA decrease, a number of data filtering steps were conducted.

A.



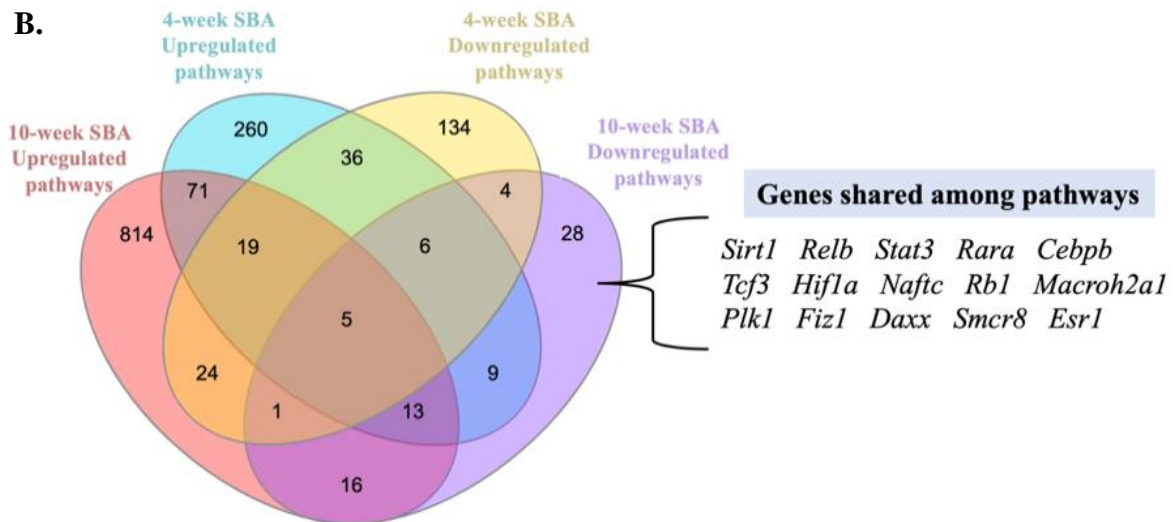


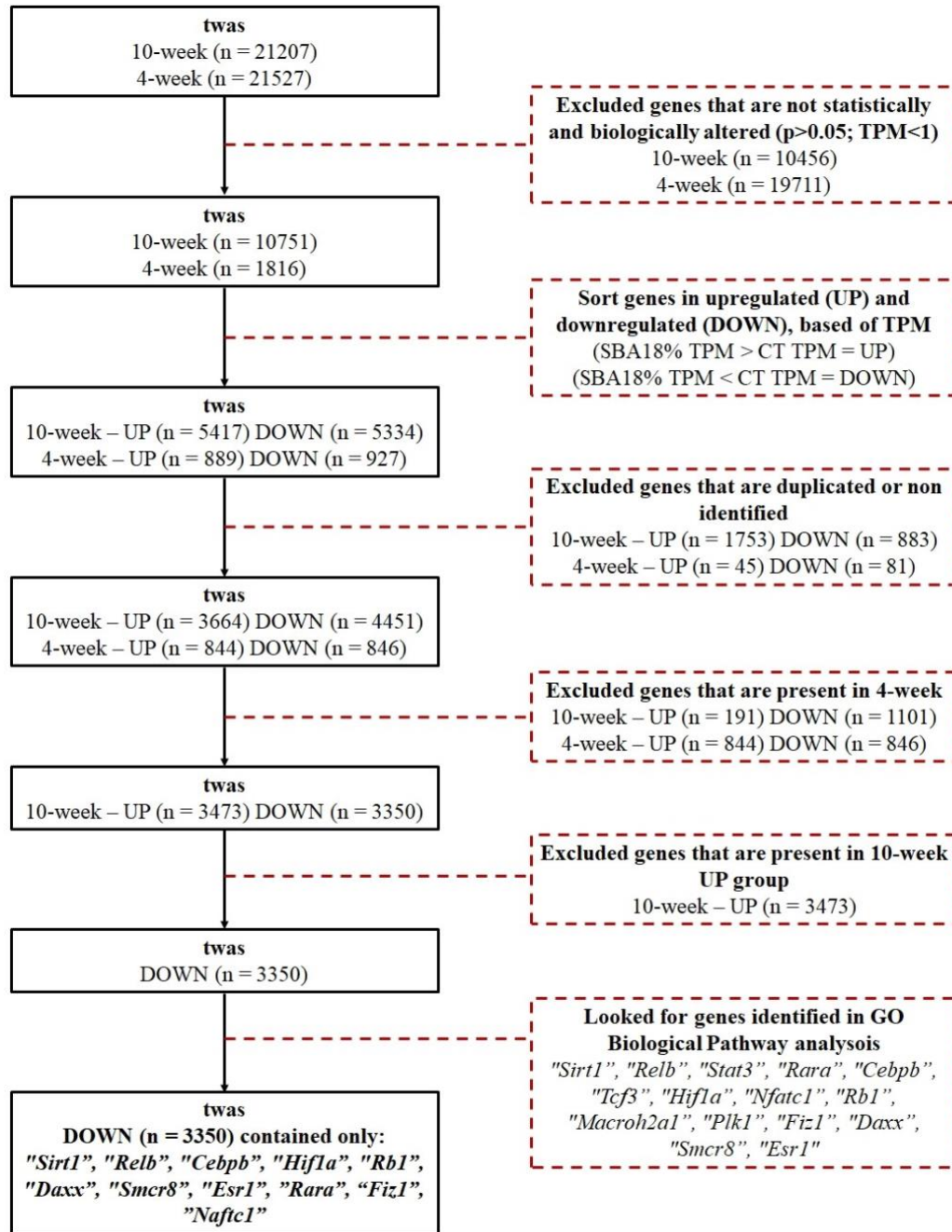
Figure 59. Summary of RNA-seq data analysis to identify *Sirt1* related genes and Venn diagram of upregulated/downregulated pathways. A. Summary of the RNA-seq data analysis aiming to identify genes that potentially are involved in *Sirt1* regulation; B. Venn diagram representing the upregulated/downregulated pathways in 4-week and 10-week SBA 18% protocols with summary of shared genes among 10-week downregulated pathways.

The first step was to identify pathways (based of ORA), in which *Sirt1* gene is present, using Bioconductor R package cluster Profiler. Initially, from all pathways established using GO Biological Processes database (10-week and 4-week groups), statistically insignificant pathways were excluded. After, based on our previous conclusion, that 4-week SBA study (cohort 1) does not result in alterations in BMSCs differentiation capacity nor in *Sirt1* mRNA level, we decided to exclude all pathways that are altered in 4-week samples. This was done to exclude pathways that were assumed to not be involved in *Sirt1* regulation. Next, we identified that only statistically significantly downregulated pathways contained *Sirt1* gene, which led us to focus only on 28 pathways where *Sirt1* was found. Moreover, all these pathways contained other 14 common genes, which have been treated as potential regulators of *Sirt1* (Fig. 59). On the other hand, there is a possibility that other genes which were excluded can also be involved in regulation of *Sirt1* expression. However, we hypothesised that genes that are present with *Sirt1* in multiple common pathways have higher possibility to be involved in its regulation, at least in one out of multiple pathways that were identified.

Following this, we were interested, do all of these 14 genes exhibit significant changes (statistical and biological) in SBA 18% condition of 10-week protocol. To do this, we used a TWAS dataset containing all data on differentially expressed genes in SBA 18% group vs. CT.

Therefore, further steps of analysis are focused on gene expression database specifically. Overall, this dataset consisted of 21 207 genes in 10-week group and the first step was to remove all genes that exhibited p-value > 0.05. RNA-seq is a very sensitive quantification tool, therefore, all genes that had the number of transcripts per kilobase million (TPM) less than 1, were eliminated, due to their lack of biological significance. After, we removed all the data of upregulated genes in SBA 18% group, as our genes of interest were found to be present specifically within downregulated pathways (Fig. 59B). Using this data exclusion method, only 3 350 genes were left, and our next step is to look for our candidate genes in current data set. Out of 14 genes, that were identified, only 10 were found among the 3 350 genes in 10-week downregulated gene dataset (Fig. 59). The last step in the selection process was the confirmation of gene transcription downregulation using qPCR.

A.



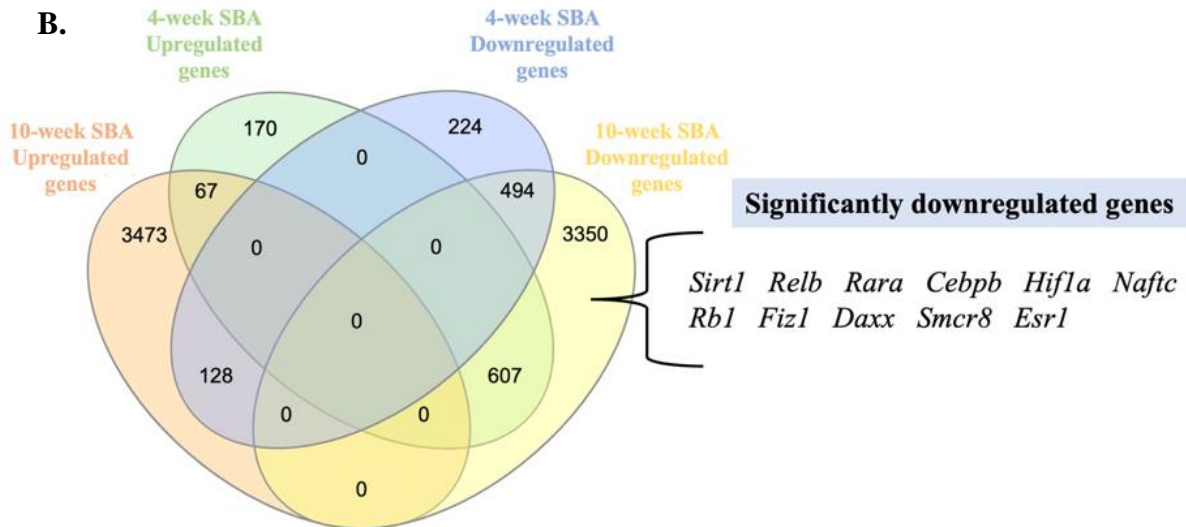


Figure 60. Summary of RNA-seq data analysis to identify *Sirt1* related genes and Venn diagram of upregulated/downregulated genes. A. Summary of the RNA-seq data analysis aiming to identify genes that potentially are involved in *Sirt1* regulation; B. Venn diagram representing the upregulated/downregulated genes in 4-week and 10-week SBA 18% protocols with summary of shared genes among 10-week downregulated genes ($p < 0.05$; $TPM > 1$).

As it was mentioned earlier, RNA-seq is a very powerful and very sensitive tool, but to double-check our findings qPCR is required to confirm a significant change in mRNA level of identified genes. Results of this experiment showed that out of 10 genes (*Relb*, *Cebpb*, *Hif1a*, *Rb1*, *Daxx*, *Smcr8*, *Esr1*, *Fiz1*, *Naftc1*, *Rara*), only 6 were significantly downregulated in same cells according to qPCR results (10-week SBA 18% condition vs CT) (Fig. 61).

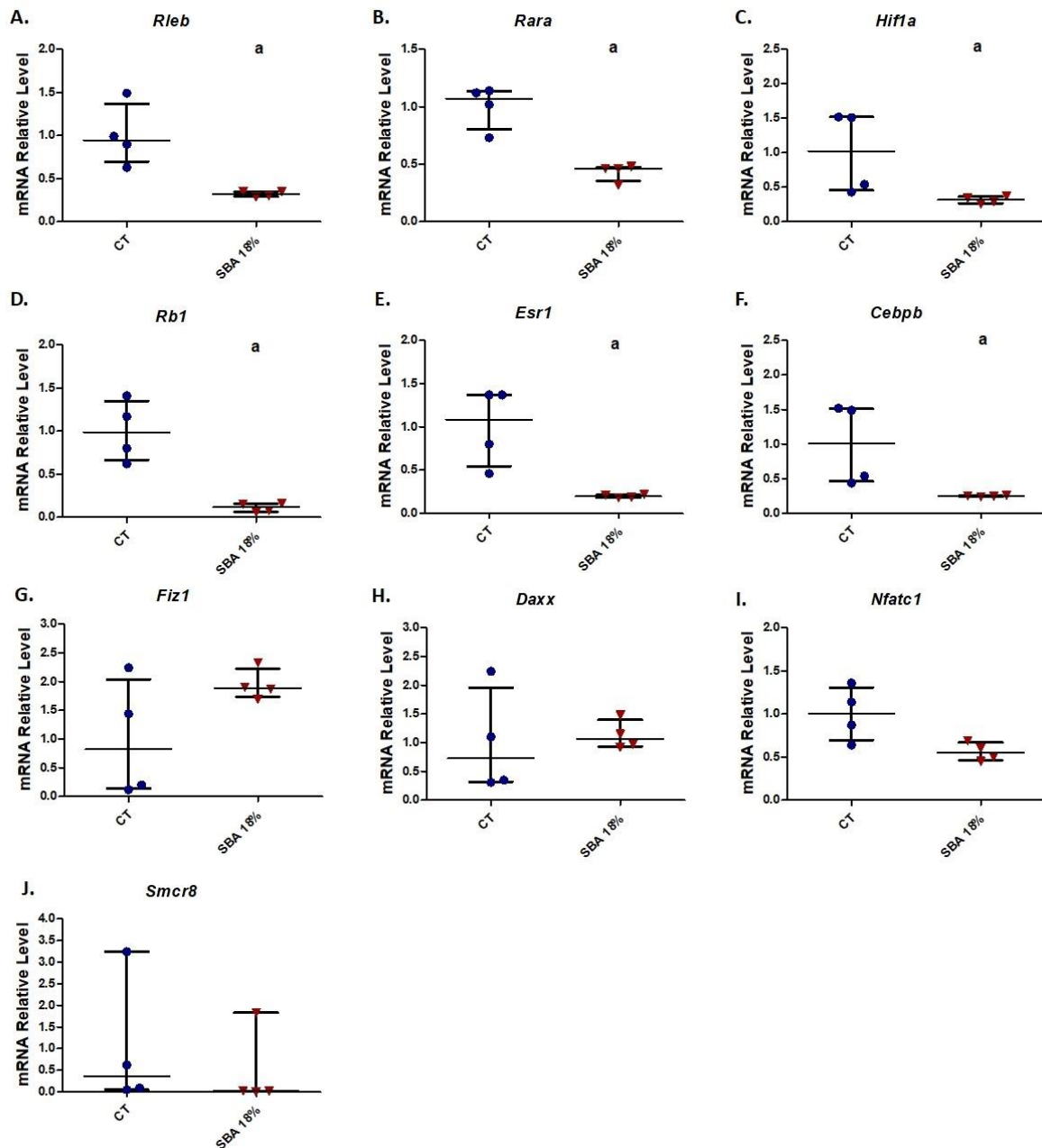


Figure 61. Relative mRNA expression of RNA sequencing identified genes. A-G. Relative mRNA level of genes Identified using RNA sequencing – *Relb*, *Rara*, *Hif1a*, *Rb1*, *Esr1*, *Cebpb*, *Fiz1*, *Daxx*, *Nfatc1*, *Smcr8*, respectively; Data represents mean \pm Interquartile range; n=4. Statistical analysis was performed using Mann-Whitney’s test; a - p<0.05.

This analysis allowed to identify genes to study primarily because they could play a role in *Sirt1* regulation in the context of the study. All 6 genes were found to be involved in gene transcription and regulation of various processes like response to hypoxia, cell cycle or inflammatory response (Table 13). Moreover, in literature, it was described that some of the identified genes are known to indirectly and directly interact with *Sirt1*. For example, *Relb* gene transcribed into a protein, which becomes a part of NF-kB homodimer. Previously,

positive effect of NF- κ B binding to *Sirt1* promoter region was widely described (701,702). For that reason, it can be hypothesised that reduction of *Relb* expression can result in reduced NF- κ B complex assembly and therefore, lead to reduced *Sirt1* expression. Also, HIF1a was shown to upregulate *Sirt1* expression through binding HER5 response element (713). On the other hand, in liver, CEBP β forming the complex with histone deacetylase 1 (HDAC1) was shown to repress SIRT1 (1003). Other identified genes were formerly reported to be downstream targets of SIRT1 – *Rara* and *Esr1* (1004,1005), and thus were not considered as gene to study first.

Gene	Full Name	Function
<i>Relb</i>	V-Rel Avian Reticuloendotheliosis Viral Oncogene Homolog B	Transcription factor, which is a proto-oncogene and is a part of NF- κ B homo- or heterodimeric complex
<i>Rara</i>	Retinoic Acid Receptor Alpha	Nuclear retinoic acid receptor, regulates transcription in a ligand-dependent manner
<i>Hif1a</i>	Hypoxia Inducible Factor 1 Subunit Alpha	Encodes the alpha subunit of transcription factor, which functions as a master regulator of cellular and systemic homeostatic response to hypoxia by activating transcription of many genes
<i>Rb1</i>	Rb Transcriptional Corepressor 1	Protein encoded by this gene is a negative regulator of the cell cycle and was the first tumour suppressor gene found. <u>Capasso <i>et al</i> showed that RB1 inactivation in BMSCs facilitates adipogenic differentiation (1006)</u>
<i>Esr1</i>	Oestrogen Receptor 1	Estrogen receptor and ligand-activated transcription factor
<i>Cebpb</i>	CCAAT Enhancer Binding Protein Beta	Transcription factor, which activity is important in the regulation of genes involved in immune and inflammatory responses

Table 13. Summary of gene function. Table summarises a name and function of genes, which were identified by RNA sequencing as potential interactors and regulators of *Sirt1* in 10-week SBA 18% condition. Information is taken from genecards.org

Capasso *et al.* in 2014 have shown that shRNA treatment targeting *Rb1* in primary human BMSCs results in facilitation of adipogenic differentiation. These results showed that *Rb1* is playing a role in BMSC differentiation commitment and potentially can be involved in regulation of *Sirt1* expression in this cell type. Therefore, functional test of *Rb1* was done as a priority to determine a possible impact of its downregulation on *Sirt1* expression.

In order to understand the relationships between identified genes and *Sirt1*, it was necessary to perform functional test using RNA interference. In this case, siRNA was used to suppress the mRNA expression of genes of interest and study its effect on *Sirt1* mRNA level. For this test, ST2 cells were treated with siRNA targeting *Rb1* (25nM) for 72h and for 7 days. After 72h of treatment, cells exhibited a significant decrease in *Rb1* relative mRNA level (76.3%) (vs. siRNA negative) (Fig. 62A). This confirmed successful transfection. However, in the same cells, no decrease in *Sirt1* mRNA level was observed (Fig. 62B). After the 7-day treatment, ST2 cells did not exhibit a significant difference in *Rb1* mRNA level (-49.1%), suggesting that after this time, *Rb1* expression started to restore (Fig. 62C). Moreover, long term transfection with *Rb1* siRNA did not result in changes in *Sirt1* mRNA level (vs. siRNA negative) (Fig. 62D). These results suggest that RB1 is not involved in regulation of *Sirt1* expression in our model. Functional test on *Rb1* was the first one conducted, however, in the prospects of current study we are aiming to test the other candidate genes, to complete the work.

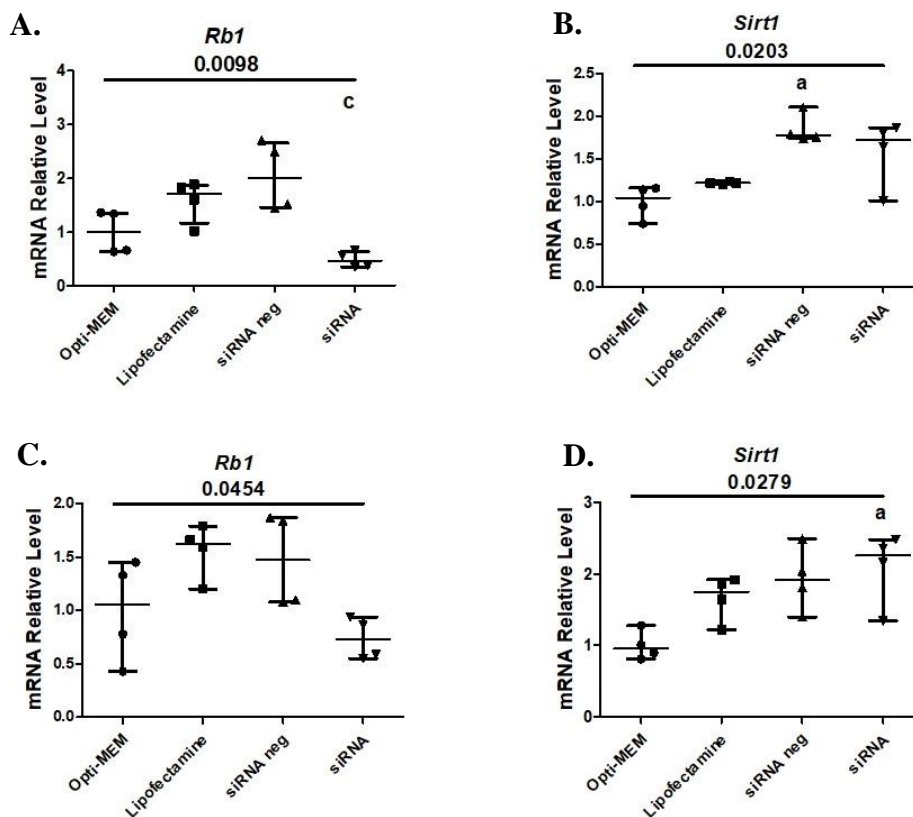


Figure 62. *Rb1* and *Sirt1* expression in ST2 cells after exposed to *Rb1* siRNA. A-B. Relative mRNA level of *Rb1* and *Sirt1* in ST2 cells treated with 50nM of Prkaa2 siRNA for 72 hours; C-D. Relative mRNA level *Rb1* and *Sirt1* in ST2 cells treated with 50nM of *Rb1* siRNA for 7 days; Data represents mean \pm Interquartile range; n=4. Statistical analysis was performed using Kruskal Wallis test and Dunn's Multiple Comparison Test; a – $p < 0.05$, when compared to Opti-MEM only condition; c – $p < 0.05$ when compared to siRNA neg condition.

IV. DISCUSSION AND CONCLUSIONS

RNA-seq allowed to identify multiple genes that might be involved in Sirt1 regulation, however Rb1 does not seem to be one of them

One of the main interests in conducting RNA-seq was to find new pathways or genes that can be involved in transcriptional regulation of *Sirt1*. Using ORA based on GO Biological Processes database, we were able to identify pathways where *Sirt1* is present. Our next step was to identify other common genes, shared among these pathways, as there is a probability that genes within the same pathway may be involved in regulation of *Sirt1* expression. The identified genes were filtered based on biological and statistical significance, and their expression level was also confirmed using qPCR. Filtering through data, allowed to identify 6 genes (*Rleb*, *Rara*, *Hif1a*, *Rb1*, *Esr1*, *Cebpb*) that can potentially regulate *Sirt1* expression, as they are present in the same pathway. The next step was to conduct functional test using siRNA transfection (Fig. 61). *Rb1* was chosen for further experiments, as Capasso *et al.* showed its involvement in suppression of adipogenic differentiation in BMSCs (1006). Furthermore, multiple studies in other cell types reported interactions between *Rb1* and *Sirt1*. Indeed, Song *et al.* described that in primary human umbilical vein endothelial cells (HUVEC), RB1 acts through stimulating SIRT1 leading to protection against endothelial senescence and dysfunction, in the context of H₂O₂ exposure (1007). Another type of endothelial cells, rat retinal capillary endothelial cells (RCECs), has been used to study an effect of RB1 treatment on high glucose-induced damage (1008). Results indicated that RB1 enhanced both SIRT activity and SIRT1/SIRT3 expression (1008). In mice hippocampus, RB1 treatment significantly increased SIRT1 protein expression (1009). Therefore, it was hypothesised that RB1 mediated suppression of adipogenesis could be fulfilled through alteration in *Sirt1* expression. However, results of *Rb1* siRNA transfection in ST2 cells showed no effect on *Sirt1* mRNA level, indicating that *Rb1* is not involved in *Sirt1* transcription regulation (Fig. 62). Other genes, which came up in RNA-seq analysis, will be further assessed using siRNA. As it was mentioned before, *Relb* can potentially regulate *Sirt1* expression, as decreased *Relb* expression will result in decreased NFκB complex assembly and subsequent reduction of *Sirt1* mRNA (701,702,1010). Besides, *Cebpb* and *Hif1a* have been described above as good candidate genes to conduct functional test and study their effect on *Sirt1* expression.

In the literature, it was widely described that HIC1 tumour suppressor negatively regulates *Sirt1* expression, through formation of co-repressor complex with CTBP1 and binding to *Sirt1* gene promoter (580,707,708,711,712). RNA-seq data showed that in BMSCs extracted from 10-week SBA 18% weight loss mice, mRNA level of *Ctbp1* gene is significantly higher comparing to CT group ($p < 0.05$). In addition, overall expression level of this gene is high (SBA18% - TPM=190; CT - TPM=181) in both conditions. Therefore, we hypothesised that increased level of *Ctbp1* expression could potentially facilitate a suppression of *Sirt1* in SBA 18% group. Thus, this gene could be a good candidate for further functional tests.

Moreover, use of siRNA as a tool for functional study has its disadvantages, one of them is the efficacy of this technique. The target selection procedure is iterative, necessitating extensive mining of routes and databases (1011). RNAi efficacies of various siRNAs targeting different portions of the same mRNA sequence vary, and only a small proportion of siRNAs have been demonstrated to be effective in human cells (1012). Among randomly chosen siRNAs, 58-78% were seen to induce silencing with better than 50% effectiveness, but only 11-18% induced silencing with 90-95% efficiency (1013). siRNA transfection has also been shown to exhibit an off-target silencing effect. It is now clearly documented that many siRNA molecules have off-targets and that most siRNA molecules are probably not as selective as previously assumed (1014–1017). The use of siRNA might have off-target effects, which are the suppression of genes other than the desired, resulting in harmful alterations of gene expression and unforeseen consequences (1018). The bulk of siRNA-mediated off-target gene silencing is caused by partial sequence similarity, particularly within the 3'UTR, with mRNAs that are not the desired recipients (1019).

Alternatively, short hairpin RNAs (shRNAs) can also be utilised to silence certain genes through the RNAi process (1020). shRNAs are stem-loop RNAs that are expressed in the nucleus, often by viral vector delivery. They are transported to the cytoplasm for additional processing, after which they are loaded into the RISC complex for particular gene silencing activity in the same way that synthetic siRNAs are (1021). The disadvantage of shRNA over siRNA could be the capacity to utilise viral vectors for delivery, which allows overcoming the problem of transfecting particular cell types (1022,1023). Additionally, the ability to regulate shRNA expression using inducible promoters, and the ability to co-express them with a reporter gene could be very useful in experimental planning (1024). Furthermore, they may have less

off-target effects (1024). The length of both the experiment and the half-life of the target protein are crucial considerations when deciding between siRNA- and shRNA-mediated gene silencing approaches. There has not been conducted large-scale research to compare the length and amount of protein knockdown accomplished by siRNA or shRNA constructs. However, preliminary results utilising transfected siRNAs and plasmids encoding shRNAs revealed that shRNAs achieves higher half-life (1024). Stable expression of a shRNA may be necessary for longer tests or when attempting to knockdown the expression of proteins with extended half-lives (1024).

Another way to identify regulators of *Sirt1* expression in BMSCs exposed to energy deficit, is to conduct study of epigenetic markers. The epigenome consists of methylated DNA and modified histone proteins. Histone modifications like acetylation are typically associated with open and accessible chromatin regions, whereas histone methylation can be associated with either open or compacted (heterochromatic) chromatin regions, depending on the specific histone amino acid that is methylated (1025–1028). Open chromatin is related with mono- or trimethylation of lysine 4 on histone H3 (H3K4me1 or H3K4me3) and trimethylation of histone H3 on lysine 36 (H3K36me3). Trimethylation of histone H3 lysines 9 and 27 (H3K9me3 and H3K27me3, respectively) is linked with compacted chromatin regions, leading in gene regulation (1029). Knowing the genome-wide pattern of single histone modifications, can reveal a lot about cell identity and disease status (1026,1030–1032). The chromatin immunoprecipitation (ChIP) test is now the preferred method for studying the epigenome. In this process, histones or transcription factors are covalently crosslinked to their genomic DNA substrates, which allows taking a snapshot of protein-DNA interactions in a particular cell. Following chromatin separation and fragmentation, protein-DNA complexes are captured using antibodies specific to the histone or transcription factor of interest. Upon crosslink reversal, the ChIP DNA is purified and examined using high-throughput sequencing (ChIP-seq), which provides the possibility to explore an entire genome in one run (1033). Identifying the chromatin state and protein binding to *Sirt1* promoter region will allow us to pinpoint the potential regulators of *Sirt1* expression in SBA condition. This is the next step which is going to be taken in current research.

PART 3 – FURTHER INVESTIGATION OF SIRT1 REGULATORS

I. INTRODUCTION

The AMPK has emerged as one of the key regulators of cellular energy homeostasis. It functions as a coordinator of metabolic pathways in mammalian cells and unicellular organisms, in order to balance nutrition supply with energy demand (1034). For the first time, back in 1981, sucrose non-fermenting 1 (SNF1) protein, the AMPK yeast ortholog, was reported as the major energy sensor in this organism (1035). After, also Woods *et al.* described SNF1 kinase, as a metabolic stress sensing kinase required for *Saccharomyces cerevisiae* survival in glucose-depleted environments (1036). AMPK is an energy-sensing protein complex that is activated when the AMP:ATP or ADP:ATP ratio increases during hypoxia, famine, glucose deprivation, or muscular contraction (1037,1038). In the context of decrease in the major carbon or nitrogen sources, this kinase is adjusting cellular metabolism to changes in the cellular environment (1039). AMPK integrates nutritional and hormonal signals to maintain cellular energy balance and execute appropriate metabolic tasks (1040). When AMPK is activated, energy-consuming biosynthesis pathways, like fatty acid synthesis, cholesterol synthesis and insulin secretion are inhibited, while ATP-producing catabolic pathways, as fatty acid uptake and oxidation, glycolysis and mitochondrial biogenesis, are activated (1041). It is achieved through AMPK-mediated suppression of ACC1 and ACC2, which leads to a decrease in FA synthesis and an increase in FA oxidation, respectively (Fig. 63) (1042). In addition, AMPK influences the transcription of particular genes involved in energy metabolism, allowing it to exercise long-term metabolic regulation. Furthermore, AMPK signalling pathways are engaged in a variety of physiological activities beyond from their primary metabolic tasks, such as cytoskeleton remodelling and transcriptional control or regulation of critical cellular processes like death or autophagy (1042,1043). The activation of autophagy in the cells can be conducted by AMPK induced activation of Unc51 like autophagy activating kinase (ULK1/2) or through the suppression of mTOR (Fig. 63) (1042).

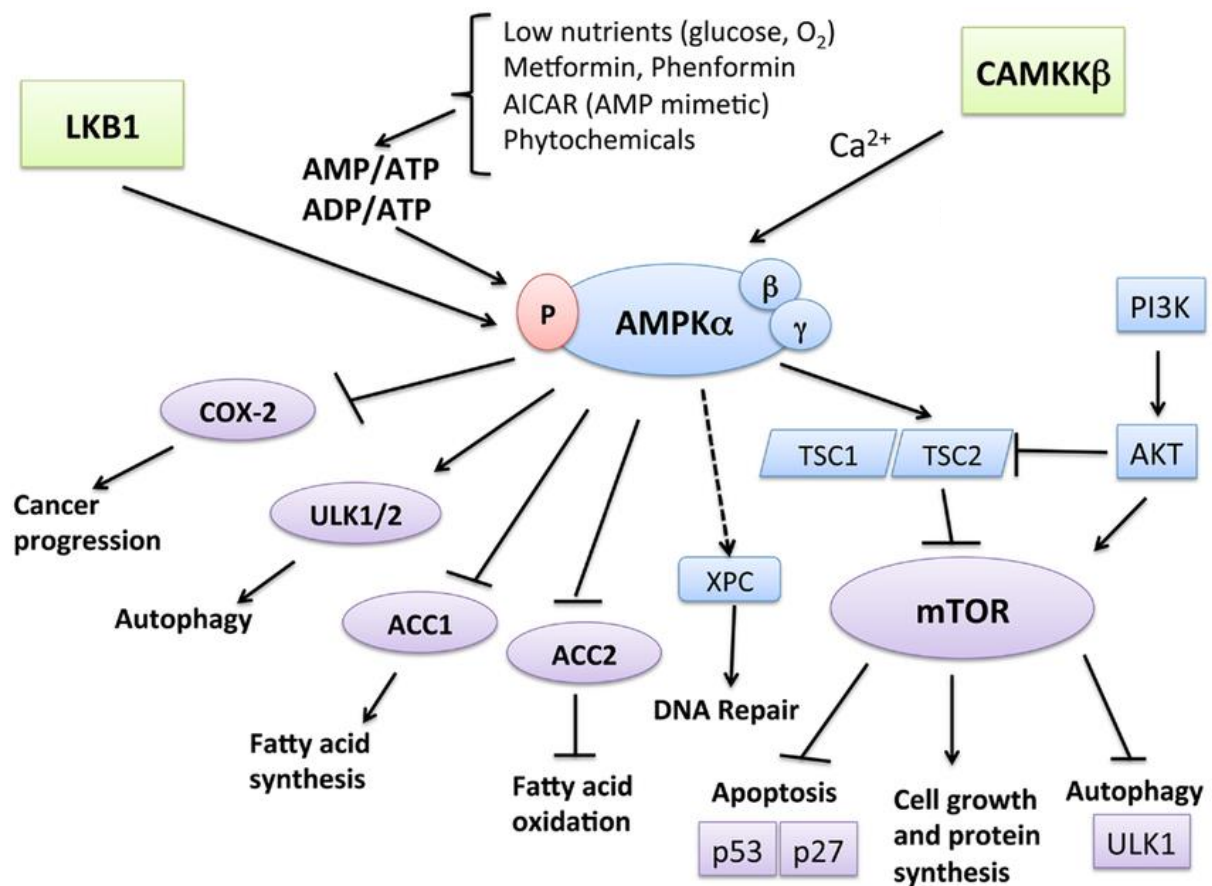


Figure 63. AMPK activity regulation and function. Diagram summarises common activators of AMPK, activation can be achieved through modulation of AMP/ATP or ADP/ATP ratio, in response to low nutrients, metformin treatment or other metabolic stressors. Moreover, increase in calcium level also leads to activation of AMPK by CAMKK β and LKB1-mediated phosphorylation induces AMPK. Activation of AMPK leads to induction of downstream signalling pathways, resulting in decrease of cancer progression, increase in autophagy and FA oxidation and DNA repair. Adapted from Kim and He, 2013 (1036).

The AMPK complex is composed of a catalytic subunit (α -subunit) and two regulatory subunits (β - and γ -subunits). The α -subunit is encoded by two isoforms in mammals, while the β - and γ -subunits are encoded by two and three isoforms, respectively. AMPK α has a highly conserved kinase domain (KD) at the N-terminus of the protein, as well as a regulatory domain (RD) at the C-terminus of the subunit (Fig. 63) (1044). AMPK α 1 and AMPK α 2 are both found in cytoplasm, however AMPK α 2 is also found in the nucleus (Fig. 63) (1045). The AMPK β subunit comprises four tandem repetitions of a structural module known as CBS, which was first discovered in cystathionine—synthase and is implicated in AMP binding (1046,1047). AMPK γ 1, γ -2, and γ -3 isoforms vary at the N-terminus of the proteins, although the C-terminus (where the CBS domains are found) is conserved. The AMPK β acts as a scaffold for

the assembly of AMPK α and AMPK γ subunits, as well as determining the complex's subcellular location and substrate selectivity. AMPK α 1 and α -2 vary only at the N-terminus yet bind with the same efficiency with AMPK β and AMPK γ subunits (1048,1049).

The expression levels of various AMPK isoforms varied between tissues, resulting in a variety of component combinations in distinct cell types. Although the various complexes are mostly functionally identical, they might have somewhat differing biochemical features (1050). Whereas AMPK α 1, AMPK β 1 and AMPK γ 1 are ubiquitously expressed, the other isoforms have a more limited pattern of expression. For example, AMPK α 2 is found in high concentrations in skeletal and cardiac muscle, and also it is found at lower concentrations in the liver and other tissue, (1051). Overall, AMPK α 1 is accounted for more than 90% of activity present in the liver of rat, whereas AMPK α 2 was shown to account only less than 10% (1052). Distinct isoforms of AMPK α -subunits exhibit not only different expression pattern, but also display structural differences. As was mentioned above, AMPK α 2 subunit was found to have a nuclear localisation signal, which are short peptides that act as a signal fragment that mediates the transport of this subunit from the cytoplasm into the nucleus (Fig. 64) (1053). Therefore, initially, it was concluded that AMPK α 1 functions predominantly in cytoplasm and AMPK α 2 in the cell nucleus (1054). For example, serum deprivation has been shown to diminish and alter the distribution of AMPK α in the nucleus and cytoplasm. Total and phosphorylated AMPK α -subunits are still mostly found in the cytoplasm (1055). However, in the nucleus, the quantity of phosphorylated AMPK α rises, while total AMPK decreases, indicating that there are additional signalling pathways in the nucleus that need AMPK activation under hunger (1055). Also, exercise has been shown to increase AMPK α 2 abundance in the nucleus of human skeletal muscle, resulting in GLUT4 expression and increased glucose transport (1056). However, despite previous attention to nuclear AMPK α 2 in muscle, it is now obvious that endogenous AMPK α 1 may be detected in the nucleus under specific conditions (1056–1059). More recent data suggests that AMPK α 1 is required for calcium-induced nuclear AMPK activation. Etoposide administration preferentially enhanced CaMKK2-dependent AMPK activity in the nucleus, but exclusively with AMPK α 1-containing complexes, even when AMPK α 2 complexes were present (1059).

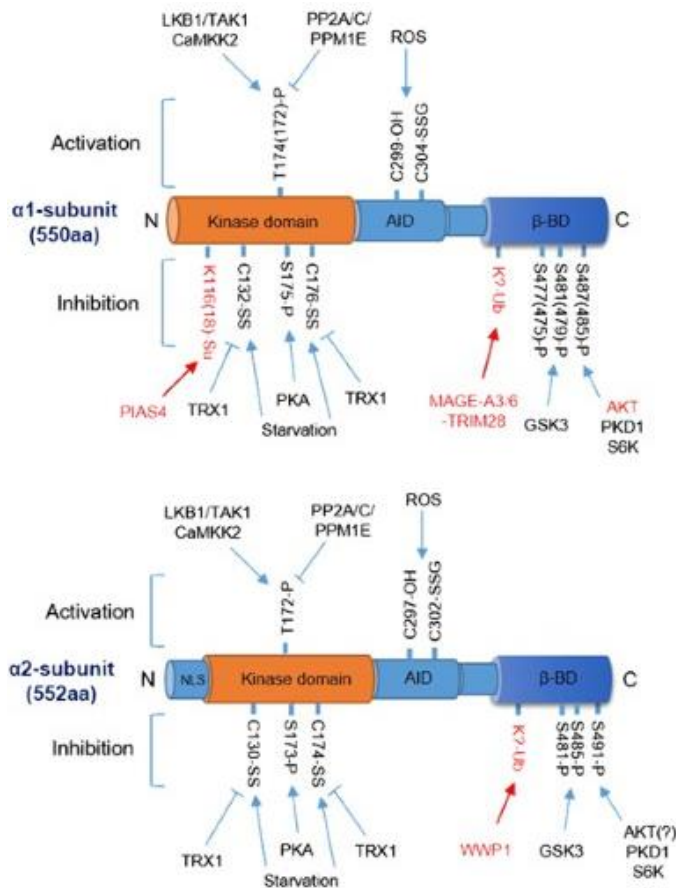


Figure 64. AMPK α -subunits structure and molecular regulation.

Modification of the AMPK α 1 (top) and α 2 (bottom) subunits by phosphorylation/dephosphorylation, ubiquitination, sumoylation and oxidation/reduction. Pathways marked in red indicate α 1- or α 2-subunit-specific modifications. Numbers of modified amino acids are based on human proteins. Adapted from Jeon *et al.*, 2016 (1028).

Binding of AMP or ADP to the α -subunit increases Thr172 phosphorylation in the process of kinase domain activation by upstream enzymes (1060). The serine/threonine kinase, liver kinase B1 (LKB1), is the primary upstream kinase responsible for Thr172 phosphorylation in response to energy stress (1061–1063). The main event required for complete AMPK activation is the phosphorylation of Thr172 in the α -subunit. *In vitro*, this phosphorylation event can raise AMPK activity up to 100-fold, while fold activation in intact cells is normally much lower (1064,1065).

Upon activation, the catalytic subunit of AMPK conducts phosphorylation of target proteins and modulate their activity. AMPK raises ATP levels by promoting lipid and glucose breakdown, while limiting its production and storage. AMPK stimulates glucose uptake by phosphorylating TBC domain family member 1 (TBC1D1) and thioredoxin-interacting protein (TXNIP), which regulate the translocation and cell-surface levels of the glucose transporters GLUT4 and GLUT1 (1066,1067). Furthermore, AMPK is able to inhibit protein synthesis, through mediating the inhibition of the mechanistic target of rapamycin complex 1 (mTORC1) (1068,1069).

SIRT1 and AMPK have been demonstrated to have many comparable roles, including the capacity to respond to stress and nutritional status, drive mitochondrial biogenesis, regulate glucose homeostasis, and regulate the activity of key transcriptional regulators such as PGC-1 and FOXO's (809). Similarly, the positive effects of both CR and resveratrol have been linked to the activation of SIRT1 and AMPK (1070–1072). As a result, the interactions between SIRT1 and AMPK has proved challenging to decipher. There is certainly a dynamic connection between these two pathways (1073–1075). AMPK has been demonstrated to activate SIRT1, most likely by an indirect rise in cellular NAD⁺ levels (973). AMPK interacts with the SIRT1 catalytic domain and induces Thr344 phosphorylation, which inhibits SIRT1-mediated deacetylation (24). AMPK can also influence SIRT1 stability by phosphorylating and activating DBC1 (25). On the other hand, SIRT1 was found to deacetylate the AMPK kinase LKB1, resulting in higher phosphorylation and activation of AMPK (1076,1077).

Given the therapeutic benefits of AMPK activation, several AMPK activating drugs have been discovered, which are also used for research purposes (1067). Abbott Laboratories created A-769662 in 2006, the first chemical for AMPK direct activation. The invention of this direct AMPK activator indicated that AMPK activation with non-nucleotide ligands is possible and sparked interest in new AMPK activation techniques. A-769662 allosterically activates AMPK on the AMPK subunit without phosphorylating Thr-172 (1078). Moreover, Scott *et al.* showed that A-769662 and AMP may activate AMPK in a synergistic (more than 1000-fold) manner (1079). A-769662 is unusual among cell-permeable activators in its capacity to directly activate AMPK in both cell-free and intact tests. Other activators, such as AICAR, metformin, and the thiazolidinediones, do not directly activate AMPK in cell-free assays and some can be pro-drug that are converted to active components inside the cell, for example, AICAR, which is converted to the AMP analogue ZMP (1080). Other work even more indirectly, like metformin, which acts by inhibiting the respiratory chain or thiazolidinediones, which is triggering release of adiponectin from adipocytes (1081). Findings of Goransson *et al.* in intact cells supported the hypothesis that A-769662 is a selective and direct activator of AMPK, as well as the idea that it has a dual action, producing both allosteric activation and dephosphorylation inhibition (1082).

On the other hand, compound C (6-[4-(2-Piperidin-1-ylethoxy) phenyl] -3-pyridin-4-ylpyrazolo [1,5-a] pyrimidine) is a currently available cell-permeable AMPK inhibitor.

Compound C, also called Dorsomorphin (DM), is a well-known competitive inhibitor of ATP binding to the catalytic α subunit of AMPK. DM was shown to induce cell death by inhibition of AMPK activity in prostate cancer cell lines (1083). Although the impact of DM on cell proliferation is not well established, it has been utilised to rescue the antiproliferative effects of AICAR and metformin (1084,1085). A lot of studies describe DM to have biochemical and cellular effects and its inhibitory impact on AMPK (1086–1091).

In this study, we aim to determine the effect of AMPK activity suppression or activation on *Sirt1* gene expression, in order to explore the regulatory relationship between AMPK and SIRT1 in primary BMSCs and ST2 cell line.

II. MATERIALS AND METHODS

1. Animals

Seven-week-old female C57BL/6J mice purchased from Charles River Laboratories (St Germain sur l'Abresle, France) were used for the BMSC extraction (1). Mice were housed 6 per cage in a controlled room temperature (22°C +/- 1°C) under a 12-hour dark/light cycle (lights off at 10 a.m.) and with free access to water. Before BMSCs harvesting, mice were acclimatized for 7 days.

2. Primary Bone Marrow Stromal Cell and ST2 Cell Culture

Primary bone marrow cells were harvested from the tibiae and femurs of the mice, as it was described in Ghali *et al.* study (808). Cells were plated for 7-10 days to reach full confluency in MEM medium (PAN BIOTECH; P04-21050) with 15% foetal bovine serum (PAN BIOTECH; P30-3306), 1% penicillin/streptomycin (PAN BIOTECH; P04-85100) and 1% stable glutamine (PANBIOTECH; P06-07100). The medium containing co-differentiation inducers was replaced every two days during the 14 days of the co-differentiation experiment. This culture duration was chosen because of its brevity, which allowed for minimizing the time for cells to change after leaving the *in vivo* state.

ST2 cells were obtained from DSMZ (ST2, ACC 333, Lot5) and incubated at 37°C and 5% CO₂, in MEM medium (PAN BIOTECH; P04-21050) supplemented with different concentration of foetal bovine serum (PAN BIOTECH; P30-3306) (5%, 7% and 10%), 1% penicillin/streptomycin (PAN BIOTECH; P04-85100) and 1% stable glutamine (PANBIOTECH; P06-07100).

3. Drug Treatments

ST2 cells and primary mouse BMSCs were exposed to AMPK activator A-769662 (Bio-technie, Cat. No. 3336) and AMPK activity inhibitor Dorsomorphin (DM) (Compound C) (Bio-technie, Cat. No. 3093). The concentration and exposure time of the drug was initially determined by literature research (1082,1092,1093). In the current study, confluent cells were treated with 50M or 200M of A-769662 for 14 hours (14h) in standard growth medium. Similarly, cells were exposed to 20M DM for 14h in standard growth medium.

4. AMPK Activity Assay

AMPK activity was measured after drug treatment, using CycLex AMPK Kinase Assay Kit (MBL International Corporation, CY-1182). In prior to experiment, protein from treated ST2 cells was extracted by washing cells three times with ice-cold PBS, following the treatment with cell lysis buffer (20mM Tris HCl, pH 7.5, 250mM NaCl, 10% glycerol, 0.5% Nonidet® P-40, 1mM EDTA, 1mM EGTA, 0.2mM PMSF, 1µg/mL pepstatin, 0.5µg/mL leupeptin, 5mM NaF, 2mM Na₃VO₄, 2mM β-glycerophosphate, 1mM DTT) for 60 min at 4 °C. Then transferred cell lysates to microcentrifuge tubes, was centrifuge at 15,000 rpm for 10 minutes at 4°C. The CycLex AMPK Kinase Assay Kit uses anti-phospho-mouse IRS-1 S789 monoclonal antibody (AS-4C4) and peroxidase coupled anti-mouse IgG antibody as a reporter molecule in a 96-well ELISA format. This assay provides a non-isotopic, sensitive and specific method to measure the activities of AMPK (1094). The protocol was conducted according to CycLex AMPK Kinase Assay Kit manufactory protocol. Absorbance was measured in each well using a spectrophotometric plate reader at a single wave of 450 nm.

5. siRNA Transfection

ST2 cells were transfected with small interfering RNA (siRNA), targeting *Prkaa1* (ref. 4390771, ID s98535) and *Prkaa2* (ref. 4390771, ID s99117), as well as non-targeting (siRNA negative control (siRNA neg) (ref. 4390846) were purchased Ambion (Life Technology Inc.). siRNA targeting *Prkaa1*, *Prkaa2* and siRNA neg were transfected to ST2 cells at a final concentration of 50nM, using Lipofectamine (Invitrogen, ref. 13778-030). Transfection solution was prepared in Opti-MEM reduced serum medium (Gibco, ref. 31985-062), four conditions were used in the study – Opti-MEM, Opti-MEM + Lipofectamine, Opti-MEM +

Lipofectamine + siRNA neg, Opti-MEM + Lipofectamine + siRNA (*Prkaa1* or *Prkaa2*). When ST2 cells reached 80% confluency, standard growth medium was change to Opti-MEM, with or without transfection agents. Cells were incubated in transfection solution for 72 hours or for 7 days, without medium change.

6. RNA Extraction and Reverse Transcription

Total RNA was extracted from BMSC culture using Extract-all (Eurobio, Les Ulis, France). At the end of cell culture, 1ml of Extract-all was added per 1 well of 12-well plate and samples were transferred to 1.5 ml collecting tube. Next step was to add 200 µl of chloroform (Thermo Scientific; J67241.AP) per each tube and spin samples at 4°C and 12 000 g for 15 min. Upper aqueous phare containing RNA was removed and the rest of the protocol was conducted according to RNeasy Mini Kit (QIAGEN; 74104) manufacturer’s protocol. Total RNA was quantified using the NanoDrop 2000 spectrophotometer (Thermo Scientific, Labteck, Palaiseau, France).

7. Real-Time PCR

Reverse transcription of samples was conducted using the Maxima First Standard cDNA Synthesis Kit for RT-qPCR (Thermofisher; K1642) manufacturer’s protocol. Quantitative PCR (qPCR) experiment required 5µl of PowerUp SYRB Green Master Mix (Applied Biosystems; A25742), 1µl of upstream primer, 1µl of downstream primer and 2µl of water, per reaction (870). The sequences of the primers (TibMolBiol, Berlin, Germany), annealing temperature, product length and GenBank reference for each of the analysed genes are shown in Table 14.

Gene	Primer Sequences	Annealing temperature	Product length	GenBank
<i>18S</i>	F: ATTCCGATAACGAACGAGAC R: GCTTATGACCCGCACTTACT	60 °C	297 bp	X03205
<i>Gapdh</i>	F: GGCATTGCTCTCAATGACAA R: TGTGAGGGGAGATGCTCAGTG	62 °C	200 bp	NM_008084
<i>Prkaa1</i>	F: ATGGCAGAAGTTTGTAGAGC R: ACGGAAATCCAACAAGTAAG	79 °C	165 bp	NM_001013367.3
<i>Prkaa2</i>	F: CGACTACATCTGCAAACATGG R: CAGTAATCCACGGCAGACAG	84 °C	157 bp	NC_000070.7
<i>Sirt1</i>	F: TAGGGAACCTTTGCCTCATC R: GGCATATTCACCACCTAGCC	51 °C	100 bp	NM_019812.2

Table 14. Primer sequences and conditions of quantitative RT–PCR (PART 3).

8. Protein Extraction

ST2 cells were washed with ice cold PBS three times and then incubated in lysis buffer (20mM HEPES (pH 7.9), 1.5mM of MgCl₂, 25% (v/v) glycerol, 0.42M KCl, 0.2mM EDTA, 0.5mM dithiothreitol (DTT), and 0.5mM phenylmethylsulfonylfluoride (PMSF) for 20 min on ice (870). After, cells were centrifuged at 4°C at maximum speed (14 000g) for 30 minutes to isolate the supernatant. Protein concentrations were measured by a bovine serum albumin (BSA) protein assay kit (Bio-Rad Life Science Group, **5000121**).

9. Western Blotting

Then 20µg proteins stained with 5µl Laemmli (Bio-Rad, 1610747), 10µL of prestained SDS-PAGE standards (low range; Bio-Rad Life Science Group) were separated by electrophoresis using SDS-PAGE 8% acrylamide gel for 2 hours at 180 V. After proteins were transferred onto activated polyvinylidene fluoride (PVDF) membrane using Trans-Blot Turbo Transfer System (Bio-Rad). PVDF membranes were blocked for 1h at room temperature using a blocking solution containing 5% of dried milk in Tris Buffered Saline with 0.1% Tween 20 (TBS-T). Membranes then were washed three times for 5 minutes in TBS-T. Blots were incubated with a 1:400 dilution of each primary antibody for overnight in 4°C. Mouse monoclonal antibodies (AMPK 1/2, SIRT1 and β-actinin) were acquired commercially (Santa Cruz Biotechnology). Membranes then were washed three times for 5 minutes in TBS-T and incubated in a blocking solution with alkaline-phosphatase-conjugated secondary antibody 1:500 (Santa Cruz Biotechnology) for 2 hours. Membranes were further washed three times for 5 minutes in TBS-T, and immunoreactive protein bands were visualized by a chemiluminescence detection kit (AP Conjugate Substrate Kit, Bio-Rad Life Science Group).

10. Statistical Analysis

The quantification of *Prkaa1* and *Prkaa2* mRNA in 10-week and 4-week SBA studies, as well as basal expression level of these isoforms was performed with 4 samples per condition. BMSC and ST2 cell treatment with A-769662 and Dorsomorphin was conducted using 4-6 samples per condition. At last, siRNA transfection experiment contained 4 replicates per condition. The median and interquartile range were calculated for the groups. Due to the low number of replicates, the normality of the data could not be tested. In siRNA transfection study we

performed Kruskal-Wallis One-Way ANOVA test, to show the significance between all the conditions. Additionally, we conducted Dunn's test in order to see the relationships between specific pairs of conditions. For the rest of studies, we performed Mann-Whitney's test to see the statistically significant relationship between the two particular conditions. All tests were performed using GraphPad Prism software. Differences with $p < 0.05$ were considered statistically significant.

III. RESULTS

1. AMPK expression is modulated in long term SBA protocol (SBA 18%)

In BMSCs extracted from 10-week SBA 18% weight loss mice (cohort 1) and plated for 48h adhesion, we observed that suppression of *Sirt1* gene expression was accompanied by the decrease in AMPK α 1 gene (*Prkaa1*) mRNA (Fig. 30B for *Sirt1* and Fig. 65A for *Prkaa2*). Interestingly, in these samples only *Prkaa1* gene suppression (-66% vs. CT) was associated with decrease in *Sirt1* mRNA (-67% vs. CT). Study on AMPK α 2 isoform (*Prkaa2*) exhibited an increase in mRNA (+230% vs. CT) (Fig. 30B for *Sirt1* and Fig. 65A for *Prkaa2*). In 4-week SBA 18% (cohort 1) samples the reverse results were observed, 62% increase in *Prkaa1* mRNA went along with significant decrease in *Prkaa2* mRNA (-45% vs. CT), however reduction in *Prkaa1* mRNA did not affect *Sirt1* expression in same samples (Fig. 36A for *Sirt1*, 65C for *Prkaa1*).

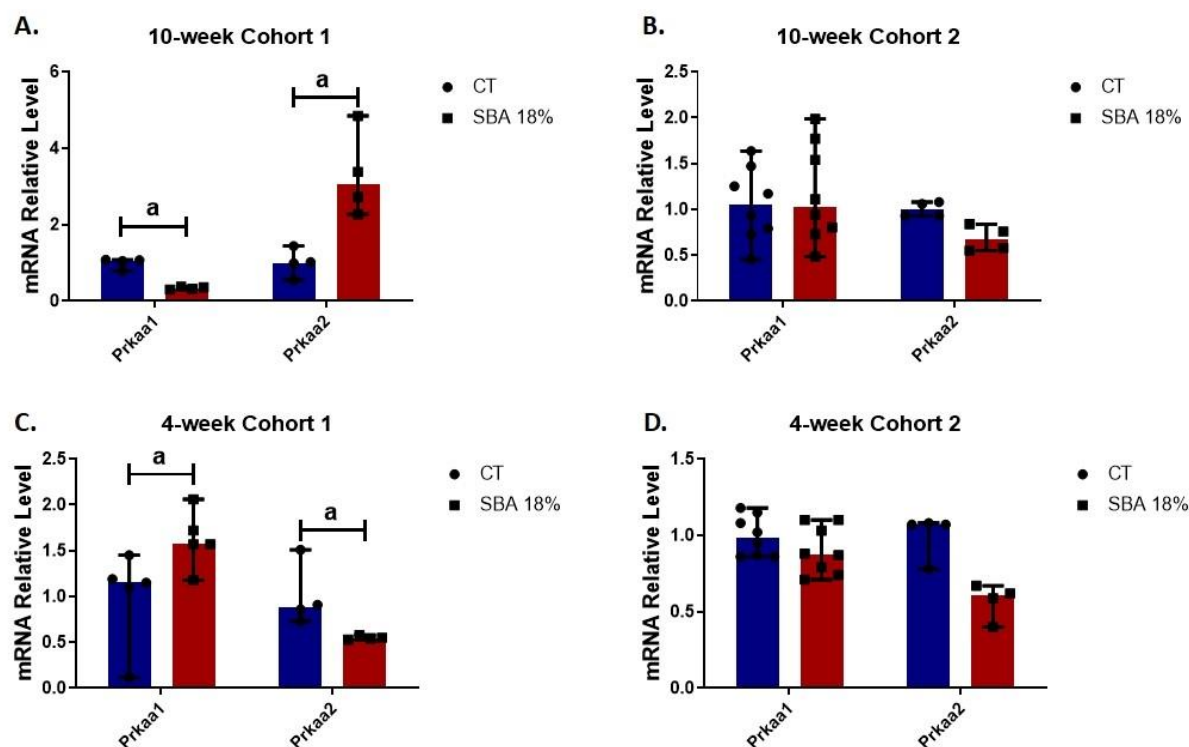


Figure 65. *Prkaa1* and *Prkaa2* expression in BMSCs extracted from SBA mice. A-B. Relative mRNA level of AMPK subunit alpha isoforms (*Prkaa1/ Prkaa2*) in primary mice BMSCs from CT and SBA 18% weigh loss mice from 10-week studies; C-D. Relative mRNA level of *Prkaa1* and *Prkaa2* compared in primary BMSCs from CT and SBA 18% weigh loss mice from 4-week studies; Data represents mean \pm Interquartile range; n=4-8. Statistical analysis was performed using Mann-Whitney's test; a - p<0.05

These findings suggested that AMPK α 1 specifically might be involved in regulation of *Sirt1* expression, additionally, the compensation between AMPK α isoform 1 and isoform 2 could be observed. Literature review and findings above, led to the hypothesis that AMPK might be involved in *Sirt1* expression regulation in BMSCs from our energy deficient mice and directed us to explore this interconnection more rigidly.

2. In primary BMSCs and ST2 cells, AMPK α 1 is more abundant than AMPK α 2

SIRT1 and AMPK are both fuel sensing molecules that are known to coexist in cells. It was widely described that in different tissues, AMPK and SIRT1 regulate each other and share multiple common target molecules (1073). Therefore, this study continues testing the effect of AMPK suppression or activation on *Sirt1* relative mRNA level, as well as expression of AMPK subunit alpha (*Prkaa1* and *Prkaa2*).

Given that in different tissue types, AMPK α 1 and AMPK α 2 has different expression patterns, in prior to activation and suppression of AMPK activity experiments, basal mRNA level of *Prkaa1* and *Prkaa2* was established in ST2 cell line and primary mouse BMSCs (1095). This was done, in order to understand, if one of the isoforms is more abundant than another in these particular cell types. Results show that in both primary BMSCs and ST2 cells, relative mRNA level of *Prkaa2* is significantly lower than *Prkaa1* (Fig. 66A,B). Suggesting that in current cell types, *Prkaa1* is predominantly expressed and can potentially have greater impact on *Sirt1* relative expression. Moreover, we confirmed that *Prkaa1* and *Prkaa2* mRNA are expressed on same level in both primary mice BMSCs and ST2 cell line, therefore study of these genes could be comparable in both cell types (Fig. 66C,D).

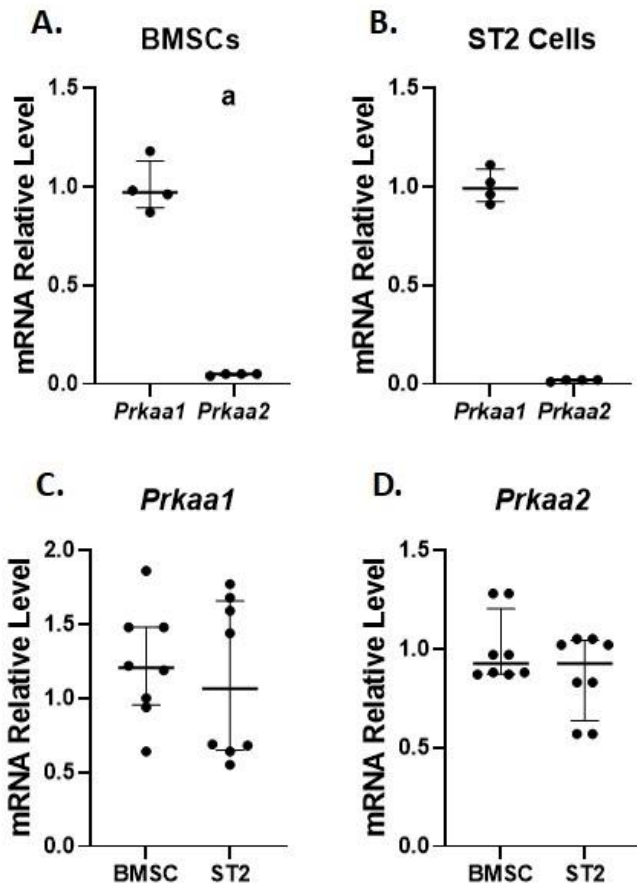


Figure 66. Basal expression of *Prkaa1* and *Prkaa2* expression in BMSCs and ST2 cells. A-B. Relative mRNA level of AMPK subunit alpha isoforms (*Prkaa1/Prkaa2*) in untreated ST2 cell line and primary mice BMSCs; C-D. Relative mRNA level of *Prkaa1* and *Prkaa2* compared in primary BMSCs and ST2 cell line; Data represents mean ± Interquartile range; n=4-8. Statistical analysis was performed using Mann-Whitney's test; a - p<0.05

3. Suppression of AMPK activity by Dorsomorphin has a negative effect on *Sirt1* expression

According to our data on *Prkaa1* expression in SBA extracted BMSCs (10-week cohort 1), we concluded that decrease in AMPK gene expression could potentially be involved in decrease of *Sirt1* mRNA in same samples (Fig. 65A). Therefore, we aimed to understand the role of AMPK suppression in *Sirt1* gene expression regulation. The following step was done to identify the effect of AMPK activity inhibition on *Sirt1* mRNA expression. In ST2 cells that were treated for 14h with DM (20M), assay showed a significant decrease of 96% in AMPK activity (vs. CT) (Fig. 67A). Exposure for 14h to DM in ST2 cells generated a significant decrease in *Sirt1* mRNA level (-79% vs. CT) (Fig. 67B). Additionally, SIRT1 protein level was studied, results of Western Blotting (WB) showed that there is no difference in band intensity between CT and 14h DM (20M) treatment conditions (Fig. 67D).

We hypothesised that 14h DM treatment did not induce changes in SIRT1 protein level, as duration of the protocol was not long enough to see changes in intracellular protein level. Average half-life of protein was established to be from 3 to 9 days, therefore we decided to test increased time of DM exposure of ST2 cells (1096). So, cells were treated for 72 hours (72h) with 20M concentration of DM. AMPK activity assay results indicated a 97% decrease in this increased treatment time condition (vs. CT) (Fig. 67A). Also, *Sirt1* mRNA quantification displayed a statistically significant decrease (-54% vs. CT) in ST2 cells (Fig. 67C). However, long term treatment of ST2 cells with DM did not result in changes in SIRT1 protein level (Fig. 76E).

In order to compare findings of ST2 cells with initial results of SBA mouse extracted BMSCs, we conducted a 14h DM (20M) treatment on primary mouse BMSCs. It was identified that *Sirt1* mRNA level was dramatically reduced by 92% (vs. CT) (Fig. 67F). Therefore, it can be concluded that in both ST2 cells and primary mouse BMSCs, exposure to DM exhibit similar effect and results in suppression of *Sirt1* mRNA. Probably, a treatment longer than those we used could result in a decrease in *Sirt1* protein, as the decreases in mRNA level observed are biologically significant.

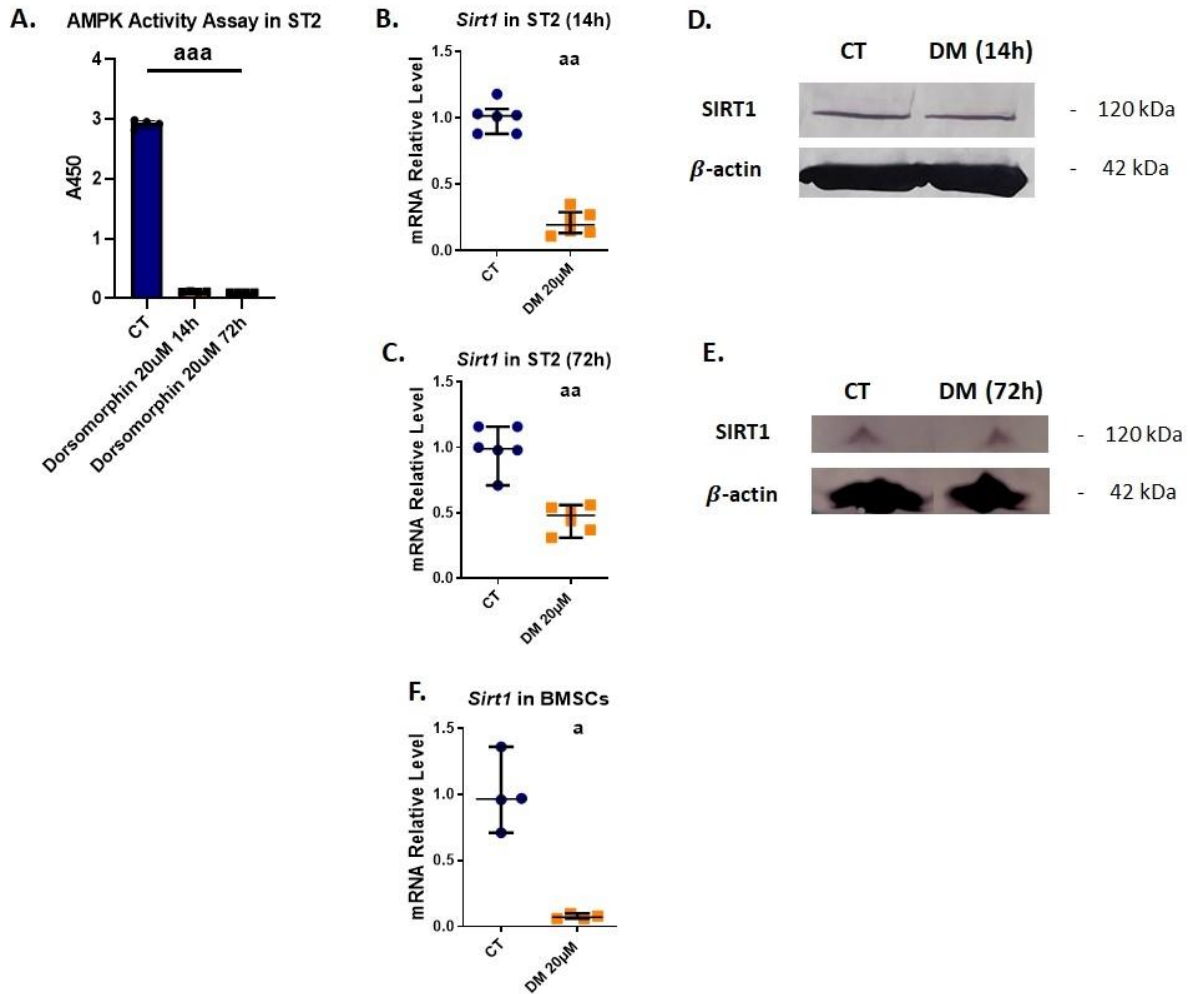


Figure 67. AMPK activity assay results and *Sirt1* expression in ST2 cells and primary BMSCs exposed to 14h and 72h DM treatment. A. AMPK enzymatic activity in CT ST2 cells and in ST2 cells treated with 20μM of DM, measured through the spectrophotometer absorbance at 450nm; B-C. Relative mRNA level of *Sirt1* in ST2 cells treated with 20μM of DM for 14h and 72h, respectively; D-E. SIRT1 protein level, in ST2 cells treated with 20μM of DM for 14h and 72h, respectively; F. Relative mRNA level of *Sirt1* in primary mice BMSCs treated with 20μM of DM; Data represents mean ± Interquartile range; n=4-6. Statistical analysis was performed using Kruskal-Wallis One-Way ANOVA test for AMPK activity assay and Mann-Whitney's test for relative gene expression data; a - p<0.05, a – p<0.005, aaa – p<0.0005.

Positive feedback has been recognised as the essential regulatory motif in the formation of switches in many biological systems (1097). Some of the examples of interlinked positive feedback loops are p53 regulation through mouse double inure homologue 2 (MDM2) (1098), or muscle cell fate specification where myoblast determination protein (MyoD) is regulated through AKT serine/threonine kinase 2 (AKT2) (1099,1100). Recently, it has been demonstrated that in skeletal muscles, exercise induces expression of GLUT4 through a positive feedback loop between AMPK and peroxisome proliferator-activated receptor β (PPAR β), which plays an important role in regulating glucose uptake (1101–1103).

Based on this previously published data, we were interested to study the effect of drug treatment on the expression of AMPK α 1 and AMPK α 2 in both ST2 cells and primary mouse BMSCs. Cells treated with DM (20M) for 14h, displayed a statistically significant suppression of *Prkaa1* (-72% vs. CT), together with 109% increase in *Prkaa2* mRNA level (vs. CT) (Fig. 68A). However, the extended treatment time (72h) resulted only in 56% decrease in *Prkaa1* mRNA (vs. CT), without affecting *Prkaa2* (Fig. 68B). These results suggest that AMPK activity suppression has a negative effect on AMPK α 1 subunit expression, confirming positive autoregulation of AMPK. Moreover, it can be theorised that in case of AMPK α 1 subunit suppression, the compensation mechanism induces AMPK α 2 subunit expression. However, both, 14h DM treatment study and 72h study on ST2 cells confirmed the hypothesis that potentially only AMPK α 1 is involved in *Sirt1* regulation, as decrease in *Sirt1* gene expression is accompanied by a specific decrease in *Prkaa1* mRNA in BMSCs from 10-week cohort1 SBA 18% group.

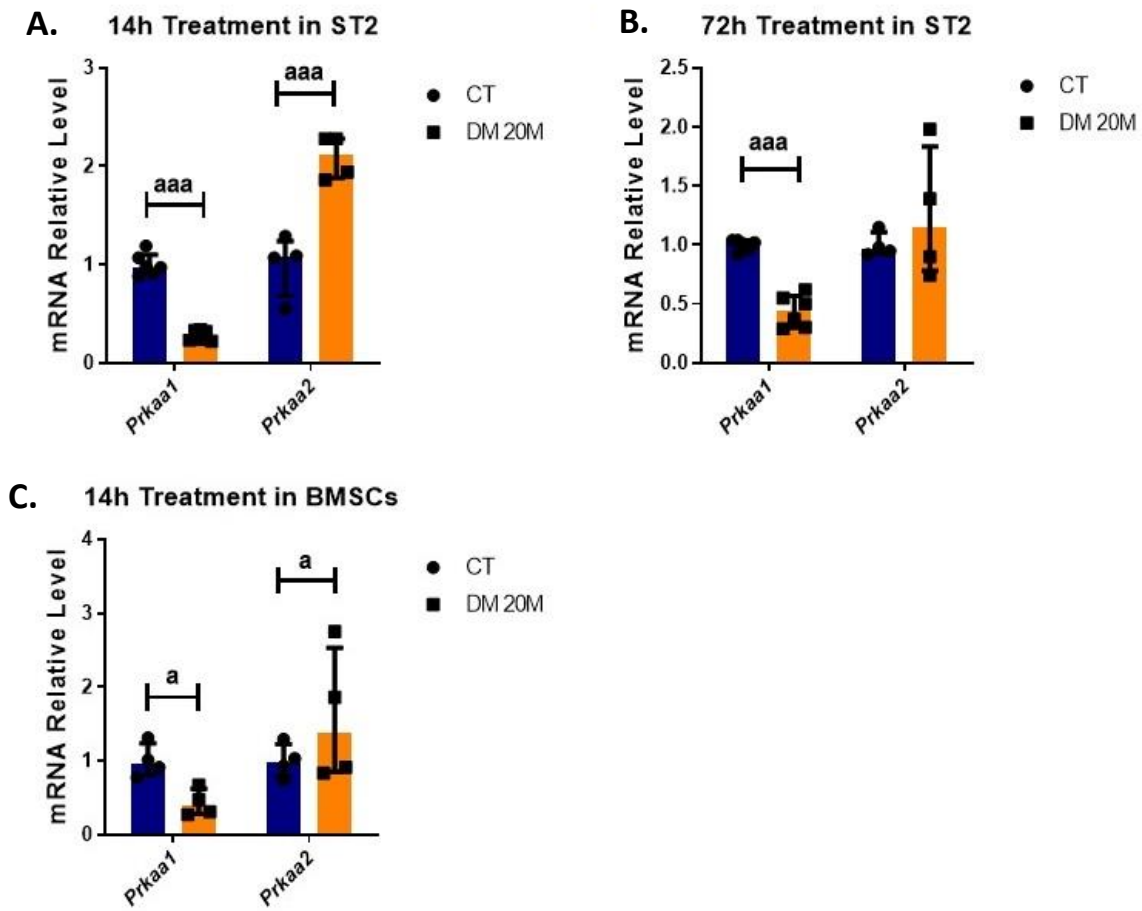


Figure 68. *Prkaa1* and *Prkaa2* expression in primary BMSCs and ST2 cells exposed to 14h and 72h DM treatment. A-B. Relative mRNA level of *Prkaa1* and *Prkaa2* in ST2 cells treated with 20 μ M DM for 14h and 72h, respectively; C. Relative mRNA level of *Prkaa1* and *Prkaa2* in primary mice BMSCs treated with 50 μ M DM for 14h; Data represents mean \pm Interquartile range; n=4. Statistical analysis was performed using Mann–Whitney’s test; a - $p < 0.05$, aaa – $p < 0.0005$.

In order to confirm the negative effect of AMPK activation on AMPK α subunit gene expression, we also tested the effect of DM in primary BMSCs. Similar to findings in ST2 cell line, in BMSCs exposed to 14h treatment with DM (20M), the mRNA level of *Prkaa1* isoform was significantly decreased (-57% vs. CT) (Fig. 68C). Nonetheless, relative mRNA level of *Prkaa2* was significantly increases in the same condition (+50% vs. CT) (Fig. 68C). This effect of AMPK activity inhibition was complementary to finding of ST2 cells, confirming once again our hypothesis that positive feedback loop exists and AMPK protein might regulate *Prkaa1* gene expression.

Overall, for the first time this study highlighted a potential relationship between AMPK activity and *Sirt1* mRNA level, suggesting that AMPK might be responsible for SIRT1 regulation in our mouse model. More specifically, AMPK α 1 isoform was shown to be potentially associated with regulation of *Sirt1* gene.

4. Only *Prkaa1* suppression with small interference RNA (siRNA) affects *Sirt1* expression

In order to validate regulatory relationships between AMPK and SIRT1, further functional tests were conducted. ST2 cells were transfected with 50nM *Prkaa1* or *Prkaa2* siRNA for 72h and for 7 days (7D). Results of 72-hour transfection have shown a significant decrease in *Prkaa1* relative mRNA expression in siRNA condition (-70% vs. Opti-MEM) (Fig. 69A). Suppression of *Prkaa1* expression led to a significantly decreased in relative level of *Sirt1* mRNA (-67% vs. Opti-MEM) (Fig. 69B). However, during long term treatment (7D) with *Prkaa1* siRNA we observed that mRNA level of *Prkaa1* started to rise (-48% vs. Opti-MEM, p=0.0616) (Fig. 69D). Moreover, the insufficient suppression of *Prkaa1*, led to no changes in *Sirt1* mRNA level, after 7D exposure to siRNA (Fig. 69E). Suggesting that after long term exposure, *Prkaa1* mRNA level start to restore and *Sirt1* mRNA production start to increase, in order to maintain cell survival. Additionally, we tested mRNA level of *Prkaa2* in 72h and 7D treatment with *Prkaa1* specific siRNA, as a negative control. We observed that 72h treatment, which significantly downregulated *Prkaa1* expression, in case of *Prkaa2* resulted in an increase of mRNA (+155% vs. Opti-MEM) (Fig. 69C). It was hypothesised that this even is taking place due to the compensation of significant loss in *Prkaa1*. Surprisingly, in samples treated for 7D with *Prkaa1* siRNA, mRNA level of *Prkaa2* was significantly decreased as well (-71% vs. Opti-MEM) (Fig. 69F). We observed that the decrease in *Prkaa2* does not affect *Sirt1* mRNA level, supporting the hypothesis that *Prkaa2* expression level is not high enough to play a role in *Sirt1* expression regulation. Overall, findings of *Prkaa1* siRNA treatment showed that 72h treatment results in decrease in *Sirt1* mRNA, confirming the regulatory effect of AMPK upon *Sirt1* expression.

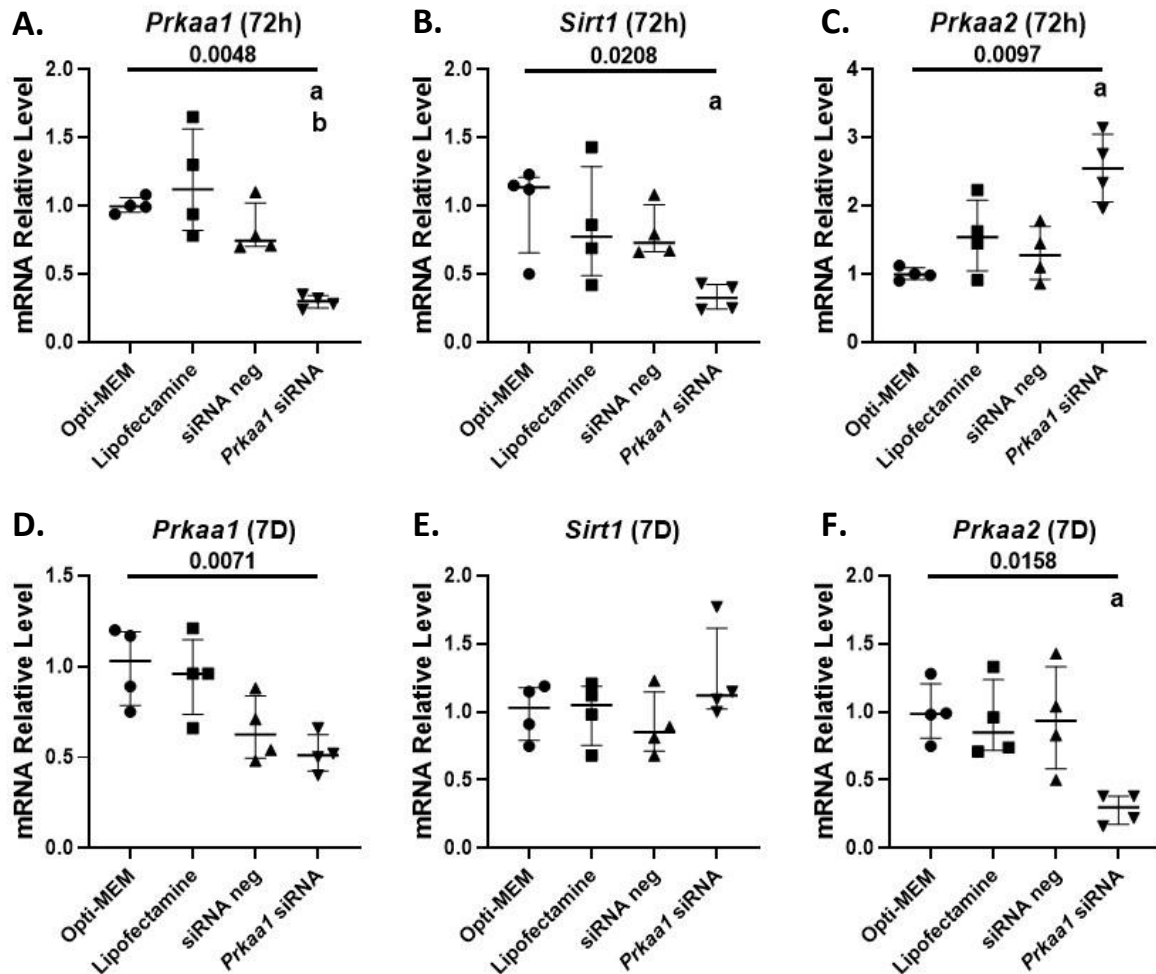


Figure 69. *Prkaa1*, *Sirt1* and *Prkaa2* expression in ST2 cells after exposed to *Prkaa1* siRNA. A-B. Relative mRNA level of AMPK subunit $\alpha 1$ (*Prkaa1*) and *Sirt1* in ST2 cells treated with 50nM of *Prkaa1* siRNA for 72 hours; C. Relative mRNA level of AMPK subunit $\alpha 2$ (*Prkaa2*) in ST2 cells treated with 50nM of *Prkaa1* siRNA for 72 hours; D-E. Relative mRNA level of *Prkaa1* and *Sirt1* in ST2 cells treated with 50nM of *Prkaa1* siRNA for 7 days; F. Relative mRNA level of *Prkaa2* in ST2 cells treated with 50nM of *Prkaa1* siRNA for 7 days; Data represents mean \pm Interquartile range; n=4. Statistical analysis was performed using Kruskal Wallis test and Dunn's Multiple Comparison Test; a – p<0.05 when compared to Opti-MEM, b – p<0.05 when compared to Lipofectamine condition.

After, we were interested to test the effect of *Prkaa2* suppression on *Sirt1* mRNA in ST2 cells. Similar to previous study, ST2 cells were transfected with 50nM *Prkaa2* siRNA for 72h and for 7 days. Results of 72h transfection have shown a significant decrease in *Prkaa2* relative mRNA expression in siRNA condition (Fig. 70A). The decrease of 72% (vs. Lipofectamine), confirms a successful reduction of *Prkaa2* expression. However, the relative mRNA level of *Sirt1* was not affected in the same cells (Fig. 70B). After 7D transfection with 50nM *Prkaa2* siRNA, ST2 cells exhibited significant decrease in *Prkaa2* mRNA (-82% vs. Lipofectamine)

(Fig. 69D). Even with extended transfection time, *Sirt1* mRNA level was not significantly affected by suppression of *Prkaa2* expression (Fig. 70E). Only, we could observe the 47% decrease in *Sirt1* mRNA ($p=0.1554$ vs. siRNA neg) in 7D condition, which potentially indicate a tendency of *Sirt1* to be decreased in the presence of *Prkaa2* siRNA (Fig. 70E).

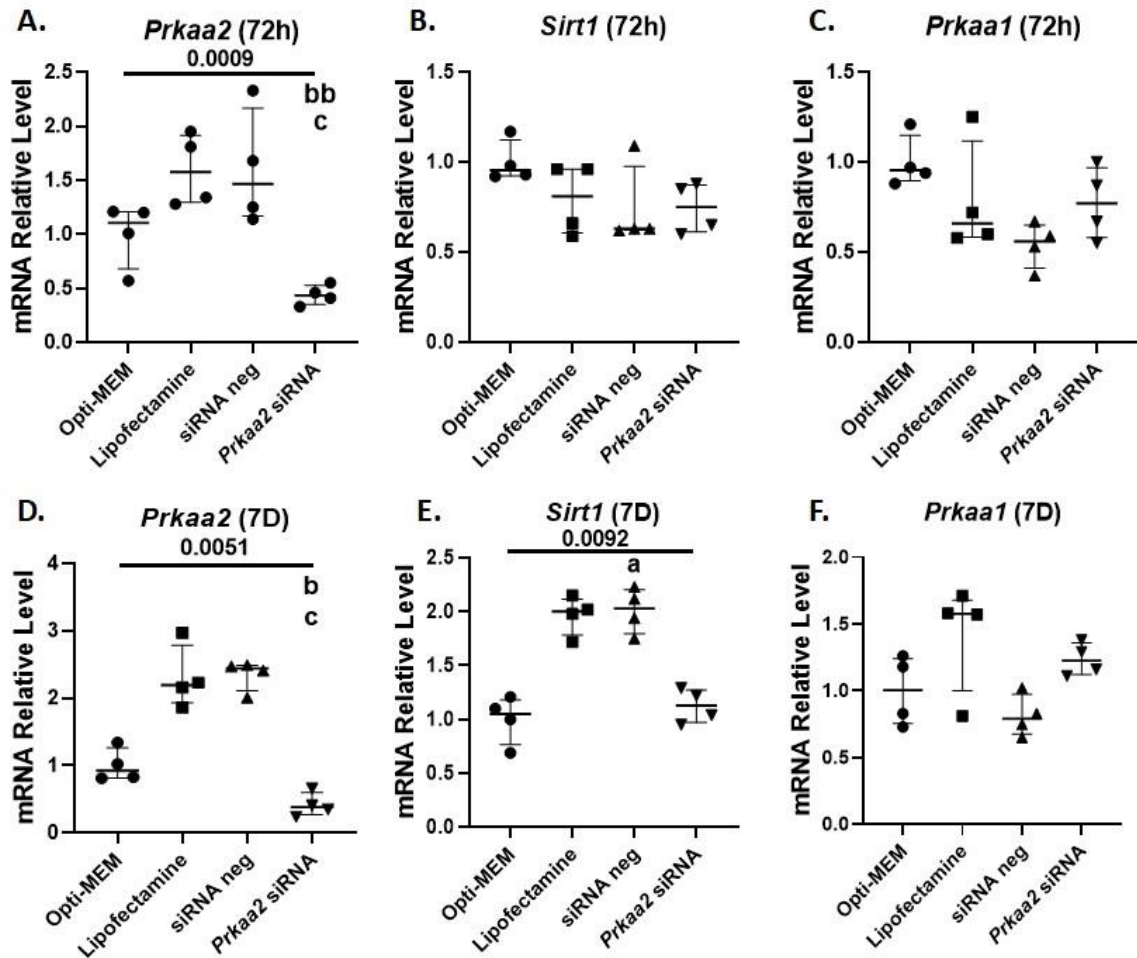


Figure 70. *Prkaa2*, *Sirt1* and *Prkaa1* expression in ST2 cells after exposed to *Prkaa2* siRNA. A-B. Relative mRNA level of *Prkaa2* and *Sirt1* in ST2 cells treated with 50nM of *Prkaa2* siRNA for 72 hours; C. Relative mRNA level of *Prkaa1* in ST2 cells treated with 50nM of *Prkaa2* siRNA for 72 hours; D-E. Relative mRNA level of *Prkaa2* and *Sirt1* in ST2 cells treated with 50nM of *Prkaa2* siRNA for 7 days; F. Relative mRNA level of *Prkaa1* in ST2 cells treated with 50nM of *Prkaa1* siRNA for 7 days; Data represents mean ± Interquartile range; n=4. Statistical analysis was performed using Kruskal Wallis test and Dunn's Multiple Comparison Test; a – $p<0.05$ when compared to Opti-MEM condition; b – $p<0.05$, bb – $p<0.005$ when compared to Lipofectamine condition; c – $p<0.05$ when compared to siRNA neg condition.

In the same samples, relative mRNA level of *Prkaa1* was tested. We found that suppression in *Prkaa2* expression does not affect *Prkaa1* expression after 72h or 7D, leading to the conclusion that current siRNA treatment specific to *Prkaa2* (Fig. 71C,F). In general, findings of *Prkaa2* siRNA transfection showed that this particular isoform does not play a role in *Sirt1* regulation, indicating once again that AMPK complex containing AMPK α 1 subunit, specifically regulates *Sirt1* gene expression.

As we observed that AMPK α 1 and α 2 subunits exhibit compensatory expression pattern, we were interested in the effect of combining *Prkaa1* and *Prkaa2* siRNA and transfect ST2 cells simultaneously, to eliminate both isoforms. After 72h of transfection, ST2 cell exhibited a statistically significant decrease in *Prkaa1* and *Prkaa2* mRNA level, -53% (vs. Lipofectamine) and -94% (vs. Lipofectamine), respectively (Fig. 71A,B). In these samples, *Sirt1* expression was also significantly downregulated, by 61% (vs. Opti-MEM) (Fig. 71C). After prolonged treatment with *Prkaa1*+*Prkaa2* siRNA, *Prkaa1* mRNA was found to be decreased by 71% (vs. Opti-MEM), which is lower than in samples treated with *Prkaa1* siRNA alone (Fig. 71D). *Prkaa2* expression was significantly affected by 7D combined treatment (-95% vs. Opti-MEM), which is also lower than samples treated with *Prkaa2* siRNA alone (Fig. 71E). Surprisingly, after 7D treatment *Sirt1* mRNA was not affected by decrease in *Prkaa1* or *Prkaa2* mRNA, suggesting that a compensatory mechanism allow the restoration of *Sirt1* mRNA level after long term treatment (Fig. 71F). Altogether, *Prkaa1*+*Prkaa2* siRNA treatment exhibited similar effect upon *Sirt1* mRNA level, as *Prkaa1* siRNA treatment alone. This can lead to the conclusion that *Prkaa1* exhibit regulatory effect on *Sirt1* mRNA during 72h treatment.

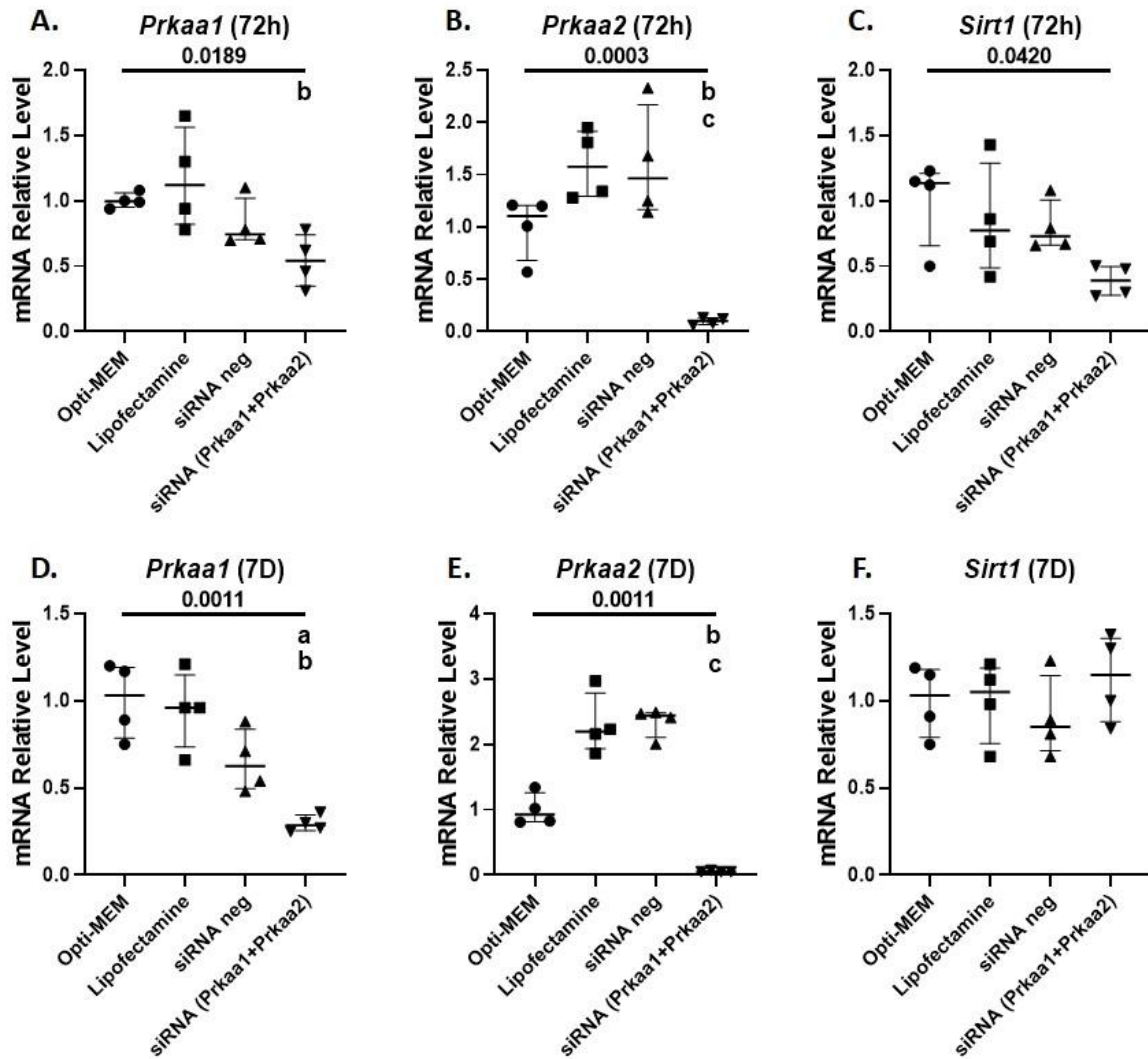


Figure 71. *Prkaa1* and *Prkaa2* expression in ST2 cells after exposed to combination of *Prkaa1* and *Prkaa2* siRNA. A-C. Relative mRNA level of *Prkaa1*, *Prkaa2* and *Sirt1* in ST2 cells treated with 50nM of *Prkaa1* and *Prkaa2* siRNA for 72 hours; D-F. Relative mRNA level of *Prkaa1*, *Prkaa2* and *Sirt1* in ST2 cells treated with 50nM of *Prkaa1* and *Prkaa2* siRNA for 7 days; Data represents mean \pm Interquartile range; n=4. Statistical analysis was performed using Kruskal Wallis test and Dunn's Multiple Comparison Test; b – $p < 0.05$ when compared to Lipofectamine condition; c – $p < 0.05$ when compared to siRNA neg.

5. Induction of AMPK activity does not affect *Sirt1* mRNA level

We showed that suppression of AMPK activity or suppression of *Prkaa1* expression can negatively impact *Sirt1* mRNA level in ST2 cells, however we were also interested to study the effect of AMPK activity induction on *Sirt1* gene expression. In order to do this, we used A-769662 compound, which is known to allosterically activate AMPK. Firstly, the effect of

200M A-769662 treatment on AMPK activity was tested in ST2 cell line. Results showed that 14h exposure to AMPK activator resulted in 24% increase in assay intensity (vs. CT), suggesting a successful rise in AMPK activity (Fig. 72A). In AMPK inhibition study we saw that ST2 cells had similar results to BMSCs, therefore we replicated the study on AMPK induction in primary mouse BMSCs. In order to determine the effect of AMPK activation in mice BMSCs, cells extracted from mice BM were treated for 14h with two different concentrations of AMPK activator (A-769662) - 50M or 200M. After, relative mRNA level of *Sirt1* was studied in BMSCs, which treated with lower (50M) and higher (200M) concentrations of A-769662 for 14h. The experiment showed that despite increased AMPK activity, both concentrations of A-769662 there was no desired effect on *Sirt1* mRNA level (Fig. 72B,C). Even 200M concentration of A-769662 induced a 36% decrease in *Sirt1* mRNA, without being statistically significant, leading to the conclusion that activation of AMPK enzymatic function is not enough to induce changes in *Sirt1* mRNA (Fig. 72C).

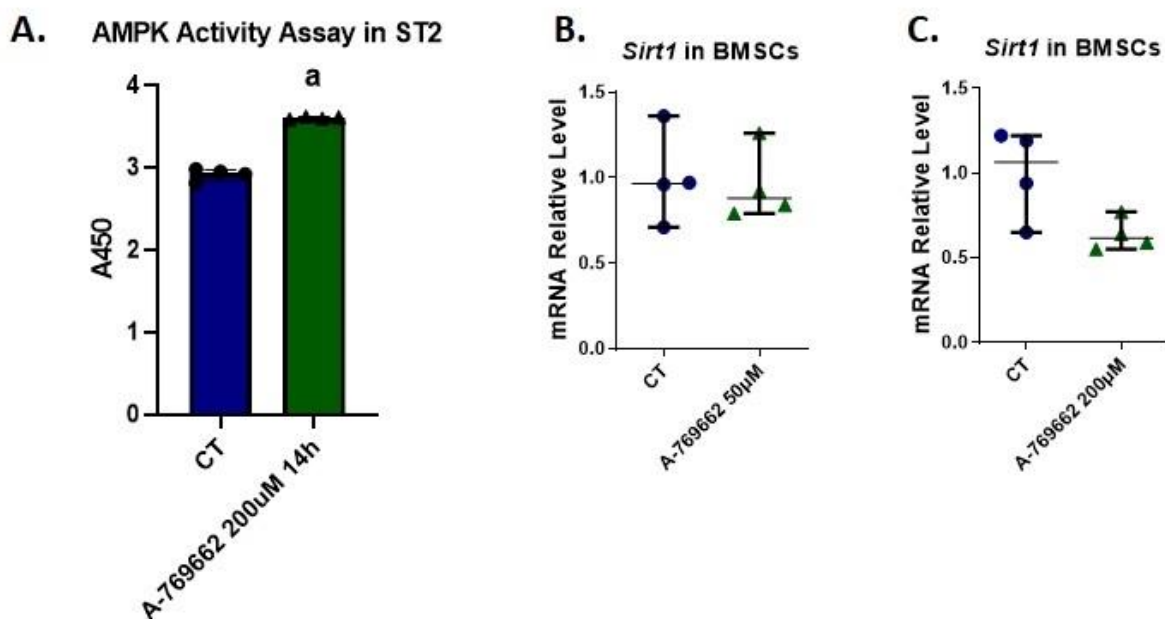


Figure 72. AMPK activity assay results and *Sirt1* expression in primary BMSCs exposed to 14h A-769662 treatment. A. AMPK enzymatic activity in CT ST2 cells and in ST2 cells treated with 200µM of A-769662, measured through the spectrophotometer absorbance at 450nm; B-C. Relative mRNA level of *Sirt1* in primary mice BMSCs treated with 50µM and 200µM of A-769662, respectively; Data represents mean ± Interquartile range; n=4. Statistical analysis was performed using Mann–Whitney’s test; a - p<0.05,

Similar to DM treatment study, we wanted to detect changes in *Prkaa1* and *Prkaa2* expression in cells treated with A-769662. Results showed that the expression level of *Prkaa1* mRNA was not altered by exposure to 50M A-769662, nor by 200M A-769662 treatment in mouse BMSCs (Fig. 73A,B). However, high concentration of AMPK activator resulted in 49% increase in *Prkaa2* mRNA (vs. CT) in BMSCs (Fig. 73B). According to these findings, it can be hypothesised that AMPK potentially is able to positively regulate the expression of AMPK subunit, through the downstream signalling. In the same time, we observed that increase in *Prkaa2* expression did not result in increase in *Sirt1* mRNA, suggesting that this isoform is not part of the complex that is involved in regulation of *Sirt1* expression (Fig. 72C).

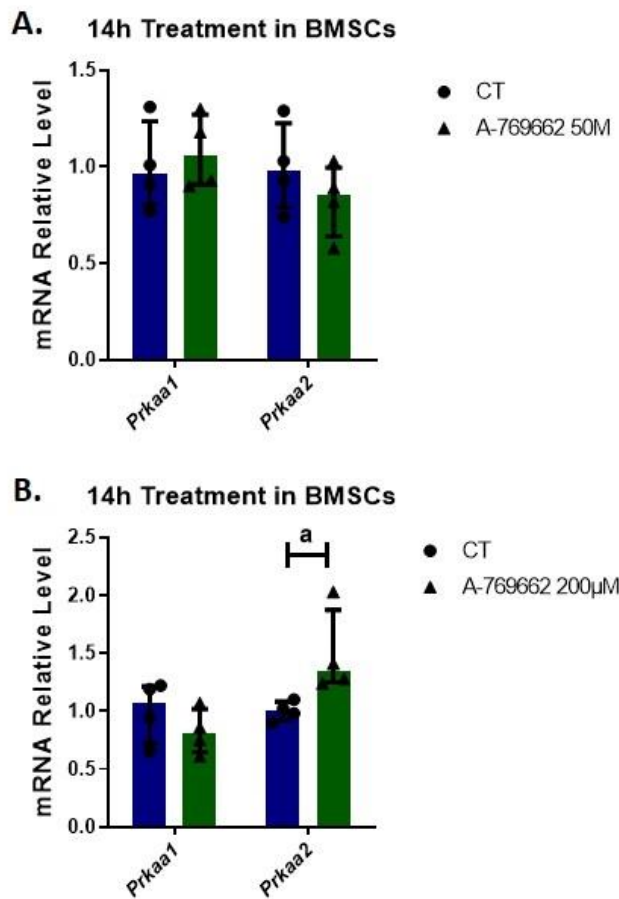


Figure 73. *Prkaa1* and *Prkaa2* expression in primary BMSCs exposed to 14h A-769662 treatment. A-B. Relative mRNA level of *Prkaa1* and *Prkaa2* in primary mice BMSCs treated with 50µM and 200µM A-769662, respectively; Data represents mean ± Interquartile range; n=4. Statistical analysis was performed using Mann–Whitney’s test; a - p<0.05,

6. DISCUSSION AND CONCLUSIONS

Previously, the relationship between SIRT1 and AMPK was established (1073). For that reason, the regulation of *Sirt1* expression by AMPK pathway was explored in ST2 cells line and primary mouse BMSCs. Study looked not only at mRNA level of *Sirt1*, but also at two isoforms of AMPK catalytic subunits (*Prkaa1* and *Prkaa2*). In the current study, we focused specifically on examination of *Prkaa1* and *Prkaa2* gene expression, as both activator and inhibitor of AMPK protein acts upon catalytic subunit. The basal expression level of *Prkaa1* and *Prkaa2* in primary BMSCs and ST2 cells showed a large predominance in *Prkaa1* isoform, suggesting that it is more transcribed in current cell types, comparing to *Prkaa2*. This finding corresponded to previously published data, where it was described that AMPK α isoform has a prevalence of 90%, in contrast to AMPK α 2, which covers only 10% of total AMPK α subunit expression (1052).

In BMSCs extracted from SBA 18% weight loss mice (10-week cohort 1) we observed a significant decrease in *Sirt1* mRNA level, as well as a decrease in AMPK1 gene (*Prkaa1*). Therefore, we were interested to see the relationship between decrease in AMPK and *Sirt1* expression. Long term (72h) and short term (14h) treatments of ST2 cells with DM have shown remarkable decrease in AMPK activity comparing to not treated cells (-96% vs. CT) (Fig. 67A). Overall, experiments demonstrated that successful inhibition of AMPK activity resulted in a decrease in *Sirt1* mRNA level in both ST2 cell line and primary mouse BMSCs (Fig. 67). However, reduction of AMPK activity did not induce changes in SIRT1 protein level, suggesting that 72h decrease in *Sirt1* mRNA is not enough to induce changes at protein expression level. These findings provide first evidence of AMPK regulatory effect upon *Sirt1* expression in mouse stromal cells. In the light of these findings, we hypothesised that AMPK might regulate *Sirt1* expression through E2F1 phosphorylation and stabilisation (976). The regulatory effect of E2F1 upon *Sirt1* expression was widely described in the literature. It was shown that DNA damage by cancer drug (etoposide) results in E2F1-dependent induction of *Sirt1* gene expression (550,714). Moreover, E2F1 transcription factor was shown to interact with two binding sites in the *Sirt1* promoter to induce *Sirt1* transcription (659).

Despite the fact that DM is widely described to be a good suppressor of AMPK activity and in current study it demonstrated an efficient result, other agents could be tested in current

condition, as DM has been shown to act upon other proteins like BMP. DM can also be utilised as a specific BMP pathway inhibitor (1104,1105). Indeed, in a comprehensive examination of inhibitor kinase specificities, DM was discovered to inhibit a variety of kinases other than AMPK (1106–1108). Taking into account the off target effect of DM, we conducted a literature research and did not find evidence that BMP pathway regulates *Sirt1* expression (1109). Therefore, we assumed that DM involvement in regulation of other protein activity does not affect our results. Nevertheless, to avoid any additional variables in the experiment, alternative suppressors of AMPK activity could be used. In 2018, Dite *et al.* published work where they described a selective inhibition of AMPK by SBI-0206965 (1110). Later, other studies also highlighted the efficient suppression of AMPK with SBI-0206965 (1111–1113).

Additionally, to explore a potential positive feedback loop of AMPK, we quantified *Prkaa1* mRNA, which showed its decrease in ST2 cell line and primary BMSCs after DM treatment (Fig. 65). One of possible mechanism of AMPK autoregulation is through AMPK facilitated phosphorylation of E2F1 transcription factor. It was reported that E2F1 directly binds to the promoter region and transactivates the expression of *Prkaa1* and *Prkaa2*, in return AMPK protein was shown to contribute to stabilisation of E2F1 (976,1114). Yang *et al.* described that AMPK α contributes to induction of apoptosis by stabilising E2F1 through the direct phosphorylation (976). Reduction in AMPK activity could have potentially reduced the rate of E2F1 phosphorylation, causing a decrease in its stability and capacity to conduct transcriptional regulation and further leading to the suppression of *Prkaa1* transcription. On the top of that, DM treatment in primary mouse BMSCs and ST2 cell line, display a compensation mechanism between *Prkaa1* and *Prkaa2* subunits. With a significant decrease in *Prkaa1* expression, an intracellular mechanism triggers activation of *Prkaa2*, which basal expression is low. This mechanism can potentially maintain basal cellular function and cell survival.

Following, an RNA interference study was conducted to validate findings of DM treatment, overcome possible drug side effects, and develop our understanding of AMPK role in *Sirt1* regulation. siRNA was used to specifically suppress *Prkaa1* and *Prkaa2* expression. ST2 cell treatment by *Prkaa1* siRNA for 72 hours, demonstrated a significant reduction in *Prkaa1* expression (-70% vs. Opti-MEM), as well as a decrease in *Sirt1* mRNA level (-67% vs. Opti-MEM) (Fig. 69A,B). However, findings of *Prkaa2* siRNA transfection showed a decrease in *Prkaa2* mRNA without affecting *Sirt1* expression (Fig. 70). These results once again demonstrated the involvement of AMPK in *Sirt1* gene expression. Furthermore, it can be

indicated that only *Prkaa1* suppression caused a statistically significant decrease in *Sirt1* mRNA and also, only reduction in *Prkaa1* mRNA was associated with decline in *Sirt1* in DM treated samples. However, in long term suppression (7D) of *Prkaa1*, only 48% decrease in *Prkaa1* mRNA was observed without affecting *Sirt1* expression (Fig. 69C,D). As was mentioned before, the basal expression level of *Prkaa2* in ST2 cells is much lower than *Prkaa1* isoform (Fig. 65B). When we combined *Prkaa1* and *Prkaa2* siRNA we observed similar results to *Prkaa1* treatment alone. *Sirt1* mRNA level was significantly reduced in cells treated for 72h, however after 7D its mRNA level was restored (Fig. 71). Multiple studies that focused on *Sirt1* mRNA expression suppression conducted the treatment for only 48 hours, therefore we postulate that in long term treatment, *Sirt1* expression is restored through alternative pathways, as this protein is crucial for cell function and survival (1115,1116).

In contrast to AMPK activity suppression study, AMPK activity induction did not result in any changes in *Sirt1* relative mRNA level in primary BMSCs (Fig. 72). Even with the higher concentration of activator tested (200M), AMPK activity was modestly increased. This modest effect appeared to be insufficient to induce an increase in *Sirt1* expression. So, if we want to study more the impact of AMPK activation on *Sirt1* mRNA level, other activators could be used. For example, it has been stated that Compound 991 (C991) and MT 63-78 are 5-10 times more potent than A-769662 and potentially can be good alternative (1117,1118). Benzimidazole derivative chemical 991 (C991), as a new and very effective AMPK activator (1119–1121). C991 binds directly to the AMPK α subunit, resulting in significant AMPK activation. It is the most powerful AMPK activator known, surpassing A769622 and AICAR (5-aminoimidazole-4-carboxamide-1-d-ribofuranoside) (1120,1121). Another more recently produced direct activators, MT 63-78, was able to inhibit prostate cancer cell proliferation *in vitro* as well as tumour growth *in vivo* (1122). It has similar effect to A-769662 and salicylates, MT 63-78 allosterically activates AMPK by directly binding to the AMPK β regulatory subunit (1118,1122,1123).

Nevertheless, our results strongly suggest that in primary mouse BMSCs and in ST2 cell line, AMPK can be responsible for regulation of *Sirt1* gene expression, however the molecular mechanism of this regulation is not yet defined.

OVERALL CONCLUSIONS AND PROSPECTIVES

Overview of findings and their contribution to the field

Throughout 3 years, our work focused on two main questions – What is the link between Bone - BMSC differentiation capacity – *Sirt1* expression (in BMSCs)? What are potential regulators of *Sirt1* expression in energy deficit context? (Fig. 74). Therefore, this project branched into two parts – 1. Focusing on SBA model and developing our understanding of how severity and length of nutrient deficit effects mice and what are transcriptomic differences between BMSCs extracted from SBA 18% and CT mice; 2. Focusing on establishment of previously unknown regulators of *Sirt1* expression and exploring previously described interactions between AMPK and SIRT1.

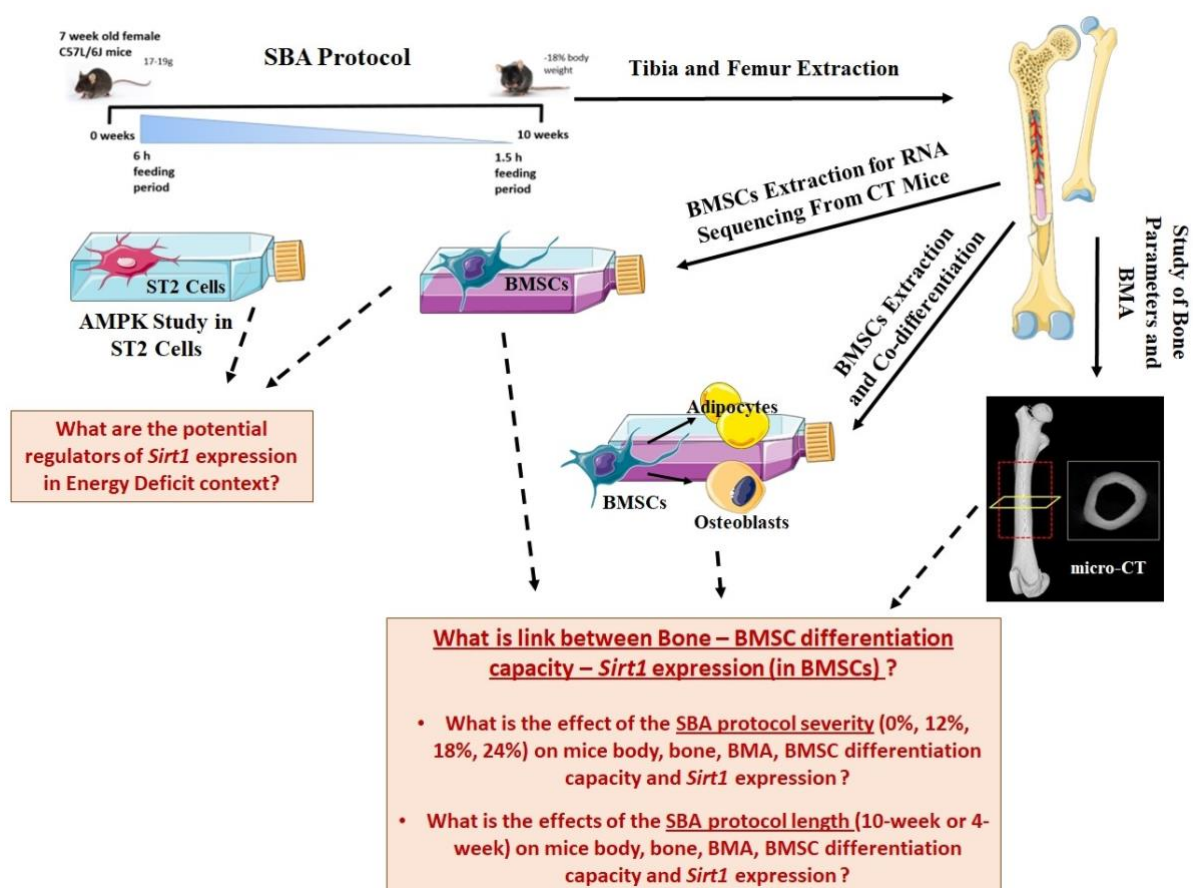


Figure 74. Project work overview and main questions addressed in this study.

Components of the diagram were taken from <https://smart.servier.com/>. Micro-CT diagram adapted from Hsu *et al.*, 2014 (182).

First of all, for the first time we identified that severity level of energy deficit plays a role not only in bone alterations, but also in BMSCs fate decision. Our long term (10-week) SBA protocol of moderate (18%) and severe (24%) weight loss induced loss of bone mineral content, trabecular thickness, as well cortical thickness, together with loss of periosteum diameter. These results suggest a decrease in bone formation, despite the fact that bone resorption was not assessed. Interestingly, that micro-CT analysis of proximal tibia BMA did not show any changes. However, when we studied the differentiation potential of BMSCs we observed a fast and upregulated adipogenesis and a low level of osteoblastogenesis, indicating a potential reduction in bone due to the switch in BMSCs differentiation potential. Switch in BMSC fate decision was accompanied by a decrease in *Sirt1* mRNA in moderate and severe weight loss conditions. Overall, we demonstrated that moderate and severe energy deficit can induce bone loss, which can be explained by a switch in BMSCs differentiation potential due to the reduction in *Sirt1* mRNA production (Fig. 75).

Secondly, we looked at moderate (18%) weight loss condition at different angle. We were interested to identify the effect of duration of energy deficit on bone and BMSCs. The preliminary study showed interesting results – weight loss in mice did not induce changes in bone parameter, BMSC differentiation, and subsequently *Sirt1* mRNA production. This strengthened our hypothesis that bone loss during energy deficit can be related to decreased osteoblastic differentiation of BMSC, that is related to reduced level of SIRT1 transcription factor (Fig. 75).

To a greater extent, we were interested in changes that take place in BMSCs extracted from 10-week and 4-week protocol, from both CT and SBA 18% weight loss mice, as these two conditions exhibit remarkably different results. As a first step of our investigation, with the help of our collaborators from EGID, we decided to conduct RNA-seq analysis to study transcriptomic differences between BMSCs from SBA and control mice, but also between long- and short-term protocols. Preliminary analysis of RNA sequencing revealed that both 10-week and 4-week protocols induced a reduced expression of genes involved in immune system development, white blood cell maturation or activation, indicating a significant number of haematopoietic cells within the extracted heterogeneous population of BMSCs. In spite of the fact that deeper analysis of data is required, it allowed us to have an overview of the events that take place within BMSCs following the energy deficiency exposure.

Additionally, we used the RNA-seq data to identify pathways and candidate genes, that might be involved in reduction of *Sirt1* expression in 10-week SBA 18% extracted BMSCs. Scanning thorough the available data we identified that – *Rleb*, *Rara*, *Hif1a*, *Esr1*, *Cebpb* or *Rb1*, could be involved in *Sirt1* regulation, as they are present within same pathways. However, functional test showed that suppression of *Rb1* expression with siRNA does not result in alteration of *Sirt1* mRNA. Therefore, we have left other 5 candidate genes to do test upon.

Additional to RNA-seq, we explored already described regulatory relationships between AMPK and SIRT1. We were interested in the effect of suppression of AMPK activity, as well as AMPK gene (*Prkaa1*) production, on *Sirt1* mRNA level. Results have confirmed that decrease activity of AMPK results in reduced production of *Sirt1* mRNA, also suppression of *Prkaa1* expression by siRNA leads to the decrease in *Sirt1* mRNA.

To test the cohort effect and confirm the preliminary findings of 4-week study, we replicated 10-week and 4-week SBA 18% weight loss protocol in mice. 10-week results showed similar findings to previously done SBA studies, on alterations in bone, but this time no change in *Sirt1* expression or BMSC differentiation was observed. Second time, replication of 4-week study demonstrated that short-term nutrient deficit can induce changes in bone parameters and induce a slight increase in BMA as well (Fig. 75). Nevertheless, lack of changes in BMSCs differentiation capacity and no effect on *Sirt1* mRNA level have been observed. Despite the fact that cohort 2 study did not confirm our previous finding, we still observed a strong effect of moderate weight loss on bone loss. These findings showed us that weight difference in mice at final day of the protocol (as it was observed between 4-week cohort 1 and cohort 2) can play a big role in bone alteration quantification, as SBA 18% data is compared to CT condition. Due to the fact that in these samples no change in BMSC differentiation capacity was observed, nor decrease in *Sirt1* expression was exhibited, other mechanism should have played a role in bone alterations. Samples from this cohort still can provide us valuable information on other mechanisms that can result in bone changes, which will be explored in future. But the link in BMSCs between alteration of differentiation and alteration of *Sirt1* mRNA level appeared to be confirmed and strong in all experimental situations.

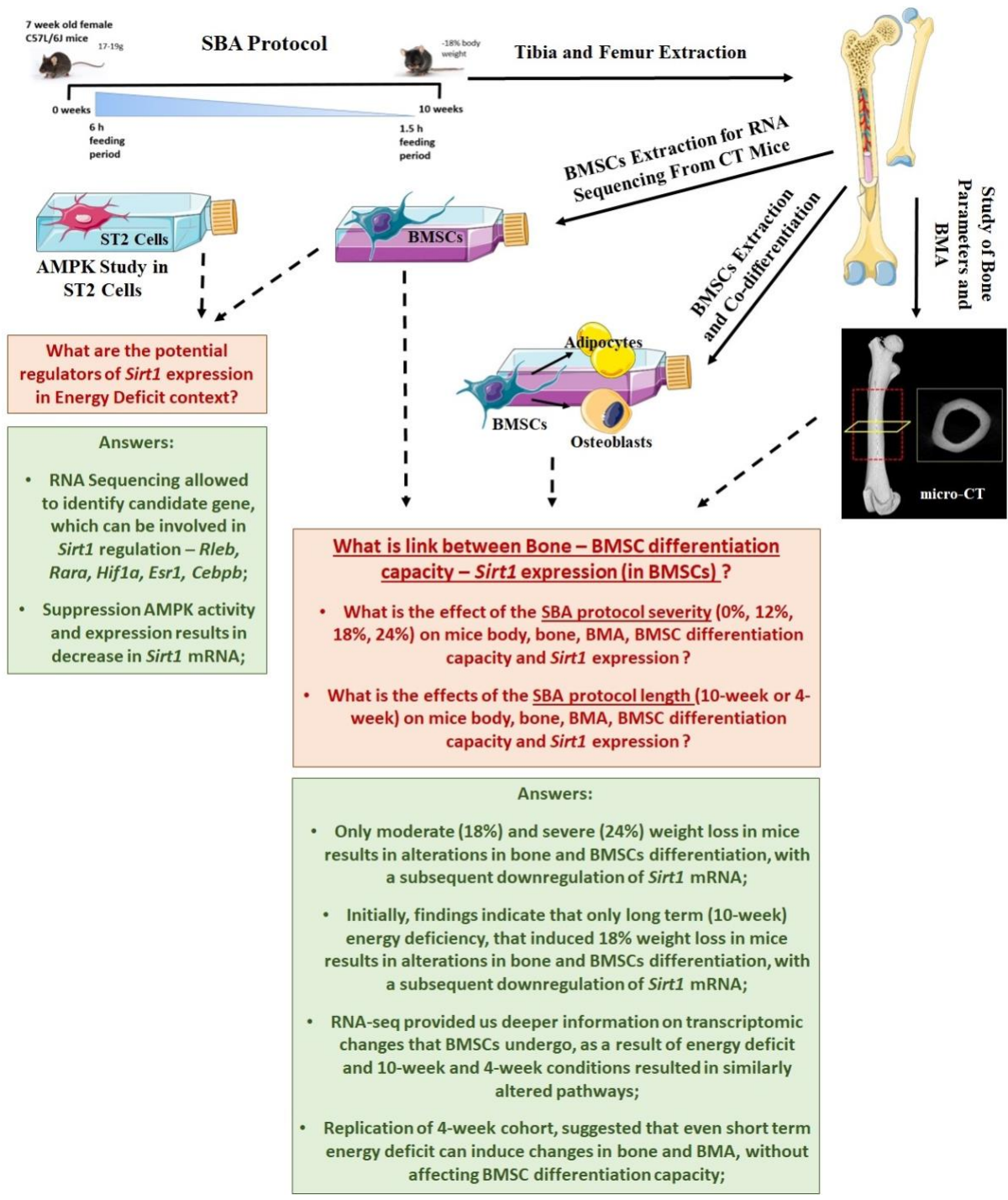


Figure 75. Project work overview and main questions addressed in this study with answers.

Components of the diagram were taken from <https://smart.servier.com/>. Micro-CT diagram adapted from Hsu *et al.*, 2014 (182).

Research on the topic of CR or severe energy deficiency provided compelling evidence of the negative relationship between BMD and BMA. In AN patients multiple cross-sectional studies indicate that AN is associated with loss of BMD, which is often accompanied by increase in BMA at different sites (femoral neck, long bone, lumbar vertebrae) (Fig. 76) (406–412). However, some studies, like Abella *et al.* have demonstrated a decrease in BMA in AN patients with severe condition of gelatinous degeneration of the bone marrow, which can be associated with BM necrosis (407). Variety of studies on CR in animal model, which used different approaches to subject mice or rat to CR, have demonstrated that decrease in bone parameters or BMD is predominantly accompanied by an increase in BMA (Fig. 76) (2,283,414). Previous studies on CR or energy deficit mainly focused on characterisation of BMAT in energy deficit condition. More specifically, extensive data was provided by Scheller *et al.* and Cawthorn *et al.* on distinguishing rBMAT and cBMAT, their regulatory and functional differences (179,196,283).

However, not all CR studies achieved increase in BMA. For example, Devlin *et al.* described a complete loss of BMADs in distal femur of mice, after 30% weight loss (vs. CT) (414). Moreover, in a rabbit model, Cawthorn *et al.* demonstrated that CR does not induce BMAT expansion (283). Suggesting that the lack of BMA alteration, that we observed in our current study on SBA model, correlates with previous findings in other CR models and species, emphasising the fact that bone loss in energy deficit is not a direct cause of increase in BMA, but rather additional factor that can enhance a bone loss. Therefore, our goal was to focus on the link between bone and molecular processes that can result in bone loss under energy insufficiency condition. We were interested in investigating molecular mechanisms that are responsible for a potential change in bone and BMA balance. Due to the fact that in BM both cell types (osteoblast and adipocyte) are derived from BMSCs and that SIRT1 plays an important role in BMSCs differentiation potential, favouring osteoblastogenesis and suppressing adipogenesis, we explored potential mechanisms of SIRT1 suppression in the context of energy deprivation. Overall, results of this work bring along valuable information about underlining process of bone loss in SBA model, like the fact that the lack of SIRT1 might play an important role in the BMSCs fate decision switch (Fig. 76). Additionally, we highlighted that AMPK might be one of the regulators of *Sirt1* expression in this cell type. Moreover, RNA-seq data opened a door to explore molecular changes that take place in BMSCs, extracted from SBA mice. A deep exploitation of the data could in future lead to the establishment of new regulatory mechanisms of BMSC differentiation.

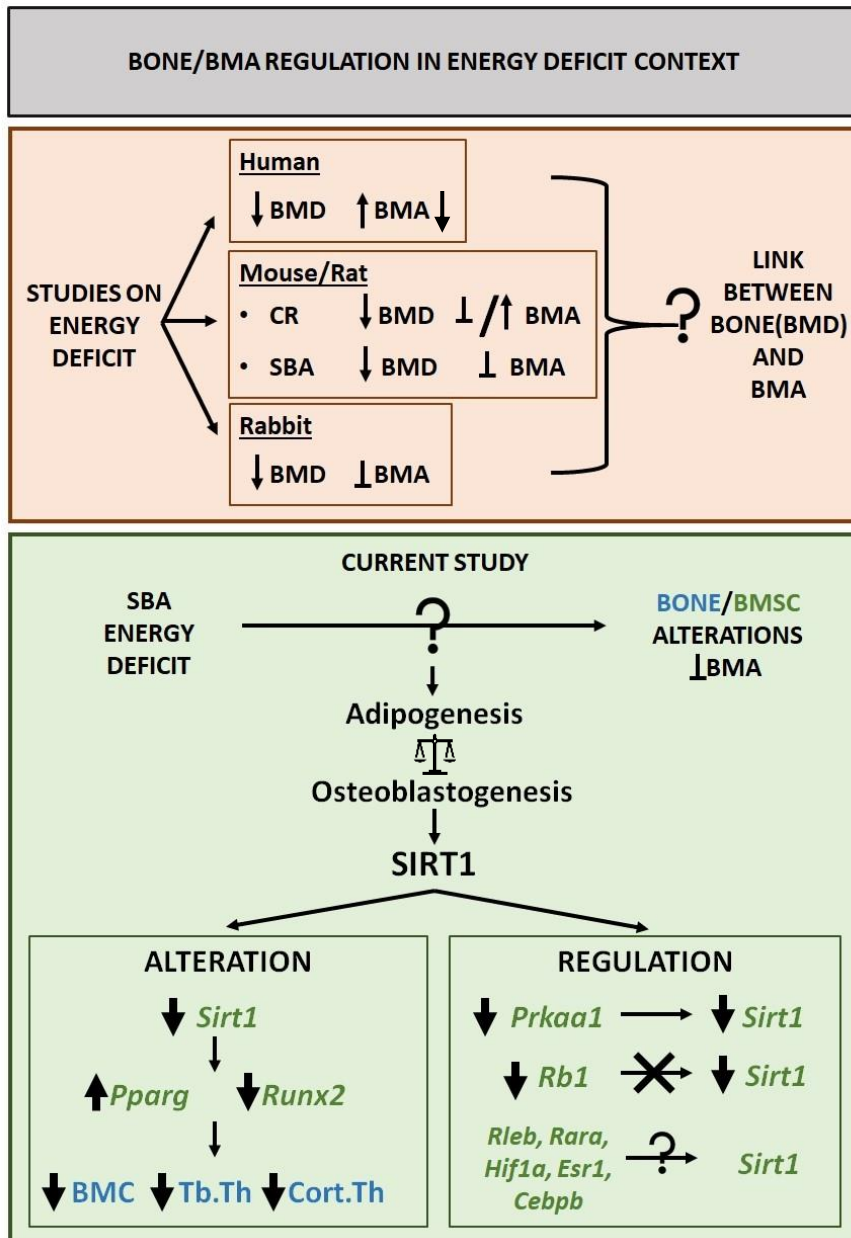


Figure 76. Bone/BMA regulation in the context of energy deficit. Diagram highlights main findings on bone alterations and BMA described in the literature, and emphasizes how this study is connected to previous findings and summarizes what were the main results obtained.

Future perspectives of current study

As this project led to several questions to investigate, it is important to emphasise on work that is necessary to be done first in the future. First of all, in a close future BMA data on 10-week and 4-week cohort 2 studies is going to be complete, which will allow having a better understanding regarding the relationship between bone and BMA in this SBA cohort. Moreover, it is crucial to replicate 10-week and 4-week SBA 18% weight loss studies again, in order to confirm or to refute results of cohort 2 study. This time, it would be important to allocate mice to groups so that initial weight of subjects will not be different between SBA and CT conditions. Moreover, it would be necessary to avoid weight gain within the protocol, after the first rapid weight loss, as this potentially can affect the outcome of the study. After inducing weight loss in mice and extracting BMSCs, it will be required to characterise the heterogeneous population using flow cytometry analysis of surface markers. For us, it would be necessary to understand what proportion of cells have haematopoietic and stromal origin (markers of trilineage differentiation - CD45⁻CD31⁻Sca1⁺CD24⁺), additionally, we would like to see the abundance of Zfp423⁺ cells that are considered to be pre-adipocytes. This will allow us to improve our understanding about origin of heterogeneity of extracted BMSCs and to see the effect of SBA protocol on proportion of cell populations (vs. CT).

RNA-seq provided big amount of data, which can be analysed from different perspectives and can improve our knowledge about transcriptomic alterations in cells extracted from BM of SBA 18% weight loss mice. These findings can shine the light on mechanisms of cell differentiation and adaptation in response to energy deficit *in vivo*. Extensive amount of work is required in data analysis and interpretation, as well as further functional tests.

In current study we used RNA-seq approach to identify new potential regulators of Sirt1 expression in BMSCs, additionally we tested previously described regulator of SIRT1 activity – AMPK. However, the long-term suppression of *Sirt1* mRNA expression, throughout the 14-day co-differentiation protocol, can take place due to epigenetic alterations of *Sirt1* promoter region. Chromatin immunoprecipitation (ChIP) experiment or ChIP sequencing (ChIP-seq) would be useful tools to investigate epigenetic alterations in cells extracted from SBA mice. This knowledge could be crucial in understanding the origin of *Sirt1* mRNA decrease in BMSCs extracted from SBA 18% weight loss mice – is epigenetic mechanism responsible for

gene expression suppression or *Sirt1* expression is negatively regulated through protein binding?

Furthermore, reduction of *Sirt1* mRNA level in BMSCs derived from BMA mice, could be due to the increase in mRNA degradation through miRNA activity. Previously it was described that miR-34a, miR-143, miR-132, miR-217 are negative regulators of SIRT1, through post transcriptional repression of *Sirt1* mRNA (721). Therefore, it would have been interesting to quantify the abundance of these miRNAs in BMSCs extracted from SBA mice, as they potentially can contribute to the reduction of *Sirt1* mRNA.

Overall, we have clear ideas about further steps of this project and exact paths that are necessary to be taken in order to achieve our goal and improve or apprehension of molecular changes that take place in SBA mice-derived BMSCs and regulation mechanism of *Sirt1* mRNA decrease.

Why is there an increase in BMAT and loss of bone in AN-affected individuals?

After 3 years of conducting a research project on the topic of AN-associated bone loss, personally for me there is no yet clear answer on question - why is there a bone loss and increase in BMA in energy deprivation condition?

In answering this question, it is important to take into account the crosstalk between different systems in the human body and emphasise the importance of hormones, growth factors and other signalling molecules in the regulation of bone homeostasis and BM microenvironment. Due to the fact that AN individuals are predominantly females and one of the severe symptoms of nutrient deficiency is amenorrhoea, oestrogen deficiency has been shown to have a strong association with BMAT accumulation and bone loss (1124). Therefore, oestrogen signalling in BM plays an important role in the growth and maturation of bone, as well as, it functions as one of the regulators of bone turnover in adult bone (1125). Oestrogen deficiency in the context of severe nutrient deprivation can probably contribute to the bone loss (1126).

Reduction in AT results in decreased source of adiponectin, that is necessary for protection against insulin resistance and atherosclerosis. It was described that in animal model, with depletion of AT, BMAT becomes the main source of circulating adiponectin (179). Moreover,

Li *et al.* showed that in the context of CR, BMAT lipolysis is required to maintain myelopoiesis, suggesting that BM fat storage is required for function of haematopoiesis (246).

Our research focused on investigating changes in the BMSCs caused by the decrease in SIRT1 production, however in other metabolic tissue, CR is known to increase production of SIRT1 and other members of sirtuin family. Therefore, I found it important to investigate the changes in sirtuin family production during different metabolic states (obesity, diabetes and AN) in other tissue. Moreover, my research on this topic was driven by understanding the effect of sirtuins on secretome production in metabolic tissue (pancreas, liver and other adipose tissue depots). Throughout the project we were focusing only on BM environment, but a variety of systemic changes can affect bone in the context of AN. Therefore, we published a review article, highlighting the effect of energy deficit on sirtuins production in metabolic tissue, understanding how it can alter the secretome of this tissue, and further affect bone homeostasis (1). Overall, our findings emphasised the fact that GH resistance, which was described before in AN patients, as well as in SBA mouse model, could take place due to SIRT1-mediated STAT5 deacetylation and deactivation, leading to reduced expression of IGF-1 gene (1127). This event can potentially have a negative impact on bone formation. Also, leptinaemia development in AN subjects, can negatively affect bone homeostasis, through sympathetic nervous system (SNS) and activity in the hypothalamus. Eleftheriou *et al.* demonstrated that leptin deficiency results in reduced production of cocaine amphetamine regulated transcript (CART). CART signals to osteoblasts and reduces RANKL expression in these cells by suppressing osteoclast maturation. Therefore, a decrease in CART results in the activation of bone resorption through upregulated osteoclast maturation (1128). All-inclusive, this review article highlighted several mechanisms through which other tissue can negatively affect bone homeostasis in AN condition (586).

Overall, to answer this difficult question – why there is an increase in BMAT and loss of bone in AN-affected individuals, we need to combine all the collected evidence together. Leading to my personal conclusion, that oestrogen deficiency, leptinaemia, GH resistance, alterations in BMSCs differentiation (potentially through downregulation of SIRT1 production), BMAT-derived adiponectin production and moreover the necessity of energy supply to maintain haematopoiesis – can lead to an increase in BMAT and bone loss in the context of energy deficit.

Personal conclusion

From the beginning we understood that during these 3 years we would not be able to reach a clear conclusion and determine (with 100% certainty) a regulating mechanism of *Sirt1* expression in BMSCs, under energy deficit condition. However, our results moved forward our understanding of energy deficit involvement in bone and BMSCs alterations. Moreover, we came up with compelling evidence of AMPK involvement in regulation of *Sirt1* expression in BMSCs, which was not described before. Maybe in the end, this project brought more questions than answers, but isn't it how science works? Great Russian physicist Sergey Vavilov once said – “When science reaches any high, from this peak opens a wide perspective on further journey, new paths, new roads are going to be open, which science will use to go forward.” I think this quite perfectly fits to the description of the work that has been done in past 3 years.

LIST OF PUBLICATIONS AND COMMUNICATIONS

Publications

- V. Avilkina, D. Leterme, G. Falgayrac, J. Delattre, F. Miellot, V. Gauthier, C. Chauveau, O. Ghali Mhenni, Severity Level and Duration of Energy Deficit in Mice Affect Bone Phenotype and Bone Marrow Stromal Cell Differentiation Capacity, *Frontiers in Endocrinology*, Volume 13, 2022, 880503, 10.3389/fendo.2022.880503
- V. Avilkina, C. Chauveau, O. Ghali Mhenni, Sirtuin function and metabolism: Role in pancreas, liver, and adipose tissue and their crosstalk impacting bone homeostasis, *Bone*, Volume 154, 2022, 116232, ISSN 8756-3282, 10.1016/j.bone.2021.116232.
- R. Labella, S. Little-Letsinger, V. Avilkina, R. Sarkis, M. Tencerova, A. Vlug, B. Palmisano, Next Generation Bone Marrow Adiposity Researchers: Report From the 1st BMAS Summer School 2021, *Frontiers in Endocrinology*, Volume 13, 2022, 879588, 10.3389/fendo.2022.879588.

Oral Poster Communications

- V. Avilkina, C. Chauveau, O. Ghali Mhenni. **Regulators of Sirtuin type 1 (SIRT1); a key player in bone marrow adiposity increase in anorexia nervosa.** *European Calcified Tissue Society Digital Masterclass 2020*
- V. Avilkina, D. Leterme, G. Falgayrac, P. Marchandise, F. Miellot, V. Gauthier, C. Chauveau, O. Ghali Mhenni. **How the severity level of energy deficit in mouse model affects the bone marrow adiposity, bone quality and bone marrow stromal cells differentiation.** *Bone Marrow Adiposity Society Digital Congress 2020*
- V. Avilkina, D. Leterme, G. Falgayrac, P. Marchandise, F. Miellot, V. Gauthier, C. Chauveau, O. Ghali Mhenni. **How the duration of energy deficit in mouse model affects the body composition, bone phenotype and bone marrow stromal cells differentiation capacity.** *European Calcified Tissue Society Digital Congress 2021*

- V. Avilkina, D. Leterme, G. Falgayrac, P. Marchandise, F. Miellot, V. Gauthier, C. Chauveau, O. Ghali Mhenni. **How the severity level and duration of energy deficit in mouse model affects the body composition, bone phenotype and bone marrow stromal cells differentiation capacity.** *Bone Marrow Adiposity Society Summer School 2021*
- V. Avilkina, D. Leterme, J. Delattre, F. Miellot, V. Gauthier, P. Froguel, A. Bonnefond, M. Derhourhi, M. Canouil, C. Chauveau, O. Ghali Mhenni. **Exploring molecular mechanisms of Sirtin type 1 (SIRT1) regulation in mouse model mimicking consequences of anorexia nervosa.** *Journees Francaises de Biologie des Tissus Mineralises Congress 2022*
- V. Avilkina, D. Leterme, J. Delattre, F. Miellot, V. Gauthier, P. Froguel, A. Bonnefond, M. Derhourhi, M. Canouil, C. Chauveau, O. Ghali Mhenni. **Exploring potential regulators of Sirtuin type 1 (SIRT1) in mouse bone marrow stromal cells (BMSCs) from energy deficit model.** *Bone Marrow Adiposity Society Digital Congress 2022*

PROJECT SUMMARY IN FRENCH

Identification des régulateurs de la sirtuine de type 1 (SIRT1) : acteur clé de l'altération osseuse et la capacité de différenciation des cellules stromales en situation de déficit énergétique (Anorexie Mentale)

1. Situation du projet de recherche dans la littérature et objectifs

L'ostéoporose est une maladie du squelette caractérisée par une diminution de la densité de l'os et des altérations de sa structure. Un déséquilibre entre formation et résorption osseuses au détriment de la formation entraîne la fragilisation de l'os et la survenue de fractures, qui représentent la manifestation principale de l'ostéoporose (OP). Une augmentation de l'adiposité médullaire est démontrée dans différents types d'OP : post-ménopausique ou liée au vieillissement (1129), cortico-induite (294) et de l'anorexie mentale (AM) (1130) (voir synthèse récente sur l'adiposité médullaire (1131)). Les deux premiers types d'OP (post ménopausique et vieillissement) ont de nombreux points communs et sont pour la plupart largement étudiés. Par contre l'AM représente un contexte ostéoporotique unique, notamment au regard de son statut non inflammatoire, de l'âge moyen de sa survenue et du faible nombre d'études qui lui sont consacrées. Les multiples conséquences incluent des perturbations neuro-endocrines majeures et une densité minérale osseuse (DMO) basse induisant des fractures chez 44% des patientes. Cette DMO n'est que rarement et partiellement corrigée par la reprise de poids et la sortie d'aménorrhée.

Notre équipe, est impliquée depuis de nombreuses années dans l'étude des altérations osseuses associées à l'AM. Nous avons ainsi montré une perte osseuse chez les patientes anorexiques (1130), une corrélation négative entre la DMO de ces patientes au niveau du col fémoral et le niveau plasmatique de l'adiponectine totale (1132) qui est soupçonnée d'être produite majoritairement par les adipocytes médullaires dans ce contexte (265) et l'existence d'une corrélation négative entre l'adiposité médullaire et la densité minérale osseuse (DMO) au niveau du col fémoral et de la hanche au sein d'une cohorte conséquente de patientes anorexiques (411).

Cette adiposité médullaire, autrefois considérée comme un tissu passif de remplissage de l'espace laissé vacant par la perte osseuse, semble jouer un rôle crucial dans la survenue de l'OP (1133). Parmi les arguments soutenant cette hypothèse, notons que les ostéoblastes et les

adipocytes médullaires proviennent d'un progéniteur commun, la cellule souche squelettique (CSS) qui fait partie des cellules stromales (CS), et que plusieurs études ont montré une relation inverse entre ostéogenèse et adipogenèse (99,1134,1135). Enfin, les adipocytes médullaires, dont la caractérisation encore en cours a fait l'objet de plusieurs présentations dans des congrès internationaux, sont capables de produire des facteurs agissant directement sur la formation et la résorption osseuses.

Parmi les régulateurs de la différenciation ostéoblastique, plusieurs études ont montré que les sirtuines et plus particulièrement la sirtuine de type 1 (une classe d'enzymes des histones désacétylases) jouent un rôle majeur dans le contrôle de la balance ostéogenèse/adipogenèse. En effet, la sirtuine de type 1 (SIRT1) est connue pour ses effets pro-ostéoblastiques et anti-adipocytaires via une désacétylation de résidus lysines de régulateurs clés des voies de différenciation et de leurs cofacteurs (634,900,1136). Sirt1 favorise la différenciation ostéoblastique en bloquant l'expression de PPAR-gamma2 (facteur de transcription majeur de l'adipogenèse) en entraînant la désacétylation de ses co-facteurs ou via la désacétylation de RUNX2 (facteur de transcription majeur de l'ostéogenèse) (900) (Fig. 77).

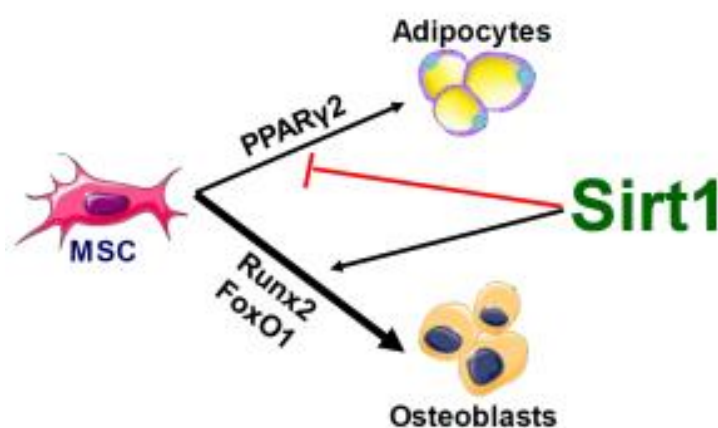


Figure 77. Régulation de la différenciation des cellules souches stromales en adipocytes et ostéoblastes par *Sirt1*.

En ce qui concerne la restriction calorique et l'expression de *Sirt1*, à ce jour, deux publications ont montré que la restriction calorique stimulait l'expression et l'activité extra-osseuses de *Sirt* (21,906).

Afin d'étudier le rôle des adipocytes de la moelle osseuse dans le développement de l'OP associée à l'AM, notre groupe a développé un modèle murin mimant les conséquences de l'anorexie mentale (modèle basé sur la restriction alimentaire couplée à la séparation « SBA » :

Separation Based Anorexia) (1). Nous avons ainsi montré une diminution durable de l'expression de *Sirt1* dans les CS des souris SBA par rapport aux CS des souris contrôles (CT). En effet, après 48h de culture (milieu de prolifération standard) ou après 14 jours de co-différenciation (milieu permettant l'obtention à la fois des adipocytes et ostéoblastes (808)), les CS des souris SBA (à 18% de perte de poids par rapport au poids initial) présentent un niveau d'ARNm de *Sirt1* inférieur de 80% à celui des CS des souris CT. Ceci s'accompagne d'une part, d'une accélération et d'une augmentation de l'adipogenèse au détriment de l'ostéogenèse et d'autre part, d'une forte acétylation des facteurs de transcriptions RUNX2 et FOXO1. L'ensemble de ces résultats suggère l'implication de SIRT1 dans la régulation de l'adiposité médullaire (2).

Ce projet de thèse repose sur l'hypothèse que la diminution de l'expression de *Sirt1*, dans les cellules stromales, est associée aux altérations osseuses et à l'adiposité médullaire et que le niveau de l'expression de *Sirt1* pourrait être lié au degré de sévérité et la durée du protocole SBA. L'objectif principal sera donc d'identifier les régulateurs de *Sirt1* et de déterminer les mécanismes moléculaires qui en sont responsables dans ce modèle. Ceci permettra à court terme une meilleure compréhension de la régulation de l'adiposité médullaire et à moyen terme de proposer de nouvelles stratégies thérapeutiques pour une meilleure prise en charge de l'ostéoporose, notamment liée à l'anorexie mentale.

Ainsi les objectifs de ce projet de recherche sont :

- 1) Etudier l'impact de différents degrés de sévérité (0%, 12%, 18% et 24% de perte de poids) et la durée du protocole SBA (10 et 4 semaines) sur les paramètres osseux, l'expression de *Sirt1* et la capacité de différenciation des CS en ostéoblastes et adipocytes;
- 2) Déterminer les mécanismes de régulation de l'expression de *Sirt1* en analysant le séquençage des ARNs après 48h de culture de CS issues des souris SBA et CT à 10 et 4 semaines de protocole et en étudiant la voie de signalisation de l'adénosine monophosphate kinase (AMPK);

Le schéma ci-dessous résume la méthodologie utilisée dans le cadre de cette thèse ainsi que les questions abordées.

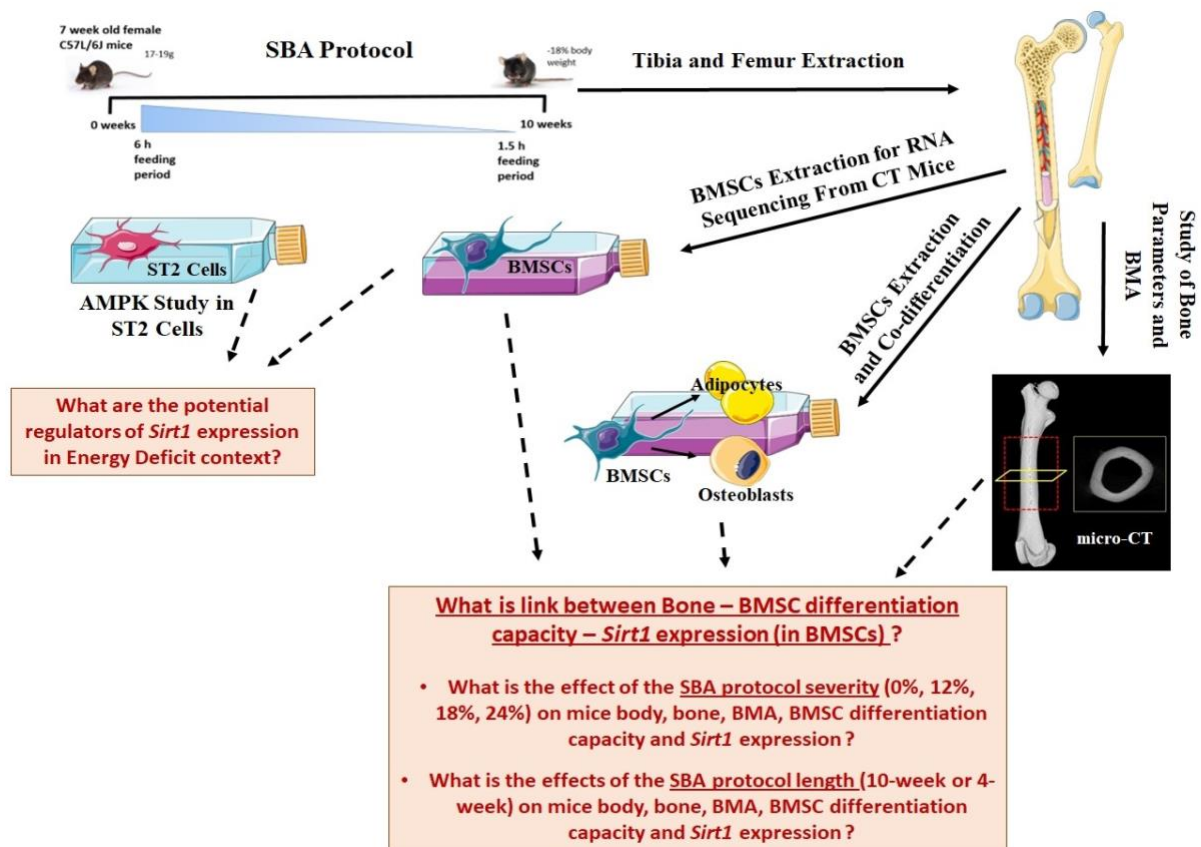


Figure 78. Méthodologie employée dans le cadre de ce projet de recherche. BMSC (Bone Marrow Stromal Cells). SBA : Separation-Based Anorexia. BMA : Bone Marrow Adiposity. ST2 : lignée cellulaire murine commerciale. Micro-CT : outil pour scanner et analyser les os (tibias).

2. Principaux résultats de la thèse

2.1 Les effets de différents degrés de sévérité et la durée de déficit énergétique sur les paramètres osseux, l'expression de *Sirt1* et la capacité de différenciation des cellules stromales dans le modèle SBA

2.1.1 Les effets du protocole SBA 10 semaines sur la composition corporelle et le phénotype osseux

Nos résultats ont montré que le protocole à 10 semaines a entraîné une forte diminution de la masse grasse pour les souris de 12%, 18% et 24% de perte de poids. Une réduction de la masse maigre n'a été observée que pour les souris de 12% (-19% vs. CT) et 24% (-22% vs. CT). En ce qui concerne, la densité minérale osseuse (DMO) du corps entier, nos résultats ont montré une diminution significative pour les souris de -12% (-17% vs. CT) et -18% (-15% vs. CT) de degré de sévérité (Fig. 25). En outre, les souris de 12%, 18% et 24% montrent une baisse

significative de la DMO au niveau des fémurs. En revanche, seulement les souris de 18% de perte de poids, présentent une diminution de la DMO au niveau des vertèbres lombaires (L3-L5) (SBA 18% -23% vs. CT) (Fig. 25).

L'analyse de la micro-architecture osseuse au niveau du tibia proximal, montre que le protocole SBA à 10 semaines, n'a pas altéré la fraction du volume osseux (Bv/Tv) pour tous les groupes de souris. Les souris ayant un fort degré de sévérité présentent une forte diminution de l'épaisseur trabéculaire (Tb.Th) (SBA 24%: -29% vs. CT) et de l'espacement trabéculaire (Tb.Sp) (-18% vs. CT). L'épaisseur corticale (Cort.Th) est significativement réduite chez les souris SBA de 18% (-16% vs. CT) et 24% (-17% vs. CT). En revanche, le protocole SBA à 10 semaines n'a pas d'effet sur l'adiposité médullaire (Fig. 79).

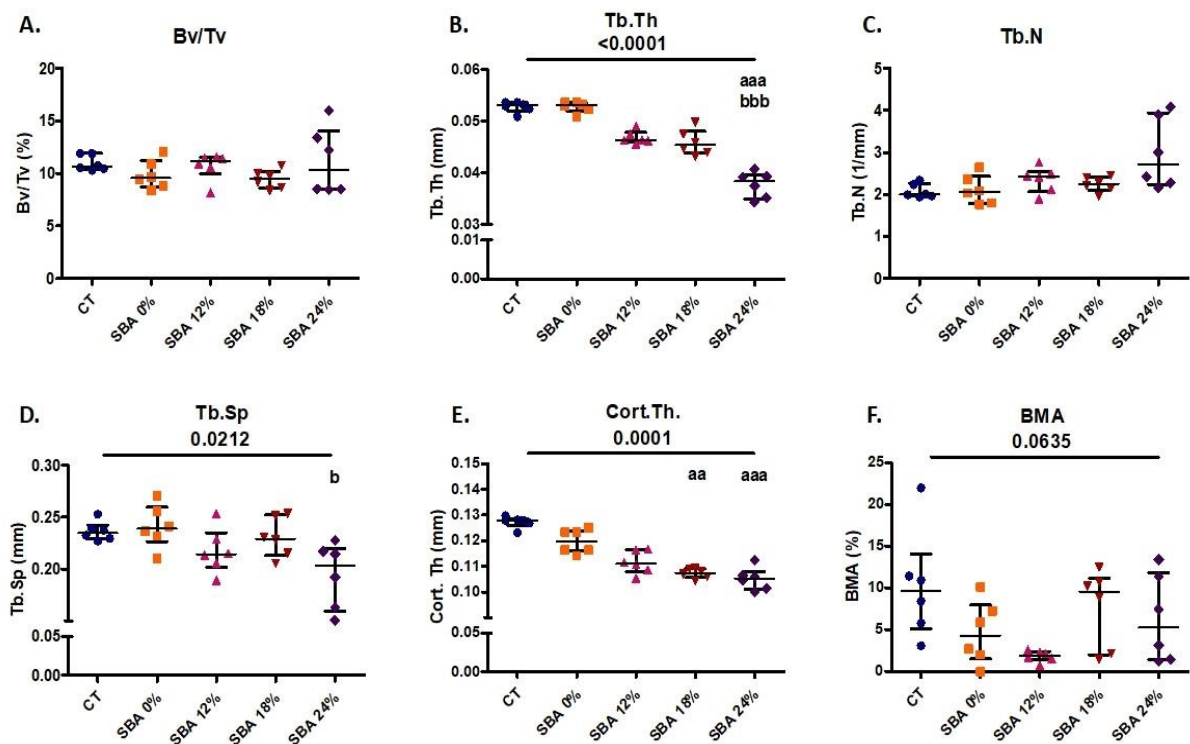


Figure 79. Impacts de différents degrés de sévérité et du protocole SBA à 10 semaines sur la micro-architecture osseuse et l'adiposité médullaire. A. fraction du volume osseux (Bv/Tv); B-E. Épaisseur trabéculaire (Tb.Th), nombre des travées (Tb.N), l'espacement trabéculaire (Tb.Sp), et l'épaisseur corticale (Cort.Th) sont évalués au niveau du tibia proximal de chaque souris et exprimés en millimètres; F. Adiposité médullaire (BMA) est exprimée en pourcentage du tissu adipeux dans la moelle. n=6. L'analyse statistique est déterminée par le test Kruskal-Wallis One-Way ANOVA et le test Dunn; a - p<0.05, aa - p<0.005 and aaa - p<0.0005 vs groupe CT (b – vs le SBA 0%).

2.1.2 Les effets du protocole SBA 10 semaines sur l'expression de Sirt1 et la capacité de différenciation des cellule stromales

Afin de déterminer l'impact de ce long protocole SBA et ces différents degrés de sévérité sur l'expression de Sirt1 et la capacité de différenciation des cellules stromales (CS), les cellules de différents groupes de SBA (0%, 12%, 18% et 24%) et du groupe contrôle ont été co-différenciées en ostéoblastes et adipocytes pendant 14 jours. La mesure de l'expression de l'ARNm de *Sirt1* et des marqueurs adipocytaires (*PPAR-gamma 2- (Pparg2)*, *leptine (lep)*, *adiponectine (Adipoq)* et le transporteur de type 4 de glucose (*Glut4*)) et ostéoblastiques (*Runx2*, *collagène de type 1 (coll1a1)*, *ostérix (Sp7)* et *ostéocalcine (Bglap)*) a été effectuée par la PCR-quantitative. En effet, nos résultats ont montré une diminution significative de l'expression de Sirt1 seulement dans les souris de -18% (-75% vs CT) et -24% (-68% vs CT) de degré de sévérité. Ceci s'accompagne d'une augmentation de l'adipogénèse au détriment de l'ostéogénèse (Fig. 80). L'ensemble de ces résultats suggère que l'altération de la capacité de différenciation des cellules stromales pourrait être associée à la diminution de l'expression de *Sirt1*.

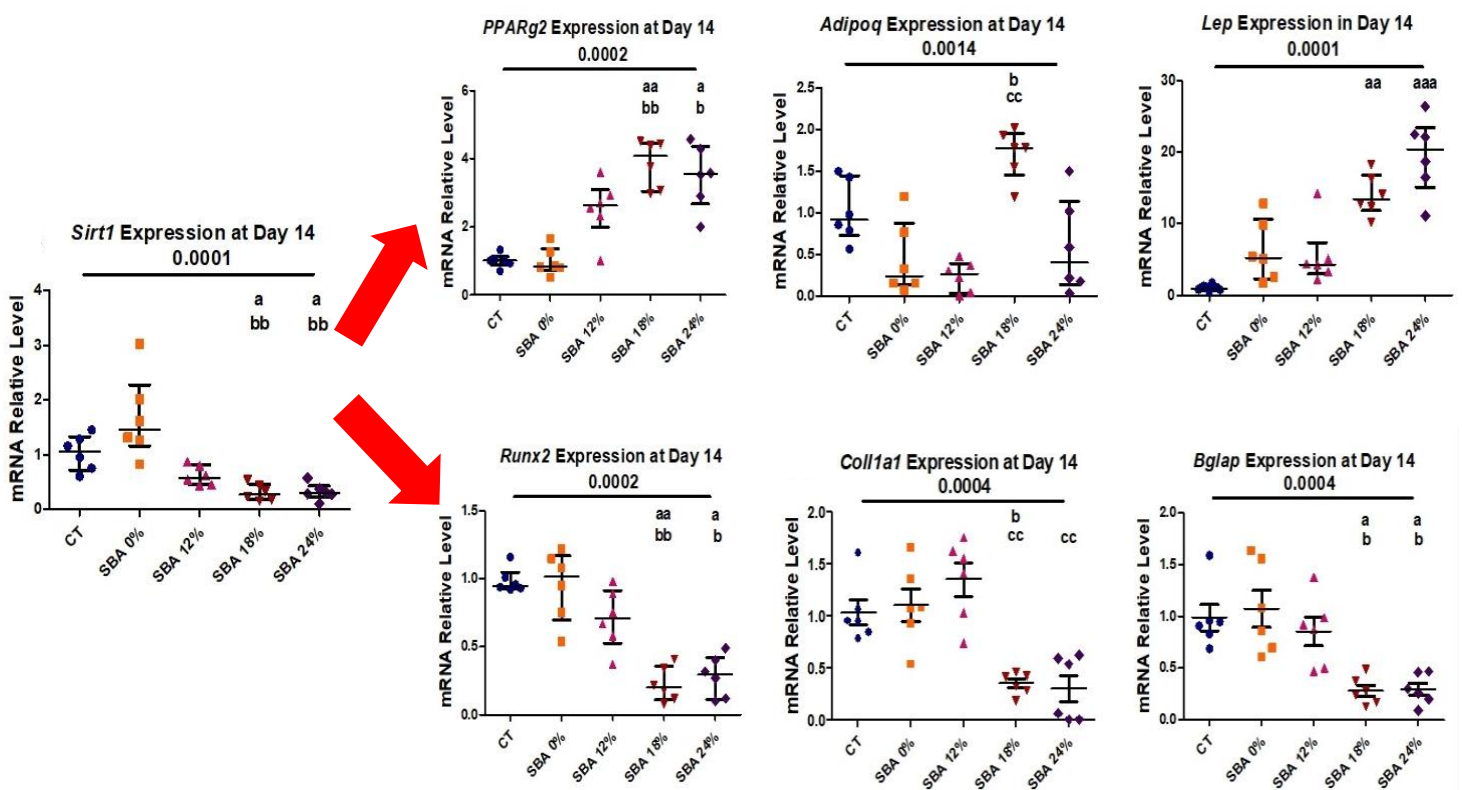


Figure 80. Impacts de différents degrés de sévérité et du protocole SBA à 10 semaines sur l'expression de Sirt1 et les marqueurs de la différenciation adipocytaire et ostéoblastique après 14 jours de différenciation. Les mesures des niveaux d'ARNm de *Sirt1* et tous ces marqueurs ont été réalisées avec la PCR-quantitative. n=6. L'analyse statistique est déterminée par le test Kruskal-Wallis One-Way ANOVA et le test Dunn; a - $p < 0.05$, aa - $p < 0.005$ and aaa - $p < 0.0005$ vs groupe CT (b – vs le SBA 0%).

Le reste de l'étude sera focalisé sur le degré de sévérité de -18% car ce degré a entraîné :

- Une forte altération de tous les paramètres osseux;
- Une accélération de l'engagement des cellule stromales vers la voie adipocytaire;
- Une diminution de tous les marqueurs de la différenciation ostéoblastique;
- Une forte diminution de l'expression de *Sirt1* (diminution durable à 48h de culture et 14 jours de différenciation).

2.1.3 Les effets du protocole SBA (-18%) à 4 semaines sur la composition corporelle, le phénotype osseux, l'expression de *Sirt1* et la capacité de différenciation des cellules stromales

Contrairement au long protocole SBA (-18%), le protocole court de 4 semaines et de -18% de degré de sévérité n'a entraîné que la diminution de la masse grasse (-50% vs. CT) et de l'épaisseur trabéculaire (-16% vs. CT). En outre, aucune modification de l'adiposité médullaire n'a été observée. En ce qui concerne l'expression de *Sirt1* et la différenciation des cellules stromales vers la voie adipocytaire et ostéoblastique, nos résultats ont montré que ce protocole n'a pas d'effet ni sur le niveau de l'expression de *Sirt1* ni sur la capacité de différenciation des CS. L'ensemble de ces résultats montre que cette durée n'est pas suffisante ni pour altérer le phénotype osseux ni pour modifier l'expression de *Sirt1* et la différenciation cellulaire. Ces résultats ont fait l'objet d'un article récemment publié dans le journal *Frontiers in Endocrinology* (882).

2.2 Les mécanismes de régulation de l'expression de *Sirt1*

L'objectif de cette partie est de déterminer les mécanismes moléculaires responsables de la diminution de l'expression de *Sirt1* en utilisant deux approches:

- a) L'analyse de séquençage des ARNm extraits des CS de souris SBA à 4 et à 10 semaines de protocole (-18% de degré de sévérité) ;
- b) L'exploration de la voie de signalisation de l'adénosine monophosphate kinase (AMPK) en utilisant un inhibiteur et un activateur de cette voie.

2.2.1 Analyse transcriptomique de l'ARNm des cellules stromales issues des souris SBA à 4 et 10 semaines de protocole et après 48h de culture (étude préliminaire)

Cette partie a été réalisée par le CNRS UMR-1283-8199 et la plateforme de génomique UMR 8199. Les données de RNASeq ont fait l'objet d'une étude préliminaire qui a permis une première mise en évidence de perturbations géniques potentiellement reliés à la régulation de *Sirt1* (Fig. 81).

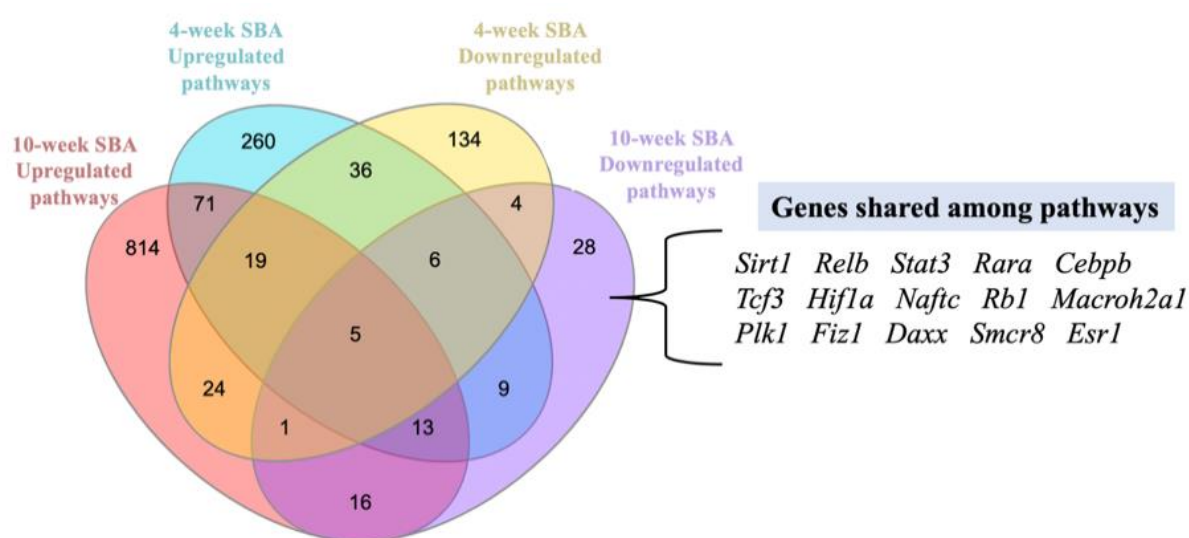


Figure 81. Synthèse de l'analyse des données du séquençage des ARNm afin d'identifier quelques gènes responsables de la diminution de l'expression de *Sirt1*. « diagramme Ven » représentant les gènes possédant une augmentation ou une diminution de leur expression dans les cellules stromales issues des souris de 4 et 10 semaines de protocole SBA à -18% de perte de poids. Les gènes possédant des voies de signalisation communes avec *Sirt1* sont les gènes identifiés dans la cohorte SBA à 10 semaines de protocole.

Après confirmation avec la PCR-quantitative, nos résultats ont montré que seulement 6 gènes présentent une diminution significative de leur niveau d'expression en ARNm (souris SBA à 10 semaines de protocole). Il s'agit des gènes *Relb*, *Rara*, *Hif1a*, *Rb1*, *Esr1* et *Cebpb* (Fig. 82). Un tableau résumant la fonction de chaque gène est représenté à Table 10.

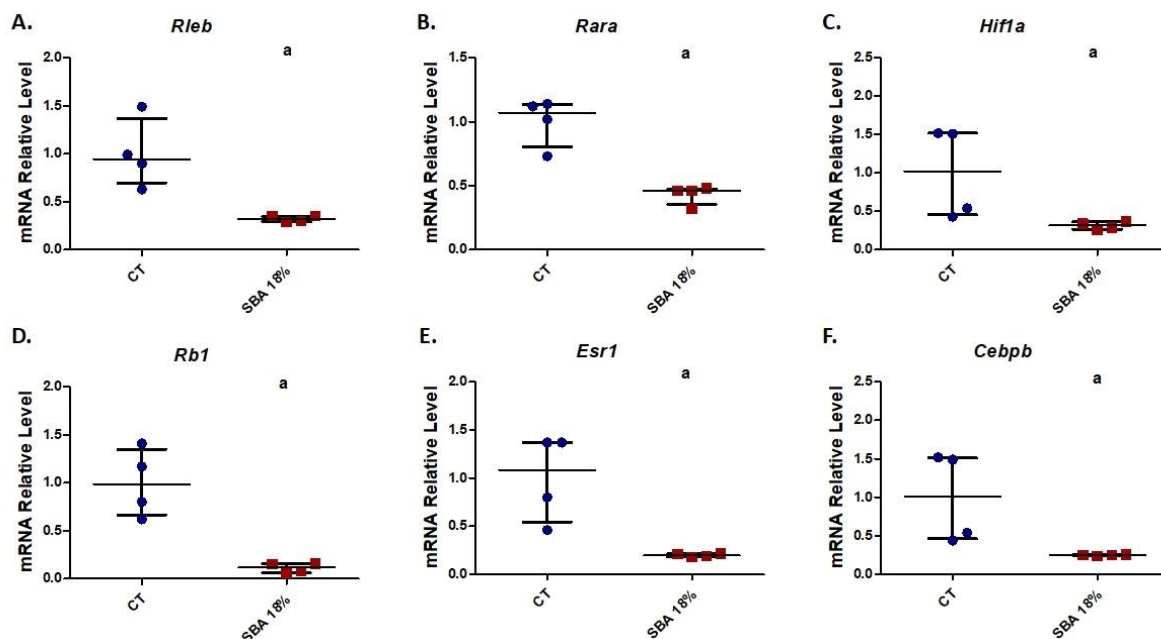


Figure 82. Mesure de l'expression des gènes identifiés par le séquençage des ARN (*Rleb*, *Rara*, *Hif1a*, *Rb1*, *Esr1* et *Cebpb*). L'analyse statistique a été réalisée par le test Mann-Whitney; a - $p < 0.05$ ($n=4$).

Afin d'étudier le lien entre ces gènes identifiés et l'expression de *Sirt1*, une transfection des cellules ST2 (cellules murines commerciales) avec un siRNA de *Rb1*, a été réalisée. Nos résultats ont montré une baisse significative de l'expression de *Rb1* de -76.3% et de -49,1% (vs le siRNA négatif) après 72 heures et 7 jours de transfection respectivement. En revanche, malgré cette diminution, le niveau de l'expression de *Sirt1* n'a pas été modifié, suggérant que *Rb1* n'est pas impliqué dans la régulation de *Sirt1* (Fig. 83).

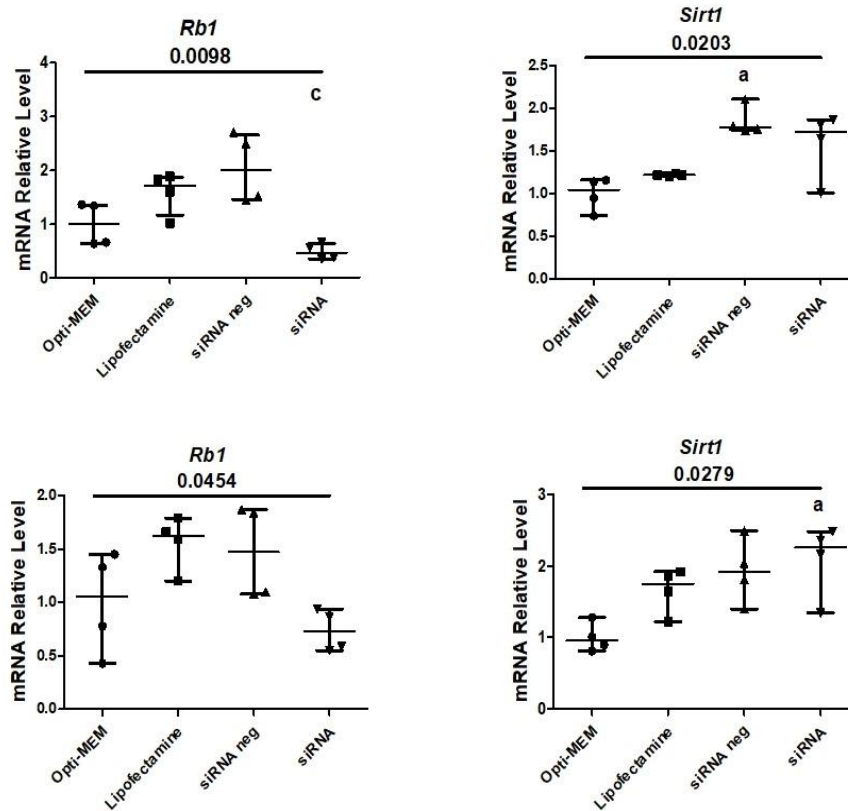


Figure 83. Etude de l'effet de la transfection avec un siRNA *Rb1* sur l'expression de *Sirt1* dans les cellules ST2. A-B. Le niveau d'ARNm de *Rb1* et *Sirt1* dans les cellules ST2 traitées avec 50nM de siRNA *Rb1* pendant 72 heures; C-D. Le niveau d'ARNm de *Rb1* et *Sirt1* dans les cellules ST2 traitées avec 50nM de siRNA *Rb1* pendant 7 jours. L'analyse statistique a été réalisée par les tests Kruskal Wallis et le Dunn's Multiple Comparison; a - $p < 0.05$ (n=4) vs l' Opti-MEM; c - $p < 0.05$ vs le siRNA négatif.

2.2.2 Etude de l'interaction entre SIRT1 et la voie de signalisation de l'AMPK

Plusieurs études ont montré une interaction entre la voie de l'AMPK et SIRT1 notamment pour réguler le métabolisme énergétique via la régulation de l'activité des facteurs de transcriptions comme PGC1 et FOXO (809). En plus, il a été montré que la restriction calorique ainsi que le resvératrol (activateur de SIRT1) stimulent l'expression de l'AMPK et *Sirt1* suggérant ainsi une connexion entre les deux voies (1040–1042).

Dans ce contexte, l'hypothèse de cette partie de la thèse, est que la diminution de l'expression de *Sirt1*, dans les cellules stromales issues des souris SBA (10 semaines et -18% de perte de poids) serait associée à une diminution de l'expression de l'AMPK.

Ainsi, nous avons mesuré le niveau d'ARNm de la sous unité alpha-1 (*Prkaa1*) et alpha -2 (*Prkaa2*) de l'AMPK dans les cellules stromales des souris SBA et contrôles. Nos résultats ont montré que la diminution de l'expression de *Sirt1* s'accompagne d'une baisse significative de l'expression de *Prkaa1* (-66% vs. CT) et d'une augmentation de l'expression de *Prkaa2* (+230% vs. CT). Ces résultats montrent que la voie de l'AMPK pourrait être impliquée dans la régulation de l'expression de *Sirt1* et qu'il existe une compensation entre les deux isoformes (Fig. 84).

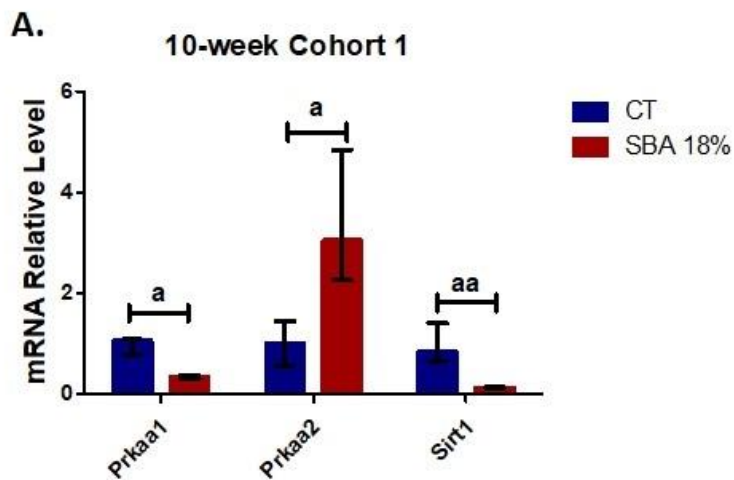


Figure 84. Mesure de l'expression de *Prkaa1* et *Prkaa2* dans les cellules stromales issues des souris SBA à 10 semaines et à -18% de degré de sévérité. L'analyse statistique a été réalisée par le test Mann-Whitney; a - $p < 0.05$ (n=4).

Afin d'explorer davantage le lien entre *Sirt1* et l'AMPK, nous avons traité pendant 14 heures les cellules ST2 et les cellules stromales issues des souris contrôles (BMSC) avec 20 μ M de dorsomorphine, inhibiteur spécifique de l'AMPK, afin d'étudier l'effet de l'inhibition de cette voie de signalisation sur l'expression de *Sirt1*. En effet, nos résultats ont montré que la diminution de l'expression de *Prkaa1* (-57% vs. CT dans les BMSC et -72% vs. CT dans les ST2) par la dorsomorphine s'accompagne d'une forte diminution de l'expression de *Sirt1* (-92% et -54% vs. CT dans les BMSC et ST2 respectivement) (Fig. 85). Ces résultats montrent que seulement l'isoforme *Prkaa1* semble être impliqué dans la régulation de *Sirt1*.

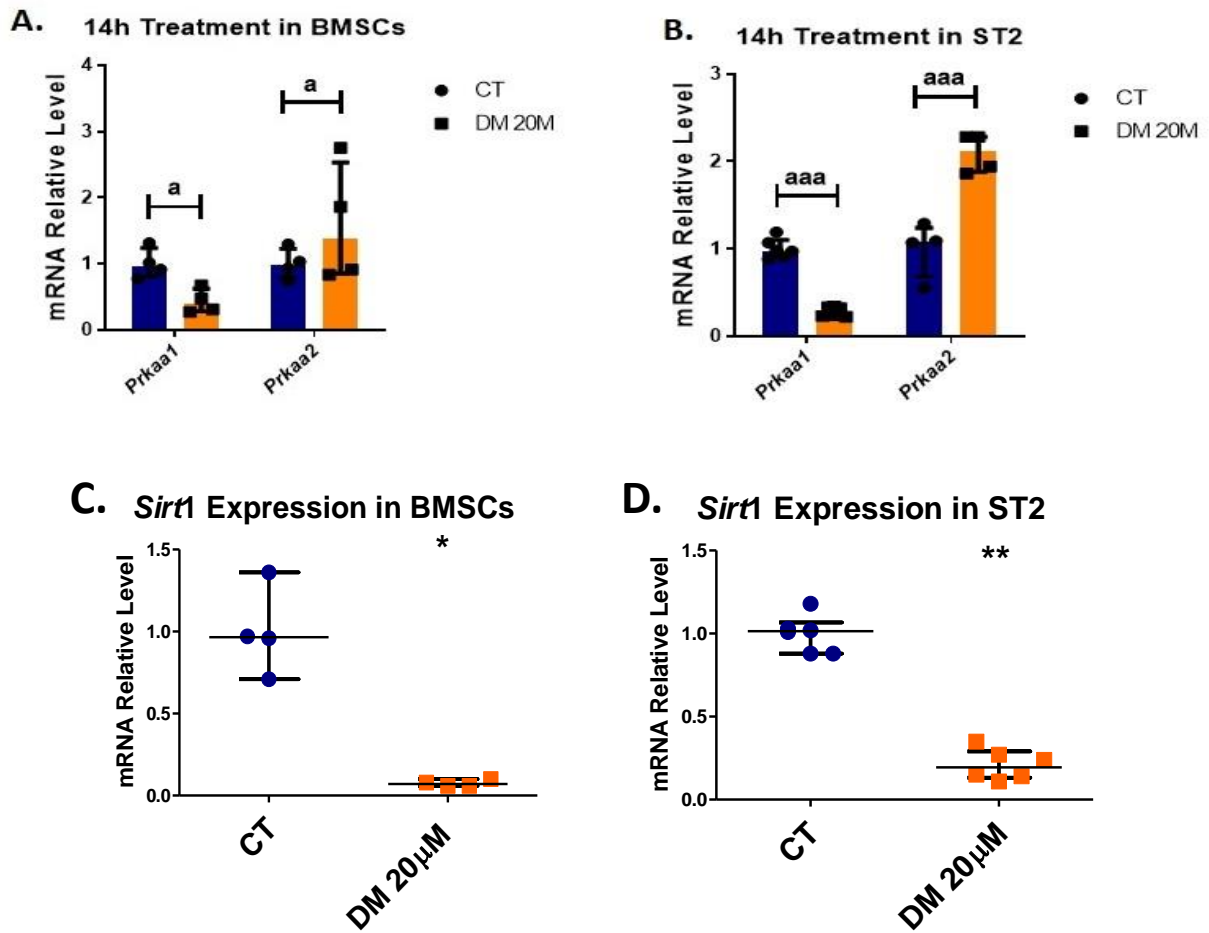


Figure 85. Effets de la dorsomorphine (DM) sur l'expression de l'AMPK (*Prkaa1* et *Prkaa2*) et *Sirt1*. A-B. Niveaux d'expressions de *Prkaa1* et *Prkaa2* dans les cellules stromales (BMSC) et ST2 traitées avec 20µM de DM pendant 14 heures; C-D. Expressions de *Sirt1* dans les cellules stromales (BMSC) et ST2 traitées avec 20µM de DM pendant 14 heures. L'analyse statistique a été réalisée par le test Mann-Whitney; a et * - $p < 0.05$, aaa et ** - $p < 0.0005$ (n=4).

Enfin, afin de confirmer l'effet négatif de *Prkaa1* sur l'expression de *Sirt1*, nous avons transfecté les cellules ST2 par 50nM d'un siRNA dirigé contre *Prkaa1* et 50nM d'un siRNA dirigé contre *Prkaa2* pendant 72 heures et 7 jours. Nos résultats ont montré que seulement la diminution de l'expression de *Prkaa1* s'accompagne d'une baisse significative de l'expression de *Sirt1* après 72h ou 7 jours de transfection (Fig. 86). En revanche, malgré la diminution de l'expression de *Prkaa2*, aucune modification de l'expression de *Sirt1* n'a été détectée. Ces résultats confirment que seulement la diminution de l'expression de *Prkaa1* est responsable de la diminution de l'expression de *Sirt1* montrant ainsi que l'AMPK est un régulateur de *Sirt1*.

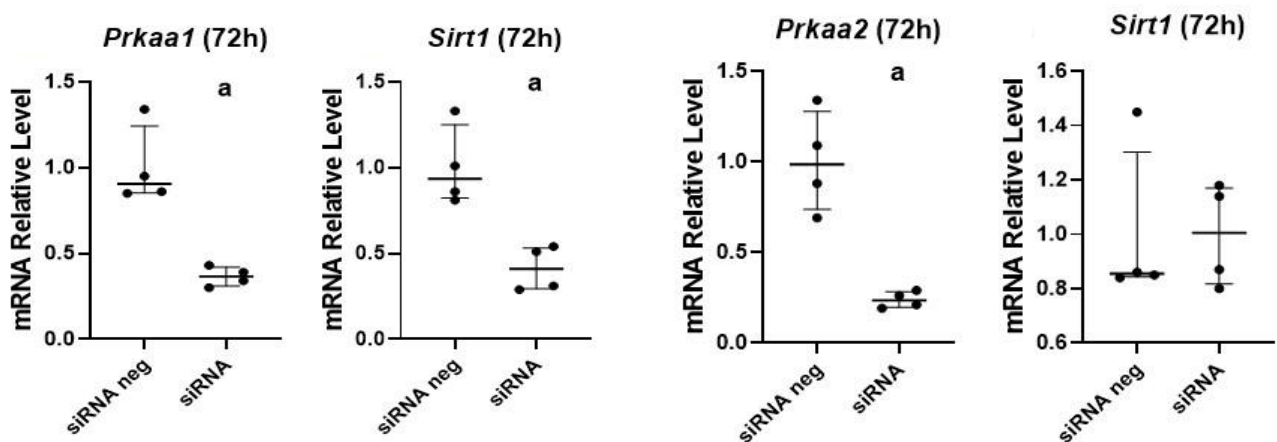


Figure 86. Effets de la transfection avec un siRNA *Prkaa1* et un siRNA *Prkaa2* sur l'expression de *Sirt1*. Les cellules ST2 ont été transfectées par 50nM d'un siRNA *Prkaa1* et 50nM d'un siRNA *Prkaa2*. Le niveau d'ARNm de *Sirt1* a été mesuré par la PCR-quantitative après 72 heures de transfection. L'analyse statistique (n=4) a été réalisée par le test Mann-Whitney; a - p<0.05 vs. siRNA négatif (siRNA neg).

3. Conclusions et perspectives

Ce projet de thèse nous a conduit aux conclusions suivantes:

- Le degré de sévérité ainsi que la durée du protocole SBA peuvent affecter les paramètres osseux, l'expression de *Sirt1* et la capacité de différenciation des cellules stromales en ostéoblastes et adipocytes;
- La diminution de l'expression de *Sirt1* chez les souris de -18% et -24% de degré de sévérité et à 10 semaines de protocole SBA s'accompagne d'une augmentation de l'adipogénèse au détriment de l'ostéogénèse;

- Les données de RNA-Seq ont fait l'objet d'une étude préliminaire qui a permis une première mise en évidence de quelques gènes potentiellement impliqués dans la régulation de *Sirt1* (*Rleb*, *Rara*, *Hif1a*, *Esr1*, *Cebpb* et *Rb1*);
- La diminution de l'expression de *Rb1* par le siRNA n'a pas impacté l'expression de *Sirt1* montrant que ce gène n'est pas un régulateur de *Sirt1*;
- L'analyse de la voie de signalisation de l'AMPK par l'emploi d'un inhibiteur comme la dorsomorphine et par transfection avec des siRNA de l'isoforme *Prkaa1* et l'isoforme *Prkaa2*, a montré que seulement *Prkaa1* est responsable de la diminution de l'expression de *Sirt1*;

Ci-dessous un schéma bilan montrant les réponses aux principales questions abordées dans le cadre de cette thèse (Fig. 87).

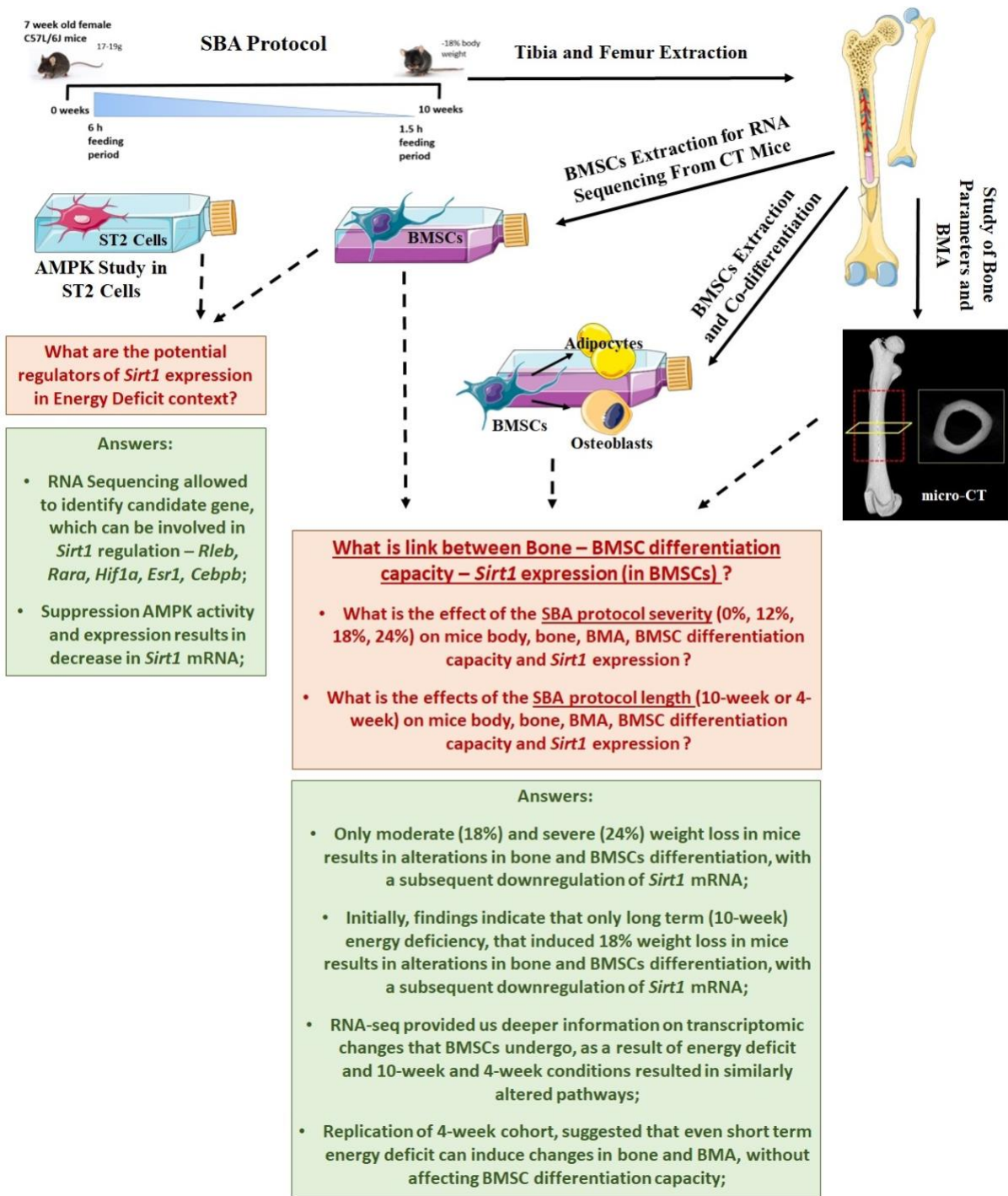


Figure 87. Bilan du travail de la thèse représentant les réponses aux principales questions abordées dans le cadre de ce projet de recherche.

Components of the diagram were taken from <https://smart.servier.com/>. Micro-CT diagram adapted from Hsu *et al.*, 2014 (182).

Perspectives

Etant donné que tous les résultats du modèle SBA, étaient obtenus à partir d'une population hétérogène, il serait intéressant de caractériser par cytométrie de flux la proportion des cellules stromales (CD45⁻CD31⁻Sca1⁺CD24⁺), hématopoïétiques et les pré-adipocytes (Zfp423⁺).

Nous envisageons de poursuivre les analyses du RNA-seq par l'utilisation des tests fonctionnels comme l'emploi des siRNA dirigés contre *Rleb*, *Rara*, *Hif1a*, *Esr1*, *Cebpb* afin d'identifier de nouveaux régulateurs de *Sirt1*.

Enfin, comme les cellules stromales des souris SBA (10 semaines et -18%) présentent une diminution durable de l'expression de *Sirt1* après 48 de culture et 14 jours de différenciation, il serait intéressant, d'étudier les régulateurs épigénétiques au niveau du promoteur de *Sirt1* par immunoprécipitation à la chromatine (ChIP) afin d'identifier de nouveaux gènes responsables de la diminution de l'expression de *Sirt1*.

BIBLIOGRAPHY

1. Zgheib S, Méquinion M, Lucas S, Leterme D, Ghali O, Tolle V, et al. Long-Term Physiological Alterations and Recovery in a Mouse Model of Separation Associated with Time-Restricted Feeding: A Tool to Study Anorexia Nervosa Related Consequences. *PLOS ONE*. 2014 Aug 4;9(8):e103775.
2. Louvet L, Leterme D, Delplace S, Miellot F, Marchandise P, Gauthier V, et al. Sirtuin 1 deficiency decreases bone mass and increases bone marrow adiposity in a mouse model of chronic energy deficiency. *Bone*. 2020 Jul 1;136:115361.
3. Friedenstein AJ, Chailakhjan RK, Lalykina KS. THE DEVELOPMENT OF FIBROBLAST COLONIES IN MONOLAYER CULTURES OF GUINEA-PIG BONE MARROW AND SPLEEN CELLS. *Cell Prolif*. 1970 Oct 1;3(4):393–403.
4. Crisan M, Yap S, Casteilla L, Chen CW, Corselli M, Park TS, et al. A Perivascular Origin for Mesenchymal Stem Cells in Multiple Human Organs. *Cell Stem Cell*. 2008 Sep 11;3(3):301–13.
5. da Silva Meirelles L, Caplan AI, Nardi NB. In Search of the In Vivo Identity of Mesenchymal Stem Cells. *Stem Cells*. 2008 Sep 1;26(9):2287–99.
6. Mafi R, Hindocha S, Mafi P, Griffin M, Khan WS. Sources of adult mesenchymal stem cells applicable for musculoskeletal applications - a systematic review of the literature. *Open Orthop J*. 2011/07/28 ed. 2011;5 Suppl 2:242–8.
7. Tuan RS, Boland G, Tuli R. Adult mesenchymal stem cells and cell-based tissue engineering. *Arthritis Res Ther*. 2002/12/11 ed. 2003;5(1):32–45.
8. Taichman RS. Blood and bone: two tissues whose fates are intertwined to create the hematopoietic stem-cell niche. *Blood*. 2005 Apr 1;105(7):2631–9.
9. Sommerfeldt DW, Rubin CT. Biology of bone and how it orchestrates the form and function of the skeleton. *Eur Spine J Off Publ Eur Spine Soc Eur Spinal Deform Soc Eur Sect Cerv Spine Res Soc*. 2001 Oct;10 Suppl 2(Suppl 2):S86–95.
10. Rucci N. Molecular biology of bone remodelling. *Clin Cases Miner Bone Metab Off J Ital Soc Osteoporos Miner Metab Skelet Dis*. 2008 Jan;5(1):49–56.
11. Clarke B. Normal bone anatomy and physiology. *Clin J Am Soc Nephrol CJASN*. 2008 Nov;3 Suppl 3(Suppl 3):S131–9.
12. Hall BK, Miyake T. The membranous skeleton: the role of cell condensations in vertebrate skeletogenesis. *Anat Embryol (Berl)*. 2004;186:107–24.
13. Maes C, Kobayashi T, Selig MK, Torrekens S, Roth SI, Mackem S, et al. Osteoblast precursors, but not mature osteoblasts, move into developing and fractured bones along with invading blood vessels. *Dev Cell*. 2010 Aug 17;19(2):329–44.

14. Kronenberg HM. Developmental regulation of the growth plate. *Nature*. 2003 May 1;423(6937):332–6.
15. Karsenty G, Wagner EF. Reaching a Genetic and Molecular Understanding of Skeletal Development. *Dev Cell*. 2002 Apr 1;2(4):389–406.
16. Berendsen AD, Olsen BR. Bone development. *Bone*. 2015 Nov;80:14–8.
17. Black C. The use of translational models to assess potential novel strategies in bone tissue engineering. 2017.
18. Buckwalter JA, Glimcher MJ, Cooper RR, Recker RR. Bone biology. I: Structure, blood supply, cells, matrix, and mineralization. *Instr Course Lect*. 1996;45:371–86.
19. Downey PA, Siegel MI. Bone Biology and the Clinical Implications for Osteoporosis. *Phys Ther*. 2006 Jan 1;86(1):77–91.
20. Zaidi M. Skeletal remodeling in health and disease. *Nat Med*. 2007 Jul 1;13(7):791–801.
21. Cohen HY, Miller C, Bitterman KJ, Wall NR, Hekking B, Kessler B, et al. Calorie Restriction Promotes Mammalian Cell Survival by Inducing the SIRT1 Deacetylase. *Science*. 2004 Jul 16;305(5682):390.
22. Roodman GD. Cell biology of the osteoclast. *Exp Hematol*. 1999 Aug 1;27(8):1229–41.
23. Manolagas SC. Birth and Death of Bone Cells: Basic Regulatory Mechanisms and Implications for the Pathogenesis and Treatment of Osteoporosis*. *Endocr Rev*. 2000 Apr 1;21(2):115–37.
24. Anderson HC. Matrix vesicles and calcification. *Curr Rheumatol Rep*. 2003 May 1;5(3):222–6.
25. Burger EH, Klein-Nulend J, Smit TH. Strain-derived canalicular fluid flow regulates osteoclast activity in a remodelling osteon—a proposal. *Bone Cell Tissue Mech*. 2003 Oct 1;36(10):1453–9.
26. Asada N, Sato M, Katayama Y. Communication of bone cells with hematopoiesis, immunity and energy metabolism. *BoneKEy Rep*. 2015 Oct 7;4:748–748.
27. Han Y, You X, Xing W, Zhang Z, Zou W. Paracrine and endocrine actions of bone—the functions of secretory proteins from osteoblasts, osteocytes, and osteoclasts. *Bone Res*. 2018 May 24;6:16–16.
28. Su N, Yang J, Xie Y, Du X, Chen H, Zhou H, et al. Bone function, dysfunction and its role in diseases including critical illness. *Int J Biol Sci*. 2019 Jan 29;15(4):776–87.
29. Xie Y, Yin T, Wiegand W, He XC, Miller D, Stark D, et al. Detection of functional haematopoietic stem cell niche using real-time imaging. *Nature*. 2009 Jan 1;457(7225):97–101.

30. Deguchi K, Yagi H, Inada M, Yoshizaki K, Kishimoto T, Komori T. Excessive Extramedullary Hematopoiesis in Cbfa1-Deficient Mice with a Congenital Lack of Bone Marrow. *Biochem Biophys Res Commun*. 1999 Feb 16;255(2):352–9.
31. Komori T, Yagi H, Nomura S, Yamaguchi A, Sasaki K, Deguchi K, et al. Targeted Disruption of Cbfa1 Results in a Complete Lack of Bone Formation owing to Maturational Arrest of Osteoblasts. *Cell*. 1997 May 30;89(5):755–64.
32. Visnjic D, Kalajzic Z, Rowe DW, Katavic V, Lorenzo J, Aguila HL. Hematopoiesis is severely altered in mice with an induced osteoblast deficiency. *Blood*. 2004 May 1;103(9):3258–64.
33. Calvi LM, Adams GB, Weibrecht KW, Weber JM, Olson DP, Knight MC, et al. Osteoblastic cells regulate the haematopoietic stem cell niche. *Nature*. 2003 Oct 1;425(6960):841–6.
34. Sugimura R, He XC, Venkatraman A, Arai F, Box A, Semerad C, et al. Noncanonical Wnt signaling maintains hematopoietic stem cells in the niche. *Cell*. 2012 Jul 20;150(2):351–65.
35. Yoshihara H, Arai F, Hosokawa K, Hagiwara T, Takubo K, Nakamura Y, et al. Thrombopoietin/MPL Signaling Regulates Hematopoietic Stem Cell Quiescence and Interaction with the Osteoblastic Niche. *Cell Stem Cell*. 2007 Dec 13;1(6):685–97.
36. Arai F, Hirao A, Ohmura M, Sato H, Matsuoka S, Takubo K, et al. Tie2/Angiopoietin-1 Signaling Regulates Hematopoietic Stem Cell Quiescence in the Bone Marrow Niche. *Cell*. 2004 Jul 23;118(2):149–61.
37. Zhu J, Garrett R, Jung Y, Zhang Y, Kim N, Wang J, et al. Osteoblasts support B-lymphocyte commitment and differentiation from hematopoietic stem cells. *Blood*. 2007 Jan 16;109(9):3706–12.
38. Terashima A, Okamoto K, Nakashima T, Akira S, Ikuta K, Takayanagi H. Sepsis-Induced Osteoblast Ablation Causes Immunodeficiency. *Immunity*. 2016 Jun 21;44(6):1434–43.
39. Tzeng YS, Li H, Kang YL, Chen WC, Cheng WC, Lai DM. Loss of Cxcl12/Sdf-1 in adult mice decreases the quiescent state of hematopoietic stem/progenitor cells and alters the pattern of hematopoietic regeneration after myelosuppression. *Blood*. 2011 Jan 13;117(2):429–39.
40. Adams GB, Chabner KT, Alley IR, Olson DP, Szczepiorkowski ZM, Poznansky MC, et al. Stem cell engraftment at the endosteal niche is specified by the calcium-sensing receptor. *Nature*. 2006 Feb 1;439(7076):599–603.
41. Kollet O, Dar A, Shivtiel S, Kalinkovich A, Lapid K, Sztainberg Y, et al. Osteoclasts degrade endosteal components and promote mobilization of hematopoietic progenitor cells. *Nat Med*. 2006 Jun 1;12(6):657–64.
42. Heissig B, Hattori K, Dias S, Friedrich M, Ferris B, Hackett NR, et al. Recruitment of stem and progenitor cells from the bone marrow niche requires MMP-9 mediated release of kit-ligand. *Cell*. 2002 May 31;109(5):625–37.

43. Mansour A, Abou-Ezzi G, Sitnicka E, Jacobsen SEW, Wakkach A, Blin-Wakkach C. Osteoclasts promote the formation of hematopoietic stem cell niches in the bone marrow. *J Exp Med*. 2012/02/20 ed. 2012 Mar 12;209(3):537–49.
44. Fulzele K, Krause DS, Panaroni C, Saini V, Barry KJ, Liu X, et al. Myelopoiesis is regulated by osteocytes through Gs α -dependent signaling. *Blood*. 2013 Feb 7;121(6):930–9.
45. Sato M, Asada N, Kawano Y, Wakahashi K, Minagawa K, Kawano H, et al. Osteocytes Regulate Primary Lymphoid Organs and Fat Metabolism. *Cell Metab*. 2013 Nov 5;18(5):749–58.
46. Moser SC, van der Eerden BCJ. Osteocalcin-A Versatile Bone-Derived Hormone. *Front Endocrinol*. 2019 Jan 10;9:794–794.
47. Kanazawa I. Osteocalcin as a hormone regulating glucose metabolism. *World J Diabetes*. 2015 Dec 25;6(18):1345–54.
48. Ferron M, Hinoi E, Karsenty G, Ducy P. Osteocalcin differentially regulates beta cell and adipocyte gene expression and affects the development of metabolic diseases in wild-type mice. *Proc Natl Acad Sci U S A*. 2008/03/24 ed. 2008 Apr 1;105(13):5266–70.
49. Lee NK, Sowa H, Hinoi E, Ferron M, Ahn JD, Confavreux C, et al. Endocrine regulation of energy metabolism by the skeleton. *Cell*. 2007 Aug 10;130(3):456–69.
50. Ducy P, Desbois C, Boyce B, Pinero G, Story B, Dunstan C, et al. Increased bone formation in osteocalcin-deficient mice. *Nature*. 1996 Aug 1;382(6590):448–52.
51. Fulzele K, Riddle RC, DiGirolamo DJ, Cao X, Wan C, Chen D, et al. Insulin receptor signaling in osteoblasts regulates postnatal bone acquisition and body composition. *Cell*. 2010 Jul 23;142(2):309–19.
52. Ferron M, Wei J, Yoshizawa T, Del Fattore A, DePinho RA, Teti A, et al. Insulin Signaling in Osteoblasts Integrates Bone Remodeling and Energy Metabolism. *Cell*. 2010 Jul 23;142(2):296–308.
53. Weivoda MM, Oursler MJ. Developments in sclerostin biology: regulation of gene expression, mechanisms of action, and physiological functions. *Curr Osteoporos Rep*. 2014 Mar;12(1):107–14.
54. Kim SP, Frey JL, Li Z, Kushwaha P, Zoch ML, Tomlinson RE, et al. Sclerostin influences body composition by regulating catabolic and anabolic metabolism in adipocytes. *Proc Natl Acad Sci U S A*. 2017/12/11 ed. 2017 Dec 26;114(52):E11238–47.
55. Fulzele K, Lai F, Dedic C, Saini V, Uda Y, Shi C, et al. Osteocyte-Secreted Wnt Signaling Inhibitor Sclerostin Contributes to Beige Adipogenesis in Peripheral Fat Depots. *J Bone Miner Res Off J Am Soc Bone Miner Res*. 2017/01/05 ed. 2017 Feb;32(2):373–84.
56. Itoh N, Ohta H, Konishi M. Endocrine FGFs: Evolution, Physiology, Pathophysiology, and Pharmacotherapy. *Front Endocrinol*. 2015 Sep 29;6:154–154.

57. White KE, Evans WE, O’Riordan JLH, Speer MC, Econs MJ, Lorenz-Depiereux B, et al. Autosomal dominant hypophosphataemic rickets is associated with mutations in FGF23. *Nat Genet.* 2000 Nov 1;26(3):345–8.
58. Garringer HJ, Malekpour M, Esteghamat F, Mortazavi SMJ, Davis SI, Farrow EG, et al. Molecular genetic and biochemical analyses of FGF23 mutations in familial tumoral calcinosis. *Am J Physiol Endocrinol Metab.* 2008/08/05 ed. 2008 Oct;295(4):E929–37.
59. PRINCE MJ, SCHAEFER PC, GOLDSMITH RS, CHAUSMER AB. Hyperphosphatemic Tumoral Calcinosis. *Ann Intern Med.* 1982 May 1;96(5):586–91.
60. MITNICK PD, GOLDFARB S, SLATOPOLSKY E, LEMANN J, GRAY RW, AGUS ZS. Calcium and Phosphate Metabolism in Tumoral Calcinosis. *Ann Intern Med.* 1980 Apr 1;92(4):482–7.
61. Shimada T, Hasegawa H, Yamazaki Y, Muto T, Hino R, Takeuchi Y, et al. FGF-23 Is a Potent Regulator of Vitamin D Metabolism and Phosphate Homeostasis. *J Bone Miner Res.* 2004 Mar 1;19(3):429–35.
62. Shimada T, Mizutani S, Muto T, Yoneya T, Hino R, Takeda S, et al. Cloning and characterization of FGF23 as a causative factor of tumor-induced osteomalacia. *Proc Natl Acad Sci U S A.* 2001/05/08 ed. 2001 May 22;98(11):6500–5.
63. Kuro-o M. Klotho as a regulator of fibroblast growth factor signaling and phosphate/calcium metabolism. *Curr Opin Nephrol Hypertens* [Internet]. 2006;15(4). Available from: https://journals.lww.com/co-nephrolhypertens/Fulltext/2006/07000/Klotho_as_a_regulator_of_fibroblast_growth_factor.13.aspx
64. Shimada T, Urakawa I, Yamazaki Y, Hasegawa H, Hino R, Yoneya T, et al. FGF-23 transgenic mice demonstrate hypophosphatemic rickets with reduced expression of sodium phosphate cotransporter type IIa. *Biochem Biophys Res Commun.* 2004 Feb 6;314(2):409–14.
65. Andrukhova O, Smorodchenko A, Egerbacher M, Streicher C, Zeitz U, Goetz R, et al. FGF23 promotes renal calcium reabsorption through the TRPV5 channel. *EMBO J.* 2014/01/16 ed. 2014 Feb 3;33(3):229–46.
66. Murali SK, Roschger P, Zeitz U, Klaushofer K, Andrukhova O, Erben RG. FGF23 Regulates Bone Mineralization in a 1,25(OH)2D3 and Klotho-Independent Manner. *J Bone Miner Res.* 2016 Jan 1;31(1):129–42.
67. Addison WN, Azari F, Sørensen ES, Kaartinen MT, McKee MD. Pyrophosphate Inhibits Mineralization of Osteoblast Cultures by Binding to Mineral, Up-regulating Osteopontin, and Inhibiting Alkaline Phosphatase Activity *. *J Biol Chem.* 2007 May 25;282(21):15872–83.
68. Mera P, Laue K, Ferron M, Confavreux C, Wei J, Galán-Díez M, et al. Osteocalcin Signaling in Myofibers Is Necessary and Sufficient for Optimum Adaptation to Exercise. *Cell Metab.* 2016 Jun 14;23(6):1078–92.

69. Mohammad Rahimi GR, Bijeh N, Rashidlamir A. Effects of exercise training on serum preptin, undercarboxylated osteocalcin and high molecular weight adiponectin in adults with metabolic syndrome. *Exp Physiol*. 2020 Mar 1;105(3):449–59.
70. Mera P, Laue K, Wei J, Berger JM, Karsenty G. Osteocalcin is necessary and sufficient to maintain muscle mass in older mice. *Mol Metab*. 2016 Jul 16;5(10):1042–7.
71. Oury F, Sumara G, Sumara O, Ferron M, Chang H, Smith CE, et al. Endocrine regulation of male fertility by the skeleton. *Cell*. 2011/02/17 ed. 2011 Mar 4;144(5):796–809.
72. Oury F, Khrimian L, Denny CA, Gardin A, Chamouni A, Goeden N, et al. Maternal and offspring pools of osteocalcin influence brain development and functions. *Cell*. 2013 Sep 26;155(1):228–41.
73. Khrimian L, Obri A, Ramos-Brossier M, Rousseaud A, Moriceau S, Nicot AS, et al. Gpr158 mediates osteocalcin's regulation of cognition. *J Exp Med*. 2017/08/29 ed. 2017 Oct 2;214(10):2859–73.
74. Nakamura M, Imaoka M, Takeda M. Interaction of bone and brain: osteocalcin and cognition. *Int J Neurosci*. 2021 Nov 2;131(11):1115–23.
75. Birsoy K, Festuccia WT, Laplante M. A comparative perspective on lipid storage in animals. *J Cell Sci*. 2013 Apr 1;126(7):1541.
76. Suchacki KJ, Cawthorn WP, Rosen CJ. Bone marrow adipose tissue: formation, function and regulation. *Curr Opin Pharmacol*. 2016/03/26 ed. 2016 Jun;28:50–6.
77. Peirce V, Carobbio S, Vidal-Puig A. The different shades of fat. *Nature*. 2014 Jun 1;510(7503):76–83.
78. Piotrowska K, Tarnowski M. Bone Marrow Adipocytes—Role in Physiology and Various Nutritional Conditions in Human and Animal Models. *Nutrients*. 2021;13(5).
79. Torres N, Vargas-Castillo AE, Tovar AR. Adipose Tissue: White Adipose Tissue Structure and Function. In: Caballero B, Finglas PM, Toldrá F, editors. *Encyclopedia of Food and Health* [Internet]. Oxford: Academic Press; 2016. p. 35–42. Available from: <http://www.sciencedirect.com/science/article/pii/B9780123849472000064>
80. Tsiloulis T, Watt MJ. Chapter Eight - Exercise and the Regulation of Adipose Tissue Metabolism. In: Bouchard C, editor. *Progress in Molecular Biology and Translational Science* [Internet]. Academic Press; 2015. p. 175–201. Available from: <http://www.sciencedirect.com/science/article/pii/S1877117315001301>
81. Jung SM, Sanchez-Gurmaches J, Guertin D. Brown Adipose Tissue Development and Metabolism. *Handb Exp Pharmacol*. 2019;251:3–36.
82. Kaisanlahti A, Glumoff T. Browning of white fat: agents and implications for beige adipose tissue to type 2 diabetes. *J Physiol Biochem*. 2019 Feb 1;75(1):1–10.
83. Li Y, Meng Y, Yu X. The Unique Metabolic Characteristics of Bone Marrow Adipose Tissue. *Front Endocrinol*. 2019;10:69.

84. El Hadi H, Di Vincenzo A, Vettor R, Rossato M. Food Ingredients Involved in White-to-Brown Adipose Tissue Conversion and in Calorie Burning. *Front Physiol.* 2019;9:1954.
85. Virtanen KA. Adipose Tissue: Structure and Function of Brown Adipose Tissue. In: Caballero B, Finglas PM, Toldrá F, editors. *Encyclopedia of Food and Health* [Internet]. Oxford: Academic Press; 2016. p. 30–4. Available from: <http://www.sciencedirect.com/science/article/pii/B9780123849472000076>
86. Napolitano A, Lowell B, Damm D, Leibel R, Ravussin E, Jimerson D, et al. Concentrations of adiponectin in blood and rates of adiponectin secretion by adipose tissue in humans with normal, elevated and diminished adipose tissue mass. *Int J Obes Relat Metab Disord.* 1994 Apr;18(4):213–8.
87. Helfer G, Wu QF. Chemerin: a multifaceted adipokine involved in metabolic disorders. *J Endocrinol.* 2018 Aug 1;238(2):R79–94.
88. Carrière A, Casteilla L. Chapter 7 - Role of Mitochondria in Adipose Tissues Metabolism and Plasticity. In: Morio B, Pénicaud L, Rigoulet M, editors. *Mitochondria in Obesity and Type 2 Diabetes* [Internet]. Academic Press; 2019. p. 173–94. Available from: <http://www.sciencedirect.com/science/article/pii/B9780128117521000079>
89. Rosen ED, Spiegelman BM. Adipocytes as regulators of energy balance and glucose homeostasis. *Nature.* 2006 Dec 1;444(7121):847–53.
90. Booth A, Magnuson A, Fouts J, Foster MT. Adipose tissue: an endocrine organ playing a role in metabolic regulation. *Horm Mol Biol Clin Investig.* 2016 Apr 1;26(1):25–42.
91. Galic S, Oakhill JS, Steinberg GR. Adipose tissue as an endocrine organ. *Endocr Asp Obes.* 2010 Mar 25;316(2):129–39.
92. Yilmaz M, Claiborn KC, Hotamisligil GS. De Novo Lipogenesis Products and Endogenous Lipokines. *Diabetes.* 2016/06/10 ed. 2016 Jul;65(7):1800–7.
93. CANNON B, NEDERGAARD J. Brown Adipose Tissue: Function and Physiological Significance. *Physiol Rev.* 2004 Jan 1;84(1):277–359.
94. Kalinovich AV, de Jong JMA, Cannon B, Nedergaard J. UCP1 in adipose tissues: two steps to full browning. *UCP1 40 Years Beyond.* 2017 Mar 1;134:127–37.
95. Fedorenko A, Lishko PV, Kirichok Y. Mechanism of fatty-acid-dependent UCP1 uncoupling in brown fat mitochondria. *Cell.* 2012 Oct 12;151(2):400–13.
96. Cousin B, Cinti S, Morrioni M, Raimbault S, Ricquier D, Penicaud L, et al. Occurrence of brown adipocytes in rat white adipose tissue: molecular and morphological characterization. *J Cell Sci.* 1992 Dec 1;103(4):931.
97. Young P, Arch JRS, Ashwell M. Brown adipose tissue in the parametrial fat pad of the mouse. *FEBS Lett.* 1984 Feb 13;167(1):10–4.
98. Zoico E, Rubele S, De Caro A, Nori N, Mazzali G, Fantin F, et al. Brown and Beige Adipose Tissue and Aging. *Front Endocrinol.* 2019;10:368.

99. Beresford JN, Bennett JH, Devlin C, Leboy PS, Owen ME. Evidence for an inverse relationship between the differentiation of adipocytic and osteogenic cells in rat marrow stromal cell cultures. *J Cell Sci.* 1992 Jun 1;102(2):341.
100. Krings A, Rahman S, Huang S, Lu Y, Czernik PJ, Lecka-Czernik B. Bone marrow fat has brown adipose tissue characteristics, which are attenuated with aging and diabetes. *Bone.* 2011/06/24 ed. 2012 Feb;50(2):546–52.
101. Lecka-Czernik B, Stechschulte LA, Czernik PJ, Sherman SB, Huang S, Krings A. Marrow Adipose Tissue: Skeletal Location, Sexual Dimorphism, and Response to Sex Steroid Deficiency. *Front Endocrinol.* 2017;8:188.
102. Kahn BB. Adipose Tissue, Inter-Organ Communication, and the Path to Type 2 Diabetes: The 2016 Banting Medal for Scientific Achievement Lecture. *Diabetes.* 2019 Jan 1;68(1):3.
103. Zhao S, Torres A, Henry RA, Trefely S, Wallace M, Lee JV, et al. ATP-Citrate Lyase Controls a Glucose-to-Acetate Metabolic Switch. *Cell Rep.* 2016 Oct 18;17(4):1037–52.
104. Tong L, Harwood HJ Jr. Acetyl-coenzyme A carboxylases: versatile targets for drug discovery. *J Cell Biochem.* 2006 Dec 15;99(6):1476–88.
105. Menendez JA, Lupu R. Fatty acid synthase and the lipogenic phenotype in cancer pathogenesis. *Nat Rev Cancer.* 2007 Oct 1;7(10):763–77.
106. Ntambi JM, Miyazaki M, Stoehr JP, Lan H, Kendziora CM, Yandell BS, et al. Loss of stearoyl-CoA desaturase-1 function protects mice against adiposity. *Proc Natl Acad Sci.* 2002 Aug 20;99(17):11482.
107. Kabashima T, Kawaguchi T, Wadzinski BE, Uyeda K. Xylulose 5-phosphate mediates glucose-induced lipogenesis by xylulose 5-phosphate-activated protein phosphatase in rat liver. *Proc Natl Acad Sci.* 2003 Apr 29;100(9):5107.
108. Davies MN, O’Callaghan BL, Towle HC. Glucose Activates ChREBP by Increasing Its Rate of Nuclear Entry and Relieving Repression of Its Transcriptional Activity *. *J Biol Chem.* 2008 Aug 29;283(35):24029–38.
109. Hurtado del Pozo C, Vesperinas-García G, Rubio MÁ, Corripio-Sánchez R, Torres-García AJ, Obregon MJ, et al. ChREBP expression in the liver, adipose tissue and differentiated preadipocytes in human obesity. *Biochim Biophys Acta BBA - Mol Cell Biol Lipids.* 2011 Dec 1;1811(12):1194–200.
110. Stoeckman AK, Ma L, Towle HC. Mlx Is the Functional Heteromeric Partner of the Carbohydrate Response Element-binding Protein in Glucose Regulation of Lipogenic Enzyme Genes*. *J Biol Chem.* 2004 Apr 9;279(15):15662–9.
111. Weiss SB, Kennedy EP. THE ENZYMATIC SYNTHESIS OF TRIGLYCERIDES. *J Am Chem Soc.* 1956 Jul 1;78(14):3550–3550.
112. Yu J, Loh K, Song Z yuan, Yang H qin, Zhang Y, Lin S. Update on glycerol-3-phosphate acyltransferases: the roles in the development of insulin resistance. *Nutr Diabetes.* 2018 May 25;8(1):34.

113. Yamashita A, Hayashi Y, Matsumoto N, Nemoto-Sasaki Y, Oka S, Tanikawa T, et al. Glycerophosphate/Acylglycerophosphate acyltransferases. *Biology*. 2014 Nov 19;3(4):801–30.
114. Carman GM, Han GS. Phosphatidic acid phosphatase, a key enzyme in the regulation of lipid synthesis. *J Biol Chem*. 2008/09/23 ed. 2009 Jan 30;284(5):2593–7.
115. Lehner R, Quiroga AD. Chapter 5 - Fatty Acid Handling in Mammalian Cells. In: Ridgway ND, McLeod RS, editors. *Biochemistry of Lipids, Lipoproteins and Membranes (Sixth Edition)* [Internet]. Boston: Elsevier; 2016. p. 149–84. Available from: <http://www.sciencedirect.com/science/article/pii/B9780444634382000055>
116. Müller G, Petry S, Aventis Pharma Germany a member of the SA group. Triacylglycerol Storage and Mobilization, Regulation of. In: *Reviews in Cell Biology and Molecular Medicine* [Internet]. American Cancer Society; 2006. Available from: <https://onlinelibrary.wiley.com/doi/abs/10.1002/3527600906.mcb.200400165>
117. Endemann G, Stanton LW, Madden KS, Bryant CM, White RT, Protter AA. CD36 is a receptor for oxidized low density lipoprotein. *J Biol Chem*. 1993 Jun 5;268(16):11811–6.
118. Summers LK, Barnes SC, Fielding BA, Beysen C, Ilic V, Humphreys SM, et al. Uptake of individual fatty acids into adipose tissue in relation to their presence in the diet. *Am J Clin Nutr*. 2000 Jun 1;71(6):1470–7.
119. Rorsman P, Ashcroft FM. Pancreatic β -Cell Electrical Activity and Insulin Secretion: Of Mice and Men. *Physiol Rev*. 2018 Jan 1;98(1):117–214.
120. Cantley LC. The Phosphoinositide 3-Kinase Pathway. *Science*. 2002 May 31;296(5573):1655.
121. Taniguchi CM, Emanuelli B, Kahn CR. Critical nodes in signalling pathways: insights into insulin action. *Nat Rev Mol Cell Biol*. 2006 Feb 1;7(2):85–96.
122. Chakrabarti P, English T, Shi J, Smas CM, Kandror KV. Mammalian target of rapamycin complex 1 suppresses lipolysis, stimulates lipogenesis, and promotes fat storage. *Diabetes*. 2010/01/12 ed. 2010 Apr;59(4):775–81.
123. Crewe C, Zhu Y, Paschoal VA, Joffin N, Ghaben AL, Gordillo R, et al. SREBP-regulated adipocyte lipogenesis is dependent on substrate availability and redox modulation of mTORC1. *JCI Insight*. 2019 Jul 16;5(15):e129397.
124. Paoletta LM, Mukherjee S, Tran CM, Bellaver B, Hugo M, Luongo TS, et al. mTORC1 restrains adipocyte lipolysis to prevent systemic hyperlipidemia. *Mol Metab*. 2020 Feb 1;32:136–47.
125. Jaworski K, Sarkadi-Nagy E, Duncan RE, Ahmadian M, Sul HS. Regulation of triglyceride metabolism. IV. Hormonal regulation of lipolysis in adipose tissue. *Am J Physiol Gastrointest Liver Physiol*. 2007/01/11 ed. 2007 Jul;293(1):G1–4.
126. Park MK. Subchapter 17A - Glucagon. In: Takei Y, Ando H, Tsutsui K, editors. *Handbook of Hormones* [Internet]. San Diego: Academic Press; 2016. p. 129-e17A-4.

Available from:

<http://www.sciencedirect.com/science/article/pii/B9780128010280001380>

127. Janah L, Kjeldsen S, Galsgaard KD, Winther-Sørensen M, Stojanovska E, Pedersen J, et al. Glucagon Receptor Signaling and Glucagon Resistance. *Int J Mol Sci.* 2019 Jul 5;20(13):3314.
128. Langin D. Control of fatty acid and glycerol release in adipose tissue lipolysis. *Mal Tissu Adipeux.* 2006 Aug 1;329(8):598–607.
129. Anthonsen MW, Rönstrand L, Wernstedt C, Degerman E, Holm C. Identification of Novel Phosphorylation Sites in Hormone-sensitive Lipase That Are Phosphorylated in Response to Isoproterenol and Govern Activation Properties in Vitro *. *J Biol Chem.* 1998 Jan 2;273(1):215–21.
130. Wang H, Hu L, Dalen K, Dorward H, Marcinkiewicz A, Russell D, et al. Activation of Hormone-sensitive Lipase Requires Two Steps, Protein Phosphorylation and Binding to the PAT-1 Domain of Lipid Droplet Coat Proteins *. *J Biol Chem.* 2009 Nov 13;284(46):32116–25.
131. Duncan RE, Ahmadian M, Jaworski K, Sarkadi-Nagy E, Sul HS. Regulation of lipolysis in adipocytes. *Annu Rev Nutr.* 2007;27:79–101.
132. Galsgaard KD, Pedersen J, Knop FK, Holst JJ, Wewer Albrechtsen NJ. Glucagon Receptor Signaling and Lipid Metabolism. *Front Physiol.* 2019;10:413.
133. Manganiello V, Vaughan M. Selective loss of adipose cell responsiveness to glucagon with growth in the rat. *J Lipid Res.* 1972 Jan 1;13(1):12–6.
134. Gravholt CH, Møller N, Jensen MD, Christiansen JS, Schmitz O. Physiological Levels of Glucagon Do Not Influence Lipolysis in Abdominal Adipose Tissue as Assessed by Microdialysis I. *J Clin Endocrinol Metab.* 2001 May 1;86(5):2085–9.
135. Xiao C, Pavlic M, Szeto L, Patterson BW, Lewis GF. Effects of Acute Hyperglucagonemia on Hepatic and Intestinal Lipoprotein Production and Clearance in Healthy Humans. *Diabetes.* 2011 Feb 1;60(2):383.
136. Pereira MJ, Thombare K, Sarsenbayeva A, Kamble PG, Almby K, Lundqvist M, et al. Direct effects of glucagon on glucose uptake and lipolysis in human adipocytes. *Mol Cell Endocrinol.* 2020 Mar 1;503:110696.
137. Camell CD, Sander J, Spadaro O, Lee A, Nguyen KY, Wing A, et al. Inflammasome-driven catecholamine catabolism in macrophages blunts lipolysis during ageing. *Nature.* 2017;550(7674):119–23.
138. Grabner GF, Xie H, Schweiger M, Zechner R. Lipolysis: cellular mechanisms for lipid mobilization from fat stores. *Nat Metab.* 2021 Nov 1;3(11):1445–65.
139. Friedman JM, Leibel RL, Siegel DS, Walsh J, Bahary N. Molecular mapping of the mouse ob mutation. *Genomics.* 1991 Dec 1;11(4):1054–62.

140. Kelesidis T, Kelesidis I, Chou S, Mantzoros CS. Narrative review: the role of leptin in human physiology: emerging clinical applications. *Ann Intern Med.* 2010 Jan 19;152(2):93–100.
141. Gettys TW. Leptin. In: Lennarz WJ, Lane MD, editors. *Encyclopedia of Biological Chemistry* [Internet]. New York: Elsevier; 2004. p. 541–5. Available from: <https://www.sciencedirect.com/science/article/pii/B0124437109003537>
142. Elias CF, Aschkenasi C, Lee C, Kelly J, Ahima RS, Bjorbaek C, et al. Leptin Differentially Regulates NPY and POMC Neurons Projecting to the Lateral Hypothalamic Area. *Neuron.* 1999 Aug 1;23(4):775–86.
143. Geerling JJ, Boon MR, Kooijman S, Parlevliet ET, Havekes LM, Romijn JA, et al. Sympathetic nervous system control of triglyceride metabolism: novel concepts derived from recent studies. *J Lipid Res.* 2013/11/27 ed. 2014 Feb;55(2):180–9.
144. Li Y, Xu S, Mihaylova MM, Zheng B, Hou X, Jiang B, et al. AMPK phosphorylates and inhibits SREBP activity to attenuate hepatic steatosis and atherosclerosis in diet-induced insulin-resistant mice. *Cell Metab.* 2011 Apr 6;13(4):376–88.
145. Miyamoto L, Ebihara K, Kusakabe T, Aotani D, Yamamoto-Kataoka S, Sakai T, et al. Leptin activates hepatic 5'-AMP-activated protein kinase through sympathetic nervous system and α 1-adrenergic receptor: a potential mechanism for improvement of fatty liver in lipodystrophy by leptin. *J Biol Chem.* 2012/09/28 ed. 2012 Nov 23;287(48):40441–7.
146. Lee M, Katerelos M, Gleich K, Galic S, Kemp BE, Mount PF, et al. Phosphorylation of Acetyl-CoA Carboxylase by AMPK Reduces Renal Fibrosis and Is Essential for the Anti-Fibrotic Effect of Metformin. *J Am Soc Nephrol JASN.* 2018/07/05 ed. 2018 Sep;29(9):2326–36.
147. Kamohara S, Burcelin R, Halaas JL, Friedman JM, Charron MJ. Acute stimulation of glucose metabolism in mice by leptin treatment. *Nature.* 1997 Sep 1;389(6649):374–7.
148. Muoio DM, Dohn GL, Fiedorek FT, Tapscott EB, Coleman RA. Leptin Directly Alters Lipid Partitioning in Skeletal Muscle. *Diabetes.* 1997 Aug 1;46(8):1360.
149. Friedman JM. Leptin and the Regulation of Body Weigh. *Keio J Med.* 2011;60(1):1–9.
150. Hebebrand J, Muller TD, Holtkamp K, Herpertz-Dahlmann B. The role of leptin in anorexia nervosa: clinical implications. *Mol Psychiatry.* 2007 Jan 1;12(1):23–35.
151. Fasshauer M, Blüher M. Adipokines in health and disease. *Trends Pharmacol Sci.* 2015 Jul 1;36(7):461–70.
152. Waki H, Yamauchi T, Kamon J, Ito Y, Uchida S, Kita S, et al. Impaired Multimerization of Human Adiponectin Mutants Associated with Diabetes: MOLECULAR STRUCTURE AND MULTIMER FORMATION OF ADIPONECTIN *. *J Biol Chem.* 2003 Oct 10;278(41):40352–63.
153. TP Combs, EB Marliss. Adiponectin signaling in the liver. *Rev Endocr Metab Disord.* 2014;15:137–47.

154. Yamauchi T, Kamon J, Waki H, Terauchi Y, Kubota N, Hara K, et al. The fat-derived hormone adiponectin reverses insulin resistance associated with both lipodystrophy and obesity. *Nat Med*. 2001 Aug 1;7(8):941–6.
155. Ruan H, Dong L. Adiponectin signaling and function in insulin target tissues. *J Mol Cell Biol*. 2016 Mar 18;8:mjw014.
156. L Qiao, B Kinney, HS Yoo, B Lee, J Schaack, J Shao. Adiponectin increases skeletal muscle mitochondrial biogenesis by suppressing mitogen-activated protein kinase phosphatase-1. *Diabetes*. 2012;61:1463–70.
157. Turer AT, Scherer PE. Adiponectin: mechanistic insights and clinical implications. *Diabetologia*. 2012 Sep 1;55(9):2319–26.
158. Lee Y ho, Magkos F, Mantzoros CS, Kang ES. Effects of leptin and adiponectin on pancreatic β -cell function. *Metabolism*. 2011 Dec;60(12):1664–72.
159. Balsan GA, Vieira JL da C, Oliveira AM de, Portal VL. Relationship between adiponectin, obesity and insulin resistance. *Rev Assoc MÃcopyrightdica Bras*. 2015;61:72–80.
160. Bylund DB, Bylund KC. Norepinephrine. In: Aminoff MJ, Daroff RB, editors. *Encyclopedia of the Neurological Sciences (Second Edition)* [Internet]. Oxford: Academic Press; 2014. p. 614–6. Available from: <http://www.sciencedirect.com/science/article/pii/B9780123851574000476>
161. Zhao J, Cannon B, Nedergaard J. α 1-Adrenergic Stimulation Potentiates the Thermogenic Action of β 3-Adrenoreceptor-generated cAMP in Brown Fat Cells *. *J Biol Chem*. 1997 Dec 26;272(52):32847–56.
162. Gaudry MJ, Campbell KL. Evolution of UCP1 Transcriptional Regulatory Elements Across the Mammalian Phylogeny. *Front Physiol*. 2017;8:670.
163. Porter C, Chondronikola M, Sidossis LS. The Therapeutic Potential of Brown Adipocytes in Humans. *Front Endocrinol*. 2015;6:156.
164. Imran KM, Yoon D, Lee TJ, Kim YS. Medicarpin induces lipolysis via activation of Protein Kinase A in brown adipocytes. *BMB Rep*. 2018 May;51(5):249–54.
165. Shih MF, Taberner PV. Selective activation of brown adipocyte hormone-sensitive lipase and cAMP production in the mouse by β 3-adrenoceptor agonists. *Biochem Pharmacol*. 1995 Aug 25;50(5):601–8.
166. Caplan AI. Mesenchymal stem cells. *J Orthop Res*. 1991 Sep 1;9(5):641–50.
167. Caplan AI. Review: Mesenchymal Stem Cells: Cell–Based Reconstructive Therapy in Orthopedics. *Tissue Eng*. 2005 Jul 1;11(7–8):1198–211.
168. Stanko P, Altanerova U, Jakubechova J, Repiska V, Altaner C. Dental Mesenchymal Stem/Stromal Cells and Their Exosomes. Heng BC, editor. *Stem Cells Int*. 2018 Apr 15;2018:8973613.

169. Wu Y, Hoogduijn MJ, Baan CC, Korevaar SS, de Kuiper R, Yan L, et al. Adipose Tissue-Derived Mesenchymal Stem Cells Have a Heterogenic Cytokine Secretion Profile. *Stem Cells Int.* 2017/05/31 ed. 2017;2017:4960831–4960831.
170. Sekiya I, Katano H, Ozeki N. Characteristics of MSCs in Synovial Fluid and Mode of Action of Intra-Articular Injections of Synovial MSCs in Knee Osteoarthritis. *Int J Mol Sci.* 2021 Mar 11;22(6):2838.
171. Bianco P, Robey PG, Simmons PJ. Mesenchymal stem cells: revisiting history, concepts, and assays. *Cell Stem Cell.* 2008 Apr 10;2(4):313–9.
172. Elsafadi M, Manikandan M, Atteya M, Hashmi JA, Iqbal Z, Aldahmash A, et al. Characterization of Cellular and Molecular Heterogeneity of Bone Marrow Stromal Cells. Mori G, editor. *Stem Cells Int.* 2016 Aug 16;2016:9378081.
173. Post S, Abdallah BM, Bentzon JF, Kassem M. Demonstration of the presence of independent pre-osteoblastic and pre-adipocytic cell populations in bone marrow-derived mesenchymal stem cells. *Bone.* 2008 Jul 1;43(1):32–9.
174. Sikora M, Śmieszek A, Marycz K. Bone marrow stromal cells (BMSCs CD45(-) /CD44(+) /CD73(+) /CD90(+)) isolated from osteoporotic mice SAM/P6 as a novel model for osteoporosis investigation. *J Cell Mol Med.* 2021/06/01 ed. 2021 Jul;25(14):6634–51.
175. Boxall SA, Jones E. Markers for Characterization of Bone Marrow Multipotential Stromal Cells. Kuçi S, editor. *Stem Cells Int.* 2012 May 14;2012:975871.
176. Kuznetsov SA, Krebsbach PH, Satomura K, Kerr J, Riminucci M, Benayahu D, et al. Single-Colony Derived Strains of Human Marrow Stromal Fibroblasts Form Bone After Transplantation In Vivo. *J Bone Miner Res.* 1997 Sep 1;12(9):1335–47.
177. Larsen KH, Frederiksen CM, Burns JS, Abdallah BM, Kassem M. Identifying a molecular phenotype for bone marrow stromal cells with in vivo bone-forming capacity. *J Bone Miner Res.* 2010 Apr 1;25(4):796–808.
178. Caplan AI, Correa D. PDGF in bone formation and regeneration: New insights into a novel mechanism involving MSCs. *J Orthop Res.* 2011 Dec 1;29(12):1795–803.
179. Cawthorn WP, Scheller EL, Learman BS, Parlee SD, Simon BR, Mori H, et al. Bone marrow adipose tissue is an endocrine organ that contributes to increased circulating adiponectin during caloric restriction. *Cell Metab.* 2014/07/03 ed. 2014 Aug 5;20(2):368–75.
180. Nehlin JO, Jafari A, Tencerova M, Kassem M. Aging and lineage allocation changes of bone marrow skeletal (stromal) stem cells. *Bone.* 2019 Jun 1;123:265–73.
181. Piney A. The Anatomy Of The Bone Marrow: With Special Reference To The Distribution Of The Red Marrow. *Br Med J.* 1922;2(3226):792–5.
182. Tavassoli M. Fatty Involution of Marrow and the Role of Adipose Tissue in Hemopoiesis. In: Tavassoli M, editor. *Handbook of the Hemopoietic Microenvironment*

- [Internet]. Totowa, NJ: Humana Press; 1989. p. 157–87. Available from:
https://doi.org/10.1007/978-1-4612-4494-3_4
183. Henke F. *Handbuch der speziellen pathologischen Anatomie und Histologie*. Vol. 2. J. Springer.; 1924.
 184. Vanden Bulcke C, Wynen M, Detobel J, La Rosa F, Absinta M, Dricot L, et al. BMAT: An open-source BIDS managing and analysis tool. *NeuroImage Clin*. 2022 Jan 1;36:103252.
 185. Suchacki KJ, Tavares AAS, Mattiucci D, Scheller EL, Papanastasiou G, Gray C, et al. Bone marrow adipose tissue is a unique adipose subtype with distinct roles in glucose homeostasis. *Nat Commun*. 2020 Jun 18;11(1):3097.
 186. Li Z, Hardij J, Bagchi DP, Scheller EL, MacDougald OA. Development, regulation, metabolism and function of bone marrow adipose tissues. *Bone*. 2018 May;110:134–40.
 187. Blebea JS, Houseni M, Torigian DA, Fan C, Mavi A, Zhuge Y, et al. Structural and Functional Imaging of Normal Bone Marrow and Evaluation of Its Age-Related Changes. *Norm Funct Struct Var PET CT MR Imaging Part II*. 2007 May 1;37(3):185–94.
 188. Suchacki KJ, Cawthorn WP. Molecular Interaction of Bone Marrow Adipose Tissue with Energy Metabolism. *Curr Mol Biol Rep*. 2018/04/28 ed. 2018;4(2):41–9.
 189. Justesen J, Stenderup K, Ebbesen EN, Mosekilde L, Steiniche T, Kassem M. Adipocyte tissue volume in bone marrow is increased with aging and in patients with osteoporosis. *Biogerontology*. 2001 Sep 1;2(3):165–71.
 190. Griffith JF, Yeung DKW, Ma HT, Leung JCS, Kwok TCY, Leung PC. Bone marrow fat content in the elderly: A reversal of sex difference seen in younger subjects. *J Magn Reson Imaging*. 2012 Jul 1;36(1):225–30.
 191. Roldan-Valadez E, Piña-Jimenez C, Favila R, Rios C. Gender and age groups interactions in the quantification of bone marrow fat content in lumbar spine using 3T MR spectroscopy: A multivariate analysis of covariance (Mancova). *Eur J Radiol*. 2013 Nov 1;82(11):e697–702.
 192. Tratwal J, Labella R, Bravenboer N, Kerckhofs G, Douni E, Scheller EL, et al. Reporting Guidelines, Review of Methodological Standards, and Challenges Toward Harmonization in Bone Marrow Adiposity Research. Report of the Methodologies Working Group of the International Bone Marrow Adiposity Society. *Front Endocrinol [Internet]*. 2020;11. Available from:
<https://www.frontiersin.org/article/10.3389/fendo.2020.00065>
 193. Parfitt AM, Foldes J, Villanueva AR, Shih MS. Difference in label length between demethylchlortetracycline and oxytetracycline: Implications for the interpretation of bone histomorphometric data. *Calcif Tissue Int*. 1991 Feb 1;48(2):74–7.
 194. Neues F, Epple M. X-ray Microcomputer Tomography for the Study of Biomineralized Endo- and Exoskeletons of Animals. *Chem Rev*. 2008 Nov 12;108(11):4734–41.

195. Ritman EL. Current Status of Developments and Applications of Micro-CT. *Annu Rev Biomed Eng.* 2011 Aug 15;13(1):531–52.
196. Scheller EL, Doucette CR, Learman BS, Cawthorn WP, Khandaker S, Schell B, et al. Region-specific variation in the properties of skeletal adipocytes reveals regulated and constitutive marrow adipose tissues. *Nat Commun.* 2015 Aug 6;6(1):7808.
197. Scheller EL, Troiano N, VanHoutan JN, Bouxsein MA, Fretz JA, Xi Y, et al. Chapter Seven - Use of Osmium Tetroxide Staining with Microcomputerized Tomography to Visualize and Quantify Bone Marrow Adipose Tissue In Vivo. In: Macdougald OA, editor. *Methods in Enzymology* [Internet]. Academic Press; 2014. p. 123–39. Available from: <https://www.sciencedirect.com/science/article/pii/B9780124116191000070>
198. Khoury BM, Bigelow EMR, Smith LM, Schlecht SH, Scheller EL, Andarawis-Puri N, et al. The use of nano-computed tomography to enhance musculoskeletal research. *Connect Tissue Res.* 2015 Mar 4;56(2):106–19.
199. Nakakoshi M, Nishioka H, Katayama E. New versatile staining reagents for biological transmission electron microscopy that substitute for uranyl acetate. *J Electron Microscop.* (Tokyo). 2011 Dec 1;60(6):401–7.
200. Makarovskiy I, Markel G, Hoffman A, Schein O, Finkelstien A, Brosh-Nissimov T, et al. Osmium tetroxide: a new kind of weapon. *Isr Med Assoc J.* 2007 Oct;9(10):750–2.
201. Kerckhofs G, Stegen S, van Gastel N, Sap A, Falgayrac G, Penel G, et al. Simultaneous three-dimensional visualization of mineralized and soft skeletal tissues by a novel microCT contrast agent with polyoxometalate structure. *Biomaterials.* 2018 Mar 1;159:1–12.
202. Hu HH, Kan HE. Quantitative proton MR techniques for measuring fat. *NMR Biomed.* 2013 Dec 1;26(12):1609–29.
203. Karampinos DC, Ruschke S, Dieckmeyer M, Diefenbach M, Franz D, Gersing AS, et al. Quantitative MRI and spectroscopy of bone marrow. *J Magn Reson Imaging.* 2018 Feb 1;47(2):332–53.
204. Styner M, Pagnotti GM, McGrath C, Wu X, Sen B, Uzer G, et al. Exercise Decreases Marrow Adipose Tissue Through β -Oxidation in Obese Running Mice. *J Bone Miner Res.* 2017 Aug 1;32(8):1692–702.
205. Li GW, Xu Z, Chang SX, Zhou L, Wang XY, Nian H, et al. Influence of Early Zoledronic Acid Administration on Bone Marrow Fat in Ovariectomized Rats. *Endocrinology.* 2014 Dec 1;155(12):4731–8.
206. Reeder SB, Cruite I, Hamilton G, Sirlin CB. Quantitative assessment of liver fat with magnetic resonance imaging and spectroscopy. *J Magn Reson Imaging.* 2011 Oct 1;34(4):729–49.
207. Reeder SB, Hu HH, Sirlin CB. Proton density fat-fraction: A standardized mr-based biomarker of tissue fat concentration. *J Magn Reson Imaging.* 2012 Nov 1;36(5):1011–4.

208. Flehr A, Källgård J, Alvéén J, Lagerstrand K, Papalini E, Wheeler M, et al. Development of a novel method to measure bone marrow fat fraction in older women using high-resolution peripheral quantitative computed tomography. *Osteoporos Int.* 2022 Jul 1;33(7):1545–56.
209. Lecka-Czernik B. Marrow fat metabolism is linked to the systemic energy metabolism. *Bone.* 2011/07/04 ed. 2012 Feb;50(2):534–9.
210. Qian G, Fan W, Ahlemeyer B, Karnati S, Baumgart-Vogt E. Peroxisomes in different skeletal cell types during intramembranous and endochondral ossification and their regulation during osteoblast differentiation by distinct peroxisome proliferator-activated receptors. *PloS One.* 2015;10(12):e0143439.
211. Li Q, Wu Y, Kang N. Marrow Adipose Tissue: Its Origin, Function, and Regulation in Bone Remodeling and Regeneration. Zhu H, editor. *Stem Cells Int.* 2018 May 31;2018:7098456.
212. Shen W, Heymsfield SB. Bone marrow adipose tissue function — is space a constraint? *Nat Rev Endocrinol.* 2020 Oct 1;16(10):543–4.
213. Ellis JM, Frahm JL, Li LO, Coleman RA. Acyl-coenzyme A synthetases in metabolic control. *Curr Opin Lipidol* [Internet]. 2010;21(3). Available from: https://journals.lww.com/co-lipidology/Fulltext/2010/06000/Acyl_coenzyme_A_synthetases_in_metabolic_control.9.aspx
214. Miranda M, Pino AM, Fuenzalida K, Rosen CJ, Seitz G, Rodríguez JP. Characterization of Fatty Acid Composition in Bone Marrow Fluid From Postmenopausal Women: Modification After Hip Fracture. *J Cell Biochem.* 2016 Oct 1;117(10):2370–6.
215. Ren J, Dimitrov I, Sherry AD, Malloy CR. Composition of adipose tissue and marrow fat in humans by ¹H NMR at 7 Tesla *. *J Lipid Res.* 2008 Sep 1;49(9):2055–62.
216. Scheller EL, Khandaker S, Learman BS, Cawthorn WP, Anderson LM, Pham HA, et al. Bone marrow adipocytes resist lipolysis and remodeling in response to β -adrenergic stimulation. *Bone.* 2018/01/31 ed. 2019 Jan;118:32–41.
217. Brasaemle DL, Barber T, Wolins NE, Serrero G, Blanchette-Mackie EJ, Londos C. Adipose differentiation-related protein is an ubiquitously expressed lipid storage droplet-associated protein. *J Lipid Res.* 1997 Nov 1;38(11):2249–63.
218. Blanchette-Mackie EJ, Dwyer NK, Barber T, Coxey RA, Takeda T, Rondinone CM, et al. Perilipin is located on the surface layer of intracellular lipid droplets in adipocytes. *J Lipid Res.* 1995 Jun 1;36(6):1211–26.
219. Attané C, Estève D, Chaoui K, Iacovoni JS, Corre J, Moutahir M, et al. Human Bone Marrow Is Comprised of Adipocytes with Specific Lipid Metabolism. *Cell Rep.* 2020 Jan 28;30(4):949-958.e6.
220. Houten SM, Wanders RJA. A general introduction to the biochemistry of mitochondrial fatty acid β -oxidation. *J Inherit Metab Dis.* 2010 Oct 1;33(5):469–77.

221. Morrison SJ, Scadden DT. The bone marrow niche for haematopoietic stem cells. *Nature*. 2014 Jan 16;505(7483):327–34.
222. Gulati GL, Ashton JK, Hyun BH. Structure and Function of the Bone Marrow and Hematopoiesis. *Bone Marrow Exam*. 1988 Dec 1;2(4):495–511.
223. Allen TD, Dexter TM, Simmons PJ. Marrow biology and stem cells. *Immunol Ser* [Internet]. 1990; Available from: <http://hdl.handle.net/10541/109764>
224. Krebsbach PH, Kuznetsov SA, Bianco P, Gehron Robey P. Bone Marrow Stromal Cells: Characterization and Clinical Application. *Crit Rev Oral Biol Med*. 1999 Apr 1;10(2):165–81.
225. Bianco P. Minireview: The Stem Cell Next Door: Skeletal and Hematopoietic Stem Cell “Niches” in Bone. *Endocrinology*. 2011 Aug 1;152(8):2957–62.
226. Naveiras O, Nardi V, Wenzel PL, Hauschka PV, Fahey F, Daley GQ. Bone-marrow adipocytes as negative regulators of the haematopoietic microenvironment. *Nature*. 2009 Jul 1;460(7252):259–63.
227. Cuminetti V, Arranz L. Bone Marrow Adipocytes: The Enigmatic Components of the Hematopoietic Stem Cell Niche. *J Clin Med*. 2019;8(5).
228. Adler BJ, Green DE, Pagnotti GM, Chan ME, Rubin CT. High Fat Diet Rapidly Suppresses B Lymphopoiesis by Disrupting the Supportive Capacity of the Bone Marrow Niche. *PLOS ONE*. 2014 Mar 4;9(3):e90639.
229. Miggitsch C, Meryk A, Naismith E, Pangrazzi L, Ejaz A, Jenewein B, et al. Human bone marrow adipocytes display distinct immune regulatory properties. *EBioMedicine*. 2019 Aug 1;46:387–98.
230. Yokota T, Meka CSR, Kouro T, Medina KL, Igarashi H, Takahashi M, et al. Adiponectin, a Fat Cell Product, Influences the Earliest Lymphocyte Precursors in Bone Marrow Cultures by Activation of the Cyclooxygenase-Prostaglandin Pathway in Stromal Cells. *J Immunol*. 2003 Nov 15;171(10):5091.
231. Masamoto Y, Arai S, Sato T, Kubota N, Takamoto I, Kadowaki T, et al. Adiponectin Enhances Quiescence Exit of Murine Hematopoietic Stem Cells and Hematopoietic Recovery Through mTORC1 Potentiation. *Stem Cells*. 2017 Jul 1;35(7):1835–48.
232. DiMascio L, Voermans C, Uqoezwa M, Duncan A, Lu D, Wu J, et al. Identification of Adiponectin as a Novel Hemopoietic Stem Cell Growth Factor. *J Immunol*. 2007 Mar 15;178(6):3511.
233. Lin FY, Wu HC, Cheng KC, Tung CL, Chang CP, Feng YH. Adiponectin is down-regulated in bone marrow interstitial fluid in hematological malignancy. *Int J Hematol*. 2015 Sep 1;102(3):312–7.
234. Colotta F, Allavena P, Sica A, Garlanda C, Mantovani A. Cancer-related inflammation, the seventh hallmark of cancer: links to genetic instability. *Carcinogenesis*. 2009 Jul 1;30(7):1073–81.

235. Fantuzzi G, Faggioni R. Leptin in the regulation of immunity, inflammation, and hematopoiesis. *J Leukoc Biol.* 2000 Oct 1;68(4):437–46.
236. Claycombe Kate, King Louis E., Fraker Pamela J. A role for leptin in sustaining lymphopoiesis and myelopoiesis. *Proc Natl Acad Sci.* 2008 Feb 12;105(6):2017–21.
237. Pietramaggiore G, Scherer SS, Alperovich M, Chen B, Orgill DP, Wagers AJ. Improved Cutaneous Healing in Diabetic Mice Exposed to Healthy Peripheral Circulation. *J Invest Dermatol.* 2009 Sep 1;129(9):2265–74.
238. Faggioni Raffaella, Jones-Carson Jessica, Reed David A., Dinarello Charles A., Feingold Kenneth R., Grunfeld Carl, et al. Leptin-deficient (ob/ob) mice are protected from T cell-mediated hepatotoxicity: Role of tumor necrosis factor α and IL-18. *Proc Natl Acad Sci.* 2000 Feb 29;97(5):2367–72.
239. Bennett BD, Solar GP, Yuan JQ, Mathias J, Thomas GR, Matthews W. A role for leptin and its cognate receptor in hematopoiesis. *Curr Biol.* 1996 Sep 1;6(9):1170–80.
240. Umemoto Y, Tsuji K, Yang FC, Ebihara Y, Kaneko A, Furukawa S, et al. Leptin Stimulates the Proliferation of Murine Myelocytic and Primitive Hematopoietic Progenitor Cells. *Blood.* 1997 Nov 1;90(9):3438–43.
241. Zhou BO, Yu H, Yue R, Zhao Z, Rios JJ, Naveiras O, et al. Bone marrow adipocytes promote the regeneration of stem cells and haematopoiesis by secreting SCF. *Nat Cell Biol.* 2017 Aug 1;19(8):891–903.
242. Li Z, Bagchi DP, Zhu J, Bowers E, Yu H, Hardij J, et al. Constitutive bone marrow adipocytes suppress local bone formation. *JCI Insight [Internet].* 2022 Sep 1; Available from: <https://doi.org/10.1172/jci.insight.160915>
243. Elbaz A, Wu X, Rivas D, Gimble JM, Duque G. Inhibition of fatty acid biosynthesis prevents adipocyte lipotoxicity on human osteoblasts in vitro. *J Cell Mol Med.* 2010 Apr 1;14(4):982–91.
244. Maurin AC, Chavassieux PM, Frappart L, Delmas PD, Serre CM, Meunier PJ. Influence of mature adipocytes on osteoblast proliferation in human primary cocultures. *Bone.* 2000 May 1;26(5):485–9.
245. Bredella MA, Fazeli PK, Miller KK, Misra M, Torriani M, Thomas BJ, et al. Increased Bone Marrow Fat in Anorexia Nervosa. *J Clin Endocrinol Metab.* 2009 Jun 1;94(6):2129–36.
246. Li Z, Bowers E, Zhu J, Yu H, Hardij J, Bagchi DP, et al. Lipolysis of bone marrow adipocytes is required to fuel bone and the marrow niche during energy deficits. Zaidi M, Cawthorn WP, editors. *eLife.* 2022 Jun 22;11:e78496.
247. Wei W, Dutchak PA, Wang X, Ding X, Wang X, Bookout AL, et al. Fibroblast growth factor 21 promotes bone loss by potentiating the effects of peroxisome proliferator-activated receptor γ . *Proc Natl Acad Sci U S A.* 2012/02/06 ed. 2012 Feb 21;109(8):3143–8.

248. Kang S, Bennett CN, Gerin I, Rapp LA, Hankenson KD, MacDougald OA. Wnt Signaling Stimulates Osteoblastogenesis of Mesenchymal Precursors by Suppressing CCAAT/Enhancer-binding Protein α and Peroxisome Proliferator-activated Receptor γ *. *J Biol Chem*. 2007 May 11;282(19):14515–24.
249. Laharrague P, Larrouy D, Fontanilles AM, Truel N, Campfield A, Tenenbaum R, et al. High expression of leptin by human bone marrow adipocytes in primary culture. *FASEB J*. 1998 Jun 1;12(9):747–52.
250. Yue R, Zhou BO, Shimada IS, Zhao Z, Morrison SJ. Leptin Receptor Promotes Adipogenesis and Reduces Osteogenesis by Regulating Mesenchymal Stromal Cells in Adult Bone Marrow. *Cell Stem Cell*. 2016 Jun 2;18(6):782–96.
251. Takeshita S, Fumoto T, Naoe Y, Ikeda K. Age-related Marrow Adipogenesis Is Linked to Increased Expression of RANKL *. *J Biol Chem*. 2014 Jun 1;289(24):16699–710.
252. Kelly KA, Tanaka S, Baron R, Gimble JM. Murine Bone Marrow Stromally Derived BMS2 Adipocytes Support Differentiation and Function of Osteoclast-Like Cells in Vitro*. *Endocrinology*. 1998;139(4):2092–101.
253. Hardaway AL, Herroon MK, Rajagurubandara E, Podgorski I. Marrow adipocyte-derived CXCL1 and CXCL2 contribute to osteolysis in metastatic prostate cancer. *Clin Exp Metastasis*. 2015 Apr 1;32(4):353–68.
254. Oury F, Yadav VK, Wang Y, Zhou B, Liu XS, Guo XE, et al. CREB mediates brain serotonin regulation of bone mass through its expression in ventromedial hypothalamic neurons. *Genes Dev*. 2010 Oct 15;24(20):2330–42.
255. Fu L, Patel MS, Karsenty G. The circadian modulation of leptin-controlled bone formation. In: Kalsbeek A, Fliers E, Hofman MA, Swaab DF, van Someren EJW, Buijs RM, editors. *Progress in Brain Research* [Internet]. Elsevier; 2006. p. 177–88. Available from: <https://www.sciencedirect.com/science/article/pii/S0079612306530109>
256. Fu L, Patel MS, Bradley A, Wagner EF, Karsenty G. The Molecular Clock Mediates Leptin-Regulated Bone Formation. *Cell*. 2005 Sep 9;122(5):803–15.
257. Zhou BO, Yue R, Murphy MM, Peyer JG, Morrison SJ. Leptin-receptor-expressing mesenchymal stromal cells represent the main source of bone formed by adult bone marrow. *Cell Stem Cell*. 2014/06/19 ed. 2014 Aug 7;15(2):154–68.
258. Thomas T, Gori F, Khosla S, Jensen MD, Burguera B, Riggs BL. Leptin Acts on Human Marrow Stromal Cells to Enhance Differentiation to Osteoblasts and to Inhibit Differentiation to Adipocytes*. *Endocrinology*. 1999 Apr 1;140(4):1630–8.
259. Hamrick MW, Della-Fera MA, Choi YH, Pennington C, Hartzell D, Baile CA. Leptin Treatment Induces Loss of Bone Marrow Adipocytes and Increases Bone Formation in Leptin-Deficient ob/ob Mice. *J Bone Miner Res*. 2005 Jun 1;20(6):994–1001.
260. Lindenmaier LB, Philbrick KA, Branscum AJ, Kalra SP, Turner RT, Iwaniec UT. Hypothalamic Leptin Gene Therapy Reduces Bone Marrow Adiposity in ob/ob Mice Fed Regular and High-Fat Diets. *Front Endocrinol*. 2016 Aug 16;7:110–110.

261. Hamrick MW, Pennington C, Newton D, Xie D, Isales C. Leptin deficiency produces contrasting phenotypes in bones of the limb and spine. *Bone*. 2004 Mar 1;34(3):376–83.
262. Martin PJ, Haren N, Ghali O, Clabaut A, Chauveau C, Hardouin P, et al. Adipogenic RNAs are transferred in osteoblasts via bone marrow adipocytes-derived extracellular vesicles (EVs). *BMC Cell Biol*. 2015 Mar 18;16:10–10.
263. Lazar I, Clement E, Dauvillier S, Milhas D, Ducoux-Petit M, LeGonidec S, et al. Adipocyte Exosomes Promote Melanoma Aggressiveness through Fatty Acid Oxidation: A Novel Mechanism Linking Obesity and Cancer. *Cancer Res*. 2016 Jul 14;76(14):4051–7.
264. Sulston RJ, Cawthorn WP. Bone marrow adipose tissue as an endocrine organ: close to the bone? *Horm Mol Biol Clin Investig*. 2016;28(1):21–38.
265. Scheller EL, Burr AA, MacDougald OA, Cawthorn WP. Inside out: Bone marrow adipose tissue as a source of circulating adiponectin. *Adipocyte*. 2016 Mar 22;5(3):251–69.
266. Combs TP, Berg AH, Rajala MW, Klebanov S, Iyengar P, Jimenez-Chillaron JC, et al. Sexual Differentiation, Pregnancy, Calorie Restriction, and Aging Affect the Adipocyte-Specific Secretory Protein Adiponectin. *Diabetes*. 2003 Feb 1;52(2):268–76.
267. Liu LF, Shen WJ, Ueno M, Patel S, Kraemer FB. Characterization of age-related gene expression profiling in bone marrow and epididymal adipocytes. *BMC Genomics*. 2011 May 5;12(1):212.
268. Isobe T, Saitoh S, Takagi S, Takeuchi H, Chiba Y, Katoh N, et al. Influence of gender, age and renal function on plasma adiponectin level: the Tanno and Sobetsu study. *Eur J Endocrinol Eur J Endocrinol*. 2005 Jul 1;153(1):91–8.
269. Imagawa A, Funahashi T, Nakamura T, Moriwaki M, Tanaka S, Nishizawa H, et al. Elevated Serum Concentration of Adipose-Derived Factor, Adiponectin, in Patients With Type 1 Diabetes. *Diabetes Care*. 2002 Sep 1;25(9):1665–6.
270. Civitarese AE, Ukropcova B, Carling S, Hulver M, DeFronzo RA, Mandarino L, et al. Role of adiponectin in human skeletal muscle bioenergetics. *Cell Metab*. 2006 Jul 1;4(1):75–87.
271. Fairfield H, Rosen CJ, Reagan MR. Connecting Bone and Fat: The Potential Role for Sclerostin. *Curr Mol Biol Rep*. 2017/04/18 ed. 2017 Jun;3(2):114–21.
272. Uchihashi K, Aoki S, Shigematsu M, Kamochi N, Sonoda E, Soejima H, et al. Organotypic culture of human bone marrow adipose tissue. *Pathol Int*. 2010 Apr 1;60(4):259–67.
273. Belaid-Choucair Z, Lepelletier Y, Poncin G, Thiry A, Humblet C, Maachi M, et al. Human Bone Marrow Adipocytes Block Granulopoiesis Through Neuropilin-1-Induced Granulocyte Colony-Stimulating Factor Inhibition. *Stem Cells*. 2008 Jun 1;26(6):1556–64.

274. Rydén M, Dicker A, Götherström C, Åström G, Tammik C, Arner P, et al. Functional characterization of human mesenchymal stem cell-derived adipocytes. *Biochem Biophys Res Commun*. 2003 Nov 14;311(2):391–7.
275. Tencerova M, Figeac F, Ditzel N, Taipaleenmäki H, Nielsen TK, Kassem M. High-Fat Diet–Induced Obesity Promotes Expansion of Bone Marrow Adipose Tissue and Impairs Skeletal Stem Cell Functions in Mice. *J Bone Miner Res*. 2018 Jun 1;33(6):1154–65.
276. Corre J, Barreau C, Cousin B, Chavoïn JP, Caton D, Fournial G, et al. Human subcutaneous adipose cells support complete differentiation but not self-renewal of hematopoietic progenitors. *J Cell Physiol*. 2006 Aug 1;208(2):282–8.
277. Zhang K, Wang C, Chen Y, Ji X, Chen X, Tian L, et al. Preservation of high-fat diet-induced femoral trabecular bone loss through genetic target of TNF- α . *Endocrine*. 2015 Sep 1;50(1):239–49.
278. Wang C, Tian L, Zhang K, Chen Y, Chen X, Xie Y, et al. Interleukin-6 gene knockout antagonizes high-fat-induced trabecular bone loss. *J Mol Endocrinol*. 2016 Oct 1;57(3):161–70.
279. Mirantes C, Passequé E, Pietras EM. Pro-inflammatory cytokines: emerging players regulating HSC function in normal and diseased hematopoiesis. *Exp Cell Res*. 2014/08/19 ed. 2014 Dec 10;329(2):248–54.
280. Tavassoli M. Marrow adipose cells. Histochemical identification of labile and stable components. *Arch Pathol Lab Med*. 1976 Jan;100(1):16–8.
281. Bigelow CL, Tavassoli M. Fatty Involution of Bone Marrow in Rabbits. *Cells Tissues Organs*. 1984;118(1):60–4.
282. Li Z, MacDougald OA. Preclinical models for investigating how bone marrow adipocytes influence bone and hematopoietic cellularity. *Emerg Role Bone Marrow Adipose Tissue*. 2021 Jul 1;35(4):101547.
283. Cawthorn WP, Scheller EL, Parlee SD, Pham HA, Learman BS, Redshaw CMH, et al. Expansion of Bone Marrow Adipose Tissue During Caloric Restriction Is Associated With Increased Circulating Glucocorticoids and Not With Hypoleptinemia. *Endocrinology*. 2015/12/22 ed. 2016 Feb;157(2):508–21.
284. Iwaniec UT, Turner RT. Failure to generate bone marrow adipocytes does not protect mice from ovariectomy-induced osteopenia. *Bone*. 2012/12/12 ed. 2013 Mar;53(1):145–53.
285. Li Z, MacDougald OA. Stem cell factor: the bridge between bone marrow adipocytes and hematopoietic cells. *Haematologica*. 2019 Sep;104(9):1689–91.
286. Lecka-Czernik B, Stechschulte LA, Czernik PJ, Dowling AR. High bone mass in adult mice with diet-induced obesity results from a combination of initial increase in bone mass followed by attenuation in bone formation; implications for high bone mass and decreased bone quality in obesity. *SI Bone Health Nutr*. 2015 Jul 15;410:35–41.

287. Styner M, Pagnotti GM, Galior K, Wu X, Thompson WR, Uzer G, et al. Exercise Regulation of Marrow Fat in the Setting of PPAR γ Agonist Treatment in Female C57BL/6 Mice. *Endocrinology*. 2015 Aug 1;156(8):2753–61.
288. Marędziak M, Śmieszek A, Chrzęstek K, Basinska K, Marycz K. Physical Activity Increases the Total Number of Bone-Marrow-Derived Mesenchymal Stem Cells, Enhances Their Osteogenic Potential, and Inhibits Their Adipogenic Properties. Dani C, editor. *Stem Cells Int*. 2015 Jun 16;2015:379093.
289. Pagnotti GM, Styner M. Exercise Regulation of Marrow Adipose Tissue. *Front Endocrinol* [Internet]. 2016;7. Available from: <https://www.frontiersin.org/article/10.3389/fendo.2016.00094>
290. Fan Y, Hanai J ichi, Le PT, Bi R, Maridas D, DeMambro V, et al. Parathyroid Hormone Directs Bone Marrow Mesenchymal Cell Fate. *Cell Metab*. 2017 Mar 7;25(3):661–72.
291. Yeung DK, Griffith JF, Antonio GE, Lee FK, Woo J, Leung PC. Osteoporosis is associated with increased marrow fat content and decreased marrow fat unsaturation: a proton MR spectroscopy study. *J Magn Reson Imaging Off J Int Soc Magn Reson Med*. 2005;22(2):279–85.
292. Bethel M, Chitteti BR, Srour EF, Kacena MA. The changing balance between osteoblastogenesis and adipogenesis in aging and its impact on hematopoiesis. *Curr Osteoporos Rep*. 2013;11(2):99–106.
293. Jacobs FA, Sadie-Van Gijzen H, Van de Vyver M, Ferris WF. Vanadate impedes adipogenesis in mesenchymal stem cells derived from different depots within bone. *Front Endocrinol*. 2016;7:108.
294. Rosen CJ, Bouxsein ML. Mechanisms of disease: is osteoporosis the obesity of bone? *Nat Clin Pract Rheumatol*. 2006;2(1):35–43.
295. Cawthorn WP, Scheller EL. Bone marrow adipose tissue: formation, function, and impact on health and disease. *Front Endocrinol*. 2017;8:112.
296. Infante A, Rodríguez CI. Osteogenesis and aging: lessons from mesenchymal stem cells. *Stem Cell Res Ther*. 2018;9(1):1–7.
297. Tencerova M, Kassem M. The bone marrow-derived stromal cells: commitment and regulation of adipogenesis. *Front Endocrinol*. 2016;7:127.
298. Akune T, Ohba S, Kamekura S, Yamaguchi M, Chung U il, Kubota N, et al. PPAR γ insufficiency enhances osteogenesis through osteoblast formation from bone marrow progenitors. *J Clin Invest*. 2004;113(6):846–55.
299. Takada I, Mihara M, Suzawa M, Ohtake F, Kobayashi S, Igarashi M, et al. A histone lysine methyltransferase activated by non-canonical Wnt signalling suppresses PPAR- γ transactivation. *Nat Cell Biol*. 2007;9(11):1273–85.
300. Fazeli PK, Horowitz MC, MacDougald OA, Scheller EL, Rodeheffer MS, Rosen CJ, et al. Marrow fat and bone—new perspectives. *J Clin Endocrinol Metab*. 2013;98(3):935–45.

301. Kajkenova O, Lecka-Czernik B, Gubrij I, Hauser SP, Takahashi K, Parfitt AM, et al. Increased adipogenesis and myelopoiesis in the bone marrow of SAMP6, a murine model of defective osteoblastogenesis and low turnover osteopenia. *J Bone Miner Res.* 1997;12(11):1772–9.
302. Moerman EJ, Teng K, Lipschitz DA, Lecka-Czernik B. Aging activates adipogenic and suppresses osteogenic programs in mesenchymal marrow stroma/stem cells: the role of PPAR- γ 2 transcription factor and TGF- β /BMP signaling pathways. *Aging Cell.* 2004;3(6):379–89.
303. Sadie-Van Gijzen H, Hough F, Ferris W. Determinants of bone marrow adiposity: the modulation of peroxisome proliferator-activated receptor- γ 2 activity as a central mechanism. *Bone.* 2013;56(2):255–65.
304. Chandra A, Lin T, Young T, Tong W, Ma X, Tseng W, et al. Suppression of sclerostin alleviates radiation-induced bone loss by protecting bone-forming cells and their progenitors through distinct mechanisms. *J Bone Miner Res.* 2017;32(2):360–72.
305. Singh L, Brennan TA, Russell E, Kim JH, Chen Q, Johnson FB, et al. Aging alters bone-fat reciprocity by shifting in vivo mesenchymal precursor cell fate towards an adipogenic lineage. *Bone.* 2016;85:29–36.
306. da Silva PF, Ogradnik M, Kucheryavenko O, Glibert J, Miwa S, Cameron K, et al. The bystander effect contributes to the accumulation of senescent cells in vivo. *Aging Cell.* 2019;18(1):e12848.
307. de Magalhães JP, Passos JF. Stress, cell senescence and organismal ageing. *Mech Ageing Dev.* 2018;170:2–9.
308. Woods GN, Ewing SK, Sigurdsson S, Kado DM, Eiriksdottir G, Gudnason V, et al. Greater Bone Marrow Adiposity Predicts Bone Loss in Older Women. *J Bone Miner Res.* 2020 Feb 1;35(2):326–32.
309. Li GW, Xu Z, Chen QW, Tian YN, Wang XY, Zhou L, et al. Quantitative evaluation of vertebral marrow adipose tissue in postmenopausal female using MRI chemical shift-based water–fat separation. *Clin Radiol.* 2014 Mar 1;69(3):254–62.
310. Beekman KM, Veldhuis-Vlug AG, van der Veen A, den Heijer M, Maas M, Kerckhofs G, et al. The effect of PPAR γ inhibition on bone marrow adipose tissue and bone in C3H/HeJ mice. *Am J Physiol-Endocrinol Metab.* 2019;316(1):E96–105.
311. Limonard EJ, Veldhuis-Vlug AG, van Dussen L, Runge JH, Tanck MW, Endert E, et al. Short-term effect of estrogen on human bone marrow fat. *J Bone Miner Res.* 2015;30(11):2058–66.
312. Beekman KM, Zwaagstra M, Veldhuis-Vlug AG, Van Essen HW, Den Heijer M, Maas M, et al. Ovariectomy increases RANKL protein expression in bone marrow adipocytes of C3H/HeJ mice. *Am J Physiol-Endocrinol Metab.* 2019;317(6):E1050–4.
313. Beekman KM, Veldhuis-Vlug AG, den Heijer M, Maas M, Oleksik AM, Tanck MW, et al. The effect of raloxifene on bone marrow adipose tissue and bone turnover in postmenopausal women with osteoporosis. *Bone.* 2019;118:62–8.

314. Elbaz A, Rivas D, Duque G. Effect of estrogens on bone marrow adipogenesis and Sirt1 in aging C57BL/6J mice. *Biogerontology*. 2009;10(6):747–55.
315. Kumar A, Ruan M, Clifton K, Syed F, Khosla S, Oursler MJ. TGF- β mediates suppression of adipogenesis by estradiol through connective tissue growth factor induction. *Endocrinology*. 2012;153(1):254–63.
316. Zhao JW, Gao ZL, Wang Y, Mei H, Li YL. Differentiation of human mesenchymal stem cells: the potential mechanism for estrogen-induced preferential osteoblast versus adipocyte differentiation. *Am J Med Sci*. 2011;341(6):460–8.
317. Okazaki R, Inoue D, Shibata M, Saika M, Kido S, Ooka H, et al. Estrogen promotes early osteoblast differentiation and inhibits adipocyte differentiation in mouse bone marrow stromal cell lines that express estrogen receptor (ER) α or β . *Endocrinology*. 2002;143(6):2349–56.
318. Rooney AM, van der Meulen MC. Mouse models to evaluate the role of estrogen receptor α in skeletal maintenance and adaptation. *Ann N Y Acad Sci*. 2017;1410(1):85–92.
319. Kim RY, Yang HJ, Song YM, Kim IS, Hwang SJ. Estrogen modulates bone morphogenetic protein-induced sclerostin expression through the Wnt signaling pathway. *Tissue Eng Part A*. 2015;21(13–14):2076–88.
320. Roforth MM, Fujita K, McGregor UI, Kirmani S, McCready LK, Peterson JM, et al. Effects of age on bone mRNA levels of sclerostin and other genes relevant to bone metabolism in humans. *Bone*. 2014;59:1–6.
321. Ueland T, Stilgren L, Bollerslev J. Bone matrix levels of dickkopf and sclerostin are positively correlated with bone mass and strength in postmenopausal osteoporosis. *Int J Mol Sci*. 2019;20(12):2896.
322. Fairfield H, Falank C, Harris E, Demambro V, McDonald M, Pettitt JA, et al. The skeletal cell-derived molecule sclerostin drives bone marrow adipogenesis. *J Cell Physiol*. 2018;233(2):1156–67.
323. Du D, Zhou Z, Zhu L, Hu X, Lu J, Shi C, et al. TNF- α suppresses osteogenic differentiation of MSCs by accelerating P2Y2 receptor in estrogen-deficiency induced osteoporosis. *Bone*. 2018;117:161–70.
324. Liu P, Ji Y, Yuen T, Rendina-Ruedy E, DeMambro VE, Dhawan S, et al. Blocking FSH induces thermogenic adipose tissue and reduces body fat. *Nature*. 2017;546(7656):107–12.
325. Chin KY. The Relationship between Follicle-stimulating Hormone and Bone Health: Alternative Explanation for Bone Loss beyond Oestrogen? *Int J Med Sci*. 2018;15(12):1373–83.
326. Zhu LL, Tourkova I, Yuen T, Robinson LJ, Bian Z, Zaidi M, et al. Blocking FSH action attenuates osteoclastogenesis. *Biochem Biophys Res Commun*. 2012;422(1):54–8.

327. Foo C, Frey S, Yang HH, Zellweger R, Filgueira L. Downregulation of beta-catenin and transdifferentiation of human osteoblasts to adipocytes under estrogen deficiency. *Gynecol Endocrinol*. 2007;23(9):535–40.
328. Gao B, Huang Q, Lin YS, Wei BY, Guo YS, Sun Z, et al. Dose-dependent effect of estrogen suppresses the osteo-adipogenic transdifferentiation of osteoblasts via canonical Wnt signaling pathway. *PLoS One*. 2014;9(6):e99137.
329. Yang Y, Luo X, Xie X, Yan F, Chen G, Zhao W, et al. Influences of teriparatide administration on marrow fat content in postmenopausal osteopenic women using MR spectroscopy. *Climacteric*. 2016;19(3):285–91.
330. Syed FA, Oursler MJ, Hefferanm T, Peterson JM, Riggs BL, Khosla S. Effects of estrogen therapy on bone marrow adipocytes in postmenopausal osteoporotic women. *Osteoporos Int*. 2008;19(9):1323–30.
331. Somjen D, Katzburg S, Kohen F, Gayer B, Posner G, Yoels I, et al. The effects of native and synthetic estrogenic compounds as well as vitamin D less-calcemic analogs on adipocytes content in rat bone marrow. *J Endocrinol Invest*. 2011;34(2):106–10.
332. Soley L, Falank C, Reagan MR. MicroRNA transfer between bone marrow adipose and multiple myeloma cells. *Curr Osteoporos Rep*. 2017;15(3):162–70.
333. Chkourko Gusky H, Diedrich J, MacDougald OA, Podgorski I. Omentum and bone marrow: how adipocyte-rich organs create tumour microenvironments conducive for metastatic progression. *Obes Rev*. 2016;17(11):1015–29.
334. Morris EV, Edwards CM. Bone marrow adipose tissue: a new player in cancer metastasis to bone. *Front Endocrinol*. 2016;7:90.
335. Morris EV, Edwards CM. The role of bone marrow adipocytes in bone metastasis. *J Bone Oncol*. 2016;5(3):121–3.
336. Diedrich JD, Rajagurubandara E, Herroon MK, Mahapatra G, Hüttemann M, Podgorski I. Bone marrow adipocytes promote the Warburg phenotype in metastatic prostate tumors via HIF-1 α activation. *Oncotarget*. 2016;7(40):64854.
337. Herroon MK, Rajagurubandara E, Hardaway AL, Powell K, Turchick A, Feldmann D, et al. Bone marrow adipocytes promote tumor growth in bone via FABP4-dependent mechanisms. *Oncotarget*. 2013;4(11):2108.
338. Wang J, Chen G liang, Cao S, Zhao M chun, Liu Y qing, Chen XX, et al. Adipogenic niches for melanoma cell colonization and growth in bone marrow. *Lab Invest*. 2017;97(6):737–45.
339. Li G, Xu Z, Zhuang A, Chang S, Hou L, Chen Y, et al. Magnetic resonance spectroscopy-detected change in marrow adiposity is strongly correlated to postmenopausal breast cancer risk. *Clin Breast Cancer*. 2017;17(3):239–44.
340. Rosen BR, Fleming DM, Kushner DC, Zaner KS, Buxton RB, Bennet WP, et al. Hematologic bone marrow disorders: quantitative chemical shift MR imaging. *Radiology*. 1988 Dec 1;169(3):799–804.

341. Falank C, Fairfield H, Reagan MR. Signaling Interplay between Bone Marrow Adipose Tissue and Multiple Myeloma cells. *Front Endocrinol* [Internet]. 2016;7. Available from: <https://www.frontiersin.org/articles/10.3389/fendo.2016.00067>
342. Shafat MS, Oellerich T, Mohr S, Robinson SD, Edwards DR, Marlein CR, et al. Leukemic blasts program bone marrow adipocytes to generate a protumoral microenvironment. *Blood*. 2017 Mar 9;129(10):1320–32.
343. Tabe Y, Yamamoto S, Saitoh K, Sekihara K, Monma N, Ikeo K, et al. Bone Marrow Adipocytes Facilitate Fatty Acid Oxidation Activating AMPK and a Transcriptional Network Supporting Survival of Acute Monocytic Leukemia Cells. *Cancer Res*. 2017 Mar 14;77(6):1453–64.
344. Shen W, Chen J, Punyanitya M, Shapses S, Heshka S, Heymsfield SB. MRI-measured bone marrow adipose tissue is inversely related to DXA-measured bone mineral in Caucasian women. *Osteoporos Int J Establ Result Coop Eur Found Osteoporos Natl Osteoporos Found USA*. 2006/12/01 ed. 2007 May;18(5):641–7.
345. Shen W, Chen J, Gantz M, Punyanitya M, Heymsfield SB, Gallagher D, et al. Ethnic and sex differences in bone marrow adipose tissue and bone mineral density relationship. *Osteoporos Int J Establ Result Coop Eur Found Osteoporos Natl Osteoporos Found USA*. 2011/12/16 ed. 2012 Sep;23(9):2293–301.
346. Di Iorgi N, Rosol M, Mittelman SD, Gilsanz V. Reciprocal relation between marrow adiposity and the amount of bone in the axial and appendicular skeleton of young adults. *J Clin Endocrinol Metab*. 2008/04/01 ed. 2008 Jun;93(6):2281–6.
347. Wren TAL, Chung SA, Dorey FJ, Bluml S, Adams GB, Gilsanz V. Bone Marrow Fat Is Inversely Related to Cortical Bone in Young and Old Subjects. *J Clin Endocrinol Metab*. 2011 Mar 1;96(3):782–6.
348. Tuljapurkar SR, McGuire TR, Brusnahan SK, Jackson JD, Garvin KL, Kessinger MA, et al. Changes in human bone marrow fat content associated with changes in hematopoietic stem cell numbers and cytokine levels with aging. *J Anat*. 2011/09/16 ed. 2011 Nov;219(5):574–81.
349. Ambrosi TH, Scialdone A, Graja A, Gohlke S, Jank AM, Bocian C, et al. Adipocyte Accumulation in the Bone Marrow during Obesity and Aging Impairs Stem Cell-Based Hematopoietic and Bone Regeneration. *Cell Stem Cell*. 2017/03/16 ed. 2017 Jun 1;20(6):771–784.e6.
350. HUI SL, EPSTEIN S, JOHNSTON CC JR. A Prospective Study of Bone Mass in Patients with Type I Diabetes*. *J Clin Endocrinol Metab*. 1985 Jan 1;60(1):74–80.
351. Picke AK, Campbell G, Napoli N, Hofbauer LC, Rauner M. Update on the impact of type 2 diabetes mellitus on bone metabolism and material properties. *Endocr Connect*. 2019 Mar 1;8(3):R55–70.
352. Botolin S, Faugere MC, Malluche H, Orth M, Meyer R, McCabe LR. Increased bone adiposity and peroxisomal proliferator-activated receptor-gamma2 expression in type I diabetic mice. *Endocrinology*. 2005/05/19 ed. 2005 Aug;146(8):3622–31.

353. Botolin S, McCabe LR. Bone Loss and Increased Bone Adiposity in Spontaneous and Pharmacologically Induced Diabetic Mice. *Endocrinology*. 2007 Jan 1;148(1):198–205.
354. Botolin S, McCabe LR. Inhibition of PPAR γ prevents type I diabetic bone marrow adiposity but not bone loss. *J Cell Physiol*. 2006 Dec 1;209(3):967–76.
355. Motyl KJ, McCabe LR. Leptin treatment prevents type I diabetic marrow adiposity but not bone loss in mice. *J Cell Physiol*. 2009 Feb 1;218(2):376–84.
356. Motyl KJ, Raetz M, Tekalur SA, Schwartz RC, McCabe LR. CCAAT/enhancer binding protein β -deficiency enhances type 1 diabetic bone phenotype by increasing marrow adiposity and bone resorption. *Am J Physiol-Regul Integr Comp Physiol*. 2011 May 1;300(5):R1250–60.
357. Poll LW, Chantelau EA. Routine MRI findings of the asymptomatic foot in diabetic patients with unilateral Charcot foot. *Diabetol Metab Syndr*. 2010 Apr 22;2(1):25.
358. Slade JM, Coe LM, Meyer RA, McCabe LR. Human bone marrow adiposity is linked with serum lipid levels not T1-diabetes. *J Diabetes Complications*. 2012 Jan 1;26(1):1–9.
359. Oei L, Zillikens MC, Dehghan A, Buitendijk GHS, Castaño-Betancourt MC, Estrada K, et al. High bone mineral density and fracture risk in type 2 diabetes as skeletal complications of inadequate glucose control: the Rotterdam Study. *Diabetes Care*. 2013/01/11 ed. 2013 Jun;36(6):1619–28.
360. Schwartz AV, Sellmeyer DE, Ensrud KE, Cauley JA, Tabor HK, Schreiner PJ, et al. Older Women with Diabetes Have an Increased Risk of Fracture: A Prospective Study. *J Clin Endocrinol Metab*. 2001 Jan 1;86(1):32–8.
361. Janghorbani M, Feskanich D, Willett WC, Hu F. Prospective Study of Diabetes and Risk of Hip Fracture: The Nurses' Health Study. *Diabetes Care*. 2006 Jul 1;29(7):1573–8.
362. Goulding A, Taylor R, Jones I, McAuley K, Manning P, Williams S. Overweight and obese children have low bone mass and area for their weight. *Int J Obes*. 2000 May 1;24(5):627–32.
363. Bredella MA, Torriani M, Ghomi RH, Thomas BJ, Brick DJ, Gerweck AV, et al. Vertebral bone marrow fat is positively associated with visceral fat and inversely associated with IGF-1 in obese women. *Obes Silver Spring Md*. 2010/05/13 ed. 2011 Jan;19(1):49–53.
364. Di Bernardo G, Messina G, Capasso S, Del Gaudio S, Cipollaro M, Peluso G, et al. Sera of overweight people promote in vitro adipocyte differentiation of bone marrow stromal cells. *Stem Cell Res Ther*. 2014 Jan 9;5(1):4–4.
365. Casado-Díaz A, Santiago-Mora R, Dorado G, Quesada-Gómez JM. The omega-6 arachidonic fatty acid, but not the omega-3 fatty acids, inhibits osteoblastogenesis and induces adipogenesis of human mesenchymal stem cells: potential implication in osteoporosis. *Osteoporos Int*. 2013 May 1;24(5):1647–61.

366. Morris J, Twaddle S. Anorexia nervosa. *BMJ*. 2007 Apr 28;334(7599):894–8.
367. Misra M, Soyka LA, Miller KK, Grinspoon S, Levitsky LL, Klibanski A. Regional body composition in adolescents with anorexia nervosa and changes with weight recovery. *Am J Clin Nutr*. 2003 Jun 1;77(6):1361–7.
368. van Eeden AE, van Hoeken D, Hoek HW. Incidence, prevalence and mortality of anorexia nervosa and bulimia nervosa. *Curr Opin Psychiatry*. 2021 Nov 1;34(6):515–24.
369. 50-year trends in the incidence of anorexia nervosa in Rochester, Minn.: a population-based study. *Am J Psychiatry*. 1991 Jul 1;148(7):917–22.
370. von Ranson KM, Iacono WG, McGue M. Disordered eating and substance use in an epidemiological sample: I. associations within individuals. *Int J Eat Disord*. 2002 May 1;31(4):389–403.
371. Andersen AE, Woodward PJ, LaFrance N. Bone mineral density of eating disorder subgroups. *Int J Eat Disord*. 1995 Dec 1;18(4):335–42.
372. Jappe LM, Cao L, Crosby RD, Crow SJ, Peterson CB, Le Grange D, et al. Stress and eating disorder behavior in anorexia nervosa as a function of menstrual cycle status. *Int J Eat Disord*. 2014 Mar 1;47(2):181–8.
373. Rojo L, Conesa L, Bermudez O, Livianos L. Influence of Stress in the Onset of Eating Disorders: Data From a Two-Stage Epidemiologic Controlled Study. *Psychosom Med* [Internet]. 2006;68(4). Available from: https://journals.lww.com/psychosomaticmedicine/Fulltext/2006/07000/Influence_of_Stress_in_the_Onset_of_Eating.17.aspx
374. Legroux-Gérot I, Vignau J, d’Herbomez M, Flipo RM, Cortet B. Predictive factors of change in BMD at 1 and 2 years in women with anorexia nervosa: a study of 146 cases. *Osteoporos Int*. 2012 Dec 1;23(12):2855–61.
375. Fazeli PK, Lawson EA, Prabhakaran R, Miller KK, Donoho DA, Clemmons DR, et al. Effects of Recombinant Human Growth Hormone in Anorexia Nervosa: A Randomized, Placebo-Controlled Study. *J Clin Endocrinol Metab*. 2010 Nov 1;95(11):4889–97.
376. Misra M, Klibanski A. Anorexia Nervosa and Its Associated Endocrinopathy in Young People. *Horm Res Paediatr*. 2016;85(3):147–57.
377. Modan-Moses D, Yaroslavsky A, Novikov I, Segev S, Toledano A, Miterany E, et al. Stunting of Growth as a Major Feature of Anorexia Nervosa in Male Adolescents. *Pediatrics*. 2003 Feb 1;111(2):270–6.
378. Rozé C, Doyen C, Le Heuzey MF, Armoogum P, Mouren MC, Léger J. Predictors of late menarche and adult height in children with anorexia nervosa. *Clin Endocrinol (Oxf)*. 2007 Sep 1;67(3):462–7.
379. Prabhakaran R, Misra M, Miller KK, Kruczek K, Sundaralingam S, Herzog DB, et al. Determinants of Height in Adolescent Girls With Anorexia Nervosa. *Pediatrics*. 2008 Jun 1;121(6):e1517–23.

380. Modan-Moses D, Yaroslavsky A, Kochavi B, Toledano A, Segev S, Balawi F, et al. Linear Growth and Final Height Characteristics in Adolescent Females with Anorexia Nervosa. *PLOS ONE*. 2012 Sep 18;7(9):e45504.
381. Misra M, Miller KK, Kuo K, Griffin K, Stewart V, Hunter E, et al. Secretory dynamics of leptin in adolescent girls with anorexia nervosa and healthy adolescents. *Am J Physiol-Endocrinol Metab*. 2005 Sep 1;289(3):E373–81.
382. Lawson EA, Miller KK, Blum JI, Meenaghan E, Misra M, Eddy KT, et al. Leptin levels are associated with decreased depressive symptoms in women across the weight spectrum, independent of body fat. *Clin Endocrinol (Oxf)*. 2012 Apr 1;76(4):520–5.
383. Matsuzaki T, Azuma K, Irahara M, Yasui T, Aono T. Mechanism of anovulation in hyperprolactinemic amenorrhea determined by pulsatile gonadotropin-releasing hormone injection combined with human chorionic gonadotropin. *Fertil Steril*. 1994 Dec 1;62(6):1143–9.
384. Amitani H, Asakawa A, Ogiso K, Nakahara T, Ushikai M, Haruta I, et al. The role of adiponectin multimers in anorexia nervosa. *Nutrition*. 2013 Jan 1;29(1):203–6.
385. Lu M, Tang Q, Olefsky JM, Mellon PL, Webster NJG. Adiponectin Activates Adenosine Monophosphate-Activated Protein Kinase and Decreases Luteinizing Hormone Secretion in L β T2 Gonadotropes. *Mol Endocrinol*. 2008 Mar 1;22(3):760–71.
386. Luo XH, Guo LJ, Xie H, Yuan LQ, Wu XP, Zhou HD, et al. Adiponectin Stimulates RANKL and Inhibits OPG Expression in Human Osteoblasts Through the MAPK Signaling Pathway. *J Bone Miner Res*. 2006 Oct 1;21(10):1648–56.
387. Biver E, Salliot C, Combescure C, Gossec L, Hardouin P, Legroux-Gerot I, et al. Influence of Adipokines and Ghrelin on Bone Mineral Density and Fracture Risk: A Systematic Review and Meta-Analysis. *J Clin Endocrinol Metab*. 2011 Sep 1;96(9):2703–13.
388. Chou SH, Mantzoros C. Bone metabolism in anorexia nervosa and hypothalamic amenorrhea. *Metab - Clin Exp*. 2018 Mar 1;80:91–104.
389. Steinman J, Shibli-Rahhal A. Anorexia Nervosa and Osteoporosis: Pathophysiology and Treatment. *J Bone Metab*. 2019/08/31 ed. 2019 Aug;26(3):133–43.
390. Vestergaard P, Emborg C, Støving RK, Hagen C, Mosekilde L, Brixen K. Fractures in patients with anorexia nervosa, bulimia nervosa, and other eating disorders—A nationwide register study. *Int J Eat Disord*. 2002 Nov 1;32(3):301–8.
391. Fazeli PK, Klibanski A. Bone metabolism in anorexia nervosa. *Curr Osteoporos Rep*. 2014 Mar;12(1):82–9.
392. Grinspoon S, Thomas E, Pitts S, Gross E, Mickley D, Miller K, et al. Prevalence and Predictive Factors for Regional Osteopenia in Women with Anorexia Nervosa. *Ann Intern Med*. 2000 Nov 21;133(10):790–4.
393. Bachmann KN, Fazeli PK, Lawson EA, Russell BM, Riccio AD, Meenaghan E, et al. Comparison of hip geometry, strength, and estimated fracture risk in women with

- anorexia nervosa and overweight/obese women. *J Clin Endocrinol Metab.* 2014 Dec;99(12):4664–73.
394. Mehler PS. Clinical guidance on osteoporosis and eating disorders: the NEDA continuing education series. *Eat Disord.* 2019 Sep 3;27(5):471–81.
395. Karaguzel G, Holick MF. Diagnosis and treatment of osteopenia. *Rev Endocr Metab Disord.* 2010 Dec 1;11(4):237–51.
396. Sattari M, Cauley JA, Garvan C, Johnson KC, LaMonte MJ, Li W, et al. Osteoporosis in the Women’s Health Initiative: Another Treatment Gap? *Am J Med.* 2017 Aug 1;130(8):937–48.
397. US Preventive Services Task Force. Vitamin D, Calcium, or Combined Supplementation for the Primary Prevention of Fractures in Community-Dwelling Adults: US Preventive Services Task Force Recommendation Statement. *JAMA.* 2018 Apr 17;319(15):1592–9.
398. Golden NH, Iglesias EA, Jacobson MS, Carey D, Meyer W, Schebendach J, et al. Alendronate for the Treatment of Osteopenia in Anorexia Nervosa: A Randomized, Double-Blind, Placebo-Controlled Trial. *J Clin Endocrinol Metab.* 2005 Jun 1;90(6):3179–85.
399. Abbasi J. Amid Osteoporosis Treatment Crisis, Experts Suggest Addressing Patients’ Bisphosphonate Concerns. *JAMA.* 2018 Jun 26;319(24):2464–6.
400. Fazeli PK, Wang IS, Miller KK, Herzog DB, Misra M, Lee H, et al. Teriparatide increases bone formation and bone mineral density in adult women with anorexia nervosa. *J Clin Endocrinol Metab.* 2014/01/23 ed. 2014 Apr;99(4):1322–9.
401. Suresh E, Abrahamsen B. Denosumab: A novel antiresorptive drug for osteoporosis. *Cleve Clin J Med.* 2015 Feb 1;82(2):105.
402. Sim L, McGovern L, Mohamed B, Swiglo B, Erwin P, Montori V. Effect on Bone Health of Estrogen Preparations in Premenopausal Women with Anorexia Nervosa: A Systematic Review and Meta-Analyses. *Int J Eat Disord.* 2009 Nov 30;43:218–25.
403. Misra M, Katzman D, Miller KK, Mendes N, Snelgrove D, Russell M, et al. Physiologic estrogen replacement increases bone density in adolescent girls with anorexia nervosa. *J Bone Miner Res Off J Am Soc Bone Miner Res.* 2011 Oct;26(10):2430–8.
404. Miller KK, Meenaghan E, Lawson EA, Misra M, Gleysteen S, Schoenfeld D, et al. Effects of risedronate and low-dose transdermal testosterone on bone mineral density in women with anorexia nervosa: a randomized, placebo-controlled study. *J Clin Endocrinol Metab.* 2011/04/27 ed. 2011 Jul;96(7):2081–8.
405. Miller KK, Grieco KA, Mulder J, Grinspoon S, Mickley D, Yehezkel R, et al. Effects of Risedronate on Bone Density in Anorexia Nervosa. *J Clin Endocrinol Metab.* 2004 Aug 1;89(8):3903–6.
406. Bredella MA, Fazeli PK, Daley SM, Miller KK, Rosen CJ, Klibanski A, et al. Marrow fat composition in anorexia nervosa. *Bone.* 2014/06/19 ed. 2014 Sep;66:199–204.

407. Abella E, Feliu E, Granada I, Millá F, Oriol A, Ribera JM, et al. Bone Marrow Changes in Anorexia Nervosa Are Correlated With the Amount of Weight Loss and Not With Other Clinical Findings. *Am J Clin Pathol*. 2002 Oct 1;118(4):582–8.
408. Ecklund K, Vajapeyam S, Mulkern RV, Feldman HA, O'Donnell JM, DiVasta AD, et al. Bone marrow fat content in 70 adolescent girls with anorexia nervosa: Magnetic resonance imaging and magnetic resonance spectroscopy assessment. *Pediatr Radiol*. 2017/04/22 ed. 2017 Jul;47(8):952–62.
409. Moore SG, Dawson KL. Red and yellow marrow in the femur: age-related changes in appearance at MR imaging. *Radiology*. 1990 Apr 1;175(1):219–23.
410. Singhal V, Tulsiani S, Campoverde KJ, Mitchell DM, Slattery M, Schorr M, et al. Impaired bone strength estimates at the distal tibia and its determinants in adolescents with anorexia nervosa. *Bone*. 2017/07/08 ed. 2018 Jan;106:61–8.
411. Badr S, Legroux-Gérot I, Vignau J, Chauveau C, Ruschke S, Karampinos DC, et al. Comparison of regional bone marrow adiposity characteristics at the hip of underweight and weight-recovered women with anorexia nervosa using magnetic resonance spectroscopy. *Bone*. 2019 Oct 1;127:135–45.
412. Fazeli PK, Faje AT, Bredella MA, Polineni S, Russell S, Resulaj M, et al. Changes in marrow adipose tissue with short-term changes in weight in premenopausal women with anorexia nervosa. *Eur J Endocrinol*. 2019 Mar;180(3):189–99.
413. Hamrick MW, Ding KH, Ponnala S, Ferrari SL, Isaacs CM. Caloric Restriction Decreases Cortical Bone Mass but Spares Trabecular Bone in the Mouse Skeleton: Implications for the Regulation of Bone Mass by Body Weight. *J Bone Miner Res*. 2008 Jun 1;23(6):870–8.
414. Devlin MJ, Cloutier AM, Thomas NA, Panus DA, Lotinun S, Pinz I, et al. Caloric restriction leads to high marrow adiposity and low bone mass in growing mice. *J Bone Miner Res Off J Am Soc Bone Miner Res*. 2010 Sep;25(9):2078–88.
415. Van Harten S, Cardoso L. Feed restriction and genetic selection on the expression and activity of metabolism regulatory enzymes in rabbits. *Animal*. 2010;4(11):1873–83.
416. Almeida A, Van Harten S, Campos A, Coelho A, Cardoso L. The effect of weight loss on protein profiles of gastrocnemius muscle in rabbits: a study using 1D electrophoresis and peptide mass fingerprinting. *J Anim Physiol Anim Nutr*. 2010;94(2):174–85.
417. Kovacova Z, Vitkova M, Kovacikova M, Klimcakova E, Bajzova M, Hnevkovska Z, et al. Secretion of adiponectin multimeric complexes from adipose tissue explants is not modified by very low calorie diet. *Eur J Endocrinol*. 2009;160(4):585.
418. Shen W, Chen J, Gantz M, Punyanitya M, Heymsfield SB, Gallagher D, et al. MRI-measured pelvic bone marrow adipose tissue is inversely related to DXA-measured bone mineral in younger and older adults. *Eur J Clin Nutr*. 2012 Sep 1;66(9):983–8.
419. Richards JB, Valdes AM, Burling K, Perks UC, Spector TD. Serum Adiponectin and Bone Mineral Density in Women. *J Clin Endocrinol Metab*. 2007 Apr 1;92(4):1517–23.

420. Piotrowska K, Zgutka K, Kupnicka P, Chlubek D, Pawlik A, Baranowska-Bosiacka I. Analysis of Bone Mineral Profile After Prolonged Every-Other-Day Feeding in C57BL/6J Male and Female Mice. *Biol Trace Elem Res*. 2019/06/08 ed. 2020 Mar;194(1):177–83.
421. Duque G, Al Saedi A, Rivas D, Miard S, Ferland G, Picard F, et al. Differential Effects of Long-Term Caloric Restriction and Dietary Protein Source on Bone and Marrow Fat of the Aging Rat. *J Gerontol A Biol Sci Med Sci*. 2020 Oct 15;75(11):2031–6.
422. Finkel T, Deng CX, Mostoslavsky R. Recent progress in the biology and physiology of sirtuins. *Nature*. 2009 Jul 30;460(7255):587–91.
423. Michan S, Sinclair D. Sirtuins in mammals: insights into their biological function. *Biochem J*. 2007 May 15;404(1):1–13.
424. Klar AJ, Fogel S, Macleod K. MAR1-a Regulator of the HMa and HMalpha Loci in *SACCHAROMYCES CEREVISIAE*. *Genetics*. 1979 Sep;93(1):37–50.
425. Shore D, Squire M, Nasmyth KA. Characterization of two genes required for the position-effect control of yeast mating-type genes. *EMBO J*. 1984 Dec 1;3(12):2817–23.
426. Ivy JM, Hicks JB, Klar AJ. Map positions of yeast genes SIR1, SIR3 and SIR4. *Genetics*. 1985 Dec;111(4):735–44.
427. Rine J, Herskowitz I. Four genes responsible for a position effect on expression from HML and HMR in *Saccharomyces cerevisiae*. *Genetics*. 1987 May;116(1):9–22.
428. Imai S ichiro, Armstrong CM, Kaerberlein M, Guarente L. Transcriptional silencing and longevity protein Sir2 is an NAD-dependent histone deacetylase. *Nature*. 2000 Feb 1;403(6771):795–800.
429. Sinclair DA, Guarente L. Extrachromosomal rDNA Circles— A Cause of Aging in Yeast. *Cell*. 1997 Dec 26;91(7):1033–42.
430. North BJ, Verdin E. Sirtuins: Sir2-related NAD-dependent protein deacetylases. *Genome Biol*. 2004/04/28 ed. 2004;5(5):224–224.
431. Frye RA. Characterization of Five Human cDNAs with Homology to the Yeast SIR2 Gene: Sir2-like Proteins (Sirtuins) Metabolize NAD and May Have Protein ADP-Ribosyltransferase Activity. *Biochem Biophys Res Commun*. 1999 Jun 24;260(1):273–9.
432. Haigis MC, Guarente LP. Mammalian sirtuins—emerging roles in physiology, aging, and calorie restriction. *Genes Dev*. 2006 Nov 1;20(21):2913–21.
433. Hou X, Rooklin D, Fang H, Zhang Y. Resveratrol serves as a protein-substrate interaction stabilizer in human SIRT1 activation. *Sci Rep*. 2016 Nov 30;6(1):38186.
434. North BJ, Verdin E. Interphase Nucleo-Cytoplasmic Shuttling and Localization of SIRT2 during Mitosis. *PLOS ONE*. 2007 Aug 29;2(8):e784.

435. Tanno M, Sakamoto J, Miura T, Shimamoto K, Horio Y. Nucleocytoplasmic Shuttling of the NAD⁺-dependent Histone Deacetylase SIRT1 *. *J Biol Chem.* 2007 Mar 2;282(9):6823–32.
436. Hallows WC, Albaugh BN, Denu JM. Where in the cell is SIRT3? – functional localization of an NAD⁺-dependent protein deacetylase. *Biochem J.* 2008 Mar 27;411(2):e11–3.
437. Haigis MC, Mostoslavsky R, Haigis KM, Fahie K, Christodoulou DC, Murphy AJ, et al. SIRT4 Inhibits Glutamate Dehydrogenase and Opposes the Effects of Calorie Restriction in Pancreatic β Cells. *Cell.* 2006 Sep 8;126(5):941–54.
438. Schwer B, North BJ, Frye RA, Ott M, Verdin E. The human silent information regulator (Sir)2 homologue hSIRT3 is a mitochondrial nicotinamide adenine dinucleotide–dependent deacetylase. *J Cell Biol.* 2002 Aug 19;158(4):647–57.
439. Frye RA. Phylogenetic Classification of Prokaryotic and Eukaryotic Sir2-like Proteins. *Biochem Biophys Res Commun.* 2000 Jul 5;273(2):793–8.
440. Greiss S, Gartner A. Sirtuin/Sir2 phylogeny, evolutionary considerations and structural conservation. *Mol Cells.* 2009 Nov 18;28(5):407.
441. Tsang AW, Escalante-Semerena JC. CobB, a New Member of the SIR2 Family of Eucaryotic Regulatory Proteins, Is Required to Compensate for the Lack of Nicotinate Mononucleotide:5,6-Dimethylbenzimidazole Phosphoribosyltransferase Activity in cobT Mutants during Cobalamin Biosynthesis in *Salmonella typhimurium* LT2 *. *J Biol Chem.* 1998 Nov 27;273(48):31788–94.
442. Tanner KG, Landry J, Sternglanz R, Denu JM. Silent information regulator 2 family of NAD- dependent histone/protein deacetylases generates a unique product, 1-O-acetyl-ADP-ribose. *Proc Natl Acad Sci U S A.* 2000 Dec 19;97(26):14178–82.
443. Landry J, Slama JT, Sternglanz R. Role of NAD⁺ in the Deacetylase Activity of the SIR2-like Proteins. *Biochem Biophys Res Commun.* 2000 Nov 30;278(3):685–90.
444. North BJ, Marshall BL, Borra MT, Denu JM, Verdin E. The Human Sir2 Ortholog, SIRT2, Is an NAD⁺-Dependent Tubulin Deacetylase. *Mol Cell.* 2003 Feb 1;11(2):437–44.
445. Michishita E, McCord RA, Berber E, Kioi M, Padilla-Nash H, Damian M, et al. SIRT6 is a histone H3 lysine 9 deacetylase that modulates telomeric chromatin. *Nature.* 2008 Mar 1;452(7186):492–6.
446. Liszt G, Ford E, Kurtev M, Guarente L. Mouse Sir2 Homolog SIRT6 Is a Nuclear ADP-riboseyltransferase*. *J Biol Chem.* 2005 Jun 3;280(22):21313–20.
447. Hawse WF, Wolberger C. Structure-based Mechanism of ADP-ribosylation by Sirtuins *. *J Biol Chem.* 2009 Nov 27;284(48):33654–61.
448. Liou GG, Tanny JC, Kruger RG, Walz T, Moazed D. Assembly of the SIR Complex and Its Regulation by O-Acetyl-ADP-Ribose, a Product of NAD-Dependent Histone Deacetylation. *Cell.* 2005 May 20;121(4):515–27.

449. Vaquero A, Scher M, Lee D, Erdjument-Bromage H, Tempst P, Reinberg D. Human SirT1 Interacts with Histone H1 and Promotes Formation of Facultative Heterochromatin. *Mol Cell*. 2004 Oct 8;16(1):93–105.
450. Vassilopoulos A, Fritz KS, Petersen DR, Gius D. The human sirtuin family: Evolutionary divergences and functions. *Hum Genomics*. 2011 Jul 1;5(5):485.
451. Michishita E, Park JY, Burneskis JM, Barrett JC, Horikawa I. Evolutionarily conserved and nonconserved cellular localizations and functions of human SIRT proteins. *Mol Biol Cell*. 2005/08/03 ed. 2005 Oct;16(10):4623–35.
452. Carafa V, Rotili D, Forgione M, Cuomo F, Serretiello E, Hailu GS, et al. Sirtuin functions and modulation: from chemistry to the clinic. *Clin Epigenetics*. 2016 May 25;8:61–61.
453. Guarente L. Sirtuins, Aging, and Medicine. *N Engl J Med*. 2011 Jun 8;364(23):2235–44.
454. Lilja S, Stoll C, Krammer U, Hippe B, Duszka K, Debebe T, et al. Five Days Periodic Fasting Elevates Levels of Longevity Related Christensenella and Sirtuin Expression in Humans. *Int J Mol Sci*. 2021;22(5).
455. Inoue T, Hiratsuka M, Osaki M, Yamada H, Kishimoto I, Yamaguchi S, et al. SIRT2, a tubulin deacetylase, acts to block the entry to chromosome condensation in response to mitotic stress. *Oncogene*. 2007 Feb 1;26(7):945–57.
456. Kim J ye, Hwang HG, Lee JY, Kim M, Kim JY. Cortactin deacetylation by HDAC6 and SIRT2 regulates neuronal migration and dendrite morphogenesis during cerebral cortex development. *Mol Brain*. 2020 Jul 25;13(1):105.
457. Dryden Sylvia C., Nahhas Fatimah A., Nowak James E., Goustin Anton-Scott, Tainsky Michael A. Role for Human SIRT2 NAD-Dependent Deacetylase Activity in Control of Mitotic Exit in the Cell Cycle. *Mol Cell Biol*. 2003 May 1;23(9):3173–85.
458. Vaquero A, Scher MB, Lee DH, Sutton A, Cheng HL, Alt FW, et al. SirT2 is a histone deacetylase with preference for histone H4 Lys 16 during mitosis. *Genes Dev*. 2006 May 15;20(10):1256–61.
459. Serrano L, Martínez-Redondo P, Marazuela-Duque A, Vazquez BN, Dooley SJ, Voigt P, et al. The tumor suppressor SirT2 regulates cell cycle progression and genome stability by modulating the mitotic deposition of H4K20 methylation. *Genes Dev*. 2013 Mar 15;27(6):639–53.
460. Jing E, Gesta S, Kahn CR. SIRT2 regulates adipocyte differentiation through FoxO1 acetylation/deacetylation. *Cell Metab*. 2007 Aug;6(2):105–14.
461. Wang F, Tong Q. SIRT2 suppresses adipocyte differentiation by deacetylating FOXO1 and enhancing FOXO1's repressive interaction with PPARgamma. *Mol Biol Cell*. 2008/11/26 ed. 2009 Feb;20(3):801–8.

462. Guo L, Guo YY, Li BY, Peng WQ, Chang XX, Gao X, et al. Enhanced acetylation of ATP-citrate lyase promotes the progression of nonalcoholic fatty liver disease. *J Biol Chem*. 2019 Aug 1;294(31):11805–16.
463. Lin R, Tao R, Gao X, Li T, Zhou X, Guan KL, et al. Acetylation stabilizes ATP-citrate lyase to promote lipid biosynthesis and tumor growth. *Mol Cell*. 2013/08/08 ed. 2013 Aug 22;51(4):506–18.
464. Rothgiesser KM, Erener S, Waibel S, Lüscher B, Hottiger MO. SIRT2 regulates NF- κ B-dependent gene expression through deacetylation of p65 Lys310. *J Cell Sci*. 2010 Dec 15;123(24):4251–8.
465. Lombard DB, Zwaans BMM. SIRT3: as simple as it seems? *Gerontology*. 2013/10/25 ed. 2014;60(1):56–64.
466. Uchida Y, Izai K, Orii T, Hashimoto T. Novel fatty acid beta-oxidation enzymes in rat liver mitochondria. II. Purification and properties of enoyl-coenzyme A (CoA) hydratase/3-hydroxyacyl-CoA dehydrogenase/3-ketoacyl-CoA thiolase trifunctional protein. *J Biol Chem*. 1992 Jan 15;267(2):1034–41.
467. Zhang Y, Zhou F, Bai M, Liu Y, Zhang L, Zhu Q, et al. The pivotal role of protein acetylation in linking glucose and fatty acid metabolism to β -cell function. *Cell Death Dis*. 2019 Jan 25;10(2):66.
468. Peterson BS, Campbell JE, Ilkayeva O, Grimsrud PA, Hirschey MD, Newgard CB. Remodeling of the Acetylproteome by SIRT3 Manipulation Fails to Affect Insulin Secretion or β Cell Metabolism in the Absence of Overnutrition. *Cell Rep*. 2018 Jul 3;24(1):209-223.e6.
469. Caton PW, Richardson SJ, Kieswich J, Bugliani M, Holland ML, Marchetti P, et al. Sirtuin 3 regulates mouse pancreatic beta cell function and is suppressed in pancreatic islets isolated from human type 2 diabetic patients. *Diabetologia*. 2013 May 1;56(5):1068–77.
470. Gao P, Jiang Y, Wu H, Sun F, Li Y, He H, et al. Inhibition of Mitochondrial Calcium Overload by SIRT3 Prevents Obesity- or Age-Related Whitening of Brown Adipose Tissue. *Diabetes*. 2020 Feb 1;69(2):165.
471. Shi T, Wang F, Stieren E, Tong Q. SIRT3, a Mitochondrial Sirtuin Deacetylase, Regulates Mitochondrial Function and Thermogenesis in Brown Adipocytes. *J Biol Chem*. 2005 Apr 8;280(14):13560–7.
472. Hirschey MD, Shimazu T, Goetzman E, Jing E, Schwer B, Lombard DB, et al. SIRT3 regulates mitochondrial fatty-acid oxidation by reversible enzyme deacetylation. *Nature*. 2010 Mar 4;464(7285):121–5.
473. Ahuja N, Schwer B, Carobbio S, Waltregny D, North BJ, Castronovo V, et al. Regulation of Insulin Secretion by SIRT4, a Mitochondrial ADP-ribosyltransferase. *J Biol Chem*. 2007 Nov 16;282(46):33583–92.
474. Argmann C, Auwerx J. Insulin Secretion: SIRT4 Gets in on the Act. *Cell*. 2006 Sep 8;126(5):837–9.

475. Huynh FK, Peterson BS, Anderson KA, Lin Z, Coakley AJ, Llaguno FMS, et al. β -Cell-specific ablation of sirtuin 4 does not affect nutrient-stimulated insulin secretion in mice. *Am J Physiol-Endocrinol Metab*. 2020 Aug 31;319(4):E805–13.
476. Csibi A, Fendt SM, Li C, Poulogiannis G, Choo AY, Chapski DJ, et al. The mTORC1 Pathway Stimulates Glutamine Metabolism and Cell Proliferation by Repressing SIRT4. *Cell*. 2013 May 9;153(4):840–54.
477. Carrico C, Meyer JG, He W, Gibson BW, Verdin E. The Mitochondrial Acylome Emerges: Proteomics, Regulation by Sirtuins, and Metabolic and Disease Implications. *Cell Metab*. 2018 Mar 6;27(3):497–512.
478. Smith HQ, Li C, Stanley CA, Smith TJ. Glutamate Dehydrogenase, a Complex Enzyme at a Crucial Metabolic Branch Point. *Neurochem Res*. 2019 Jan 1;44(1):117–32.
479. Mathias RA, Greco TM, Oberstein A, Budayeva HG, Chakrabarti R, Rowland EA, et al. Sirtuin 4 Is a Lipoamidase Regulating Pyruvate Dehydrogenase Complex Activity. *Cell*. 2014 Dec 18;159(7):1615–25.
480. Laurent G, German NJ, Saha AK, de Boer VCJ, Davies M, Koves TR, et al. SIRT4 coordinates the balance between lipid synthesis and catabolism by repressing malonyl CoA decarboxylase. *Mol Cell*. 2013 Jun 6;50(5):686–98.
481. Kang HS, Okamoto K, Kim YS, Takeda Y, Bortner CD, Dang H, et al. Nuclear Orphan Receptor TAK1/TR4-Deficient Mice Are Protected Against Obesity-Linked Inflammation, Hepatic Steatosis, and Insulin Resistance. *Diabetes*. 2011 Jan 1;60(1):177.
482. Foster DW. Malonyl-CoA: the regulator of fatty acid synthesis and oxidation. *J Clin Invest*. 2012 Jun;122(6):1958–9.
483. Du J, Zhou Y, Su X, Yu JJ, Khan S, Jiang H, et al. Sirt5 Is a NAD-Dependent Protein Lysine Demalonylase and Desuccinylase. *Science*. 2011 Nov 11;334(6057):806–9.
484. Haschler TN, Horsley H, Balys M, Anderson G, Taanman JW, Unwin RJ, et al. Sirtuin 5 depletion impairs mitochondrial function in human proximal tubular epithelial cells. *Sci Rep*. 2021 Jul 30;11(1):15510.
485. Zhou B, Xiao M, Hu H, Pei X, Xue Y, Miao G, et al. Cardioprotective Role of SIRT5 in Response to Acute Ischemia Through a Novel Liver-Cardiac Crosstalk Mechanism. *Front Cell Dev Biol* [Internet]. 2021;9. Available from: <https://www.frontiersin.org/articles/10.3389/fcell.2021.687559>
486. Tan M, Peng C, Anderson KA, Chhoy P, Xie Z, Dai L, et al. Lysine Glutarylation Is a Protein Posttranslational Modification Regulated by SIRT5. *Cell Metab*. 2014 Apr 1;19(4):605–17.
487. Park J, Chen Y, Tishkoff DX, Peng C, Tan M, Dai L, et al. SIRT5-Mediated Lysine Desuccinylation Impacts Diverse Metabolic Pathways. *Mol Cell*. 2013 Jun 27;50(6):919–30.

488. Nishida Y, Rardin MJ, Carrico C, He W, Sahu AK, Gut P, et al. SIRT5 Regulates both Cytosolic and Mitochondrial Protein Malonylation with Glycolysis as a Major Target. *Mol Cell*. 2015 Jul 16;59(2):321–32.
489. Etchegaray JP, Zhong L, Mostoslavsky R. The Histone Deacetylase SIRT6: At the Crossroads Between Epigenetics, Metabolism and Disease. *Curr Top Med Chem*. 2013;13(23):2991–3000.
490. Raj S, Dsouza LA, Singh SP, Kanwal A. Sirt6 Deacetylase: A Potential Key Regulator in the Prevention of Obesity, Diabetes and Neurodegenerative Disease. *Front Pharmacol*. 2020;11:598326.
491. Onn L, Portillo M, Ilic S, Cleitman G, Stein D, Kaluski S, et al. SIRT6 is a DNA double-strand break sensor. Chua K, Tyler JK, editors. *eLife*. 2020 Jan;9:e51636.
492. Mostoslavsky R, Chua KF, Lombard DB, Pang WW, Fischer MR, Gellon L, et al. Genomic Instability and Aging-like Phenotype in the Absence of Mammalian SIRT6. *Cell*. 2006 Jan 27;124(2):315–29.
493. Kawahara T, Rapicavoli N, Wu A, Qu K, Quake S, Chang H. Dynamic Chromatin Localization of Sirt6 Shapes Stress- and Aging-Related Transcriptional Networks. *PLoS Genet*. 2011 Jun 1;7:e1002153.
494. Santos-Barriopedro I, Bosch-Presegué L, Marazuela-Duque A, de la Torre C, Colomer C, Vazquez BN, et al. SIRT6-dependent cysteine monoubiquitination in the PRE-SET domain of Suv39h1 regulates the NF- κ B pathway. *Nat Commun*. 2018 Jan 9;9(1):101–101.
495. Kanfi Y, Peshti V, Gil R, Naiman S, Nahum L, Levin E, et al. SIRT6 protects against pathological damage caused by diet-induced obesity. *Aging Cell*. 2010 Apr 1;9(2):162–73.
496. X Xiong, G Wang, R Tao, P Wu, T Kono, K Li, et al. Sirtuin 6 regulates glucose-stimulated insulin secretion in mouse pancreatic beta cells. *Diabetologia*. 2016;59:151–60.
497. Xiong X, Zhang C, Zhang Y, Fan R, Qian X, Dong XC. Fabp4-Cre-mediated Sirt6 deletion impairs adipose tissue function and metabolic homeostasis in mice. *J Endocrinol*. 2017/04/06 ed. 2017 Jun;233(3):307–14.
498. Kim HS, Xiao C, Wang RH, Lahusen T, Xu X, Vassilopoulos A, et al. Hepatic-specific disruption of SIRT6 in mice results in fatty liver formation due to enhanced glycolysis and triglyceride synthesis. *Cell Metab*. 2010 Sep 8;12(3):224–36.
499. Elhanati S, Kanfi Y, Varvak A, Roichman A, Carmel-Gross I, Barth S, et al. Multiple Regulatory Layers of SREBP1/2 by SIRT6. *Cell Rep*. 2013 Sep 12;4(5):905–12.
500. Beauharnois J, Bolívar B, Welch J. Sirtuin 6: A review of biological effects and potential therapeutic properties. *Mol Biosyst*. 2013 Apr 17;9.
501. Li Y, Jin J, Wang Y. SIRT6 Widely Regulates Aging, Immunity, and Cancer. *Front Oncol*. 2022 Apr 1;12:861334.

502. Gertler A, Cohen H. SIRT6, a protein with many faces. *Biogerontology*. 2013 Nov 10;14.
503. Ford E, Voit R, Liszt G, Magin C, Grummt I, Guarente L. Mammalian Sir2 homolog SIRT7 is an activator of RNA polymerase I transcription. *Genes Dev*. 2006 May 1;20(9):1075–80.
504. Grummt I, Pikaard CS. Epigenetic silencing of RNA polymerase I transcription. *Nat Rev Mol Cell Biol*. 2003 Aug 1;4(8):641–9.
505. Grob A, Roussel P, Wright JE, McStay B, Hernandez-Verdun D, Sirri V. Involvement of SIRT7 in resumption of rDNA transcription at the exit from mitosis. *J Cell Sci*. 2009 Feb 15;122(4):489–98.
506. Chen S, Seiler J, Santiago-Reichert M, Felbel K, Grummt I, Voit R. Repression of RNA polymerase I upon stress is caused by inhibition of RNA-dependent deacetylation of PAF53 by SIRT7. *Mol Cell*. 2013 Nov 7;52:303–13.
507. Yamagata K, Yoshizawa T. Chapter Four - Transcriptional Regulation of Metabolism by SIRT1 and SIRT7. In: Loos F, editor. *International Review of Cell and Molecular Biology* [Internet]. Academic Press; 2018. p. 143–66. Available from: <https://www.sciencedirect.com/science/article/pii/S1937644817300849>
508. Shin J, He M, Liu Y, Paredes S, Villanova L, Brown K, et al. SIRT7 represses Myc activity to suppress ER stress and prevent fatty liver disease. *Cell Rep*. 2013/11/07 ed. 2013 Nov 14;5(3):654–65.
509. Zhang XA, Fathima S, AU Azhar, Gohar AU, Wei, Jeanne Y, TI. Alternative Splicing Increases Sirtuin Gene Family Diversity and Modulates Their Subcellular Localization and Function. *Int J Mol Sci*. 2021;22(2).
510. Chang HC, Guarente L. SIRT1 and other sirtuins in metabolism. *Trends Endocrinol Metab*. 2013/12/30 ed. 2014 Mar;25(3):138–45.
511. Zhao X, Allison D, Condon B, Zhang F, Gheyi T, Zhang A, et al. The 2.5 Å Crystal Structure of the SIRT1 Catalytic Domain Bound to Nicotinamide Adenine Dinucleotide (NAD⁺) and an Indole (EX527 Analogue) Reveals a Novel Mechanism of Histone Deacetylase Inhibition. *J Med Chem*. 2013 Feb 14;56(3):963–9.
512. Hoff KG, Avalos JL, Sens K, Wolberger C. Insights into the sirtuin mechanism from ternary complexes containing NAD⁺ and acetylated peptide. *Structure*. 2006;14(8):1231–40.
513. Davenport AM, Huber FM, Hoelz A. Structural and Functional Analysis of Human SIRT1. *J Mol Biol*. 2014 Feb 6;426(3):526–41.
514. Min J, Landry J, Sternglanz R, Xu RM. Crystal structure of a SIR2 homolog–NAD complex. *Cell*. 2001;105(2):269–79.
515. Kang H, Suh JY, Jung YS, Jung JW, Kim MK, Chung JH. Peptide Switch Is Essential for Sirt1 Deacetylase Activity. *Mol Cell*. 2011 Oct 21;44(2):203–13.

516. Pan M, Yuan H, Brent M, Ding EC, Marmorstein R. SIRT1 Contains N- and C-terminal Regions That Potentiate Deacetylase Activity *. *J Biol Chem.* 2012 Jan 1;287(4):2468–76.
517. Ramu M, Anuja K, Alcaín F. SIRT1 and SIRT2 Activity Control in Neurodegenerative Diseases. Vol. 11, *Frontiers in Pharmacology.* 2021.
518. Westerheide SD, Anckar J, Stevens Jr SM, Sistonen L, Morimoto RI. Stress-inducible regulation of heat shock factor 1 by the deacetylase SIRT1. *Science.* 2009;323(5917):1063–6.
519. Daitoku H, Hatta M, Matsuzaki H, Aratani S, Ohshima T, Miyagishi M, et al. Silent information regulator 2 potentiates Foxo1-mediated transcription through its deacetylase activity. *Proc Natl Acad Sci.* 2004;101(27):10042–7.
520. Yeung F, Hoberg JE, Ramsey CS, Keller MD, Jones DR, Frye RA, et al. Modulation of NF- κ B-dependent transcription and cell survival by the SIRT1 deacetylase. *EMBO J.* 2004;23(12):2369–80.
521. Hendler A, Akiva E, Sandhu M, Goldberg D, Arbely E, Jackson CJ, et al. Human SIRT1 Multispecificity Is Modulated by Active-Site Vicinity Substitutions during Natural Evolution. *Mol Biol Evol.* 2021 Feb 1;38(2):545–56.
522. Rifai K, Judes G, Idrissou M, Daures M, Bignon YJ, Penault-Llorca F, et al. SIRT1-dependent epigenetic regulation of H3 and H4 histone acetylation in human breast cancer. *Oncotarget Vol 9 No 55* [Internet]. 2018 [cited 2018 Jan 1]; Available from: <https://www.oncotarget.com/article/25771/text/>
523. Yamamoto H, Schoonjans K, Auwerx J. Sirtuin functions in health and disease. *Mol Endocrinol.* 2007;21(8):1745–55.
524. Muth V, Nadaud S, Grummt I, Voit R. Acetylation of TAFI68, a subunit of TIF-IB/SL1, activates RNA polymerase I transcription. *EMBO J.* 2001;20(6):1353–62.
525. Vaquero A, Scher M, Erdjument-Bromage H, Tempst P, Serrano L, Reinberg D. SIRT1 regulates the histone methyl-transferase SUV39H1 during heterochromatin formation. *Nature.* 2007 Nov 1;450(7168):440–4.
526. Bosch-Presegué L, Vaquero A. Sirtuin-dependent epigenetic regulation in the maintenance of genome integrity. *FEBS J.* 2015 May 1;282(9):1745–67.
527. Bouras T, Fu M, Sauve AA, Wang F, Quong AA, Perkins ND, et al. SIRT1 deacetylation and repression of p300 involves lysine residues 1020/1024 within the cell cycle regulatory domain 1. *J Biol Chem.* 2005;280(11):10264–76.
528. Fulco M, Schiltz RL, Iezzi S, King MT, Zhao P, Kashiwaya Y, et al. Sir2 regulates skeletal muscle differentiation as a potential sensor of the redox state. *Mol Cell.* 2003;12(1):51–62.
529. Zhao X, Sternsdorf T, Bolger TA, Evans RM, Yao TP. Regulation of MEF2 by histone deacetylase 4-and SIRT1 deacetylase-mediated lysine modifications. *Mol Cell Biol.* 2005;25(19):8456–64.

530. Lee D, Goldberg AL. SIRT1 Protein, by Blocking the Activities of Transcription Factors FoxO1 and FoxO3, Inhibits Muscle Atrophy and Promotes Muscle Growth *. *J Biol Chem*. 2013 Oct 18;288(42):30515–26.
531. O'Hagan HM, Wang W, Sen S, Shields CD, Lee SS, Zhang YW, et al. Oxidative damage targets complexes containing DNA methyltransferases, SIRT1, and polycomb members to promoter CpG Islands. *Cancer Cell*. 2011;20(5):606–19.
532. Jeong J, Juhn K, Lee H, Kim SH, Min BH, Lee KM, et al. SIRT1 promotes DNA repair activity and deacetylation of Ku70. *Exp Mol Med*. 2007;39(1):8–13.
533. O'Hagan HM, Mohammad HP, Baylin SB. Double strand breaks can initiate gene silencing and SIRT1-dependent onset of DNA methylation in an exogenous promoter CpG island. *PLoS Genet*. 2008;4(8):e1000155.
534. O'Hagan HM. Chromatin modifications during repair of environmental exposure-induced DNA damage: A potential mechanism for stable epigenetic alterations. *Environ Mol Mutagen*. 2014;55(3):278–91.
535. Ding N, Bonham EM, Hannon BE, Amick TR, Baylin SB, O'Hagan HM. Mismatch repair proteins recruit DNA methyltransferase 1 to sites of oxidative DNA damage. *J Mol Cell Biol*. 2016;8(3):244–54.
536. Han C, Srivastava AK, Cui T, Wang QE, Wani AA. Differential DNA lesion formation and repair in heterochromatin and euchromatin. *Carcinogenesis*. 2016;37(2):129–38.
537. Kumar R, Horikoshi N, Singh M, Gupta A, Misra HS, Albuquerque K, et al. Chromatin modifications and the DNA damage response to ionizing radiation. *Front Oncol*. 2013;2:214.
538. Oberdoerffer P, Michan S, McVay M, Mostoslavsky R, Vann J, Park SK, et al. SIRT1 Redistribution on Chromatin Promotes Genomic Stability but Alters Gene Expression during Aging. *Cell*. 2008 Nov 28;135(5):907–18.
539. Wang RH, Sengupta K, Li C, Kim HS, Cao L, Xiao C, et al. Impaired DNA damage response, genome instability, and tumorigenesis in SIRT1 mutant mice. *Cancer Cell*. 2008;14(4):312–23.
540. Yuan Z, Zhang X, Sengupta N, Lane WS, Seto E. SIRT1 regulates the function of the Nijmegen breakage syndrome protein. *Mol Cell*. 2007;27(1):149–62.
541. Hughes KJ, Meares GP, Hansen PA, Corbett JA. FoxO1 and SIRT1 regulate β -cell responses to nitric oxide. *J Biol Chem*. 2011;286(10):8338–48.
542. Brunet A, Sweeney LB, Sturgill JF, Chua KF, Greer PL, Lin Y, et al. Stress-dependent regulation of FOXO transcription factors by the SIRT1 deacetylase. *science*. 2004;303(5666):2011–5.
543. Giannakou ME, Partridge L. The interaction between FOXO and SIRT1: tipping the balance towards survival. *Trends Cell Biol*. 2004;14(8):408–12.

544. Guarente L. Sirtuins in aging and disease. In Cold Spring Harbor Laboratory Press; 2007. p. 483–8.
545. Luo J, Nikolaev AY, Imai S, Ichiro, Chen D, Su F, Shiloh A, et al. Negative Control of p53 by Sir2 α Promotes Cell Survival under Stress. *Cell*. 2001 Oct 19;107(2):137–48.
546. Cheng HL, Mostoslavsky R, Saito S, Manis JP, Gu Y, Patel P, et al. Developmental defects and p53 hyperacetylation in Sir2 homolog (SIRT1)-deficient mice. *Proc Natl Acad Sci*. 2003;100(19):10794–9.
547. Vaziri H, Dessain SK, Eaton EN, Imai SI, Frye RA, Pandita TK, et al. hSIR2/SIRT1 functions as an NAD-dependent p53 deacetylase. *Cell*. 2001;107(2):149–59.
548. Han MK, Song EK, Guo Y, Ou X, Mantel C, Broxmeyer HE. SIRT1 regulates apoptosis and Nanog expression in mouse embryonic stem cells by controlling p53 subcellular localization. *Cell Stem Cell*. 2008;2(3):241–51.
549. Khan FM, Marquardt S, Gupta SK, Knoll S, Schmitz U, Spitschak A, et al. Unraveling a tumor type-specific regulatory core underlying E2F1-mediated epithelial-mesenchymal transition to predict receptor protein signatures. *Nat Commun*. 2017 Aug 4;8(1):198.
550. Wang C, Chen L, Hou X, Li Z, Kabra N, Ma Y, et al. Interactions between E2F1 and SirT1 regulate apoptotic response to DNA damage. *Nat Cell Biol*. 2006 Sep 1;8(9):1025–31.
551. Dai JM, Wang ZY, Sun DC, Lin RX, Wang SQ. SIRT1 interacts with p73 and suppresses p73-dependent transcriptional activity. *J Cell Physiol*. 2007;210(1):161–6.
552. Kuo SJ, Lin HY, Chien SY, Chen DR. SIRT1 suppresses breast cancer growth through downregulation of the Bcl-2 protein. *Oncol Rep*. 2013 Jul 1;30(1):125–30.
553. Nakae J, Cao Y, Daitoku H, Fukamizu A, Ogawa W, Yano Y, et al. The LXXLL motif of murine forkhead transcription factor FoxO1 mediates Sirt1-dependent transcriptional activity. *J Clin Invest*. 2006;116(9):2473–83.
554. Li J, Wang E, Rinaldo F, Datta K. Upregulation of VEGF-C by androgen depletion: the involvement of IGF-IR-FOXO pathway. *Oncogene*. 2005;24(35):5510–20.
555. Hariharan N, Maejima Y, Nakae J, Paik J, DePinho RA, Sadoshima J. Deacetylation of FoxO by Sirt1 Plays an Essential Role in Mediating Starvation-Induced Autophagy in Cardiac Myocytes. *Circ Res*. 2010 Dec 10;107(12):1470–82.
556. Wang F, Chan CH, Chen K, Guan X, Lin HK, Tong Q. Deacetylation of FOXO3 by SIRT1 or SIRT2 leads to Skp2-mediated FOXO3 ubiquitination and degradation. *Oncogene*. 2012 Mar 1;31(12):1546–57.
557. Motta MC, Divecha N, Lemieux M, Kamel C, Chen D, Gu W, et al. Mammalian SIRT1 Represses Forkhead Transcription Factors. *Cell*. 2004 Feb 20;116(4):551–63.
558. Hori YS, Kuno A, Hosoda R, Horio Y. Regulation of FOXOs and p53 by SIRT1 Modulators under Oxidative Stress. *PLOS ONE*. 2013 Sep 11;8(9):e73875.

559. Kroemer G, Mariño G, Levine B. Autophagy and the integrated stress response. *Mol Cell*. 2010;40(2):280–93.
560. Kim J, Kim YC, Fang C, Russell RC, Kim JH, Fan W, et al. Differential regulation of distinct Vps34 complexes by AMPK in nutrient stress and autophagy. *Cell*. 2013;152(1–2):290–303.
561. Lee IH, Cao L, Mostoslavsky R, Lombard DB, Liu J, Bruns NE, et al. A role for the NAD-dependent deacetylase Sirt1 in the regulation of autophagy. *Proc Natl Acad Sci*. 2008;105(9):3374–9.
562. Lee IH. Mechanisms and disease implications of sirtuin-mediated autophagic regulation. *Exp Mol Med*. 2019 Sep 6;51(9):1–11.
563. Huang R, Xu Y, Wan W, Shou X, Qian J, You Z, et al. Deacetylation of nuclear LC3 drives autophagy initiation under starvation. *Mol Cell*. 2015;57(3):456–66.
564. Vikram A, Lewarchik CM, Yoon JY, Naqvi A, Kumar S, Morgan GM, et al. Sirtuin 1 regulates cardiac electrical activity by deacetylating the cardiac sodium channel. *Nat Med*. 2017 Mar 1;23(3):361–7.
565. Yang HY, Lin FZ, Yang HW, Yu PL, Huang SM, Chen YC, et al. The effect of Sirt1 deficiency on Ca²⁺ and Na⁺ regulation in mouse ventricular myocytes. *J Cell Mol Med*. 2020 Jun 1;24(12):6762–72.
566. Yu D, Homiack DR, Sawyer EJ, Schrader LA. BK channel deacetylation by SIRT1 in dentate gyrus regulates anxiety and response to stress. *Commun Biol*. 2018 Jun 28;1(1):82.
567. Yang Y, Zhang S, Fan C, Yi W, Jiang S, Di S, et al. Protective role of silent information regulator 1 against hepatic ischemia: effects on oxidative stress injury, inflammatory response, and MAPKs. *Expert Opin Ther Targets*. 2016;20(5):519–31.
568. Chen G, Yu W, Chen X. SirT1 activator represses the transcription of TNF- α in THP-1 cells of a sepsis model via deacetylation of H4K16. *Mol Med Rep*. 2016;14(6):5544–50.
569. Zhang Y, Li Y, Li J, Li B, Chong Y, Zheng G, et al. SIRT1 alleviates isoniazid-induced hepatocyte injury by reducing histone acetylation in the IL-6 promoter region. *Int Immunopharmacol*. 2019;67:348–55.
570. Hayden MS, Ghosh S. Shared principles in NF- κ B signaling. *Cell*. 2008;132(3):344–62.
571. Sun SC, Ley SC. New insights into NF- κ B regulation and function. *Trends Immunol*. 2008;29(10):469–78.
572. Lei M, Wang J guo, Xiao D ming, Fan M, Wang D ping, Xiong J yi, et al. Resveratrol inhibits interleukin 1 β -mediated inducible nitric oxide synthase expression in articular chondrocytes by activating SIRT1 and thereby suppressing nuclear factor- κ B activity. *Eur J Pharmacol*. 2012;674(2–3):73–9.

573. Liu TF, Yoza BK, El Gazzar M, Vachharajani VT, McCall CE. NAD⁺-dependent SIRT1 deacetylase participates in epigenetic reprogramming during endotoxin tolerance. *J Biol Chem*. 2011;286(11):9856–64.
574. Hwang J woong, Yao H, Caito S, Sundar IK, Rahman I. Redox regulation of SIRT1 in inflammation and cellular senescence. *Free Radic Biol Med*. 2013;61:95–110.
575. Yang XD, Tajkhorshid E, Chen LF. Functional interplay between acetylation and methylation of the RelA subunit of NF- κ B. *Mol Cell Biol*. 2010;30(9):2170–80.
576. Yu Q, Dong L, Li Y, Liu G. SIRT1 and HIF1 α signaling in metabolism and immune responses. *Cancer Lett*. 2018;418:20–6.
577. Yoshizaki T, Schenk S, Imamura T, Babendure JL, Sonoda N, Bae EJ, et al. SIRT1 inhibits inflammatory pathways in macrophages and modulates insulin sensitivity. *Am J Physiol-Endocrinol Metab*. 2010;298(3):E419–28.
578. Kauppinen A, Suuronen T, Ojala J, Kaarniranta K, Salminen A. Antagonistic crosstalk between NF- κ B and SIRT1 in the regulation of inflammation and metabolic disorders. *Cell Signal*. 2013;25(10):1939–48.
579. Planavila A, Iglesias R, Giralt M, Villarroya F. Sirt1 acts in association with PPAR α to protect the heart from hypertrophy, metabolic dysregulation, and inflammation. *Cardiovasc Res*. 2011 May 1;90(2):276–84.
580. Lim JH, Lee YM, Chun YS, Chen J, Kim JE, Park JW. Sirtuin 1 Modulates Cellular Responses to Hypoxia by Deacetylating Hypoxia-Inducible Factor 1 α . *Mol Cell*. 2010 Jun 25;38(6):864–78.
581. Joo HY, Yun M, Jeong J, Park ER, Shin HJ, Woo SR, et al. SIRT1 deacetylates and stabilizes hypoxia-inducible factor-1 α (HIF-1 α) via direct interactions during hypoxia. *Biochem Biophys Res Commun*. 2015 Jul 10;462(4):294–300.
582. Bejjani F, Evanno E, Zibara K, Piechaczyk M, Jariel-Encontre I. The AP-1 transcriptional complex: Local switch or remote command? *Biochim Biophys Acta BBA - Rev Cancer*. 2019 Aug 1;1872(1):11–23.
583. Gao Z, Ye J. Inhibition of transcriptional activity of c-JUN by SIRT1. *Biochem Biophys Res Commun*. 2008 Nov 28;376(4):793–6.
584. Zhang R, Chen HZ, Liu JJ, Jia YY, Zhang ZQ, Yang RF, et al. SIRT1 Suppresses Activator Protein-1 Transcriptional Activity and Cyclooxygenase-2 Expression in Macrophages *. *J Biol Chem*. 2010 Mar 5;285(10):7097–110.
585. Cantó C, Auwerx J. Caloric restriction, SIRT1 and longevity. *Trends Endocrinol Metab TEM*. 2009/08/25 ed. 2009 Sep;20(7):325–31.
586. Avilkina V, Chauveau C, Ghali Mhenni O. Sirtuin function and metabolism: Role in pancreas, liver, and adipose tissue and their crosstalk impacting bone homeostasis. *Bone*. 2022 Jan 1;154:116232.

587. Moynihan KA, Grimm AA, Plueger MM, Bernal-Mizrachi E, Ford E, Cras-Méneur C, et al. Increased dosage of mammalian Sir2 in pancreatic β cells enhances glucose-stimulated insulin secretion in mice. *Cell Metab.* 2005 Aug 1;2(2):105–17.
588. Desai T, Koulajian K, Ivovic A, Breen DM, Luu L, Tsiani EL, et al. Pharmacologic or genetic activation of SIRT1 attenuates the fat-induced decrease in beta-cell function in vivo. *Nutr Diabetes.* 2019 Mar 19;9(1):11.
589. Robson-Doucette CA, Sultan S, Allister EM, Wikstrom JD, Koshkin V, Bhattacharjee A, et al. Beta-cell uncoupling protein 2 regulates reactive oxygen species production, which influences both insulin and glucagon secretion. *Diabetes.* 2011/10/07 ed. 2011 Nov;60(11):2710–9.
590. Bordone L, Motta MC, Picard F, Robinson A, Jhala US, Apfeld J, et al. Sirt1 regulates insulin secretion by repressing UCP2 in pancreatic beta cells. *PLoS Biol.* 2005/12/27 ed. 2006 Feb;4(2):e31–e31.
591. Kitamura YI, Kitamura T, Kruse JP, Raum JC, Stein R, Gu W, et al. FoxO1 protects against pancreatic β cell failure through NeuroD and MafA induction. *Cell Metab.* 2005 Sep 1;2(3):153–63.
592. Vetterli L, Brun T, Giovannoni L, Bosco D, Maechler P. Resveratrol potentiates glucose-stimulated insulin secretion in INS-1E beta-cells and human islets through a SIRT1-dependent mechanism. *J Biol Chem.* 2010/12/16 ed. 2011 Feb 25;286(8):6049–60.
593. Wang RH, Xu X, Kim HS, Xiao Z, Deng CX. SIRT1 Deacetylates FOXA2 and Is Critical for Pdx1 Transcription and β -Cell Formation. *Int J Biol Sci.* 2013;9(9):934–46.
594. Chen D, Bruno J, Easlon E, Lin SJ, Cheng HL, Alt FW, et al. Tissue-specific regulation of SIRT1 by calorie restriction. *Genes Dev.* 2008/06/11 ed. 2008 Jul 1;22(13):1753–7.
595. Corezola do Amaral ME, Kravets V, Dwulet JM, Farnsworth NL, Piscopio R, Schleicher WE, et al. Caloric restriction recovers impaired β -cell- β -cell gap junction coupling, calcium oscillation coordination, and insulin secretion in prediabetic mice. *Am J Physiol-Endocrinol Metab.* 2020 Aug 24;319(4):E709–20.
596. Wang RH, Kim HS, Xiao C, Xu X, Gavrilova O, Deng CX. Hepatic Sirt1 deficiency in mice impairs mTorc2/Akt signaling and results in hyperglycemia, oxidative damage, and insulin resistance. *J Clin Invest.* 2011/10/03 ed. 2011 Nov;121(11):4477–90.
597. Zhou B, Li C, Qi W, Zhang Y, Zhang F, Wu JX, et al. Downregulation of miR-181a upregulates sirtuin-1 (SIRT1) and improves hepatic insulin sensitivity. *Diabetologia.* 2012 Jul 1;55(7):2032–43.
598. Banks AS, Kon N, Knight C, Matsumoto M, Gutiérrez-Juárez R, Rossetti L, et al. SirT1 Gain of Function Increases Energy Efficiency and Prevents Diabetes in Mice. *Cell Metab.* 2008 Oct 8;8(4):333–41.
599. Baur JA, Pearson KJ, Price NL, Jamieson HA, Lerin C, Kalra A, et al. Resveratrol improves health and survival of mice on a high-calorie diet. *Nature.* 2006 Nov 1;444(7117):337–42.

600. Feige JN, Lagouge M, Canto C, Strehle A, Houten SM, Milne JC, et al. Specific SIRT1 Activation Mimics Low Energy Levels and Protects against Diet-Induced Metabolic Disorders by Enhancing Fat Oxidation. *Cell Metab.* 2008 Nov 5;8(5):347–58.
601. Li Y, Xu S, Giles A, Nakamura K, Lee JW, Hou X, et al. Hepatic overexpression of SIRT1 in mice attenuates endoplasmic reticulum stress and insulin resistance in the liver. *FASEB J.* 2011 May 1;25(5):1664–79.
602. Milne JC, Lambert PD, Schenk S, Carney DP, Smith JJ, Gagne DJ, et al. Small molecule activators of SIRT1 as therapeutics for the treatment of type 2 diabetes. *Nature.* 2007 Nov 1;450(7170):712–6.
603. Paul W Caton, Nanda K Nayuni, Julius Kieswich, Noorafza Q Khan, Muhammed M Yaqoob, Roger Corder. Metformin suppresses hepatic gluconeogenesis through induction of SIRT1 and GCN5. *J Endocrinol.* 2010 Apr 1;205(1):97–106.
604. Sun C, Zhang F, Ge X, Yan T, Chen X, Shi X, et al. SIRT1 Improves Insulin Sensitivity under Insulin-Resistant Conditions by Repressing PTP1B. *Cell Metab.* 2007 Oct 3;6(4):307–19.
605. Yang J, Kong X, Martins-Santos MES, Aleman G, Chaco E, Liu GE, et al. Activation of SIRT1 by Resveratrol Represses Transcription of the Gene for the Cytosolic Form of Phosphoenolpyruvate Carboxykinase (GTP) by Deacetylating Hepatic Nuclear Factor 4 α *. *J Biol Chem.* 2009 Oct 2;284(40):27042–53.
606. Fröjdö S, Durand C, Molin L, Carey AL, El-Osta A, Kingwell BA, et al. Phosphoinositide 3-kinase as a novel functional target for the regulation of the insulin signaling pathway by SIRT1. *Mol Cell Endocrinol.* 2011 Mar 30;335(2):166–76.
607. Guarente L. Calorie restriction and sirtuins revisited. *Genes Dev.* 2013 Oct 1;27(19):2072–85.
608. Hayashida S, Arimoto A, Kuramoto Y, Kozako T, Honda S ichiro, Shimeno H, et al. Fasting promotes the expression of SIRT1, an NAD⁺-dependent protein deacetylase, via activation of PPAR α in mice. *Mol Cell Biochem.* 2010 Jun 1;339(1):285–92.
609. Rhee J, Ge H, Yang W, Fan M, Handschin C, Cooper M, et al. Partnership of PGC-1 α and HNF4 α in the Regulation of Lipoprotein Metabolism. *J Biol Chem.* 2006 May 26;281(21):14683–90.
610. Rodgers JT, Lerin C, Haas W, Gygi SP, Spiegelman BM, Puigserver P. Nutrient control of glucose homeostasis through a complex of PGC-1 α and SIRT1. *Nature.* 2005 Mar 1;434(7029):113–8.
611. Zhou M, Luo J, Zhang H. Role of Sirtuin 1 in the pathogenesis of ocular disease (Review). *Int J Mol Med.* 2018 Aug 1;42(1):13–20.
612. Daitoku H, Yamagata K, Matsuzaki H, Hatta M, Fukamizu A. Regulation of PGC-1 Promoter Activity by Protein Kinase B and the Forkhead Transcription Factor FKHR. *Diabetes.* 2003 Mar 1;52(3):642.

613. Daitoku H, Sakamaki J ichi, Fukamizu A. Regulation of FoxO transcription factors by acetylation and protein–protein interactions. *PI3K-AKT-FoxO Axis Cancer Aging*. 2011 Nov 1;1813(11):1954–60.
614. Frescas D, Valenti L, Accili D. Nuclear Trapping of the Forkhead Transcription Factor FoxO1 via Sirt-dependent Deacetylation Promotes Expression of Glucogenetic Genes. *J Biol Chem*. 2005 May 27;280(21):20589–95.
615. Puigserver P, Rhee J, Donovan J, Walkey CJ, Yoon JC, Oriente F, et al. Insulin-regulated hepatic gluconeogenesis through FOXO1–PGC-1 α interaction. *Nature*. 2003 May 1;423(6939):550–5.
616. Xiong X, Tao R, DePinho RA, Dong XC. Deletion of hepatic FoxO1/3/4 genes in mice significantly impacts on glucose metabolism through downregulation of gluconeogenesis and upregulation of glycolysis. *PloS One*. 2013 Aug 28;8(8):e74340–e74340.
617. Zhang W, Patil S, Chauhan B, Guo S, Powell DR, Le J, et al. FoxO1 Regulates Multiple Metabolic Pathways in the Liver: EFFECTS ON GLUCONEOGENIC, GLYCOLYTIC, AND LIPOGENIC GENE EXPRESSION. *J Biol Chem*. 2006 Apr 14;281(15):10105–17.
618. Nie Y, Erion DM, Yuan Z, Dietrich M, Shulman GI, Horvath TL, et al. STAT3 inhibition of gluconeogenesis is downregulated by SirT1. *Nat Cell Biol*. 2009/03/22 ed. 2009 Apr;11(4):492–500.
619. Liu Y, Dentin R, Chen D, Hedrick S, Ravnskjaer K, Schenk S, et al. A fasting inducible switch modulates gluconeogenesis via activator/coactivator exchange. *Nature*. 2008/10/05 ed. 2008 Nov 13;456(7219):269–73.
620. Qiang L, Lin HV, Kim-Muller JY, Welch CL, Gu W, Accili D. Proatherogenic abnormalities of lipid metabolism in SirT1 transgenic mice are mediated through Creb deacetylation. *Cell Metab*. 2011/11/10 ed. 2011 Dec 7;14(6):758–67.
621. Tateya S, Rizzo-De Leon N, Cheng AM, Dick BP, Lee WJ, Kim ML, et al. The role of vasodilator-stimulated phosphoprotein (VASP) in the control of hepatic gluconeogenic gene expression. *PloS One*. 2019 Apr 24;14(4):e0215601–e0215601.
622. Purushotham A, Schug TT, Xu Q, Surapureddi S, Guo X, Li X. Hepatocyte-specific deletion of SIRT1 alters fatty acid metabolism and results in hepatic steatosis and inflammation. *Cell Metab*. 2009 Apr;9(4):327–38.
623. Pawlak M, Lefebvre P, Staels B. Molecular mechanism of PPAR α action and its impact on lipid metabolism, inflammation and fibrosis in non-alcoholic fatty liver disease. *J Hepatol*. 2015 Mar 1;62(3):720–33.
624. Ponugoti B, Kim DH, Xiao Z, Smith Z, Miao J, Zang M, et al. SIRT1 Deacetylates and Inhibits SREBP-1C Activity in Regulation of Hepatic Lipid Metabolism. *J Biol Chem*. 2010 Oct 29;285(44):33959–70.
625. Yamazaki Y, Usui I, Kanatani Y, Matsuya Y, Tsuneyama K, Fujisaka S, et al. Treatment with SRT1720, a SIRT1 activator, ameliorates fatty liver with reduced

- expression of lipogenic enzymes in MSG mice. *Am J Physiol Endocrinol Metab.* 2009 Oct 1;297:E1179-86.
626. Li Y, Zou S, Ding H, Hao N, Huang Y, Tang J, et al. Low Expression of Sirtuin 1 in the Dairy Cows with Mild Fatty Liver Alters Hepatic Lipid Metabolism. *Animals.* 2020;10(4).
627. Walker AK, Yang F, Jiang K, Ji JY, Watts JL, Purushotham A, et al. Conserved role of SIRT1 orthologs in fasting-dependent inhibition of the lipid/cholesterol regulator SREBP. *Genes Dev.* 2010 Jul 1;24(13):1403–17.
628. Li X, Zhang S, Blander G, Tse JG, Krieger M, Guarente L. SIRT1 Deacetylates and Positively Regulates the Nuclear Receptor LXR. *Mol Cell.* 2007 Oct 12;28(1):91–106.
629. Westerterp M, Fotakis P, Ouimet M, Bochem AE, Zhang H, Molusky MM, et al. Cholesterol Efflux Pathways Suppress Inflammasome Activation, NETosis, and Atherogenesis. *Circulation.* 2018 Aug 28;138(9):898–912.
630. Rodgers JT, Puigserver P. Fasting-dependent glucose and lipid metabolic response through hepatic sirtuin 1. *Proc Natl Acad Sci U S A.* 2007/07/23 ed. 2007 Jul 31;104(31):12861–6.
631. Shen T, Xu B, Lei T, Chen L, Zhang C, Ni Z. Sitagliptin reduces insulin resistance and improves rat liver steatosis via the SIRT1/AMPK α pathway. *Exp Ther Med.* 2018 Oct 1;16(4):3121–8.
632. Chawla A, Schwarz EJ, Dimaculangan DD, Lazar MA. Peroxisome proliferator-activated receptor (PPAR) gamma: adipose-predominant expression and induction early in adipocyte differentiation. *Endocrinology.* 1994 Aug 1;135(2):798–800.
633. Mayoral R, Osborn O, McNelis J, Johnson AM, Oh DY, Izquierdo CL, et al. Adipocyte SIRT1 knockout promotes PPAR γ activity, adipogenesis and insulin sensitivity in chronic-HFD and obesity. *Mol Metab.* 2015 Mar 5;4(5):378–91.
634. Picard F, Kurtev M, Chung N, Topark-Ngarm A, Senawong T, Machado de Oliveira R, et al. Sirt1 promotes fat mobilization in white adipocytes by repressing PPAR- γ . *Nature.* 2004 Jun 1;429(6993):771–6.
635. Qiang L, Wang L, Kon N, Zhao W, Lee S, Zhang Y, et al. Brown Remodeling of White Adipose Tissue by SirT1-Dependent Deacetylation of Ppar γ . *Cell.* 2012 Aug 3;150(3):620–32.
636. Jiang S, Wang W, Miner J, Fromm M. Cross Regulation of Sirtuin 1, AMPK, and PPAR γ in Conjugated Linoleic Acid Treated Adipocytes. *PLOS ONE.* 2012 Nov 14;7(11):e48874.
637. Makowski L, Brittingham KC, Reynolds JM, Suttles J, Hotamisligil GS. The fatty acid-binding protein, aP2, coordinates macrophage cholesterol trafficking and inflammatory activity. Macrophage expression of aP2 impacts peroxisome proliferator-activated receptor gamma and IkappaB kinase activities. *J Biol Chem.* 2005/01/31 ed. 2005 Apr 1;280(13):12888–95.

638. Tontonoz P, Hu E, Graves RA, Budavari AI, Spiegelman BM. mPPAR gamma 2: tissue-specific regulator of an adipocyte enhancer. *Genes Dev.* 1994 May 15;8(10):1224–34.
639. Fernandez S, Viola JM, Torres A, Wallace M, Trefely S, Zhao S, et al. Adipocyte ACLY Facilitates Dietary Carbohydrate Handling to Maintain Metabolic Homeostasis in Females. *Cell Rep.* 2019 May 28;27(9):2772-2784.e6.
640. Chu Y, Yang C, Chen X, Zheng W, Yang Y, Tang Y. Structure–function analysis of human protein Ero1-L α . *Biochem Biophys Res Commun.* 2009 Nov 27;389(4):645–50.
641. Qiang L, Wang H, Farmer SR. Adiponectin Secretion Is Regulated by SIRT1 and the Endoplasmic Reticulum Oxidoreductase Ero1-L α . *Mol Cell Biol.* 2007 Jul 1;27(13):4698.
642. Qiao L, Shao J. SIRT1 Regulates Adiponectin Gene Expression through Foxo1-C/Enhancer-binding Protein Transcriptional Complex. *J Biol Chem.* 2007 Jan 1;281:39915–24.
643. Cypess AM, Kahn CR. Brown fat as a therapy for obesity and diabetes. *Curr Opin Endocrinol Diabetes Obes.* 2010 Apr;17(2):143–9.
644. Kuryłowicz A, Puzianowska-Kuźnicka M. Induction of Adipose Tissue Browning as a Strategy to Combat Obesity. *Int J Mol Sci.* 2020;21(17).
645. Trayhurn P. Brown Adipose Tissue-A Therapeutic Target in Obesity? *Front Physiol.* 2018 Nov 23;9:1672–1672.
646. Abdesselem H, Madani A, Hani A, Al-Noubi M, Goswami N, Ben Hamidane H, et al. SIRT1 Limits Adipocyte Hyperplasia through c-Myc Inhibition. *J Biol Chem.* 2015/12/11 ed. 2016 Jan 29;291(5):2119–35.
647. Rimmelé P, Bigarella CL, Liang R, Izac B, Dieguez-Gonzalez R, Barbet G, et al. Aging-like Phenotype and Defective Lineage Specification in SIRT1-Deleted Hematopoietic Stem and Progenitor Cells. *Stem Cell Rep.* 2014 Jul 8;3(1):44–59.
648. Singh SK, Williams CA, Klarmann K, Burkett SS, Keller JR, Oberdoerffer P. Sirt1 ablation promotes stress-induced loss of epigenetic and genomic hematopoietic stem and progenitor cell maintenance. *J Exp Med.* 2013 Apr 29;210(5):987–1001.
649. Leko V, Varnum-Finney B, Li H, Gu Y, Flowers D, Nourigat C, et al. SIRT1 is dispensable for function of hematopoietic stem cells in adult mice. *Blood.* 2012 Feb 23;119(8):1856–60.
650. Rimmelé P, Lofek-Czubek S, Ghaffari S. Resveratrol increases the bone marrow hematopoietic stem and progenitor cell capacity. *Am J Hematol.* 2014 Dec 1;89(12):E235–8.
651. Zhang QS, Deater M, Schubert K, Marquez-Loza L, Pelz C, Sinclair DA, et al. The Sirt1 activator SRT3025 expands hematopoietic stem and progenitor cells and improves hematopoiesis in Fanconi anemia mice. *Stem Cell Res.* 2015 Jul 1;15(1):130–40.

652. Park S Min, Kim J, Hong C Mi, Shin D Hoon, Kim J Yeon, Park D Youn, et al. SIRT1 is dispensable for maturation of hematopoietic stem cell in the bone marrow niche. *Exp Ther Med*. 2019 Sep 1;18(3):2341–5.
653. Wang Z, Zhang C, Warden CD, Liu Z, Yuan YC, Guo C, et al. Loss of SIRT1 inhibits hematopoietic stem cell aging and age-dependent mixed phenotype acute leukemia. *Commun Biol*. 2022 Apr 28;5(1):396.
654. Artsi H, Gurt I, El-Haj M, Müller R, Kuhn GA, Ben Shalom G, et al. Sirt1 Promotes a Thermogenic Gene Program in Bone Marrow Adipocytes: From Mice to (Wo)Men. *Front Endocrinol*. 2019;10:126.
655. Bäckesjö CM, Li Y, Lindgren U, Haldosén LA. Activation of Sirt1 Decreases Adipocyte Formation During Osteoblast Differentiation of Mesenchymal Stem Cells. *J Bone Miner Res*. 2006 Jul 1;21(7):993–1002.
656. Li Y, He X, Li Y, He J, Anderstam B, Andersson G, et al. Nicotinamide phosphoribosyltransferase (Nampt) affects the lineage fate determination of mesenchymal stem cells: A possible cause for reduced osteogenesis and increased adipogenesis in older individuals. *J Bone Miner Res*. 2011 Nov 1;26(11):2656–64.
657. Peltz L, Gomez J, Marquez M, Alencastro F, Atashpanjeh N, Quang T, et al. Resveratrol Exerts Dosage and Duration Dependent Effect on Human Mesenchymal Stem Cell Development. *PLOS ONE*. 2012 May 16;7(5):e37162.
658. Simic P, Zainabadi K, Bell E, Sykes DB, Saez B, Lotinun S, et al. SIRT1 regulates differentiation of mesenchymal stem cells by deacetylating β -catenin. *EMBO Mol Med*. 2013/01/30 ed. 2013 Mar;5(3):430–40.
659. Brooks CL, Gu W. How does SIRT1 affect metabolism, senescence and cancer? *Nat Rev Cancer*. 2009 Feb 1;9(2):123–8.
660. Haigis MC, Sinclair DA. Mammalian Sirtuins: Biological Insights and Disease Relevance. *Annu Rev Pathol Mech Dis*. 2010 Jan 1;5(1):253–95.
661. Shahgaldi S, Kahmini FR. A comprehensive review of Sirtuins: With a major focus on redox homeostasis and metabolism. *Life Sci*. 2021 Oct 1;282:119803.
662. Buler M, Andersson U, Hakkola J. Who watches the watchmen? Regulation of the expression and activity of sirtuins. *FASEB J*. 2016;30(12):3942–60.
663. Kawanishi FATOS. S. Oikawa S. H₂O₂ accelerates cellular senescence by accumulation of acetylated p53 via decrease in the function of SIRT1 by NAD⁺ depletion. *Cell Physiol Biochem*. 2007;20:45–54.
664. Caito S, Rajendrasozhan S, Cook S, Chung S, Yao H, Friedman AE, et al. SIRT1 is a redox-sensitive deacetylase that is post-translationally modified by oxidants and carbonyl stress. *FASEB J*. 2010;24(9):3145–59.
665. Alam F, Syed H, Amjad S, Baig M, Khan TA, Rehman R. Interplay between oxidative stress, SIRT1, reproductive and metabolic functions. *Curr Res Physiol*. 2021 Jan 1;4:119–24.

666. Cai W, Ramdas M, Zhu L, Chen X, Striker GE, Vlassara H. Oral advanced glycation endproducts (AGEs) promote insulin resistance and diabetes by depleting the antioxidant defenses AGE receptor-1 and sirtuin 1. *Proc Natl Acad Sci.* 2012;109(39):15888–93.
667. Rajendrasozhan S, Yang SR, Kinnula VL, Rahman I. SIRT1, an antiinflammatory and antiaging protein, is decreased in lungs of patients with chronic obstructive pulmonary disease. *Am J Respir Crit Care Med.* 2008;177(8):861–70.
668. Yang Y, Fu W, Chen J, Olashaw N, Zhang X, Nicosia SV, et al. SIRT1 sumoylation regulates its deacetylase activity and cellular response to genotoxic stress. *Nat Cell Biol.* 2007 Nov 1;9(11):1253–62.
669. Zee RS, Yoo CB, Pimentel DR, Perlman DH, Burgoyne JR, Hou X, et al. Redox regulation of sirtuin-1 by S-glutathiolation. 2010;
670. Kim HJ, Kim JH, Noh S, Hur HJ, Sung MJ, Hwang JT, et al. Metabolomic analysis of livers and serum from high-fat diet induced obese mice. *J Proteome Res.* 2011;10(2):722–31.
671. Boulangé CL, Claus SP, Chou CJ, Collino S, Montoliu I, Kochhar S, et al. Early metabolic adaptation in C57BL/6 mice resistant to high fat diet induced weight gain involves an activation of mitochondrial oxidative pathways. *J Proteome Res.* 2013;12(4):1956–68.
672. Putti R, Migliaccio V, Sica R, Lionetti L. Skeletal muscle mitochondrial bioenergetics and morphology in high fat diet induced obesity and insulin resistance: focus on dietary fat source. *Front Physiol.* 2016;6:426.
673. Nijhawan P, Behl T. Role of sirtuins in obesity. *Obes Med.* 2020 Mar 1;17:100156.
674. Yan LJ. Pathogenesis of chronic hyperglycemia: from reductive stress to oxidative stress. *J Diabetes Res.* 2014;2014.
675. Lin SJ, Ford E, Haigis M, Liszt G, Guarente L. Calorie restriction extends yeast life span by lowering the level of NADH. *Genes Dev.* 2004 Jan 1;18(1):12–6.
676. Santos L, Escande C, Denicola A. Potential modulation of sirtuins by oxidative stress. *Oxid Med Cell Longev.* 2016;2016.
677. Noriega LG, Feige JN, Canto C, Yamamoto H, Yu J, Herman MA, et al. CREB and ChREBP oppositely regulate SIRT1 expression in response to energy availability. *EMBO Rep.* 2011;12(10):1069–76.
678. Chalkiadaki A, Guarente L. Metabolic signals regulate SIRT1 expression. *EMBO Rep.* 2011;12(10):985–6.
679. Revollo JR, Li X. The ways and means that fine tune Sirt1 activity. *Trends Biochem Sci.* 2013 Mar 1;38(3):160–7.

680. Kong W, Chen L lu, Zheng J, Zhang H hao, Hu X, Zeng T shu, et al. Resveratrol supplementation restores high-fat diet-induced insulin secretion dysfunction by increasing mitochondrial function in islet. *Exp Biol Med*. 2015;240(2):220–9.
681. Wu L, Zhou L, Lu Y, Zhang J, Jian F, Liu Y, et al. Activation of SIRT1 protects pancreatic β -cells against palmitate-induced dysfunction. *Biochim Biophys Acta BBA - Mol Basis Dis*. 2012 Nov 1;1822(11):1815–25.
682. Chalkiadaki A, Guarente L. High-fat diet triggers inflammation-induced cleavage of SIRT1 in adipose tissue to promote metabolic dysfunction. *Cell Metab*. 2012;16(2):180–8.
683. de Kreutzenberg SV, Ceolotto G, Papparella I, Bortoluzzi A, Semplicini A, Man CD, et al. Downregulation of the longevity-associated protein sirtuin 1 in insulin resistance and metabolic syndrome: potential biochemical mechanisms. *Diabetes*. 2010;59(4):1006–15.
684. Wu T, Liu Y hua, Fu Y cai, Liu X mu, Zhou X hui. Direct evidence of sirtuin downregulation in the liver of non-alcoholic fatty liver disease patients. *Ann Clin Lab Sci*. 2014;44(4):410–8.
685. Niu B, He K, Li P, Gong J, Zhu X, Ye S, et al. SIRT1 upregulation protects against liver injury induced by a HFD through inhibiting CD36 and the NF- κ B pathway in mouse kupffer cells. *Mol Med Rep*. 2018 Aug 1;18(2):1609–15.
686. Ding RB, Bao J, Deng CX. Emerging roles of SIRT1 in fatty liver diseases. *Int J Biol Sci*. 2017 Jul 6;13(7):852–67.
687. Lin SJ, Kaeberlein M, Andalis AA, Sturtz LA, Defossez PA, Culotta VC, et al. Calorie restriction extends *Saccharomyces cerevisiae* lifespan by increasing respiration. *Nature*. 2002;418(6895):344–8.
688. Schmidt MT, Smith BC, Jackson MD, Denu JM. Coenzyme specificity of Sir2 protein deacetylases: implications for physiological regulation. *J Biol Chem*. 2004;279(38):40122–9.
689. Anderson RM, Bitterman KJ, Wood JG, Medvedik O, Sinclair DA. Nicotinamide and PNC1 govern lifespan extension by calorie restriction in *Saccharomyces cerevisiae*. *Nature*. 2003;423(6936):181–5.
690. Ghislain M, Talla E, François JM. Identification and functional analysis of the *Saccharomyces cerevisiae* nicotinamidase gene, PNC1. *Yeast*. 2002;19(3):215–24.
691. Revollo JR, Grimm AA, Imai S ichiro. The NAD biosynthesis pathway mediated by nicotinamide phosphoribosyltransferase regulates Sir2 activity in mammalian cells. *J Biol Chem*. 2004;279(49):50754–63.
692. Imai S, Yoshino J. The importance of NAMPT/NAD/SIRT1 in the systemic regulation of metabolism and ageing. *Diabetes Obes Metab*. 2013 Sep 1;15(s3):26–33.
693. Higgins CB, Mayer AL, Zhang Y, Franczyk M, Ballentine S, Yoshino J, et al. SIRT1 selectively exerts the metabolic protective effects of hepatocyte nicotinamide phosphoribosyltransferase. *Nat Commun*. 2022 Feb 28;13(1):1074.

694. Revollo JR, Körner A, Mills KF, Satoh A, Wang T, Garten A, et al. Nampt/PBEF/visfatin regulates insulin secretion in β cells as a systemic NAD biosynthetic enzyme. *Cell Metab.* 2007;6(5):363–75.
695. Fulco M, Cen Y, Zhao P, Hoffman EP, McBurney MW, Sauve AA, et al. Glucose restriction inhibits skeletal myoblast differentiation by activating SIRT1 through AMPK-mediated regulation of Nampt. *Dev Cell.* 2008;14(5):661–73.
696. Yang H, Yang T, Baur JA, Perez E, Matsui T, Carmona JJ, et al. Nutrient-Sensitive Mitochondrial NAD⁺ Levels Dictate Cell Survival. *Cell.* 2007 Sep 21;130(6):1095–107.
697. Dor Y, Cedar H. Principles of DNA methylation and their implications for biology and medicine. *The Lancet.* 2018 Sep 1;392(10149):777–86.
698. Islam S, Uehara O, Matsuoka H, Kuramitsu Y, Adhikari BR, Hiraki D, et al. DNA hypermethylation of sirtuin 1 (SIRT1) caused by betel quid chewing—a possible predictive biomarker for malignant transformation. *Clin Epigenetics.* 2020 Jan 13;12(1):12.
699. Chen Z, Gong L, Zhang P, Li Y, Liu B, Zhang L, et al. Epigenetic Down-Regulation of Sirt 1 via DNA Methylation and Oxidative Stress Signaling Contributes to the Gestational Diabetes Mellitus-Induced Fetal Programming of Heart Ischemia-Sensitive Phenotype in Late Life. *Int J Biol Sci.* 2019;15(6):1240–51.
700. Voelter-Mahlknecht S, Mahlkecht U. Cloning, chromosomal characterization and mapping of the NAD-dependent histone deacetylases gene sirtuin 1. *Int J Mol Med.* 2006 Jan 1;17(1):59–67.
701. Zhang HN, Li L, Gao P, Chen HZ, Zhang R, Wei YS, et al. Involvement of the p65/RelA subunit of NF- κ B in TNF- α -induced SIRT1 expression in vascular smooth muscle cells. *Biochem Biophys Res Commun.* 2010 Jul 2;397(3):569–75.
702. Katto J, Engel N, Abbas W, Herbein G, Mahlkecht U. Transcription factor NF κ B regulates the expression of the histone deacetylase SIRT1. *Clin Epigenetics.* 2013 Jul 19;5(1):11.
703. Han L, Zhou R, Niu J, McNutt MA, Wang P, Tong T. SIRT1 is regulated by a PPAR γ -SIRT1 negative feedback loop associated with senescence. *Nucleic Acids Res.* 2010 Nov 1;38(21):7458–71.
704. Nemoto S, Fergusson MM, Finkel T. Nutrient Availability Regulates SIRT1 Through a Forkhead-Dependent Pathway. *Science.* 2004 Dec 17;306(5704):2105–8.
705. Yuan F, Liu L, Lei Y, Tang P. p53 inhibits the upregulation of sirtuin 1 expression induced by c-Myc. *Oncol Lett.* 2017 Oct 1;14(4):4396–402.
706. Ford J, Jiang M, Milner J. Cancer-Specific Functions of SIRT1 Enable Human Epithelial Cancer Cell Growth and Survival. *Cancer Res.* 2005 Nov 15;65(22):10457–63.

707. Zhang Q, Wang SY, Fleuriet C, Leprince D, Rocheleau JV, Piston DW, et al. Metabolic regulation of SIRT1 transcription via a HIC1:CtBP corepressor complex. *Proc Natl Acad Sci.* 2007 Jan 16;104(3):829–33.
708. Chen WY, Wang DH, Yen RC, Luo J, Gu W, Baylin SB. Tumor Suppressor HIC1 Directly Regulates SIRT1 to Modulate p53-Dependent DNA-Damage Responses. *Cell.* 2005 Nov 4;123(3):437–48.
709. Chen W, Cooper TK, Zahnow CA, Overholtzer M, Zhao Z, Ladanyi M, et al. Epigenetic and genetic loss of Hic1 function accentuates the role of p53 in tumorigenesis. *Cancer Cell.* 2004 Oct 1;6(4):387–98.
710. Kwon HS, Ott M. The ups and downs of SIRT1. *Trends Biochem Sci.* 2008 Oct 1;33:517–25.
711. Huffman DM, Grizzle WE, Bamman MM, Kim JS, Eltoum IA, Elgavish A, et al. SIRT1 Is Significantly Elevated in Mouse and Human Prostate Cancer. *Cancer Res.* 2007 Jul 17;67(14):6612–8.
712. Pascual G, Fong AL, Ogawa S, Gamliel A, Li AC, Perissi V, et al. A SUMOylation-dependent pathway mediates transrepression of inflammatory response genes by PPAR- γ . *Nature.* 2005 Sep 1;437(7059):759–63.
713. Chen R, Dioum EM, Hogg RT, Gerard RD, Garcia JA. Hypoxia Increases Sirtuin 1 Expression in a Hypoxia-inducible Factor-dependent Manner *. *J Biol Chem.* 2011 Apr 22;286(16):13869–78.
714. Laine A, Westermarck J. Molecular Pathways: Harnessing E2F1 Regulation for Prosenescence Therapy in p53-Defective Cancer Cells. *Clin Cancer Res.* 2014 Jul 14;20(14):3644–50.
715. Sasaki T, Kim HJ, Kobayashi M, Kitamura YI, Yokota-Hashimoto H, Shiuchi T, et al. Induction of Hypothalamic Sirt1 Leads to Cessation of Feeding via Agouti-Related Peptide. *Endocrinology.* 2010 Jun 1;151(6):2556–66.
716. Yuan J, Minter-Dykhouse K, Lou Z. A c-Myc–SIRT1 feedback loop regulates cell growth and transformation. *J Cell Biol.* 2009 Apr 13;185(2):203–11.
717. Jin J, Iakova P, Jiang Y, Medrano EE, Timchenko NA. The reduction of SIRT1 in livers of old mice leads to impaired body homeostasis and to inhibition of liver proliferation. *Hepatology.* 2011 Sep 2;54(3):989–98.
718. Jin Q, Zhang F, Yan T, Liu Z, Wang C, Ge X, et al. C/EBP α regulates SIRT1 expression during adipogenesis. *Cell Res.* 2010 Apr 1;20(4):470–9.
719. Abdelmohsen K, Pullmann R Jr, Lal A, Kim HH, Galban S, Yang X, et al. Phosphorylation of HuR by Chk2 Regulates SIRT1 Expression. *Mol Cell.* 2007 Feb 23;25(4):543–57.
720. O'Brien J, Hayder H, Zayed Y, Peng C. Overview of MicroRNA Biogenesis, Mechanisms of Actions, and Circulation. *Front Endocrinol [Internet].* 2018;9. Available from: <https://www.frontiersin.org/articles/10.3389/fendo.2018.00402>

721. Choi SE, Kemper JK. Regulation of SIRT1 by MicroRNAs. *Mol Cells*. 2013 Nov 1;36(5):385–92.
722. Yamakuchi M, Ferlito M, Lowenstein CJ. miR-34a repression of SIRT1 regulates apoptosis. *Proc Natl Acad Sci*. 2008;105(36):13421–6.
723. Raver-Shapira N, Marciano E, Meiri E, Spector Y, Rosenfeld N, Moskovits N, et al. Transcriptional Activation of miR-34a Contributes to p53-Mediated Apoptosis. *Mol Cell*. 2007 Jun 8;26(5):731–43.
724. Lou G, Liu Y, Wu S, Xue J, Yang F, Fu H, et al. The p53/miR-34a/SIRT1 Positive Feedback Loop in Quercetin-Induced Apoptosis. *Cell Physiol Biochem*. 2015;35(6):2192–202.
725. Xu M, Lu L, Mao B, Lü X, Wu X, Li L, et al. Mutual inhibition between miR-34a and SIRT1 contributes to regulation of DNA double-strand break repair. *Chin Sci Bull*. 2013 Mar 1;58(9):979–85.
726. Choi SE, Fu T, Seok S, Kim DH, Yu E, Lee KW, et al. Elevated microRNA-34a in obesity reduces NAD⁺ levels and SIRT1 activity by directly targeting NAMPT. *Aging Cell*. 2013 Dec 1;12(6):1062–72.
727. Li N, Muthusamy S, Liang R, Sarojini H, Wang E. Increased expression of miR-34a and miR-93 in rat liver during aging, and their impact on the expression of Mgst1 and Sirt1. *Mech Ageing Dev*. 2011;132(3):75–85.
728. Wang Y, Pang WJ, Wei N, Xiong Y, Wu WJ, Zhao CZ, et al. Identification, stability and expression of Sirt1 antisense long non-coding RNA. *Gene*. 2014;539(1):117–24.
729. Chu J, Li H, Xing Y, Jia J, Sheng J, Yang L, et al. LncRNA MNX1-AS1 promotes progression of esophageal squamous cell carcinoma by regulating miR-34a/SIRT1 axis. *Biomed Pharmacother*. 2019;116:109029.
730. Tan P, Guo YH, Zhan JK, Long LM, Xu ML, Ye L, et al. LncRNA-ANRIL inhibits cell senescence of vascular smooth muscle cells by regulating miR-181a/Sirt1. *Biochem Cell Biol*. 2019;97(5):571–80.
731. Sun X, Bai Y, Yang C, Hu S, Hou Z, Wang G. RETRACTED ARTICLE: Long noncoding RNA SNHG15 enhances the development of colorectal carcinoma via functioning as a ceRNA through miR-141/SIRT1/Wnt/ β -catenin axis. *Artif Cells Nanomedicine Biotechnol*. 2019;47(1):2536–44.
732. Wang G qiang, Wang Y, Xiong Y, Chen XC, Ma M ling, Cai R, et al. Sirt1 AS lncRNA interacts with its mRNA to inhibit muscle formation by attenuating function of miR-34a. *Sci Rep*. 2016;6(1):1–13.
733. Li B, Hu Y, Li X, Jin G, Chen X, Chen G, et al. Sirt1 antisense long noncoding RNA promotes cardiomyocyte proliferation by enhancing the stability of Sirt1. *J Am Heart Assoc*. 2018;7(21):e009700.

734. Poljsak B, Milisav I. NAD⁺ as the link between oxidative stress, inflammation, caloric restriction, exercise, DNA repair, longevity, and health span. *Rejuvenation Res.* 2016;19(5):406–13.
735. Anderson KA, Madsen AS, Olsen CA, Hirschey MD. Metabolic control by sirtuins and other enzymes that sense NAD⁺, NADH, or their ratio. *Biochim Biophys Acta BBA-Bioenerg.* 2017;1858(12):991–8.
736. Vachharajani VT, Liu T, Wang X, Hoth JJ, Yoza BK, McCall CE. Sirtuins Link Inflammation and Metabolism. Shevach EM, editor. *J Immunol Res.* 2016 Jan 20;2016:8167273.
737. Tafani M, Sansone L, Limana F, Arcangeli T, De Santis E, Polese M, et al. The interplay of reactive oxygen species, hypoxia, inflammation, and sirtuins in cancer initiation and progression. *Oxid Med Cell Longev.* 2016;2016.
738. Meijer TW, Kaanders JH, Span PN, Bussink J. Targeting hypoxia, HIF-1, and tumor glucose metabolism to improve radiotherapy efficacy. *Clin Cancer Res.* 2012;18(20):5585–94.
739. Slade D. PARP and PARG inhibitors in cancer treatment. *Genes Dev.* 2020;34(5–6):360–94.
740. Bai P, Cantó C, Oudart H, Brunyánszki A, Cen Y, Thomas C, et al. PARP-1 inhibition increases mitochondrial metabolism through SIRT1 activation. *Cell Metab.* 2011;13(4):461–8.
741. Mai A, Massa S, Lavu S, Pezzi R, Simeoni S, Ragno R, et al. Design, synthesis, and biological evaluation of sirtinol analogues as class III histone/protein deacetylase (Sirtuin) inhibitors. *J Med Chem.* 2005;48(24):7789–95.
742. Solomon JM, Pasupuleti R, Xu L, McDonagh T, Curtis R, DiStefano PS, et al. Inhibition of SIRT1 catalytic activity increases p53 acetylation but does not alter cell survival following DNA damage. *Mol Cell Biol.* 2006;26(1):28–38.
743. Park JA, Park S, Park WY, Han MK, Lee Y. Splitomicin, a SIRT1 Inhibitor, Enhances Hematopoietic Differentiation of Mouse Embryonic Stem Cells. *Int J Stem Cells.* 2019/03/30 ed. 2019 Mar;12(1):21–30.
744. Rotili D, Tarantino D, Carafa V, Lara E, Meade S, Botta G, et al. Identification of tri- and tetracyclic pyrimidinediones as sirtuin inhibitors. *ChemMedChem.* 2010;5(5):674–7.
745. Bitterman KJ, Anderson RM, Cohen HY, Latorre-Esteves M, Sinclair DA. Inhibition of silencing and accelerated aging by nicotinamide, a putative negative regulator of yeast sir2 and human SIRT1. *J Biol Chem.* 2002;277(47):45099–107.
746. Avalos JL, Bever KM, Wolberger C. Mechanism of sirtuin inhibition by nicotinamide: altering the NAD⁺ cosubstrate specificity of a Sir2 enzyme. *Mol Cell.* 2005;17(6):855–68.

747. Howitz KT, Bitterman KJ, Cohen HY, Lamming DW, Lavu S, Wood JG, et al. Small molecule activators of sirtuins extend *Saccharomyces cerevisiae* lifespan. *Nature*. 2003;425(6954):191–6.
748. Smith JJ, Kenney RD, Gagne DJ, Frushour BP, Ladd W, Galonek HL, et al. Small molecule activators of SIRT1 replicate signaling pathways triggered by calorie restriction in vivo. *BMC Syst Biol*. 2009;3(1):1–14.
749. Hubbard BP, Sinclair DA. Small molecule SIRT1 activators for the treatment of aging and age-related diseases. *Trends Pharmacol Sci*. 2014 Mar 1;35(3):146–54.
750. Greer EL, Brunet A. Different dietary restriction regimens extend lifespan by both independent and overlapping genetic pathways in *C. elegans*. *Aging Cell*. 2009;8(2):113–27.
751. Viswanathan M, Guarente L. Regulation of *Caenorhabditis elegans* lifespan by sir-2.1 transgenes. *Nature*. 2011;477(7365):E1–2.
752. Wang Z, Zhang L, Liang Y, Zhang C, Xu Z, Zhang L, et al. Cyclic AMP mimics the anti-ageing effects of calorie restriction by up-regulating sirtuin. *Sci Rep*. 2015;5(1):1–10.
753. Kim EJ, Kho JH, Kang MR, Um SJ. Active regulator of SIRT1 cooperates with SIRT1 and facilitates suppression of p53 activity. *Mol Cell*. 2007;28(2):277–90.
754. Autiero I, Costantini S, Colonna G. Human sirt-1: molecular modeling and structure-function relationships of an unordered protein. *PloS One*. 2009;4(10):e7350.
755. Kokkola T, Suuronen T, Molnár F, Määttä J, Salminen A, Jarho EM, et al. AROS has a context-dependent effect on SIRT1. *FEBS Lett*. 2014;588(9):1523–8.
756. Knight JR, Allison SJ, Milner J. Active regulator of SIRT1 is required for cancer cell survival but not for SIRT1 activity. *Open Biol*. 2013;3(11):130130.
757. Yang Y, Hou H, Haller EM, Nicosia SV, Bai W. Suppression of FOXO1 activity by FHL2 through SIRT1-mediated deacetylation. *EMBO J*. 2005;24(5):1021–32.
758. Hasegawa K, Yoshikawa K. Necdin regulates p53 acetylation via Sirtuin1 to modulate DNA damage response in cortical neurons. *J Neurosci*. 2008;28(35):8772–84.
759. Ao N, Liu Y, Feng H, Bian X, Li Z, Gu B, et al. Ubiquitin-specific peptidase USP22 negatively regulates the STAT signaling pathway by deubiquitinating SIRT1. *Cell Physiol Biochem*. 2014;33(6):1863–75.
760. Langley E, Pearson M, Faretta M, Bauer UM, Frye RA, Minucci S, et al. Human SIR2 deacetylates p53 and antagonizes PML/p53-induced cellular senescence. *EMBO J*. 2002;21(10):2383–96.
761. Jang MJ, Park UH, Kim JW, Choi H, Um SJ, Kim EJ. CACUL1 reciprocally regulates SIRT1 and LSD1 to repress PPAR γ and inhibit adipogenesis. *Cell Death Dis*. 2017;8(12):1–14.

762. Olmos Y, Sánchez-Gómez FJ, Wild B, García-Quintans N, Cabezudo S, Lamas S, et al. Sirt1 regulation of antioxidant genes is dependent on the formation of a FoxO3a/PGC-1 α complex. *Antioxid Redox Signal*. 2013;19(13):1507–21.
763. Zhao W, Kruse JP, Tang Y, Jung SY, Qin J, Gu W. Negative regulation of the deacetylase SIRT1 by DBC1. *Nature*. 2008;451(7178):587–90.
764. Kim JE, Chen J, Lou Z. DBC1 is a negative regulator of SIRT1. *Nature*. 2008;451(7178):583–6.
765. Ji Yu E, Kim SH, Heo K, Ou CY, Stallcup MR, Kim JH. Reciprocal roles of DBC1 and SIRT1 in regulating estrogen receptor α activity and co-activator synergy. *Nucleic Acids Res*. 2011;39(16):6932–43.
766. Magni M, Buscemi G, Zannini L. Cell cycle and apoptosis regulator 2 at the interface between DNA damage response and cell physiology. *Mutat Res Mutat Res*. 2018;776:1–9.
767. Carling D. AMPK signalling in health and disease. *Curr Opin Cell Biol*. 2017;45:31–7.
768. Lee CW, Wong LLY, Tse EYT, Liu HF, Leong VYL, Lee JMF, et al. AMPK promotes p53 acetylation via phosphorylation and inactivation of SIRT1 in liver cancer cells. *Cancer Res*. 2012;72(17):4394–404.
769. Lau AW, Liu P, Inuzuka H, Gao D. SIRT1 phosphorylation by AMP-activated protein kinase regulates p53 acetylation. *Am J Cancer Res*. 2014;4(3):245.
770. Sasaki T, Maier B, Koclega KD, Chruszcz M, Gluba W, Stukenberg PT, et al. Phosphorylation regulates SIRT1 function. *PloS One*. 2008;3(12):e4020.
771. Becker W, Joost HG. Structural and functional characteristics of Dyrk, a novel subfamily of protein kinases with dual specificity. *Prog Nucleic Acid Res Mol Biol*. 1998;62:1–17.
772. Boni J, Rubio-Perez C, López-Bigas N, Fillat C, de la Luna S. The DYRK family of kinases in cancer: molecular functions and therapeutic opportunities. *Cancers*. 2020;12(8):2106.
773. Guo X, Williams JG, Schug TT, Li X. DYRK1A and DYRK3 promote cell survival through phosphorylation and activation of SIRT1. *J Biol Chem*. 2010;285(17):13223–32.
774. Lu J, Xu Q, Ji M, Guo X, Xu X, Fargo DC, et al. The phosphorylation status of T522 modulates tissue-specific functions of SIRT 1 in energy metabolism in mice. *EMBO Rep*. 2017;18(5):841–57.
775. Utani K, Fu H, Jang SM, Marks AB, Smith OK, Zhang Y, et al. Phosphorylated SIRT1 associates with replication origins to prevent excess replication initiation and preserve genomic stability. *Nucleic Acids Res*. 2017;45(13):7807–24.

776. Kang H, Jung JW, Kim MK, Chung JH. CK2 is the regulator of SIRT1 substrate-binding affinity, deacetylase activity and cellular response to DNA-damage. *PloS One*. 2009;4(8):e6611.
777. Choi SE, Kwon S, Seok S, Xiao Z, Lee KW, Kang Y, et al. Obesity-linked phosphorylation of SIRT1 by casein kinase 2 inhibits its nuclear localization and promotes fatty liver. *Mol Cell Biol*. 2017;37(15):e00006-17.
778. Conrad E, Polonio-Vallon T, Meister M, Matt S, Bitomsky N, Herbel C, et al. HIPK2 restricts SIRT1 activity upon severe DNA damage by a phosphorylation-controlled mechanism. *Cell Death Differ*. 2016;23(1):110–22.
779. Nin V, Escande C, Chini CC, Giri S, Camacho-Pereira J, Matalonga J, et al. Role of Deleted in Breast Cancer 1 (DBC1) Protein in SIRT1 Deacetylase Activation Induced by Protein Kinase A and AMP-activated Protein Kinase *. *J Biol Chem*. 2012 Jul 6;287(28):23489–501.
780. Nasrin N, Kaushik VK, Fortier E, Wall D, Pearson KJ, De Cabo R, et al. JNK1 phosphorylates SIRT1 and promotes its enzymatic activity. *PloS One*. 2009;4(12):e8414.
781. Gao Z, Zhang J, Kheterpal I, Kennedy N, Davis RJ, Ye J. Sirtuin 1 (SIRT1) protein degradation in response to persistent c-Jun N-terminal kinase 1 (JNK1) activation contributes to hepatic steatosis in obesity. *J Biol Chem*. 2011;286(25):22227–34.
782. Ford J, Ahmed S, Allison S, Jiang M, Milner J. JNK2-dependent regulation of SIRT1 protein stability. *Cell Cycle*. 2008;7(19):3091–7.
783. Wang W, Li F, Xu Y, Wei J, Zhang Y, Yang H, et al. JAK1-mediated Sirt1 phosphorylation functions as a negative feedback of the JAK1-STAT3 pathway. *J Biol Chem*. 2018 Jul 13;293(28):11067–75.
784. Geng C, Zhang Y, Gao Y, Tao W, Zhang H, Liu X, et al. Mst1 regulates hepatic lipid metabolism by inhibiting Sirt1 ubiquitination in mice. *Biochem Biophys Res Commun*. 2016 Mar 18;471(4):444–9.
785. Shen T, Cai LD, Liu YH, Li S, Gan WJ, Li XM, et al. Ube2v1-mediated ubiquitination and degradation of Sirt1 promotes metastasis of colorectal cancer by epigenetically suppressing autophagy. *J Hematol Oncol* *J Hematol Oncol*. 2018 Jul 17;11(1):95.
786. Yu L, Dong L, Li H, Liu Z, Luo Z, Duan G, et al. Ubiquitination-mediated degradation of SIRT1 by SMURF2 suppresses CRC cell proliferation and tumorigenesis. *Oncogene*. 2020 May 1;39(22):4450–64.
787. Peng L, Yuan Z, Li Y, Ling H, Izumi V, Fang B, et al. Ubiquitinated Sirtuin 1 (SIRT1) Function Is Modulated during DNA Damage-induced Cell Death and Survival *. *J Biol Chem*. 2015 Apr 3;290(14):8904–12.
788. Kim M, Kwon YE, Song JO, Bae SJ, Seol JH. CHFR negatively regulates SIRT1 activity upon oxidative stress. *Sci Rep*. 2016 Nov 24;6(1):37578.

789. Han C, Gu Y, Shan H, Mi W, Sun J, Shi M, et al. O-GlcNAcylation of SIRT1 enhances its deacetylase activity and promotes cytoprotection under stress. *Nat Commun.* 2017 Nov 14;8(1):1491.
790. Chattopadhyay T, Maniyadath B, Bagul HP, Chakraborty A, Shukla N, Budnar S, et al. Spatiotemporal gating of SIRT1 functions by O-GlcNAcylation is essential for liver metabolic switching and prevents hyperglycemia. *Proc Natl Acad Sci.* 2020 Mar 24;117(12):6890–900.
791. Han X, Niu J, Zhao Y, Kong Q, Tong T, Han L. HDAC4 stabilizes SIRT1 via sumoylation SIRT1 to delay cellular senescence. *Clin Exp Pharmacol Physiol.* 2016 Jan 1;43(1):41–6.
792. Stomberski CT, Hess DT, Stamler JS. Protein S-Nitrosylation: Determinants of Specificity and Enzymatic Regulation of S-Nitrosothiol-Based Signaling. *Antioxid Redox Signal.* 2019 Apr 1;30(10):1331–51.
793. Fernando VZ XunzhenAU Walia, YashnaAU Sharma, VandanaAU Letson, JoshuaAU Furuta, SaoriTI S Nitrosylation: An Emerging Paradigm of Redox Signaling. *Antioxidants.* 2019;8(9).
794. Kornberg MD, Sen N, Hara MR, Juluri KR, Nguyen JVK, Snowman AM, et al. GAPDH mediates nitrosylation of nuclear proteins. *Nat Cell Biol.* 2010 Nov 1;12(11):1094–100.
795. Shinozaki S, Chang K, Sakai M, Shimizu N, Yamada M, Tanaka T, et al. Inflammatory stimuli induce inhibitory S-nitrosylation of the deacetylase SIRT1 to increase acetylation and activation of p53 and p65. *Sci Signal.* 2014 Nov 11;7(351):ra106–ra106.
796. Nakazawa H, Chang K, Shinozaki S, Yasukawa T, Ishimaru K, Yasuhara S, et al. iNOS as a Driver of Inflammation and Apoptosis in Mouse Skeletal Muscle after Burn Injury: Possible Involvement of Sirt1 S-Nitrosylation-Mediated Acetylation of p65 NF- κ B and p53. *PLOS ONE.* 2017 Jan 18;12(1):e0170391.
797. Speakman JR, Mitchell SE. Caloric restriction. *Caloric Restrict.* 2011 Jun 1;32(3):159–221.
798. Cerqueira FM, Kowaltowski AJ. Commonly adopted caloric restriction protocols often involve malnutrition. *Ageing Res Rev.* 2010 Oct 1;9(4):424–30.
799. Austad SN. Does Caloric Restriction in the Laboratory Simply Prevent Overfeeding and Return House Mice to Their Natural Level of Food Intake? *Sci Aging Knowl Environ.* 2001 Nov 7;2001(6):pe3–pe3.
800. Vaughan KL, Kaiser T, Peadar R, Anson RM, de Cabo R, Mattison JA. Caloric Restriction Study Design Limitations in Rodent and Nonhuman Primate Studies. *J Gerontol Ser A.* 2018 Jan 1;73(1):48–53.
801. Tropp J, Markus EJ. Effects of mild food deprivation on the estrous cycle of rats. *Physiol Behav.* 2001 Jul 1;73(4):553–9.

802. Tatsumi S, Ito M, Asaba Y, Tsutsumi K, Ikeda K. Life-Long Caloric Restriction Reveals Biphasic and Dimorphic Effects on Bone Metabolism in Rodents. *Endocrinology*. 2008 Feb 1;149(2):634–41.
803. Hao S, Avraham Y, Bonne O, Berry EM. Separation-induced body weight loss, impairment in alternation behavior, and autonomic tone: effects of tyrosine. *Pharmacol Biochem Behav*. 2001 Feb 1;68(2):273–81.
804. van Leeuwen SD, Bonne OB, Avraham Y, Berry EM. Separation as a New Animal Model for Self-Induced Weight Loss. *Physiol Behav*. 1997 Jul 1;62(1):77–81.
805. GROSS HA, Lake CR, EBERT MH, ZIEGLER MG, KOPIN IJ. Catecholamine metabolism in primary anorexia nervosa. *J Clin Endocrinol Metab*. 1979;49(6):805–9.
806. Kaye WH, Ebert MH, Raleigh M, Lake CR. Abnormalities in CNS monoamine metabolism in anorexia nervosa. *Arch Gen Psychiatry*. 1984;41(4):350–5.
807. Golden NH, Shenker IR. Amenorrhea in anorexia nervosa neuroendocrine control of hypothalamic dysfunction. *Int J Eat Disord*. 1994 Jul 1;16(1):53–60.
808. Ghali O, Broux O, Falgayrac G, Haren N, van Leeuwen JPTM, Penel G, et al. Dexamethasone in osteogenic medium strongly induces adipocyte differentiation of mouse bone marrow stromal cells and increases osteoblast differentiation. *BMC Cell Biol*. 2015 Mar 13;16:9–9.
809. Fulco M, Sartorelli V. Comparing and contrasting the roles of AMPK and SIRT1 in metabolic tissues. *Cell Cycle*. 2008;7(23):3669–79.
810. Robinette TM, Nicholatos JW, Francisco AB, Brooks KE, Diao RY, Sorbi S, et al. SIRT1 accelerates the progression of activity-based anorexia. *Nat Commun*. 2020 Jun 4;11(1):2814–2814.
811. Mariani S, di Giorgio MR, Martini P, Persichetti A, Barbaro G, Basciani S, et al. Inverse Association of Circulating SIRT1 and Adiposity: A Study on Underweight, Normal Weight, and Obese Patients. *Front Endocrinol*. 2018 Aug 7;9:449–449.
812. Wang Z, Gerstein M, Snyder M. RNA-Seq: a revolutionary tool for transcriptomics. *Nat Rev Genet*. 2009 Jan 1;10(1):57–63.
813. Van Dijk EL, Auger H, Jaszczyszyn Y, Thermes C. Ten years of next-generation sequencing technology. *Trends Genet*. 2014;30(9):418–26.
814. Goodwin S, McPherson JD, McCombie WR. Coming of age: ten years of next-generation sequencing technologies. *Nat Rev Genet*. 2016;17(6):333–51.
815. Moon M, Nakai K. Stable feature selection based on the ensemble L 1-norm support vector machine for biomarker discovery. *BMC Genomics*. 2016;17(13):65–74.
816. Zubovic L, Piazza S, Tebaldi T, Cozzuto L, Palazzo G, Sidarovich V, et al. The altered transcriptome of pediatric myelodysplastic syndrome revealed by RNA sequencing. *J Hematol Oncol J Hematol Oncol*. 2020;13(1):1–5.

817. Oshlack A, Robinson MD, Young MD. From RNA-seq reads to differential expression results. *Genome Biol.* 2010;11(12):1–10.
818. Govindarajan M, Wohlmuth C, Waas M, Bernardini MQ, Kislinger T. High-throughput approaches for precision medicine in high-grade serous ovarian cancer. *J Hematol OncolJ Hematol Oncol.* 2020;13(1):1–20.
819. Hong M, Tao S, Zhang L, Diao LT, Huang X, Huang S, et al. RNA sequencing: new technologies and applications in cancer research. *J Hematol OncolJ Hematol Oncol.* 2020 Dec 4;13(1):166.
820. Finotello F, Di Camillo B. Measuring differential gene expression with RNA-seq: challenges and strategies for data analysis. *Brief Funct Genomics.* 2015;14(2):130–42.
821. Ozsolak F, Milos PM. RNA sequencing: advances, challenges and opportunities. *Nat Rev Genet.* 2011;12(2):87–98.
822. Camarena L, Bruno V, Euskirchen G, Poggio S, Snyder M. Molecular mechanisms of ethanol-induced pathogenesis revealed by RNA-sequencing. *PLoS Pathog.* 2010;6(4):e1000834.
823. Griffith M, Griffith OL, Mwenifumbo J, Goya R, Morrissy AS, Morin RD, et al. Alternative expression analysis by RNA sequencing. *Nat Methods.* 2010;7(10):843–7.
824. Picardi E, Horner DS, Chiara M, Schiavon R, Valle G, Pesole G. Large-scale detection and analysis of RNA editing in grape mtDNA by RNA deep-sequencing. *Nucleic Acids Res.* 2010;38(14):4755–67.
825. Wilhelm BT, Briau M, Austin P, Faubert A, Boucher G, Chagnon P, et al. RNA-seq analysis of 2 closely related leukemia clones that differ in their self-renewal capacity. *Blood J Am Soc Hematol.* 2011;117(2):e27–38.
826. Wang ET, Sandberg R, Luo S, Khrebtkova I, Zhang L, Mayr C, et al. Alternative isoform regulation in human tissue transcriptomes. *Nature.* 2008;456(7221):470–6.
827. Chung M, Bruno VM, Rasko DA, Cuomo CA, Muñoz JF, Livny J, et al. Best practices on the differential expression analysis of multi-species RNA-seq. *Genome Biol.* 2021 Apr 29;22(1):121.
828. Sengupta S, Bolin JM, Ruotti V, Nguyen BK, Thomson JA, Elwell AL, et al. Single Read and Paired End mRNA-Seq Illumina Libraries from 10 Nanograms Total RNA. *J Vis Exp JoVE.* 2011;
829. Holt RA, Jones SJ. The new paradigm of flow cell sequencing. *Genome Res.* 2008;18(6):839–46.
830. Haas BJ, Papanicolaou A, Yassour M, Grabherr M, Blood PD, Bowden J, et al. De novo transcript sequence reconstruction from RNA-seq using the Trinity platform for reference generation and analysis. *Nat Protoc.* 2013 Aug 1;8(8):1494–512.

831. Nagalakshmi U, Wang Z, Waern K, Shou C, Raha D, Gerstein M, et al. The transcriptional landscape of the yeast genome defined by RNA sequencing. *Science*. 2008;320(5881):1344–9.
832. Mortazavi A, Williams BA, McCue K, Schaeffer L, Wold B. Mapping and quantifying mammalian transcriptomes by RNA-Seq. *Nat Methods*. 2008;5(7):621–8.
833. Pertea M, Kim D, Pertea GM, Leek JT, Salzberg SL. Transcript-level expression analysis of RNA-seq experiments with HISAT, StringTie and Ballgown. *Nat Protoc*. 2016;11(9):1650–67.
834. Wu J, Anczukow O, Krainer AR, Zhang MQ, Zhang C. OLEgo: fast and sensitive mapping of spliced mRNA-Seq reads using small seeds. *Nucleic Acids Res*. 2013;41(10):5149–63.
835. Bonfert T, Kirner E, Csaba G, Zimmer R, Friedel CC. ContextMap 2: fast and accurate context-based RNA-seq mapping. *BMC Bioinformatics*. 2015;16(1):1–15.
836. Wu TD, Reeder J, Lawrence M, Becker G, Brauer MJ. GMAP and GSNAP for genomic sequence alignment: enhancements to speed, accuracy, and functionality. In: *Statistical genomics*. Springer; 2016. p. 283–334.
837. Ji P, Zhang Y, Wang J, Zhao F. MetaSort untangles metagenome assembly by reducing microbial community complexity. *Nat Commun*. 2017;8(1):1–14.
838. Pertea M, Pertea GM, Antonescu CM, Chang TC, Mendell JT, Salzberg SL. StringTie enables improved reconstruction of a transcriptome from RNA-seq reads. *Nat Biotechnol*. 2015;33(3):290–5.
839. Yuan L, Yu Y, Zhu Y, Li Y, Li C, Li R, et al. GAAP: Genome-organization-framework-Assisted Assembly Pipeline for prokaryotic genomes. *BMC Genomics*. 2017;18(1):1–8.
840. Han Y, Gao S, Muegge K, Zhang W, Zhou B. Advanced Applications of RNA Sequencing and Challenges. *Bioinforma Biol Insights*. 2015 Jan 1;9s1:BBIS28991.
841. Li B, Dewey CN. RSEM: accurate transcript quantification from RNA-Seq data with or without a reference genome. *BMC Bioinformatics*. 2011;12(1):1–16.
842. Allard JS, Heilbronn LK, Smith C, Hunt ND, Ingram DK, Ravussin E, et al. In Vitro Cellular Adaptations of Indicators of Longevity in Response to Treatment with Serum Collected from Humans on Calorie Restricted Diets. *PLOS ONE*. 2008 Sep 15;3(9):e3211.
843. de Cabo R, Fürer-Galbán S, Anson RM, Gilman C, Gorospe M, Lane MA. An in vitro model of caloric restriction. *Exp Gerontol*. 2003 Jun 1;38(6):631–9.
844. Li Y, Tollefsbol TO. Analysis of Biomarkers of Caloric Restriction in Aging Cells. In: Tollefsbol TO, editor. *Biological Aging: Methods and Protocols* [Internet]. Totowa, NJ: Humana Press; 2013. p. 19–29. Available from: https://doi.org/10.1007/978-1-62703-556-9_3

845. García-Matas S, Paul RK, Molina-Martínez P, Palacios H, Gutierrez VM, Corpas R, et al. In vitro caloric restriction induces protective genes and functional rejuvenation in senescent SAMP8 astrocytes. *Aging Cell*. 2015 Jun 1;14(3):334–44.
846. Mbugi EV, Meijerink M, Veenemans J, Jeurink PV, McCall M, Olomi RM, et al. Effect of nutrient deficiencies on in vitro Th1 and Th2 cytokine response of peripheral blood mononuclear cells to *Plasmodium falciparum* infection. *Malar J*. 2010 Jun 14;9(1):162.
847. Li Y, Tollefsbol TO. p16(INK4a) suppression by glucose restriction contributes to human cellular lifespan extension through SIRT1-mediated epigenetic and genetic mechanisms. *PloS One*. 2011 Feb 24;6(2):e17421–e17421.
848. Roecklein B, Torok-Storb B. Functionally distinct human marrow stromal cell lines immortalized by transduction with the human papilloma virus E6/E7 genes. *Blood*. 1995 Feb 15;85(4):997–1005.
849. Katagiri T, Yamaguchi A, Ikeda T, Yoshiki S, Wozney JM, Rosen V, et al. The non-osteogenic mouse pluripotent cell line, C3H10T1/2, is induced to differentiate into osteoblastic cells by recombinant human bone morphogenetic protein-2. *Biochem Biophys Res Commun*. 1990 Oct 15;172(1):295–9.
850. Negishi Y, Kudo A, Obinata A, Kawashima K, Hirano H, Yanai N, et al. Multipotency of a Bone Marrow Stromal Cell Line, TBR31-2, Established from ts-SV40 T Antigen Gene Transgenic Mice. *Biochem Biophys Res Commun*. 2000 Feb 16;268(2):450–5.
851. Ogawa M, Nishikawa S, Ikuta K, Yamamura F, Naito M, Takahashi K, et al. B cell ontogeny in murine embryo studied by a culture system with the monolayer of a stromal cell clone, ST2: B cell progenitor develops first in the embryonal body rather than in the yolk sac. *EMBO J*. 1988 May 1;7(5):1337–43.
852. Kodama HA, Amagai Y, Koyama H, Kasai S. A new preadipose cell line derived from newborn mouse calvaria can promote the proliferation of pluripotent hemopoietic stem cells in vitro. *J Cell Physiol*. 1982 Jul 1;112(1):89–95.
853. Yamaguchi A, Ishizuya T, Kintou N, Wada Y, Katagiri T, Wozney JM, et al. Effects of BMP-2, BMP-4, and BMP-6 on Osteoblastic Differentiation of Bone Marrow-Derived Stromal Cell Lines, ST2 and MC3T3-G2/PA6. *Biochem Biophys Res Commun*. 1996 Mar 18;220(2):366–71.
854. Abdallah BM, Alzahrani AM, Abdel-Moneim AM, Ditzel N, Kassem M. A simple and reliable protocol for long-term culture of murine bone marrow stromal (mesenchymal) stem cells that retained their in vitro and in vivo stemness in long-term culture. *Biol Proced Online*. 2019 Feb 1;21(1):3.
855. Cui Y, Luan J, Li H, Zhou X, Han J. Exosomes derived from mineralizing osteoblasts promote ST2 cell osteogenic differentiation by alteration of microRNA expression. *FEBS Lett*. 2016 Jan 1;590(1):185–92.
856. Otsuka E, Yamaguchi A, Hirose S, Hagiwara H. Characterization of osteoblastic differentiation of stromal cell line ST2 that is induced by ascorbic acid. *Am J Physiol-Cell Physiol*. 1999 Jul 1;277(1):C132–8.

857. Abdallah BM. Marrow adipocytes inhibit the differentiation of mesenchymal stem cells into osteoblasts via suppressing BMP-signaling. *J Biomed Sci.* 2017 Feb 7;24(1):11.
858. Liu S, Xu R, Gerin I, Cawthorn WP, MacDougald OA, Chen XW, et al. SRA Regulates Adipogenesis by Modulating p38/JNK Phosphorylation and Stimulating Insulin Receptor Gene Expression and Downstream Signaling. *PLOS ONE.* 2014 Apr 17;9(4):e95416.
859. Chartoumpakis D V, Ziros P G, Sykiotis G P, Zaravinos A, Psyrogiannis A I, Kyriazopoulou V E, et al. Nrf2 activation diminishes during adipocyte differentiation of ST2 cells. *Int J Mol Med.* 2011 Nov 1;28(5):823–8.
860. DING J, NAGAI K, WOO JT. Insulin-Dependent Adipogenesis in Stromal ST2 Cells Derived from Murine Bone Marrow. *Biosci Biotechnol Biochem.* 2003 Jan 1;67(2):314–21.
861. Adamo A, Delfino P, Gatti A, Bonato A, Takam Kanga P, Bazzoni R, et al. HS-5 and HS-27A Stromal Cell Lines to Study Bone Marrow Mesenchymal Stromal Cell-Mediated Support to Cancer Development. *Front Cell Dev Biol [Internet].* 2020;8. Available from: <https://www.frontiersin.org/articles/10.3389/fcell.2020.584232>
862. YASUDA H, HIGASHIO K, SUDA T. CHAPTER 38 - Vitamin D and Osteoclastogenesis. In: FELDMAN D, editor. *Vitamin D (Second Edition)* [Internet]. Burlington: Academic Press; 2005. p. 665–85. Available from: <https://www.sciencedirect.com/science/article/pii/B9780122526879500413>
863. Takahashi N, Mizoguchi T, Nakamichi Y, Kobayashi Y, Nakamura M, Udagawa N, et al. Osteoclast Cell Lineage: Characteristics and Behavior of Osteoclast Precursors In Vivo. In: *Reference Module in Biomedical Sciences* [Internet]. Elsevier; 2014. Available from: <https://www.sciencedirect.com/science/article/pii/B9780128012383002221>
864. Tong, Kishi, Matsuda, Muraguchi. A bone marrow-derived stroma cell line, ST2, can support the differentiation of fetal thymocytes from the CD4–CD8–double negative to the CD4+ CD8+ double positive differentiation stage in vitro. *Immunology.* 1999 Aug 1;97(4):672–8.
865. Dutta S, Sengupta P. Men and mice: Relating their ages. *Life Sci.* 2016 May 1;152:244–8.
866. Coutel X, Olejnik C, Marchandise P, Delattre J, Béhal H, Kerckhofs G, et al. A Novel microCT Method for Bone and Marrow Adipose Tissue Alignment Identifies Key Differences Between Mandible and Tibia in Rats. *Calcif Tissue Int.* 2018 Aug 1;103(2):189–97.
867. Coutel X, Delattre J, Marchandise P, Falgayrac G, Béhal H, Kerckhofs G, et al. Mandibular bone is protected against microarchitectural alterations and bone marrow adipose conversion in ovariectomized rats. *Bone.* 2019 Oct 1;127:343–52.
868. Yang R, Davies CM, Archer CW, Richards RG. Immunohistochemistry of matrix markers in Technovit 9100 New-embedded undecalcified bone sections. *Eur Cell Mater.* 2003;6:57–71; discussion 71.

869. Bruedigam C, Driel M van, Koedam M, Peppel J van de, van der Eerden BCJ, Eijken M, et al. Basic Techniques in Human Mesenchymal Stem Cell Cultures: Differentiation into Osteogenic and Adipogenic Lineages, Genetic Perturbations, and Phenotypic Analyses. *Curr Protoc Stem Cell Biol*. 2011 Jun 1;17(1):1H.3.1-1H.3.20.
870. Ghali O, Chauveau C, Hardouin P, Broux O, Devedjian JC. TNF- α 's effects on proliferation and apoptosis in human mesenchymal stem cells depend on RUNX2 expression. *J Bone Miner Res*. 2010 Jul 1;25(7):1616–26.
871. Barger SR, Reilly NS, Shutova MS, Li Q, Maiuri P, Heddleston JM, et al. Membrane-cytoskeletal crosstalk mediated by myosin-I regulates adhesion turnover during phagocytosis. *Nat Commun*. 2019 Mar 19;10(1):1249.
872. McIntosh BB, Ostap EM. Myosin-I molecular motors at a glance. *J Cell Sci*. 2016 Jul 15;129(14):2689–95.
873. Nandi A, Yan LJ, Jana CK, Das N. Role of Catalase in Oxidative Stress- and Age-Associated Degenerative Diseases. Signorini C, editor. *Oxid Med Cell Longev*. 2019 Nov 11;2019:9613090.
874. Gupta R, Karpatkin S, Basch RS. Hematopoiesis and stem cell renewal in long-term bone marrow cultures containing catalase. *Blood*. 2006 Mar 1;107(5):1837–46.
875. Guo DC, Pannu H, Tran-Fadulu V, Papke CL, Yu RK, Avidan N, et al. Mutations in smooth muscle α -actin (ACTA2) lead to thoracic aortic aneurysms and dissections. *Nat Genet*. 2007 Dec 1;39(12):1488–93.
876. Iwata H, Manabe I, Fujii K, Yamamoto T, Takeda N, Eguchi K, et al. Bone Marrow-Derived Cells Contribute to Vascular Inflammation but Do Not Differentiate Into Smooth Muscle Cell Lineages. *Circulation*. 2010 Nov 16;122(20):2048–57.
877. Missler M, Zhang W, Rohlmann A, Kattenstroth G, Hammer RE, Gottmann K, et al. α -Neurexins couple Ca²⁺ channels to synaptic vesicle exocytosis. *Nature*. 2003;423(6943):939–48.
878. Kinzfohl J, Hangoc G, Broxmeyer HE. Neurexophilin 1 suppresses the proliferation of hematopoietic progenitor cells. *Blood*. 2011 Jul 21;118(3):565–75.
879. Brocker C, Carpenter C, Nebert DW, Vasiliou V. Evolutionary divergence and functions of the human acyl-CoA thioesterase gene (ACOT) family. *Hum Genomics*. 2010 Aug 1;4(6):411.
880. Cavalli M, Diamanti K, Dang Y, Xing P, Pan G, Chen X, et al. The Thioesterase ACOT1 as a Regulator of Lipid Metabolism in Type 2 Diabetes Detected in a Multi-Omics Study of Human Liver. *OMICS J Integr Biol*. 2021 Oct 1;25(10):652–9.
881. Franklin MP, Sathyanarayan A, Mashek DG. Acyl-CoA Thioesterase 1 (ACOT1) Regulates PPAR α to Couple Fatty Acid Flux With Oxidative Capacity During Fasting. *Diabetes*. 2017 Jun 12;66(8):2112–23.
882. Avilkina V, Leterme D, Falgayrac G, Delattre J, Miellot F, Gauthier V, et al. Severity Level and Duration of Energy Deficit in Mice Affect Bone Phenotype and Bone

- Marrow Stromal Cell Differentiation Capacity. *Front Endocrinol* [Internet]. 2022;13. Available from: <https://www.frontiersin.org/articles/10.3389/fendo.2022.880503>
883. Ghali O, Al Rassy N, Hardouin P, Chauveau C. Increased Bone Marrow Adiposity in a Context of Energy Deficit: The Tip of the Iceberg? *Front Endocrinol*. 2016 Sep 16;7:125–125.
884. Mitchell SE, Tang Z, Kerbois C, Delville C, Konstantopoulos P, Bruel A, et al. The effects of graded levels of calorie restriction: I. impact of short term calorie and protein restriction on body composition in the C57BL/6 mouse. *Oncotarget*. 2015 Jun 30;6(18):15902–30.
885. Scheller EL, Troiano N, Vanhoutan JN, Boussein MA, Fretz JA, Xi Y, et al. Use of osmium tetroxide staining with microcomputerized tomography to visualize and quantify bone marrow adipose tissue in vivo. *Methods Enzymol*. 2014;537:123–39.
886. Hsu JT, Chen YJ, Ho JT, Huang HL, Wang SP, Cheng FC, et al. A Comparison of Micro-CT and Dental CT in Assessing Cortical Bone Morphology and Trabecular Bone Microarchitecture. *PLOS ONE*. 2014 Sep 16;9(9):e107545.
887. Zhong L, Yao L, Seale P, Qin L. Marrow adipogenic lineage precursor: A new cellular component of marrow adipose tissue. *Emerg Role Bone Marrow Adipose Tissue*. 2021 Jul 1;35(4):101518.
888. Zhong L, Yao L, Tower RJ, Wei Y, Miao Z, Park J, et al. Single cell transcriptomics identifies a unique adipose lineage cell population that regulates bone marrow environment. *Elife*. 2020;9:e54695.
889. Zou W, Rohatgi N, Brestoff JR, Li Y, Barve RA, Tycksen E, et al. Ablation of fat cells in adult mice induces massive bone gain. *Cell Metab*. 2020;32(5):801–13.
890. Zou W, Rohatgi N, Brestoff JR, Zhang Y, Scheller EL, Craft CS, et al. Congenital lipodystrophy induces severe osteosclerosis. *PLoS Genet*. 2019;15(6):e1008244.
891. Yu W, Zhong L, Yao L, Wei Y, Gui T, Li Z, et al. Bone marrow adipogenic lineage precursors promote osteoclastogenesis in bone remodeling and pathologic bone loss. *J Clin Invest*. 2021;131(2).
892. Nakashima T, Hayashi M, Fukunaga T, Kurata K, Oh-Hora M, Feng JQ, et al. Evidence for osteocyte regulation of bone homeostasis through RANKL expression. *Nat Med*. 2011;17(10):1231–4.
893. Xiong J, Onal M, Jilka RL, Weinstein RS, Manolagas SC, O'Brien CA. Matrix-embedded cells control osteoclast formation. *Nat Med*. 2011 Oct 1;17(10):1235–41.
894. Xiong J, Piemontese M, Onal M, Campbell J, Goellner JJ, Dusevich V, et al. Osteocytes, not osteoblasts or lining cells, are the main source of the RANKL required for osteoclast formation in remodeling bone. *PLoS One*. 2015;10(9):e0138189.
895. Benova A, Ferencakova M, Bardova K, Funda J, Prochazka J, Spoutil F, et al. Novel thiazolidinedione analog reduces a negative impact on bone and mesenchymal stem cell

- properties in obese mice compared to classical thiazolidinediones. *Mol Metab.* 2022 Nov 1;65:101598.
896. Pittenger Mark F., Mackay Alastair M., Beck Stephen C., Jaiswal Rama K., Douglas Robin, Mosca Joseph D., et al. Multilineage Potential of Adult Human Mesenchymal Stem Cells. *Science.* 1999 Apr 2;284(5411):143–7.
897. Song L, Liu M, Ono N, Bringham FR, Kronenberg HM, Guo J. Loss of wnt/ β -catenin signaling causes cell fate shift of preosteoblasts from osteoblasts to adipocytes. *J Bone Miner Res Off J Am Soc Bone Miner Res.* 2012 Nov;27(11):2344–58.
898. Baek K, Bloomfield SA. Blocking β -adrenergic signaling attenuates reductions in circulating leptin, cancellous bone mass, and marrow adiposity seen with dietary energy restriction. *J Appl Physiol.* 2012 Dec 1;113(11):1792–801.
899. Bianco P, Robey PG, Saggio I, Riminucci M. ‘Mesenchymal’ stem cells in human bone marrow (skeletal stem cells): a critical discussion of their nature, identity, and significance in incurable skeletal disease. *Hum Gene Ther.* 2010 Sep;21(9):1057–66.
900. Shakibaei M, Shayan P, Busch F, Aldinger C, Buhrmann C, Lueders C, et al. Resveratrol mediated modulation of Sirt-1/Runx2 promotes osteogenic differentiation of mesenchymal stem cells: potential role of Runx2 deacetylation. *PloS One.* 2012/04/23 ed. 2012;7(4):e35712–e35712.
901. Tseng PC, Hou SM, Chen RJ, Peng HW, Hsieh CF, Kuo ML, et al. Resveratrol promotes osteogenesis of human mesenchymal stem cells by upregulating RUNX2 gene expression via the SIRT1/FOXO3A axis. *J Bone Miner Res.* 2011 Oct 1;26(10):2552–63.
902. Chiara B, Ilaria C, Antonietta C, Francesca C, Marco M, Lucia A, et al. SIRT1 Inhibition Affects Angiogenic Properties of Human MSCs. Li Z, editor. *BioMed Res Int.* 2014 Aug 27;2014:783459.
903. Orecchia A, Scarponi C, Di Felice F, Cesarini E, Avitabile S, Mai A, et al. Sirtinol Treatment Reduces Inflammation in Human Dermal Microvascular Endothelial Cells. *PLOS ONE.* 2011 Sep 12;6(9):e24307.
904. Artsi H, Cohen-Kfir E, Gurt I, Shahar R, Bajayo A, Kalish N, et al. The Sirtuin1 Activator SRT3025 Down-Regulates Sclerostin and Rescues Ovariectomy-Induced Bone Loss and Biomechanical Deterioration in Female Mice. *Endocrinology.* 2014 Sep 1;155(9):3508–15.
905. Herranz D, Muñoz-Martin M, Cañamero M, Mulero F, Martinez-Pastor B, Fernandez-Capetillo O, et al. Sirt1 improves healthy ageing and protects from metabolic syndrome-associated cancer. *Nat Commun.* 2010 Apr 12;1(1):3.
906. Zainabadi K, Liu CJ, Caldwell ALM, Guarente L. SIRT1 is a positive regulator of in vivo bone mass and a therapeutic target for osteoporosis. *PloS One.* 2017 Sep 22;12(9):e0185236–e0185236.

907. Chen D, Steele AD, Hutter G, Bruno J, Govindarajan A, Easlou E, et al. The role of calorie restriction and SIRT1 in prion-mediated neurodegeneration. *Exp Gerontol.* 2008/08/30 ed. 2008 Dec;43(12):1086–93.
908. Méquignon M, Caron E, Zgheib S, Stievenard A, Zizzari P, Tolle V, et al. Physical activity: Benefit or weakness in metabolic adaptations in a mouse model of chronic food restriction? *Am J Physiol Endocrinol Metab.* 2014 Dec 2;308:ajpendo.00340.2014.
909. Kostogrys R, Franczyk-Zarow M, Manterys A, Wybranska I. Effect of caloric restriction on liver function in young and old ApoE/LDLr^{-/-} mice. *Rocz Panstw Zakl Hig.* 2018 Mar 1;69:37–43.
910. Verrijken A, Francque S, Mertens I, Talloen M, Peiffer F, Van Gaal L. Visceral adipose tissue and inflammation correlate with elevated liver tests in a cohort of overweight and obese patients. *Int J Obes.* 2010 May 1;34(5):899–907.
911. Bruss MD, Khambatta CF, Ruby MA, Aggarwal I, Hellerstein MK. Calorie restriction increases fatty acid synthesis and whole body fat oxidation rates. *Am J Physiol-Endocrinol Metab.* 2010 Jan 1;298(1):E108–16.
912. Mundi MS, Koutsari C, Jensen MD. Effects of Increased Free Fatty Acid Availability on Adipose Tissue Fatty Acid Storage in Men. *J Clin Endocrinol Metab.* 2014 Dec 1;99(12):E2635–42.
913. Raclot T, Groscolas R. Selective mobilization of adipose tissue fatty acids during energy depletion in the rat. *J Lipid Res.* 1996 Jan 1;36(10):2164–73.
914. Gupta R, Mepani R, Kleiner S, Lo J, Khandekar M, Cohen P, et al. Zfp423 Expression Identifies Committed Preadipocytes and Localizes to Adipose Endothelial and Perivascular Cells. *Cell Metab.* 2012 Feb 8;15:230–9.
915. Arpornmaeklong P, Brown SE, Wang Z, Krebsbach PH. Phenotypic Characterization, Osteoblastic Differentiation, and Bone Regeneration Capacity of Human Embryonic Stem Cell-Derived Mesenchymal Stem Cells. *Stem Cells Dev.* 2009 Sep 1;18(7):955–68.
916. De Filippo E, Marra M, Alfinito F, Di Guglielmo ML, Majorano P, Cerciello G, et al. Hematological complications in anorexia nervosa. *Eur J Clin Nutr.* 2016 Nov 1;70(11):1305–8.
917. Cleary BS, Gaudiani JL, Mehler PS. Interpreting the Complete Blood Count in Anorexia Nervosa. *Eat Disord.* 2010 Mar 2;18(2):132–9.
918. Hütter G, Ganepola S, Hofmann WK. The hematology of anorexia nervosa. *Int J Eat Disord.* 2009 May 1;42(4):293–300.
919. Fajardo-Orduña GR, Mayani H, Montesinos JJ. Hematopoietic Support Capacity of Mesenchymal Stem Cells: Biology and Clinical Potential. *Arch Med Res.* 2015 Nov 1;46(8):589–96.
920. Liu L, Sun Q, Hu K, Huang Y, Fan C, Sun Z, et al. Establishment of a rhesus haploidentical hematopoietic stem cell and mesenchymal stem cell transplantation

model by nonmyeloablative conditioning. *Zhonghua Xue Ye Xue Za Zhi Zhonghua Xueyexue Zazhi*. 2005;26(7):385–8.

921. Almeida-Porada G, Porada CD, Tran N, Zanjani ED. Cotransplantation of human stromal cell progenitors into preimmune fetal sheep results in early appearance of human donor cells in circulation and boosts cell levels in bone marrow at later time points after transplantation. *Blood J Am Soc Hematol*. 2000;95(11):3620–7.
922. Muguruma Y, Yahata T, Miyatake H, Sato T, Uno T, Itoh J, et al. Reconstitution of the functional human hematopoietic microenvironment derived from human mesenchymal stem cells in the murine bone marrow compartment. *Blood*. 2006;107(5):1878–87.
923. Kim DH, Yoo KH, Yim YS, Choi J, Lee SH, Jung HL, et al. Cotransplanted bone marrow derived mesenchymal stem cells (MSC) enhanced engraftment of hematopoietic stem cells in a MSC-dose dependent manner in NOD/SCID mice. *J Korean Med Sci*. 2006;21(6):1000–4.
924. Angelopoulou M, Novelli E, Grove JE, Rinder HM, Civin C, Cheng L, et al. Cotransplantation of human mesenchymal stem cells enhances human myelopoiesis and megakaryocytopoiesis in NOD/SCID mice. *Exp Hematol*. 2003;31(5):413–20.
925. Delalat B, Pourfathollah AA, Soleimani M, Mozdarani H, Ghaemi SR, Movassaghpour AA, et al. Isolation and ex vivo expansion of human umbilical cord blood-derived CD34+ stem cells and their cotransplantation with or without mesenchymal stem cells. *Hematology*. 2009;14(3):125–32.
926. Omatsu Y, Sugiyama T, Kohara H, Kondoh G, Fujii N, Kohno K, et al. The essential functions of adipo-osteogenic progenitors as the hematopoietic stem and progenitor cell niche. *Immunity*. 2010;33(3):387–99.
927. Kunisaki Y, Bruns I, Scheiermann C, Ahmed J, Pinho S, Zhang D, et al. Arteriolar niches maintain haematopoietic stem cell quiescence. *Nature*. 2013;502(7473):637–43.
928. Dazzi F, Ramasamy R, Glennie S, Jones SP, Roberts I. The role of mesenchymal stem cells in haemopoiesis. *Blood Rev*. 2006;20(3):161–71.
929. AU - Maridas DE, AU - Rendina-Ruedy E, AU - Le PT, AU - Rosen CJ. Isolation, Culture, and Differentiation of Bone Marrow Stromal Cells and Osteoclast Progenitors from Mice. *J Vis Exp*. 2018 Jan 6;(131):e56750.
930. Gordon MY. Plastic-adherent cells in human bone marrow generate long-term hematopoiesis in vitro. *Leukemia*. 1994;8(5):865–70.
931. James S, Fox J, Afsari F, Lee J, Clough S, Knight C, et al. Multiparameter Analysis of Human Bone Marrow Stromal Cells Identifies Distinct Immunomodulatory and Differentiation-Competent Subtypes. *Stem Cell Rep*. 2015 Jun 9;4(6):1004–15.
932. Guo W, Spiller KV, Tang J, Karner CM, Hilton MJ, Wu C. Hypoxia depletes contaminating CD45+ hematopoietic cells from murine bone marrow stromal cell (BMSC) cultures: Methods for BMSC culture purification. *Stem Cell Res*. 2021 May 1;53:102317.

933. Herrmann M, Hildebrand M, Menzel U, Fahy N, Alini M, Lang S, et al. Phenotypic Characterization of Bone Marrow Mononuclear Cells and Derived Stromal Cell Populations from Human Iliac Crest, Vertebral Body and Femoral Head. *Int J Mol Sci.* 2019;20(14).
934. Burk AS, Monzel C, Yoshikawa HY, Wuchter P, Saffrich R, Eckstein V, et al. Quantifying Adhesion Mechanisms and Dynamics of Human Hematopoietic Stem and Progenitor Cells. *Sci Rep.* 2015 Mar 31;5(1):9370.
935. Pawar M, Pawar V, Renugalakshmi A, Albrakati A, Uthman US, Dewan H, et al. Glucose and Serum Deprivation Led to Altered Proliferation, Differentiation Potential and AMPK Activation in Stem Cells from Human Deciduous Tooth. *J Pers Med.* 2022;12(1).
936. Rostovskaya M, Anastassiadis K. Differential Expression of Surface Markers in Mouse Bone Marrow Mesenchymal Stromal Cell Subpopulations with Distinct Lineage Commitment. *PLOS ONE.* 2012 Dec 7;7(12):e51221.
937. Zhu D, Gao J, Tang C, Xu Z, Sun T. Single-Cell RNA Sequencing of Bone Marrow Mesenchymal Stem Cells from the Elderly People. *Int J Stem Cells.* 2022/05/30 ed. 2022 May;15(2):173–82.
938. Li R, Li Y, Kristiansen K, Wang J. SOAP: short oligonucleotide alignment program. *Bioinformatics.* 2008;24(5):713–4.
939. Li H, Ruan J, Durbin R. Mapping short DNA sequencing reads and calling variants using mapping quality scores. *Genome Res.* 2008;18(11):1851–8.
940. Smith AD, Xuan Z, Zhang MQ. Using quality scores and longer reads improves accuracy of Solexa read mapping. *BMC Bioinformatics.* 2008;9(1):1–8.
941. Cloonan N, Forrest AR, Kolle G, Gardiner B, Faulkner GJ, Brown MK, et al. Stem cell transcriptome profiling via massive-scale mRNA sequencing. *Nat Methods.* 2008;5(7):613–9.
942. Robinson MD, Oshlack A. A scaling normalization method for differential expression analysis of RNA-seq data. *Genome Biol.* 2010;11(3):1–9.
943. Büttner M, Miao Z, Wolf FA, Teichmann SA, Theis FJ. A test metric for assessing single-cell RNA-seq batch correction. *Nat Methods.* 2019;16(1):43–9.
944. Chen G, Shi T, Shi L. Characterizing and annotating the genome using RNA-seq data. *Sci China Life Sci.* 2017;60(2):116–25.
945. Jaitin DA, Kenigsberg E, Keren-Shaul H, Elefant N, Paul F, Zaretsky I, et al. Massively parallel single-cell RNA-seq for marker-free decomposition of tissues into cell types. *Science.* 2014;343(6172):776–9.
946. Gross A, Schoendube J, Zimmermann S, Steeb M, Zengerle R, Koltay P. Technologies for single-cell isolation. *Int J Mol Sci.* 2015;16(8):16897–919.

947. Wen L, Tang F. Boosting the power of single-cell analysis. *Nat Biotechnol.* 2018;36(5):408–9.
948. Pennisi E. Single-cell sequencing tackles basic and biomedical questions. 2012;
949. McDavid A, Finak G, Chattopadhyay PK, Dominguez M, Lamoreaux L, Ma SS, et al. Data exploration, quality control and testing in single-cell qPCR-based gene expression experiments. *Bioinformatics.* 2013;29(4):461–7.
950. Warren MP. Endocrine Manifestations of Eating Disorders. *J Clin Endocrinol Metab.* 2011 Feb 1;96(2):333–43.
951. Warren MP. Effects of undernutrition on reproductive function in the human. *Endocr Rev.* 1983;4(4):363–77.
952. Baker JH, Sisk CL, Thornton LM, Brandt H, Crawford S, Fichter MM, et al. Primary Amenorrhea in Anorexia Nervosa: Impact on Characteristic Masculine and Feminine Traits. *Eur Eat Disord Rev.* 2014 Jan 1;22(1):32–8.
953. Cheng CH, Chen LR, Chen KH. Osteoporosis Due to Hormone Imbalance: An Overview of the Effects of Estrogen Deficiency and Glucocorticoid Overuse on Bone Turnover. *Int J Mol Sci.* 2022;23(3).
954. Lubkowska A, Dobek A, Mieszkowski J, Garczynski W, Chlubek D. Adiponectin as a Biomarker of Osteoporosis in Postmenopausal Women: Controversies. Mannello F, editor. *Dis Markers.* 2014 Jan 23;2014:975178.
955. Almeida M, Iyer S, Martin-Millan M, Bartell SM, Han L, Ambrogini E, et al. Estrogen receptor- α signaling in osteoblast progenitors stimulates cortical bone accrual. *J Clin Invest.* 2013 Jan 2;123(1):394–404.
956. Solmi M, Veronese N, Favaro A, Santonastaso P, Manzato E, Sergi G, et al. Inflammatory cytokines and anorexia nervosa: A meta-analysis of cross-sectional and longitudinal studies. *Psychoneuroendocrinology.* 2015;51:237–52.
957. Dalton B, Bartholdy S, Robinson L, Solmi M, Ibrahim MA, Breen G, et al. A meta-analysis of cytokine concentrations in eating disorders. *J Psychiatr Res.* 2018;103:252–64.
958. Nilsson IAK, Millischer V, Göteson A, Hübel C, Thornton LM, Bulik CM, et al. Aberrant inflammatory profile in acute but not recovered anorexia nervosa. *Brain Behav Immun.* 2020 Aug 1;88:718–24.
959. Ochi S, Shinohara M, Sato K, Guber HJ, Koga T, Kodama T, et al. Pathological role of osteoclast costimulation in arthritis-induced bone loss. *Proc Natl Acad Sci.* 2007 Jul 3;104(27):11394–9.
960. Lapointe M. The Effects of Dietary Ingestion of Nickel Recovery Slag as a Grit Source on Avian Bone. 2020.

961. Zhang L, Fishman MC, Huang PL. Estrogen Mediates the Protective Effects of Pregnancy and Chorionic Gonadotropin in a Mouse Model of Vascular Injury. *Arterioscler Thromb Vasc Biol.* 1999 Sep 1;19(9):2059–65.
962. Semba I, Matsuuchi H, Miura Y. Histomorphometric analysis of osteoclastic resorption in bone directly invaded by gingival squamous cell carcinoma. *J Oral Pathol Med.* 1996 Sep 1;25(8):429–35.
963. Samee N, Geoffroy V, Marty C, Schiltz C, Vieux-rochas M, Levi G, et al. Dlx5, a Positive Regulator of Osteoblastogenesis, is Essential for Osteoblast-Osteoclast Coupling. *Am J Pathol.* 2008 Oct 1;173:773–80.
964. THOMSEN JS, LAIB A, KOLLER B, PROHASKA S, MOSEKILDE LI, GOWIN W. Stereological measures of trabecular bone structure: comparison of 3D micro computed tomography with 2D histological sections in human proximal tibial bone biopsies. *J Microsc.* 2005 May 1;218(2):171–9.
965. Botha D, Bhagwandin A, Lynnerup N, Steyn M. The use of stereological methods in the histomorphometric assessment of bone for age-at-death estimation. *Forensic Sci Int.* 2018 Sep 1;290:353.e1-353.e7.
966. Saper CB. Unbiased Stereology: Three-Dimensional Measurement in Microscopy by C.V. Howard and M.G. Reed. *Trends Neurosci.* 1999 Feb 1;22(2):94–5.
967. Maille A, Pillay N, Schradin C. Seasonal variation in attention and spatial performance in a wild population of the African striped mouse (*Rhabdomys pumilio*). *Anim Cogn.* 2015 Nov 1;18(6):1231–42.
968. Xiaoling Li. SIRT1 and energy metabolism. *Acta Biochim Biophys Sin.* 2013 Jan 1;45(1):51–60.
969. Schwartz JP, Passonneau JV, Johnson GS, Pastan I. The Effect of Growth Conditions on NAD⁺ and NADH Concentrations and the NAD⁺:NADH Ratio in Normal and Transformed Fibroblasts. *J Biol Chem.* 1974 Jul 10;249(13):4138–43.
970. Bernardini C, Algieri C, Mantia LD, Zannoni A, Salaroli R, Trombetti F, et al. Relationship between serum concentration, functional parameters and cell bioenergetics in IPEC-J2 cell line. *Histochem Cell Biol.* 2021 Jul 1;156(1):59–67.
971. Korzeniewski B. Influence of substrate activation (hydrolysis of ATP by first steps of glycolysis and β -oxidation) on the effect of enzyme deficiencies, inhibitors, substrate shortage and energy demand on oxidative phosphorylation. *Biophys Chem.* 2003 May 1;104(1):107–19.
972. Kim J, Yang G, Kim Y, Kim J, Ha J. AMPK activators: mechanisms of action and physiological activities. *Exp Mol Med.* 2016 Apr 1;48(4):e224–e224.
973. Cantó C, Gerhart-Hines Z, Feige JN, Lagouge M, Noriega L, Milne JC, et al. AMPK regulates energy expenditure by modulating NAD⁺ metabolism and SIRT1 activity. *Nature.* 2009 Apr 1;458(7241):1056–60.

974. Sadria M, Layton AT. Interactions among mTORC, AMPK and SIRT: a computational model for cell energy balance and metabolism. *Cell Commun Signal*. 2021 May 20;19(1):57.
975. Wang C, Chen L, Hou X, Li Z, Kabra N, Ma Y, et al. Interactions between E2F1 and SirT1 regulate apoptotic response to DNA damage. *Nat Cell Biol*. 2006 Sep 1;8(9):1025–31.
976. Yang W, Park IJ, Yun H, Im DU, Ock S, Kim J, et al. AMP-activated Protein Kinase $\alpha 2$ and E2F1 Transcription Factor Mediate Doxorubicin-induced Cytotoxicity by Forming a Positive Signal Loop in Mouse Embryonic Fibroblasts and Non-carcinoma Cells*. *J Biol Chem*. 2014 Feb 21;289(8):4839–52.
977. Fire A, Xu S, Montgomery MK, Kostas SA, Driver SE, Mello CC. Potent and specific genetic interference by double-stranded RNA in *Caenorhabditis elegans*. *nature*. 1998;391(6669):806–11.
978. Dana H, Mahmoodi Chalbatani G, Mahmoodzadeh H, Karimloo R, Rezaiean O, Moradzadeh A, et al. Molecular Mechanisms and Biological Functions of siRNA. *Int J Biomed Sci IJBS*. 2017 Jun 1;13.
979. Bartel DP. MicroRNAs: genomics, biogenesis, mechanism, and function. *cell*. 2004;116(2):281–97.
980. Meister G, Tuschl T. Mechanisms of gene silencing by double-stranded RNA. *Nature*. 2004;431(7006):343–9.
981. Elbashir SM, Harborth J, Lendeckel W, Yalcin A, Weber K, Tuschl T. Duplexes of 21-nucleotide RNAs mediate RNA interference in cultured mammalian cells. *nature*. 2001;411(6836):494–8.
982. Oh YK, Park TG. siRNA delivery systems for cancer treatment. *Adv Drug Deliv Rev*. 2009;61(10):850–62.
983. Rubin MA. Targeted therapy of cancer: new roles for pathologists—prostate cancer. *Mod Pathol*. 2008;21(2):S44–55.
984. Gabriela N. Tenea, Liliana Burlibasa. RNAi Towards Functional Genomics Studies. In: Germana Meroni, Francesca Petrera, editors. *Functional Genomics [Internet]*. Rijeka: IntechOpen; 2012 [cited 2022 Oct 12]. p. Ch. 4. Available from: <https://doi.org/10.5772/47762>
985. Natalya S. Petrova, Marina A. Zenkova, Elena L. Chernolovskaya. Structure - Functions Relations in Small Interfering RNAs. In: Adriano O. Andrade, Adriano Alves Pereira, Eduardo L. M. Naves, Alcimar B. Soares, editors. *Practical Applications in Biomedical Engineering [Internet]*. Rijeka: IntechOpen; 2013 [cited 2022 Oct 12]. p. Ch. 8. Available from: <https://doi.org/10.5772/53945>
986. Agrawal N, Dasaradhi P, Mohmmmed A, Malhotra P, Bhatnagar RK, Mukherjee SK. RNA interference: biology, mechanism, and applications. *Microbiol Mol Biol Rev*. 2003;67(4):657–85.

987. Pecot CV, Calin GA, Coleman RL, Lopez-Berestein G, Sood AK. RNA interference in the clinic: challenges and future directions. *Nat Rev Cancer*. 2011;11(1):59–67.
988. Felgner PL, Gadek TR, Holm M, Roman R, Chan HW, Wenz M, et al. Lipofection: a highly efficient, lipid-mediated DNA-transfection procedure. *Proc Natl Acad Sci*. 1987 Nov 1;84(21):7413–7.
989. Scherer LJ, Rossi JJ. Approaches for the sequence-specific knockdown of mRNA. *Nat Biotechnol*. 2003 Dec 1;21(12):1457–65.
990. Kurreck J. Antisense technologies. *Eur J Biochem*. 2003 Apr 1;270(8):1628–44.
991. Miyagishi M, Hayashi M, Taira K. Comparison of the Suppressive Effects of Antisense Oligonucleotides and siRNAs Directed Against the Same Targets in Mammalian Cells. *Antisense Nucleic Acid Drug Dev*. 2003 Feb 1;13(1):1–7.
992. Kretschmer-Kazemi Far R, Sczakiel G. The activity of siRNA in mammalian cells is related to structural target accessibility: a comparison with antisense oligonucleotides. *Nucleic Acids Res*. 2003 Aug 1;31(15):4417–24.
993. Grünweller A, Wyszko E, Bieber B, Jahnel R, Erdmann VA, Kurreck J. Comparison of different antisense strategies in mammalian cells using locked nucleic acids, 2'-O-methyl RNA, phosphorothioates and small interfering RNA. *Nucleic Acids Res*. 2003 Jun 15;31(12):3185–93.
994. Xu Y, Zhang HY, Thormeyer D, Larsson O, Du Q, Elmén J, et al. Effective small interfering RNAs and phosphorothioate antisense DNAs have different preferences for target sites in the luciferase mRNAs. *Biochem Biophys Res Commun*. 2003 Jul 4;306(3):712–7.
995. Bertrand JR, Pottier M, Vekris A, Opolon P, Maksimenko A, Malvy C. Comparison of antisense oligonucleotides and siRNAs in cell culture and in vivo. *Biochem Biophys Res Commun*. 2002 Aug 30;296(4):1000–4.
996. Lebedeva I, Stein C. Antisense Oligonucleotides: Promise and Reality. *Annu Rev Pharmacol Toxicol*. 2001 Apr 1;41(1):403–19.
997. Hafner M, Zawatzky R, Hirtreiter C, Buurman WA, Echtenacher B, Hehlhans T, et al. Antimetastatic Effect of CpG DNA Mediated by Type I IFN1. *Cancer Res*. 2001 Jul 1;61(14):5523–8.
998. Roman M, Martin-Orozco E, Goodman JS, Nguyen MD, Sato Y, Ronaghy A, et al. Immunostimulatory DNA sequences function as T helper-1-promoting adjuvants. *Nat Med*. 1997 Aug 1;3(8):849–54.
999. Rothenfusser S, Tuma E, Wagner M, Endres S, Hartmann G. Recent advances in immunostimulatory CpG oligonucleotides. *Curr Opin Mol Ther*. 2003 Apr;5(2):98–106.
1000. Jackson AL, Bartz SR, Schelter J, Kobayashi SV, Burchard J, Mao M, et al. Expression profiling reveals off-target gene regulation by RNAi. *Nat Biotechnol*. 2003 Jun 1;21(6):635–7.

1001. Chi JT, Chang HY, Wang NN, Chang DS, Dunphy N, Brown PO. Genomewide view of gene silencing by small interfering RNAs. *Proc Natl Acad Sci*. 2003 May 27;100(11):6343–6.
1002. Semizarov D, Frost L, Sarthy A, Kroeger P, Halbert DN, Fesik SW. Specificity of short interfering RNA determined through gene expression signatures. *Proc Natl Acad Sci*. 2003 May 27;100(11):6347–52.
1003. Jin J, Iakova P, Jiang Y, Lewis K, Sullivan E, Jawanmardi N, et al. Transcriptional and translational regulation of C/EBP β -HDAC1 protein complexes controls different levels of p53, SIRT1, and PGC1 α proteins at the early and late stages of liver cancer. *J Biol Chem*. 2013/04/05 ed. 2013 May 17;288(20):14451–62.
1004. Kang MR, Lee SW, Um E, Kang HT, Hwang ES, Kim EJ, et al. Reciprocal roles of SIRT1 and SKIP in the regulation of RAR activity: implication in the retinoic acid-induced neuronal differentiation of P19 cells. *Nucleic Acids Res*. 2009/11/24 ed. 2010 Jan;38(3):822–31.
1005. Elangovan S, Ramachandran S, Venkatesan N, Ananth S, Gnana-Prakasam JP, Martin PM, et al. SIRT1 is essential for oncogenic signaling by estrogen/estrogen receptor α in breast cancer. *Cancer Res*. 2011/09/15 ed. 2011 Nov 1;71(21):6654–64.
1006. Capasso S, Alessio N, Di Bernardo G, Cipollaro M, Melone MA, Peluso G, et al. Silencing of RB1 and RB2/P130 during adipogenesis of bone marrow stromal cells results in dysregulated differentiation. *Cell Cycle Georget Tex*. 2013/11/26 ed. 2014;13(3):482–90.
1007. Song Z, Liu Y, Hao B, Yu S, Zhang H, Liu D, et al. Ginsenoside Rb1 Prevents H₂O₂-Induced HUVEC Senescence by Stimulating Sirtuin-1 Pathway. *PLOS ONE*. 2014 Nov 11;9(11):e112699.
1008. Fan C, Ma Q, Xu M, Qiao Y, Zhang Y, Li P, et al. Ginsenoside Rb1 Attenuates High Glucose-Induced Oxidative Injury via the NAD-PARP-SIRT Axis in Rat Retinal Capillary Endothelial Cells. *Int J Mol Sci*. 2019;20(19).
1009. Jiang N, Zhang Y, Yao C, Huang H, Wang Q, Huang S, et al. Ginsenosides Rb1 Attenuates Chronic Social Defeat Stress-Induced Depressive Behavior via Regulation of SIRT1-NLRP3/Nrf2 Pathways. *Front Nutr [Internet]*. 2022;9. Available from: <https://www.frontiersin.org/articles/10.3389/fnut.2022.868833>
1010. Baud V, Collares D. Post-Translational Modifications of RelB NF- κ B Subunit and Associated Functions. *Cells*. 2016;5(2).
1011. Yiu SM, Wong PW, Lam TW, Mui Y, Kung H, Lin M, et al. Filtering of ineffective siRNAs and improved siRNA design tool. *Bioinformatics*. 2005;21(2):144–51.
1012. Naito Y, Ui-Tei K. Designing functional siRNA with reduced off-target effects. In: *siRNA Design*. Springer; 2013. p. 57–68.
1013. Chalk AM, Wahlestedt C, Sonnhammer EL. Improved and automated prediction of effective siRNA. *Biochem Biophys Res Commun*. 2004;319(1):264–74.

1014. Suter SR, Sheu-Gruttadauria J, Schirle NT, Valenzuela R, Ball-Jones AA, Onizuka K, et al. Structure-Guided Control of siRNA Off-Target Effects. *J Am Chem Soc.* 2016 Jul 20;138(28):8667–9.
1015. Kobayashi Y, Tian S, Ui-Tei K. The siRNA Off-Target Effect Is Determined by Base-Pairing Stabilities of Two Different Regions with Opposite Effects. *Genes.* 2022;13(2).
1016. Neumeier J, Meister G. siRNA Specificity: RNAi Mechanisms and Strategies to Reduce Off-Target Effects. *Front Plant Sci [Internet].* 2021;11. Available from: <https://www.frontiersin.org/articles/10.3389/fpls.2020.526455>
1017. Jackson AL, Linsley PS. Recognizing and avoiding siRNA off-target effects for target identification and therapeutic application. *Nat Rev Drug Discov.* 2010 Jan 1;9(1):57–67.
1018. Lam JK, Worsley AJ. What is the future of siRNA therapeutics? *J Drug Des Res.* 2014;
1019. Birmingham A, Anderson EM, Reynolds A, Iisley-Tyree D, Leake D, Fedorov Y, et al. 3' UTR seed matches, but not overall identity, are associated with RNAi off-targets. *Nat Methods.* 2006;3(3):199–204.
1020. Rao DD, Vorhies JS, Senzer N, Nemunaitis J. siRNA vs. shRNA: similarities and differences. *Adv Drug Deliv Rev.* 2009;61(9):746–59.
1021. Taxman DJ, Moore CB, Guthrie EH, Huang MTH. Short Hairpin RNA (shRNA): Design, Delivery, and Assessment of Gene Knockdown. In: Sioud M, editor. *RNA Therapeutics: Function, Design, and Delivery [Internet].* Totowa, NJ: Humana Press; 2010. p. 139–56. Available from: https://doi.org/10.1007/978-1-60761-657-3_10
1022. Yin H, Kanasty RL, Eltoukhy AA, Vegas AJ, Dorkin JR, Anderson DG. Non-viral vectors for gene-based therapy. *Nat Rev Genet.* 2014;15(8):541–55.
1023. Davidson BL, McCray PB. Current prospects for RNA interference-based therapies. *Nat Rev Genet.* 2011;12(5):329–40.
1024. O'Keefe EP. siRNAs and shRNAs: Tools for Protein Knockdown by Gene Silencing. *Mater Methods.* 2013;3.
1025. Barski A, Cuddapah S, Cui K, Roh TY, Schones DE, Wang Z, et al. High-resolution profiling of histone methylations in the human genome. *Cell.* 2007;129(4):823–37.
1026. Kouzarides T. Chromatin modifications and their function. *Cell.* 2007;128(4):693–705.
1027. Heintzman ND, Hon GC, Hawkins RD, Kheradpour P, Stark A, Harp LF, et al. Histone modifications at human enhancers reflect global cell-type-specific gene expression. *Nature.* 2009;459(7243):108–12.
1028. Heintzman ND, Stuart RK, Hon G, Fu Y, Ching CW, Hawkins RD, et al. Distinct and predictive chromatin signatures of transcriptional promoters and enhancers in the human genome. *Nat Genet.* 2007;39(3):311–8.

1029. Squazzo SL, Iyengar S, Blahnik K, Rinn JL, Chang HY, Green R, et al. Genome-Wide Analysis of KAP1 Binding Suggests Autoregulation of KRAB-ZNFs. *PLoS Genet.* 2007;3(6).
1030. Rinn JL, Kertesz M, Wang JK, Squazzo SL, Xu X, Brugmann SA, et al. Functional demarcation of active and silent chromatin domains in human HOX loci by noncoding RNAs. *cell.* 2007;129(7):1311–23.
1031. Lanzuolo C, Orlando V. The function of the epigenome in cell reprogramming. *Cell Mol Life Sci.* 2007;64(9):1043–62.
1032. Hemberger M, Dean W, Reik W. Epigenetic dynamics of stem cells and cell lineage commitment: digging Waddington’s canal. *Nat Rev Mol Cell Biol.* 2009;10(8):526–37.
1033. Nakato R, Sakata T. Methods for ChIP-seq analysis: A practical workflow and advanced applications. *Adv Epigenetics Methods Biomed.* 2021 Mar 1;187:44–53.
1034. Jeon SM. Regulation and function of AMPK in physiology and diseases. *Exp Mol Med.* 2016 Jul 1;48(7):e245–e245.
1035. Carlson M, Osmond BC, Botstein D. Mutants of yeast defective in sucrose utilization. *Genetics.* 1981;98(1):25–40.
1036. Woods A, Munday MR, Scott J, Yang X, Carlson M, Carling D. Yeast SNF1 is functionally related to mammalian AMP-activated protein kinase and regulates acetyl-CoA carboxylase in vivo. *J Biol Chem.* 1994;269(30):19509–15.
1037. Hedbacker K, Carlson M. SNF1/AMPK pathways in yeast. *Front Biosci J Virtual Libr.* 2008;13:2408.
1038. Kahn BB, Alquier T, Carling D, Hardie DG. AMP-activated protein kinase: ancient energy gauge provides clues to modern understanding of metabolism. *Cell Metab.* 2005;1(1):15–25.
1039. Hardie DG. The AMP-activated protein kinase pathway—new players upstream and downstream. *J Cell Sci.* 2004;117(23):5479–87.
1040. Viollet B, Guigas B, Leclerc J, Hébrard S, Lantier L, Mounier R, et al. AMP-activated protein kinase in the regulation of hepatic energy metabolism: from physiology to therapeutic perspectives. *Acta Physiol.* 2009;196(1):81–98.
1041. Viollet B, Foretz M, Guigas B, Horman S, Dentin R, Bertrand L, et al. Activation of AMP-activated protein kinase in the liver: a new strategy for the management of metabolic hepatic disorders. *J Physiol.* 2006;574(1):41–53.
1042. Kim I, He YY. Targeting the AMP-Activated Protein Kinase for Cancer Prevention and Therapy. *Front Oncol.* 2013 Jul 15;3:175.
1043. Ke R, Xu Q, Li C, Luo L, Huang D. Mechanisms of AMPK in the maintenance of ATP balance during energy metabolism. *Cell Biol Int.* 2018;42(4):384–92.

1044. Hardie DG, Carling D, Carlson M. THE AMP-ACTIVATED/SNF1 PROTEIN KINASE SUBFAMILY: Metabolic Sensors of the Eukaryotic Cell? *Annu Rev Biochem.* 1998 Jun 1;67(1):821–55.
1045. SALT IP, JOHNSON G, ASHCROFT SJH, HARDIE DG. AMP-activated protein kinase is activated by low glucose in cell lines derived from pancreatic β cells, and may regulate insulin release. *Biochem J.* 1998 Nov 1;335(3):533–9.
1046. Bateman A. The structure of a domain common to archaebacteria and the homocystinuria disease protein. *Trends Biochem Sci.* 1997 Jan 1;22(1):12–3.
1047. Scott JW, Hawley SA, Green KA, Anis M, Stewart G, Scullion GA, et al. CBS domains form energy-sensing modules whose binding of adenosine ligands is disrupted by disease mutations. *J Clin Invest.* 2004 Jan 15;113(2):274–84.
1048. Gimeno-Alcañiz JV, Sanz P. Glucose and type 2A protein phosphatase regulate the interaction between catalytic and regulatory subunits of AMP-activated protein kinase. *J Mol Biol.* 2003;333(1):201–9.
1049. Thornton C, Snowden MA, Carling D. Identification of a Novel AMP-activated Protein Kinase β Subunit Isoform That Is Highly Expressed in Skeletal Muscle *. *J Biol Chem.* 1998 May 15;273(20):12443–50.
1050. Ross FA, MacKintosh C, Hardie DG. AMP-activated protein kinase: a cellular energy sensor that comes in 12 flavours. *FEBS J.* 2016;283(16):2987–3001.
1051. Garcia D, Shaw RJ. AMPK: Mechanisms of Cellular Energy Sensing and Restoration of Metabolic Balance. *Mol Cell.* 2017 Jun 15;66(6):789–800.
1052. Woods Angela, Azzout-Marniche Dalila, Foretz Marc, Stein Silvie C., Lemarchand Patricia, Ferré Pascal, et al. Characterization of the Role of AMP-Activated Protein Kinase in the Regulation of Glucose-Activated Gene Expression Using Constitutively Active and Dominant Negative Forms of the Kinase. *Mol Cell Biol.* 2000 Sep 15;20(18):6704–11.
1053. Lu J, Wu T, Zhang B, Liu S, Song W, Qiao J, et al. Types of nuclear localization signals and mechanisms of protein import into the nucleus. *Cell Commun Signal.* 2021 May 22;19(1):60.
1054. Suzuki Atsushi, Okamoto Shiki, Lee Suni, Saito Kumiko, Shiuchi Tetsuya, Minokoshi Yasuhiko. Leptin Stimulates Fatty Acid Oxidation and Peroxisome Proliferator-Activated Receptor α Gene Expression in Mouse C2C12 Myoblasts by Changing the Subcellular Localization of the $\alpha 2$ Form of AMP-Activated Protein Kinase. *Mol Cell Biol.* 2007 Jun 15;27(12):4317–27.
1055. Kodiha M, Rassi JG, Brown CM, Stochaj U. Localization of AMP kinase is regulated by stress, cell density, and signaling through the MEK \rightarrow ERK1/2 pathway. *Am J Physiol-Cell Physiol.* 2007;293(5):C1427–36.
1056. McGee SL, Howlett KF, Starkie RL, Cameron-Smith D, Kemp BE, Hargreaves M. Exercise increases nuclear AMPK $\alpha 2$ in human skeletal muscle. *Diabetes.* 2003;52(4):926–8.

1057. Steinberg GR, Watt MJ, McGee SL, Chan S, Hargreaves M, Febbraio MA, et al. Reduced glycogen availability is associated with increased AMPK α 2 activity, nuclear AMPK α 2 protein abundance, and GLUT4 mRNA expression in contracting human skeletal muscle. *Appl Physiol Nutr Metab*. 2006;31(3):302–12.
1058. Lamia KA, Sachdeva UM, DiTacchio L, Williams EC, Alvarez JG, Egan DF, et al. AMPK regulates the circadian clock by cryptochrome phosphorylation and degradation. *Science*. 2009;326(5951):437–40.
1059. Vara-Ciruelos D, Dandapani M, Gray A, Egbani EO, Evans AM, Hardie DG. Genotoxic Damage Activates the AMPK- α 1 Isoform in the Nucleus via Ca²⁺/CaMKK2 Signaling to Enhance Tumor Cell Survival. *Etoposide-Induced AMPK Activation Enhances Cell Survival*. *Mol Cancer Res*. 2018;16(2):345–57.
1060. Gowans GJ, Hawley SA, Ross FA, Hardie DG. AMP is a true physiological regulator of AMP-activated protein kinase by both allosteric activation and enhancing net phosphorylation. *Cell Metab*. 2013;18(4):556–66.
1061. Hawley S, Boudeau J, Reid J, Mustard K, Udd L, Makela T, et al. Complexes between the LKB1 tumor suppressor, STRAD/and MO25/are upstream kinases in the AMP-activated protein kinase cascade [article online]. *J Biol*. 2003;2:28.
1062. Shaw RJ, Kosmatka M, Bardeesy N, Hurley RL, Witters LA, DePinho RA, et al. The tumor suppressor LKB1 kinase directly activates AMP-activated kinase and regulates apoptosis in response to energy stress. *Proc Natl Acad Sci*. 2004;101(10):3329–35.
1063. Woods A, Johnstone SR, Dickerson K, Leiper FC, Fryer LG, Neumann D, et al. LKB1 is the upstream kinase in the AMP-activated protein kinase cascade. *Curr Biol*. 2003;13(22):2004–8.
1064. Joseph BK, Liu HY, Francisco J, Pandya D, Donigan M, Gallo-Ebert C, et al. Inhibition of AMP kinase by the protein phosphatase 2A heterotrimer, PP2A^{pp2r2d}. *J Biol Chem*. 2015;290(17):10588–98.
1065. Garcia-Haro L, Garcia-Gimeno MA, Neumann D, Beullens M, Bollen M, Sanz P. The PP1-R6 protein phosphatase holoenzyme is involved in the glucose-induced dephosphorylation and inactivation of AMP-activated protein kinase, a key regulator of insulin secretion, in MIN6 β cells. *FASEB J*. 2010;24(12):5080–91.
1066. Wu N, Zheng B, Shaywitz A, Dagon Y, Tower C, Bellinger G, et al. AMPK-dependent degradation of TXNIP upon energy stress leads to enhanced glucose uptake via GLUT1. *Mol Cell*. 2013;49(6):1167–75.
1067. Hardie DG. AMPK: a target for drugs and natural products with effects on both diabetes and cancer. *Diabetes*. 2013;62(7):2164–72.
1068. Agarwal S, Bell CM, Rothbart SB, Moran RG. AMP-activated Protein Kinase (AMPK) Control of mTORC1 Is p53- and TSC2-independent in Pemetrexed-treated Carcinoma Cells *. *J Biol Chem*. 2015 Nov 13;290(46):27473–86.
1069. Wang Y, Liu Z, Shu S, Cai J, Tang C, Dong Z. AMPK/mTOR Signaling in Autophagy Regulation During Cisplatin-Induced Acute Kidney Injury. *Front Physiol*

- [Internet]. 2020;11. Available from:
<https://www.frontiersin.org/articles/10.3389/fphys.2020.619730>
1070. Boily G, He X, Pearce B, Jardine K, McBurney M. SirT1-null mice develop tumors at normal rates but are poorly protected by resveratrol. *Oncogene*. 2009;28(32):2882–93.
1071. Boily G, Seifert EL, Bevilacqua L, He XH, Sabourin G, Estey C, et al. SirT1 regulates energy metabolism and response to caloric restriction in mice. *PloS One*. 2008;3(3):e1759.
1072. Um JH, Park SJ, Kang H, Yang S, Foretz M, McBurney MW, et al. AMP-activated protein kinase-deficient mice are resistant to the metabolic effects of resveratrol. *Diabetes*. 2010;59(3):554–63.
1073. Ruderman NB, Xu XJ, Nelson L, Cacicedo JM, Saha AK, Lan F, et al. AMPK and SIRT1: a long-standing partnership? *Am J Physiol Endocrinol Metab*. 2010/01/26 ed. 2010 Apr;298(4):E751–60.
1074. Chen H, Liu X, Chen H, Cao J, Zhang L, Hu X, et al. Role of SIRT1 and AMPK in mesenchymal stem cells differentiation. *Ageing Res Rev*. 2014 Jan 1;13:55–64.
1075. Li S, Qian Q, Ying N, Lai J, Feng L, Zheng S, et al. Activation of the AMPK-SIRT1 pathway contributes to protective effects of Salvianolic acid A against lipotoxicity in hepatocytes and NAFLD in mice. *Front Pharmacol* [Internet]. 2020;11. Available from:
<https://www.frontiersin.org/articles/10.3389/fphar.2020.560905>
1076. Price NL, Gomes AP, Ling AJY, Duarte FV, Martin-Montalvo A, North BJ, et al. SIRT1 Is Required for AMPK Activation and the Beneficial Effects of Resveratrol on Mitochondrial Function. *Cell Metab*. 2012 May 2;15(5):675–90.
1077. Lan F, Cacicedo JM, Ruderman N, Ido Y. SIRT1 modulation of the acetylation status, cytosolic localization, and activity of LKB1: possible role in AMP-activated protein kinase activation. *J Biol Chem*. 2008;283(41):27628–35.
1078. Sanders MJ, Ali ZS, Hegarty BD, Heath R, Snowden MA, Carling D. Defining the mechanism of activation of AMP-activated protein kinase by the small molecule A-769662, a member of the thienopyridone family. *J Biol Chem*. 2007;282(45):32539–48.
1079. Scott JW, Ling N, Issa SM, Dite TA, O'Brien MT, Chen ZP, et al. Small molecule drug A-769662 and AMP synergistically activate naive AMPK independent of upstream kinase signaling. *Chem Biol*. 2014;21(5):619–27.
1080. Corton JM, Gillespie JG, Hawley SA, Hardie DG. 5-Aminoimidazole-4-carboxamide ribonucleoside: a specific method for activating AMP-activated protein kinase in intact cells? *Eur J Biochem*. 1995;229(2):558–65.
1081. Hardie DG. AMP-activated protein kinase as a drug target. *Annu Rev Pharmacol Toxicol*. 2007;47:185–210.
1082. Göransson O, McBride A, Hawley SA, Ross FA, Shpiro N, Foretz M, et al. Mechanism of action of A-769662, a valuable tool for activation of AMP-activated protein kinase. *J Biol Chem*. 2007/09/12 ed. 2007 Nov 9;282(45):32549–60.

1083. Park HU, Suy S, Danner M, Dailey V, Zhang Y, Li H, et al. AMP-activated protein kinase promotes human prostate cancer cell growth and survival. *Mol Cancer Ther.* 2009;8(4):733–41.
1084. Tang YC, Williams BR, Siegel JJ, Amon A. Identification of aneuploidy-selective antiproliferation compounds. *Cell.* 2011;144(4):499–512.
1085. Isakovic A, Harhaji L, Stevanovic D, Markovic Z, Sumarac-Dumanovic M, Starcevic V, et al. Dual antiglioma action of metformin: cell cycle arrest and mitochondria-dependent apoptosis. *Cell Mol Life Sci.* 2007;64(10):1290–302.
1086. Ríos M, Foretz M, Viollet B, Prieto A, Fraga M, Costoya JA, et al. AMPK Activation by Oncogenesis Is Required to Maintain Cancer Cell Proliferation in Astrocytic Tumors. *Cancer Res.* 2013 Apr 15;73(8):2628–38.
1087. Dowling RJO, Zakikhani M, Fantus IG, Pollak M, Sonenberg N. Metformin Inhibits Mammalian Target of Rapamycin–Dependent Translation Initiation in Breast Cancer Cells. *Cancer Res.* 2007 Nov 15;67(22):10804–12.
1088. Liu X, Chhipa RR, Pooya S, Wortman M, Yachyshin S, Chow LML, et al. Discrete mechanisms of mTOR and cell cycle regulation by AMPK agonists independent of AMPK. *Proc Natl Acad Sci.* 2014 Jan 28;111(4):E435–44.
1089. Vucicevic L, Misirkic M, Kristina J, Vilimanovich U, Sudar E, Isenovic E, et al. Compound C induces protective autophagy in cancer cells through AMPK inhibition-independent blockade of Akt/mTOR pathway. *Autophagy.* 2011 Jan 1;7(1):40–50.
1090. Hwang JT, Ha J, Park IJ, Lee SK, Baik HW, Kim YM, et al. Apoptotic effect of EGCG in HT-29 colon cancer cells via AMPK signal pathway. *Cancer Lett.* 2007 Mar 8;247(1):115–21.
1091. Pan W, Yang H, Cao C, Song X, Wallin B, Kivlin R, et al. AMPK mediates curcumin-induced cell death in CaOV3 ovarian cancer cells. *Oncol Rep.* 2008 Dec 1;20(6):1553–9.
1092. Zhu Y, Zhou J, Ao R, Yu B. A-769662 Protects Osteoblasts from Hydrogen Dioxide-Induced Apoptosis through Activating of AMP-Activated Protein Kinase (AMPK). *Int J Mol Sci.* 2014;15(6).
1093. Hao J, Daleo MA, Murphy CK, Yu PB, Ho JN, Hu J, et al. Dorsomorphin, a selective small molecule inhibitor of BMP signaling, promotes cardiomyogenesis in embryonic stem cells. *PloS One.* 2008 Aug 6;3(8):e2904–e2904.
1094. Choi S, Yang SY, Choi GJ, Kim BG, Kang H. Comparison of pressure- and volume-controlled ventilation during laparoscopic colectomy in patients with colorectal cancer. *Sci Rep.* 2019 Nov 18;9(1):17007.
1095. Wang Y gang, Han X guo, Yang Y, Qiao H, Dai K rong, Fan Q ming, et al. Functional differences between AMPK $\alpha 1$ and $\alpha 2$ subunits in osteogenesis, osteoblast-associated induction of osteoclastogenesis, and adipogenesis. *Sci Rep.* 2016 Sep 7;6(1):32771.

1096. Toyama BH, Hetzer MW. Protein homeostasis: live long, won't prosper. *Nat Rev Mol Cell Biol.* 2013 Jan 1;14(1):55–61.
1097. Ferrell Jr JE, Xiong W. Bistability in cell signaling: How to make continuous processes discontinuous, and reversible processes irreversible. *Chaos Interdiscip J Nonlinear Sci.* 2001;11(1):227–36.
1098. Harris SL, Levine AJ. The p53 pathway: positive and negative feedback loops. *Oncogene.* 2005;24(17):2899–908.
1099. Kaneko S, Feldman RI, Yu L, Wu Z, Gritsko T, Shelley SA, et al. Positive feedback regulation between Akt2 and MyoD during muscle differentiation: cloning of Akt2 promoter. *J Biol Chem.* 2002;277(26):23230–6.
1100. Thayer MJ, Tapscott SJ, Davis RL, Wright WE, Lassar AB, Weintraub H. Positive autoregulation of the myogenic determination gene MyoD1. *Cell.* 1989;58(2):241–8.
1101. Koh JH, Hancock CR, Han DH, Holloszy JO, Nair KS, Dasari S. AMPK and PPAR β positive feedback loop regulates endurance exercise training-mediated GLUT4 expression in skeletal muscle. *Am J Physiol-Endocrinol Metab.* 2019 May 1;316(5):E931–9.
1102. Holloszy JO. Regulation of mitochondrial biogenesis and GLUT4 expression by exercise. *Compr Physiol.* 2011;1(2):921–40.
1103. Gan Z, Burkart-Hartman EM, Han DH, Finck B, Leone TC, Smith EY, et al. The nuclear receptor PPAR β/δ programs muscle glucose metabolism in cooperation with AMPK and MEF2. *Genes Dev.* 2011;25(24):2619–30.
1104. Yu PB, Hong CC, Sachidanandan C, Babitt JL, Deng DY, Hoyng SA, et al. Dorsomorphin inhibits BMP signals required for embryogenesis and iron metabolism. *Nat Chem Biol.* 2008;4(1):33–41.
1105. Boergermann J, Kopf J, Yu P, Knaus P. Dorsomorphin and LDN-193189 inhibit BMP-mediated Smad, p38 and Akt signalling in C2C12 cells. *Int J Biochem Cell Biol.* 2010;42(11):1802–7.
1106. Bain J, Plater L, Elliott M, Shpiro N, Hastie CJ, Mclauchlan H, et al. The selectivity of protein kinase inhibitors: a further update. *Biochem J.* 2007;408(3):297–315.
1107. Vogt J, Traynor R, Sapkota GP. The specificities of small molecule inhibitors of the TGF β s and BMP pathways. *Cell Signal.* 2011;23(11):1831–42.
1108. Liu X, Chhipa RR, Nakano I, Dasgupta B. The AMPK Inhibitor Compound C Is a Potent AMPK-Independent Antiglioma Agent. *Mol Cancer Ther.* 2014 Mar 9;13(3):596–605.
1109. Bartoli-Leonard F, Wilkinson FL, Langford-Smith AWW, Alexander MY, Weston R. The Interplay of SIRT1 and Wnt Signaling in Vascular Calcification. *Front Cardiovasc Med [Internet].* 2018;5. Available from: <https://www.frontiersin.org/articles/10.3389/fcvm.2018.00183>

1110. Dite T, Langendorf C, Hoque A, Galic S, Rebello R, Ovens A, et al. AMP-activated protein kinase selectively inhibited by the type II inhibitor SBI-0206965. *J Biol Chem*. 2018 Apr 25;293:jbc.RA118.003547.
1111. Knudsen JR, Madsen AB, Persson KW, Henríquez-Olguín C, Li Z, Jensen TE. The ULK1/2 and AMPK Inhibitor SBI-0206965 Blocks AICAR and Insulin-Stimulated Glucose Transport. *Int J Mol Sci*. 2020;21(7).
1112. Strembitska A, Mancini SJ, Gamwell JM, Palmer TM, Baillie GS, Salt IP. A769662 inhibits insulin-stimulated Akt activation in human macrovascular endothelial cells independent of AMP-activated protein kinase. *Int J Mol Sci*. 2018;19(12):3886.
1113. Choumessi AT, Johanns M, Beaufay C, Herent MF, Stroobant V, Vertommen D, et al. Two isoprenylated flavonoids from *Dorstenia psilurus* activate AMPK, stimulate glucose uptake, inhibit glucose production and lower glycemia. *Biochem J*. 2019;476(24):3687–704.
1114. Ma T, Chen Y, Vingtdoux V, Zhao H, Viollet B, Marambaud P, et al. Inhibition of AMP-Activated Protein Kinase Signaling Alleviates Impairments in Hippocampal Synaptic Plasticity Induced by Amyloid β . *J Neurosci*. 2014 Sep 3;34(36):12230.
1115. Allison SJ, Milner J. RNA Interference by Single- and Double-stranded siRNA With a DNA Extension Containing a 3' Nuclease-resistant Mini-hairpin Structure. *Mol Ther - Nucleic Acids* [Internet]. 2014 Jan 1 [cited 2022 Nov 14];3. Available from: <https://doi.org/10.1038/mtna.2013.68>
1116. Li Y, Chen X, Cui Y, Wei Q, Chen S, Wang X. Effects of SIRT1 silencing on viability, invasion and metastasis of human glioma cell lines. *Oncol Lett*. 2019 Apr 1;17(4):3701–8.
1117. Xiao B, Sanders MJ, Carmena D, Bright NJ, Haire LF, Underwood E, et al. Structural basis of AMPK regulation by small molecule activators. *Nat Commun*. 2013;4(1):1–10.
1118. Zadra G, Photopoulos C, Tyekucheva S, Heidari P, Weng QP, Fedele G, et al. A novel direct activator of AMPK inhibits prostate cancer growth by blocking lipogenesis. *EMBO Mol Med*. 2014;6(4):519–38.
1119. Xu Y yi, Chen F li, Ji F, Fei H dong, Xie Y, Wang S guo. Activation of AMP-activated protein kinase by compound 991 protects osteoblasts from dexamethasone. *Biochem Biophys Res Commun*. 2018 Jan 1;495(1):1014–21.
1120. Bultot L, Jensen TE, Lai YC, Madsen AL, Collodet C, Kviklyte S, et al. Benzimidazole derivative small-molecule 991 enhances AMPK activity and glucose uptake induced by AICAR or contraction in skeletal muscle. *Am J Physiol-Endocrinol Metab*. 2016;311(4):E706–19.
1121. Johanns M, dit Ruys SP, Houddane A, Vertommen D, Herinckx G, Hue L, et al. Direct and indirect activation of eukaryotic elongation factor 2 kinase by AMP-activated protein kinase. *Cell Signal*. 2017;36:212–21.

1122. Scott JW, van Denderen BJ, Jorgensen SB, Honeyman JE, Steinberg GR, Oakhill JS, et al. Thienopyridone drugs are selective activators of AMP-activated protein kinase β 1-containing complexes. *Chem Biol.* 2008;15(11):1220–30.
1123. Hawley SA, Fullerton MD, Ross FA, Schertzer JD, Chevtzoff C, Walker KJ, et al. The ancient drug salicylate directly activates AMP-activated protein kinase. *Science.* 2012;336(6083):918–22.
1124. Rharass T, Lucas S. MECHANISMS IN ENDOCRINOLOGY: Bone marrow adiposity and bone, a bad romance? *Eur J Endocrinol.* 2018 Oct 1;179(4):R165–82.
1125. Kalervo Väänänen H, Härkönen PL. Estrogen and bone metabolism. *Maturitas.* 1996 May 1;23:S65–9.
1126. Legroux-Gerot I, Vignau J, Collier F, Cortet B. Factors Influencing Changes in Bone Mineral Density in Patients with Anorexia Nervosa-Related Osteoporosis: The Effect of Hormone Replacement Therapy. *Calcif Tissue Int.* 2008 Nov 1;83(5):315–23.
1127. Yamamoto M, Iguchi G, Fukuoka H, Suda K, Bando H, Takahashi M, et al. SIRT1 regulates adaptive response of the growth hormone--insulin-like growth factor-I axis under fasting conditions in liver. *Proc Natl Acad Sci.* 2013 Sep 10;110(37):14948.
1128. Eleftheriou F, Ahn JD, Takeda S, Starbuck M, Yang X, Liu X, et al. Leptin regulation of bone resorption by the sympathetic nervous system and CART. *Nature.* 2005 Mar 1;434(7032):514–20.
1129. Briot K, Cortet B, Thomas T, Audran M, Blain H, Breuil V, et al. 2012 update of French guidelines for the pharmacological treatment of postmenopausal osteoporosis. *Joint Bone Spine.* 2012 May 1;79(3):304–13.
1130. Legroux-Gerot I, Vignau J, Collier F, Cortet B. Bone loss associated with anorexia nervosa. *Joint Bone Spine.* 2005 Dec 1;72(6):489–95.
1131. Penel G, Kerckhofs G, Chauveau C. Brief Report From the 4th International Meeting on Bone Marrow Adiposity (BMA2018). *Front Endocrinol [Internet].* 2019;10. Available from: <https://www.frontiersin.org/articles/10.3389/fendo.2019.00691>
1132. Legroux-Gérot I, Vignau J, Viltart O, Hardouin P, Chauveau C, Cortet B. Adipokines and bone status in a cohort of anorexic patients. *Joint Bone Spine.* 2019 Jan 1;86(1):95–101.
1133. Gimble JM. The function of adipocytes in the bone marrow stroma. *New Biol.* 1990;2(4):304–12.
1134. Nuttall ME, Shah F, Singh V, Thomas-Porch C, Frazier T, Gimble JM. Adipocytes and the Regulation of Bone Remodeling: A Balancing Act. *Calcif Tissue Int.* 2014 Jan 1;94(1):78–87.
1135. Schilling T, Nöth U, Klein-Hitpass L, Jakob F, Schütze N. Plasticity in adipogenesis and osteogenesis of human mesenchymal stem cells. *Mol Cell Endocrinol.* 2007 Jun 15;271(1):1–17.

1136. Cohen-Kfir E, Artsi H, Levin A, Abramowitz E, Bajayo A, Gurt I, et al. Sirt1 Is a Regulator of Bone Mass and a Repressor of Sost Encoding for Sclerostin, a Bone Formation Inhibitor. *Endocrinology*. 2011 Dec 1;152(12):4514–24.